frontiers
RESEARCH TOPICS

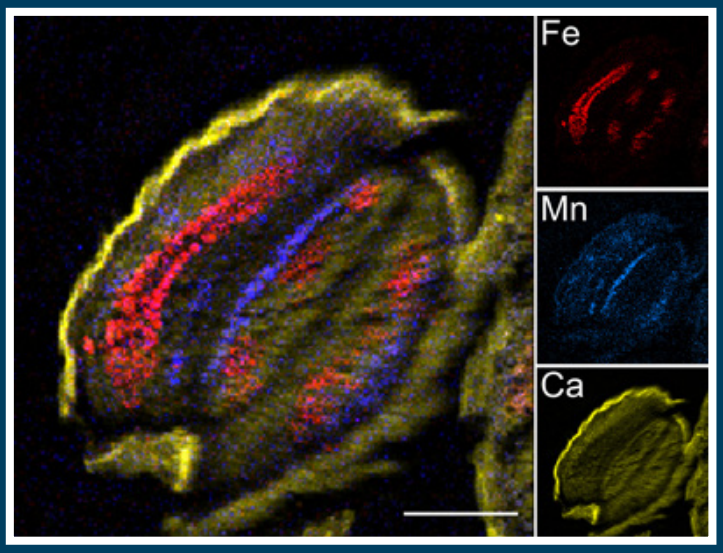

CELLULAR IRON HOMEOSTASIS AND METABOLISM IN PLANT

Topic Editors
Gianpiero Vigani, Khurram Bashir, Katrin Philippar, Jean-François Briat and Graziano Zocchi

frontiers in PLANT SCIENCE

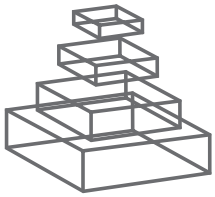

frontiers

ISSN 1664-8714
ISBN 978-2-88919-216-8
DOI 10.3389/978-2-88919-216-8

ABOUT FRONTIERS

Frontiers is more than just an open-access publisher of scholarly articles: it is a pioneering approach to the world of academia, radically improving the way scholarly research is managed. The grand vision of Frontiers is a world where all people have an equal opportunity to seek, share and generate knowledge. Frontiers provides immediate and permanent online open access to all its publications, but this alone is not enough to realize our grand goals.

FRONTIERS JOURNAL SERIES

The Frontiers Journal Series is a multi-tier and interdisciplinary set of open-access, online journals, promising a paradigm shift from the current review, selection and dissemination processes in academic publishing.
All Frontiers journals are driven by researchers for researchers; therefore, they constitute a service to the scholarly community. At the same time, the Frontiers Journal Series operates on a revolutionary invention, the tiered publishing system, initially addressing specific communities of scholars, and gradually climbing up to broader public understanding, thus serving the interests of the lay society, too.

DEDICATION TO QUALITY

Each Frontiers article is a landmark of the highest quality, thanks to genuinely collaborative interactions between authors and review editors, who include some of the world's best academicians. Research must be certified by peers before entering a stream of knowledge that may eventually reach the public - and shape society; therefore, Frontiers only applies the most rigorous and unbiased reviews.
Frontiers revolutionizes research publishing by freely delivering the most outstanding research, evaluated with no bias from both the academic and social point of view.
By applying the most advanced information technologies, Frontiers is catapulting scholarly publishing into a new generation.

WHAT ARE FRONTIERS RESEARCH TOPICS?

Frontiers Research Topics are very popular trademarks of the Frontiers Journals Series: they are collections of at least ten articles, all centered on a particular subject. With their unique mix of varied contributions from Original Research to Review Articles, Frontiers Research Topics unify the most influential researchers, the latest key findings and historical advances in a hot research area!
Find out more on how to host your own Frontiers Research Topic or contribute to one as an author by contacting the Frontiers Editorial Office: researchtopics@frontiersin.org

CELLULAR IRON HOMEOSTASIS AND METABOLISM IN PLANT

Topic Editors:
Gianpiero Vigani, Università degli Studi di Milano, Italy
Khurram Bashir, Riken, Yokohama, Japan
Katrin Philippar, Ludwig-Maximilians-University Munich, Germany
Jean-François Briat, Centre National de la Recherche Scientifique (CNRS), France
Graziano Zocchi, Università degli Studi di Milano, Italy

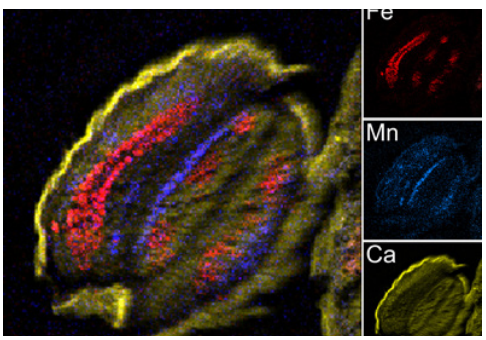

µPIXE elemental reconstituted image of Arabidopsis thaliana dry seed section. Total X-ray spectra of areas scanned with 3 MeV proton beam were collected. Specific distributions of Fe, Mn, and Ca in a 30 µm thick longitudinal section of Arabidopsis dry seed are shown overlaid (large image) and separately (small images). False color images and reconstitution were obtained using ImageJ free software. Scale bar: 100 µm; red, Fe; blue, Mn; yellow, Ca.

image taken from: Fig 2 of the following article >> Schnell Ramos, M., Khodja, H., Mary, V., Thomine, S. (2013). Using µPIXE for quantitative mapping of metal concentration in Arabidopsis thaliana seeds. Front. *Plant Sci.* doi: 10.3389/fpls.2013.00168

Iron (Fe) is an essential element for all living organisms because it is a cofactor for fundamental biochemical activities such as energy metabolism, oxygen transport and DNA synthesis. Hence both a deficiency and an excess of this transition metal has a strong impact on plant growth. As a consequence, plants must tightly regulate Fe homeostasis and metabolism to allow an effective Fe acquisition, distribution and utilization in the cell in both roots and leaves.

Mitochondria and chloroplasts represent the plant cellular compartments in which Fe is the most requested micronutrient. Indeed, several proteins involved in their Fe uptake mechanism are located in the inner membrane of both mitochondria and chloroplasts. As well, several enzymes belonging both to the respiratory chain and to the TCA cycle are Fe-containing proteins: complex I (NADH:ubiquinone oxidoreductase, Fe/S), complex II (succinate:ubiquinone oxidoreductase, Fe/S and heme), complex III (ubiquinol–cytochrome c oxidoreductase or bc1 complex, Fe/S and heme) and complex IV (cytochrome c oxidase, heme) as well as cytochrome c (heme), AOX (alternative oxidase, di-iron), aconitase (Fe/S), biotin synthase (Fe/S) and ferredoxins (Fe/S). Moreover, important proteins of Fe homeostasis such as

frataxin as well as crucial steps of the Fe-S cluster assembly for the entire cell take place in the mitochondrion. Similarly, in the chloroplast is located up to 80% of the cellular iron in leaves. In the photosynthetic apparatus Fe is an essential component of photosystem II (PSII) (iron), PSI (Fe/S, iron), cytochrome b6f (Fe/S and heme) and ferredoxins (Fdx, Fe/S) as well as of enzymes catalyzing chlorophyll synthesis. Similar to mitochondria, Fe is required in chloroplasts for heme and Fe/S cluster synthesis and it is stored in ferritin.

An impaired Fe content in plants induces Fe homeostasis-controlling mechanisms and a complex reprogramming of cellular metabolism, as mitochondria and chloroplasts are the site of essential pathways for plant growth. Indeed, under Fe deficiency, the defective respiratory and photosynthetic pathways lead to remarkable changes in carbon metabolism, including the activation of glycolysis, accumulation of organic acids and induction of several pathways involved in the synthesis of organic Fe-chelating compounds, useful to improve Fe uptake and transport within the plant.

Other than mitochondria and chloroplasts, also vacuoles play a key role in the intracellular compartmentalization of Fe. Sequestration and storage of Fe in vacuole and its remobilization (efflux) are important for plant to maintain cytosolic Fe homeostasis. Numerous ion transporters are located in the tonoplast, as well as organic acid transporters and proton pumps. Since vacuole transporters are involved in ion, organic acid and proton exchange between cytosol and lumen, the vacuole exerts an important role both in Fe homeostasis and in the metabolic changes induced by different Fe availability in plants.

The Research Topic will provide an overview on the new insights of both the Fe homeostasis processes and the metabolism reprogramming occurring in mitochondria, chloroplasts and vacuoles under different Fe nutritional status of plants (both deficiency and excess). We warmly welcome all types of articles, such as original research articles, methods articles, reviews, mini-reviews or perspective articles.

Table of Contents

frontiers in
PLANT SCIENCE

EDITORIAL
published: 03 December 2013
doi: 10.3389/fpls.2013.00490

Cellular iron homeostasis and metabolism in plant

Gianpiero Vigani[1]*, Graziano Zocchi[1]*, Khurram Bashir[2]*, Katrin Philippar[3]* and Jean François Briat[4]*

[1] *Dipartimento di Scienze Agrarie e Ambientali-Produzione, Territorio e Agroenergia, Università degli Studi di Milano, Milano, Italy*
[2] *Center for Sustainable Resource Sciences, RIKEN Yokohama campus, RIKEN, Yokohama, Japan*
[3] *Department Biology I-Plant Biochemistry and Physiology, Ludwig-Maximilians-University Munich, Munich, Germany*
[4] *Biochimie and Physiologie Moléculaire des Plantes, Centre National de la Recherche Scientifique, Institut National de la Recherche Agronomique, Université Montpellier 2, Montpellier, France*
**Correspondence: gianpiero.vigani@unimi.it; graziano.zocchi@unimi.it; bashirkhurram@hotmail.com; philippar@lmu.de; briat@supagro.inra.fr*

Edited by:
Nicolaus Von Wirén, IPK Gatersleben, Germany

Keywords: plant Fe homeostasis, plant metabolism, chloroplast, mitochondrion, vacuole, Fe transporters, Fe-S clusters, plant Fe localization

Iron (Fe) homeostasis represents an important topic in the plant mineral nutrition, since Fe is an essential cofactor for fundamental biochemical activities. Due to the low availability of Fe in most soils, plants are often limited in Fe content. As a consequence, plants must tightly regulate an effective Fe acquisition, distribution, and utilization in root and leaf cells in order to allow for sustainable Fe homeostasis and metabolism. In the past several years, there has been significant progress in understanding how the Fe deficiency responses are regulated and controlled in plants. However, several questions remain still open (Vigani et al., 2013a). Thereby, further work is required in order to fully understand the Fe homeostasis and metabolism in plants.

The aim of this Research Topic is to provide an overview on the new insights of both Fe homeostasis processes and metabolic reprogramming occurring in cellular compartments under different Fe nutritional conditions. Our intent was to recruit a panel of leading experts in the field of plant Fe homeostasis to prepare focused papers advancing our current knowledge in this field and contributing to the development of a comprehensive understanding of iron homeostasis in plants. Within this special issue of Frontiers, 9 original research articles, 4 reviews/mini-reviews and 2 perspective articles are collected.

Four papers are based on "Omic" approaches, which in the past few years provided a huge amount of information about transcriptomic, proteomic, and metabolomic effects induced by Fe deficiency. In particular, Lan et al. (2013) investigated the role of protein phosphorylation in the regulation of cellular Fe homeostasis, by using RNA-seq analysis. The authors revealed networks comprising 87 known or annotated protein kinase and phosphatase genes that could be subdivided into several co-expressed gene modules, assigned to the leucine-rich repeat protein kinase superfamily or associated with biological processes such as "hypotonic salinity response," "potassium ion import," and "cellular potassium ion homeostasis." Furthermore, Rodriguez-Celma et al. (2013), observed a dramatic down-regulation of genes belonging to photosynthesis and tetrapyrrole metabolisms by transcriptomic analysis performed on Fe-deficient Arabidopsis leaves, indicating the presence of a carefully orchestrated balance of potentially toxic tetrapyrrole intermediates and functional end products to avoid photo-oxidative damage. In addition, this study indicated six novel players with putative roles in Fe homeostasis, named Iron Responsive Proteins (IRP) 1–6.

At the proteomic level, the review paper by López-Millán et al. (2013) summarized the new findings that this approach provided during the recent years. Indeed, proteomics has been a powerful tool in the elucidation of general metabolic rearrangements upon Fe deficiency. Fe deficiency has a profound impact on carbon metabolism and on the arrangement of the photosynthetic machinery, with many of these changes conserved amongst plant species. In this context, Khandakar et al. (2013) performed a small-scale proteomic approach on *Hypocampus alba*, confirming the main metabolic strategy of Fe-deficient plants to adjust the metabolism by an economical use of Fe and ATP. The latter including the use of energy to re-programme root morphology and function in response to Fe restriction, which should be a principal strategy for plant roots facing severely suboptimal Fe availability. Additionally they showed also that Fe deficiency affected the alkaloid biosynthesis pathways.

An important topic concerning the nutrient mapping in plant tissues arises in the past recent years. About this issue, two original research papers, dealing with the Fe localization in both tissues and sub-cellular compartments have been published in the present research topic. By using Particle-Induced X-ray Emission (μPIXE) analysis, Schnell Ramos et al. (2013) determined the metal distribution in Arabidopsis seeds. μPIXE induced by a focused ion beam allows multi-elemental mapping in biological samples with high spatial resolution and high sensitivity. This fully quantitative approach revealed important Fe stores outside the endodermal cells. Imaging of imbibed seeds indicates a dynamic localization of metals as Fe and Zn concentrations increase in the subepidermal cell layer of cotyledons after imbibition. Other than quantitative approaches, also qualitative Fe localization techniques have been improved. Indeed, Roschzttardtz et al. (2013) have taken advantage of the Perls/DAB Fe staining procedure to perform a systematic analysis of Fe distribution in roots, leaves, and reproductive organs of the model plant *Arabidopsis thaliana*, using wild-type and mutant genotypes affected in Fe transport and storage. This study has established a reliable atlas of Fe distribution in the Arabidopsis organs, proving and refining long-assumed intracellular locations and uncovering new ones. The authors suggested that the characterization of the "iron map" in Arabidopsis will contribute to identify further actors of Fe movement in plant tissues and cell compartments.

One of the Fe-dependent pathways essential to the cell is the Fe-S cluster assembly. In the present research topic Couturier et al. (2013) reviewed the new actors of this pathways that have been discovered in the past few years, such as glutaredoxin redox enzymes. Further, BolAA and NEET proteins as well as MIP18, MMS19, TAH18, DRE2 are required for the cytosolic machinery of plant Fe-S cluster biogenesis systems.

It is clear that Fe-S clusters biogenesis is strictly related to a correct supply of both Fe and S. In this context Fiorieri et al. (2013) discussed that the interaction between these two nutrients might be of particular importance because Fe starvation influences S nutrition and *vice versa*. As a future perspective they concluded that a co-regulation between Fe and S metabolism exists and that Fe-S cluster availability might be involved in sensing and signaling mechanisms of combined Fe and S deficiencies. Accordingly, also Couturier et al. (2013) suggested the possible involvement of Grx-BolA complexes either in the regulation of Fe-S cluster biogenesis or in the sensing of Fe-S cluster status in organelles where both proteins are simultaneously present.

These findings underline a big open question in the plant Fe homeostasis field: the identification of the cellular Fe sensing and signaling mechanism(s). How such sensing is achieved and how it leads to metabolic adjustments in case of nutrient shortage is mostly unknown. In this research topic, the perspective article by Vigani et al. (2013b) provided a tentative answer, suggesting a possible involvement of some prolyl hydroxylase (P4Hs) belonging to the 2-OG-dioxygenase family proteins in mediating the Fe-induced metabolic adjustment in plants.

Investigating Fe homeostasis at sub-cellular level represents an intriguing topic that provided important discoveries in the past few years. Fe is essential for central organelles such as mitochondria and chloroplasts. Therefore, Fe deficiency responses require wide adjustments of all cellular compartments. Here, papers unraveling mitochondrial as well as vacuolar involvement in Fe homeostasis have been reported. In particular, a timely review by Jain and Connolly (2013) focused on the recent findings related to mitochondrial Fe homeostasis. In particular the authors described the recent identification of both a mitochondrial Fe uptake transporter in rice and a possible role for metal-reductases in Fe uptake by mitochondria. In addition, the authors underlined the recent advances in mitochondrial iron homeostasis with an emphasis on the roles of frataxin and ferritin in Fe trafficking and storage within mitochondria. However, the presence and the role of plant mitochondrial ferritin has been often questioned. In this research topic Vigani et al. (2013c) provided a proof that ferritin is a functional Fe-storage protein in cucumber mitochondria showing that the native 24-mer ferritin complex indeed truly binds Fe(III).

Changes in Fe content in the cell do not affect only Fe-dependent compartments such as mitochondria and chloroplast but also vacuoles. Indeed, the role of the vacuole in Fe-deficient cells is crucial, since the vacuole is involved in homeostasis of both protons and metal concentrations. Dell'Orto et al. (2013) showed the different behavior of cucumber and soybean, developing Fe deficiency responses mainly in relation to the vacuolar proton pump activities. Furthermore, vacuolar sequestration of heavy metals is particularly important during Fe deficiency, when the increased activity of the IRT1 transporter causes excessive uptake of Mn, Ni, and Zn, as well as some other heavy metals. Indeed, Chu et al. (2013) characterized the function and the sub-cellular localization of two new transporters YLS in Arabidopsis plants, demonstrating their localization on tonoplast and endoplasmic reticulum and their involvement in the regulation of homeostasis of heavy metals in the cell. However, these results do not agree with a recently published Plant Cell paper which reported that these YSL transporters (namely YSL4 and YSL6) are chloroplast transporters involved in Fe efflux from this organelle (Divol et al., 2013). These discrepancies between these two studies are so far unexplained and will require additional work to be clarified.

The subcellular analysis of plant Fe homeostasis would benefit from a model organism such as the green algae *Chlamydomonas*. Glaesener et al. (2013) reviewed the progress made on Fe homeostasis in *Chlamydomonas*, detailing the analytical procedures to investigate on it.

Finally, it is important to keep in mind that plants are in interaction with other organisms in their environment, in particular with those living in the soil. Indeed, the complex interactions between plant and soil microbiome make the study on plant Fe nutrition more complex as well as more intriguing. A typical example for this interaction is the legume-rhizobia symbiosis. Brear et al. (2013) underlined the importance of Fe in the legume-rhizobium symbiosis, specifically Fe movement within the symbiotic organ, the nodule. The authors described how the analysis of legume genomes would allow the identification of relevant Fe transporters into the nodule.

ACKNOWLEDGMENTS

We acknowledge all the authors and co-authors for their contributions, and we are indebted to the reviewers for their very useful advices, and to the Frontiers Team members for their help.

REFERENCES

Brear, E. M., Day, D. A., and Collina Smith, P. M. (2013). Iron: an essential micronutrient for the legume-rhizobium symbiosis. *Front. Plant Sci.* 4:359. doi: 10.3389/fpls.2013.00359

Chu, H. H., Conte, S. S., Rodriguez, D. C., Vasques, K., Punshon, T., Salt, D. E., et al. (2013). *Arabidopsis thaliana* Yellow Stripe1-Like4 and Yellow Stripe1-Like6 localize to internal cellular membranes and are involved in metal ion homeostasis. *Front. Plant Sci.* 4:283. doi: 10.3389/fpls.2013.00283

Couturier, J., Touraine, B., Briat, J. F., Gaymard, F., and Rouhier, N. (2013). The iron-sulfur cluster assembly machineries in plants: current knowledge and open questions. *Front. Plant Sci.* 4:259. doi: 10.3389/fpls.2013.00259

Dell'Orto, M., De Nisi, P., Vigani, G., and Zocchi, G. (2013). Fe deficiency differentially affects the vacuolar proton pumps in cucumber and soybean roots. *Front. Plant Sci.* 4:326. doi: 10.3389/fpls.2013.00326

Divol, F., Couch, D., Conéjéro, G., Roschzttardtz, H., Mari, S., and Curie, C. (2013). The Arabidopsis Yellow Stripe LIKE4 and 6 transporters control iron release from the chloroplast. *Plant Cell* 25, 1040–1055. doi: 10.1105/tpc.112.107672

Fiorieri, I., Wirtz, M., and Hell, R. (2013). Toward new perspectives on the interaction of iron and sulfur metabolism in plants. *Front. Plant Sci.* 4:357. doi: 10.3389/fpls.2013.00357

Glaesener, A. G., Merchant, S. S., and Blaby-Haas, C. E. (2013). Iron economy in *Chlamydomonas reinhardtii*. *Front. Plant Sci.* 4:337. doi: 10.3389/fpls.2013.00337

Jain, A., and Connolly, E. L. (2013). Mitochondrial iron transport and homeostasis in plants. *Front. Plant Sci.* 4:348. doi: 10.3389/fpls.2013.00348

Khandakar, J., Haraguchi, I., Yamaguchi, K., and Kitamura, Y. (2013). A small-scale proteomic approach reveals a survival strategy, including a reduction in alkaloid biosynthesis, in *Hyoscyamus albus* roots subjected to iron deficiency. *Front. Plant Sci.* 4:331. doi: 10.3389/fpls.2013.00331

Lan, P., Li, W., and Schmidt, W. (2013). A digital compendium of genes mediating the reversible phosphorylation of proteins in Fe-deficient Arabidopsis roots. *Front. Plant Sci.* 4:173. doi: 10.3389/fpls.2013.00173

López-Millán, A. F., Grusak, M. A., Abadia, A., and Abadía, J. (2013). Iron deficiency in plants: an insight from proteomic approaches. *Front. Plant Sci.* 4:254. doi: 10.3389/fpls.2013.00254

Rodriguez-Celma, J., Pan, I. C., Li, W., Lan, P., Buckhout, T. J., and Schmidt, W. (2013). The transcriptional response of Arabidopsis leaves to Fe deficiency. *Front. Plant Sci.* 4:276. doi: 10.3389/fpls.2013.00276

Roschzttardtz, H., Conéjéro, G., Divol, F., Alcon, C., Verdeil, J. L., Curie, C., et al. (2013). New insights into Fe localization in plant tissues. *Front. Plant Sci.* 4:350. doi: 10.3389/fpls.2013.00350

Schnell Ramos, M., Khodja, H., Mary, V., and Thomine, S. (2013). Using μPIXE for quantitative mapping of metal concentration in *Arabidopsis thaliana* seeds. *Front. Plant Sci.* 4:168. doi: 10.3389/fpls.2013.00168

Vigani, G., Zocchi, G., Bashir, K., Phillipar, K., and Briat, J. F. (2013a). Signal from choloroplast and mitochondria for iron homeostasis regulation. *Trends Plant Sci.* 18, 305–311. doi: 10.1016/j.tplants.2013.01.006

Vigani, G., Morandini, P., and Murgia, I. (2013b). Searching iron sensors in plants by exploring the link among 2'-OG-dependent dioxygenases, the iron deficiency response and metabolic adjustments occurring under iron deficiency. *Front. Plant Sci.* 4:169. doi: 10.3389/fpls.2013.00169

Vigani, G., Tarantino, D., and Murgia, I. (2013c). Mitochondrial ferritin is a functional iron-storage protein in cucumber (*Cucumis sativus*) roots. *Front. Plant Sci.* 4:316. doi: 10.3389/fpls.2013.00316

Received: 06 November 2013; accepted: 14 November 2013; published online: 03 December 2013.

Citation: Vigani G, Zocchi G, Bashir K, Philippar K and Briat JF (2013) Cellular iron homeostasis and metabolism in plant. Front. Plant Sci. ***4****:490. doi: 10.3389/fpls.2013.00490*

This article was submitted to Plant Nutrition, a section of the journal Frontiers in Plant Science.

frontiers in
PLANT SCIENCE

ORIGINAL RESEARCH ARTICLE
published: 03 June 2013
doi: 10.3389/fpls.2013.00173

A digital compendium of genes mediating the reversible phosphorylation of proteins in Fe-deficient *Arabidopsis* roots

***Ping Lan*[1,2]*, *Wenfeng Li*[2] *and Wolfgang Schmidt*[2]**

[1] State Key Laboratory of Soil and Sustainable Agriculture, Institute of Soil Science, Chinese Academy Sciences, Nanjing, China
[2] Institute of Plant and Microbial Biology, Academia Sinica, Taipei, Taiwan

Edited by:
Gianpiero Vigani, Università degli Studi di Milano, Italy

Reviewed by:
Sebastien Thomine, Centre National de la Recherche Scientifique, France
Petra Bauer, Saarland University, Germany

***Correspondence:**
Ping Lan, Institute of Soil Science, Chinese Academy Sciences 71# East Beijing Road, Nanjing 210008, China
e-mail: plan@issas.ac.cn

Post-translational modifications of proteins such as reversible phosphorylation provide an important but understudied regulatory network that controls important nodes in the adaptation of plants to environmental conditions. Iron (Fe) is an essential mineral nutrient for plants, but due to its low solubility often a limiting factor for optimal growth. To understand the role of protein phosphorylation in the regulation of cellular Fe homeostasis, we analyzed the expression of protein kinases (PKs) and phosphatases (PPs) in *Arabidopsis* roots by mining differentially expressed PK and PP genes. Transcriptome analysis using RNA-seq revealed that subsets of 203 PK and 39 PP genes were differentially expressed under Fe-deficient conditions. Functional modules of these PK and PP genes were further generated based on co-expression analysis using the MACCU toolbox on the basis of 300 publicly available root-related microarray data sets. Results revealed networks comprising 87 known or annotated PK and PP genes that could be subdivided into one large and several smaller highly co-expressed gene modules. The largest module was composed of 58 genes, most of which have been assigned to the leucine-rich repeat protein kinase superfamily and associated with the biological processes "hypotonic salinity response," "potassium ion import," and "cellular potassium ion homeostasis." The comprehensive transcriptional information on PK and PP genes in iron-deficient roots provided here sets the stage for follow-up experiments and contributes to our understanding of the post-translational regulation of Fe deficiency and potassium ion homeostasis.

Keywords: protein phosphorylation, RNA-seq, co-expression, iron deficiency, potassium homeostasis

INTRODUCTION

Iron (Fe) is an essential element for all living organisms. In plants, Fe is required for basic redox reactions in photosynthesis and respiration and for many vital enzymatic reactions such as DNA replication, lipid metabolism, and nitrogen fixation. Although Fe is one of the most abundant elements in the earth's crust, its bioavailability is severely restricted due to an extremely low solubility at neutral or basic pH. Approximately 30% of the cultivated plants are grown on calcareous soils, making Fe deficiency a major constraint for crop yield and quality (Rellan-Alvarez et al., 2011). Excess Fe is cytotoxic due to the formation of potentially harmful reactive oxygen species. Thus, plants must tightly regulate Fe homeostasis to allow an effective acquisition, distribution, and utilization of Fe.

Plants have evolved sophisticated mechanisms to promote Fe availability. Fe is acquired by two distinct strategies, referred to as strategy I and strategy II (Romheld and Marschner, 1986). In strategy II plants such as maize (*Zea mays*), Fe(III) is chelated by phytosiderophores that are synthesized and secreted by plant roots and the Fe-phytosiderophore complex is taken up by an oligopeptide transporter, YELLOW-STRIPE1 (Curie et al., 2001). Strategy II is confined to the grasses. In strategy I plants such as *Arabidopsis* (*Arabidopsis thaliana*), Fe acquisition is controlled by two basic helix-loop-helix (bHLH) transcription factors, FER-LIKE IRON DEFICIENCY-INDUCED TRANSCRIPTION FACTOR (FIT) and POPEYE (PYE), regulating non-overlapping subsets of genes with various roles in Fe uptake and metabolism (Colangelo and Guerinot, 2004; Bauer et al., 2007; Long et al., 2010; Schmidt and Buckhout, 2011). Disruption of FIT or PYE function leads to severe growth reduction and chlorosis under Fe-limited conditions, implicating that the function of these genes is critical for regulating Fe homeostasis. FIT forms heterodimers with bHLH38 and bHLH39 and positively regulates a subset of Fe-responsive genes, including three key genes required for Fe acquisition that encode the ferric chelate reductase FERRIC REDUCTION OXIDASE2 (FRO2), the Fe transporter IRT1 (Eide et al., 1996; Robinson et al., 1999; Vert et al., 2002; Colangelo and Guerinot, 2004; Yuan et al., 2008), and the H^+-translocating P-type ATPase AHA2 (Santi and Schmidt, 2009; Ivanov et al., 2012). Recent studies showed that the transcription factors bHLH100 and bHLH101, belonging to the Ib subgroup bHLH proteins, are also involved in *Arabidopsis* Fe-deficiency responses by interacting with FIT (Wang et al., 2013) or via a FIT-independent manner (Sivitz et al., 2012). *PYE* is preferentially expressed in the pericycle and aids in maintaining Fe homeostasis by positively regulating a separate set of genes. The expression of *BRUTUS* (*BTS*),

encoding a putative E3 ligase protein that negatively regulates some of the Fe-deficiency responses, is tightly correlated with *PYE* gene activity. Both proteins interact with the PYE homologs IAA-LEU-RESISTANT3 (ILR3) and bHLH115, suggesting a complex and dynamic regulatory circuit that adapts plants to fluctuating availability of Fe (Long et al., 2010).

For long-distance transport, Fe is exported from the cell by the ferroportin ortholog IREG1/FPN1 and transported in the xylem as a complex with citrate (Morrissey et al., 2009). The MATE transporter FRD3 was shown to be important for the proper transport of Fe from roots to leaves. *frd3* mutants showed constitutive up-regulated Fe-deficiency responses, chlorotic leaves, and ectopic accumulation of Fe in the root vasculature (Rogers and Guerinot, 2002; Durrett et al., 2007). FRD3 loads citrate into the xylem, which is crucial for the transport of Fe to the shoot. A recent report further showed that FRD3 promotes Fe nutrition of symplastically disconnected tissues such as pollen throughout the development (Roschzttardtz et al., 2011).

The signaling processes that are upstream of or parallel to FIT, PYE, and BTS are largely unknown. All three genes are regulated by the plant's Fe status, indicating that other components are involved in Fe sensing and signaling. The turnover of FIT is 26S proteasome-dependent (Lingam et al., 2011; Meiser et al., 2011; Sivitz et al., 2011), and the activity of IRT1 is post-translationally regulated by monoubiquitin (Barberon et al., 2011). Other post-translational processes, such as protein phosphorylation, were shown to be involved in the Fe-deficiency response (Lan et al., 2012b), but only for a few cases clear-cut evidence for a regulatory function of such modifications has been provided (Arnaud et al., 2006). An estimated one-third of all eukaryotic proteins are putatively regulated by reversible phosphorylation via protein kinases (PKs) and phosphatases (PPs), demonstrating the importance of this process. Phosphorylation can affect the configuration, activity, localization, interaction, and stability of proteins, thereby regulating crucial processes in metabolism and development. Transcriptional profiling experiments on Fe-deficient roots revealed several differentially expressed protein kinase genes, suggesting that alterations in protein phosphorylation patterns induced by Fe deficiency are involved in the control of Fe homeostasis (Colangelo and Guerinot, 2004; Dinneny et al., 2008; Buckhout et al., 2009; Garcia et al., 2010; Yang et al., 2010). Biological roles of these differentially expressed PKs and PPs, however, cannot be inferred solely based on the transcript level without functional characterization by genetic approaches. None the less, studying hundreds of differentially expressed genes without any selection filter would be extremely laborious. Co-expression analysis provides a way to filter and select genes of interest for the biological question under study (Ihmels et al., 2004; Kharchenko et al., 2005). The expression of genes within the same metabolic pathway shows often similar pattern; thus, co-expression analysis can aid in discovering upstream regulators or downstream substrates of a particular metabolic pathways (Ihmels et al., 2004; Kharchenko et al., 2005).

In order to gain insights into the regulation of the responses to Fe deficiency at the post-translational level, we analyzed the expression of PK and PP genes in Fe-deficient roots using the RNA-seq technology. Genes encoding PKs and PPs that were differentially expressed upon Fe starvation were clustered into groups of closely correlated modules based on their co-expression relationships under various sets of experimental conditions. Using this approach, we discovered PKs with potentially critical regulatory functions in cellular Fe and potassium (K) ion homeostasis under Fe-deficient conditions.

RESULTS

EXPRESSION OF PK AND PP GENES IN Fe-DEFICIENT *ARABIDOPSIS* ROOTS

Transcriptional changes in the expression of PK and PP genes upon Fe deficiency in *Arabidopsis* roots were mined in a previously published RNA-seq data set (Li et al., submitted). The flowchart was shown as **Figure 1**. Out of 1,118 PK (GO: 0004672) and 205 PP genes (GO: 0004721) annotated in the TAIR10 release

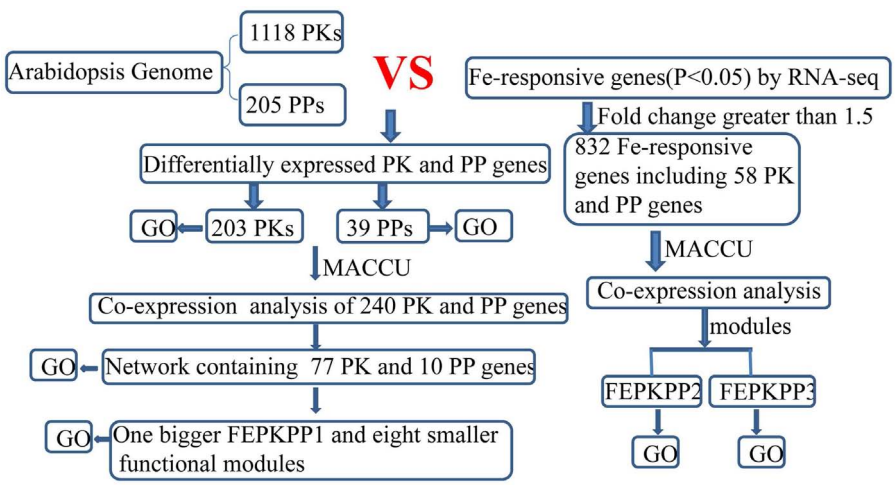

FIGURE 1 | Flowchart for mining differentially expressed PK and PP genes and subsequent co-expression analysis in *Arabidopsis* iron-deficient roots.

of the *Arabidopsis* genome, 203 PK and 39 PP genes were differentially expressed between Fe-sufficient and Fe-deficient plants ($P < 0.05$; Table S1 in Supplementary Material). Among the 203 PK genes, 88 and 37 genes were induced and repressed by Fe deficiency with fold-changes greater than 1.2 (**Figures 2A,B**), transcripts of 53 genes were changed more than 1.5-fold upon Fe deficiency (**Table 1**). Interestingly, 38 out of these 53 genes belong to the receptor-like kinase (RLK) and receptor-like cytoplasmic protein kinase (RLCK) superfamily (**Table 1**). The second most predominant group (eight genes) encodes PKs from the CAMK_AMPK/CDPK subfamily (**Table 1**). Among the 39 differentially expressed PP genes, 18 genes were up- or down-regulated by Fe deficiency with fold-changes greater than 1.2 (**Figures 2C,D**), transcripts of seven genes were changed more than 1.5-fold upon Fe deficiency (**Table 2**). Two genes, At2g46700 and At3g49370, are annotated to possess both PK and PP activity and are listed in both **Tables 1** and **2**.

GENE ONTOLOGY ENRICHMENT ANALYSIS OF THE DIFFERENTIALLY EXPRESSED PK AND PP GENES

Gene Ontology (GO) enrichment analysis revealed that the products of most of the 203 PKs localizes to the plasma membrane, the endomembrane system, and the micropyle (inset of Figure S1 in Supplementary Material, $P < 0.01$), and are involved in diverse biological processes ($P < 0.01$, Figure S1 in Supplementary Material). To gain insights into the physiological roles of the differentially expressed PKs, a GO enrichment analysis of PK genes that showed expression changes of more than 1.5-fold was performed. The results showed that that the categories "regulation of potassium ion transport," "tapetal cell fate specification," "response to nickel ion," and "cellular response to potassium ion starvation" were over-represented (Figure S2 in Supplementary Material). Most of the products of these genes are localized in the endomembrane system.

Among the 39 differentially expressed PP genes, the processes "hypotonic salinity response," "photosystem stoichiometry adjustment," and "cellular potassium ion homeostasis" etc. were enriched (Figure S3A in Supplementary Material). Gene products are localized in the protein serine/threonine phosphatase complex, on the plasma membrane, and in the calcineurin complex (Figure S3B in Supplementary Material). Within the seven PP genes with more than 1.5-fold change, none of the cellular components or biological processes was enriched.

CO-EXPRESSION ANALYSIS OF Fe-RESPONSIVE PK AND PP GENES

Co-expression networks of differentially expressed PK and PP genes were generated using the MACCU software (Lin et al., 2011). Pairwise co-expressed genes were selected with a Pearson correlation coefficient cutoff of 0.7 (Lin et al., 2011; Wang et al.,

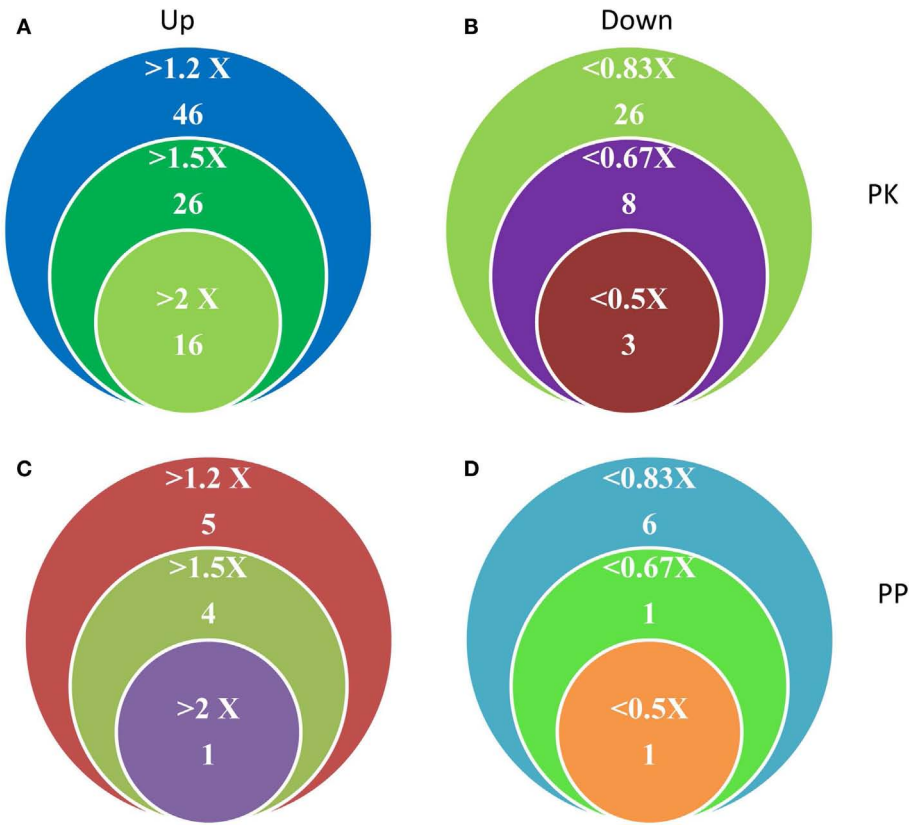

FIGURE 2 | Differentially expressed PK and PP genes in Fe-deficient *Arabidopsis* roots. **(A,B)** Number and expression levels of PK genes. **(C,D)** Number and expression levels of PP genes.

Table 1 | Differentially expressed protein kinase genes upon iron deficiency with fold change of more than 1.5-fold.

AGI	Function	Mean (−Fe/+Fe)	SD	Subfamily
AT2G19410	Protein kinase family protein	10.26	0.95	RLCK
AT5G53450	ORG1 (OBP3-responsive gene 1); ATP binding/kinase/protein kinase	5.24	0.18	
AT5G01060	Protein kinase family protein	5.01	0.85	RLCK
AT1G51870	Protein kinase family protein	4.10	2.00	RLK
AT1G77280	Protein kinase family protein	4.09	0.46	RLCK
AT4G38830	Protein kinase family protein	3.54	0.49	RLK
AT1G16120	WAKL1 (wall associated kinase-like 1)	2.76	0.57	RLK
AT5G39000	protein kinase family protein	2.75	0.63	RLK
AT1G16150	WAKL4 (WALL ASSOCIATED KINASE-LIKE 4)	2.72	0.39	RLK
AT5G23170	Protein kinase family protein	2.62	0.40	RLCK
AT1G05700	Leucine-rich repeat protein kinase	2.60	0.40	RLK
AT1G51830	ATP binding/kinase/protein serine/threonine kinase	2.58	0.19	RLK
AT4G26890	MAPKKK16; ATP binding/kinase/protein kinase/protein serine/threonine kinase/protein tyrosine kinase	2.18	0.13	Group-C
AT5G07280	EMS1 (EXCESS MICROSPOROCYTES1); kinase/transmembrane receptor protein kinase	2.14	0.27	RLK
AT1G33260	Protein kinase family protein	2.03	0.19	RLCK
AT1G51860	Leucine-rich repeat protein kinase	2.02	0.32	RLK
AT1G72540	Protein kinase, putative	1.97	0.33	RLCK
AT2G28990	Leucine-rich repeat protein kinase	1.96	0.08	RLK
AT5G60280	Lectin protein kinase family protein	1.93	0.36	RLK
AT4G18700	CIPK12 (CBL-INTERACTING PROTEIN KINASE 12); ATP binding/kinase/protein kinase/protein serine/threonine kinase	1.91	0.12	CAMK_AMPK
AT2G45590	Protein kinase family protein	1.89	0.32	RLCK
AT2G30360	SIP4 (SOS3-INTERACTING PROTEIN 4); kinase/protein kinase	1.89	0.21	CAMK_CDPK
AT3G46330	MEE39 (maternal effect embryo arrest 39)	1.78	0.28	RLK
AT1G51620	Protein kinase family protein	1.78	0.55	RLCK
AT1G08650	PPCK1 (PHOSPHOENOLPYRUVATE CARBOXYLASE KINASE); kinase/protein serine/threonine kinase	1.78	0.16	CAMK_CDPK
AT5G35580	ATP binding/kinase/protein kinase/protein serine/threonine kinase/protein tyrosine kinase	1.73	0.44	RLCK
AT3G49370	CDPK-related kinase	1.71	0.30	CAMK_AMPK
AT1G01140	CIPK9 (CBL-INTERACTING PROTEIN KINASE 9); ATP binding/kinase/protein kinase/protein serine/threonine kinase	1.71	0.37	CAMK_CDPK
AT3G27580	ATPK7; kinase/protein serine/threonine kinase	1.69	0.21	AGC_S6K
AT1G16160	WAKL5 (wall associated kinase-like 5)	1.64	0.34	RLK
AT3G45330	Lectin protein kinase family protein	1.62	0.19	RLK
AT5G55560	Protein kinase family protein	1.62	0.34	Other_WNK
AT1G07560	Leucine-rich repeat protein kinase	1.61	0.21	RLK
AT3G57740	Protein kinase family protein	1.61	0.39	RLCK
AT5G25440	Protein kinase family protein	1.59	0.16	RLCK
AT1G51800	Leucine-rich repeat protein kinase	1.58	0.12	RLK
AT1G66930	Serine/threonine protein kinase family protein	1.57	0.15	RLK
AT1G74360	Leucine-rich repeat transmembrane protein kinase	1.56	0.22	RLK
AT5G16900	Leucine-rich repeat protein kinase	1.56	0.15	RLK
AT4G04700	CPK27; ATP binding/calcium ion binding/kinase/protein kinase/protein serine/threonine kinase/protein tyrosine kinase	1.56	0.16	CAMK_CDPK
AT5G35750	AHK2 (*ARABIDOPSIS* HISTIDINE KINASE 2); cytokinin receptor/osmosensor/protein histidine kinase	1.56	0.03	
AT2G46700	CDPK-related kinase	1.52	0.11	CAMK_AMPK
AT3G50230	Leucine-rich repeat transmembrane protein kinase	0.64	0.09	RLK
AT5G49760	Leucine-rich repeat family protein/protein kinase family protein	0.63	0.04	RLK

(Continued)

Table 1 | Continued

AGI	Function	Mean (−Fe/+Fe)	SD	Subfamily
AT1G61480	S-locus protein kinase, putative	0.62	0.04	RLK
AT5G49780	ATP binding/kinase/protein serine/threonine kinase	0.62	0.03	RLK
AT2G25090	CIPK16 (CBL-INTERACTING PROTEIN KINASE 16); ATP binding/kinase/protein kinase/protein serine/threonine kinase	0.61	0.09	CAMK_AMPK
AT5G59660	Leucine-rich repeat protein kinase	0.60	0.05	RLK
AT1G07150	MAPKKK13; ATP binding/kinase/protein kinase/protein serine/threonine kinase	0.60	0.13	Group-C
AT2G18470	Protein kinase family protein	0.53	0.11	RLK
AT1G74490	Protein kinase, putative	0.46	0.09	RLCK
AT1G21230	WAK5 (WALL ASSOCIATED KINASE 5)	0.44	0.14	RLK
AT4G40010	SNRK2.7 (SNF1-RELATED PROTEIN KINASE 2.7)	0.44	0.08	Group-A

The corresponding mean ratios, defined as the transcript level (Reads Per Kilobase per Million mapped reads) in the –Fe treatment divided by the level in the +Fe treatment ($P < 0.05$).

Table 2 | Differentially expressed protein phosphatase genes upon iron deficiency with fold change of more than 1.5-fold.

AGI	Function	Mean (−Fe/+Fe)	SD	Alias
AT2G01880	PAP7 (PURPLE ACID PHOSPHATASE 7); acid phosphatase/protein serine/threonine phosphatase	3.11	0.42	PAP7
AT2G32960	Tyrosine specific protein phosphatase family protein	1.95	0.19	PFA-DSP2
AT3G49370	CDPK-related kinase	1.71	0.30	
AT2G01890	PAP8 (PURPLE ACID PHOSPHATASE 8); acid phosphatase/protein serine/threonine phosphatase	1.57	0.04	PAP8
AT2G46700	CDPK-related kinase	1.52	0.11	CRK3
AT5G26010	Catalytic/protein serine/threonine phosphatase	0.65	0.07	
AT5G59220	Protein phosphatase 2C, putative/PP2C, putative	0.45	0.04	SAG113

The corresponding mean ratios, defined as the transcript level (Reads Per Kilobase per Million mapped reads) in the −Fe treatment divided by the level in the +Fe treatment ($P < 0.05$).

2012). The 300 publicly available microarrays that were mined for analyzing co-expression relationship discriminated root-related experiments and the co-expression relationships reported here are restricted to roots. Because protein phosphorylation is reversible, both PK and PP genes were used to generate the network. The total number of differentially expressed PK and PP genes was 240. Co-expression relationships between these genes were visualized using Cytoscape[1]. The network of PK and PP genes responsive to Fe deficiency consists of 87 nodes (77 PKs genes and 10 PPs genes) and 248 edges (correlations between genes; **Figure 3**). The network can be further divided into one larger and eight smaller clusters. GO enrichment analysis revealed that the biological processes "defense response to fungus," "stomatal movement," "regulation of cell growth," and "response to nickel ion" were most strongly enriched (**Figure 4A**), the products of these genes were chiefly localized on the plasma membrane, in the endomembrane system, in the calcineurin complex, in the micropyle, and in the protein serine/threonine phosphatase complex (**Figure 4B**). The largest module of the network, named FEPKPP1, consists of 51 PK and seven PP genes (Table S2 in Supplementary Material). More than 76% of the genes in this module belong to the RLK superfamily, including 33 RLKs and 11 RLCKs. GO analysis showed that genes involved in the biological processes "detection of molecule of fungal origin," "hypotonic salinity response," and "potassium ion import and cellular potassium ion homeostasis," and the localizations "plasma membrane," "micropyle," and "calcineurin complex" were enriched in this cluster (**Figures 5A,B**).

Co-expression analysis of the 58 differentially expressed PK and PP genes with fold-changes greater than 1.5 using the criteria mentioned above yielded a network consisting of 14 nodes and 32 edges; none of the PP genes was associated with the network (Figure S4 in Supplementary Material). The network can be divided into one larger and one smaller cluster. GO enrichment analysis of the bigger module revealed that, similar to cluster FEPKPP1, the biological processes "detection of molecule of fungal origin," "hypotonic salinity response," and "potassium ion import and cellular potassium ion homeostasis" were enriched.

A GENOME-WIDE FUNCTIONAL NETWORK ASSOCIATED WITH Fe-RESPONSIVE PK AND PP GENES

A co-expression network of 832 Fe-responsive genes including 58 PK and PP genes with fold-changes greater than 1.5 was generated as described above. In the network shown in **Figure 6** only

[1]http://www.cytoscape.org

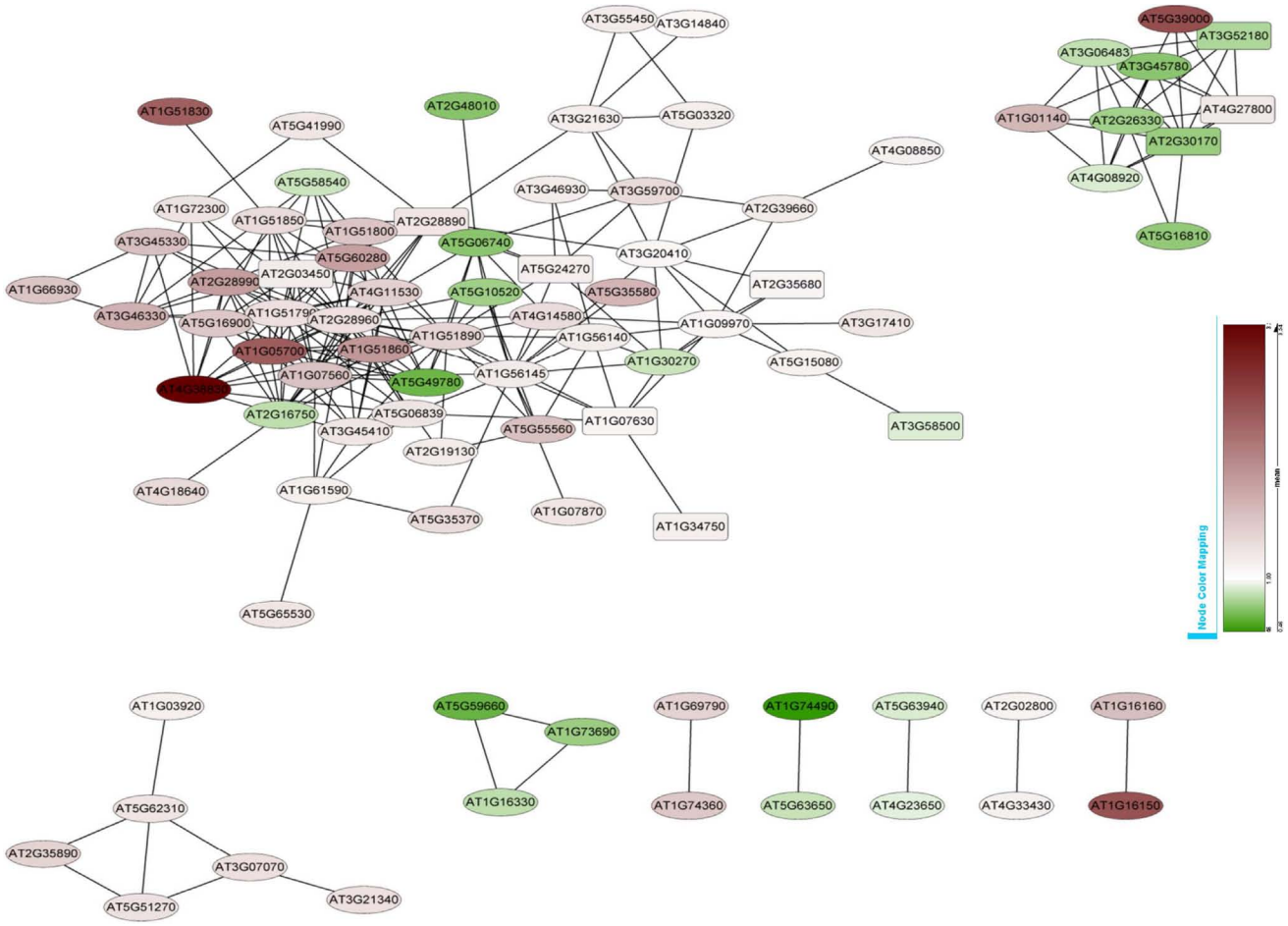

FIGURE 3 | Co-expression relationships of the differentially expressed PK and PP genes. Red nodes indicate up-regulated genes, green nodes denote genes that are repressed by Fe deficiency. Round-shaped nodes represent protein kinase genes, rectangles indicate protein phosphatase genes.

nodes that were not connected by at least one edge to a bait (PK or PP) gene and edges linked to two preys (all other differentially expressed genes) were excluded. Also this network could be divided into two clusters, one of which comprises 64 nodes and 440 edges with 14 PK genes (**Figure 6A**, herein named FEPKPP2), and a smaller cluster consisting of 36 nodes and 564 edges with only one PK genes (**Figure 6B**, herein named FEPKPP3). The majority of the prey genes in this cluster were induced by Fe starvation; only transcripts derived from five out of 50 prey genes showed decreased abundance (Table S3 in Supplementary Material). None of the products of these prey genes are identified as Fe-responsive phosphoproteins (Lan et al., 2012b), possibly due to most of these products are membrane proteins not easy to be detected by phosphoproteomics. GO enrichment analysis of the module FEPKPP2 revealed that the biological processes "defense response," "innate immune response," and "cobalt ion transport and cellular homeostasis" were enriched (**Figure 7A**), with the majority of the gene products localized to the tonoplast or intrinsic to the plasma membrane (**Figure 7B**). This stands in contrast to the genes in the module FEPKPP3 where 30 out of the 35 prey genes showed decreased transcript abundance upon Fe deficiency (Table S4 in Supplementary Material). GO enrichment analysis of this module revealed that the biological processes "photosynthesis," "cellular response to nitric oxide," "cellular response to iron ion," "cell redox homeostasis," "photosystem II repair," and "vitamin B6 biosynthetic process" were enriched (**Figure 8A**). The gene products mainly localized to the chloroplast thylakoid membrane, photosystem I reaction center, the chloroplast envelope, plastoglobules, the chloroplast thylakoid lumen, and the chloroplast stroma (**Figure 8B**).

DISCUSSION

The possible function of post-translational modifications of proteins in the Fe-deficiency response remains poorly understood. PKs and PPs play key roles in the regulation of nearly all aspects of metabolism and development. Due to the use of microarray probe sets that have significant cross hybridization potential and are unable to distinguish highly similar genes of this subfamily, transcriptional information on the expression of PK and PP genes in response to Fe deficiency is lacking in *Arabidopsis*. The RNA-seq technology has proven to provide precise "digital" information on

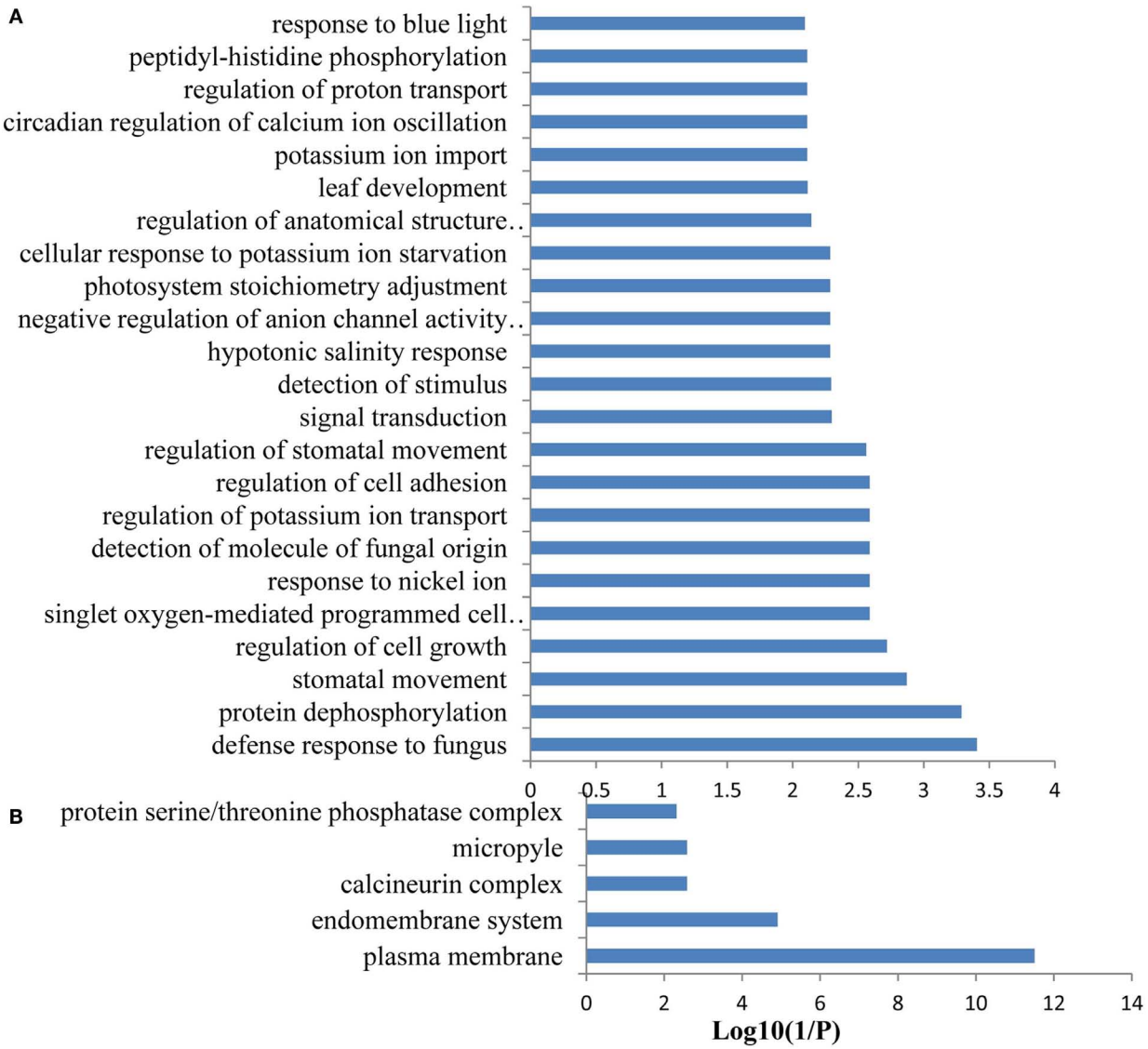

FIGURE 4 | Gene ontology (GO) enrichment analysis of the genes forming the network. GO enrichment of the 87 PK and PP genes which involved in the co-expression network was performed with the Gene Ontology Browsing Utility (GOBU) (Lin et al., 2006) using the TopGo "elim" method (Alexa et al., 2006) with $P < 0.01$. **(A)** GO of the biological process and **(B)** GO of the subcellular localization.

gene expression, and is able to discriminate genes of high sequence identity (Ozsolak and Milos, 2011). Using this technology, we here present comprehensive information on the transcriptional expression of PK and PP genes in Fe-deficient *Arabidopsis* roots. Based on our criteria, less than 20% of the annotated PK and PP genes were differentially expressed upon Fe deficiency and only around 5% PK and PP genes were differentially expressed with fold-changes greater than 1.5. GO enrichment analysis of the 203 differentially expressed PK genes revealed that these PKs were involved in various biological processes (Figure S1 in Supplementary Material). Considering only the 53 PK genes with fold-changes greater than 1.5, the GO categories "regulation of potassium ion transport," "tapetal cell fate specification," "response to nickel ion," and "cellular response to potassium ion starvation" were over-represented (Figure S2 in Supplementary Material). The subtle transcriptional response of these genes suggests that under conditions of Fe-deficiency protein phosphorylation may function to fine-tune basic housekeeping processes. Alternatively, transcription is not usually the main level for regulation of PK and PP activities, which occurs mostly at the post-translational level. The shift in overrepresented GO categories in robustly up-regulated PK genes may indicate post-translational regulation of processes that are critical for cellular Fe homeostasis such as potassium ion transport and response to potassium and nickel ions. Interestingly, 87% of the robustly regulated PK genes belong to the RLK/RLCK and CAMK_AMPK/CDPK subfamilies (**Table 1**), implicating that

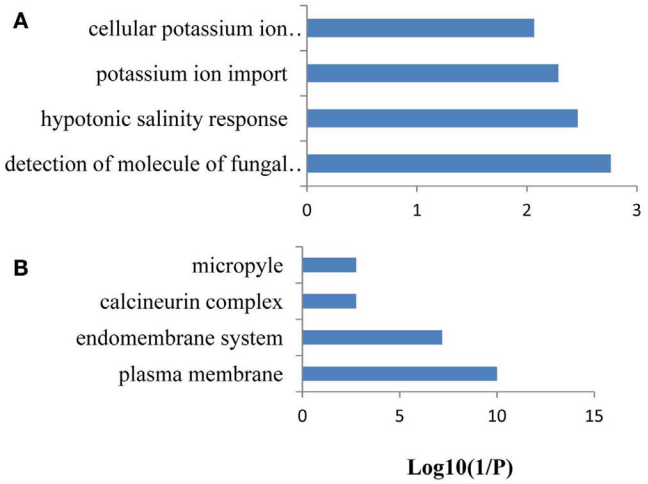

FIGURE 5 | Gene ontology (GO) enrichment analysis of the genes from FEPKPP1. GO enrichment of the 58 PK and PP genes in the module FEPKPP1 was performed with the GOBU toolbox using the TopGo "elim" method with $P < 0.01$. **(A)** GO biological process and **(B)** GO subcellular localization.

PKs from these families may be important for adaptation to Fe deficiency in *Arabidopsis* roots. This finding is consistent with our previous quantitative phosphoproteomic study that predicted two pro-directed kinases [A protein kinase that phosphorylates certain Ser/Thr residues that precede a Pro residue (Ser/Thr-Pro motifs) (Lu and Zhou, 2007)] belonging to RLK superfamily to play critical roles in regulating Fe-responsive phosphopeptides (Lan et al., 2012b). RLKs are defined by the presence of a signal peptide, an extracellular domain, which is absent in the RLCK subfamily, a transmembrane domain region that anchors the receptor in the cell membrane, and a carboxyl-terminal serine/threonine kinase domain (Wang et al., 2007). More than 2% of the predicted *Arabidopsis* coding sequences encode RLKs, which have diverse functions in development, pathogen resistance, hormone perception, and environmental adaption (Wang et al., 2007).

The strong overrepresentation of PK and PP genes encoding proteins involved in potassium homeostasis was an unexpected result. The link between potassium uptake and Fe deficiency remains elusive. One possible explanation is that PKs are required in the regulation of both potassium and Fe homeostasis. Some PKs may play broader roles in nutrient signaling. For example, CIPK23 was reported to be required for both nitrate sensing and activation of the potassium channel AKT1 (Xu et al., 2006; Ho et al., 2009). Alternatively, there might be undiscovered cross-talks between Fe and K deficiency signaling. Evidence for such cross-talk has been inferred from microarray analysis that revealed that the Fe transporter *LeIRT1* is up-regulated by K deficiency (Wang et al., 2002). Moreover, expression of the K transporter gene *LeKC1* was strongly increased by Fe deficiency and K starvation, further supporting such a scenario (Wang et al., 2002). An ameliorating effect of K supply on Fe deficiency has been described three decades ago (Barak and Chen, 1983), and was associated with a change in the cation/anion uptake balance.

Genes showing similar expression pattern under diverse conditions often have correlative functions (Eisen et al., 1998), and the processes in which genes with unknown functions are involved can be inferred from their co-expression relationships with genes with known functions (Aoki et al., 2007; Usadel et al., 2009). In the present study, the global expression of PK and PP genes in *Arabidopsis* roots was analyzed to gain insights into the interplay of transcriptional responses to Fe deficiency. By mining public databases, PK and PP genes that were differentially expressed upon Fe starvation were clustered into groups of closely correlated modules based on their co-expression relationships under various sets of experimental conditions. Using this approach, we discovered nine potentially critical regulatory modules with various putative roles under Fe deficiency (**Figures 3** and **4**). Interestingly, only 35% of the differentially expressed PK and PP genes were constituents of the co-expression network, suggesting that the majority of PKs and PPs responsive to Fe deficiency are functionally diverse and involved in a variety of biological processes and metabolic pathways. It is noteworthy that, compared to the 26% of the differentially expressed PP genes that are involved in the network, the group of PKs is clearly better represented (38% of the differentially expressed PK genes are included in the network), even though the percentage of differentially expressed PP gene is slightly higher than that of PK genes (39 out of 205 PP genes VS 203 out of 1,118 PK genes). Some modules contain only a few or no PP genes at all (**Figure 2**). These observations support the assumption that the regulation of biological processes requires a cascaded and/or coordinated protein phosphorylation by different PKs to adapt to environmental stresses, while the PP-mediated removal of phosphate from a phosphorylated protein is less specific.

To explore potential upstream regulators and downstream targets of the PK and PP genes, a co-expression network was constructed from the 774 Fe-responsive genes (excluding PK and PP genes) with fold change greater than 1.5-fold and the 58 PK and PP genes as baits. Co-expression network generated in this study was mainly associated with PK and PP genes, which is different from those previously reported gene co-expression networks where they consider the global Fe supply dependent co-expression networks in *Arabidopsis* roots (Schmidt and Buckhout, 2011; Ivanov et al., 2012). This network could be divided into two sub-modules, named FEPKPP2 and FEPKPP3 (**Figure 6**). Interestingly, in the module FEPKPP2 90% of the prey genes were induced by Fe deficiency while the transcript abundance of 86% prey genes in module FEPKPP3 were decreased (Tables S3 and S4 in Supplementary Material). Products of most prey genes in FEPKPP2 are localized on the tonoplast and on the plasma membrane. Several transporters, such as the Co, Ni, and Fe ion transporter IREG2 (Schaaf et al., 2006; Morrissey et al., 2009), the Zn detoxification protein MPT3 (Arrivault et al., 2006), and the proton-translocating ATPase AHA7 were induced upon Fe deficiency and were tightly co-expressed with PKs. For example, IREG2 was directly co-expressed with the PKs At4g38830 (ATMPK8), At5g16900 (ATMPK9), At3g46330, and At1g07560, indicating that these PKs might be required for IREG2 regulation. MPT3 was directly co-expressed with the LRR subfamily PKs At1g07560 and At1g51860, suggesting that these PKs play major roles in detoxification of excess zinc by MPT3. AHA7, reported to

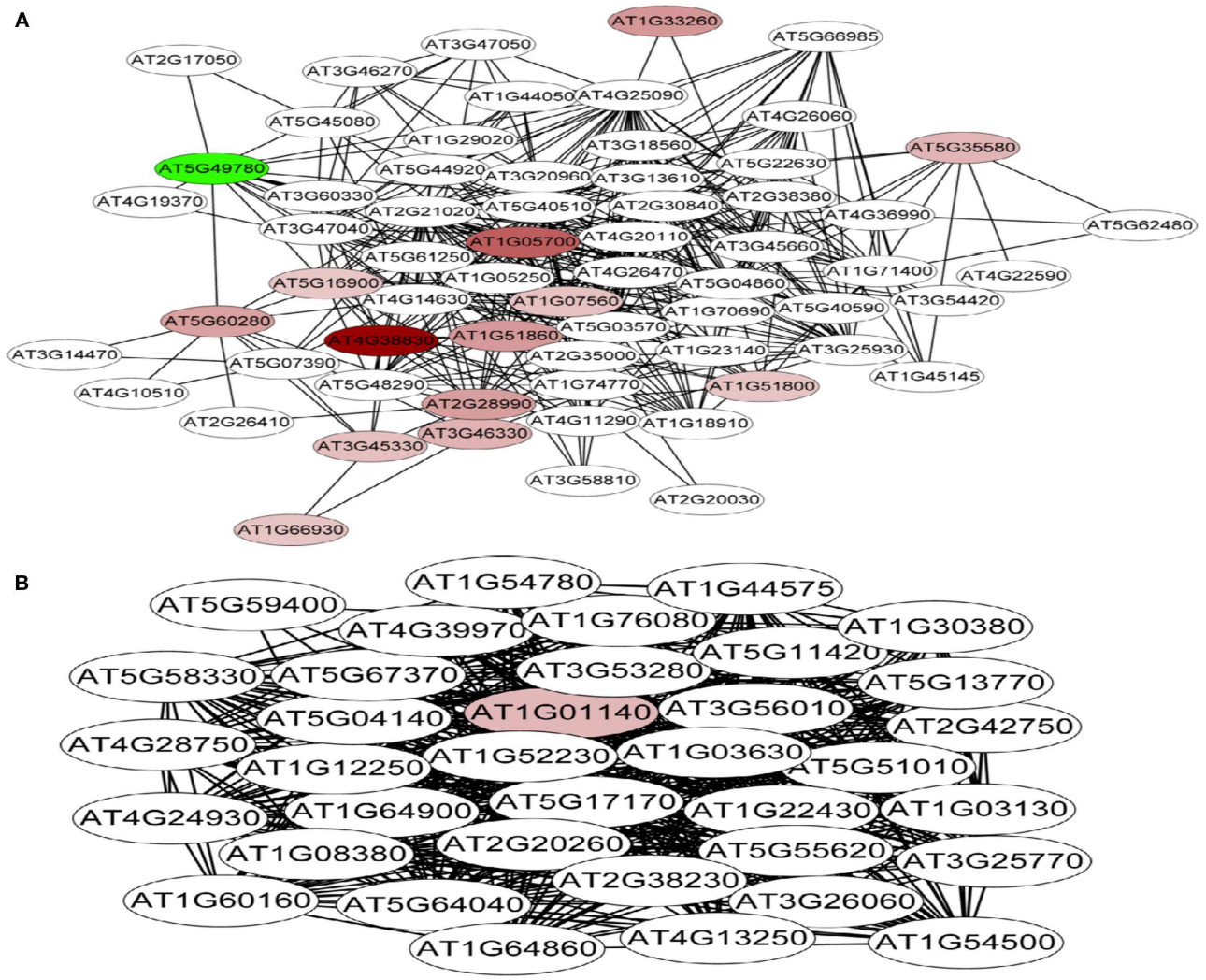

FIGURE 6 | Co-expression relationships of Fe-responsive genes with fold-changes greater than 1.5-fold in *Arabidopsis* roots. **(A)** Module FEPKPP2 and **(B)** module FEPKPP3. Red nodes indicate up-regulated PK genes, green nodes denote PK genes that are repressed by Fe deficiency, white nodes indicate fished genes.

be involved in Fe-deficiency-induced root hair formation (Santi and Schmidt, 2009), was directly co-expressed with ATMPK8, indicating that ATMPK8-mediated AHA7 phosphorylation might be critical for the morphological changes in Fe-deficient roots. The module FEPKPP3 is composed of 36 genes, with only one PK gene, *CIPK9*, closely co-expressed with the prey genes. This suggests that CIPK9 has broad substrate specificity and is involved in diverse processes. A recent study has shown that CIPK9 is involved in K homeostasis under low K stress (Liu et al., 2013). *CIPK9* was induced by Fe deficiency but the majority of the prey genes were repressed by Fe starvation. For example, seven photosynthesis-related prey genes (At1g54780, At2g20260, At1g52230, At1g03130, At5g64040, At1g08380, and At1g30380) that were co-expressed with *CIPK9* showed decreased transcript abundance upon by Fe deficiency. Photosynthesis has been shown to be down-regulated in response to Fe deficiency also in leaves and, unexpectedly, also in roots (Buckhout et al., 2009), indicating that this is a conserved component of the Fe-deficiency response that may be implicated in Fe signaling pathways. Alternatively, some of the photosynthesis-related genes may have acquired novel functions in roots that are associated with the re-calibration of cellular Fe homeostasis. GO enrichment analysis of this module also revealed that the biological processes "cellular response to nitric oxide" and "cellular response to iron ion" were enriched (**Figure 8A**), due to two genes At5g55620 and At3g53280 in this module. These two genes are strongly induced by both nitric oxide treatment and Fe deficiency (Garcia et al., 2010).

CONCLUSION

In summary, we provide genome-wide information on the transcriptional expression of PK and PP genes in Fe-deficient *Arabidopsis* roots and on the biological processes putatively controlled

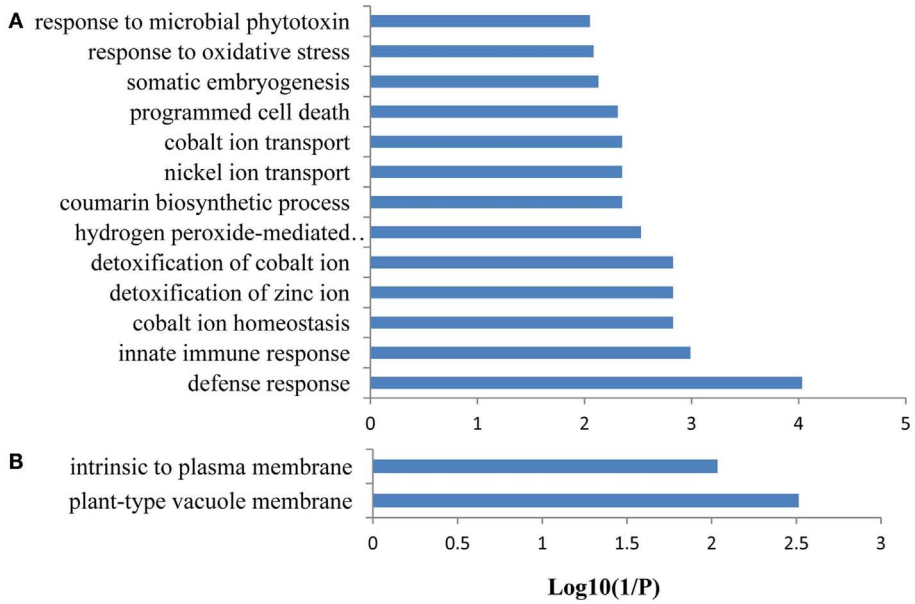

FIGURE 7 | Gene ontology (GO) enrichment analysis of the genes from FEPKPP2. GO enrichment of the 64 Fe-responsive genes in the module FEPKPP2 was performed with the GOBU toolbox using the TopGo "elim" method with $P < 0.01$. **(A)** GO biological process and **(B)** GO subcellular localization.

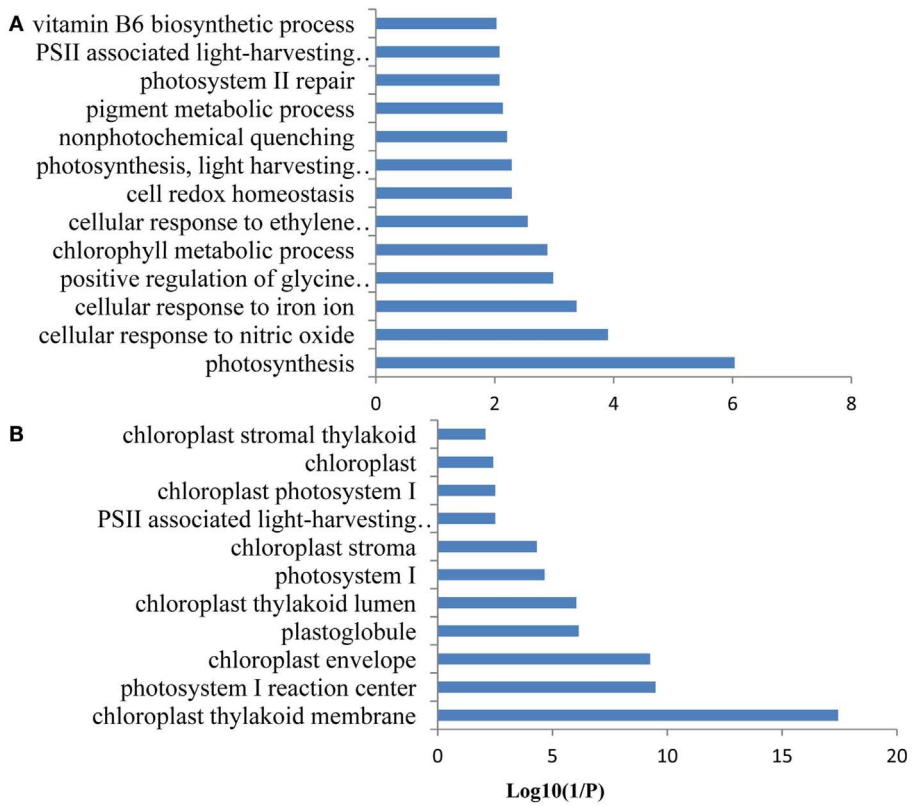

FIGURE 8 | Gene ontology (GO) enrichment analysis of the genes from FEPKPP3. GO enrichment of the 36 Fe-responsive genes in the module FEPKPP3 was performed with the GOBU toolbox using the TopGo "elim" method with $P < 0.01$. **(A)** GO biological process and **(B)** GO subcellular localization.

by reversible phosphorylation. A root-specific co-expression network of Fe-responsive genes encoding PKs and PPs predicted ATMPK8, ATMPK9, and CIPK9 as putative novel players in the control of cellular Fe homeostasis. The results further show that the control of ion transport across the plasma membrane and the vacuolar membrane as well as plastid development and function PK are dependent. The approach applied here will be useful to direct further studies and to decipher the mechanisms by which ion transporters and plastid function is controlled post-translationally in Fe-deficient plants.

MATERIALS AND METHODS

METHODS

Data collection and processing

Transcriptome data of roots from 13-day-old *Arabidopsis* seedlings grown in the presence or absence of Fe by RNA-seq were downloaded from a public database (NCBI: SRA045009) and analyzed as described in (Lan et al., 2012a). Microarray data of 2,671 ATH1 arrays from the NASCarray database[2] were downloaded and normalized using the RMA function of the Affy package of the Bioconductor software. Three hundred root-related arrays were manually identified as described in (Lin et al., 2011), and were used as a data base for co-expression analysis. PK and PP genes were retrieved on the basis of the TAIR 10 release of *Arabidopsis* genome.

Gene ontology analysis

Enrichment analysis of GO categories was performed with the Gene Ontology Browsing Utility (GOBU) (Lin et al., 2006) using the TopGo "elim" method (Alexa et al., 2006) from the aspects of "biological process" and "subcellular localization." The elim algorithm iteratively removes the genes mapped to significant terms from higher level GO terms, and thus avoids unimportant functional categories being enriched.

GENERATION OF CO-EXPRESSION NETWORKS AND MODULES OF Fe-RESPONSIVE PK AND PP GENES USING THE MACCU TOOLBOX

To generate root-specific networks of Fe-responsive PK and PP genes, differentially expressed PK and PP genes were identified using a Student t-test at a $P < 0.05$. Gene networks were constructed based on 300 publicly available root-related microarrays using the MACCU toolbox as described in (Lin et al., 2011), with a Pearson correlation threshold of 0.7. The generated co-expression networks were visualized by Cytoscape (see text footnote 1). If one cluster of genes did not have any connection (edges) to any other cluster in the co-expression network, we referred to such a cluster as a module.

[2]http://affymetrix.arabidopsis.info/

CONSTRUCTION OF Fe-RESPONSIVE ROOT NETWORKS WITH PK AND PP GENES

To obtain root-related, Fe-responsive gene networks comprising PK and PP genes, subsets of 774 Fe-responsive genes with fold-changes greater than 1.5-fold were mined. Next, 58 Fe-responsive PK and PP genes were extracted (bait genes), combined with the root Fe-responsive genes (preys), and used for generating co-expression network. The resulting networks show only those nodes (genes) and edges (relationships between genes) that were linked by at least one edge with a bait gene. Edges linked to two preys were excluded.

ACKNOWLEDGMENTS

The study was financially supported by a starting career grant from Institute of Soil Science, Chinese Academy Sciences (Y225070000). Work in the Schmidt lab was supported by grants from Academia Sinica and NSC. We thank Drs. Wen-Dar Lin and Jorge Rodríguez-Celma for their help in using the MACCU software.

SUPPLEMENTARY MATERIAL

The Supplementary Material for this article can be found online at: http://www.frontiersin.org/Plant_Nutrition/10.3389/fpls.2013.00173/abstract

Table S1 | Differentially expressed protein kinase and phosphatase genes upon iron deficiency. The corresponding response ratios, defined as the transcript level (Reads Per Kilobase per Million mapped reads) in the −Fe treatment divided by the level in the +Fe treatment, are shown in three biological repeats, as well as the mean ($P < 0.05$).

Table S2 | Genes associated with the major module FEPKPP1.

Table S3 | Genes associated with the module FEPKPP2.

Table S4 | Genes associated with the module FEPKPP3.

Figure S1 | Gene ontology (GO) enrichment analysis of the 203 differentially expressed PK genes. GO enrichment of the "biological process" of the 203 Fe-responsive PK genes was performed with the GOBU toolbox using the TopGo "elim" method with $P < 0.01$. Inset indicates GO of the subcellular localization.

Figure S2 | Gene ontology of 53 PK genes with fold-changes greater than 1.5-fold. GO enrichment of the 53 Fe-responsive PK genes with fold-changes greater than 1.5-fold was performed with the GOBU toolbox using the TopGo "elim" method with $P < 0.01$.

Figure S3 | Gene ontology of the 39 differentially expressed PP genes. GO enrichment of the 39 Fe-responsive PP genes was performed with the GOBU toolbox using the TopGo "elim" method with $P < 0.01$. **(A)** GO biological process and **(B)** GO subcellular localization.

Figure S4 | Co-expression relationships of Fe-responsive PK and PP genes with fold-changes greater 1.5-fold in *Arabidopsis* roots.

REFERENCES

Alexa, A., Rahnenfuhrer, J., and Lengauer, T. (2006). Improved scoring of functional groups from gene expression data by decorrelating GO graph structure. *Bioinformatics* 22, 1600–1607. doi:10.1093/bioinformatics/btl140

Aoki, K., Ogata, Y., and Shibata, D. (2007). Approaches for extracting practical information from gene co-expression networks in plant biology. *Plant Cell Physiol.* 48, 381–390. doi:10.1093/pcp/pcm013

Arnaud, N., Murgia, I., Boucherez, J., Briat, J. F., Cellier, F., and Gaymard, F. (2006). An iron-induced nitric oxide burst precedes ubiquitin-dependent protein degradation for *Arabidopsis* AtFer1 ferritin gene expression. *J. Biol. Chem.* 281, 23579–23588. doi:10.1074/jbc.M602135200

Arrivault, S., Senger, T., and Kramer, U. (2006). The *Arabidopsis* metal tolerance protein AtMTP3 maintains metal homeostasis by mediating Zn exclusion from the shoot under Fe deficiency and Zn oversupply. *Plant J.* 46, 861–879. doi:10.1111/j.1365-313X.2006.02746.x

Barak, P., and Chen, Y. (1983). The effect of potassium fertilization on iron deficiency. *Commun. Soil Sci. Plant Anal.* 14, 945–950. doi:10.1080/00103628309367422

Barberon, M., Zelazny, E., Robert, S., Conejero, G., Curie, C., Friml, J., et al. (2011). Monoubiquitin-dependent endocytosis of the iron-regulated transporter 1 (IRT1) transporter controls iron uptake in plants. *Proc. Natl. Acad. Sci. U.S.A.* 108, E450–458. doi:10.1073/pnas.1100659108

Bauer, P., Ling, H. Q., and Guerinot, M. L. (2007). FIT, the FER-LIKE IRON DEFICIENCY INDUCED TRANSCRIPTION FACTOR in *Arabidopsis*. *Plant Physiol. Biochem.* 45, 260–261. doi:10.1016/j.plaphy.2007.03.006

Buckhout, T. J., Yang, T. J., and Schmidt, W. (2009). Early iron-deficiency-induced transcriptional changes in *Arabidopsis* roots as revealed by microarray analyses. *BMC Genomics* 10:147. doi:10.1186/1471-2164-10-147

Colangelo, E. P., and Guerinot, M. L. (2004). The essential basic helix-loop-helix protein FIT1 is required for the iron deficiency response. *Plant Cell* 16, 3400–3412. doi:10.1105/tpc.104.024315

Curie, C., Panaviene, Z., Loulergue, C., Dellaporta, S. L., Briat, J. F., and Walker, E. L. (2001). Maize yellow stripe1 encodes a membrane protein directly involved in Fe(III) uptake. *Nature* 409, 346–349. doi:10.1038/35053080

Dinneny, J. R., Long, T. A., Wang, J. Y., Jung, J. W., Mace, D., Pointer, S., et al. (2008). Cell identity mediates the response of *Arabidopsis* roots to abiotic stress. *Science* 320, 942–945. doi:10.1126/science.1153795

Durrett, T. P., Gassmann, W., and Rogers, E. E. (2007). The FRD3-mediated efflux of citrate into the root vasculature is necessary for efficient iron translocation. *Plant Physiol.* 144, 197–205. doi:10.1104/pp.107.097162

Eide, D., Broderius, M., Fett, J., and Guerinot, M. L. (1996). A novel iron-regulated metal transporter from plants identified by functional expression in yeast. *Proc. Natl. Acad. Sci. U.S.A.* 93, 5624–5628. doi:10.1073/pnas.93.11.5624

Eisen, M. B., Spellman, P. T., Brown, P. O., and Botstein, D. (1998). Cluster analysis and display of genome-wide expression patterns. *Proc. Natl. Acad. Sci. U.S.A.* 95, 14863–14868. doi:10.1073/pnas.95.25.14863

Garcia, M. J., Lucena, C., Romera, F. J., Alcantara, E., and Perez-Vicente, R. (2010). Ethylene and nitric oxide involvement in the up-regulation of key genes related to iron acquisition and homeostasis in *Arabidopsis*. *J. Exp. Bot.* 61, 3885–3899. doi:10.1093/jxb/erq203

Ho, C. H., Lin, S. H., Hu, H. C., and Tsay, Y. F. (2009). CHL1 functions as a nitrate sensor in plants. *Cell* 138, 1184–1194. doi:10.1016/j.cell.2009.07.004

Ihmels, J., Levy, R., and Barkai, N. (2004). Principles of transcriptional control in the metabolic network of *Saccharomyces cerevisiae*. *Nat. Biotechnol.* 22, 86–92. doi:10.1038/nbt918

Ivanov, R., Brumbarova, T., and Bauer, P. (2012). Fitting into the harsh reality: regulation of iron-deficiency responses in dicotyledonous plants. *Mol. Plant.* 5, 27–42. doi:10.1093/mp/ssr065

Kharchenko, P., Church, G. M., and Vitkup, D. (2005). Expression dynamics of a cellular metabolic network. *Mol. Syst. Biol.* 1, 2005.0016. doi:10.1038/msb4100023

Lan, P., Li, W., and Schmidt, W. (2012a). Complementary proteome and transcriptome profiling in phosphate-deficient *Arabidopsis* roots reveals multiple levels of gene regulation. *Mol. Cell Proteomics* 11, 1156–1166. doi:10.1074/mcp.M112.020461

Lan, P., Li, W., Wen, T. N., and Schmidt, W. (2012b). Quantitative phosphoproteome profiling of iron-deficient *Arabidopsis* roots. *Plant Physiol.* 159, 403–417. doi:10.1104/pp.112.193987

Lin, W.-D., Chen, Y.-C., Ho, J.-M., and Hsiao, C.-D. (2006). GOBU: toward an integration interface for biological objects. *J. Inf. Sci. Eng.* 22, 19.

Lin, W. D., Liao, Y. Y., Yang, T. J., Pan, C. Y., Buckhout, T. J., and Schmidt, W. (2011). Coexpression-based clustering of *Arabidopsis* root genes predicts functional modules in early phosphate deficiency signaling. *Plant Physiol.* 155, 1383–1402. doi:10.1104/pp.110.166520

Lingam, S., Mohrbacher, J., Brumbarova, T., Potuschak, T., Fink-Straube, C., Blondet, E., et al. (2011). Interaction between the bHLH transcription factor FIT and ETHYLENE INSENSITIVE3/ETHYLENE INSENSITIVE3-LIKE1 reveals molecular linkage between the regulation of iron acquisition and ethylene signaling in *Arabidopsis*. *Plant Cell* 23, 1815–1829. doi:10.1105/tpc.111.084715

Liu, L. L., Ren, H. M., Chen, L. Q., Wang, Y., and Wu, W. H. (2013). A protein kinase, calcineurin B-like protein-interacting protein Kinase9, interacts with calcium sensor calcineurin B-like Protein3 and regulates potassium homeostasis under low-potassium stress in *Arabidopsis*. *Plant Physiol.* 161, 266–277. doi:10.1104/pp.112.206896

Long, T. A., Tsukagoshi, H., Busch, W., Lahner, B., Salt, D. E., and Benfey, P. N. (2010). The bHLH transcription factor POPEYE regulates response to iron deficiency in *Arabidopsis* roots. *Plant Cell* 22, 2219–2236. doi:10.1105/tpc.110.074096

Lu, K. P., and Zhou, X. Z. (2007). The prolyl isomerase PIN1: a pivotal new twist in phosphorylation signalling and disease. *Nat. Rev. Mol. Cell Biol.* 8, 904–916. doi:10.1038/nrm2261

Meiser, J., Lingam, S., and Bauer, P. (2011). Posttranslational regulation of the iron deficiency basic helix-loop-helix transcription factor FIT is affected by iron and nitric oxide. *Plant Physiol.* 157, 2154–2166. doi:10.1104/pp.111.183285

Morrissey, J., Baxter, I. R., Lee, J., Li, L., Lahner, B., Grotz, N., et al. (2009). The ferroportin metal efflux proteins function in iron and cobalt homeostasis in *Arabidopsis*. *Plant Cell* 21, 3326–3338. doi:10.1105/tpc.109.069401

Ozsolak, F., and Milos, P. M. (2011). RNA sequencing: advances, challenges and opportunities. *Nat. Rev. Genet.* 12, 87–98. doi:10.1038/nrg2934

Rellan-Alvarez, R., El-Jendoubi, H., Wohlgemuth, G., Abadia, A., Fiehn, O., Abadia, J., et al. (2011). Metabolite profile changes in xylem sap and leaf extracts of strategy I plants in response to iron deficiency and resupply. *Front. Plant Sci.* 2:66. doi:10.3389/fpls.2011.00066

Robinson, N. J., Procter, C. M., Connolly, E. L., and Guerinot, M. L. (1999). A ferric-chelate reductase for iron uptake from soils. *Nature* 397, 694–697. doi:10.1038/17800

Rogers, E. E., and Guerinot, M. L. (2002). FRD3, a member of the multidrug and toxin efflux family, controls iron deficiency responses in *Arabidopsis*. *Plant Cell* 14, 1787–1799. doi:10.1105/tpc.001495

Romheld, V., and Marschner, H. (1986). Evidence for a specific uptake system for iron phytosiderophores in roots of grasses. *Plant Physiol.* 80, 175–180. doi:10.1104/pp.80.1.175

Roschzttardtz, H., Seguela-Arnaud, M., Briat, J. F., Vert, G., and Curie, C. (2011). The FRD3 citrate effluxer promotes iron nutrition between symplastically disconnected tissues throughout *Arabidopsis* development. *Plant Cell* 23, 2725–2737. doi:10.1105/tpc.111.088088

Santi, S., and Schmidt, W. (2009). Dissecting iron deficiency-induced proton extrusion in *Arabidopsis* roots. *New Phytol.* 183, 1072–1084. doi:10.1111/j.1469-8137.2009.02908.x

Schaaf, G., Honsbein, A., Meda, A. R., Kirchner, S., Wipf, D., and Von Wiren, N. (2006). AtIREG2 encodes a tonoplast transport protein involved in iron-dependent nickel detoxification in *Arabidopsis thaliana* roots. *J. Biol. Chem.* 281, 25532–25540. doi:10.1074/jbc.M601062200

Schmidt, W., and Buckhout, T. J. (2011). A hitchhiker's guide to the *Arabidopsis* ferrome. *Plant Physiol. Biochem.* 49, 462–470. doi:10.1016/j.plaphy.2010.12.001

Sivitz, A., Grinvalds, C., Barberon, M., Curie, C., and Vert, G. (2011). Proteasome-mediated turnover of the transcriptional activator FIT is required for plant iron-deficiency responses. *Plant J.* 66, 1044–1052. doi:10.1111/j.1365-313X.2011.04565.x

Sivitz, A. B., Hermand, V., Curie, C., and Vert, G. (2012). *Arabidopsis* bHLH100 and bHLH101 control iron homeostasis via a FIT-independent pathway. *PLoS ONE* 7::e44843. doi:10.1371/journal.pone.0044843

Usadel, B., Obayashi, T., Mutwil, M., Giorgi, F. M., Bassel, G. W., Tanimoto, M., et al. (2009). Co-expression tools for plant biology: opportunities for hypothesis generation and caveats. *Plant Cell Environ.* 32, 1633–1651. doi:10.1111/j.1365-3040.2009.02040.x

Vert, G., Grotz, N., Dedaldechamp, F., Gaymard, F., Guerinot, M. L., Briat, J. F., et al. (2002). IRT1, an *Arabidopsis* transporter essential for iron uptake from the soil and for plant growth. *Plant Cell* 14, 1223–1233. doi:10.1105/tpc.001388

Wang, H., Chevalier, D., Larue, C., Ki Cho, S., and Walker, J. C. (2007). The protein phosphatases and protein kinases of *Arabidopsis thaliana*. *Arabidopsis Book* 5, e0106.

Wang, N., Cui, Y., Liu, Y., Fan, H., Du, J., Huang, Z., et al. (2013). Requirement and functional redundancy of Ib subgroup bHLH proteins for iron deficiency responses and uptake in *Arabidopsis thaliana*. *Mol. Plant.* 6, 503–513. doi:10.1093/mp/sss089

Wang, S., Yin, Y., Ma, Q., Tang, X., Hao, D., and Xu, Y. (2012). Genome-scale identification of cell-wall related genes in *Arabidopsis* based on co-expression network analysis. *BMC Plant Biol.* 12:138. doi:10.1186/1471-2229-12-138

Wang, Y. H., Garvin, D. F., and Kochian, L. V. (2002). Rapid induction of regulatory and transporter genes in response to phosphorus, potassium, and iron deficiencies in tomato roots. Evidence for cross talk and root/rhizosphere-mediated signals. *Plant Physiol.* 130, 1361–1370.

Xu, J., Li, H. D., Chen, L. Q., Wang, Y., Liu, L. L., He, L., et al. (2006). A protein kinase, interacting with two calcineurin B-like proteins, regulates K+ transporter AKT1 in *Arabidopsis*. *Cell* 125, 1347–1360. doi:10.1016/j.cell.2006.06.011

Yang, T. J., Lin, W. D., and Schmidt, W. (2010). Transcriptional profiling of the *Arabidopsis* iron deficiency response reveals conserved transition metal homeostasis networks. *Plant Physiol.* 152, 2130–2141. doi:10.1104/pp.109.152728

Yuan, Y., Wu, H., Wang, N., Li, J., Zhao, W., Du, J., et al. (2008). FIT interacts with AtbHLH38 and AtbHLH39 in regulating iron uptake gene expression for iron homeostasis in *Arabidopsis*. *Cell Res.* 18, 385–397. doi:10.1038/cr.2008.26

Conflict of Interest Statement: The authors declare that the research was conducted in the absence of any commercial or financial relationships that could be construed as a potential conflict of interest.

Received: 08 April 2013; accepted: 15 May 2013; published online: 03 June 2013.
*Citation: Lan P, Li W and Schmidt W (2013) A digital compendium of genes mediating the reversible phosphorylation of proteins in Fe-deficient Arabidopsis roots. Front. Plant Sci. **4**:173. doi: 10.3389/fpls.2013.00173*
This article was submitted to Frontiers in Plant Nutrition, a specialty of Frontiers in Plant Science.

frontiers in
PLANT SCIENCE

ORIGINAL RESEARCH ARTICLE
published: 23 July 2013
doi: 10.3389/fpls.2013.00276

The transcriptional response of *Arabidopsis* leaves to Fe deficiency

Jorge Rodríguez-Celma[1], I Chun Pan[1], Wenfeng Li[1], Ping Lan[1], Thomas J. Buckhout[2] and Wolfgang Schmidt[1,3,4]*

[1] *Academia Sinica, Institute of Plant and Microbial Biology, Taipei, Taiwan*
[2] *Institute of Biology, Humboldt University Berlin, Berlin, Germany*
[3] *Biotechnology Center, National Chung-Hsing University, Taichung, Taiwan*
[4] *Genome and Systems Biology Degree Program, College of Life Science, National Taiwan University, Taipei, Taiwan*

Edited by:
Jean-Francois Briat, Centre National de la Recherche Scientifique, France

Reviewed by:
Petra Bauer, Saarland University, Germany
Naoko K. Nishizawa, The University of Tokyo, Japan

***Correspondence:**
Wolfgang Schmidt, Academia Sinica, Institute of Plant and Microbial Biology, Academia Road 128, Taipei 11529, Taiwan
e-mail: wosh@gate.sinica.edu.tw

Due to its ease to donate or accept electrons, iron (Fe) plays a crucial role in respiration and metabolism, including tetrapyrrole synthesis, in virtually all organisms. In plants, Fe is a component of the photosystems and thus essential for photosynthesis. Fe deficiency compromises chlorophyll (Chl) synthesis, leading to interveinal chlorosis in developing leaves and decreased photosynthetic activity. To gain insights into the responses of photosynthetically active cells to Fe deficiency, we conducted transcriptional profiling experiments on leaves from Fe-sufficient and Fe-deficient plants using the RNA-seq technology. As anticipated, genes associated with photosynthesis and tetrapyrrole metabolism were dramatically down-regulated by Fe deficiency. A sophisticated response comprising the down-regulation of *HEMA1* and *NYC1*, which catalyze the first committed step in tetrapyrrole biosynthesis and the conversion of Chl *b* to Chl *a* at the commencement of Chl breakdown, respectively, and the up-regulation of *CGLD27*, which is conserved in plastid-containing organisms and putatively involved in xanthophyll biosynthesis, indicates a carefully orchestrated balance of potentially toxic tetrapyrrole intermediates and functional end products to avoid photo-oxidative damage. Comparing the responses to Fe deficiency in leaves to that in roots confirmed subgroup 1b bHLH transcription factors and POPEYE/BRUTUS as important regulators of Fe homeostasis in both leaf and root cells, and indicated six novel players with putative roles in Fe homeostasis that were highly expressed in leaves and roots and greatly induced by Fe deficiency. The data further revealed down-regulation of organ-specific subsets of genes encoding ribosomal proteins, which may be indicative of a change in ribosomal composition that could bias translation. It is concluded that Fe deficiency causes a massive reorganization of plastid activity, which is adjusting leaf function to the availability of Fe.

Keywords: Fe deficiency, chlorophyll metabolism, ribosomes, Fe homeostasis, reactive oxygen species, RNA-seq

INTRODUCTION

In leaves, the vast majority of Fe is associated with the chloroplast, serving as a cofactor in all three photosynthetic electron transfer complexes. Iron deficiency is manifested in the interveinal chlorosis of developing leaves, which has been described more than one-hundred years ago as a diagnostic symptom of Fe deficiency (Gris, 1844). Chlorosis is caused by compromised chloroplast development and impaired chlorophyll (Chl) biosynthesis and is associated with dramatically decreased photosynthetic rates (Terry, 1980). The first step in tetrapyrrole biosynthesis is the formation of 5-aminolevulinic acid (ALA). Synthesis of ALA is regarded as the rate-limiting step in tetrapyrrole synthesis, and the glutamyl-tRNA reductase is the point of regulation (Tanaka et al., 2011). Interrupting the Chl biosynthesis pathway is detrimental to the plant due to severe oxidative damage caused by the generation of singlet oxygen by free tetrapyrroles upon illumination (op den Camp et al., 2003). A sensitive Fe sensing system associated with chloroplast function would allow plants to anticipate the inability to complete tetrapyrrole synthesis, to shut off the first committed step in the pathway and thus to avoid potentially detrimental consequences.

How Fe is sensed by plants is not known. In *Arabidopsis* roots, the earliest hub of the Fe signaling cascade is the bHLH protein FER-LIKE IRON DEFICIENCY INDUCED TRANSCRIPTION FACTOR (FIT), which positively controls a set of genes that are involved in the acquisition and distribution of Fe. Among them are the key genes that mediate rhizosphere acidification (AHA2; Santi and Schmidt, 2009), the solubilization of un-available Fe pools (*F6'H1* and *PDR9*; Rodríguez-Celma et al., 2013), the reduction of Fe(III) chelates (*FRO2*; Robinson et al., 1999) and the uptake of the resulting Fe(II) (*IRT1*; Eide et al., 1996; Ling et al., 2002; Colangelo and Guerinot, 2004; Jakoby et al., 2004). FIT forms heterodimers with four Fe-responsive bHLH proteins, bHLH38, bHLH39, bHLH100, and bHLH101 (Yuan et al., 2005, 2008; Wang et al., 2012), presumably controlling different subsets of genes. Another bHLH transcription factor, POPEYE (PYE),

negatively regulates a non-overlapping set of genes involved in Fe mobilization in roots and translocation of Fe to above-ground plant parts in association with the bHLH protein IAA-LEUCINE RESISTANT3 (ILR3/bHLH105) (Long et al., 2010). ILR3 also interacts with the putative DNA-binding E3 ubiquitin-protein ligase BRUTUS (BTS), which positively regulates the same set of genes. This dual regulation is thought to allow a fine-tuning of the expression of genes involved in Fe acquisition and cellular Fe homeostasis (Long et al., 2010).

Little information is available on putative candidates involved in sensing and signaling of Fe in chloroplasts or leaves. Sensing of the Fe status in the plastid would not only allow a close coupling of Chl synthesis, chloroplast development and photosynthesis rate, thus optimizing plant performance, but would also enable the plants to communicate the Fe status of the chloroplast to roots and to adjust Fe uptake to demand. Furthermore, the mechanisms that underlie Fe uptake in leaves have not been thoroughly described. Fe is transported to leaves as Fe^{3+}-citrate chelate (Rellán-Álvarez et al., 2010), and might then be reduced either enzymatically by members of the FRO family or non-enzymatically by ascorbate. Based on their expression patterns and chlorotic mutant phenotypes, the YELLOW STRIPE-LIKE (YSL) transporters YSL1, YSL2, and YSL3 have been implicated in the uptake of Fe that has arrived in leaves via xylem transport (Didonato et al., 2004; Waters et al., 2006). Land plants evolved from chlorophyte algae, suggesting that conserved responses to Fe deficiency should be present in both groups. Indeed, a recent survey on transcriptional responses of *Chlamydomonas reinhardtii* revealed an overlap with Fe-responsive genes of *Arabidopsis thaliana*, including the metal transporters *IRT1*, *IRT2*, *NRAMP4*, and the P-type H^+-ATPase *AHA2* (Urzica et al., 2012). However, the development of multicellularity in plants is accompanied by functional diversity of cells, tissues and organs. The contrasting roles of leaves and roots as sinks and sources for Fe are indicative of fundamentally different transcriptional responses in these organs.

To dissect the Fe deficiency response of leaf cells, we analyzed the changes in the transcriptome upon exposure to Fe deficiency in *Arabidopsis* leaves and compared this response with a previously published RNA-seq data set collected following the same treatment. The analysis revealed a suite of genes functioning in photosynthesis, chloroplast development and Chl synthesis that was rapidly and robustly regulated by Fe in leaves, indicating that the control of plastid function is a conserved and integral component of the *Arabidopsis* response to Fe deficiency. Our analysis further suggests that the composition of ribosomes by Fe is affected in an organ-specific manner, probably biasing translation. Lastly, we show that a small subset of highly expressed genes is robustly regulated by Fe deficiency in both roots and leaves, suggesting putative roles of the encoded proteins in Fe metabolism and the regulation of Fe homeostasis.

MATERIALS AND METHODS

PLANT GROWTH CONDITIONS

Arabidopsis thaliana plants were grown in a growth chamber on an agar-based medium as described by Estelle and Somerville (1987). Seeds of the accession Columbia (Col-0) were obtained from the Arabidopsis Biological Resource Center (Ohio State University). Seeds were surface-sterilized by immersing them in 5% (v/v) NaOCl for 5 min and 70% ethanol for 7 min, followed by four rinses in sterile water. Seeds were placed onto Petri dishes and kept for 1 d at 4°C in the dark, before the plates were transferred to a growth chamber and grown at 21°C under continuous illumination (50 μmol m^{-2} s^{-1}; Phillips TL lamps). The medium was composed of (mM): KNO_3 (5), $MgSO_4$ (2), $Ca(NO_3)_2$ (2), KH_2PO_4 (2.5) and (μM): H_3BO_3 (70), $MnCl_2$ (14), $ZnSO_4$ (1), $CuSO_4$ (0.5), NaCl (10), Na_2MoO_4 (0.2), FeEDTA (40), 4.7 mM MES, supplemented with sucrose (43 mM) and solidified with 0.4% Gelrite pure (Kelco). The pH was adjusted to 5.5.

For RNA-seq analysis, plants were pre-cultivated for 10 d in a complete medium, and then transferred to fresh agar medium either with 40 μM Fe(III)-EDTA (+Fe plants) or without Fe and with 100 μM 3-(2-pyridyl)-5,6-diphenyl-1,2,4-triazine sulfonate (ferrozine; −Fe plants) to trap residual Fe. Plants were grown for 3 d on Fe-free media before analysis. Three independent experiments were conducted for each growth type. For RT-PCR analysis, 10-day-old plants were transferred to hydroponic solution (Buckhout et al., 2009) for 3 d and then transferred to Fe-free solution for 15, 30, and 45 min, or for 1, 2, 4, and 6 h.

RNA-SEQ

For RNA-seq, total RNA was extracted from the leaves and roots using the RNeasy Plant Mini Kit (Qiagen), following the manufacturer's instructions. For analysis, equal amounts of total RNA were collected and cDNA libraries for sequencing were prepared from total RNA following the manufacturer's protocol (Illumina). The cDNA libraries were subsequently enriched by PCR amplification. The resulting cDNA libraries were subjected to sequencing on a single lane of an Illumina Genome Analyzer II. RNA-seq and data collection was done following the protocol of Mortazavi et al. (2008). The length of the cDNA library varied from 250 to 300 bp with a 5′-adapter of 20 bp and a 3′-adapter of 33 bp at both ends.

To quantify gene expression levels, 75-mers sequences were aligned to the genomic sequence annotated in TAIR10 using the BLAT program (Kent, 2002), and RPKM (Reads Per Kilobase of exon model per Million mapped reads) values were computed using RACKJ (Read Analysis & Comparison Kit in Java, http://rackj.sourceforge.net/) software. Only those genes whose expression level in RPKM was over the square root of the mean expression value of the whole dataset (∼4.5 RPKM) were considered as relevant for further analyses. Differentially expressed genes were selected based on Student's *t*-test ($P < 0.05$) and delta RPKM changes bigger than the mean expression value of the whole dataset (∼20 RPKM) and/or 2-fold change in expression level between treatments.

BIOINFORMATICS

For gene clustering, we used the MACCU software (http://maccu.sourceforge.net/) to build co-expression networks based on co-expression relationships with a Pearson's coefficient greater than or equal to 0.60. In order to capture the tissue-specific co-expression relationships, Pearson's coefficients were computed based on robust multi-array averaged array data derived from leaf- and root-specific experiments for each tissue

downloaded from NASCArrays (http://affymetrix.arabidopsis.info/). Visualization of the networks was performed with the Cytoscape software version 2.8.2 (http://www.cytoscape.org/).

RT-PCR

For RT-PCR, total RNA was extracted from the leaves using Trizol (Invitrogen) and DNase treated with the Turbo DNA-free Kit (Ambion) following the manufacturer's instructions. cDNA was synthesized using QuantiTect Reverse Transcription Kit (Qiagen) following the manufacturer's instructions. Real-time PCR was performed using Power SYBR Green PCR Master Mix (Applied Biosystems) on an Applied Biosystems 7500 Fast Real-Time PCR System with programs recommended by the manufacturer. Samples were normalized first to an endogenous reference *(AtEF1α)* and then the relative target gene was determined by performing a comparative ΔΔCt. The following primers were used: *AtEF1α* (At5g60390) fwd: GAGCCCAAGTTTTTGAAGA, rev: CTAACAGCGAAACGTCCCA, and *HEMA1* (At1g58290) fwd: GATCTCCTTCTTCCACATCGCAA, rev: CCGCCATTGAAAC CCAAAATC.

RESULTS

To dissect processes that are triggered by decreased Fe supply, we analyzed the transcriptome of Fe-sufficient and Fe-deficient leaves using the RNA-seq technology. A total of approximately 60 million reads was collected from three independent sequencing runs per growth type and aligned to the TAIR10 annotation of the *Arabidopsis* genome. A set of 413 genes was differentially expressed between Fe-deficient and Fe-sufficient plants (*t*-test $P < 0.05$ with either a FC > 2 or a ΔRPKM > 20.6), out of a total of 24841 genes detected in leaves from Fe-sufficient and Fe-deficient plants (**Figure 1**).

As anticipated from the high Fe demand of the photosynthetic electron chain, the strongest regulation was observed for photosynthesis-related genes. The expression of the PSI subunits *PSAF* and *PSAN* and of the ferredoxin *FED2* was decreased by more than 1000 RPKM; transcript levels of several other photosynthesis-associated genes such as the light harvesting complexes-related proteins *LHCB6*, *LHCA3*, *LHCA2*, and *LHCB4.1* were reduced by ca. 500 RPKM when grown on media lacking Fe. Furthermore, genes encoding Chl-binding proteins were strongly down-regulated. Interestingly, a subset of seven unknown proteins (At1g47400, At2g14247, At1g13609, At1g47395, At3g56360, At2g30766, and At5g67370) was most strongly up-regulated in leaves. In addition, the protein kinase *ORG1*, the oligopeptide transporter *OPT3* and the Ib subgroup transcription factors *bHLH38*, *bHLH39*, *bHLH100*, and *bHLH101* were strongly induced by Fe deficiency.

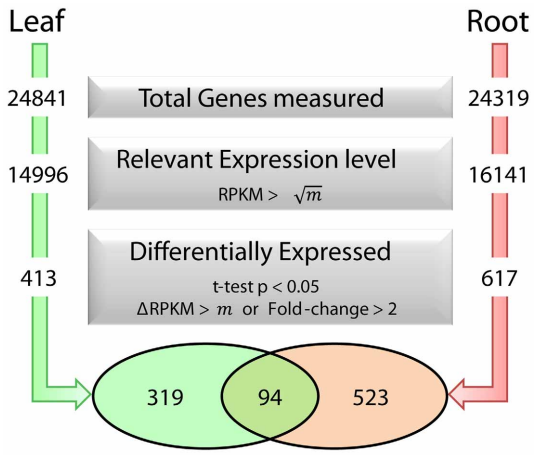

FIGURE 1 | Fe deficiency-induced transcriptional changes in leaves and roots and selection parameters used to identify differentially expressed genes. *m* represents the average RPKM value for all genes detected in each dataset.

CHLOROPHYLL SYNTHESIS, CHL *b* TO CHL *a* CONVERSION AND XANTHOPHYLL SYNTHESIS COMPRISE A "PHOTOOXIDATIVE DAMAGE AVOIDANCE" MODULE

The universal symptom of Fe–deficient plants is interveinal chlorosis of developing leaves, which is the cause of the decreased Chl content. We found that the Glu-tRNA reductase (HEMA1), which catalizes the reduction of glutamyl-tRNA to glutamate-1-semialdehyde, the first committed step in tetrapyrrole biosynthesis, was massively down-regulated in Fe-deficient plants (**Figure 2**). The product of this first subdivision of Chl synthesis is 5-aminolevulinic acid (ALA). Down-regulation of *HEMA1* was robust and occurred rapidly after exposure of the plants to media lacking Fe. We observed a 2-fold decrease in transcript abundance in leaves of hydroponically grown plants after transfer of the plants to Fe-free media within 2 h (**Figure 2**, inset), suggesting a prompt adjustment of ALA biosynthesis to the available Fe. The second subdivision of the Chl biosynthesis pathway comprises six steps common to the heme, siroheme and Chl branches in which ALA is converted to protoporphyrin IX (Proto IX). None of the genes encoding enzymes mediating these common steps in tetrapyrrole biosynthesis was affected by Fe deficiency at the transcriptional level. Strong down-regulation occurred in three genes in the Chl branch, namely *GUN5*, *PORB*, and *CHLP* (**Figure 2**). This branch starts with the insertion of Mg^{2+} into Proto IX, mediated by magnesium chelatase (GUN5). PORB is one out of three *Arabidopsis* protochlorophyllide (Pchlide) oxidoreductases that catalize the reduction of the C17-C18 double bond in the D pyrrole ring to yield chlorophyllide *a*. *CHLP* encodes a geranylgeranyl reductase that catalyzes the reduction of geranylgeranyl pyrophosphate to phytyl pyrophosphate (**Figure 2**). A marked decrease in expression was also observed for *NON-YELLOW COLORING1* (*NYC1*), mediating the conversion of Chl *b* to Chl *a*. This conversion is important for Chl breakdown and is critical in light regulation (Tanaka et al., 2011). It can be assumed that the rate of Chl breakdown is adjusted to the decreased Chl synthesis under Fe-deficient conditions. Enzymes of the heme branch were not transcriptionally regulated by Fe. This is contrary to the anticipation since a lack of Fe will compromise the activity of ferrochelatases, inserting Fe^{2+} into proto IX to form protoheme. A weak down-regulation was observed for UPM1, catalyzing two steps in the siroheme branch.

CONSERVED IN THE GREEN LINEAGE AND DIATOMS27 (*CGLD27*) belongs to a group of strongly up-regulated leaf

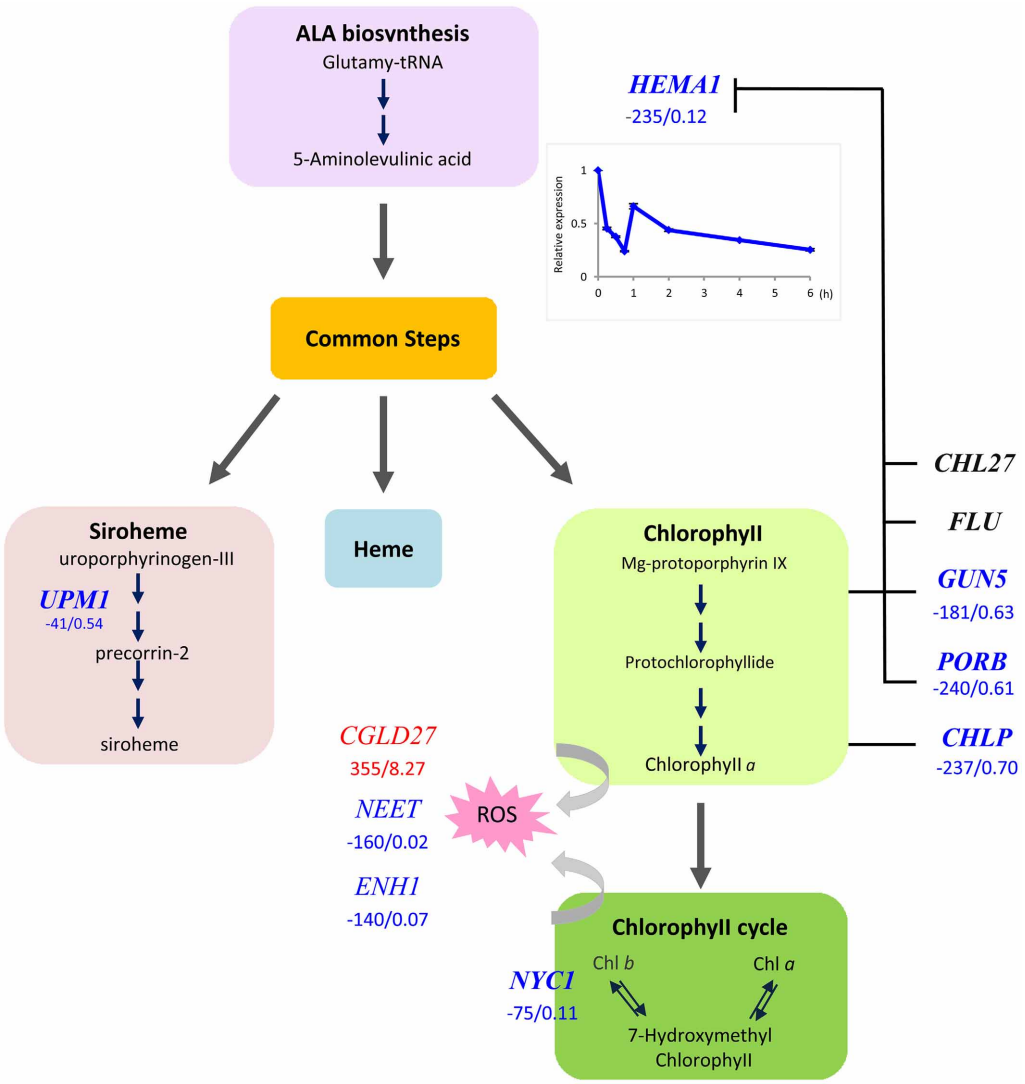

FIGURE 2 | Flow chart of the tetrapyrrole pathway toward siroheme, heme, and chlorophyll. Enzymes that were transcriptionally affected by Fe deficiency are indicated by red (up-regulated genes) or blue letters (down-regulated genes). Numbers indicate delta RPKM and fold change of samples from Fe deficient compared with Fe-sufficient plants. Arrows denote steps that are likely regulated by the [Fe]. Inset shows the time-course of *HEMA1* expression in leaves after transfer to Fe-deplete media.

genes. *CGLD27* has been described as one out of 14 Fe-responsive orthologs in *Chlamydomonas* and *Arabidopsis*, indicating that *CGLD27* is a common and potentially important component of the Fe deficiency response of the plant lineage (Urzica et al., 2012). *CGLD27 is* conserved in cyanobacteria and plastid-containing organisms but not in non-photosynthetic organisms, and CGLD27 likely targeted to plastids. Homozygous mutants are more sensitive to low Fe concentrations in the media (Urzica et al., 2012). The protein was predicted to function in carotenoid-xanthophyll metabolism (Kourmpetis et al., 2010) and is co-expressed with the ZETA-CAROTENE DESATURASE (ZDS; At3g04870) involved in the biosynthesis of carotenes and xanthophylls. It is tempting to speculate that CGLD27 has a function in photoprotection by quenching free radicals and singlet oxygen. Together the results indicate that HEMA1, NYC1, and CGLD27 may represent key players in preventing photooxidative damage in Fe-deficient leaf cells.

Two other genes encoding proteins that are targeted to chloroplast, AtNEET and NAP1 were strongly down-regulated in leaves from Fe-deficient plants. For both genes ancient roles in Fe metabolism were proposed (Xu et al., 2005; Nechushtai et al., 2012), indicating that these proteins may play a role in coordinating tetrapyrrole synthesis and ROS detoxification with the amount of available Fe.

CO-EXPRESSION NETWORKS FROM ROOTS AND SHOOTS ALLOWS AN INTEGRATIVE VIEW OF THE *ARABIDOPSIS* FE DEFICIENCY RESPONSE

Co-expression networks can group genes to functionally related modules and can assign putative functions to unknown proteins. To identify modules with functions in the leaf response to Fe

deficiency, we subjected the differentially expressed genes identified in our data set to a co-expression analysis using the MACCU software package (Lin et al., 2011). In an attempt to identify conserved and potentially co-regulated processes common to both leaves and roots, we compared transcriptional changes induced by growth on Fe depleted media in leaves with those of roots by re-analyzing a previously published data set of roots from plants grown under the same conditions (Rodríguez-Celma et al., 2013). In roots from Fe-deficient plants, 617 genes were found to be differentially expressed when similar criteria were applied (**Figure 1**). We then analyzed the co-expression of genes in leaves and roots separately using databases of publically available microarray experiments that discriminate for leaf- and root-related processes. Finally, we merged the two sub-networks, yielding a large hybrid network comprising 725 genes that can be subdivided in several subclusters (**Figure 3**, Table S1 and Figure S1). Two subclusters (Hub_1 and Hub_2) connect the two major clusters. The cluster Root_C2 contains genes involved in the acquisition of Fe and in regulation of Fe homeostasis. The largest changes in transcript abundance were observed for genes that mediate the acquisition of Fe (*IRT1* and *AHA2*), genes catalyzing the first steps in the general phenylpropanoid pathway (*F6'H1*, *PAL1*, *PAL2*), the detoxification of transition metals (*MTPA2*) and in the regulation of Fe homeostasis (*FIT*). Also, several genes with yet undefined function in Fe homeostasis were highly responsive to the change in growth regime. The most strongly down-regulated gene was *PYK10*, encoding a β-glucosidase located in the ER (Nitz et al., 2001). *PYK10* was suggested to restrict colonization of the beneficial endophytic fungus *Piriformospora indica*, thereby conferring resistance to heavy metal ions and promoting nutrient uptake (Sherameti et al., 2008). It can be assumed that lowered expression of *PYK10* compensates for reduced interaction between roots and the fungus due to decreased Fe content of root cells. While this assumption awaits further experimental support, the data might hint at an understudied aspect of the Fe-deficiency response that may be of importance for the fitness of plants under natural conditions.

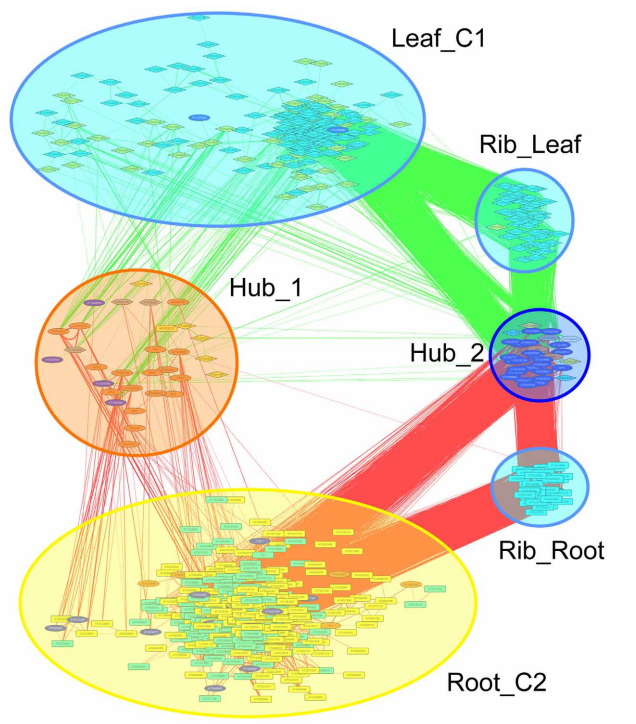

FIGURE 3 | Merged co-expression network of differentially expressed genes in roots and leaves. Differentially expressed genes were first clustered separately for roots and shoots based on their co-expression relationships with a Pearson's coefficient of ≥0.60 against a customized data base that was constructed from experiments conducted with roots or leaves, respectively, using the MACCU software package, and then the two networks were combined. Yellow nodes denote genes that were up-regulated in roots or shoots, orange nodes indicate genes with increased expression in both organs. Light blue nodes denote genes that were down-regulated in roots or shoots, dark blue nodes indicate genes with decreased expression in both organs. Red and green lines represent co-expression edges derived from the root or leaf networks, respectively.

The cluster Leaf_C1 contained several genes associated with PS, LHCs and with Chl synthesis that have been described above. Genes derived from the root and shoot network were connected by three relatively large subclusters containing ribosome genes. Notably, two of the ribosomal subclusters (Rib_Leaf and Rib_Root) were comprised of genes that were exclusively derived from the root and shoot network, and the third subcluster contained genes from both subnetworks. Inspection of the genes in these subclusters revealed that the down-regulation of genes encoding ribosomal proteins was differential between leaves or roots. Notably, in leaves proteins belonging to paralogs families of the large subunit were affected by Fe deficiency, while in roots the majority of regulated ribosomal genes encoded ribosomal proteins from the 40S subunit (Table S2). This suggests that the composition of ribosomes is changed by Fe deficiency and that this change occurs in an organ-specific manner (**Figure 4**).

A CONSERVED SET OF FE-REGULATED GENES IS HIGHLY EXPRESSED IN BOTH LEAVES AND ROOTS

Using conservative criteria (FC > 2, $P < 0.05$ and ΔRPKM > 40), we mined the data sets for genes that are strongly Fe-regulated in both leaves and roots. A set of 17 genes fulfilled these criteria, among them the transcription factors *bHLH38*, *bHLH39* and *bHLH100*, *FRO3*, *OPT3,* the nicotianamine synthase *NAS4*, the Fe storage protein *FER1*, the Fe superoxide dismutase *FDS1* and the protein kinase *ORG1* (**Table 1**), some of which were reported to be Fe-regulated in previous microarray experiments (Ivanov et al., 2011). Furthermore, six proteins in this set have unknown functions (**Table 1**). The high expression levels and the robust regulation of the genes encoding these proteins indicate putatively important functions in Fe metabolism. We have named them IRON-RESPONSIVE PROTEIN (IRP) 1–6, as candidates for follow-up experiments (**Table 1**). The encoded proteins can be organized in three groups of two proteins. IRP1 (At1g47400) and IRP2 (At1g47395) are peptides of 50 amino acids with a conserved region. The second group comprises IRP3 (At2g14247) and IRP4 (At1g13609), small proteins of 78 amino acids and no conserved domain. IRP5 (At3g56360) and IRP6 (At5g05250) are 25.1 and 25.9 kDa proteins, respectively, with predicted myristoylation sites.

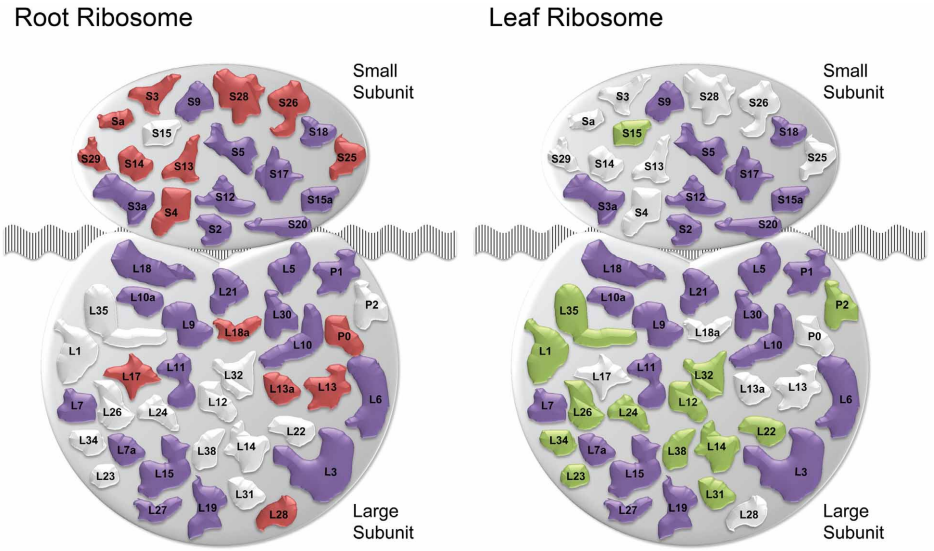

FIGURE 4 | Fe deficiency-induced changes in ribosomal composition. Schematic of ribosomal composition changes for roots and leaves. Red and green shapes represent ribosomal protein families down-regulated specifically in roots and leaves, respectively. Purple colored shapes represent families down-regulated in both organs. White colored shapes denote families not regulated in the corresponding tissue ribosomes.

Table 1 | Genes that were differentially expressed between Fe-sufficient and Fe-deficient plants in both leaves and roots with a ΔRPKM > 40 and FC > 2 at $P < 0.05$.

ID	Symbol	Description	Leaf ΔRPKM	Leaf FC (log_2)	Root ΔRPKM	Root FC (log_2)
At1g47400	IRP1	Iron-responsive protein 1	397.47	6.44	63.29	4.11
At1g47395	IRP2	Iron-responsive protein 2	797.71	6.30	139.65	3.89
At2g14247	IRP3	Iron-responsive protein 3	432.04	6.30	142.85	2.37
At1g13609	IRP4	Iron-responsive protein 4	682.77	7.97	80.11	6.27
At3g56360	IRP5	Iron-responsive protein 5	318.11	2.04	82.54	1.24
At5g05250	IRP6	Iron-responsive protein 6	238.88	4.04	58.06	2.72
At3g56970	bHLH38	Basic helix-loop-helix protein 38	275.66	10.17	144.41	6.19
At3g56980	bHLH39	Basic helix-loop-helix protein 39	154.59	9.45	120.43	4.96
At2g41240	BHLH100	Basic helix-loop-helix protein 100	363.10	12.12	105.43	8.14
At1g23020	FRO3	Ferric reduction oxidase 3	124.84	2.55	87.69	2.91
At4g16370	OPT3	Oligopeptide transporter 3	300.81	2.49	80.60	2.77
At5g53450	ORG1	OBP3-responsive gene 1	390.12	4.39	57.89	2.39
At1g56430	NAS4	Nicotianamine synthase 4	92.59	2.70	43.08	2.39
At4g08390	SAPX	Stromal ascorbate peroxidase	−98.62	−3.41	−50.32	−1.06
At4g25100	FSD1	Fe superoxide dismutase 1	−239.22	−4.26	−57.45	−2.15
At5g01600	FER1	Ferritin 1	−233.03	−4.85	−60.79	−2.29
At1g48300	DGAT3	Diacylglycerol acyltransferase 3	260.16	1.65	143.56	1.18

To put the conserved genes into a functional context and to assign putative functions for the unknown proteins, we constructed a co-expression network using the set of 17 conserved genes as baits and fished for first degree co-expressed nodes (**Figure 5**). The resulting network was comprised 99 genes with several central players in Fe homeostasis such as *OPT3*, *FRO3*, *NAS4*, *IRT1*, *MTPA2*, and the phosphoenolpyruvate carboxylase *PPC1*. Also, four major regulators of Fe homeostasis were found within this network, including *BTS*, *PYE*, *bHLH39*, and *bHLH101*. Notably, with the exception of *IRT1*, *MTPA2*, and *PPC1*, which appear more important for root Fe acquisition, all the genes listed above plus *HEMA1* and *FER4* were located in HUB_1 (**Figure 3**) that connects the genes that are specific for roots or leaves, indicating a function of these genes in both organs and/or in systemic Fe homeostatic regulation. This network also contained 16 genes encoding ribosomal proteins and two orthologs of the mammalian receptor for activated C-kinase 1 (*RACK1*), *RACK1A*, and *RACK1B*. In both mammals and plants, *RACK1* genes have been associated with protein translation and ribosome biogenesis (Nilsson et al., 2004; Guo et al., 2011). Together these results indicate conserved players in cellular Fe homeostasis. They establish a link between several novel genes

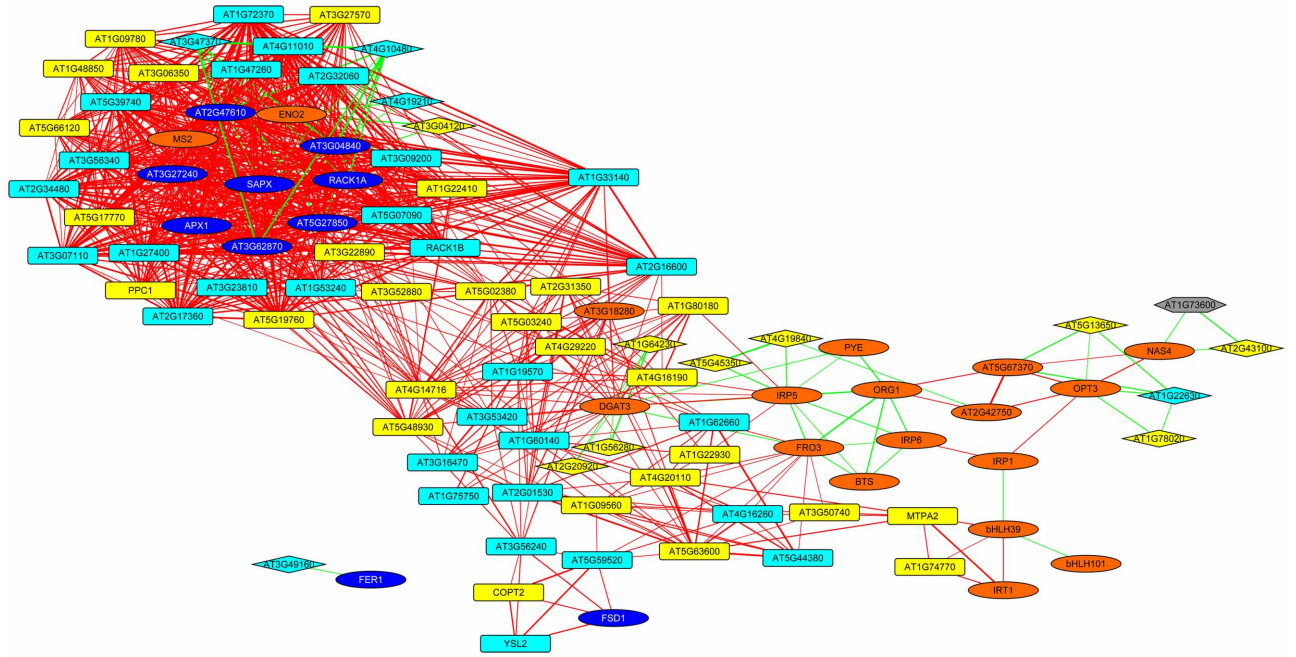

FIGURE 5 | Co-expression network around genes that are differentially expressed in roots and leaves. The genes listed in **Table 1** were used as baits and first-degree neighbors were added based on a database comprising publicly available microarray experiments. Yellow nodes denote genes that were up-regulated in roots or shoots, orange nodes indicate genes with increased expression in both organs. Light blue nodes denote genes that were down-regulated in roots or shoots, dark blue nodes indicate genes with decreased expression in both organs. Red and green lines represent co-expression edges derived from the root or leaf networks, respectively. Squared and diamond shaped nodes represent genes differentially expressed in roots and leaves, respectively.

encoding proteins with unknown functions and a regulatory network.

DISCUSSION

While the transcriptional response of roots to Fe deficiency is well explored at the whole-genome level, information on transcriptional profile changes that occur in Fe-deficient leaves is scarce. The largest sinks for Fe are PSI and PSII, and the major fraction of Fe is located in the chloroplasts. It seems reasonable to assume that photosynthetic cells have evolved mechanisms that adjust the synthesis of light harvesting complexes to that of Fe-containing enzymes and complexes to avoid accumulation of ROS and to recalibrate Fe homeostasis in leaf cells.

PHOTOOXIDATIVE DAMAGE IN FE-DEFICIENT LEAF CELLS IS AVOIDED BY ELABORATE MECHANISMS

Decreased Chl content is a hallmark of Fe-deficient plants and has been associated with compromised photosynthesis caused by decreased tetrapyrrole biosynthesis. The fast and pronounced down-regulation of *HEMA1* expression suggests a rapid and dramatic decline of tetrapyrrole synthesis at an early stage of Fe deficiency. Our data support a scenario in which plastid Fe sensing links Chl synthesis to the activity of the photosystems to avoid the production of toxic radicals upon illumination of free tetrapyrrole intermediates. Notably, Fe-deficient *Clamydomonas* cells are not sensitive to high light and photosynthetic mutants grow better on low Fe media (Moseley et al., 2002), demonstrating that Fe-deficient plants are protected against photo-oxidative damage. ALA synthesis is rate-limiting in tetrapyrrole synthesis and sophisticatedly regulated (Tanaka et al., 2011; Brzezowski and Grimm, 2013). Interestingly, in acetate-grown *Chlamydomonas* cells tetrapyrrole synthesis was up-regulated upon Fe deficiency, while photoautotrophic cells showed lower mRNA levels of the enzymes involved in the pathway (Moseley et al., 2002), suggesting that Chl synthesis is not restricted by decreased Fe supply. Similar to other regulators of tetrapyrrole synthesis such as light, phytohormones and the circadian clock, the control sites with regard to Fe availability are at the beginning, at the branch points and at the end of the pathway. This avoids the accumulation of photoreactive porphyrin and of free Chl intermediates, and adjusts the metabolic flow to demand. The metabolites Mg-protoporphyrin and divinylprotochlorophylide *a* negatively regulate HEMA1 activity (Tanaka and Tanaka, 2007). Recently, it has been shown that in the presence of Pchlide a complex comprising the fluorescence protein FLU, PORB, CHL27, and CHLP interacts with HEMA1 and inhibits ALA synthesis (**Figure 2**; Kauss et al., 2012). In the absence of Pchlide, such interaction is compromised and allows ALA synthesis (Kauss et al., 2012). How are Chl synthesis and photosynthetic activity synchronized to avoid accumulation of ROS in Fe-deficient leaves? A possible scenario involves a Chl-mediated disconnection of the LHC1 antenna from PSI as described for *Chlamydomonas* (Moseley et al., 2002). A finely tuned Chl synthesis and binding of Chl to PSI would allow an efficient adaptation of the photosynthetic machinery

to the available Fe pools. The diiron Mg-protoporphyrin IX monomethylester oxidative cyclase CHL27 has been suggested as a candidate plastid Fe sensor (Tottey et al., 2003). Another potential candidate that links photosynthesis, ROS and Fe metabolism is the NEET protein At5g51720 (AtNEET). AtNEET harbors two redox active 2Fe-2S clusters and is dramatically down-regulated (40-fold; 98% decrease in transcript level) in leaves of Fe-deficient plants. *AtNEET* is tightly co-expressed with *FER3* and *FER4*, encoding plastid ferritins. Furthermore, *AtNEET* is co-expressed with *ENH1*, which may play a role in ROS detoxification (Zhu et al., 2007). Reduced levels of *AtNEET* transcript levels caused late greening, increased the sensitivity to low Fe levels, and conferred insensitivity to high Fe concentrations (Nechushtai et al., 2012). NEET proteins are conserved in plants and mammals and an ancient role of AtNEET in Fe homeostasis has been suggested (Nechushtai et al., 2012). However, a clear role in plastid Fe metabolism has not yet been defined. Another candidate for a plastid Fe sensor is the NON-INTRINSIC ABC PROTEIN (NAP1), a protein with similarities to prokaryotic *SufB* proteins which are involved in Fe-S cluster repair (Xu et al., 2005). AtNAP1 complements an *E. coli SufB* mutant, indicating that AtNAP1 is an evolutionary conserved SufB protein (Xu et al., 2005), and regulation of cellular sulfur level has been previously shown to be related to Fe homeostasis (Ivanov et al., 2011). AtNAP1 is transcriptionally and post-transcriptionally regulated by Fe, and may function in plastid Fe homeostasis (Xu et al., 2005). A strong down-regulation of *AtNAP1* was observed in the present study (Table S1), supporting the assumption of a role of AtNAP1 in plastid Fe sensing or signaling.

FE DEFICIENCY ALTERS RIBOSOME COMPOSITION IN AN ORGAN-SPECIFIC MANNER

While considered as housekeeping genes encoding structural components, plant cytosolic ribosomes are more heterogenous and plastic than their mammalian counterparts. Plant ribosomal proteins are encoded by multiple divergent paralogs, which allows, in theory, for 10^{34} structurally different ribosomes (Hummel et al., 2012), a number that can be increased by numerous post-translational modifications. Generally, ribosome biogenesis appears to be down-regulated in both roots and leaves from Fe-deficient plants. A large part of transcriptional activity is used for this process and the decrease in the abundance of ribosomal subunits may be interpreted in terms of biasing translation toward proteins encoding products that are needed in large amounts to recalibrate cellular Fe homeostasis. It also appears, however, that the down-regulation is not general but highly organ-specific, indicating a carefully controlled change in ribosomal composition. Paralog composition has also been shown to be altered by growth conditions (Hummel et al., 2012), which is most likely the case in Fe-deficient plants. The fact that the change in the expression of paralogous isoforms is typical of leaves and roots suggests that this change is not due to a general down-regulation of translation, but rather may adjust the protein composition of the cell to the prevailing conditions. This would also offer an explanation for the relatively low concordance of proteomic and transcriptomic changes in response to environmental conditions (Lan et al., 2012). Importantly, our results indicate that translational bias, mediated by a change in composition of ribosomes, is part of the Fe deficiency response of both leaves and roots.

ESTABLISHED AND NOVEL PLAYERS CONTROL CELLULAR FE HOMEOSTASIS IN LEAVES AND ROOTS

Despite the different function of leaf and root cells, many of the major regulators of Fe deficiency responses that have been identified in roots were also found in leaves, indicating that the subgroup 1b transcription factors and PYE/BTS are controlling cellular Fe homeostasis in most if not all plant cells (Ivanov et al., 2011). A notable exception was FIT, the expression of which appears to be root-specific. It seems plausible that different combinations of heterodimers are regulating non-overlapping sets of genes, a scenario which does not exclude other levels of regulation. A novel finding was the differential expression of ribosomal proteins, which possibly altered the composition of ribosomes in an organ and growth type-specific manner, a regulatory layer which has yet to be explored. Our data also revealed several new players that may play conserved roles in Fe metabolism in both leaves and roots. Some of these genes have no corresponding probe set on the ATH1 gene chip and can thus not be properly inserted into co-expression networks. The three genes for which a co-expression relationship can be inferred from public data bases (*IRP1*, *IRP5*, and *IRP6*), are closely co-expressed with each other and several genes with important functions in Fe homeostasis (e.g., *NRAMP4*, *FRO3*, *NAS4*, *bHLH39*, *OPT3*, *ORG1*, and *PYE*), associating putative roles in Fe metabolism of these proteins in both leaves and roots.

No transporter from the YLS, ZIP, or IREG family that could mediate the transport of Fe(II) has been found to be Fe-regulated in leaf cells. Such a function could be fulfilled by OPT3, as inferred from the strong phenotype of the *opt3-2* mutant (Stacey et al., 2008), the general characteristics and expression patterns of OPT transporters (Lubkowitz, 2011), the massive up-regulation of the genes upon Fe deficiency and the central position in the co-expression networks.

Several lines of evidence support a concept of anticipated changes that have been proven for the sequestering of surplus metals that are associated with an up-regulation of IRT1 activity (Yang et al., 2010). For example, down-regulation of *PYK10* can be interpreted as an anticipation of a Fe deficiency-induced decrease in colonization efficiency of *P. indica*. Also, the fast orchestrated regulation of tetrapyrrole synthesis, Chl *b* to a Chl *a* conversion and, putatively, the biosynthesis of xanthophyll to avoid oxidative damage may be interpreted as anticipatory changes. Understanding of the regulation of these response modules is desirable in order to gain a holistic understanding of the responses to Fe deficiency and also in order to develop tools to generate plants with improved Fe efficiency.

ACKNOWLEDGMENTS

This work was supported by grants from Academia Sinica.

SUPPLEMENTARY MATERIAL

The Supplementary Material for this article can be found online at http://www.frontiersin.org/Plant_Nutrition/10.3389/fpls.2013.00276/abstract

REFERENCES

Brzezowski, P., and Grimm, B. (2013). Chlorophyll metabolism. *eLS*. doi: 10.1002/9780470015902.a0020084.pub2

Buckhout, T. J., Yang, T. J. W., and Schmidt, W. (2009). Early iron-deficiency-induced transcriptional changes in Arabidopsis roots as revealed by microarray analyses. *BMC Genomics* 10:147. doi: 10.1186/1471–2164-10-147

Colangelo, E. P., and Guerinot, M. L. (2004). The essential basic helix-loop-helix protein FIT1 is required for the iron deficiency response. *Plant Cell* 16, 3400–3412. doi: 10.1105/tpc.104.024315

Didonato, R. J., Jr., Roberts, L. A., Sanderson, T., Eisley, R. B., and Walker, E. L. (2004). Arabidopsis Yellow Stripe-Like2 (YSL2): a metal-regulated gene encoding a plasma membrane transporter of nicotianamine-metal complexes. *Plant J.* 39, 403–414. doi: 10.1111/j.1365-313X.2004.02128.x

Eide, D., Broderius, M., Fett, J., and Guerinot, M. L. (1996). A novel iron-regulated metal transporter from plants identified by functional expression in yeast. *Proc. Natl. Acad. Sci. U.S.A.* 93, 5624–5628. doi: 10.1073/pnas.93.11.5624

Estelle, M. A., and Somerville, C. (1987). Auxin-resistant mutants of *Arabidopsis thaliana* with an altered morphology. *Mol. Gen. Genet.* 206, 200–206. doi: 10.1007/BF00333575

Gris, E. (1844). Nouvelles expériences sur l'action des composés ferrugineux solubles, et de la debilite des plantes. *CR Acad. Sci. Paris* 19, 1118–1119.

Guo, J., Wang, S., Valerius, O., Hall, H., Zeng, Q., Li, J. F., et al. (2011). Involvement of Arabidopsis RACK1 in protein translation and its regulation by abscisic acid. *Plant Physiol.* 155, 370–383. doi: 10.1104/pp.110.160663

Hummel, M., Cordewener, J. H. G., De Groot, J. C. M., Smeekens, S., America, A. H. P., and Hanson, J. (2012). Dynamic protein composition of *Arabidopsis thaliana* cytosolic ribosomes in response to sucrose feeding as revealed by label free MSE proteomics. *Proteomics* 12, 1024–1038. doi: 10.1002/pmic.201100413

Ivanov, R., Brumbarova, T., and Bauer, P. (2011). Fitting into the harsh reality: regulation of iron-deficiency responses in dicotyledonous plants. *Mol. Plant* 5, 27–42. doi: 10.1093/mp/ssr065

Jakoby, M., Wang, H. Y., Reidt, W., Weisshaar, B., and Bauer, P. (2004). FRU (BHLH029) is required for induction of iron mobilization genes in *Arabidopsis thaliana*. *FEBS Lett.* 577, 528–534. doi: 10.1016/j.febslet.2004.10.062

Kauss, D., Bischof, S., Steiner, S., Apel, K., and Meskauskiene, R. (2012). FLU, a negative feedback regulator of tetrapyrrole biosynthesis, is physically linked to the final steps of the Mg(++)-branch of this pathway. *FEBS Lett.* 586, 211–216. doi: 10.1016/j.febslet.2011.12.029

Kent, W. J. (2002). BLAT - the BLAST-like alignment tool. *Genome Res.* 12, 656–664. doi: 10.1101/gr.229202

Kourmpetis, Y. A., Van Dijk, A. D., Bink, M. C., Van Ham, R. C., and TerBraak, C. J. (2010). Bayesian Markov Random Field analysis for protein function prediction based on network data. *PLoS ONE* 5:e9293. doi: 10.1371/journal.pone.0009293

Lan, P., Li, W., and Schmidt, W. (2012). Complementary proteome and transcriptome profiling in phosphate-deficient Arabidopsis roots reveals multiple levels of gene regulation. *Mol. Cell. Proteomics* 11, 1156–1166. doi: 10.1074/mcp.M112.020461

Lin, W. D., Liao, Y. Y., Yang, T. J., Pan, C. Y., Buckhout, T. J., and Schmidt, W. (2011). Coexpression-based clustering of Arabidopsis root genes predicts functional modules in early phosphate deficiency signaling. *Plant Physiol.* 155, 1383–1402. doi: 10.1104/pp.110.166520

Ling, H. Q., Bauer, P., Bereczky, Z., Keller, B., and Ganal, M. (2002). The tomato *fer* gene encoding a bHLH protein controls iron-uptake responses in roots. *Proc. Natl. Acad. Sci. U.S.A.* 99, 13938–13943. doi: 10.1073/pnas.212448699

Long, T. A., Tsukagoshi, H., Busch, W., Lahner, B., Salt, D. E., and Benfey, P. N. (2010). The bHLH transcription factor POPEYE regulates response to iron deficiency in Arabidopsis roots. *Plant Cell* 22, 2219–2236. doi: 10.1105/tpc.110.074096

Lubkowitz, M. (2011). The oligopeptide transporters: a small gene family with a diverse group of substrates and functions? *Mol. Plant* 4, 407–415. doi:10.1093/mp/ssr004

Mortazavi, A., Williams, B. A., McCue, K., Schaeffer, L., and Wold, B. (2008). Mapping and quantifying mammalian transcriptomes by RNA-Seq. *Nat. Methods* 5, 621–628. doi: 10.1038/nmeth.1226

Moseley, J. L., Allinger, T., Herzog, S., Hoerth, P., Wehinger, E., Merchant, S., et al. (2002). Adaptation to Fe-deficiency requires remodeling of the photosynthetic apparatus. *EMBO J.* 21, 6709–6720. doi: 10.1093/emboj/cdf666

Nechushtai, R., Conlan, A. R., Harir, Y., Song, L., Yogev, O., Eisenberg-Domovich, Y., et al. (2012). Characterization of Arabidopsis NEET reveals an ancient role for NEET proteins in iron metabolism. *Plant Cell* 24, 2139–2154. doi: 10.1105/tpc.112.097634

Nilsson, J., Sengupta, J., Frank, J., and Nissen, P. (2004). Regulation of eukaryotic translation by the RACK1 protein: a platform for signalling molecules on the ribosome. *EMBO Rep.* 5, 1137–1141. doi: 10.1038/sj.embor.7400291

Nitz, I., Berkefeld, H., Puzio, P. S., and Grundler, F. M. (2001). PYK10, a seedling and root specific gene and promoter from *Arabidopsis thaliana*. *Plant Sci.* 161, 337–346. doi: 10.1016/S0168-9452(01)00412-5

op den Camp, R. G., Przybyla, D., Ochsenbein, C., Laloi, C., Kim, C., Danon, A., et al. (2003). Rapid induction of distinct stress responses after the release of singlet oxygen in Arabidopsis. *Plant Cell* 15, 2320–2332. doi: 10.1105/tpc.014662

Rellán-Álvarez, R., Giner-Martínez-Sierra, J., Orduna, J., Orera, I., Rodríguez-Castrillón, J. A., García-Alonso, J. I., et al. (2010). Identification of a tri-iron(III), tri-citrate complex in the xylem sap of iron-deficient tomato resupplied with iron: new insights into plant iron long-distance transport. *Plant Cell Physiol.* 51, 91–102. doi: 10.1093/pcp/pcp170

Robinson, N. J., Procter, C. M., Connolly, E. L., and Guerinot, M. L. (1999). A ferric-chelate reductase for iron uptake from soils. *Nature* 397, 694–697.

Rodríguez-Celma, J., Lin, W.-D., Fu, G.-M., Abadia, J., López-Millán, A.-F., and Schmidt, W. (2013). Mutually exclusive alterations in secondary metabolism are critical for the uptake of insoluble iron compounds by Arabidopsis and *Medicago truncatula*. *Plant Physiol.* 162, 1473–1485. doi: 10.1104/pp.113.220426

Santi, S., and Schmidt, W. (2009). Dissecting iron deficiency-induced proton extrusion in Arabidopsis roots. *New Phytol.* 183, 1072–1084. doi: 10.1111/j.1469-8137.2009.02908.x

Sherameti, I., Venus, Y., Drzewiecki, C., Tripathi, S., Dan, V. M., Nitz, I., et al. (2008). PYK10, a beta-glucosidase located in the endoplasmatic reticulum, is crucial for the beneficial interaction between Arabidopsis thaliana and the endophytic fungus *Piriformospora indica*. *Plant J.* 54, 428–439. doi: 10.1111/j.1365-313X.2008.03424.x

Stacey, M. G., Patel, A., McClain, W. E., Mathieu, M., Remley, M., Rogers, E. E., et al. (2008). The Arabidopsis AtOPT3 protein functions in metal homeostasis and movement of iron to developing seeds. *Plant Physiol.* 146, 589–601. doi: 10.1104/pp.107.108183

Tanaka, R., Kobayashi, K., and Masuda, T. (2011). Tetrapyrrole metabolism in *Arabidopsis thaliana*. *Arabidopsis Book* 9:e0145. doi: 10.1199/tab.0145

Tanaka, R., and Tanaka, A. (2007). Tetrapyrrole biosynthesis in higher plants. *Annu. Rev. Plant Biol.* 58, 321–346. doi: 10.1146/annurev.arplant.57.032905.105448

Terry, N. (1980). Limiting factors in photosynthesis: I. Use of iron stress to control photochemical capacity *in vivo*. *Plant Physiol.* 65, 114–120. doi: 10.1104/pp.65.1.114

Tottey, S., Block, M. A., Allen, M., Westergren, T., Albrieux, C., Scheller, H. V., et al. (2003). Arabidopsis CHL27, located in both envelope and thylakoid membranes, is required for the synthesis of protochlorophyllide. *Proc. Natl. Acad. Sci. U.S.A.* 100, 16119–16124. doi: 10.1073/pnas.2136793100

Urzica, E. I., Casero, D., Yamasaki, H., Hsieh, S. I., Adler, L. N., Karpowicz, S. J., et al. (2012). Systems and trans-system level analysis identifies conserved iron deficiency responses in the plant lineage. *Plant Cell* 24, 3921–3948. doi: 10.1105/tpc.112.102491

Wang, L., Cui, Y., Liu, Y., Fan, H., Du, J., Huang, Z., et al. (2012). Requirement and Functional Redundancy of Ib subgroup bHLH proteins for iron deficiency responses and uptake in *Arabidopsis thaliana*. *Mol. Plant* 6, 503–513. doi: 10.1093/mp/sss089

Waters, B. M., Chu, H. H., Didonato, R. J., Roberts, L. A., Eisley, R. B., Lahner, B., et al. (2006). Mutations in Arabidopsis yellow stripe-like1 and yellow stripe-like3 reveal their roles in metal ion homeostasis and loading of metal ions in seeds.

Plant Physiol. 141, 1446–1458. doi: 10.1104/pp.106.082586

Xu, X. M., Adams, S., Chua, N. H., and Moller, S. G. (2005). AtNAP1 represents an atypical SufB protein in *Arabidopsis plastids*. *J. Biol. Chem.* 280, 6648–6654.

Yang, T. J. W., Lin, W. D., and Schmidt, W. (2010). Transcriptional profiling of the Arabidopsis Iron deficiency response reveals conserved transition metal homeostasis networks. *Plant Physiol.* 152, 2130–2141. doi: 10.1104/pp.109.152728

Yuan, Y., Wu, H., Wang, N., Li, J., Zhao, W., Du, J., et al. (2008). FIT interacts with AtbHLH38 and AtbHLH39 in regulating iron uptake gene expression for iron homeostasis in Arabidopsis. *Cell Res.* 18, 385–397. doi: 10.1038/cr.2008.26

Yuan, Y. X., Zhang, J., Wang, D. W., and Ling, H. Q. (2005). AtbHLH29 of Arabidopsis thaliana is a functional ortholog of tomato FER involved in controlling iron acquisition in strategy I plants. *Cell Res.* 15, 613–621. doi: 10.1038/sj.cr.7290331

Zhu, J., Fu, X., Koo, Y. D., Zhu, J. K., Jenney, F. E. Jr., et al. (2007). An enhancer mutant of Arabidopsis salt overly sensitive 3 mediates both ion homeostasis and the oxidative stress response. *Mol. Cell. Biol.* 27, 5214–5224. doi: 10.1128/MCB.01989-06

Conflict of Interest Statement: The authors declare that the research was conducted in the absence of any commercial or financial relationships that could be construed as a potential conflict of interest.

Received: 29 May 2013; paper pending published: 19 June 2013; accepted: 04 July 2013; published online: 23 July 2013.
*Citation: Rodríguez-Celma J, Pan IC, Li W, Lan P, Buckhout TJ and Schmidt W (2013) The transcriptional response of Arabidopsis leaves to Fe deficiency. Front. Plant Sci. **4**:276. doi: 10.3389/fpls.2013.00276*
This article was submitted to Frontiers in Plant Nutrition, a specialty of Frontiers in Plant Science.

frontiers in
PLANT SCIENCE

REVIEW ARTICLE
published: 25 July 2013
doi: 10.3389/fpls.2013.00254

Iron deficiency in plants: an insight from proteomic approaches

Ana-Flor López-Millán[1]*, Michael A. Grusak[2], Anunciación Abadía[1] and Javier Abadía[1]

[1] Plant Nutrition Department, Aula Dei Experimental Station (CSIC), Zaragoza, Spain
[2] Department of Pediatrics, USDA-ARS Children's Nutrition Research Center, Baylor College of Medicine, Houston, TX, USA

Edited by:
Gianpiero Vigani, Università degli Studi di Milano, Italy

Reviewed by:
Sabine Lüthje, University of Hamburg, Germany
Jesus V. Jorrin Novo, University of Cordoba, Spain

***Correspondence:**
Ana-Flor López-Millán, Plant Nutrition Department, Aula Dei Experimental Station (CSIC), Avenida Montañana 1005, E-50059, Zaragoza, Spain
e-mail: anaflor@eead.csic.es

Iron (Fe) deficiency chlorosis is a major nutritional disorder for crops growing in calcareous soils, and causes decreases in vegetative growth as well as marked yield and quality losses. With the advances in mass spectrometry techniques, a substantial body of knowledge has arisen on the changes in the protein profiles of different plant parts and compartments as a result of Fe deficiency. Changes in the protein profile of thylakoids from several species have been investigated using gel-based two-dimensional electrophoresis approaches, and the same techniques have been used to investigate changes in the root proteome profiles of tomato (*Solanum lycopersicum*), sugar beet (*Beta vulgaris*), cucumber (*Cucumis sativus*), *Medicago truncatula* and a *Prunus* rootstock. High throughput proteomic studies have also been published using Fe-deficient *Arabidopsis thaliana* roots and thylakoids. This review summarizes the major conclusions derived from these "-omic" approaches with respect to metabolic changes occurring with Fe deficiency, and highlights future research directions in this field. A better understanding of the mechanisms involved in root Fe homeostasis from a holistic point of view may strengthen our ability to enhance Fe-deficiency tolerance responses in plants of agronomic interest.

Keywords: iron, metabolism, proteomics, root, thylakoid

INTRODUCTION

Iron (Fe) is the sixth most abundant element in the universe and the fourth most abundant in the earth's crust (Morgan and Anders, 1980). For most living organisms on earth, Fe is an essential element. However, its chemical properties in oxygenated environments limit its availability. As a consequence, Fe deficiency is a widespread phenomenon among the animal and plant kingdoms. According to the WHO, anemia (including Fe-deficiency induced anemia) affects more than 2 billion people worldwide (McLean et al., 2009). In crops, and especially in those grown on calcareous soils, Fe deficiency is a major nutritional disorder that causes decreases in vegetative growth and marked yield and quality losses (Abadía et al., 2011). A substantial body of knowledge has arisen during the genomic era with regard to the molecular aspects of plant Fe acquisition mechanisms that are induced in response to limited Fe availability (Palmer and Guerinot, 2009; Schmidt and Buckhout, 2011; Hindt and Guerinot, 2012). In all plants except grasses, the adaptation mechanism to Fe limitation suggests the need for increased reducing power (NADH) for the root plasma membrane (PM) Fe reductase, and increased energy (ATP) for the PM H^+-ATPase (Römheld and Marschner, 1983). Proteomic approaches are an excellent tool to elucidate the general metabolic reprogramming needed to sustain these requirements. Understanding how plants respond to Fe limitation at the proteomic level provides a new layer of information on Fe homeostasis processes that can ultimately help to reduce the effects of Fe deficiency in crops. This review summarizes, in a comprehensive manner, the major conclusions regarding metabolic adaptations that occur under Fe deficiency conditions in roots and thylakoids of several plant species, and highlights future research directions in the field. Also, the review provides a clear overview on the limitations of the different proteomic techniques available to study a prevalent abiotic stress case in crops.

CHANGES INDUCED BY FE DEFICIENCY IN THE ROOT PROTEOME

When Fe is scarce, Strategy I plants develop morphological and biochemical changes leading to an increase in their Fe acquisition capacity. Morphological changes include swelling of root tips and formation of lateral roots, root hairs, and transfer cells that increase the root's surface area. Biochemical changes result in an increased ability to acquire Fe, and include the induction of a plasma-membrane Fe(III)-reductase and an Fe(II) transporter, an enhanced proton extrusion capacity, and the release of low molecular weight compounds such as carboxylates, flavins and phenolic compounds (Abadía et al., 2011).

The most common approach used to study changes in the root proteome upon Fe starvation has been a gel-based approach, using two-dimensional (2-DE) IEF SDS/PAGE electrophoresis. All of the studies reviewed here have been conducted using root extracts of Strategy I plants, whereas proteomic studies in Strategy II plants have only been conducted in root plasma membrane of maize (Hopff et al., 2013). Small gels (7 cm) were used in studies

involving *Beta vulgaris* (Rellán-Álvarez et al., 2010), *Medicago truncatula* (Rodríguez-Celma et al., 2011a) and *Prunus dulcis* × *Prunus persica* (Rodríguez-Celma et al., 2013a), whereas larger gels were used for *Cucumis sativus* (24 cm, Donnini et al., 2010) and *Solanum lycopersicum* (24 cm in Li et al., 2008 and 13 cm in Brumbarova et al., 2008). When using small gels the average number of proteins detected in root extracts ranged between 140 for *B. vulgaris* to ∼335 for *P. dulcis* × *P. persica* and *M. truncatula*, whereas in larger gels the number of spots ranged from 1400 in *S. lycopersicum* to 2200 in *C. sativus*. Independently of the total number of spots, the number of spots whose relative abundance changed significantly as a result of the different Fe deficiency treatments was within the same range among plant species, with 17, 31, and 61 spots for *P. dulcis* × *P. persica*, *M. truncatula* and *B. vulgaris*, 57 for *C. sativus*, and 41 (Li et al., 2008) and 24 (Brumbarova et al., 2008) for *S. lycopersicum*, respectively. The protein identification rates ranged between 71 and 95%, except for *B. vulgaris* where only 36% of the proteins changing in abundance upon Fe limitation were identified, underlying the importance of using plant species with sufficient genomic information for proteomic studies. In *A. thaliana* root extracts, a high-throughput study of changes induced by Fe limitation was performed using HPLC-MS and iTRAQ (Isobaric Tag for Relative and Absolute Quantification). In this study, 4454 proteins were identified in *A. thaliana* root extracts and 2882 were reliably quantified; from these, a subset of 101 proteins were identified whose abundance changed upon Fe deficiency (Lan et al., 2011). Finally, a phosphoproteomics study with *A. thaliana* found that among 425 phosphorylated proteins, 45 changed in abundance with Fe deficiency (Lan et al., 2012).

The comparison of proteomes from multiple plant species is not straightforward. This is because of difficulties in handling homology between species, in particular when public genomic data sets are not comprehensive, or in some cases are lacking, as it occurs with *B. vulgaris*. Furthermore, the reliability of protein identification using database comparisons always has some uncertainty and clearly depends on the stringency of the criteria selected for positive identification, including number of peptides matched and sequence coverage. In addition, because any given proteomic profile is a snapshot of a dynamic process, differences in plant developmental stage and in the manner Fe limitation is imposed can likely lead to final protein profile pictures that may differ significantly. Also, we should keep in mind that changes in spot intensity can be related to post-translational modifications, adding a new layer of complexity to the interpretation of proteomic studies. As a compromise, we used an approach where identified proteins found to change in each plant species were matched to proteins existing in *A. thaliana*. BLAST searches were run for every protein species found in the different studies and those matches with *E*-values below e^{-30} were retained as positive *Arabidopsis* orthologs; if any of the accession numbers overlapped between two or more entries of the same plant species, they were considered redundant and only a single representative entry was retained (**Table S1**). Also, in an attempt to reduce variability associated with differences in the treatments, the proteomes of *B. vulgaris* and *M. truncatula* plants grown in the absence of Fe, but in the presence of $CaCO_3$, were in principle excluded from the comparison (although data are also provided in **Table S1**).

Based on this approach, 199 non-redundant *Arabidopsis* orthologs were found to change in relative abundance with Fe deficiency: 101, 17, 37, 27, and 32 of them were derived from the *Arabidopsis* (Lan et al., 2011), *M. truncatula*, *S. lycopersicum*, *P. dulcis* × *P. persica*, and *C. sativus* studies, respectively. These non-redundant root proteins and the results from the BLAST searches are listed in **Table S1**. Results showing proteins grouped by function (generally as described by authors, although with some modifications) are summarized in **Figure 1A** and **Table S2** (in the latter case with red and green backgrounds indicating proteins increasing or decreasing in relative abundance, respectively). This comparison did not yield a single specific protein species changing in all plant species as a result of Fe limitation, whereas only 15 proteins did show changes in two or more plant species (**Figure 1B**; **Table S2**). Among them, six were related to stress defense, three were related to C metabolism, and three to N metabolism. The remaining three protein species were a β-xylosidase involved in cell wall modification, the translation initiation factor ELF5A-1, and the chaperone HSP70-1. In spite of the low number of common protein overlaps, changes in metabolic pathways do follow a similar trend. It should be noted that changes in Fe homeostasis and transport proteins upon Fe deficiency were only detected in *Arabidopsis* using HPLC-MS, because most of these proteins are membrane associated and therefore difficult to solubilize and detect with gel-based 2-DE approaches.

COMMON CHANGES AMONG PLANT SPECIES

Oxidative stress and defense

Oxidative stress was the category containing more specific proteins (five) changing as a result of Fe deficiency in more than one plant species. These changes included increases in superoxide dismutases (CuZnSOD and MnSOD), monodehydroascorbate reductase (MDAR1), peroxidase 12 (PER12) and a decrease in catalase (CAT-2) (**Figure 1B**; **Table S2**). These observations point to the strong impact of Fe deficiency on redox homeostasis, not only because free Fe ions induce reactive oxygen species (ROS) formation via Fenton reactions, but also because many proteins involved in oxidative stress such as peroxidases and catalase are Fe-containing proteins. Some of the changes observed, such as the compensatory mechanism of the SOD isoenzymes in *P. dulcis* × *P. persica*, *M. truncatula* and *Arabidopsis*, as well as the decrease in catalase in *S. lycopersicum* and *P. dulcis* × *P. persica*, are likely associated with the decrease in Fe availability. The increases and decreases reported in some of the plant species for the different peroxidase species (i.e., increases in PER12, PER3 and decreases in PER53 and PER21, all of them containing Fe), indicate the complex interplay between Fe and redox homeostasis mechanisms. Increases in MDAR (in *S. lycopersicum* and *Arabidopsis*) and ascorbate peroxidase (APX; in *S. lycopersicum*) also indicate an induction of the glutathione-ascorbate cycle in response to Fe deficiency.

With regard to defense proteins, only GLP5 (Germin-Like-Protein 5) increased in two species, *S. lycopersicum*

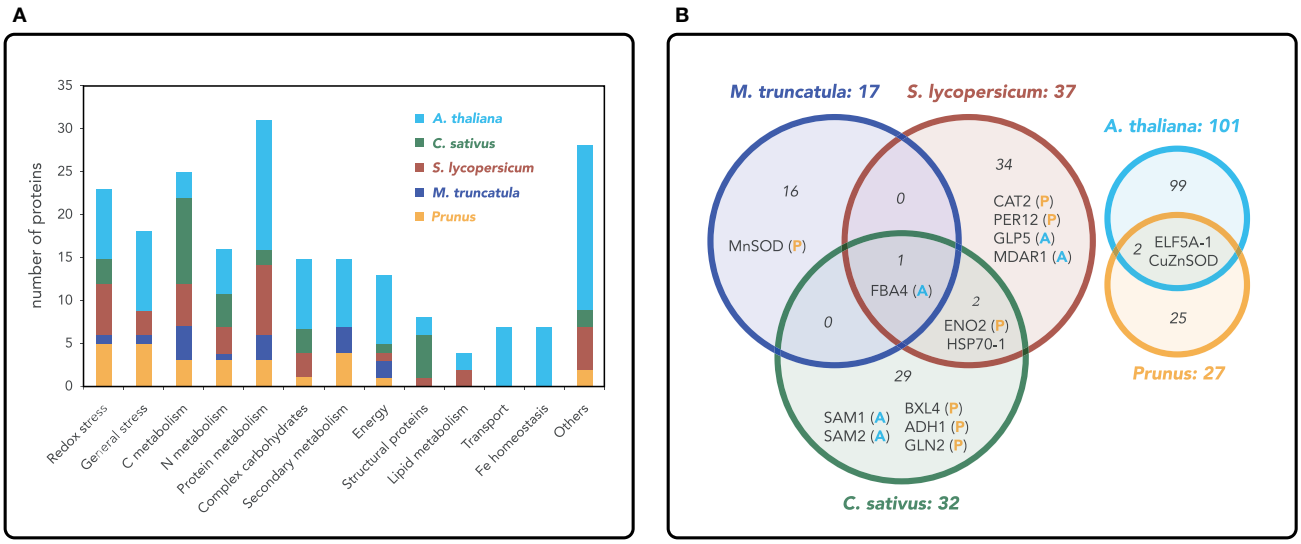

FIGURE 1 | (A) Functional classification of proteins in root extracts that shows changes in relative abundance as a result of Fe deficiency. The number of proteins and functional assignments were obtained from proteomic studies in roots of *Arabidopsis thaliana* (yellow; Lan et al., 2011), *Cucumis sativus* (green; Donnini et al., 2010), *Solanum lycopersicum* (red; Brumbarova et al., 2008; Li et al., 2008), *Medicago truncatula* (blue; Rodríguez-Celma et al., 2011a) and the Prunus rootstock *Prunus dulcis* × *Prunus persica* (orange; Rodríguez-Celma et al., 2013a). **(B)** Proteins with changes in relative abundance as a result of Fe deficiency in two or more plant species are shown in a Venn diagram. Since the comparison of five species in a single Venn diagram was not fully clear, we used two Venn graphs: in the one in the left, a comparison is made between *C. sativus*, *S. lycopersicum*, and *M. truncatula* (letters next to the protein species acronyms indicate whether changes also occur in *A. thaliana* and the Prunus rootstock), whereas the one in the right shows the contrast between *A. thaliana* and the Prunus rootstock. Numbers within the circles indicate the total number of proteins changing in relative abundance as a result of Fe deficiency in each plant species.

and *Arabidopsis* (**Figure 1B**; **Table S2**). This protein is plasmodesmata-localized and it is involved in regulating primary root growth by controlling phloem-mediated allocation of resources between the primary and lateral root meristems (Ham et al., 2012). Six glutathione S transferase (GST) proteins changed as a result of Fe deficiency, although no specific overlaps were observed between plant species. The GSTs decreasing in abundance in *P. dulcis* × *P. persica* (GSTF9 and GSTF4) belong to the phi class, whereas the GSTs increasing in abundance belong to the lambda (GSTL1 in *Arabidopsis* and GSTL3 in *P. dulcis* × *P. persica*) and tau (GSTU19 in *M. truncatula* and GSTU25 in *Arabidopsis*) classes. The phi class has been linked to tolerance to oxidative stress, whereas the lambda family likely has an oxidoreductase activity and the tau subclass of GST binds fatty acid derivatives (Dixon and Edwards, 2010). Even though the specific functions of these GSTs are not well known, these proteomic data suggest that glutathionylation could be a common detoxifying strategy in Fe-deficient roots.

C metabolism

Carbon metabolism, and in particular glycolysis, is the metabolic pathway showing the most consistent changes with Fe deficiency at the proteomic level within all plant species studied (also including those grown in the presence of $CaCO_3$) (**Figure 1B**, **Table S2**). Two or more proteins belonging to this pathway increased in abundance in all plant species, except for *Arabidopsis*, where only one protein increased, a fructose bisphosphate aldolase for which increases were also found in *S. lycopersicum* and *C. sativus* (and also in *M. truncatula* and *B. vulgaris* grown with $CaCO_3$). Enolase also showed a consistent increase in all species (in *M. truncatula* in the presence of $CaCO_3$) except *Arabidopsis*. Furthermore, these two proteins were the only ones increasing with Fe deficiency in three of the five plant species studied, highlighting the fact that the metabolic reprogramming of carbon metabolism that occurs upon Fe deficiency is well conserved among species. Increases in the abundance of enzymes from the TCA cycle with Fe deficiency were found in *C. sativus* and *M. truncatula*, whereas an increase in PEPC was detected in *S. lycopersicum*. These proteomic results are in agreement with transcriptomic and biochemical studies that report increases in glycolysis and TCA cycle enzymes upon Fe limitation (see Zocchi, 2006 for a review). Increases in the activity of these pathways could (1) fulfill the increased demand for reducing power and ATP from the up-regulated Fe acquisition mechanisms, including the PM Fe reductase and ATPase, and (2) account for the increases in carboxylates consistently reported in Fe-deficient roots. These holistic proteomic approaches highlight the importance of general metabolic pathways in the elicitation of the stress response mechanisms. In only one case, a protein of the TCA cycle, aconitase in *C. sativus*, showed a relative decrease in abundance with Fe deficiency. Although aconitase is an Fe containing protein, this decrease has only been reported for *C. sativus*, whereas contrasting changes in aconitase activity as a result of Fe deficiency have been reported in other plant species (Abadía et al., 2002). These apparent inconsistencies with regard to aconitase could be explained by the different ways Fe

treatments were imposed: in the *C. sativus* study, seedlings were always grown in the absence of Fe, whereas in the other studies plants were pre-grown with Fe before imposing the Fe-deficiency treatment.

Two enzymes involved in fermentation, alcohol dehydrogenase in *P. dulcis* × *P. persica* and *C. sativus* and formate dehydrogenase in *S. lycopersicum* (and in *B. vulgaris* grown in the presence of $CaCO_3$) increased in relative abundance in Fe-deficient roots. These results are also in agreement with previous studies, and have been associated with low intracellular O_2 caused by an increased consumption of O_2 in Fe-deficient roots (López-Millán et al., 2000, 2009).

N metabolism

Iron deficiency also has an impact on N metabolism. Three proteins related to N metabolism changed in at least two plant species: glutamine synthetase (GLN2) increased in *P. dulcis* × *P. persica* and *C. sativus*, S-adenosylmethionine synthase 1 (SAM 1) increased in *C. sativus* and *Arabidopsis*, and SAM2 decreased in *C. sativus* and increased in *Arabidopsis* (**Figure 1B**, **Table S2**). In some species, increases were also observed in enzymes involved in ammonia release [urease (UREG) and dihydrolipoamide dehydrogenase (LPD1) in *M. truncatula* and an omega amidase in *C. sativus*], assimilation (GLN1 in *Arabidopsis*, GLN2 in *P. dulcis* × *P. persica* and *C. sativus*) and amino group transfer (alanine aminotransferase in *C. sativus* and aspartate aminotransferase in *M. truncatula* grown with $CaCO_3$). Overall, these changes indicate an increase in N recycling that could help to overcome the reduced N assimilation caused by a decrease in the Fe-containing enzyme nitrite reductase. Decreases in nitrite reductase have been found in *M. truncatula* and *S. lycopersicum* at the protein level and in *C. sativus* at the biochemical level (Borlotti et al., 2012).

Fe deficiency has a conserved impact on SAM metabolism among plant species. Increases in proteins involved in SAM synthesis have been found at the proteomic level in *S. lycopersicum*, *M. truncatula*, *C. sativus* and *Arabidopsis*. Several authors have already pointed out the central role of SAM in the Fe-deficiency response, not only as a methyl group donor but also as a precursor for the synthesis of nicotianamine, an important Fe chelator, and ethylene, a hormone with a role in the regulation of Fe acquisition in roots (Waters et al., 2007; Donnini et al., 2010; Lan et al., 2011).

SPECIES- OR TREATMENT-SPECIFIC CHANGES

Cell wall

A significant number of proteins involved in the metabolism of glycosyl compounds are Fe-responsive in all plant species except in *M. truncatula* (one in *P. dulcis* × *P. persica*, four in *S. lycopersicum*, three in *C. sativus* and eight in *Arabidopsis*), and most of them are localized in the apoplast, suggesting that Fe shortage leads to modifications in cell wall structure and metabolism. Although a more detailed biochemical study is needed to understand these changes, these responses to Fe deficiency seem to be species-specific. In *C. sativus*, decreases were measured for two enzymes involved in the hydrolysis of O-glycosyl compounds (1,4-β-xylosidase and UDP-glucose dehydrogenase) and an invertase, whereas in *P. dulcis* × *P. persica* only 1,4-β-xylosidase was found to decrease. In *Arabidopsis*, in addition to decreases in proteins involved in the transfer of glycosyl groups, lignin catabolism, and hydrolysis, increases were measured in five more proteins: four involved in lignin or cellulose biosynthesis and a β-glucosidase involved in cellulose degradation. A similar situation was observed in *S. lycopersicum,* with two cell wall-related proteins increasing and two decreasing. In the studies with *C. sativus*, the authors explained these changes as a decrease in cell wall biosynthesis that could potentially lead to increased carbon flux toward other metabolic processes such as glycolysis (Donnini et al., 2010); however, the nature of the proteins identified may also reflect hydrolysis of the cell wall as a means to supply carbon skeletons. Irrespective of the specific changes occurring, it can be concluded that cell wall remodeling occurs upon Fe limitation; whereas this may provide carbon for glycolysis or other processes, it is also likely to cause changes in the dynamics of intercellular metabolite trafficking.

Secondary metabolism

An interesting observation highlighted by our comparison relates to the species-specific changes observed in proteins of secondary metabolism. Even though no overlaps were seen among proteins changing in abundance with Fe deficiency in the different plant species, proteins participating in the riboflavin synthesis pathway increased in *M. truncatula* (and in *B. vulgaris* grown in the presence of $CaCO_3$), whereas increases in several proteins involved in the phenylpropanoid pathway were observed in *Arabidopsis* roots and in isoprenoid and flavonoid synthesis in *P. dulcis* × *P. persica*. These proteomic results are in agreement with biochemical and transcriptomic data (Rellán-Álvarez et al., 2010; Lan et al., 2011; Rodríguez-Celma et al., 2011b, 2013b) and suggest that Fe deficiency induces the synthesis of different secondary metabolites in roots whose function in the Fe deficiency response deserves further attention.

Energy and ATP-coupled transport processes

Contrasting results are reported in root proteomes regarding energy-related proteins. In *Arabidopsis*, significant increases in the abundance of proteins participating in the mitochondrial transport chain, including several subunits of complex I, were observed upon Fe deficiency, whereas in *M. truncatula* and *C. sativus*, decreases were found for a subunit of complex I and in subunit B of the mitochondrial ATPase. Also, the abundance of two vacuolar ATPases was decreased in Fe-deficient *Arabidopsis*, whereas a higher abundance was reported for a vacuolar ATPase in Fe-deficient *S. lycopersicum*. The decrease in complex I has been confirmed at the biochemical level also in *C. sativus* (Vigani et al., 2009; Vigani, 2012). These apparent discrepancies could be species-specific or may be explained by the different growing conditions, because *Arabidopsis* was grown in agar under continuous illumination conditions (including the root) that can alter electron transfer reactions.

Protein metabolism

It is more difficult to extract general conclusions about changes in protein metabolism related processes induced by Fe deficiency. In *Arabidopsis*, several translation elongation and initiation factors

increased in abundance upon Fe limitation, and abundance decreases were also found for some ribosomal components (Lan et al., 2011). In *P. dulcis* × *P. persica*, an abundance increase in a translation initiation factor was found, but similar changes were not observed in other species. In two species, *M. truncatula* and *S. lycopersicum*, an increase in proteolysis may take place upon Fe-deficiency based on increases measured in some proteases and in the reorganization of the proteasome machinery. In *C. sativus*, no changes were measured in proteolytic enzymes, but decreases were observed in structural proteins such as actin and globulins. The authors hypothesized that these proteins could be used as a source of C and N during Fe-deficient conditions that cause macronutrient starvation (Donnini et al., 2010).

THE SHOOT PROTEOME

Changes induced by Fe deficiency in the shoot proteome have only been reported for *S. lycopersicum* (Herbik et al., 1996). In that study, although apparent differences were observed in the protein profiles of Fe-sufficient and Fe-deficient leaves, protein identification was not pursued because the aim of the work was to identify differences between a mutant *S. lycopersicum* genotype (chloronerva) and wild type.

THE THYLAKOID PROTEOME

Thylakoid membranes contain the multiprotein photosynthetic complexes photosystems I and II, which include the reaction centers responsible for converting light energy into chemical bond energy, as well as cytochrome b_6/f and ATPase complexes. Fe-deficient plants have a reduced number of granal and stromal lamellae per chloroplast and decreased amounts of many thylakoid membrane components including proteins, electron carriers and lipids and this is consistent with marked decreases in photosynthetic rates (Terry, 1980; Terry and Abadía, 1986; Morales et al., 1990).

Changes induced in the thylakoid proteome by Fe-deficiency have been studied in *B. vulgaris* and *Spinacia oleracea* using 2-DE blue native (BN) SDS/PAGE in combination with mass spectrometry (Andaluz et al., 2006; Timperio et al., 2007) and by HPLC and tandem mass spectrometry in *A. thaliana* (Laganowsky et al., 2009). These studies clearly demonstrate that Fe deficiency causes decreases in the relative amounts of electron transfer proteins, including the core and light harvesting components of the PSI and PSII complexes and in cytochrome b6/f, with the largest decreases seen in PSI. The time course studies performed in *S. oleracea* also indicate that Fe deficiency affects supercomplex organization, by inducing a transient decrease in trimeric and dimeric organization of the light harvesting complex of PSII. These changes might constitute an adaptive strategy to facilitate energy dissipation in Fe-deficient plants (Timperio et al., 2007).

Contrasting results were obtained for ATP synthase, showing no Fe-deficiency induced changes in *B. vulgaris* and *A. thaliana* and decreases in *S. oleracea*. Also, the relative amounts of proteins involved in leaf C fixation, including Rubisco, increased in *B. vulgaris*, whereas Rubisco decreased significantly in *S. oleracea*. These results may be species-specific or more likely are related to plant culture conditions, because *S. oleracea* was grown without Fe from germination, whereas *B. vulgaris* and *Arabidopsis* had a preculture period in the presence of Fe. Other changes observed in proteins present in thylakoid preparations upon Fe limitation included increases in enzymes involved in ROS protection, such as ascorbate peroxidase in *A. thaliana* and SOD in *B. vulgaris*.

The analyses of exact masses of thylakoid membrane proteins in *Arabidopsis* also revealed that several proteins undergo post-translational modifications upon Fe deficiency; for example, the PSII oxygen evolving complex in Fe-deficient *Arabidopsis* thylakoids was found mostly in its doubly phosphorylated form, while in Fe-sufficient samples the non-phosphorylated form was predominant (Laganowsky et al., 2009).

Results provided in these papers underscore that 2-DE BN SDS/PAGE and HPLC-MS are the techniques more suitable for proteomic studies involving membranes, because they allow the resolution of highly hydrophobic integral membrane proteins. However, the use of other approaches such as 2-DE IEF SDS/PAGE also provides useful complementary information about other sets of proteins tightly linked to membranes.

CONCLUSION AND FUTURE PERSPECTIVES

As proteomic and transcriptomic techniques have evolved toward high-throughput methodologies such as iTRAQ or the new Illumina technology, it has become more evident that a strict correlation does not exist between observed changes in protein and gene expression profiles. The comparison between changes in proteomic and transcriptomic profiles was out of the scope of this review; however, we have compared the datasets obtained from *Arabidopsis* Fe-deficient root extracts using iTRAQ and RNA sequencing. This comparison is only possible in *Arabidopsis*, where the genome is available and both studies have been reported; for other plant species, such as *Medicago*, the genome is still not finished and there are no reports of iTRAQ profiles. The total number of *Arabidopsis* transcripts identified was ∼26 K, from which 2679 (10%) were differentially expressed upon Fe deficiency (Rodríguez-Celma et al., 2013b), whereas the total number of proteins identified by iTRAQ was 4454, from which 101 (2%) were differentially accumulated upon Fe deficiency (Lan et al., 2011). Among these, forty-seven protein species (50% of the differentially accumulated proteins) showed changes in both protein accumulation and gene expression (**Table S3**). The results of this comparison indicate that both omic approaches are complementary and that the gap in information between them is not only due to methodological limitations, but also reflects the complex regulation of stress responses such as Fe deficiency.

As shown in this review, proteomics has been a powerful tool in the elucidation of general metabolic rearrangements upon Fe deficiency. Different proteomic approaches have demonstrated that Fe deficiency has a profound impact on C metabolism and on the arrangement of the photosynthetic machinery, with many of these changes conserved amongst plant species. However, species- and treatment-specific changes have also been revealed that deserve further attention. The full potential of proteomic approaches is quite far from being fully exploited and detailed studies on specific changes unveiled with this holistic technique may yield new insights into the adaptation of plants to Fe deficiency. Future directions for proteomic studies should

focus on the analysis of sub-proteomes crucial for Fe homeostasis, such as those of plant fluids, isolated organelles, and purified membrane preparations. Recent examples have been published for plasma membrane (Meisrimler et al., 2011; Hopff et al., 2013) and phloem sap (Lattanzio et al., 2013). These studies will help to elucidate the specific roles subcellular compartments may play in Fe homeostasis, and also will allow the discovery of proteins with new functions in these processes, which might remain hidden using other, less targeted approaches.

ACKNOWLEDGMENTS

The writing of this review was supported in part by the Spanish Ministry of Economy and Competitivity (MINECO; projects AGL2010-16515 and AGL2012-31988, co-financed with FEDER), the Aragón Government (Group A03), and by the US Department of Agriculture, Agricultural Research Service (Agreement number 58-6250-0-008). The contents of this publication do not necessarily reflect the views or policies of the US Department of Agriculture, nor does mention of trade names, commercial products, or organizations imply endorsement by the US Government.

SUPPLEMENTARY MATERIAL

The Supplementary Material for this article can be found online at: http://www.frontiersin.org/Plant_Nutrition/10.3389/fpls.2013.00254/abstract

Table S1 | Tables of BLAST results from proteins identified in roots from *Prunus dulcis* × *Prunus persica* (Rodríguez-Celma et al., 2013a), *Medicago truncatula* (Rodríguez-Celma et al., 2011a), *Beta vulgaris* (Rellán-Álvarez et al., 2010), *Cucumis sativus* (Donnini et al., 2010), and *Solanum lycopersicum* (Herbik et al., 1996; Brumbarova et al., 2008; Li et al., 2008). Spot nomenclature in the first column is that used in the original papers. BLAST searches were performed in the NCBI website (http://blast.ncbi.nlm.nih.gov/Blast.cgi) against the *Arabidopsis* database (taxid:3701) in March 2013. BLAST annotations were assigned as not hit when BLAST E-values were higher than $1e^{-30}$. If any of the accession numbers overlapped between two or more entries of the same plant species, they were considered redundant and only a single representative entry was retained.

Table S2 | Comparison of changes observed upon Fe deficiency in the non-redundant *Arabidopsis* root proteomes obtained from *Arabidopsis thaliana* (Lan et al., 2011) and from BLAST results in *Cucumis sativus, Solanum lycopersicum, Medicago truncatula* and *Prunus dulcis* × *Prunus persica*. Red and green backgrounds indicate increases and decreases, respectively, in protein abundance upon Fe deficiency. A blue background in the first column marks proteins showing changes in two or more plant species (not considering the *M. truncatula* and *B. vulgaris* treatments including $CaCO_3$, which are included in the Table in the last two columns in white characters).

Table S3 | List of *Aradidopsis thaliana* gene identifiers showing changes in both protein accumulation (Lan et al., 2011) and gene expression (Rodríguez-Celma et al., 2013b).

REFERENCES

Abadía, J., López-Millán, A. F., Rombolà, A., and Abadía, A. (2002). Organic acids and Fe deficiency: a review. *Plant Soil* 241, 75–86. doi: 10.1023/A:1016093317898

Abadía, J., Vázquez, S., Rellán-Álvarez, R., El-Jendoubi, H., Abadía, A., Álvarez-Fernández, A., et al. (2011). Towards a knowledge-based correction of iron chlorosis. *Plant Physiol. Biochem.* 49, 471–482. doi: 10.1016/j.plaphy.2011.01.026

Andaluz, S., López-Millán, A. F., De las Rivas, J., Aro, E. M., Abadía, J., and Abadía, A. (2006). Proteomic profiles of thylakoid membranes and changes in response to iron deficiency. *Photosynth. Res.* 89, 141–155. doi: 10.1007/s11120-006-9092-6

Borlotti, A., Vigani, G., and Zocchi, G. (2012). Iron deficiency affects nitrogen metabolism in cucumber (*Cucumis sativus* L.) plants. *BMC Plant Biol.* 12:189. doi: 10.1186/1471-2229-12-189

Brumbarova, T., Matros, A., Mock, H. P., and Bauer, P. (2008). A proteomic study showing differential regulation of stress, redox regulation and peroxidase proteins by iron supply and the transcription factor FER. *Plant J.* 54, 321–334. doi: 10.1111/j.1365-313X.2008.03421.x

Dixon, D. P., and Edwards, R. (2010). *Glutathione Transferases. Arabidopsis Book* 8:e0131. doi: 10.1199/tab.0131

Donnini, S., Prinsi, B., Negri, A. S., Vigani, G., Espen, L., and Zocchi, G. (2010). Proteomic characterization of iron deficiency responses in *Cucumis sativus* L. roots. *BMC Plant Biol.* 10:268. doi: 10.1186/1471-2229-10-268

Ham, B. K., Li, G., Kang, B. H., Zeng, F., and Lucas, W. J. (2012). Overexpression of Arabidopsis plasmodesmata germin-like proteins disrupts root growth and development. *Plant Cell* 24, 3630–3648. doi: 10.1105/tpc.112.101063

Herbik, A., Giritch, A., Horstmann, C., Becker, R., Balzer, H. J., Baumlein, H., et al. (1996). Iron and copper nutrition-dependent changes in protein expression in a tomato wild type and the nicotianamine-free mutant chloronerva. *Plant Physiol.* 111, 533–540. doi: 10.1104/pp.111.2.533

Hindt, M. N., and Guerinot, M. L. (2012). Getting a sense for signals: regulation of the plant iron deficiency response. *Biochim. Biophys. Acta* 1823, 1521–1530. doi: 10.1016/j.bbamcr.2012.03.010

Hopff, D., Wienkoop, S., and Lüthje, S. (2013). The plasma membrane proteome of maize roots grown under low and high iron conditions. *J. Proteomics* doi: 10.1016/j.jprot.2013.01.006. [Epub ahead of print].

Laganowsky, A., Gomez, S. M., Whitelegge, J. P., and Nishio, J. N. (2009). Hydroponics on a chip: analysis of the Fe deficient Arabidopsis thylakoid membrane proteome. *J. Proteomics* 72, 397–415. doi: 10.1016/j.jprot.2009.01.024

Lan, P., Li, W., Wen, T. N., and Schmidt, W. (2012). Quantitative phosphoproteome profiling of iron-deficient Arabidopsis roots. *Plant Physiol.* 159, 403–417. doi: 10.1104/pp.112.193987

Lan, P., Li, W., Wen, T. N., Shiau, J. Y., Wu, Y. C., Lin, W., et al. (2011). iTRAQ protein profile analysis of Arabidopsis roots reveals new aspects critical for iron homeostasis. *Plant Physiol.* 155, 821–834. doi: 10.1104/pp.110.169508

Lattanzio, G., Andaluz, S., Matros, A., Calvete, J. J., Kehr, J., Abadía, A., et al. (2013). Protein profile of *Lupinus texensis* phloem sap exudates: searching for Fe and Zn containing proteins. *Proteomics* doi: 10.1002/pmic.201200515. [Epub ahead of print].

Li, J., Wu, X. D., Hao, S. T., Wang, X. J., and Ling, H. Q. (2008). Proteomic response to iron deficiency in tomato root. *Proteomics* 8, 2299–2311. doi: 10.1002/pmic.200700942

López-Millán, A. F., Morales, F., Andaluz, S., Gogorcena, Y., Abadía, A., De Las Rivas, J., et al. (2000). Responses of sugar beet roots to iron deficiency. Changes in carbon assimilation and oxygen use. *Plant Physiol.* 124, 885–898. doi: 10.1104/pp.124.2.885

López-Millán, A. F., Morales, F., Gogorcena, Y., Abadía, A., and Abadía, J. (2009). Metabolic responses in iron deficient tomato plants. *J. Plant Physiol.* 166, 375–384. doi: 10.1016/j.jplph.2008.06.011

McLean, E., Cogswell, M., Egli, I., Wojdyla, D., and de Benoist, B. (2009). Worldwide prevalence of anaemia, WHO vitamin and mineral nutrition information system, 1993-2005. *Public Health Nutr.* 12, 444–454. doi: 10.1017/S1368980008002401

Meisrimler, C. N., Planchon, S., Renaut, J., Sergeant, K., and Lüthje, S. (2011). Alteration of plasma membrane-bound redox systems of iron deficient pea roots by chitosan. *J. Proteomics* 74, 1437–1449. doi: 10.1016/j.jprot.2011.01.012

Morales, F., Abadía, A., and Abadía, J. (1990). Characterization of the xanthophyll cycle and other

photosynthetic pigment changes induced by iron deficiency in sugar beet (*Beta vulgaris* L.). *Plant Physiol.* 94, 607–613. doi: 10.1104/pp.94.2.607

Morgan, J. W., and Anders, E. (1980). Chemical composition of Earth, Venus, and Mercury. *Proc. Natl. Acad. Sci. U.S.A.* 77, 6973–6977. doi: 10.1073/pnas.77.12.6973

Palmer, C. M., and Guerinot, M. L. (2009). Facing the challenges of Cu, Fe and Zn homeostasis in plants. *Nat. Chem. Biol.* 5, 333–340. doi: 10.1038/nchembio.166

Rellán-Álvarez, R., Andaluz, S., Rodríguez-Celma, J., Wohlgemuth, G., Zocchi, G., Álvarez-Fernández, A., et al. (2010). Changes in the proteomic and metabolic profiles of *Beta vulgaris* root tips in response to iron deficiency and resupply. *BMC Plant Biol.* 10:120. doi: 10.1186/1471-2229-10-120

Rodríguez-Celma, J., Lattanzio, G., Grusak, M. A., Abadía, A., Abadía, J., and López-Millán, A. F. (2011a). Root responses of Medicago truncatula plants grown in two different iron deficiency conditions: changes in root protein profile and riboflavin biosynthesis. *J. Proteome Res.* 10, 2590–2601. doi: 10.1021/pr2000623

Rodríguez-Celma, J., Vázquez-Reina, S., Orduna, J., Abadía, A., Abadía, J., Álvarez-Fernández, A., et al. (2011b). Characterization of flavins in roots of Fe-deficient strategy I plants, with a focus on Medicago truncatula. *Plant Cell Physiol.* 52, 2173–2189. doi: 10.1093/pcp/pcr149

Rodríguez-Celma, J., Lattanzio, G., Jiménez, S., Briat, J. F., Abadía, J., Abadía, A., et al. (2013a). Changes induced by Fe deficiency and Fe resupply in the root protein profile of a peach-almond hybrid rootstock. *J. Proteome Res.* 12, 1162–1172. doi: 10.1021/pr300763c

Rodríguez-Celma, J., Lin, W.-D., Fu, G.-M., Abadía, J., López-Míllán, A.-F., and Schmidt, W. (2013b). Mutually exclusive alterations in secondary metabolism are critical for the uptake of insoluble iron compounds by Arabidopsis and Medicago truncatula. *Plant Physiol.* 162, 1473–1485. doi: 10.1104/pp.113.220426

Römheld, V., and Marschner, H. (1983). Mechanism of iron uptake by peanut plants: I. Fe reduction, chelate splitting, and release of phenolics. *Plant Physiol.* 71, 949–954. doi: 10.1104/pp.71.4.949

Schmidt, W., and Buckhout, T. J. (2011). A hitchhiker's guide to the Arabidopsis ferrome. *Plant Physiol. Biochem.* 49, 462–470. doi: 10.1016/j.plaphy.2010.12.001

Terry, N. (1980). Limiting factors in photosynthesis. I. Use of iron stress to control photochemical capacity *in vivo*. *Plant Physiol.* 65, 114–120. doi: 10.1104/pp.65.1.114

Terry, N., and Abadía, J. (1986). Function of iron in chloroplast. *J. Plant Nutr.* 9, 609–646. doi: 10.1080/01904168609363470

Timperio, A. M., D'Amici, G. M., Barta, C., Loreto, F., and Zolla, L. (2007). Proteomics, pigment composition, and organization of thylakoid membranes in iron-deficient spinach leaves. *J. Exp. Bot.* 58, 3695–3710.

Vigani, G. (2012). Discovering the role of mitochondria in the iron deficiency-induced metabolic responses of plants. *J. Plant Physiol.* 169, 1–11. doi: 10.1016/j.jplph.2011.09.008

Vigani, G., Maffi, D., and Zocchi, G. (2009). Iron availability affects the function of mitochondria in cucumber roots. *New Phytol.* 182, 127–136. doi: 10.1111/j.1469-8137.2008.02747.x

Waters, B. M., Lucena, C., Romera, F. J., Jester, G. G., Wynn, A. N., Rojas, C. L., et al. (2007). Ethylene involvement in the regulation of the H(+)-ATPase CsHA1 gene and of the new isolated ferric reductase CsFRO1 and iron transporter CsIRT1 genes in cucumber plants. *Plant Physiol. Biochem.* 45, 293–301. doi: 10.1016/j.plaphy.2007.03.011

Zocchi, G. (2006). "Metabolic changes in iron-stressed dicotyledoneus plants," in *Iron Nutrition in Plants and Rhizospheric Microorganisms*, eds L. L. Barton and J., Abadía (Dordrecht: Springer), 359–370.

Conflict of Interest Statement: The authors declare that the research was conducted in the absence of any commercial or financial relationships that could be construed as a potential conflict of interest.

Received: 24 April 2013; accepted: 23 June 2013; published online: 25 July 2013.

*Citation: López-Millán A-F, Grusak MA, Abadía A and Abadía J (2013) Iron deficiency in plants: an insight from proteomic approaches. Front. Plant Sci. **4**:254. doi: 10.3389/fpls.2013.00254*

This article was submitted to Frontiers in Plant Nutrition, a specialty of Frontiers in Plant Science.

frontiers in
PLANT SCIENCE

ORIGINAL RESEARCH ARTICLE
published: 28 August 2013
doi: 10.3389/fpls.2013.00331

A small-scale proteomic approach reveals a survival strategy, including a reduction in alkaloid biosynthesis, in *Hyoscyamus albus* roots subjected to iron deficiency

Jebunnahar Khandakar[1], Izumi Haraguchi[2], Kenichi Yamaguchi[1,2,3] and Yoshie Kitamura[1,2]*

[1] Graduate School of Science and Technology, Nagasaki University, Nagasaki, Japan
[2] Graduate School of Fisheries Science and Environmental Studies, Nagasaki University, Nagasaki, Japan
[3] Division of Biochemistry, Faculty of Fisheries, Nagasaki University, Nagasaki, Japan

Edited by:
Gianpiero Vigani, Università degli Studi di Milano, Italy

Reviewed by:
Ana-Flor Lopez-Millan, Consejo Superior de Investigaciones Científicas, Spain
Silvia Donnini, Università degli Studi di Milano, Italy

***Correspondence:**
Yoshie Kitamura, Laboratory of Environmental and Functional Botany, Graduate School of Fisheries Science and Environmental Studies, Nagasaki University, 1-14 Bunkyo-machi, Nagasaki 852-8521, Japan
e-mail: k-yoshie@nagasaki-u.ac.jp

Hyoscyamus albus is a well-known source of the tropane alkaloids, hyoscyamine and scopolamine, which are biosynthesized in the roots. To assess the major biochemical adaptations that occur in the roots of this plant in response to iron deficiency, we used a small-scale proteomic approach in which 100 mg of root tips were treated with and without Fe, respectively, for 5 days. Two-dimensional mini gels showed that 48 spots were differentially accumulated between the two conditions of Fe availability and a further 36 proteins were identified from these spots using MALDI-QIT-TOF mass spectrometry. The proteins that showed elevated levels in the roots lacking Fe were found to be associated variously with carbohydrate metabolism, cell differentiation, secondary metabolism, and oxidative defense. Most of the proteins involved in carbohydrate metabolism were increased in abundance, but mitochondrial NAD-dependent malate dehydrogenase was decreased, possibly resulting in malate secretion. Otherwise, all the proteins showing diminished levels in the roots were identified as either Fe-containing or ATP-requiring. For example, a significant decrease was observed in the levels of hyoscyamine 6β-hydroxylase (H6H), which requires Fe and is involved in the conversion of hyoscyamine to scopolamine. To investigate the effects of Fe deficiency on alkaloid biosynthesis, gene expression studies were undertaken both for H6H and for another Fe-dependent protein, Cyp80F1, which is involved in the final stage of hyoscyamine biosynthesis. In addition, tropane alkaloid contents were determined. Reduced gene expression was observed in the case of both of these proteins and was accompanied by a decrease in the content of both hyoscyamine and scopolamine. Finally, we have discussed energetic and Fe-conservation strategies that might be adopted by the roots of *H. albus* to maintain iron homeostasis under Fe-limiting conditions.

Keywords: *Hyoscyamus albus*, roots, Fe deficiency, small-scale proteomics, hyoscyamine 6β-hydroxylase, tropane alkaloid biosynthesis, malic acid secretion

INTRODUCTION

The tropane alkaloids, hyoscyamine and scopolamine, are secondary metabolites produced by some members of the Solanaceae family, such as *Atropa*, *Datura*, *Duboisia,* and *Hyoscyamus*. These alkaloids have anticholinergic effects and, therefore, atropine (*dl*-hyoscyamine) and scopolamine are used as mydriatics and analgesics, respectively (Evans, 1996). Tropane alkaloid biosynthesis has been intensively studied, and it is well known that these compounds are biosynthesized in the roots and then transported to the aerial parts of the plant (Manske and Holmes, 1965). Biosynthesis begins with the conversion of putrescine to *N*-methylputrescine, catalyzed by putrescine *N*-methyltransferase (Walton et al., 1994; Biastoff et al., 2009) and ultimately leads to the end-product, scopolamine, which is generated from hyoscyamine by the bi-functional enzyme, hyoscyamine 6β-hydroxylase (H6H) (Hashimoto et al., 1993). The important step to produce hyoscyamine from littorine, *via* a molecular rearrangement catalyzed by a cytochrome P450 enzyme (Cyp80F1) (Li et al., 2006) has recently been investigated at the gene-expression level. Since tropane alkaloids are commercially important plant-derived drugs, manipulation of their biotechnological production using hairy-root cultures or by metabolic engineering has been actively investigated (Zeef et al., 2000; Rahman et al., 2006; Wilhelmson et al., 2006; Zhang et al., 2007). Nevertheless, many important aspects of their biosynthesis, especially in relation to developmental and environmental factors, remain poorly understood.

Iron (Fe) availability is one of the major nutrient constraints for plant growth and development, especially in neutral and alkaline soils, owing to the low solubility of Fe (Lindsay and Schwab, 1982). Insufficient levels of Fe induce a range of morphological and metabolic changes required to withstand the resultant stress and to maintain Fe homeostasis (Thimm et al., 2001; Zaharieva et al., 2004). Higher plants take up Fe through their roots, so that Fe deficiency initially and most directly affects the roots; and therefore survival under Fe deficiency depends

upon the root system, although aerial parts also suffer from serious damage (Rodríguez-Celma et al., 2013a). Using a hairy-root culture system of *H. albus*, we have found that cultured roots are able to grow under Fe deficiency, although the roots show morphological changes, such as shorter, swollen root tips, that have been observed also in the roots of other plants (Rodríguez-Celma et al., 2011a). Interestingly, *H. albus* roots secrete flavin (riboflavin) into the rhizosphere under these conditions (Higa et al., 2008, 2010), in the same way as other, taxonomically unrelated, dicotyledonous plants, including *Beta vulgaris* (Susin et al., 1994), *Medicago truncatula* (Rodríguez-Celma et al., 2011a,b), *Cucumis sativus* (Shinmachi et al., 1997) and *Helianthus annuus* (Raju and Marschner, 1973).

In order to address the range of metabolic and respiratory adaptations of *H. albus* hairy roots to Fe deficiency, we have initially investigated the characteristics of mitochondrial respiration in these roots, and especially their electron transport chains (ETC) (Higa et al., 2010). The plant mtETC consists of complex I to complex IV, which are components found in all organisms (Dudkina et al., 2006), in addition to a plant-specific alternative oxidase (AOX) and NAD(P)H dehydrogenases (ADX). During electron transport from complex I to complex IV, proton gradients are generated, resulting in the synthesis of ATP, the universal energy currency, through the action of ATP synthase (complex V). Our feeding experiments with respiratory-component-specific inhibitors have indicated that the mtETC changes in response to Fe deficiency (Higa et al., 2010): under these conditions, electrons mainly flow through the alternative dehydrogenase (ADX) to complexes III and IV, whereas both complexes I and II and the AOX are less active. It is noteworthy that complexes I and II contain a large number of Fe ions, whilst AOX does not contribute to the generation of a proton gradient (Ohnishi, 1998; Taiz and Zeiger, 2002; Vigani et al., 2009). On this basis, we have proposed that riboflavin secretion occurs as a result of the underuse of flavoprotein complexes I and/or II (Higa et al., 2010), although both increased *de novo* riboflavin synthesis and hydrolysis of FMN could be involved in riboflavin secretion (Higa et al., 2012). On the other hand, it has been proposed that flavins accumulated in the roots may act as electron donors or as cofactors for Fe (III) reductase (López-Millán et al., 2000; Rodríguez-Celma et al., 2011a,b), because the Fe reductase contains FAD as a cofactor (Schagerlöf et al., 2006). Very recently, Rodríguez-Celma et al. (2013b) proposed a hypothesis that flavins function as Fe-binding compounds in the utilization from usually unavailable Fe pools. In spite of several possible hypotheses including those mentioned above, the actual cause and function of secreted/accumulated flavins under Fe deficiency remain uncertain.

As outlined above, our results have indicated that the mtETC machinery undergoes a shift to a less Fe-dependent mode under Fe-deficient conditions. We contend that this adaptation is likely to be a more extensive phenomenon involving wide-ranging adaptations at the cellular and tissue levels. To explore this idea, we decided to undertake a global protein expression survey using a proteomic approach. Proteomics has become a powerful tool to study many aspects of plant biology, including Fe-deficiency stress (López-Millán et al., 2013). Both in model plants such as *Arabidopsis* (Lan et al., 2011) and *Medicago* (Rodríguez-Celma et al., 2011a), and in crop plants such as *B. vulgaris* (Rellán-Alvarez et al., 2010), *C. sativus* (Donnini et al., 2010), *Prunus* hybrid (Rodríguez-Celma et al., 2013a), and *Lycopersicum esculentum* (Brumbarova et al., 2008; Li et al., 2008), adaptations to Fe deficiency have been examined by a proteomic approach. However, there have been very few investigations reported with medicinal plants, many of which are technically less amenable to study (Aghaei and Komatsu, 2013). Furthermore, most studies have used medium- or large-scale extractions and required large amounts of sample, which are often unavailable for less amenable plant species, or when very detailed, organ- or tissue-specific analyses need to be made. We faced precisely these difficulties in undertaking the proteomic analysis of cultured root tips of *H. albus*; the amount of tissue available was very small and no proteomic analyses had been reported for any *Hyoscyamus* spp. Here we report the application of a small-scale proteomics for comparison of protein profiles from *H. albus* root tips subjected to two different Fe statuses.

MATERIALS AND METHODS

ROOT CULTURE AND SAMPLE COLLECTION

Hairy roots of *Hyoscyamus albus* L. (Solanaceae) used in these experiments had been established previously (Higa et al., 2008). Roots were maintained on MS basal liquid medium (Murashige and Skoog, 1962) containing 3% sucrose. A primary root tip with a few lateral roots (*ca*. 2 cm in length) isolated from ca. 2-week-old root cultures was pre-propagated in the normal liquid B5 medium (Gamborg et al., 1968), containing 1% sucrose, for 2 weeks. After pre-propagation, root cultures were separated into sub-sets by exchanging the medium for fresh B5 medium containing 1% sucrose, either with Fe or without Fe; culture was then continued for 5 days. Fe deficiency stress was imposed by the elimination of Fe(III)-EDTA (100 μM in the final concentration) from B5 basal medium, prior to autoclaving at 121°C for 15 min. All cultures were performed in 100 mL conical flasks containing 25 mL of liquid medium and incubated at 25°C with agitation at 80 rpm on a rotary shaker (SHK-420N Iwaki, Tokyo, Japan) under the sterile conditions until harvest. For protein and transcript analyses, root tips were harvested at day 5, frozen in liquid nitrogen and stored at −80°C until further use. In the case of alkaloid analysis, the roots cultured ±Fe for 5 days were harvested by vacuum filtration. The root tips were then excised and the tips and the remaining parts of the roots were separated and each dried to constant weight at 50°C, before being ground to a powder using a mortar and pestle. The culture medium was also collected for 5 days and analyzed for organic acids. All analyses were carried out by HPLC using three biological replicates (more details were in Alkaloid Extraction and Analysis and Organic acid Analysis).

PROTEIN EXTRACTION

Protein was extracted from root tips using bead-beating, followed by acid guanidinium-phenol-chloroform treatment (the optimization of this protocol to *H. albus* roots and its effectiveness will be reported elsewhere). A 100 mg (fresh weight) of frozen root tips, together with 20% w/w dithiothreitol (DTT, Bio-Rad, Hercules, CA, USA) and 10% w/w polyvinylpolypyrrolidone (PVPP, Sigma-Aldrich, St. Louis, MO, USA), and one

stainless-steel bead crusher (SK-100-D10, Tokken, Inc., Chiba, Japan) were placed in the 2-mL stainless-steel tube (Tokken, Inc., Chiba, Japan). The tubes were then mounted in the Master Rack aluminum block (BMS, Tokyo, Japan) under liquid nitrogen and agitated for 1 min in the ShakeMaster Auto ver 1.5 (BMS, Tokyo, Japan). To the tube, 1 mL of TRIzol reagent (Invitrogen, Boston, MA, USA) was added and protein extraction was performed in accordance with manufacturer's instructions. The resulting pellet was then incubated with 1 mL ethanol for 20 min at room temperature, the solution was centrifuged (7500 × *g*, 5 min, at 4°C), and the pellets were dried for 5–10 min on the bench with the centrifuge tube lids open. To each pellet, 100 μL of resuspension solution (8 M urea, 50 mM DTT, 2% w/v CHAPS, 0.2% v/v carrier ampholyte, 0.001% w/v bromophenol blue) was added; then the mixture was homogenized with a plastic pestle, and sonicated for 1 min (10 s × 6; output level 4) in the ice-cold cup of a horn-type sonicator (Astrason Ultrasonic Processor XL2020, Misonix, NY, USA) and finally incubated for 1 h at room temperature. Protein concentration in the solution was determined by a modified Bradford assay (Quick Start® Protein Assay Kit, Bio-Rad), using bovine serum albumin (BSA) as a standard.

2-D GEL ELECTROPHORESIS

The first dimensional iso-electrofocusing (IEF) separation was carried out using 7-cm ReadyStrip® IPG Strips (linear pH gradient, pH 5–8, Bio-Rad) using a Protean® IEF Cell (Bio-Rad,). The IPG strips were passively rehydrated for 12 h at 20°C in 125 μL of resuspension solution (8 M urea, 50 mM DTT, 2% w/v CHAPS, 0.2% v/v carrier ampholyte, 0.001% w/v bromophenol blue), containing protein sample (20 μg/strip). IEF was carried out at 20°C, for a total of 20,000 Vh (15 min with a 0–250 V linear gradient; 2 h with a 250–4000 V linear gradient; and finally 4000 V, held constant until 20,000 Vh had been reached). After IEF, proteins in the strips were reduced and alkylated by gentle stirring for 10 min in equilibration buffer (6 M urea, 0.375 M Tris-HCl, pH 8.8, 2% w/v SDS, 20% v/v glycerol), supplemented with 2% w/v DTT, and for an additional 10 min in the same equilibration buffer supplemented with 2.5% w/v iodoacetamide. The second dimensional electrophoresis was performed with the Mini-PROTEAN Tetra® electrophoresis cell (Bio-Rad, Hercules, CA, USA). The equilibrated IPG strips were placed on top of Mini-Protean TGX® precast gels (AnykD IPG/Prep®, Bio-Rad), sealed with ReadyPrep® overlay agarose (Bio-Rad) and electrophoresed at 200 V in 25 mM Tris base, 192 mM glycine and 0.1% w/v SDS, for *ca.* 30 min at room temperature. Gels were stained with Flamingo® fluorescent stain (Bio-Rad) and the gel images for figure presentation were captured using a GELSCAN® laser scanner (iMeasure, Nagano, Japan).

IMAGE ANALYSIS, SPOT DETECTION AND STATISTICAL ANALYSIS

For 2-DE pattern analyses, four biological replicates for each condition and four technical replicates for each protein sample were compared between Fe-replete and Fe-deficient conditions. Differences in spot abundance were statistically evaluated by ANOVA ($p < 0.05$) after normalization, using the Prodigy SameSpots® software package (Non-linear Dynamics, Newcasle, UK). A criterion of an abundance ratio (≥1.5-fold) was used to define significant differences.

PROTEIN IN-GEL DIGESTION AND MALDI-QIT-TOF/MS ANALYSIS

Protein spots were manually excised from 2D-gels using a spot image analyzer (FluoroPhoreStar 3000®, Anatech, Tokyo, Japan) equipped with a gel picker (1.8-mm diameter). In-gel tryptic digestion and peptide extraction were carried out as previously described by Yamaguchi (2011). The dried samples were dissolved in 2 μL of DHBA solution (5 mg mL^{-1} of 2, 5-dihydroxybenzoic acid, in 33% v/v acetonitrile and 0.1% v/v trifluoroacetic acid), and 1 μL samples of the solutions were spotted onto a stainless 384-well MALDI target plate (Shimadzu GLC, Tokyo, Japan). For peptides obtained from faint spots, the dried sample was dissolved in 2 μL of 1 10^{-1} diluted DHBA solution, and 1 μL of the solution was spotted onto a μFocus MALDI target plate (Hudson Surface Technology, NJ, USA). MS and MS/MS spectra were obtained using a MALDI-QIT-TOF mass spectrometer (AXIMA Resonance, Shimadzu, Kyoto, Japan) in the positive mode. All the spectra were externally calibrated using human angiotensin II (m/z: 1046.54) and human ACTH fragment 18–39 (m/z: 2465.20) in a ProteoMass® Peptide and Protein MALDI-MS Calibration Kit (Sigma-Aldrich, St. Louis, MO, USA). MS/MS ion searches were performed using MASCOT® version 2.3 (Matrix Science, London, UK) against SwissProt 2012_06 (536,489 sequences; 190,389,898 residues), EST_Solanaceae 2012_04 (2,984,694 sequences; 560,101,884 residues) and NCBInr 20130614 (26236801 sequences; 9088244489 residues) in our own MASCOT server. Search parameters used were: enzyme, trypsin; fixed modifications, carbamidomethyl (Cys); variable modifications, oxidation (H, W, and M); mass values, monoisotopic; peptide mass tolerance, ± 0.5 Da; fragment mass tolerance, ± 0.5 Da, max missed cleavage, 1. Positive identification was assigned with Mascot scores above the threshold level ($p < 0.05$), at least two peptide (protein score > 44) or single peptide (peptide score > 47), 2% sequence coverage, and similar theoretical and observed mass and *pI* values. In the case of single peptide identification, annotated MS/MS spectra of Mascot search results (peptide view) were shown in Supplemental data 2.

DETERMINATION OF *PI*, MW AND SUBCELLULAR LOCALIZATION

Theoretical isoelectric points (*pI*) and sequence mass of the precursor protein were calculated using ProtParam (http://www.expasy.ch/tools/protparam.html). Observed *pI* was calculated from the horizontal migration of the spot. Observed mass was estimated from the vertical migration of the spot, according to Weber and Osborn (1969). Subcellular location of proteins was predicted by WoLF-PSORT (http://wolfpsort.org/), if it has not been reported.

RNA EXTRACTION AND SEMI-QUANTITATIVE RT-PCR

Total RNA was isolated from frozen roots of *H. albus* (100 mg) using an RNeasy® Plant Mini Kit (Qiagen, Tokyo, Japan) and following the manufacturer's instructions. The concentrations of RNAs were determined using a NanoDrop ND-1000 spectrometer (NanoDrop Technologies, DE, USA). For the analysis of the expression of genes involved in tropane alkaloid biosynthesis, we

focused on the genes encoding the enzymes H6H and Cyp80F1. Primers for *H6H* were designed by the alignment of conserved cDNA sequences of *H. niger* and other tropane alkaloid-producing plants, previously deposited in the database (GenBank accessions, M62719 and EU530633). In the case of Cyp80F1, primer pairs were used, according to the previous report (Li et al., 2006). The expression of *riboflavin synthase* (*RibD*) was also determined as a representative gene involved in riboflavin biosynthesis, according to our previous report (GenBank accession, AB712370) (Higa et al., 2012). Primers used were as follows: *H6H*, forward (5′-GGTCTCTTTCAGGTGATCAA-3′) and reverse (5′-CTTCACAGATGTAGTCCAGCA-3′); *Cyp80F1*, forward (5′-CACAGTTGAATGGACATTGGTGGAGC-3′) and reverse (5′-GAACAGTAATGGCGCCGGAGGATGC-3′); *RibD*, forward (5′-GTTGTCGGAATTTAGTGTCGG-3′) and reverse (5′-TCCCAGTCTTGACCTTCACC-3′). The universal primer pairs for 18S ribosomal RNA were used as a control for semi-quantification, according to the manufacture's recommendations (Applied Biosystems, CA, USA). RT-PCR was performed using an mRNA-selective PCR kit (Takara Bio, Shiga, Japan) with the primers mentioned above. A sample aliquot containing 1.0 μg RNA for both *H6H* and *Cyp80F1* or 0.5 μg RNA for *RibD* was subjected to reverse transcription (25 min for *H6H* and *Cyp80F1*; 30 min for *RibD*, at 45°C). The PCR conditions were, as follows: 1 min at 85°C, 1 min at 45°C, 1 min at 72°C, 23 cycles for *H6H* and *Cyp80F1*; 1 min at 85°C, 1 min at 47°C, 1 min at 72°C, 21 cycles for *RibD*. RT-PCR products were loaded onto 3% (w/v) agarose gels and stained with ethidium bromide. A 100-bp DNA ladder (Takara) was used as a molecular marker. Pictures were taken with a gray-scale digital camera (CFW-1310M, Scion Corp., MD, USA) and band intensities were measured using Image J software (NIH, MD, USA).

ALKALOID EXTRACTION AND ANALYSIS

Alkaloids were extracted from dried root tissues (*ca*. 50 mg) according to the reported method (Sauerwein and Shimomura, 1991). Alkaloid analysis was performed by HPLC as described in a previous report (Hank et al., 2004), with some modifications. We added 5 mM homatropine (60 μL) to extracts at the initial stage, as an internal standard, and the MeOH extracts (20 μL) were applied to an HPLC system (Shimadzu LC-10, Kyoto, Japan) fitted with a Wakosil-II 5C8 RS column (4.6 × 150 mm, Wako Corporation, Osaka, Japan). The eluent conditions were as follows: flow rate, 1 mL min^{-1}; column temp, 40°C; solvent A; 30 mM phosphate buffer (pH 6.2), containing 0.1% triethylamine, and MeOH 75/10 (v/v); solvent B, CH_3CN; isocratic elution, with A: B = 80: 20. Alkaloids were detected at 210 nm with a UV detector (Shimadzu SPD-10AVP) and a photodiode array (Shimadzu SPD-M20A). Quantification was based on standard curves using the reference standard and the internal standard.

ORGANIC ACID ANALYSIS

Organic acids in the culture medium, including malic acid and citric acid, were measured by HPLC (Intelligent HPLC system, Jasco, Tokyo, Japan), according to the reported method (Nisperos-Carriedo et al., 1992). Before applying, insoluble particles in the culture medium were removed with 0.2 μm membrane filters (Millex-LG, Merck Millipore, MA, USA) and then 10–20 μL eluent was applied to an Inertsil ODS-3 column (4.6 × 150 mm, GL sciences Inc, Japan). The HPLC conditions were as follows: flow rate, 0.5 mL min^{-1}; column temp, 25°C; detection, 220 nm; solvent A, MeOH; solvent B, 2% NaH_2PO_4 (pH 2.3, adjusted with H_3PO_4); isocratic elution, with A: B = 2: 98. Quantification was based on standard curves established with standard compounds.

RESULTS AND DISCUSSION

SMALL-SCALE PROTEOMIC APPROACH

Since the effects of Fe deficiency appear prominently in root tips both in our system and in other plant systems (Rellán-Alvarez et al., 2010), we decided to collect root tips for proteomic analysis. In order to eliminate bacterial contamination or other environmental factors that can affect plant metabolism and to guarantee reproducible data, we used sterile root cultures as our source material. Our previous study had shown that both flavin mononucleotide (FMN) hydrolase activity and respiration activity in root tips of *H. albus* were significantly higher at day 5 after transfer to Fe-deficient medium (Higa et al., 2012). We tried to harvest root tips at day 5, cultured in both Fe-deficient and -replete media, for proteomic analysis.

By this method, the total protein amounts soluble in CHAPS buffer that were obtained from Fe-deficient and Fe-replete samples, respectively, were 5.57 ± 0.56 and 4.92 ± 0.60 mg g^{-1} fr. wt (from four biologically independent experiments). Fe-deficient root tips contained slightly higher amounts of protein (by *ca*. 13%) than Fe-replete ones (**Table 1**).

CHANGES IN THE PROTEIN PROFILE UNDER IRON DEFICIENCY

Using our small-scale proteomic approach, 219 ± 4 spots and 218 ± 4 spots (from four biological samples, analyzed in four times) were resolved from protein extracts obtained from

Table 1 | Summarized results of protein yields and profiles from *H. albus* root tips.

Protein yield and spot number	+Fe	−Fe
Root tips (mg FW)	100	100
Protein yields (mg protein g^{-1} FW)	4.92 ± 0.60	5.57 ± 0.56
No. of spots detected	218 ± 4	219 ± 4
Comparative protein profile	**−Fe/+Fe**	
No. of spots changed*	48	
(Increased in abundance)		(30)
(Decreased in abundance)		(18)
No. of spots identified	36	
(Increased in abundance)		(22)
(Decreased in abundance)		(14)

*Twenty μg of proteins extracted from 100 mg of H. albus root tips cultured under Fe-replete and Fe-deficient conditions for 5 days were separated on small gels (7 × 7 cm). *To analyze differential protein accumulation between the two conditions of Fe availability, a threshold value (ANOVA at $p < 0.05$) was set at ≥ 1.5-fold change after normalization using Prodigy SameSpots®.*

Fe-deficient and Fe-replete root tips, respectively (**Figure 1**; **Table 1**). To analyze differential protein accumulation between the two conditions of Fe availability, we first set ≥1.5-fold change as a threshold value (ANOVA at $p < 0.05$) after normalization using Prodigy SameSpots®. Using these parameters, a total of 48 spots were detected; of these, 30 were increased in abundance and 18 were decreased under Fe deficiency (**Table 1**).

After in-gel digestion of each protein spot, followed by peptide extraction, the solutions were applied to matrix-assisted laser desorption/ionization–quadrupole ion trap–time of flight (MALDI-QIT-TOF) mass spectrometry for analysis of MS/MS. In this way, a total of 36 proteins were identified (**Tables 2**, **3**; Supplemental data 1 and 2); of these, 22 were increased in abundance, while the others were decreased under Fe deficiency (**Figure 1**; **Tables 1**–**3**). The results of this small-scale proteomic analysis revealed that most of the identified proteins have already been reported in the previous proteomic studies, but 10 proteins seemed not to be matched to the previously identified proteins from other dicotyledonous plants under Fe deficiency (Li et al., 2008; Donnini et al., 2010; Rellán-Alvarez et al., 2010; Wang et al., 2010; Lan et al., 2011; Rodríguez-Celma et al., 2011a, 2013a). These proteins included chaperonin 21 (spot 9), peroxidase 27 putative (spot 1), peroxiredoxin (spot 62), galactose oxidase/kelch repeat-containing protein (Glx, spot 5), elongation factor Tu (spot 46), aspartic protease (spot 60), soluble inorganic pyrophosphatase (spot 49), sinapyl alcohol dehydrogenase (spot 66), hyoscyamine 6β-hydroxylase (H6H, spot 30), and acetoacetyl-CoA thiolase (spot 52) (**Figure 1**; **Tables 2**, **3**). Some of these proteins, like H6H, could be highly dependent on plant species and materials. However, the comparison of proteomes from various plant species is not simple, because protein identification is restricted to the availability of public database and its reliability depends on the stringency of the criteria selected for positive identification at least (López-Millán et al., 2013).

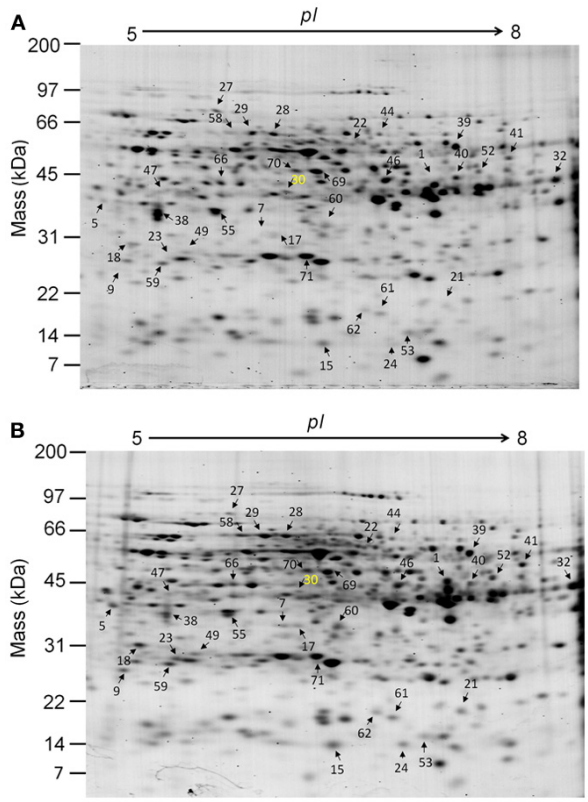

FIGURE 1 | 2-D Gel electrophoretic separations of *Hyoscyamus albus* root-tip proteins extracted from cultures exposed to Fe-replete (A) and Fe-deficient (B) conditions. Twenty μg of proteins extracted from 100 mg of *H. albus* root tips cultured under Fe-replete **(A)** and Fe-deficient **(B)** conditions for 5 days were separated on 7 cm IPG strips (pH5-8 linear gradient) using isoelectric focusing (IEF) in the first dimension, followed by AnyKd® gels in the second dimension. Gels were stained with Flamingo fluorescent stain. The prodigy rank number was used as a spot number; the number shown in yellow color is identified as hyoscyamine 6β-hydroxylase (H6H), the others are shown in black color. Molecular mass (kDa) and *pI* are indicated on the left-hand and upper axes, respectively.

The efficient identification of a diverse range of proteins using only small amounts of protein sample (20 μg per gel) must be a reflection of our particular extraction methodology, coupled with the highly-sensitive MALDI-QIT-TOF MS and MS/MS analysis (detection limit, *ca*. 500 amol).

Based on function, 36 differentially accumulated proteins in *H. albus* root tips were roughly classified into six groups: carbohydrate metabolism (8 proteins, 22%), defense response (8 proteins, 22%), structure/development (5 proteins, 14%), amino acid/protein metabolism (6 proteins, 17%), ETC/ATP synthesis (2 proteins, 6%) and secondary metabolism/others (7 proteins, 19%), although there is some overlap between categories. They were further divided into two groups of proteins that were either increased or decreased in abundance, respectively, under Fe deficiency (**Figure 2**; **Tables 1**, **2**). In the categories of carbohydrate metabolism, defense response and structure/development, 75–80% of proteins identified were increased in abundance. On the other hand, the number of decreased proteins was higher than that of increased proteins in amino acid/protein metabolism. In the case of ETC/ATP synthesis, only decreased proteins were detected (**Figure 2**).

Our principal findings are now discussed in detail below.

Carbohydrate metabolism and malate secretion under Fe deficiency

Our proteomic results showed that the accumulation of a subset of enzymes involved in glycolysis and TCA cycle was increased, including fructose bisphosphate aldolase (spot 32), phosphoglycerate mutase (spots 28, and 29), enolase (spot 22), UDP-glucose pyrophosphorylase (spot 58) and fumarase (spot 41) (**Table 2**). Indeed, under Fe deficiency, both Fe(III)-chelate reductase (FC-R) and H^+-ATPase activities are greatly enhanced (Curie and Briat, 2003), leading to a strong demand for energy in the form of NADPH and ATP. In plant cells, the typical energy production process is that hexose or sucrose is metabolized to pyruvate by glycolysis, and then pyruvate is either subjected to fermentation, or fully oxidized via the tricarboxylic acid (TCA) cycle. *H. albus* roots can continue to grow under Fe deficiency (Higa et al., 2008, 2010), so obviously energy generation can be maintained. Enhancement of glycolysis is likely to be the most conspicuous initial indicator of high energy production, as recently reported (Donnini et al., 2010; Rellán-Alvarez et al., 2010; Rodríguez-Celma et al., 2011a).

Table 2 | MS/MS-based cross-species identification and characterization of the protein spots that showed significant volume increase under iron-deficient conditions.

Spot No.	Protein name	Species	Accession no (NCBI)	Theoretical mass (kDa)/pI	Observed mass (kDa)/pI	PS/NMP[†]	SC (%)[‡]	Fold (−Fe/+Fe)	Subcellular localization
CARBOHYDRATE METABOLISM									
58	UDP-Glucose pyrophosphorylase	*Solanum tuberosum*	P19595	51.87/5.70	77.8/6.2	52/1[a]	7[b]	1.7	Cytoplasm
28	Phosphoglycerate mutase	*Solanum tuberosum*	AAD24857.1	61.26/5.42	77.8/6.3	64/3	6	1.8	Cytoplasm
29	Phosphoglycerate mutase	*Solanum tuberosum*	AAD24857.1	61.26/5.42	76.0/6.3	48/2	3	1.7	Cytoplasm
22	Enolase	*Solanum lycopersicum*	NP_001234080.1	47.79/5.68	47.6/6.7	75/2	8	2.0	Cytoplasm
32	Fructose bisphosphate aldolase like protein	*Solanum tuberosum*	ABB29926.1	38.53/8.32	45.4/7.9	53/2	11	1.7	Cytoplasm
41	Fumarase	*Solanum tuberosum*	CAA62817.1	53.38/6.51	60.7/7.7	56/1[a]	2	1.6	Mitochondria
DEFENSE RESPONSE									
7	Pyridoxine biosynthesis protein isoform A	*Lotus japonicus*	AAZ67141.1	33.09/5.92	41.2/6.3	57/2	9	2.9	Cytoplasm
9	Chaperonin 21 precursor	*Solanum lycopersicum*	NP_001234423.1	26.56/6.85	29.4/5.3	63/2	9	2.8	Plastid
1	Peroxidase 27 precursor putative	*Ricinus communis*	XP_002527239.1	35.67/8.89	46.5/7.1	52/1[a]	5	9.4	Secreted
62	Peroxiredoxin	*Ipomoea batatas*	AAP42502.1	20.76/8.80	23.1/6.8	94/3	21	1.5	Mitochondria
61	Glutathione peroxidase	*Solanum lycopersicum*	NP_001234567.1	18.84/6.58	20.9/6.8	89/3	21	1.5	Secreted
15	Superoxide dismutase [Cu-Zn]	*Nicotiana plumbaginifolia*	P27082.2	15.23/5.47	16.5/6.5	101/2	20	2.1	Cytoplasm
STRUCTURE / DEVELOPMENT									
59	Actin	*Bos taurus*	P62739	42.01/5.24	30.8/5.7	59/2	9[b]	1.5	Cytoplasm
21	Ubiquitin-conjugating enzyme E2 13 variant	*Solanum tuberosum*	ABA40444.1	16.56/6.20	17.3/6.8	79/3	29	2.1	Cytoplasm
53	Actin depolymerizing factor 3	*Gossypium hirsutum*	ABD66505.1	16.11/6.74	17.35/6.8	74/2	14	1.6	Cytoplasm
5	Galactose oxidase/ kelch repeat-containing protein	*Medicago truncatula*	XP_003596164.1	35.49/5.43	35.6/5.3	50/2	8	3.3	Cytoplasm
AMINO ACID/PROTEIN METABOLISM									
17	Cysteine protease 14	*Trifolium repens*	AAP32193.1	39.66/5.63	37.4/6.3	49/1[a]	5	2.0	Vacuole
60	Aspartic Protease	*Nicotiana tabacum*	ABG37021.1	54.78/5.53	41.2/6.6	67/2	7	1.5	Secreted
SECONDARY METABOLISM/OTHERS									
18	Caffeoyl-CoA-*O*- methyltransferase 6	*Nicotiana tabacum*	Q42945.1	27.79/5.30	32.4/5.5	59/1[a]	4	1.6	Cytoplasm
23	Caffeoyl-CoA-*O*-methyltransferase 1	*Nicotiana tabacum*	O24144	26.96/5.41	32.4/5.6	78/2	8[b]	2.0	Cytoplasm
49	Soluble inorganic pyrophsphatase	*Solanum tuberosum*	Q43187.1	24.26/5.59	34.0/5.7	58/1[a]	8[b]	1.6	Cytoplasm
24	6,7-Dimethyl-8-ribityllumazine synthase	*Nicotiana tabacum*	AAQ04061.1	24.42/8.18 (15.1/5.53)*	16.7/6.6	55/1[a]	17[b]	2.0	Plastid

[†]*Protein score (PS) and number of matched peptide (NMP) were obtained from Mascot search.*

[‡]*Percentage of sequence coverage (SC) of identified peptides related to the corresponding sequence in database.*

[a]*Annotated MS/MS spectra are provided in Supplemental data.*

[b]*Based on SwissProt full sequence identified by Mascot search.*

**Due to the presence of significantly long (86 aa) transit peptide in the precursor sequence, theoretical mass/pI of the predicted mature protein is also indicated in parenthesis.*

Table 3 | MS/MS-based cross-species identification and characterization of the protein spots that showed significant volume decreased under iron-deficient conditions.

Spot No.	Protein name	Species	Accession no (NCBI)	Theoretical mass (kDa)/pI	Observed mass (kDa)/pI	PS/NMP[†]	SC (%)[‡]	Fold (+Fe/−Fe)	Subcellular localization
CARBOHYDRATE METABOLISM									
40	Fructose bisphosphate aldolase like protein	*Solanum tuberosum*	ABC01905.1	38.62/7.51	47.6/7.5	66/2	9	1.7	Cytoplasm
55	NAD-dependent malate dehydrogenase	*Nicotiana tabacum*	CAB45387.1	43.31/8.03	41.2/6.0	70/2	7	1.6	Mitochondria
DEFENSE RESPONSE									
71	Ascorbate peroxidase	*Nicotiana tabacum*	BAA12918.1	27.45/5.43	32.4/6.5	203/6	33	1.5	Cytoplasm
38	Predicted cationic peroxidase	*Vitis vinifera*	XP_002268412.1	34.25/9.36	43.3/5.7	48/1[a]	4	1.7	Vacuole
STRUCTURE/DEVELOPMENT									
47	Annexin p34	*Solanum lycopersicum*	NP_001234104.1	35.80/5.37	35.7/6.0	48/2	9	1.6	Cytoplasm
AMINO ACID/PROTEIN METABOLISM									
46	Elongation factor Tu	*Arabidopsis thaliana*	Q9ZT91	49.41/6.25	57.8/6.8	217/5	17[b]	1.6	Mitochondria
70	*S*-adenosylmetionine synthase	*Brassica rapa*	Q5DNB1.1	43.16/5.8	48.2/6.3	50/2	7[b]	1.5	Cytoplasm
69	*S*-adenosylmetionine synthase 2	*Solanum tuberosum*	Q38JH8	42.70/5.6	47.9/6.4	52/2	8[b]	1.5	Cytoplasm
44	Nitrite reductase	*Nicotiana tabacum*	BAD15364.1	65.46/6.67	77.3/7.1	57/2	5	1.6	Mitochondria
SECONDARY METABOLISM/OTHERS									
66	Sinapyl alcohol dehydrogenase	*Populus trichocarpa*	XP_002322822.1	38.94/6.23	55.1/6.1	68/2	5	1.5	Cytoplasm
30	Hyoscyamine 6β-hydroxylase	*Atropa belladonna*	AEM91979.1	39.22/5.44	37.4/6.4	64/4	16	1.8	Cytoplasm
52	Acetoacetyl-CoA thiolase	*Nicotiana tabacum*	AAU95618.1	41.27/6.47	55.1/7.3	59/2	7	1.7	Cytoplasm
ETC/ATP SYNTHESIS									
27	NADH dehydrogenase Fe-S protein 1	*Solanum tuberosum*	Q43644	79.97/5.87	89.3/6.1	45/2	4[b]	1.6	Mitochondria
39	ATP Synthase subunit alpha	*Celtis yunnanensis*	ADL63175.1	55.05/6.23	66.8/7.3	61/2	8	1.7	Mitochondria

[†]*Protein score (PS) and number of matched peptide (NMP) were obtained from Mascot search.*

[‡]*Percentage of sequence coverage (SC) of identified peptides related to the corresponding sequence in database.*

[a]*Annotated MS/MS spectra are provided in Supplemental data.*

[b]*Based on SwissProt full sequence identified by Mascot search.*

In comparison to such proteins increased in abundance, a mitochondrial NAD-dependent malate dehydrogenase (MDH, spot 55) was decreased in relative intensity under Fe depletion (**Table 3**). It is interesting to note that an accumulation of large amounts of malate together with relatively small amounts of citrate was detected in the culture medium of *H. albus* roots (**Figure 3**). This is similar to the behavior of some other "strategy I" plant roots (Brown and Tiffin, 1965; Alhendawi et al., 1997; Abadía et al., 2002; Zocchi, 2006; Rellán-Alvarez et al., 2010) subjected to Fe-limiting conditions. The observed increase of fumarase (spot 41) could also contribute to malate secretion.

The defense system working under Fe deficiency

Our proteomic results revealed that the accumulations of predicted cationic peroxidase (spot 38) and ascorbate peroxidase (APX, spot 71) were decreased under Fe deficiency, while glutathione peroxidase (GPX, spot 61), CuZn-superoxide dismutase (SOD, spot 15), peroxidase 27 putative (spot 1), peroxiredoxin (PRX, spot 62) and pyridoxine biosynthesis protein isoform A (spot 7) all showed increased accumulation (**Tables 2**, **3**). Generally, environmental stress enhances the production of reactive oxygen species (ROS) in plant cells, which can cause oxidative damage to lipids, proteins, and DNA, thereby promoting cell damage. Since the detoxification of ROS is essential for survival, many antioxidant enzymes (e.g., catalase, APX, SOD, GPX, and PRX) are involved in ROS-scavenging. Recently, pyridoxine biosynthesis protein is also revealed to be an efficient quencher of various ROS such as singlet oxygen and superoxide (Ehrenshaft et al., 1999; Chen and Xiong, 2005; Ristilä et al., 2011).

Our results suggest that increased accumulation of the Fe-independent enzymes, GPX, PRX, CuZnSOD and pyridoxine biosynthesis protein isoform A, may compensate for a decreased accumulation of the heme-containing ROS scavengers such as peroxidases and APX. On the other hand, the role of the newly detected putative peroxidase 27 (spot 1), a member of the class of pathogenesis-related proteins (Okushima et al., 2000), is not clear at present, because very little is known about this protein. It might play a crucial role in iron homeostasis under Fe deficiency.

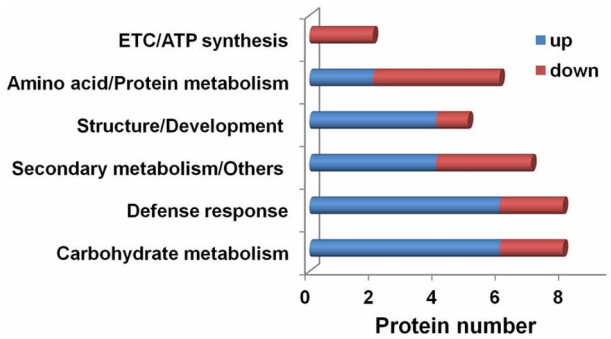

FIGURE 2 | Classification of differentially accumulated proteins from the root tips of *H. albus* roots cultured under Fe-deficient and Fe-replete conditions. A total of 36 identified proteins were found to be differentially accumulated and were classified into six functional categories, viz: carbohydrate metabolism; defense response; amino acid/protein metabolism; structure/development; electron transport chains (ETC)/ATP synthesis; and secondary metabolism/others. Blue and red bars indicate up and down proteins in abundance, respectively.

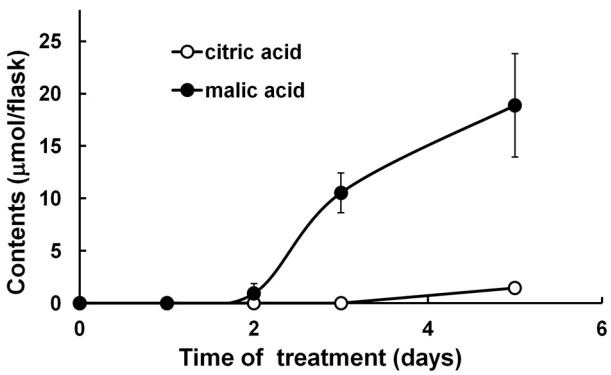

FIGURE 3 | Citric and malic acids released into the culture medium by *H. albus* roots under Fe-deficient conditions. After *H. albus* root cultures had been exposed to Fe-deficient culture medium, 500 μL of the medium was collected at days 1, 2, 3, and 5, respectively. Results are the means of three independent experiments, and bars indicate standard deviations of the means.

Amino acid and protein metabolism under Fe deficiency

Two protease enzymes, cysteine protease 14 (spot 17) and aspartic protease (spot 60), were increased under Fe-deficient conditions (**Table 2**). Conversely, nitrite reductase (spot 44), responsible for assimilation of NO_2^- (Takahashi et al., 2001) was found to be decreased by Fe deficiency (**Table 3**). In addition, decrease was observed of *S*-adenosyl-L-methionine synthetase (SAM, spots 69 and 70), which catalyzes the biosynthesis of SAM from methionine and ATP, and H6H (spot 30), which is involved in tropane alkaloid biosynthesis (Hashimoto and Yamada, 1987) (**Table 3**). Our proteomic data therefore suggested the possibility of a shift under Fe-deficient conditions away from the *de novo* synthesis of amino acids and toward an enhanced reutilization of amino acids produced by proteolysis. There might also have been some shift in the utilization of amino acids, toward essential cellular housekeeping and away from non-essential functions such as secondary product biosynthesis. It is well known that tropane alkaloids are derived from ornithine and phenylalanine. In *Cucumis sativus* plants, the assay of the nitrate reductase activity revealed the reduction of nitrate assimilation in both roots and leaves under Fe limitation (Borlotti et al., 2012). Based on this and the previous results, the authors hypothesized that the decreased proteins, actin, tubulin and globulin in this case, might be recycled and used as a source of amino acids, carbon skeletons and $N\text{-}NH_4^+$ under Fe deficiency (Donnini et al., 2010; Borlotti et al., 2012). Although the proteins detected in *H. albus* roots under Fe limitation were different from those in *C. sativus* roots, similar outline of an adaptation mechanism has been suggested from our results, too.

Nitrite reductase contains Fe-S clusters (Taiz and Zeiger, 2002), SAM synthetase requires ATP, as mentioned above, and H6H is a Fe-dependent enzyme. All these enzymes appeared from our proteomic data to be decreased in response to Fe deficiency,

in agreement with our hypothesis that plants can survive under Fe deficiency by prioritizing the use of Fe and ATP for essential processes.

Fe deficiency induces morphological changes

In *H. albus* roots, ubiquitin-conjugating enzyme (UBC) E2 variant 13 (synonymous with UBC13) (spot 21) showed an increase in abundance under Fe deficiency (**Table 2**). In addition, actin (spot 59) and actin depolymerizing factor 3 (ADF, spot 53) were both increased under Fe deficiency (**Table 2**). Furthermore, an increase of galactose oxidase/kelch repeat-containing protein (Glx, spot 5), which is a member of the Cu-dependent Glx family of proteins involved in the oxidation of primary alcohols to aldehydes, was observed (**Table 2**). In contrast, one annexins p34 (spot 47), members of a multi-gene family, was decreased under Fe deficiency (**Table 3**). *Arabidopsis* responds to Fe deficiency by forming branched roots, and over-expression of UBC13 enhances this process (Li and Schmidt, 2010). In fact, *H. albus* roots showed morphological changes such as swelling of the root tips and increases in the numbers of lateral roots under Fe deficiency (Higa et al., 2008), same as previous report (Ling et al., 2002). An increase of ADF was also found in *Arabidopsis* (Lan et al., 2011). Changes in the actin cytoskeleton may be involved in adaptations to stresses, beginning with signal transduction and perception (Samaj et al., 2004). This possibility is supported by the fact that ADFs function in the remodeling of the actin cytoskeleton in response to environmental cues (Bamburg, 1999; Ruzicka et al., 2007). One annexins p34 (spot 47), which is capable of binding to F-actin (Hoshino et al., 2004) and of hydrolyzing ATP and GTP (Shin and Brown, 1999), was decreased under Fe deficiency (**Table 3**), possibly because of diminished availability of ATP or GTP.

One of the remarkable differences between our study and other proteomic studies of responses to Fe deficiency was the presence and enhanced expression of Glx (spot 5) (**Table 2**). However, the physiological role of this protein remains elusive. Recently, Liman et al. (2013) reported that Glx is required for aerial hyphae formation and for their further differentiation into hyphal spores in *Streptomyces coelicolor*. Similarly, this protein might play an important role in plant cell differentiation or in morphological changes.

Fe deficiency affects secondary metabolism and others

A major secondary metabolic pathway in *H. albus* is tropane alkaloid biosynthesis. The decrease of H6H in response to Fe deficiency has already been described above. In addition, two isoforms of caffeoyl-CoA-*O*-methyltransferase (1 and 6: spots 23 and 18, respectively) involved in phenylpropanoid biosynthesis were increased under Fe deficiency (**Table 2**). This enzyme catalyzes the conversion of caffeoyl-CoA to feruloyl-CoA. On the other hand, sinapyl alcohol dehydrogenase (spot 66), involved in lignin biosynthesis and known to generate free-radical intermediates (Taiz and Zeiger, 2002), was found to decrease (**Table 3**). These results suggest that the phenylpropanoid pathway leading to lignin biosynthesis via sinapyl alcohol could be rerouted to produce other phenolics such as the coumarin derivative, scopoletin, found in *Arabidopsis* roots under Fe deficiency (Lan et al., 2011). However, in the case of *Arabidopsis*, increased lignification was suggested, because of the up-regulation of various enzymes, including PAL, involved in lignin biosynthesis (Lan et al., 2011; Rodríguez-Celma et al., 2013b). Lignifications usually occur after cell wall expansion ceases and synthesis of secondary cell wall starts (Taiz and Zeiger, 2002). Since under Fe deficiency, *H. albus* root tips start changing morphologically such as swelling, it is likely that liginification is suppressed under this situation. To confirm such metabolic changes in *H. albus* roots, further work is necessary.

One increased protein, 6,7-dimethyl-8-ribityllumazine synthase (RibC, spot 24) that we identified was associated with riboflavin production (**Table 2**). We will describe about this in the section Effects of Iron Deficiency on Tropane Alkaloid and Riboflavin Biosyntheses. Other increased and decreased proteins include soluble inorganic pyrophosphatase (spot 49) and acetoacetyl-CoA thiolase (spot 52), respectively (**Tables 2**, **3**). Inorganic pyrophosphatase catalyzes the conversion of one molecule of pyrophosphate to two phosphate ions. This is a highly exergonic reaction and involved in many biochemical reactions, including lipid degradation and glycolysis (Jelitto et al., 1992). Acetoacetyl-CoA thiolases catalyze a reversible Claisen-type condensation of two acetyl-CoA molecules to form acetoacetyl-CoA and the first step of the mevalonate pathway (Ahumada et al., 2008). These changes are likely to be involved in the survival strategy of *H. albus*.

Changes in ETC and ATP synthesis by Fe deficiency

It was found that a component of the mitochondrial ETC, complex I, NADH dehydrogenase Fe-S protein 1 (spot 27), which requires many Fe ions (Ohnishi, 1998), was decreased in abundance (**Table 3**). An abundance decrease of ATP synthase subunit alpha (spot 39) was also observed (**Table 3**). Decreased acuumulation of a subunit of complex I under Fe deficiency has also been reported in *M. truncatula* (Rodríguez-Celma et al., 2011a). This result was consistent with our own previous results obtained through inhibitor-feeding experiments (Higa et al., 2010), and with the results of enzyme assay and western analysis in cucumber roots (Vigani et al., 2009).

As mentioned previously, our proteomic data showed that most of the proteins that were decreased required either Fe or ATP for activity. This is also applied to complex I as well. In addition, the observed decrease of ATP synthase subunit alpha (spot 39) suggested a reduced capacity for ATP synthesis as well.

EFFECTS OF IRON DEFICIENCY ON TROPANE ALKALOID AND RIBOFLAVIN BIOSYNTHESES

Because of the importance of *H. albus* as a source of medicinal compounds, we investigated further the effects of Fe deficiency on tropane alkaloid production. H6H (EC1.14.11.11), required Fe as a cofactor for activity, is a bi-functional monooxygenase and converts hyoscyamine to 6β-hydroxyhyoscyamine and thence to scopolamine (Hashimoto et al., 1993). In addition, hyoscyamine biosynthesis via the rearrangement of littorine is found to be catalyzed by a Fe-dependent cytochrome P450, Cyp80F1 (Li et al., 2006). Therefore, we decided to investigate whether these Fe-dependent enzymes were down-regulated at

the expression level and whether tropane alkaloid content was decreased. The expression of both *Cyp80F1* and *H6H* was examined by RT-PCR, using hairy roots treated with/without Fe for 5 days (**Figure 4**). The results showed that the transcript accumulations of both enzymes in Fe-deficient root tips were reduced in comparison to those in Fe-replete root tips (**Figure 4A**). Semi-quantitative analysis showed that H6H (*ca*. 50% diminished) was more strongly affected than Cyp80F1 (*ca*. 35% diminished) (**Figure 4B**).

The effect of Fe deficiency on alkaloid production was also examined by HPLC, using not only root tips but also the older parts of the roots, because it is known that alkaloids can be transported *via* the xylem (Manske and Holmes, 1965). The results showed that the root tips accumulated smaller amounts of scopolamine and hyoscyamine than the older parts, and that the hyoscyamine content was always substantial, regardless of the root material (**Figure 5**). The results confirmed that the content of both hyoscyamine and scopolamine was decreased under Fe deficiency, but that the scopolamine content was more strongly affected than hyoscyamine content (**Figure 5**), in agreement with the results for transcript accumulation (**Figures 4A,B**). This might reflect the known requirement for Fe ions in the conversion of hyoscyamine to scopolamine.

Flavins are heterocyclic compounds same as alkaloids. In contrast to tropane alkaloid biosynthesis described above, accumulation of RibC that is involved in riboflavin synthsis was increased in the root tips treated without Fe for 5 days (**Table 2**). This result agreed with our previous findings that the riboflavin secretion we observed occurred as a result of the enhancement both of *de novo* riboflavin synthesis and of the hydrolysis of FMN (Higa et al., 2012), although protein that functions in the hydrolysis of FMN was not identified. To reconfirm the previous results, we again determined the gene expression of *riboflavin synthase* (*RibD*) as a direct enzyme involved in *de novo* riboflavin synthesis, by the same way used for analyses of *Cyp80F1* and *H6H* (**Figure 4C**). The semi-quantitative analysis showed an apparent increase (*ca*. 6 times) in *HaRibD* accumulation under Fe deficiency (**Figure 4D**). This coincided with the previous reports on both *M. truncatula* and *B. vulgaris*, in which increase of the riboflavin-biosynthetic enzyme, RibC was confirmed by proteomic data as well as by analysis at the mRNA level (Rellán-Alvarez et al., 2010; Rodríguez-Celma et al., 2011a).

In this paper, we reported the application of a small-scale proteomic approach that permitted the extraction and separation of proteins from 100 mg (fresh weight) of *H. albus* root tips. Two-dimensional separation using mini-gels, followed by spot-picking and analysis by Matrix-assisted laser desorption/ionization–quadrupole ion trap–time of flight (MALDI-QIT-TOF) mass spectrometry allowed the identification of 36 differentially accumulated proteins in Fe-deficient roots compared to Fe-replete roots. To the best of our knowledge, this is the first reported application of the use of MALDI-QIT-TOF mass spectrometry for the analysis of proteins from plant roots in relation to Fe deficiency. The proteome profile supported our hypothesis that the adaptation of *H. albus* roots under Fe depletion is characterized by metabolic and respiratory shifts that achieve greater economy in the use of Fe, one example of which was the suppression of tropane alkaloid biosynthesis.

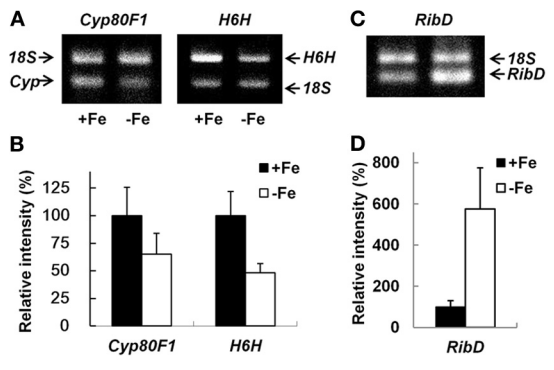

FIGURE 4 | Transcript accumulations of *H6H, Cyp80F1* and *RibD* in the root tips of *H. albus* roots cultured under Fe-deficient and Fe-replete conditions. Representative expression profiles are shown in **(A)** and **(C)** and semiquantitative analysis of the expressions with three biological replicates and standard deviations are in **(B)** and **(D)**, respectively. H6H, hyoscyamine 6β-hydoroxylase, catalyzes the conversion from hyoscyamine to scopolamine, Cyp80F1, a cytochrome P450, is involved in littorine rearrangement to produce hyoscyamine and RibD, riboflavin synthase, is involved in *de nono* synthesis of ribofalvin. RNA was extracted from 0.1 g of fresh root tips, and 500–1000 ng RNA was used for RT-PCR. Using primers specific for *H6H*, *Cyp80F1* and *RibD*, corresponding fragments of 512 bp, 202 bp and 215 bp, respectively, were amplified. Ribosomal RNA 18S universal primer pairs were used as an internal standard for normalization (product fragment, 315 bp). −Fe, no addition of Fe; +Fe, with addition of 0.1 mM Fe(III)-EDTA.

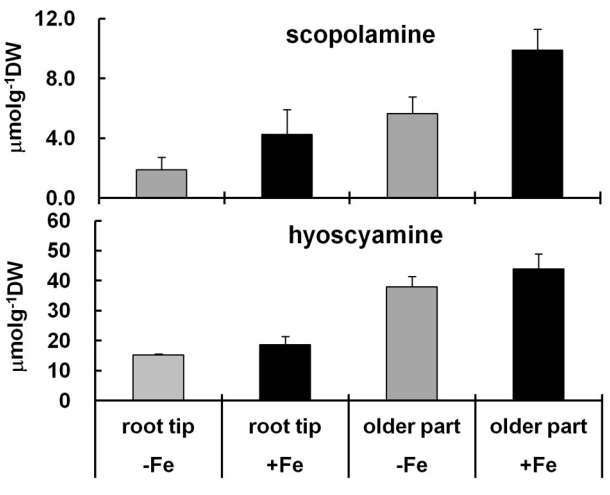

FIGURE 5 | Alkaloid contents of the tips and of the remaining older parts of *H. albus* roots cultured under Fe deficiency and Fe repletion. Roots were treated with and without Fe for 5 days, and then harvested. Roots were separated into the tips (*ca*. 1.0–1.5 cm in length) and the remaining parts, and then dried at 50°C overnight. Results are means of three independent experiments, and bars indicate standard deviations of the means.

One of the suggestions emerging from our proteomic data is that malate secretion seemed to occur as a result of a decreased abundance of mitochondrial NAD-dependent MDH under Fe deficiency (**Table 3**). Although the secretion of both malate and citrate is a well-known phenomenon, the mechanism of origin of malate remains uncertain. It has been suggested that the observed up-regulation of cytosolic phosphoenolpyruvate carboxylase (PEPC) (López-Millán et al., 2000) generates oxaloacetate and malate, which can be imported into mitochondria and thence generate citrate; citrate might then efflux from the mitochondria to be transported in the xylem and/or exuded (Zocchi, 2006). In the case of *H. albus* roots, it is uncertain whether malate that is secreted is derived from the mitochondria and/or the cytosol. In any event, an apparent decrease of mtMDH must cause metabolic changes in the mitochondria. Recently, in the case of breakdown of the TCA cycle, non-cyclic flux models have been proposed (Sweetlove et al., 2010; Vigani, 2012). The TCA cycle provides not only organic acids, but also amino acid precursors. Our proteomic data indicate, however, that under Fe deficiency amino acids for cell development are generated mainly by proteolysis, with the result that *de novo* synthesis may be reduced. This suggests that the TCA cycle may not be fully working under Fe deficiency.

Secreted citrate and malate have been suggested to function as carriers of Fe ions and as cytosolic pH stats after H^+ efflux by H^+-ATPase (Zocchi, 2006). However, for plants and from the perspective of energy consumption, the secretion of malate (a C_4 compound) is more economical than that of citrate (a C_6 compound). Since a flux of carbon from plants to the soil increases both the size of the microbial population and the mobilization of soil micronutrients (Dakora and Phillips, 2002), malate might in principle be used to invite fungi or bacteria as "vehicles" for the supply of Fe ions for plant roots. In addition to citrate and malate, flavin (riboflavin) secretion also occurred in the culture media of *H. albus* roots under Fe deficiency (Higa et al., 2008, 2010, 2012), same as *B. vulgaris* (Susin et al., 1994), *M. truncatula* (Rodríguez-Celma et al., 2011a,b), and *C. sativus* (Shinmachi et al., 1997). Together with organic acids or independently, flavins may aid the availability of soil Fe for plant roots *via* changing the soil microflora as indicated by Vorwieger et al. (2007). They suggested that riboflavin acts as a plant-generated signal to manipulate rhizosphere microbiology. Recent evidence that chemical diversity exists among secreted/accumulated flavins depending on plant species (Rodríguez-Celma et al., 2011b) also supports their ecological role. Another possible role of flavins produced by *M. truncatula* roots in the rhizosphere has been proposed, according to the result on the coexpression and promoter analysis of genes that are responsive to Fe deficiency: as iron-binding compounds, flavins chelate Fe(III) from non-soluble ferrihydroxides and provide these chelates to Fe reductase (Rodríguez-Celma et al., 2013b). The authors also mentioned that in the case of *Arabidopsis*, phenylpropanoids function as iron-binding compounds, and flavins and phenylpropanoids are produced by a mutually exclusive metabolism in these plants.

Further extensive studies are clearly required, however, in order to elucidate the ecological significance of organic acid and flavin secretions into the rhizosphere.

CONCLUSION

Hyoscyamus albus is an important medicinal plant, as a source of both hyoscyamine and scopolamine. Using our original small-scale proteomic approach with 100 mg of root tips, we determined the effects of Fe deficiency on protein expression. The differentially-accumulated proteins (36) identified by MALDI-QIT-TOF mass spectrometry were divided into six groups according to function, *viz*: carbohydrate metabolism, defense responses, amino acid/protein metabolism, structure/development, ETC /ATP synthesis and, lastly, other miscellaneous functions, including secondary metabolism.

There was evidence of the enhanced accumulation of some glycolytic proteins under Fe-deficient conditions, presumably to maintain energy supply, but the decrease of mitochondrial MDH under Fe deficiency seemed correlated with malate secretion into the rhizosphere. For defense against environmental stresses, there was evidence that Fe-independent ROS scavenging machinery might substitute for Fe-dependent mechanisms. Our data also confirmed that the response to Fe deficiency caused morphological changes such as root branching. Furthermore, the proteins necessary for such remodeling of root development seemed to derive their amino acids through proteolysis, rather than through amino acid biosynthesis *de novo*. Fe deficiency also affected secondary metabolism, including alkaloid metabolism. Most proteins exhibiting decreases in abundance required either Fe or ATP for activity. Representative examples were the mitochondrial ETC component complex I and H6H, which is involved in tropane alkaloid biosynthesis. A further determination of transcript accumulation for H6H supported the decrease in tropane alkaloid content observed in Fe-deficient roots. On the contrary, the increase of RibC accumulation indicated that riboflavin secretion occurs at least through the enhancement of *de novo* synthesis.

Economy in the use of Fe and ATP, including the use of energy to re-programme root morphology and function in response to Fe restriction, must be a principal strategy for plant roots faced with severely suboptimal Fe availability. In contrast, another strategy of expenditure of carbon and nitrogen sources in the rhizosphere need to be solved.

ACKNOWLEDGMENTS

We wish to thank all of the members of Dr. Tatsuya Oda's laboratory, especially Ms. Moemi Shibata-Yamawaki, for their helpful cooperation in sample preparation for small-scale proteomics. We also appreciate the excellent English edition by Dr. Nicholas Walton (Norwich, UK). This work was supported by a Grant-in-Aid (C, 24580479) from the Japan Society for the Promotion of Science.

SUPPLEMENTARY MATERIAL

The Supplementary Material for this article can be found online at: http://www.frontiersin.org/Plant_Nutrition/10.3389/fpls.2013.00331/abstract

REFERENCES

Abadía, J., Lopez-Millan, A.-F., Rombola, A., and Abadía, A. (2002). Organic acids and Fe deficiency: a review. *Plant Soil* 241, 75–86. doi: 10.1023/A:1016093317898

Aghaei, K., and Komatsu, S. (2013). Crop and medicinal plants proteomics in response to salt stress. *Front. Plant Sci.* 4:8. doi: 10.3389/fpls.2013.00008

Ahumada, I., Cairó, A., Hemmerlin, A., González, V., Pateraki, I., Bach, T. J., et al. (2008). Characterisation of the gene family encoding acetoacetyl-CoA thiolase in *Arabidopsis*. *Funct. Plant Biol.* 35, 1100–1111. doi: 10.1071/FP08012

Alhendawi, R. A., Römheld, V., Kirkby, E. A., and Marschner, H. (1997). Influence of increasing bicarbonate concentrations on plant growth, organic acid accumulation in roots and iron uptake by barley, sorghum, and maize. *J. Plant Nutr.* 20, 1731–1753. doi: 10.1080/01904169709365371

Bamburg, J. R. (1999). Proteins of the ADF/cofilin family: essential regulators of actin dynamics. *Annu. Rev. Cell Dev. Biol.* 15, 185–230. doi: 10.1146/annurev.cellbio.15.1.185

Biastoff, S., Brandt, W., and Dräger, B. (2009). Putrescine N-methyltransferase:the start for alkaloids. *Phytochemistry* 70, 1708–1718. doi: 10.1016/j.phytochem.2009.06.012

Borlotti, A., Vigani, G., and Zocchi, G. (2012). Iron deficiency affects nitrogen metabolism in cucumber (*Cucumis sativus* L.). plants. *BMC Plant Biol.* 12:189. doi: 10.1186/1471-2229-12-189

Brown, J. C., and Tiffin, L. O. (1965). Iron stress as related to the iron and citrate occurring in stem exudate. *Plant Physiol.* 40, 395–400. doi: 10.1104/pp.40.2.395

Brumbarova, T., Matros, A., Mock, H. P., and Bauer, P. (2008). A proteomic study showing differential regulation of stress, redox regulation and peroxidase proteins by iron supply and the transcription factor FER. *Plant J.* 54, 321–334. doi: 10.1111/j.1365-313X.2008.03421.x

Chen, H., and Xiong, L. (2005). Pyridoxine is required for post-embryonic root development and tolerance to osmotic and oxidative stresses. *Plant J.* 44, 396–408. doi: 10.1111/j.1365-313X.2005.02538.x

Curie, C., and Briat, J. F. (2003). Iron transport and signaling in plants. *Annu. Rev. Plant Biol.* 54, 183–206. doi: 10.1007/978-3-642-14369-4_4

Dakora, F. D., and Phillips, D. A. (2002). Root exudates as mediators of mineral acquisition in low-nutrient environments. *Plant Soil* 245, 35–47. doi: 10.1023/A:1020809400075

Donnini, S., Prinsi, B., Negri, A. S., Vigani, G., Espen, L., and Zocchi, G. (2010). Proteomic characterization of iron deficiency responses in *Cucumis sativus* L. roots. *BMC Plant Biol.* 10:268. doi: 10.1186/1471-2229-10-268

Dudkina, N. V., Heinemeyer, J., Sunderhaus, S., Boekema, E. J., and Braun, H. P. (2006). Respiratory chain supercomplexes in the plant mitochondrial membrane. *Trends Plant Sci.* 11, 232–240. doi: 10.1016/j.tplants.2006.03.007

Ehrenshaft, M., Bilski, P., Li, M. Y., Chignell, C. F., and Daub, M. E. (1999). A highly conserved sequence is a novel gene involved in *de novo* vitamin B_6 biosynthesis. *Proc. Natl. Acad. Sci. U.S.A.* 96, 9374–9378. doi: 10.1073/pnas.96.16.9374

Evans, W. C. (1996). *Trease and Evans Pharmacognosy*. London: WB Saunders.

Gamborg, O. L., Miller, R. A., and Ojima, K. (1968). Nutrient requirements of suspension cultures of soybean root cells. *Exp. Cell Res.* 50, 151–158. doi: 10.1016/0014-4827(68)90403-5

Hank, H., Szoke, É., Tóth, K., László, I., and Kursinszki, L. (2004). Investigation of tropane alkaloids in genetically transformed *Atropa belladonna* L. cultures. *Chromatographia* 60, S55–S59.

Hashimoto, T., Matsuda, J., and Yamada, Y. (1993). Two-step epoxidation of hyoscyamine to scopolamine is catalyzed by bifunctional hyoscyamine 6β-hydroxylase. *FEBS Lett.* 329, 35–39. doi: 10.1016/0014-5793(93)80187-Y

Hashimoto, T., and Yamada, Y. (1987). Purification and characterization of hyoscyamine 6β-hydroxylase from root cultures of Hyoscyamus niger L. Hydroxylase and epoxidase activities in the enzyme preparation. *Eur. J. Biochem.* 164, 277–285.

Higa, A., Khandakar, J., Mori, Y., and Kitamura, Y. (2012). Increased de novo riboflavin synthesis and hydrolysis of FMN are involved in riboflavin secretion from *Hyoscyamus albus* hairy roots under iron deficiency. *Plant Physiol. Biochem.* 58, 166–173. doi: 10.1016/j.plaphy.2012.07.001

Higa, A., Miyamoto, E., ur Rahman, L., and Kitamura, Y. (2008). Root tip-dependent, active riboflavin secretion by *Hyoscyamus albus* hairy roots under iron deficiency. *Plant Physiol. Biochem.* 46, 452–460. doi: 10.1016/j.plaphy.2008.01.004

Higa, A., Mori, Y., and Kitamura, Y. (2010). Iron deficiency induces changes in riboflavin secretion and the mitochondrial electron transport chain in hairy roots of *Hyoscyamus albus*. *J Plant Physiol.* 167, 870–878. doi: 10.1016/j.jplph.2010.01.011

Hoshino, D., Hayashi, A., Temmei, Y., Kanzawa, N., and Tsuchiya, T. (2004). Biochemical and immunohistochemical characterization of *Mimosa* annexin. *Planta* 219, 867–875. doi: 10.1007/s00425-004-1285-7

Jelitto, T., Sonnewald, U., Willmitzer, L., Hajirezeai, M., and Stitt, M. (1992). Inorganic pyrophosphate content and metabolites in potato and tobacco plants expressing *E. coli* pyrophosphatase in their cytosol. *Planta* 188, 238–244. doi: 10.1007/BF00216819

López-Millán, A.-F., Grusak, M. A., Abadía, A., and Abadía, J. (2013). Iron deficiency in plants: an insight from proteomic approaches. *Front. Plant Sci.* 4:254. doi: 10.3389/fpls.2013.00254

López-Millán, A. F., Morales, F., Andaluz, S., Gogorcena, Y., Abadía, A., De Las Rivas, J., et al. (2000). Responses of sugar beet roots to iron deficiency. Changes in carbon assimilation and oxygen use. *Plant Physiol.* 124, 885–898. doi: 10.1104/pp.124.2.885

Lan, P., Li, W., Wen, T. N., Shiau, J. Y., Wu, Y. C., Lin, W., et al. (2011). iTRAQ protein profile analysis of *Arabidopsis* roots reveals new aspects critical for iron homeostasis. *Plant Physiol.* 155, 821–834. doi: 10.1104/pp.110.169508

Li, J., Wu, X. D., Hao, S. T., Wang, X. J., and Ling, H. Q. (2008). Proteomic response to iron deficiency in tomato root. *Proteomics* 8, 2299–2311. doi: 10.1002/pmic.200700942

Li, R., Reed, D. W., Liu, E., Nowak, J., Pelcher, L. E., Page, J. E., et al. (2006). Functional genomic analysis of alkaloid biosynthesis in *Hyoscyamus niger* reveals a cytochrome P450 involved in littorine rearrangement. *Chem. Biol.* 13, 513–520. doi: 10.1016/j.chembiol.2006.03.005

Li, W., and Schmidt, W. (2010). A lysine-63-linked ubiquitin chain-forming conjugase, UBC13, promotes the developmental responses to iron deficiency in *Arabidopsis* roots. *Plant J.* 62, 330–343. doi: 10.1111/j.1365-313X.2010.04150.x

Liman, R., Facey, P. D., van Keulen, G., Dyson, P. J., and Del Sol, R. (2013). A laterally acquired galactose oxidase-like gene is required for aerial development during osmotic stress in *Streptomyces coelicolor*. *PLoS ONE* 8:e54112. doi: 10.1371/journal.pone.0054112

Lindsay, W., and Schwab, A. (1982). The chemistry of iron in soils and its availability to plants. *J. Plant Nutr.* 5, 821–840. doi: 10.1080/01904168209363012

Ling, H. Q., Bauer, P., Bereczky, Z., Keller, B., and Ganal, M. (2002). The tomato fer gene encoding a bHLH protein controls iron-uptake responses in roots. *Proc. Natl. Acad. Sci. U.S.A.* 99, 13938–13943. doi: 10.1073/pnas.212448699

Manske, R. R. H. F., and Holmes, H. H. L. (1965). *The Alkaloids: Chemistry and Physiology V1: Chemistry and Physiology*. New York, NY: Academic Press.

Murashige, T., and Skoog, F. (1962). A revised medium for rapid growth and bioassay with tobacco tissue cultures. *Physiol. Plant.* 15, 473–497. doi: 10.1111/j.1399-3054.1962.tb08052.x

Nisperos-Carriedo, M. O., Buslig, B. S., and Shaw, P. E. (1992). Simultaneous detection of dehydroascorbic, ascorbic, and some organic acids in fruits and vegetables by HPLC. *J. Agri. Food Chem.* 40, 1127–1130. doi: 10.1021/jf00019a007

Ohnishi, T. (1998). Iron-sulfur clusters/semiquinones in complex I. *Biochim. Biophys. Acta* 1364, 186–206. doi: 10.1016/S0005-2728(98)00027-9

Okushima, Y., Koizumi, N., Kusano, T., and Sano, H. (2000). Secreted proteins of tobacco cultured BY2 cells: identification of a new member of pathogenesis-related proteins. *Plant Mol. Biol.* 42, 479–488. doi: 10.1023/A:1006393326985

Rahman, L.u., Kitamura, Y., Yamaguchi, J., Mukai, M., Akiyama, K., et al. (2006). Exogenous plant H6H but not bacterial HCHL gene is expressed in *Duboisia leichhardtii* hairy roots and affects tropane alkaloid production. *Enzyme Microbial. Technol.* 39, 1183–1189. doi: 10.1016/j.enzmictec.2006.02.029

Raju, K. V., and Marschner, H. (1973). Regulation of iron uptake from relatively insoluble iron compounds by sunflower plants. *Zeitschrift für Pflanzenernährung und Bodenkunde* 133, 227–241. doi: 10.1002/jpln.19731330305

Rellán-Alvarez, R., Andaluz, S., Rodríguez-Celma, J., Wohlgemuth,

G., Zocchi, G., Alvarez-Fernández, A., et al. (2010). Changes in the proteomic and metabolic profiles of *Beta vulgaris* root tips in response to iron deficiency and resupply. *BMC Plant Biol.* 10:120. doi: 10.1186/1471-2229-10-120

Ristilä, M., Strid, H., Eriksson, L. A., Strid, A., and Sävenstrand, H. (2011). The role of the pyridoxine (vitamin B_6). biosynthesis enzyme PDX1 in ultraviolet-B radiation responses in plants. *Plant Physiol. Biochem*. 49, 284–292. doi: 10.1016/j.plaphy.2011.01.003

Rodríguez-Celma, J., Lattanzio, G., Grusak, M. A., Abadía, A., Abadía, J., and López-Millán, A. F. (2011a). Root responses of *Medicago truncatula* plants grown in two different iron deficiency conditions: changes in root protein profile and riboflavin biosynthesis. *J. Proteome Res.* 10, 2590–2601. doi: 10.1021/pr2000623

Rodríguez-Celma, J., Vázquez-Reina, S., Orduna, J., Abadía, A., Abadía, J., Álvarez-Fernández, A., et al. (2011b). Characterization of flavins in roots of Fe-deficient strategy I plants, with a focus on *Medicago truncatula*. *Plant Cell Physiol*. 52, 2173–2189. doi: 10.1093/pcp/pcr149

Rodríguez-Celma, J., Lattanzio, G., Jiménez, S., Briat, J.-F., Abadía, J., Abadía, A., et al. (2013a). Changes induced by Fe deficiency and Fe resupply in the root protein profile of a peach-almond hybrid rootstock. *J. Proteome Res*. 12, 1162–1172. doi: 10.1021/pr300763c

Rodríguez-Celma, J., Lin, W.-D., Fu, G.-M., Abadia, J., López-Míllán, A.-F., and Schmidt, W. (2013b). Mutually exclusive alterations in secondary metabolism are critical for the uptake of insoluble iron compounds by *Arabidopsis* and *Medicago truncatula*. *Plant Physiol.* 162, 1473–1485. doi: 10.1104/pp.113.220426

Ruzicka, D. R., Kandasamy, M. K., McKinney, E. C., Burgos-Rivera, B., and Meagher, R. B. (2007). The ancient subclasses of *Arabidopsis* Actin Depolymerizing Factor genes exhibit novel and differential expression. *Plant J.* 52, 460–472. doi: 10.1111/j.1365-313X.2007.03257.x

Samaj, J., Baluska, F., Voigt, B., Schlicht, M., Volkmann, D., and Menzel, D. (2004). Endocytosis, actin cytoskeleton, and signaling. *Plant Physiol.* 135, 1150–1161. doi: 10.1104/pp.104.040683

Sauerwein, M., and Shimomura, K. (1991). Alkaloid production in hairy roots of *Hyoscyamus albus* transformed with *Agrobacterium rhizogenes*. *Phytochemistry* 30, 3277–3280. doi: 10.1016/0031-9422(91)83192-N

Schagerlöf, U., Wilson, G., Hebert, H., Al-Karadaghi, S., and Hägerhäll, C. (2006). Transmembrane topology of FRO2, a ferric chelate reductase from *Arabidopsis thaliana*. *Plant Mol Biol.* 62, 215–221. doi: 10.1007/s11103-006-9015-0

Shin, H., and Brown, R. M. (1999). GTPase activity and biochemical characterization of a recombinant cotton fiber annexin. *Plant Physiol.* 119, 925–934. doi: 10.1104/pp.119.3.925

Shinmachi, F., Hasegawa, I., Noguchi, A., and Yazaki, J. (1997). "Characterization of iron deficiency response system with riboflavin secretion in some dicotyledonous plants," in *Plant Nutrition for Sustainable Food Production and Environment*, eds T. Ando, K. Fujita, T. Mae, H. Matsumoto, S. Mori, and J. Sekiya (Dordecht: Kluwer Academic Publisher), 277–278.

Susin, S., Abian. J., Peleato, M. L., Sanchez-Baeza, F., Abadía, A., Gelpi, E., et al. (1994). Flavin excretion from roots of iron-deficient sugar beet (Beta vulgaris L.). *Planta* 193, 514–519. doi: 10.1007/BF02411556

Sweetlove, L. J., Beard, K. F., Nunes-Nesi, A., Fernie, A. R., and Ratcliffe, R. G. (2010). Not just a circle: flux modes in the plant TCA cycle. *Trends Plant Sci*. 15, 462–470. doi: 10.1016/j.tplants.2010.05.006

Taiz, L., and Zeiger, E. (2002). *Plant Physiology*. Sunderland, MA: Sinauer Associates.

Takahashi, M., Sasaki, Y., Ida, S., and Morikawa, H. (2001). Nitrite reductase gene enrichment improves assimilation of NO_2 in *Arabidopsis*. *Plant Physiol.* 126, 731–741. doi: 10.1104/pp.126.2.731

Thimm, O., Essigmann, B., Kloska, S., Altmann, T., and Buckhout, T. J. (2001). Response of *Arabidopsis* to iron deficiency stress as revealed by microarray analysis. *Plant Physiol.* 127, 1030–1043. doi: 10.1104/pp.010191

Vigani, G. (2012). Discovering the role of mitochondria in the iron deficiency-induced metabolic responses of plants. *J. Plant Physiol.* 169, 1–11. doi: 10.1016/j.jplph.2011.09.008

Vigani, G., Maffi, D., and Zocchi, G. (2009). Iron availability affects the function of mitochondria in cucumber roots. *New Phytol.* 182, 127–136. doi: 10.1111/j.1469-8137.2008.02747.x

Vorwieger, A., Gryczka, C., Czihal, A., Douchkov, D., Tiedemann, J., Mock, H. P., et al. (2007). Iron assimilation and transcription factor controlled synthesis of riboflavin in plants. *Planta* 226, 147–158. doi: 10.1007/s00425-006-0476-9

Walton, N. J., Peerless, A. C., Robins, R. J., Rhodes, M. J., Boswell, H. D., and Robins, D. J. (1994). Purification and properties of putrescine N-methyltransferase from transformed roots of *Datura stramonium* L. *Planta* 193, 9–15. doi: 10.1007/BF00191600

Wang, J., Ruan, S., Wu, W., Xu, X., Wang, Y., and Han, Z.-H. (2010). Proteomics approach to identify differentially expressed proteins induced by iron deficiency in roots of *malus*. *Pak. J. Bot.* 42, 3055–3064.

Weber, K., and Osborn, M. (1969). The reliability of molecular weight determinations by dodecyl sulfate-polyacrylamide gel electrophoresis. *J. Biol. Chem*. 244, 4406–4412.

Wilhelmson, A., Häkkinen, S. T., Kallio, P. T., Oksman-Caldentey, K. M., and Nuutila, A. M. (2006). Heterologous expression of *Vitreoscilla* hemoglobin (VHb). and cultivation conditions affect the alkaloid profile of *Hyoscyamus muticus* hairy roots. *Biotechnol. Prog.* 22, 350–358. doi: 10.1021/bp050322c

Yamaguchi, K. (2011). "Preparation and proteomic analysis of chloroplast ribosomes," in *Chloroplast Research in Arabidopsis*, ed R. P. Javis (New York, NY: Humana Press), 241–264. doi: 10.1007/978-1-61779-237-3_13

Zaharieva, T., Gogorcena, Y., and Abadıa, J. (2004). Dynamics of metabolic responses to iron deficiency in sugar beet roots. *Plant Sci*. 166, 1045–1050. doi: 10.1016/j.plantsci.2003.12.017

Zeef, L. A., Christou, P., and Leech, M. J. (2000). Transformation of the tropane alkaloid-producing medicinal plant *Hyoscyamus muticus* by particle bombardment. *Transgenic Res.* 9, 163–168. doi: 10.1023/A:1008912330067

Zhang, L., Yang, B., Lu, B., Kai, G., Wang, Z., Xia, Y., et al. (2007). Tropane alkaloids production in transgenic *Hyoscyamus niger* hairy root cultures over-expressing putrescine N-methyltransferase is methyl jasmonate-dependent. *Planta* 225, 887–896. doi: 10.1007/s00425-006-0402-1

Zocchi, G. (2006). "Metabolic changes in iron-stressed dicotyledonous plants," in *Iron Nutrition in Plants and Rhizospheric Microorganisms*, eds L. L. Barton and J. Abadía (Dordrecht: Springer), 359–370. doi: 10.1007/1-4020-4743-6_18

Conflict of Interest Statement: The authors declare that the research was conducted in the absence of any commercial or financial relationships that could be construed as a potential conflict of interest.

Received: 17 May 2013; accepted: 06 August 2013; published online: 28 August 2013.

*Citation: Khandakar J, Haraguchi I, Yamaguchi K and Kitamura Y (2013) A small-scale proteomic approach reveals a survival strategy, including a reduction in alkaloid biosynthesis, in Hyoscyamus albus roots subjected to iron deficiency. Front. Plant Sci. **4**:331. doi: 10.3389/fpls.2013.00331*

This article was submitted to Plant Nutrition, a section of the journal Frontiers in Plant Science.

frontiers in
PLANT SCIENCE

ORIGINAL RESEARCH ARTICLE
published: 03 June 2013
doi: 10.3389/fpls.2013.00168

Using μPIXE for quantitative mapping of metal concentration in *Arabidopsis thaliana* seeds

Magali Schnell Ramos[1,2]*, Hicham Khodja[3], Viviane Mary[1] and Sébastien Thomine[1]

[1] Institut des Sciences du Végétal, UPR2355, Centre National de la Recherche Scientifique, Gif-sur-Yvette, France
[2] Chimica Agraria, Dipartimento di Scienze Agrarie e Ambientali, Università degli Studi di Udine, Udine, Italy
[3] Laboratoire d'Etude des Eléments légers, SIS2M, UMR 3299, CEA-CNRS, CEA Saclay, Gif-sur-Yvette, France

Edited by:
Jean-François Briat, Centre National de la Recherche Scientifique, France

Reviewed by:
Stéphane Mari, Institut National pour la Recherche Agronomique, France
Marie-Pierre Isaure, Université de Pau et des Pays de l'Adour and CNRS, France

***Correspondence:**
Magali Schnell Ramos, Chimica Agraria, Dipartimento di Scienze Agrarie e Ambientali, Università degli Studi di Udine, Via delle Scienze 208, 33100 Udine, Italy
e-mail: magali.schnell@uniud.it

Seeds are a crucial stage in plant life. They contain the nutrients necessary to initiate the development of a new organism. Seeds also represent an important source of nutrient for human beings. Iron (Fe) and zinc (Zn) deficiencies affect over a billion people worldwide. It is therefore important to understand how these essential metals are stored in seeds. In this work, Particle-Induced X-ray Emission with the use of a focused ion beam (μPIXE) has been used to map and quantify essential metals in Arabidopsis seeds. In agreement with Synchrotron radiation X-ray fluorescence (SXRF) imaging and Perls/DAB staining, μPIXE maps confirmed the specific pattern of Fe and Mn localization in the endodermal and subepidermal cell layers in dry seeds, respectively. Moreover, μPIXE allows absolute quantification revealing that the Fe concentration in the endodermal cell layer reaches ~800 $\mu g \cdot g^{-1}$ dry weight. Nevertheless, this cell layer accounts only for about half of Fe stores in dry seeds. Comparison between Arabidopsis wild type (WT) and mutant seeds impaired in Fe vacuolar storage (*vit1-1*) or release (*nramp3nramp4*) confirmed the strongly altered Fe localization pattern in *vit1-1*, whereas no alteration could be detected in *nramp3nramp4* dry seeds. Imaging of imbibed seeds indicates a dynamic localization of metals as Fe and Zn concentrations increase in the subepidermal cell layer of cotyledons after imbibition. The complementarities between μPIXE and other approaches as well as the importance of being able to quantify the patterns for the interpretation of mutant phenotypes are discussed.

Keywords: iron, seed, Arabidopsis, μPIXE, elemental mapping, quantitative

INTRODUCTION

Thanks to their redox properties or Lewis acid strength under physiological conditions, iron (Fe), manganese (Mn), copper (Cu), or zinc (Zn) act as major cofactors in many enzymes such as proteases or antioxidant enzymes as well as in electron transfer chains of mitochondrial respiration or chloroplast photosynthesis (Marschner, 2012). While micronutrients are essential at adequate concentrations, excess leads to toxicity. Moreover, certain trace metals such as cadmium (Cd) or mercury (Hg) have no known function as nutrients and are potentially toxic at low concentrations (Clemens, 2006; Clemens et al., 2013). Therefore, mechanisms for tight regulation of metal homeostasis are vital (Kraemer and Clemens, 2006; Marschner, 2012).

Seeds are a crucial stage in the life of a plant. They contain the macro- and micronutrients necessary to initiate the development of a new organism. More specifically, essential micronutrients need to be safely stored and readily remobilized during early germination. Seeds also represent an important source of nutrient for human beings. Fe and Zn deficiencies affect over a billion people worldwide (Murgia et al., 2012). Consequently, studies on seed transition metal content are necessary. Despite its relatively high abundance, Fe availability remains limited for living organisms. In seeds, Fe is stored either as highly bio-available phytoferritins localized in plastids, or as poorly bio-available Fe-phytate salts, localized in vacuolar inclusions called globoids (Harrison and Arosio, 1996; Briat and Lobreaux, 1997; Otegui et al., 2002; Lanquar et al., 2005). The balance between those two forms is different according to plant species and is greatly modified during germination. Besides, in seeds, phytate salts are also the main storage form of potassium (K), magnesium (Mg), calcium (Ca), and Zn (Mikus et al., 1992).

In Arabidopsis, VIT1, a vacuolar Fe transporter required for Fe storage in the vacuole during seed formation, was identified by Kim et al. (2006). Synchrotron radiation X-ray fluorescence (SXRF) tomographic imaging demonstrated that loss of VIT1 function disrupts the cell specific localization of Fe in dry seeds. Whereas Fe is stored in endodermal cells surrounding the provascular tissues in wild type (WT), it co-localizes with Mn in the subepidermal cell layer of *vit1-1* knockout mutant embryos (Kim et al., 2006; Roschzttardtz et al., 2009). Fe mislocalization results in drastically decreased viability of *vit1-1* seedlings under Fe deficiency. While VIT1 mediates Fe influx into the vacuole, NRAMP3 and NRAMP4 metal transporters have been shown to act redundantly to export Fe out of the vacuole (Lanquar et al., 2005). Energy-Dispersive X-ray (EDX) technique indicated that the *nramp3nramp4* double knockout mutant is defective in Fe retrieval from seed vacuolar globoids during germination. As a consequence, *nramp3nramp4* mutant seedlings display an early

developmental arrest when germinated on low Fe. Furthermore, the drastic morphological and biological changes that occur during germination must be accompanied by a relocation of nutrients to the sites where they are required for metabolism. Although several reports have addressed metal patterning in dry seed, the changes in metal localization and their kinetics upon seed germination have not been addressed at the tissue level. Three imaging techniques have been used to investigate Fe distribution in Arabidopsis WT and mutant seeds EDX (Lanquar et al., 2005), SXRF (Kim et al., 2006), and Perls/DAB staining (Roschzttardtz et al., 2009). However, those techniques provided either non-quantitative data (EDX, Perls/DAB) or approximate quantification (SXRF) of metal concentrations in the different seed tissues.

Particle-Induced X-ray Emission induced by a focused ion beam (μPIXE) allows multi-elemental mapping in biological samples with high spatial resolution (1 μm range) and high sensitivity (down to $\mu g \cdot g^{-1}$ range). Importantly, μPIXE technique presents the unique advantage of providing quantitative results when used simultaneously with Rutherford Backscattering (RBS) and Scanning Transmission Ion Microscopy (STIM) analyses (Deves et al., 2005). The combined measurements of trace element amount by PIXE, charge monitoring and organic element determination by RBS and sample local mass determination by STIM are often referred as "fully" quantitative results in the literature in opposition to "semi"-quantitative results obtained by other imaging techniques.

In plants, μPIXE has been used for the localization and quantification of essential macro- and micronutrients in specific tissues and organs such as elemental mapping of buckwheat seeds (Vogel-Mikus et al., 2009), Fe in barley roots (Schneider et al., 2002), Fe and Zn in Phaseolus seeds (Cvitanich et al., 2010, 2011), Cu in *Brassica carinata* leaf and root (Cestone et al., 2012). μPIXE was also used to image and quantify non-essential elements. In the context of environmental contamination, μPIXE was used to study cesium (Cs) in Arabidopsis leaf, stem, and trichome (Isaure et al., 2006), Cd and Ni in soybean seed (Malan et al., 2012), and uranium (U) in leaf and root of oilseed rape, sunflower, and wheat (Laurette et al., 2012). In the context of metal hyperaccumulation, it was used to analyze Cd in leaf and seed of *Thalspi praecox* (Vogel-Mikus et al., 2007, 2008) or nickel (Ni) in *Berkheya coddii* leaves (Budka et al., 2005).

Here, the μPIXE approach was used to quantitatively analyse metal distribution in Arabidopsis seeds. A sample preparation protocol suitable for μPIXE analysis of *Arabidopsis thaliana* dry but also imbibed seeds was established. Analysis of some nutritionally important elements by μPIXE mapping confirmed the previously established pattern in WT dry seed metal distribution, exhibiting Mn accumulation at the abaxial side of cotyledons as well as Fe localization around the provascular tissues. Local Fe, Mn, and Zn concentrations were determined in these tissues in WT and both *nramp3nramp4* and *vit1-1* mutant seeds. Moreover, a comparison between elemental maps obtained with dry or imbibed seeds revealed early changes in metal localization. The μPIXE results are put in perspective with other elemental analysis techniques raising questions regarding the input of element quantification in the interpretation of mutant phenotypes. Finally, μPIXE results obtained for WT dry and imbibed seeds are discussed with respect to the possible use of this technique to study dynamic element redistribution.

MATERIALS AND METHODS

PLANT MATERIAL

Mature (dry) and imbibed seeds of Arabidopsis (*Arabidopsis thaliana* accession Columbia-0) WT, *nramp3nramp4* (*nr3nr4*) and *vit1-1* mutants were used. Generation of both mutants has been described previously in Ravet et al. (2009b) and Kim et al. (2006), respectively. Dry seeds of all genotypes were harvested from plants grown on potting soil (Tonerde PAM argile, Brill France) in a greenhouse under a 16 h photoperiod with regular watering (2–3 times per week). Seeds were imbibed in deionized water on an orbital shaker (40 rotations$\cdot min^{-1}$), under continuous light (60 μmol photon$\cdot m^{-2} \cdot s^{-1}$) at 21°C for 48 h.

AAS ANALYSES OF DRY SEEDS

Three to four replicates of circa 20 mg of dry seeds were digested in 2 ml of 70% nitric acid in a DigiBlock ED36 (LabTech, Italy) at 80°C for 1 h, 100°C for 1 h, and 120°C for 2 h. After dilution to 12 ml with ultrapure water, K, Ca, Mn, Fe, Cu, and Zn contents of the samples were determined by atomic absorption spectrometry using an AA240FS flame spectrometer (Agilent, USA).

SAMPLE PREPARATION FOR μPIXE ANALYSIS

In order to avoid losses of elements and their redistribution in the analysed samples, cryotechniques were used. The seeds were fixed by high pressure cryofixation (Leica EM PACT2, Leica Microsystems, Germany) and stored in liquid nitrogen. Subsequent steps were performed in a cryostat (CM3050-S, Leica Microsystems, Germany) at −30°C: seeds were recovered from their cryofixation container in cold isopentane, embedded in an inert matrix (Tissue-Tek® OCT compound, Sakura Finetek, USA) and cut with a tungsten blade in sections of approximately 30 μm. Sections were individually mounted on a cold aluminium sample holder covered with a pioloform film (1 g pioloform, 75 ml chloroform). Samples were carefully transferred to a freeze-dryer (Alpha 1-4, Christ Martin, Germany), freeze-dried at −10°C, under a vacuum of 0.37 mbar for 48 h and brought back to room temperature (RT) by steps of 5°C per hour. Finally, samples were covered by a second pioloform film and stored in an anhydrous environment at RT until μPIXE analyses. Section integrity of seed sample was verified by putting a few freshly cut sections directly on a microscope slide (Menzel-Gläser SUPERFROST®, Thermo Fisher Scientific, USA) stored in the cryostat. After sectioning, the microscope slides mounted with seed sections were quickly brought to RT in a vacuum desiccator and checked under a light microscope.

MULTI-ELEMENTAL LOCALIZATION BY μPIXE

Microanalyses of Arabidopsis sections were performed at the Saclay nuclear microprobe, France (Khodja et al., 2001). The sample holder with seed sections and reference samples were attached to a motorized vacuum goniometer in the analyzing chamber. After closing the chamber and establishing a vacuum (typically 10^{-6} mbar), rough positioning of the samples was

achieved using an optical camera. The proton beam of 3.0 MeV and 200 pA current was focused down to a $1.5 \times 1.5\,\mu m^2$ spot, used to rapidly scan large areas of the sample and finally adjusted to scan the seed section areas (usually $500 \times 500\,\mu m^2$) during circa 4 h. Simultaneous PIXE, RBS, and STIM analyses were performed. A 40 mm^2-Bruker XFlash SDD detector placed at 75° relative to the beam path and at 21 mm working distance of the scanned sample was used to collect X-rays emitted by non-organic elements. A 50 μm Mylar foil was placed in front of the detector to stop backscattered protons and attenuate X-ray signals from major elements. Backscattered particles were collected by a 180 mm^2-surface barrier detector positioned at 170° and 35 mm from incident beam. Energy-loss maps based on STIM were obtained by collecting scattered particles at 30° using a surface barrier detector located behind the sample. In total, 11 seed sections were analyzed: 5 from WT, 5 from *nramp3nramp4* mutant and 1 from *vit1-1* mutant.

MULTI-ELEMENTAL QUANTIFICATION BY μPIXE

In order to generate μPIXE qualitative elemental images, PIXE spectra of the scanned Arabidopsis sections were processed using RISMIN software (Daudin et al., 2003). Distinct regions of particular interest (ROIs) such as seed morphological structures or areas enriched for one particular element were selected as ROIs on the elemental images and the corresponding X-ray spectra were extracted. Associated RBS and STIM spectra and images were used to assess thickness and matrix composition of the different ROIs using SIMNRA (Mayer, 1999) and a modified version of RISMIN software. Finally, all elemental quantifications were obtained by processing the extracted data using SIMNRA and GUPIX (Campbell et al., 2000) softwares. Concentrations of the elements present in the selected ROIs (whole seed section, Fe- and Mn-enriched areas) are presented, either as elemental concentrations of one representative sample (**Table 2**), or as average elemental concentrations of three to four representative samples (**Figures 5A,B**).

DATA ANALYSES

Average elemental concentrations presented in (**Figures 5A,B**) as well as elemental fractions presented in **Table 3**, were analysed by a Kruskal–Wallis test followed by a Tukey *post-hoc* test for multiple comparisons ($p < 0.05$). For both dry and imbibed seeds, fractions of Fe and Mn that accumulate in their respective enriched areas compared to the whole seed section element content were calculated as followed: [element concentration in enriched area·area of enriched area]/[element concentration in whole seed section·area of whole seed section].

RESULTS

SAMPLE PREPARATION FOR ANALYSES

Seed samples were prepared as recommended in Mesjasz-Przybylowicz and Przybylowicz (2002) and described in Materials and Methods. The chosen section thickness was 30 μm to obtain the best compromise between 3 requirements: (1) analysing a sufficient amount of matter by μPIXE to obtain accurate quantification, (2) the ability to record RBS and STIM complementary signals, and (3) to resolve Arabidopsis seed morphology (30 μm corresponds to circa 2 cell layers). A cryogenic approach was used to prevent element leakage or redistribution within the sample sections (Mesjasz-Przybylowicz and Przybylowicz, 2002). Due to Arabidopsis seed small size, high-pressure freezing was used. In order to confirm that cryosectioning did not alter seed structure, some sections were put aside and directly observed under light microscopy after being rapidly brought back to RT. In agreement with previous reports, Arabidopsis dry seed morphological structure could be clearly defined for 30 μm thick longitudinal and transversal sections (**Figure 1**) (e.g., Vaughan and Whitehouse, 1971). After high-pressure freezing, samples could be either freeze-dried or freeze-substituted as no module for frozen-hydrated state specimen analysis was available (Tylko et al., 2007). Freeze-drying technique has been demonstrated to be neither suitable for observations at the cellular level since it may alter the morphology of the samples, nor for metal speciation since water extraction induces metal speciation artifacts (Sarret et al., 2009). However, freeze-drying is appropriate for elemental mapping, in particular for Fe, at the tissue level and thus, was used in this research (Schneider et al., 2002; Sarret et al., 2013). Furthermore, preliminary tests showed that the substitution of vitrified water by EPOXY resin lead to partial to complete leakage of some elements (data not shown).

ARABIDOPSIS SEED ELEMENTAL DISTRIBUTION USING μPIXE TECHNIQUE

Freeze-dried 30 μm thick sections of *Arabidopsis thaliana* dry and imbibed seeds were analysed by Particle-Induced X-ray Emission induced by a focused ion beam (μPIXE) and elemental images were generated (**Figure 2**). Some macroelements, such as K, and microelements such as Zn are apparently evenly distributed over the dry seed section (**Figure A1**). Mapping of Ca, which is evenly distributed in the embryo and accumulates to a higher level in

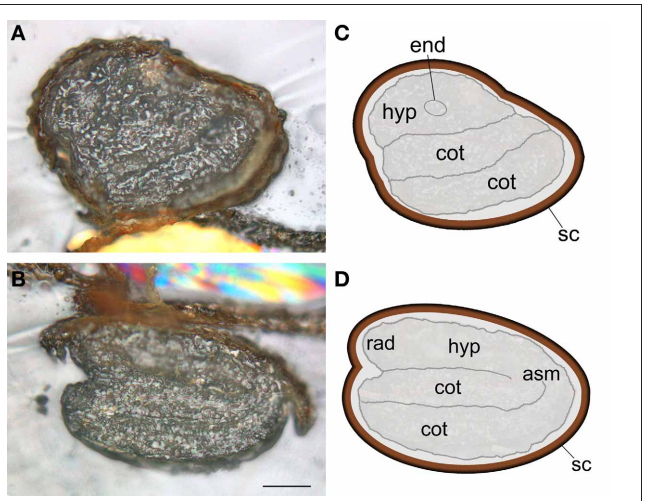

FIGURE 1 | *Arabidopsis thaliana* dry seed structure. Light microscopy images of transversal **(A)** and longitudinal **(B)** sections with respective schematic representations **(C,D)**. Thirty micrometer sections were obtained at −30°C using a cryomicrotome. Scale bar: 100 μm; asm, apical shoot meristem; cot, cotyledon; end, endodermis; hyp, hypocotyl; rad, radicle; sc, seed coat.

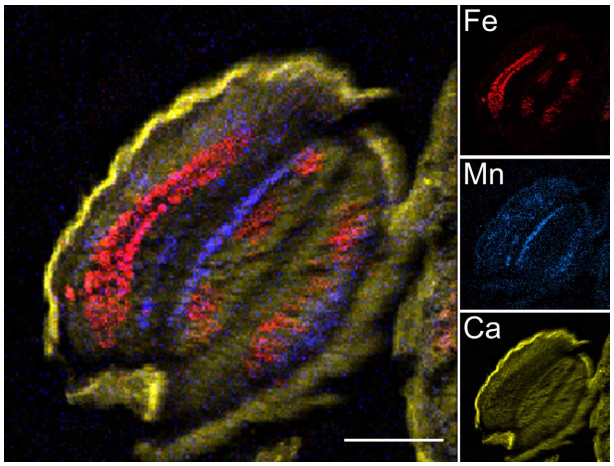

FIGURE 2 | μPIXE elemental reconstituted image of *Arabidopsis thaliana* dry seed section. Total X-ray spectra of areas scanned with 3 MeV proton beam were collected. Specific distributions of Fe, Mn, and Ca in a 30 μm thick longitudinal section of Arabidopsis dry seed are shown overlaid (large image) and separately (small images). False color images and reconstitution were obtained using ImageJ free software. Scale bar: 100 μm; red, Fe; blue, Mn; yellow, Ca.

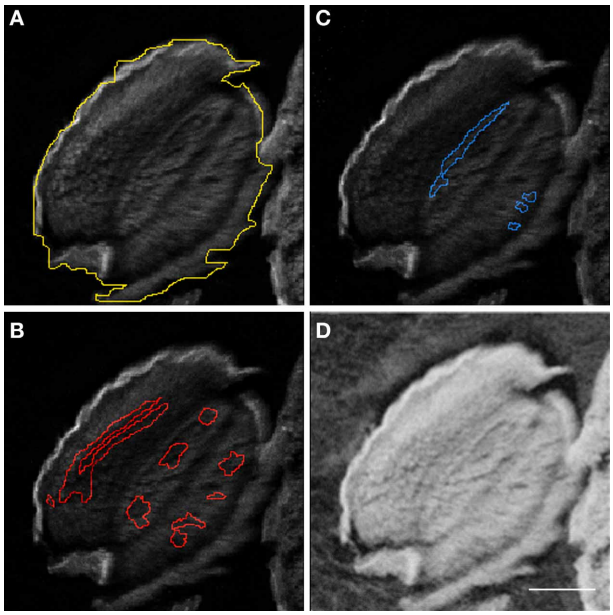

FIGURE 3 | Regions of interest for μPIXE elemental quantification. Element distribution maps allowed selection of regions of interest (ROI). *Arabidopsis thaliana* whole seed **(A)**, Fe- **(B)**, and Mn- **(C)** ROIs are shown using the Ca distribution map as background. The associated STIM image **(D)** shows the local mass of the sample which is necessary for quantification. Scale bar: 100 μm.

the seed coat, allows the visualization of general seed morphology, recalling the light microscopy image (compare **Figures 1B**, **2**, Ca inset). Other elements, such as Fe and Mn, exhibited more specific localization in particular structures, organs or tissues. The elemental map of Fe highlighted the provascular tissue in the cotyledons, hypocotyl and radicle while the Mn elemental map showed concentration on the abaxial (lower) side of the cotyledons (**Figure 2**, Fe and Mn insets). Subsequently, elemental images were used to select regions specifically enriched in Fe or Mn within sections (regions of interest, ROIs; **Figure 3**) to determine the element concentrations within ROIs.

SEED ELEMENTAL CONTENT ANALYSES

Dry seed bulk sample analyses of Arabidopsis WT, *nramp3nramp4* and *vit1-1* were performed by atomic absorption spectroscopy (AAS) to determine seed concentrations of various macro- and microelements (**Table 1**). As previously reported, for all quantified elements, no notable differences were observed between seeds of the different genotypes (Lanquar et al., 2005; Kim et al., 2006; Young et al., 2006). Some seeds of the analysed batches were set aside and analysed by μPIXE to determine elemental concentration in the ROI corresponding to the whole seed section (**Table 1**). In general, seed element average concentrations obtained by μPIXE for each genotype were in the same range of concentrations but usually higher when compared to AAS analyses (**Table 1**). This difference can be partly explained by the huge difference in the sample sizes used for each technique. AAS elemental content analyses of circa 1800 Arabidopsis dry seeds (20 mg aliquots) are compared with μPIXE analyses of few 30 μm-thick seed sections (approximately 2 cell layers). Single seed elemental variability, seed cell heterogeneity as well as low replicate number inherent to the technique have a larger impact on the seed elemental content measured by μPIXE.

Elemental images obtained for the three genotypes showed that Fe distribution is strongly perturbed in *vit1-1* mutant whereas it is not affected in *nramp3nramp4* dry seed at the same stage (**Figure 4**). Similar elemental distribution patterns were obtained using SXRF microtomography (Kim et al., 2006; Donner et al., 2012). ROIs corresponding to whole seed section, Fe- or Mn-enriched areas were selected on the images of each genotype and the corresponding PIXE, RBS, and STIM extracted spectra were analysed (**Table 2**). In WT and *nramp3nramp4* dry seed sections, element quantification within the ROIs confirmed the accumulation of Fe around the provascular tissues of the radicle and cotyledons (from 159 $\mu g \cdot g^{-1}$ dry weight (DW) in the whole section, up to 751 $\mu g \cdot g^{-1}{}_{DW}$ in Fe-enriched area) and of Mn at the abaxial side of cotyledons (from 44 $\mu g \cdot g^{-1}{}_{DW}$ up to 386 $\mu g \cdot g^{-1}{}_{DW}$). Surprisingly, slight accumulation of Zn also occurred in the Fe-enriched area (from 141 $\mu g \cdot g^{-1}{}_{DW}$ up to 311 $\mu g \cdot g^{-1}{}_{DW}$). In *vit1-1* dry seed, Fe (up to 360 $\mu g \cdot g^{-1}{}_{DW}$) and Mn (up to 172 $\mu g \cdot g^{-1}{}_{DW}$) concentrated in a single Fe- and Mn-enriched area at the abaxial side of the cotyledons, while no Fe accumulation around provascular tissues was observed. Here also, Zn (up to 224 $\mu g \cdot g^{-1}{}_{DW}$) exhibited a slight accumulation within the combined enriched area.

The concentrations of Fe, Mn, and Zn in whole longitudinal and transversal seed sections as well as Fe- and Mn-enriched areas from dry and imbibed samples of WT and *nramp3nramp4* were measured. Statistical analyses of the results did not reveal any significant difference between WT and *nramp3nramp4* in any of the ROIs analysed. **Figure 5** shows the average concentrations

Table 1 | AAS analysis and μPIXE quantification of various elements in three different *Arabidopsis thaliana* seed genotypes.

El.	AAS—dry seed				μPIXE—seed section					
	WT	*nr3nr4*	*vit1-1*		WT		*nr3nr4*		*vit1-1*	
	$\mu g \cdot g^{-1}{}_{DW}$	$\mu g \cdot g^{-1}{}_{DW}$	$\mu g \cdot g^{-1}{}_{DW}$	LOD	$\mu g \cdot g^{-1}{}_{DW}$	LOD	$\mu g \cdot g^{-1}{}_{DW}$	LOD	$\mu g \cdot g^{-1}{}_{DW}$	LOD
K	11881 ± 188	11272 ± 463	11909 ± 663	0.008	17648	36	19989	30	27274	52
Ca	4200 ± 208	4590 ± 288	4445 ± 329	0.001	9165	85	11223	82	9757	77
Mn	32 ± 4	34 ± 3	33 ± 3	0.001	44	4	58	4	65	8
Fe	78 ± 5	73 ± 1	80 ± 13	0.006	159	3	189	3	157	8
Cu	10 ± 1	12 ± 1	11 ± 0	0.001	10	2	20	2	68	3
Zn	58 ± 5	59 ± 7	62 ± 5	0.001	141	2	197	2	169	6

AAS of bulk samples. Values are means ± SE (n = 3–4 dry seed batches for each genotypes). X-ray and RBS spectra of the whole seed section were selected using RISMIN software and analysed using SIMNRA and GUPIX softwares. Concentrations of one representative measured sample are presented; LOD, limit of detection of the measurements ($\mu g \cdot g^{-1}{}_{DW}$).

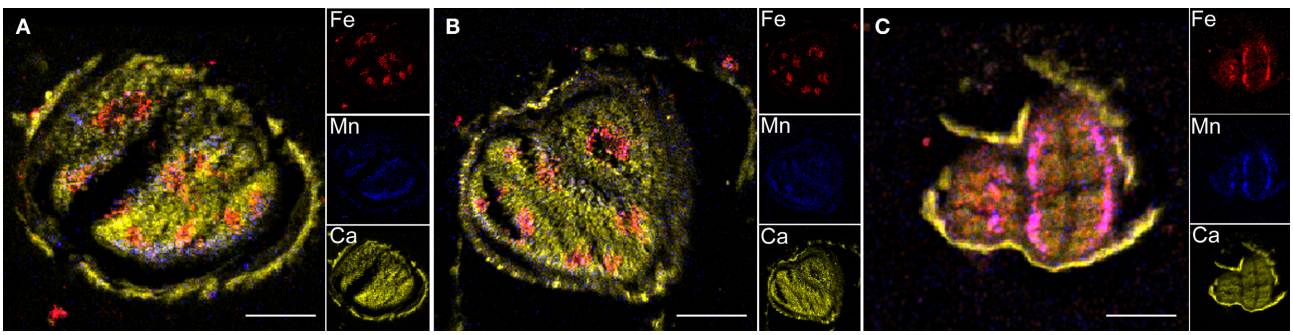

FIGURE 4 | Transversal sections of *Arabidopsis thaliana* dry and imbibed seeds. Specific distributions of Fe, Mn, and Ca in section of WT **(A)** and *nr3nr4* **(B)** imbibed seeds and *vit1-1* **(C)** dry seeds are shown overlaid (large image) and separately (small images). Scale bar: 100 μm; red, Fe; blue, Mn; yellow, Ca.

of Fe, Mn, and Zn in the whole seed section, Fe- and Mn-enriched areas from dry and imbibed samples. In both sample types, Fe (751 ± 134 $\mu g \cdot g^{-1}{}_{DW}$ and 910 ± 74 $\mu g \cdot g^{-1}{}_{DW}$) significantly accumulated in Fe-enriched provascular area as expected (**Figures 5A,B**). As already indicated in **Table 2**, Zn average concentrations were also significantly higher in Fe-enriched areas of both dry and imbibed seeds (298 ± 9 $\mu g \cdot g^{-1}{}_{DW}$ and 284 ± 18 $\mu g \cdot g^{-1}{}_{DW}$). Mn accumulated at significantly higher concentration in the Mn-enriched area at the abaxial side of the cotyledons of both dry and imbibed seeds (**Figures 2**, **4**, **5** and **Table 2**). Interestingly, after 48 h of imbibition, Fe (577 ± 61 $\mu g \cdot g^{-1}{}_{DW}$) and Zn (268 ± 14 $\mu g \cdot g^{-1}{}_{DW}$) were also significantly more concentrated within Mn-enriched area at the abaxial side of the cotyledons. These changes were not detectable visually on the elemental maps.

Finally, combining the relative areas of Fe- and Mn-enriched areas and the metal concentration within these areas, we calculated the fractions of Fe and Mn accumulated in their corresponding enriched areas, namely the provascular tissue region for Fe and the abaxial side of the cotyledons for Mn (**Table 3**). These calculations revealed that at most 69 and 54% of Fe and Mn, respectively, were localized within these areas. A significant fraction of seed Fe and Mn stores is thus localized outside the areas where these metals are the most concentrated.

DISCUSSION

Images of Arabidopsis dry seed sections obtained by μPIXE confirmed Fe, Mn, and Zn distribution patterns observed previously in WT, *nramp3nramp4* and *vit1-1* mutant dry seeds. In addition, valuable information about local metal concentrations could be obtained from the analyses of the different types of spectra collected at the microprobe installation.

μPIXE COMPLEMENTS OTHER TECHNIQUES FOR ELEMENTAL IMAGING OF SEEDS

Fe distribution in Arabidopsis seeds has been already reported using different imaging techniques: EDX microanalysis on a transmission electron microscope (Lanquar et al., 2005), Fe histochemical localization using Perls staining with DAB enhancing (Roschzttardtz et al., 2009) and SXRF microtomography (Kim et al., 2006; Chu et al., 2010; Donner et al., 2012). The respective advantages and limitations of these different approaches have been recently discussed in several reviews (Deves et al., 2005; Lobinski et al., 2006; Ortega et al., 2009; Punshon et al., 2009, 2012; Donner et al., 2012; Sarret et al., 2013).

Combined together, the information about Fe localization obtained by EDX, histochemical staining and SXRF techniques indicate that in Arabidopsis dry seed, Fe is concentrated in the endodermal cells of the embryo and, at subcellular level,

Table 2 | μPIXE quantification of various elements in three different *Arabidopsis thaliana* seed genotypes with emphasis on Fe- and Mn-enriched areas.

El.	Seed section		Fe-enriched area		Mn-enriched area	
	$\mu g \cdot g^{-1}_{DW}$	LOD	$\mu g \cdot g^{-1}_{DW}$	LOD	$\mu g \cdot g^{-1}_{DW}$	LOD
WT						
K	17648	36	21393	71	15851	121
Ca	9165	85	7509	140	9060	155
Mn	44	4	22	12	386	13
Fe	159	3	751	5	90	20
Cu	10	2	9	7	n.d.	n.d.
Zn	141	2	311	11	156	15
nr3nr4						
K	19989	30	19443	81	15582	57
Ca	11223	82	10672	128	10315	90
Mn	58	4	85	13	106	7
Fe	189	3	520	11	218	6
Cu	20	2	24	7	9	5
Zn	197	2	281	11	200	5

El.	Seed section		Fe- and Mn-enriched area	
	$\mu g \cdot g^{-1}_{DW}$	LOD	$\mu g \cdot g^{-1}_{DW}$	LOD
vit1-1				
K	27274	25	22519	52
Ca	9757	63	8826	77
Mn	65	3	172	8
Fe	157	3	360	8
Cu	68	2	60	3
Zn	169	1	224	6

Concentrations of one representative measured sample of dry seed are presented; LOD, limit of detection of the measurements ($\mu g \cdot g^{-1}_{DW}$); n.d., not detected.

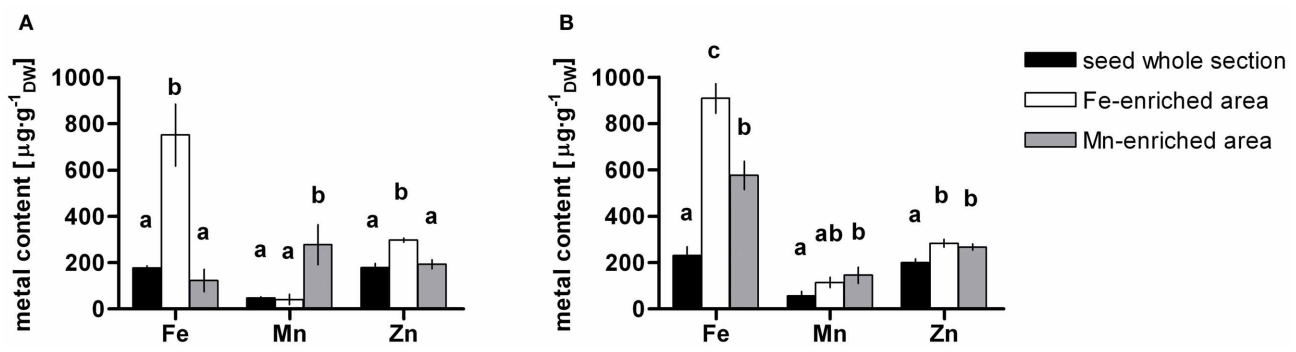

FIGURE 5 | Metal content in *Arabidopsis thaliana* dry (A) and imbibed (B) seed. Fe, Mn, and Zn contents in whole seed section (black bars) as well as in selected Fe- (white bars) and Mn- (gray bars) enriched areas were quantified. Dry seeds were cryofixed directly **(A)** or after 48 h imbibition **(B)**. Values are means ± SE ($n = 3$–4 scanned sections). Different letters denote statistically significant differences based on Kruskal–Wallis test followed by Tukey *post-hoc* test comparing values of dry and imbibed seeds for each metal ($P < 0.05$).

is associated with vacuolar globoids (Lanquar et al., 2005; Kim et al., 2006; Roschzttardtz et al., 2009). Fe concentrations close to 1000 $\mu g \cdot g^{-1}_{DW}$ in provascular tissues were quantified by μPIXE (**Table 2** and **Figure 5**). As globoids represent no more than 10% of the cell volume but constitute the main site for Fe storage in seed cells (Lanquar et al., 2005), endodermal vacuole globoids possibly contain close to 1% Fe. Besides, it has been hypothesized that Fe in the vacuole is mainly stored as Fe^{3+} but this still remains to be demonstrated using XAS (Pich et al., 2001; Otegui et al., 2002). Based on analyses of mutant phenotypes and metal

Table 3 | Fractions of Fe and Mn in *Arabidopsis thaliana* dry and imbibed seed.

El.	Dry		Imbibed	
	% metal	% area	% metal	% area
Fe	50.7 ± 11.2	13.4 ± 5.4	68.9 ± 5.8	17.1 ± 1.5
Mn	30.3 ± 7.0	8.3 ± 6.0	54.4 ± 2.8*	22.4 ± 7.3

The fractions of Fe and Mn quantified in their corresponding enriched areas relative to the whole seed section element content were calculated for dry and imbibed seed. Proportion of each enriched area was also calculated. Values are means ± SE (n = 3–4 scanned sections). Asterisk denotes statistically significant differences based on Mann–Whitney U test ($p < 0.05$).

localization, a mechanism of Fe loading into seed endodermal vacuoles mediated by VIT1 and its release into vasculature cells by NRAMP3 and NRAMP4 during germination has been suggested (Morrissey and Guerinot, 2009; Roschzttardtz et al., 2009). Accordingly, recent data indicated that no more than 5% of total seed Fe is associated with the plastidial ferritin in Arabidopsis seed (Ravet et al., 2009a). Concentration of Fe in endodermal vacuoles in the vicinity of the provascular strand cells allows rapid and easy mobilization of Fe to the growing parts of the seedling during germination. Nevertheless, our determination of Fe fractions in dry seed sections by μPIXE revealed that only about 50% of this metal is actually stored around the seed embryo provascular tissue (**Table 3**). This result indicates that Arabidopsis seeds likely contain two pools of Fe: a pool of concentrated Fe associated to endodermal vacuoles, previously identified by several imaging techniques (Kim et al., 2006; Roschzttardtz et al., 2009), and a less concentrated pool spread in all seed tissues, which have so far been overseen. This finding does not contradict the previous assessments about the central role of vacuoles in Fe storage in Arabidopsis (Roschzttardtz et al., 2009). However, it points to the existence of significant Fe stores outside of the endodermal cells that have to be taken into account in seed Fe storage models. Moreover, our results suggest that, besides VIT1, which is expressed near the vasculature, other vacuolar Fe uptake systems drive Fe accumulation into the vacuoles of other embryo cells.

Imaging techniques also showed heterogeneous distribution of Mn and Zn in plant seeds (Kim et al., 2006; Vogel-Mikus et al., 2007; Takahashi et al., 2009; Cvitanich et al., 2011). Our analyses by μPIXE showed that up to 30% of the Mn present in Arabidopsis dry seed is stored in subepidermal cells. Until now, the transporters which mediate Mn accumulation in those particular cells remain unknown. In the case of Zn, our quantification of Zn in seed sections by μPIXE indicated that Zn is slightly more concentrated in the embryo provascular tissue. This is in agreement with SXRF microtomography of Arabidopsis seeds (Kim et al., 2006) and μPIXE analysis of Phaseolus seeds (Cvitanich et al., 2011).

METAL REDISTRIBUTION IN ARABIDOPSIS SEED DURING GERMINATION MONITORED BY μPIXE

During germination, seed undergoes drastic morphological and biological changes, necessarily inducing a redistribution of macro- and micronutrients (Bewley, 1997; Bolte et al., 2011). Whereas mature dry seed is an excellent plant sample stage for imaging by SXRF or μPIXE due to its natural dehydration state, monitoring of seed germination by X-ray imaging techniques remains challenging. Here, a μPIXE analysis of Arabidopsis WT and *nramp3nramp4* mutant after seed imbibition was undertaken. Whereas EDX microanalyses revealed *nramp3nramp4* mutant defect in Fe remobilization from globoids in 2-day old seedling, μPIXE failed to detect any qualitative or quantitative modification of the Fe pattern between the two genotypes at the same stage (Lanquar et al., 2005). As a matter of fact, elemental maps obtained on dry seeds or after imbibitions did not show any obvious difference. Two hypotheses may account for this apparent discrepancy: (1) even though the experiment was performed after 2 days in both case, seedling development may have been slower in the case of the μPIXE experiment, due to differences in the conditions or seed age. Attempts to analyse sections of WT and mutant seeds at later stage were hampered by difficulties to obtain intact sections; (2) after 2 days, Fe may have been remobilized from the globoids, preventing its detection by EDX, but may have remained in the same tissues explaining why no change could be detected at the μm resolution of the μPIXE analysis.

Nevertheless, quantification of Fe, Mn, and Zn in seed sections by μPIXE indicates significant distribution modifications after 48 h of imbibition. During imbibition, Fe and Zn concentrations increase in subepidermal cells of cotyledons, corresponding to the Mn-enriched area, while the fraction of Mn accumulating in those cells significantly increases from 30 to more than 50% of total Mn content. Although the origin of the metals could not be identified as no significant decrease of Fe, Mn, or Zn occurs in other areas, it is likely that during seed imbibition metals are already beginning to be redistributed toward the future photosynthetic cell layers. As the Fe concentration in the endodermal area is unchanged after imbibition, it is tempting to speculate that the Fe that accumulates in the sub epidermal area originates from the "diluted pool" spread in all seed tissues, which would therefore represent a more loosely bound Fe pool. The endodermal pool would be released at later stages of germination.

In conclusion, our study using μPIXE complemented other approaches to analyse metal distribution in Arabidopsis seeds. This fully quantitative approach revealed unsuspected important Fe stores outside the endodermal cells. Analysis after seed imbibition provided a first glimpse at the rapid metal redistribution that occurs during germination.

ACKNOWLEDGMENTS

The authors are very thankful to Marie Carrière and Béatrice Satiat-Jeunemaître for their help to design and initiate the project and to Spencer Brown for critical reading of the manuscript. They thank Alain Brunelle and Alexandre Seyer for kindly providing access and training on the cryostat. Magali Schnell Ramos and Sébastien Thomine were supported by funding from the CNRS, Italian M.U.R.S.T. (FIRB: "Futuro in Ricerca") and ANR grants ANR-07-BLAN-0110 and ANR-2011-BSV6-00401. This work has benefited from the facilities and expertise of the Imagif Cell Biology Unit of the Gif campus (www.imagif.cnrs.fr) which is supported by the Conseil Général de l'Essonne.

REFERENCES

Bewley, J. D. (1997). Seed germination and dormancy. *Plant Cell* 9, 1055–1066. doi: 10.1105/tpc.9.7.1055

Bolte, S., Lanquar, V., Soler, M. N., Beebo, A., Satiat-Jeunemaitre, B., Bouhidel, K., et al. (2011). Distinct lytic vacuolar compartments are embedded inside the protein storage vacuole of dry and germinating *Arabidopsis thaliana* seeds. *Plant Cell Physiol.* 52, 1142–1152. doi: 10.1093/pcp/pcr065

Briat, J. F., and Lobreaux, S. (1997). Iron transport and storage in plants. *Trends Plant Sci.* 2, 187–193. doi: 10.1016/S1360-1385(97)85225-9

Budka, D., Mesjasz-Przybylowicz, J., Tylko, G., and Przybylowicz, W. J. (2005). Freeze-substitution methods for Ni localization and quantitative analysis in *Berkheya coddii* leaves by means of PIXE. *Nucl. Instrum. Methods Phys. Res. B* 231, 338–344. doi: 10.1016/j.nimb.2005.01.080

Campbell, J. L., Hopman, T. L., Maxwell, J. A., and Nejedly, Z. (2000). Guelph PIXE software package III: alternative proton database *Nucl. Instrum. Methods Phys. Res. B* 170, 193–204. doi: 10.1016/S0168-583X(00)00156-7

Cestone, B., Vogel-Mikus, K., Quartacci, M. F., Rascio, N., Pongrac, P., Pelicon, P., et al. (2012). Use of micro-PIXE to determine spatial distributions of copper in Brassica carinata plants exposed to CuSO 4 or CuEDDS. *Sci. Total Environ.* 427–428, 339–346. doi: 10.1016/j.scitotenv.2012.03.065

Chu, H. H., Chiecko, J., Punshon, T., Lanzirotti, A., Lahner, B., Salt, D. E., et al. (2010). Successful reproduction requires the function of Arabidopsis YELLOW STRIPE-LIKE1 and YELLOW STRIPE-LIKE3 metal-nicotianamine transporters in both vegetative and reproductive structures. *Plant Physiol.* 154, 197–210. doi: 10.1104/pp.110.159103

Clemens, S. (2006). Toxic metal accumulation, responses to exposure and mechanisms of tolerance in plants. *Biochimie* 88, 1707–1719. doi: 10.1016/j.biochi.2006.07.003

Clemens, S., Aarts, M. G. M., Thomine, S., and Verbruggen, N. (2013). Plant science: the key to preventing slow cadmium poisoning. *Trends Plant Sci.* 18, 92–99. doi: 10.1016/j.tplants.2012.08.003

Cvitanich, C., Przybylowicz, W. J., Mesjasz-Przybylowicz, J., Blair, M. W., Astudillo, C., Orlowska, E., et al. (2011). Micro-PIXE investigation of bean seeds to assist micronutrient biofortification. *Nucl. Instrum. Methods Phys. Res. B* 269, 2297–2302. doi: 10.1016/j.nimb.2011.02.047

Cvitanich, C., Przybylowicz, W. J., Urbanski, D. F., Jurkiewicz, A. M., Mesjasz-Przybylowicz, J., Blair, M. W., et al. (2010). Iron and ferritin accumulate in separate cellular locations in Phaseolus seeds. *BMC Plant Biol.* 10:26. doi: 10.1186/1471-2229-10-26

Daudin, L., Khodja, H., and Gallien, J. P. (2003). Development of "position-charge-time" tagged spectrometry for ion beam microanalysis. *Nucl. Instrum. Methods Phys. Res. B* 210, 153–158. doi: 10.1016/S0168-583X(03)01008-5

Deves, G., Isaure, M. P., Le Lay, P., Bourguignon, J., and Ortega, R. (2005). Fully quantitative imaging of chemical elements in *Arabidopsis thaliana* tissues using STIM, PIXE and RBS. *Nucl. Instrum. Methods Phys. Res. B* 231, 117–122. doi: 10.1016/j.nimb.2005.01.044

Donner, E., Punshon, T., Guerinot, M. L., and Lombi, E. (2012). Functional characterisation of metal(loid) processes in planta through the integration of synchrotron techniques and plant molecular biology. *Anal. Bioanal. Chem.* 402, 3287–3298. doi: 10.1007/s00216-011-5624-9

Harrison, P. M., and Arosio, P. (1996). The ferritins: molecular properties, iron storage function and cellular regulation. *Biochim. Biophys. Acta Bioenerg.* 1275, 161–203. doi: 10.1016/j.jsb.2008.12.001

Isaure, M. P., Fraysse, A., Deves, G., Le Lay, P., Fayard, B., Susini, J., et al. (2006). Micro-chemical imaging of cesium distribution in *Arabidopsis thaliana* plant and its interaction with potassium and essential trace elements. *Biochimie* 88, 1583–1590. doi: 10.1016/j.biochi.2006.08.006

Khodja, H., Berthoumieux, E., Daudin, L., and Gallien, J. P. (2001). The Pierre Süe Laboratory nuclear microprobe as a multi-disciplinary analysis tool. *Nucl. Instrum. Methods Phys. Res. B* 181, 83–86. doi: 10.1016/S0168-583X(01)00564-X

Kim, S. A., Punshon, T., Lanzirotti, A., Li, A., Alonso, J. M., Ecker, J. R., et al. (2006). Localization of iron in Arabidopsis seed requires the vacuolar membrane transporter VIT1. *Science* 314, 1295–1298. doi: 10.1126/science.1132563

Kraemer, U., and Clemens, S. (2006). Functions and homeostasis of zinc, copper, and nickel in plants. *Top. Curr. Genet.* 14, 216–271. doi: 10.1007/4735_96

Lanquar, V., Lelievre, F., Bolte, S., Hames, C., Alcon, C., Neumann, D., et al. (2005). Mobilization of vacuolar iron by AtNRAMP3 and AtNRAMP4 is essential for seed germination on low iron. *EMBO J.* 24, 4041–4051. doi: 10.1038/sj.emboj.7600864

Laurette, J., Larue, C., Mariet, C., Brisset, F., Khodja, H., Bourguignon, J., et al. (2012). Influence of uranium speciation on its accumulation and translocation in three plant species: oilseed rape, sunflower and wheat. *Environ. Exp. Bot.* 77, 96–107. doi: 10.1016/j.envexpbot.2011.11.007

Lobinski, R., Moulin, C., and Ortega, R. (2006). Imaging and speciation of trace elements in biological environment. *Biochimie* 88, 1591–1604. doi: 10.1016/j.biochi.2006.10.003

Malan, H. L., Mesjasz-Przybylowicz, J., Przybylowicz, W. J., Farrant, J. M., and Linder, P. W. (2012). Distribution patterns of the metal pollutants Cd and Ni in soybean seeds. *Nucl. Instrum. Methods Phys. Res. B.* 273, 157–160. doi: 10.1016/j.nimb.2011.07.064

Marschner, H. (2012). *Mineral Nutrition of Higher Plants*. San Diego, CA: Academic Press.

Mayer, M. (1999). SIMNRA, a simulation program for the analysis of NRA, RBS and ERDA. *AIP Conf. Proc.* 475, 541–544. doi: 10.1063/1.59188

Mesjasz-Przybylowicz, J., and Przybylowicz, W. J. (2002). Micro-PIXE in plant sciences: present status and perspectives. *Nucl. Instrum. Methods Phys. Res. B* 189, 470–481. doi: 10.1016/S0168-583X(01)01127-2

Mikus, M., Bobak, M., and Lux, A. (1992). Structure of protein bodies and elemental composition of phytin from dry germ of maize (*Zea-Mays L*). *Botanica Acta* 105, 26–33.

Morrissey, J., and Guerinot, M. L. (2009). Iron uptake and transport in plants: the good, the bad, and the ionome. *Chem. Rev.* 109, 4553–4567. doi: 10.1021/cr900112r

Murgia, I., Arosio, P., Tarantino, D., and Soave, C. (2012). Biofortification for combating 'hidden hunger' for iron. *Trends Plant Sci.* 17, 47–55. doi: 10.1016/j.tplants.2011.10.003

Ortega, R., Deves, G., and Carmona, A. (2009). Bio-metals imaging and speciation in cells using proton and synchrotron radiation X-ray microspectroscopy. *J. R. Soc. Interface* 6, S649–S658. doi: 10.1098/rsif.2009.0166.focus

Otegui, M. S., Capp, R., and Staehelin, L. A. (2002). Developing seeds of Arabidopsis store different minerals in two types of vacuoles and in the endoplasmic reticulum. *Plant Cell* 14, 1311–1327. doi: 10.1105/tpc.010486

Pich, A., Manteuffel, R., Hillmer, S., Scholz, G., and Schmidt, W. (2001). Fe homeostasis in plant cells: does nicotianamine play multiple roles in the regulation of cytoplasmic Fe concentration? *Planta* 213, 967–976. doi: 10.1007/s004250100573

Punshon, T., Guerinot, M. L., and Lanzirotti, A. (2009). Using synchrotron X-ray fluorescence microprobes in the study of metal homeostasis in plants. *Ann. Bot.* 103, 665–672. doi: 10.1093/aob/mcn264

Punshon, T., Hirschi, K., Yang, J., Lanzirotti, A., Lai, B., and Guerinot, M. L. (2012). The role of CAX1 and CAX3 in elemental distribution and abundance in Arabidopsis seed. *Plant Physiol.* 158, 352–362. doi: 10.1104/pp.111.184812

Ravet, K., Touraine, B., Boucherez, J., Briat, J. F., Gaymard, F., and Cellier, F. (2009a). Ferritins control interaction between iron homeostasis and oxidative stress in Arabidopsis. *Plant J.* 57, 400–412. doi: 10.1111/j.1365-313X.2008.03698.x

Ravet, K., Touraine, B., Kim, S. A., Cellier, F., Thomine, S., Guerinot, M. L., et al. (2009b). Post-translational regulation of AtFER2 ferritin in response to intracellular iron trafficking during fruit development in Arabidopsis. *Mol. Plant* 2, 1095–1106. doi: 10.1093/mp/ssp041

Roschzttardtz, H., Conejero, G., Curie, C., and Mari, S. (2009). Identification of the endodermal vacuole as the iron storage compartment in the Arabidopsis embryo. *Plant Physiol.* 151, 1329–1338. doi: 10.1104/pp.109.144444

Sarret, G., Smits, E. A. H., Michel, H. C., Isaure, M. P., Zhao, F. J., and Tappero, R. (2013). *Advances in Agronomy*. San Diego, CA: Academic Press.

Sarret, G., Willems, G., Isaure, M. P., Marcus, M. A., Fakra, S. C., Frerot, H., et al. (2009). Zinc distribution and speciation in *Arabidopsis halleri* x *Arabidopsis lyrata* progenies presenting various zinc accumulation capacities. *New Phytol.* 184, 581–595. doi: 10.1111/j.1469-8137.2009.02996.x

Schneider, T., Strasser, O., Gierth, M., Scheloske, S., and Povh, B. (2002). Micro-PIXE investigations of apoplastic iron in freeze-dried root cross-sections of soil grown barley. *Nucl. Instrum. Methods Phys. Res. B* 189, 487–493. doi: 10.1016/S0168-583X(01)01129-6

Takahashi, M., Nozoye, T., Kitajima, N., Fukuda, N., Hokura, A., Terada, Y., et al. (2009). *In vivo* analysis of metal distribution and expression of metal transporters in rice seed during germination process by microarray and X-ray Fluorescence Imaging of Fe, Zn, Mn, and Cu. *Plant Soil* 325, 39–51. doi: 10.1007/s11104-009-0045-7

Tylko, G., Mesjasz-Przybylowicz, J., and Przybylowicz, W. J. (2007). In-vacuum micro-PIXE analysis of biological specimens in frozen–hydrated state. *Nucl. Instrum. Methods Phys. Res. B* 260, 141–148. doi: 10.1016/j.nimb.2007.02.017

Vaughan, J. G., and Whitehouse, J. M. (1971). Seed structure and the taxonomy of the Cruciferae. *Bot. J. Linn. Soc.* 64, 383–409. doi: 10.1111/j.1095-8339.1971.tb02153.x

Vogel-Mikus, K., Pelicon, P., Vavpetic, P., Kreft, I., and Regvar, M. (2009). Elemental analysis of edible grains by micro-PIXE: common buckwheat case study. *Nucl. Instrum. Methods Phys. Rev. B* 267, 2884–2889. doi: 10.1016/j.nimb.2009.06.104

Vogel-Mikus, K., Pongrac, P., Kump, P., Necemer, M., Simcic, J., Pelicon, P., et al. (2007). Localisation and quantification of elements within seeds of Cd/Zn hyperaccumulator *Thlaspi praecox* by micro-PIXE. *Environ. Pollut.* 147, 50–59. doi: 10.1016/j.envpol.2006.08.026

Vogel-Mikus, K., Regvar, M., Mesjasz-Przybylowicz, J., Przybylowicz, W. J., Simcic, J., Pelicon, P., et al. (2008). Spatial distribution of cadmium in leaves of metal hyperaccumulating *Thlaspi praecox* using micro-PIXE. *New Phytol.* 179, 712–721. doi: 10.1111/j.1469-8137.2008.02519.x

Young, L. W., Westcott, N. D., Attenkofer, K., and Reaney, M. J. T. (2006). A high-throughput determination of metal concentrations in whole intact *Arabidopsis thaliana* seeds using synchrotron-based X-ray fluorescence spectroscopy. *J. Synchrotron. Radiat.* 13, 304–313. doi: 10.1107/S0909049506019571

Conflict of Interest Statement: The authors declare that the research was conducted in the absence of any commercial or financial relationships that could be construed as a potential conflict of interest.

Received: 05 March 2013; paper pending published: 21 March 2013; accepted: 13 May 2013; published online: 03 June 2013.

Citation: Schnell Ramos M, Khodja H, Mary V and Thomine S (2013) Using μPIXE for quantitative mapping of metal concentration in Arabidopsis thaliana seeds. Front. Plant Sci. ***4****:168. doi: 10.3389/fpls.2013.00168*

This article was submitted to Frontiers in Plant Nutrition, a specialty of Frontiers in Plant Science.

APPENDIX

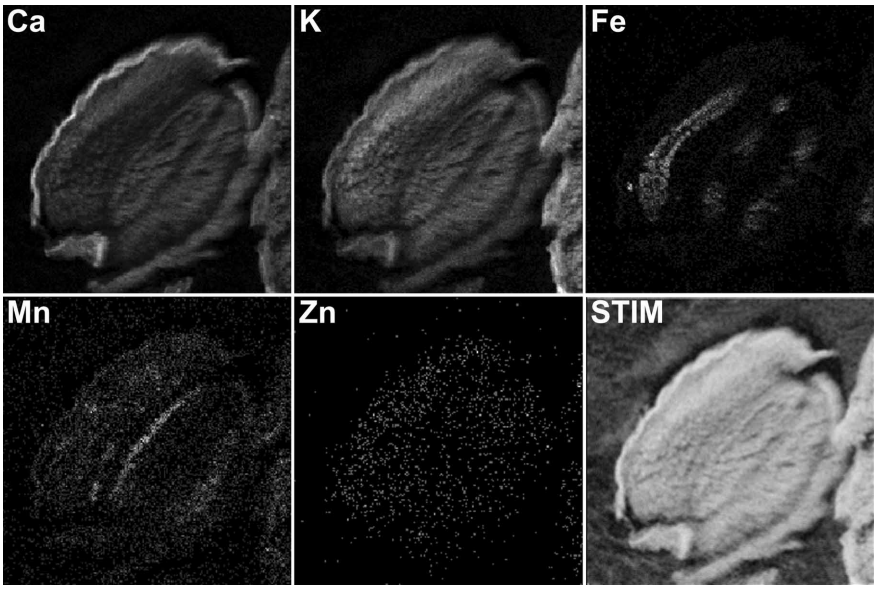

FIGURE A1 | μPIXE elemental reconstituted image of *Arabidopsis thaliana* dry seed section. Total X-ray spectra of areas scanned with 3 MeV proton beam were collected. Specific distributions of Ca, K, Fe, Mn, and Zn in a 30 μm thick longitudinal section of Arabidopsis dry seed are separately. The associated STIM image shows the local mass of the sample. Scale bar: 100 μm.

frontiers in
PLANT SCIENCE

ORIGINAL RESEARCH ARTICLE
published: 06 September 2013
doi: 10.3389/fpls.2013.00350

New insights into Fe localization in plant tissues

Hannetz Roschzttardtz†, Geneviève Conéjéro, Fanchon Divol†, Carine Alcon, Jean-Luc Verdeil†, Catherine Curie and Stéphane Mari*

Biochimie et Physiologie Moléculaire des Plantes, Centre National de la Recherche Scientifique, Institut National pour la Recherche Agronomique, Laboratoire de Biochimie et Physiologie Moléculaire des Plantes, INRA/SupAgro,Université Montpellier 2, Montpellier, France

Edited by:
Katrin Philippar, Ludwig-Maximilians-University Munich, Germany

Reviewed by:
Takanori Kobayashi, Ishikawa Prefectural University, Japan
James Stangoulis, Flinders University, Australia

***Correspondence:**
Stéphane Mari, Institut National pour le Recherche Agronomique, Laboratoire de Biochimie et Physiologie Moléculaire des Plantes, INRA/SupAgro, place Viala, bâtiment 7, Montpellier, F-34060, France
e-mail: mari@supagro.inra.fr

†Present address:
Hannetz Roschzttardtz, Department of Botany, University of Wisconsin-Madison, Madison, USA; Fanchon Divol and Jean-Luc Verdeil,Centre de Coopération Internationale en Recherche Agronomique et Développement, Montpellier, France

Deciphering cellular iron (Fe) homeostasis requires having access to both quantitative and qualitative information on the subcellular pools of Fe in tissues and their dynamics within the cells. We have taken advantage of the Perls/DAB Fe staining procedure to perform a systematic analysis of Fe distribution in roots, leaves and reproductive organs of the model plant *Arabidopsis thaliana*, using wild-type and mutant genotypes affected in iron transport and storage. Roots of soil-grown plants accumulate iron in the apoplast of the central cylinder, a pattern that is strongly intensified when the citrate effluxer FRD3 is not functional, thus stressing the importance of citrate in the apoplastic movement of Fe. In leaves, Fe level is low and only detected in and around vascular tissues. In contrast, Fe staining in leaves of iron-treated plants extends in the surrounding mesophyll cells where Fe deposits, likely corresponding to Fe-ferritin complexes, accumulate in the chloroplasts. The loss of ferritins in the *fer1,3,4* triple mutant provoked a massive accumulation of Fe in the apoplastic space, suggesting that in the absence of iron buffering in the chloroplast, cells activate iron efflux and/or repress iron influx to limit the amount of iron in the cell. In flowers, Perls/DAB staining has revealed a major sink for Fe in the anthers. In particular, developing pollen grains accumulate detectable amounts of Fe in small-size intracellular bodies that aggregate around the vegetative nucleus at the binuclear stage and that were identified as amyloplasts. In conclusion, using the Perls/DAB procedure combined to selected mutant genotypes, this study has established a reliable atlas of Fe distribution in the main Arabidopsis organs, proving and refining long-assumed intracellular locations and uncovering new ones. This "iron map" of Arabidopsis will serve as a basis for future studies of possible actors of iron movement in plant tissues and cell compartments.

Keywords: iron, Arabidopsis, root, chloroplast, ferritin, pollen, amyloplast, mitochondria

INTRODUCTION

Iron (Fe) is an essential metal that plays a central role in many cellular mechanisms. The transition between two redox states, ferrous and ferric iron, involving the gain or loss of one electron, is a key feature for a wide variety of reactions requiring Fe, such as the electron transport chains of the photosynthesis or respiration, the synthesis of nucleotides and chlorophyll. Plants, as sessile organisms, have to continuously adapt to changing conditions. Regarding Fe, dicotyledonous plants such as *Arabidopsis thaliana* have developed efficient strategies to acquire Fe from the soil, where the availability of this metal is often extremely low, by the expression of the root ferric chelate reductase encoded by FRO2 and the Fe^{2+} transporter encoded by IRT1 (Eide et al., 1996; Robinson et al., 1999; Vert et al., 2002). In the meantime, Fe excess can be harmful and induce oxidative stress due to the high reactivity of Fe^{2+} with O_2 to produce reactive oxygen species. When challenged with high Fe concentrations, plants induce the expression of ferritins (Lobreaux et al., 1992). Ferritins are plastidial proteins with the capacity of complexing several thousands of Fe atoms when associated in 24-mer multimers. By analogy with animal systems, plant ferritin was thought to play a key role in buffering Fe excess in plants (Briat and Lobreaux, 1998; Briat and Lebrun, 1999). The function of ferritins may be more complex since these proteins have recently been shown to play a more direct role in the protection against oxidative damage (Ravet et al., 2009). Overall, plants have to maintain a strict Fe homeostasis to achieve proper growth and development. This is achieved through the tight regulation of the physiological functions of root absorption, long distance circulation, storage and remobilization.

Many genes involved in Fe homeostasis have been identified by genetic or transcriptomic approaches. Over the last 15 years, a wealth of important advances has been obtained to understand the mechanism of Fe homeostasis, including the identification of molecular actors of Fe transport, circulation and sequestration. On the contrary, the precise localization of the Fe pools as well as the dynamics of these pools at the tissue, cellular and sub-cellular levels remain elusive.

In roots, the apoplast has been proposed to play an important role in the storage of Fe following absorption (Bienfait et al., 1985). Although it has been shown biochemically, by reduction and complexation, that the Fe binding and exchanging capacities of the apoplast can be extremely high, these measurements do not reflect the real quantity of apoplastic Fe found in roots of plants grown in soil (Strasser et al., 1999). Beside the biochemical approach described by Bienfait et al. (1985), Fe can also be detected by histochemical staining with the Perls reagent. Specific

for Fe^{3+}, the Perls staining procedure was a valuable tool to show that roots of FRD3 mutant plants, impaired in citrate loading in the xylem, accumulated high amounts of Fe in the central cylinder, in both Arabidopsis and rice mutant genotypes (Green and Rogers, 2004; Yokosho et al., 2009). However, the spatial resolution of the Perls images was not high enough to identify Fe location at the cellular or the sub-cellular level in these roots.

In leaves it is predictable that an important portion of Fe will be located in chloroplasts, since a complete electron transfer chain contains 22 atoms of Fe (Wollman et al., 1999). It could thus be expected that Fe would be evenly distributed in the leaf mesophyll tissues. Actually, several studies have reported that Fe is highly concentrated in the vasculature of leaves from Arabidopsis (Stacey et al., 2008), peach-almond hybrids (Jimenez et al., 2009) and tobacco (Takahashi et al., 2003). In contrast, by performing sub-cellular fractionation and organelle purification of Arabidopsis leaves, approximately 70% of the total Fe measured was found in the chloroplastic fraction, of which one half was attributed to the thylakoids (Shikanai et al., 2003). Overall, clear information on the localization of Fe pools in leaves, at the cellular and sub-cellular levels is still missing. The discrepancies between the reports cited above may be due to (i) the complexity of the organ in terms of cell types, and (ii) the technical bias such as the low penetration of Perls in hydrophobic tissues or substantial metal loss during organelle fractionation.

The Arabidopsis embryo has recently emerged as an ideal model to study iron distribution and localization. The three dimensional imaging of metals in seeds, obtained by micro X-ray fluorescence (μXRF) and tomography, beautifully showed the specific accumulation of Fe around the pro-vascular system of the embryo, whereas manganese (Mn) was concentrated in the abaxial part of the cotyledons and zinc (Zn) uniformly distributed in all embryonic cells (Kim et al., 2006). This pattern of Fe was further shown to depend on the activity of the tonoplastic iron transporter VIT1, since in a *vit1* knockout mutant the vascular distribution was abolished. To reach a sub-cellular resolution, Energy Dispersive X-ray microanalysis (EDX) and inelastic scattered microscopy techniques were used (Lanquar et al., 2005). The authors have identified a Fe pool in globoid structures that are engulfed in the vacuoles (Lanquar et al., 2005). Furthermore, this Fe pool was shown to be remobilized from the vacuoles during germination by the efflux transport activity of the NRAMP3 and NRAMP4 tonoplastic proteins (Lanquar et al., 2005). More recently, we have reported the development of a highly sensitive histochemical staining of Fe that combines Perls staining with a second step of intensification with diamino benzidine (DAB) and H_2O_2 (Roschzttardtz et al., 2009). With this simple and quick method (termed Perls/DAB from now on) we have shown that both Fe2+ and Fe3+ could be detected, with a definition and sensitivity comparable to μXRF (Roschzttardtz et al., 2009). The problems of dye penetration in tissues were overcome by applying the staining procedure directly on the histological sections, hence dramatically increasing the image resolution, although in this case the loosely bound iron forms could be washed away and lost during fixation and dehydration steps (Roschzttardtz et al., 2011a).

In Arabidopsis embryos, a detailed histological analysis with Perls/DAB, combined with suited developmental mutants, enabled to establish that the Fe accumulated around the provascular system was in fact located in a single cell layer corresponding to the endodermis. Moreover, we could show that in endodermal cells Fe was located within the vacuoles, most likely in the globoid structures described above. This vacuolar storage of iron is not a general feature of seeds. We have recently shown that in pea embryos an important pool of Fe is actually located in the nucleus, the highest local concentration of Fe being in the nucleolus (Roschzttardtz et al., 2011a). This unexpected discovery could actually be extended to many cell types in different species, uncovering a potential new role of Fe in the nucleolus.

Besides providing basic information on the localization of an essential metal in plant cells, the different reports on embryo Fe localization have illustrated convincingly the pivotal contribution of imaging approaches to the comprehension of the function of genes (VIT1, NRAMP3, NRAMP4) that would not have been possible otherwise. However, basic questions remain unaddressed, such as to what extent apoplastic and vacuolar compartments can buffer Fe, how much Fe is located in plastids and mitochondria, or have other cellular compartments been completely overlooked in terms of Fe storage?

Our previous work has illustrated the power of the Perls/DAB staining method to pinpoint Fe-containing compartments in plant cells. We therefore, sought to extend the use of the Perls/DAB method to the rest of the plant, in order to establish an atlas of Fe distribution and localization in the model plant Arabidopsis. Here we report on Fe distribution in roots, leaves and flowers with a particular emphasis on pollen grains. In order to avoid potential artifacts originating from the source of iron in the growth medium, the plants were only grown on soil. Apart from wild-type plants, two mutants were included in this study, *frd3*, impaired in Fe translocation from roots to shoots and the triple *fer1,3,4* mutant, devoid of ferritin proteins in leaves (Ravet et al., 2008, 2009).

MATERIALS AND METHODS

PLANT MATERIAL AND GROWTH CONDITIONS

Arabidopsis thaliana plants were grown on soil (Humin Substrate N2 Neuhaus; Klasmann-Deilmann, Geeste, Germany) in a greenhouse at 23°C. The plants were irrigated with H_2O or supplemented with iron (irrigation with 2 mM FeEDDHA for 48 h), as indicated in the legend of each Figure. The genotypes used in this study were Col-0 (wild-type), the triple ferritin mutant *atfer1,3,4* (Ravet et al., 2008) and the *frd3-7* mutant (Roschzttardtz et al., 2011b). The *atfer1,3,4* mutant is devoid of ferritin proteins in all plant organs except in seeds and has no macroscopic phenotype in standard conditions, although the mutant plants are more sensitive to oxidative stress (Ravet et al., 2008). The *frd3* mutant, severely impaired in root-to-shoot translocation of Fe, accumulates high amounts of Fe in the stele (Green and Rogers, 2004; Durrett et al., 2007).

HISTOCHEMICAL STAINING OF Fe WITH THE PERLS/DAB PROCEDURE

For organ staining, the flowers were vacuum infiltrated with equal volumes of 4% (v/v) HCl and 4% (w/v) K-ferrocyanide (Perls

stain solution) for 15 min and incubated for 30 min at room temperature (Stacey et al., 2008). The DAB intensification was performed according to Roschzttardtz et al. (2009). After washing with distillated water, the flowers were incubated in a methanol solution containing 0.01 M NaN_3 and 0.3% (v/v) H_2O_2 for 1 h, and then washed with 0.1 M phosphate buffer (pH 7.4). For the intensification reaction the flowers were incubated between 10 and 30 min in a 0.1 M phosphate buffer (pH 7.4) solution containing 0.025% (w/v) DAB (tetrahydrochloride, Sigma, St Louis, Mo, USA), 0.005% (v/v) H_2O_2, and 0.005% (w/v) $CoCl_2$*$6H_2O$ (intensification solution). Rinsing with distilled water stopped the reaction.

For the *in situ* Perls/DAB/H_2O_2 intensification, different organs were vacuum infiltrated with the fixation solution containing 2% (w/v) paraformaldehyde, 1% (v/v) glutaraldehyde, 1% (w/v) caffeine in 100 mM phosphate buffer (pH 7) for 30 min and incubated for 15 h in the same solution. For leaves, the fixation solution alos contained 0.01% (v/v) triton X-100. The roots were previously rinsed with distilled water and traces of soil were eliminated using a binocular magnifying lens. The fixed samples were washed with 0.1 M Na-phosphate buffer (pH 7.4) three times, and dehydrated in successive baths of 50, 70, 90, 95, and 100% Ethanol, butanol/ethanol 1:1 (v/v) and 100% butanol. Then, the tissues were embedded in the Technovit 7100 resin (Kulzer) according to the manufacturer's instructions and thin sections (3 μm) were cut. The sections were deposited on glass slides that were incubated for 45 min in Perls stain solution. The intensification procedure was then applied as described above.

FERRITIN INMUNOLOCALIZATION

The rosette leaves from 3 week-old plants grown in greenhouse were vacuum infiltrated with 4% (w/v) paraformaldehyde in 10 mM PBS pH 7.2 buffer (7 mM $NaHPO_4$, 3 mM NaH_2PO_4, 120 mM NaCl, 2.7 mM KCl) for 1 h and incubated overnight in the same solution. The samples were washed with 100 mM glycine in 10 mM phosphate buffer (pH 7.5) three times, and dehydrated in successive baths of 50, 70, 95, and 100% ethanol, butanol/ethanol 1:1 (v/v), and 100% butanol. The tissue embedding was performed with successive baths of increasing concentrations of Safesolv (Labonord, France) in butanol and then with Safesolv/Paraplast pura wax (Parrafin X-TRA, McCormick Scientific) baths at increasing pure wax concentration. Paraplast blocks were cut with a razor blade at 8 μm thickness (Leica microtome RM 2265). The cross sections were transferred on silanized slides (DakoCytomation, http://www.dako.com) and completely dried. The samples were then dewaxed and rehydrated following the converse steps. After blocking overnight by incubation with 5% BSA (w/v) in PBS, the samples were treated with trypsin (0.1%) for 10 min at room temperature, and washed in PBS (2 × 5 min). Trypsine activity was inhibited by adding trypsin inhibitor (0.05%) during 5 min at room temperature and washed in PBS (2 × 10 min). After overnight incubation (4°C) with rabbit anti-Ferritin polyclonal antibody (1/500), the sections were washed with PBS (3 × 10 min) and incubated with anti-rabbit IgG F(ab')$_2$ fragment conjugated to the Alexa Fluor 488 fluorochrome (Invitrogen) for 1 h at room temperature in the dark. After washing in PBS (3 × 10 min), the sections were incubated with DAPI solution staining during 10 min at room temperature. After washing in PBS (3 × 10 min), the sections were mounted in Mowiol anti-fading medium and kept at 4°C until analyzed.

LASER SCANNING CONFOCAL MICROSCOPY

The microscope imaging was performed in Montpellier RIO Imaging Platform (http://www/mri/cnrs.fr) with a confocal microscope (LSM 510, Meta; Carl Zeiss MicroImaging, http://www.zeiss.de). An Argon laser at 488 nm provided excitation for the Alexa 488, and 405 nm was used for DAPI staining. The fluorescence emission signals were detected in Multi Track using a band-pass filter of 505–530 nm for the Alexa Fluor 488, a long-pass filter of 650 nm for the far-red autofluorescence of the chloroplast and a band-pass filter of 420–480 nm for DAPI. The sections were observed with a x63 oil Zeiss objective. Pictures were processed using the Zeiss LSM Image Browser software.

MITOCHONDRIA STAINING WITH DiOC6

Thin sections of resin-embedded anthers (2 μm thick) were stained with 3,3′-Dihexyloxacarbocyanine Iodide (DiOC6) as previously described (Nagata et al., 2000). Sections were incubated with 100 μg of DiOC6 per mL of ethanol for 1 min, rinsed with 50% (v:v) ethanol for 1 min and with distilled water for 1 min. The sections were then mounted in Mowiol anti-fading medium and kept at 4°C until analyzed. Observations were realized with an epifluorescence microscope (Olympus BX61, Ex = 470 nm ± 20, dichroïc mirror 495 nm, Em = 500–530 nm).

POLYSACCHARIDE STAINING WITH PERIODIC ACID-SCHIFF REAGENT

Thin sections of resin-embedded anthers (2 μm thick) were incubated 10 min in 1% (w/v) periodic acid solution and then rinsed with distilled water. Subsequently, the sections were stained with Schiff's reagent (Labonord, France) for 20 min and rinsed rapidly once with 0.25% (w/v) sodium metabisulfite, 0.05 N HCl, followed by once with distilled water, and observed under a light microscope.

RESULTS

IRON DISTRIBUTION IN ROOTS

Once absorbed in root epidermal cells by the IRT1 ferrous iron transporter, iron must be translocated to the shoot through the vascular system. In order to determine where iron is located during this process, roots of Arabidopsis plants grown in soil were stained with Perls/DAB, which specifically stains iron (Roschzttardtz et al., 2009). Although staining intensity varied from root to root (data not shown) we observed that Fe accumulated in the stele (**Figure 1A**). The staining appeared consistently higher around the pericycle cells and the xylem tracheary elements. We also used a genetic model for iron accumulation in the root, the *frd3* mutant, which had been reported to accumulate high levels of iron in the root vascular region (Green and Rogers, 2004). FRD3 encodes a membrane protein that controls citrate loading of the xylem (Rogers and Guerinot, 2002; Green and Rogers, 2004; Durrett et al., 2007) To visualize more precisely the impact of the loss of FRD3 on the distribution of iron, root sections of *frd3-7* grown in soil were stained with Perls/DAB. As in WT roots, Fe staining was restricted to the vascular tissue,

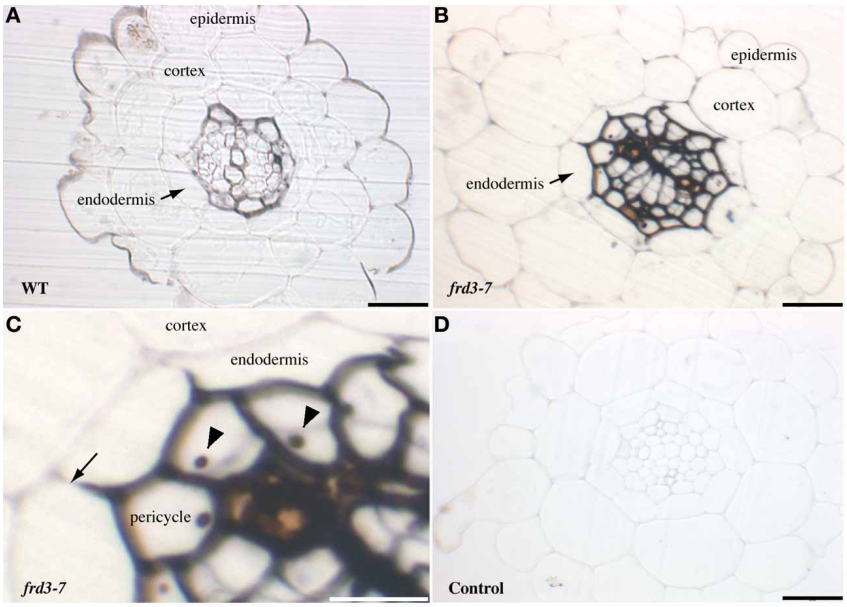

FIGURE 1 | Iron detection in Arabidopsis roots. Sections of 4-week old WT **(A)** or *frd3-7* **(B–D)** mutant plants stained with Perls/DAB. Panel **(C)** corresponds to a magnified image of panel **(B)**, both showing iron restriction within the boundary of the Casparian strip (arrow), nucleoli are indicated by arrowheads. **(D)**, control section stained with DAB without previous Perls reaction. Scale bars: 50 μm **(A,B,D)** or 25 μm **(C)**.

however, the intensity of the signal was dramatically increased compared to WT (**Figures 1B,C**). These results are compatible with the current hypothesis that in the absence of citrate efflux activity in the xylem parenchyma cells, iron is prone to precipitation and is retained in the apoplastic compartment. Interestingly, iron staining in *frd3* roots outlined exactly the inner most half of the endodermal cells, thus revealing the role of the casparian strip in restraining apoplastic Fe in the inner layers of the root (**Figure 1C**). Beside the cell wall compartment, some pericyle cells contained a Fe-rich structure that most likely corresponded to the nucleolus (**Figure 1C**).

IRON DISTRIBUTION IN LEAVES

The chloroplast is a well-known sink compartment for iron since each chain of electron transport contains as many as 22 Fe atoms that are used as cofactors. Indeed, iron deficiency impairs photosynthesis and provokes a characteristic chlorosis of the leaves. Moreover, the ubiquitous storage protein Ferritin is located in plastids in plants where it accumulates in response to iron overload. Although it is assumed, for these reasons, that the chloroplast represents an important iron storage compartment in the leaf, little is known about iron localization in this organ.

Rosette leaves of 4 week-old plants grown in soil were used to visualize the main iron pools by Perls/DAB staining, either in normal iron (irrigation with water) or in iron excess (irrigation with 2 mM FeEDDHA for 48 h) conditions. Since previous reports indicated that Fe was more concentrated around the veins, we tried to realize longitudinal/tangential sections in order to have more informative pictures of the vascular system and the surrounding cells. All the leaf sections presented (**Figures 2–4**) correspond to the spongy mesophyll region of the leaves, where round cells are loosely arranged, with numerous air spaces. Leaf thin sections of plants grown on standard Fe exhibited a fuzzy staining in the chloroplasts of some of the mesophyll cells, as well as in the vasculature at the level of the xylem vessels and neighboring parenchyma cells (**Figures 2A,C**). No staining was detected in the control slide without Perls (**Figures 2E,F**). Leaves treated with iron showed a stronger staining in the plastids with defined black dots within the organelle indicating the presence of elevated iron concentration (**Figures 2B,D**). In addition, Fe excess triggers the appearance of numerous dots of Fe in parenchyma cells of the vasculature region (**Figure 2B**). Because the ferritin protein is accumulated to buffer Fe in excess conditions, we tested whether Fe distribution was altered in the *Atfer134* triple mutant that retains no detectable ferritins in leaves (Ravet et al., 2008). *Atfer134* leaf sections prepared from plants grown on Fe excess showed a large quantity of iron in plastids, compared to optimal Fe plants that did not show detectable staining of Fe (**Figures 3A,B**). Moreover, the Fe-rich dots observed in wild-type plastids and in the vascular parenchyma were absent in *Atfer1,3,4* (**Figures 3B,D**). These results strongly suggest that Perls/DAB detects Fe-ferritin in leaves in two locations, in the chloroplast of mesophyll cells and in xylem parenchyma cells in a sub-cellular compartment that remains to be identifed. Interestingly, the *Atfer134* mutant accumulated a dramatic amount of iron in the extracellular space, suggesting a profound effect of the loss of ferritin on iron homeostasis in leaf cells (**Figures 3B,D**).

To further support the view that Perls/DAB-stained dots in mesophyll chloroplasts and in vasculature cells are Fe-ferritin complexes, we performed inmunolocalization of ferritins in rosette leaves of plants treated or not with FeEDDHA (**Figure 4**). No signal was detected in *Atfer134* even in iron excess conditions

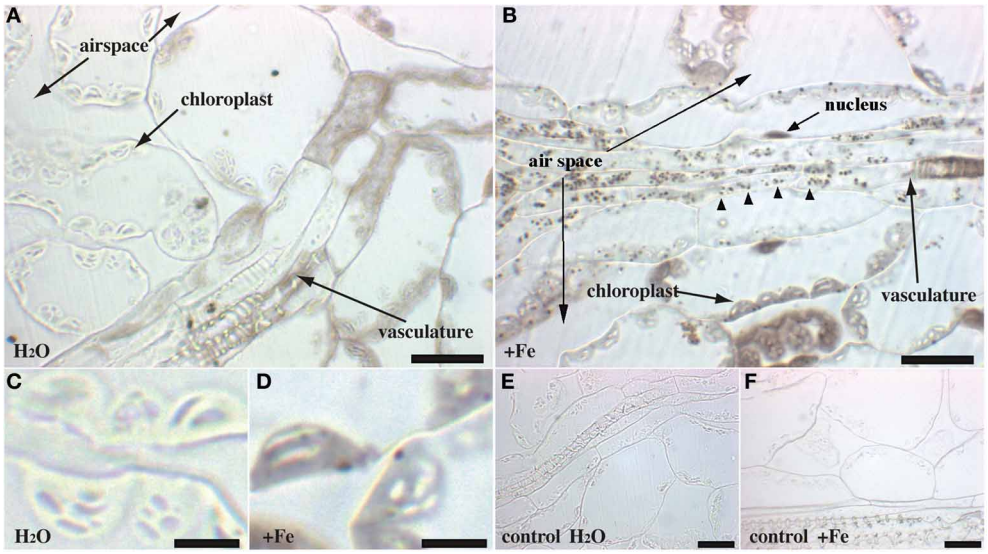

FIGURE 2 | Iron excess in Arabidopsis rosette leaves. Sections of 4-week old WT plants irrigated with either water **(A,C,E)** or Fe-EDDHA 2 mM during 48 h **(B,D,F)** were stained with either Perls/DAB **(A–D)** or DAB alone as a negative control **(E,F)**. The panels **(C,D)** correspond to a magnified image of regions of panels **(A,B)**, respectively. Arrowheads in panel **(B)** indicate Fe-rich structures in the vascular tissues. Scale bars: 20 μm **(A,B,E,F)** or 5 μm **(C,D)**.

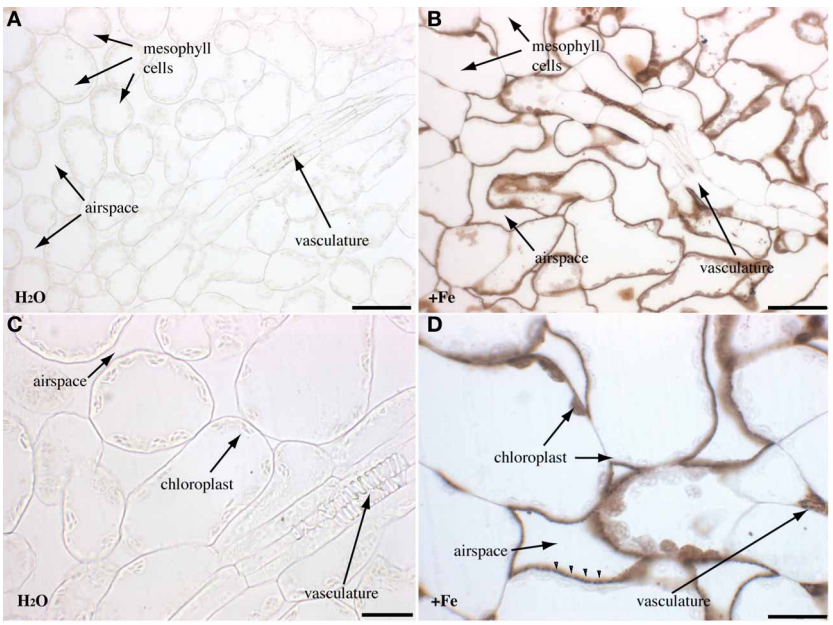

FIGURE 3 | Iron excess in rosette leaves of the *Atfer134* triple mutant. Sections of 4-week old *Atfer134* plants irrigated with either water **(A,C)** or Fe-EDDHA 2 mM during 48 h **(B,D)** were stained with either Perls/DAB **(A,B,D)** or DAB alone as a negative control. **(C)** Fe accumulation in the extracellular space is indicated by arrowheads in panel **(D)**. Scale bars: 50 μm **(A,B)** or 20 μm **(C,D)**.

(**Figures 4A,D**). In wild-type leaves, the ferritin was detected in xylem-associated cells in standard conditions but not in mesophyll cells (**Figures 4B,C**). In iron excess conditions, however, punctuate labeling appeared in chloroplasts of the mesophyll cells (**Figures 4E,F**). The presence of ferritin in the vasculature is therefore compatible with the presence of Fe-ferritin in these cells in response to iron excess. Whether ferritins are located in plastids in these cells like in mesophyll cells remains to be established.

IRON DISTRIBUTION IN THE FLOWER

Iron accumulation or distribution in flowers is still uncharacterized. However, the importance of iron in flowers is illustrated by the frequent sterility observed in iron homeostasis defective

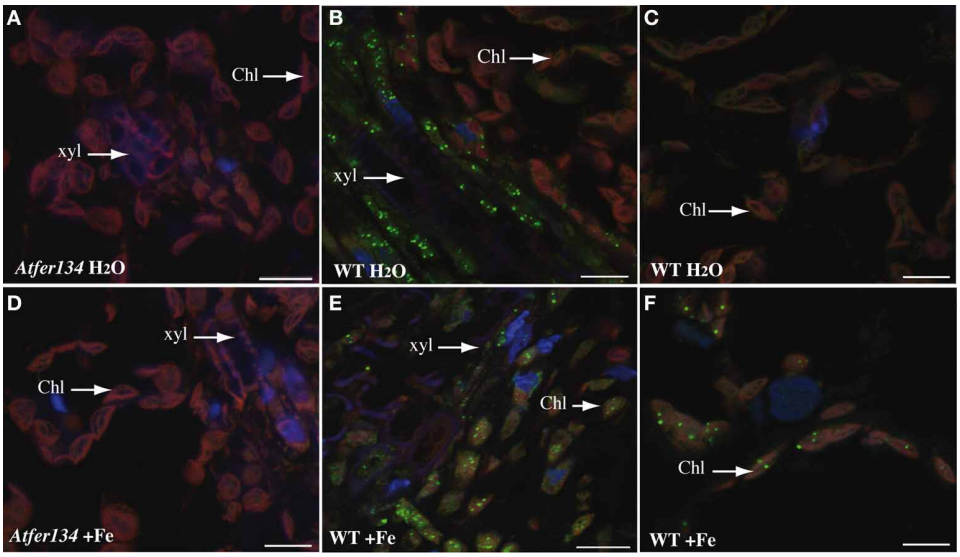

FIGURE 4 | Immunolocalization of Ferritin in Arabidopsis leaves. Sections of rosette leaves from 3 week-old WT **(B,C,E,F)** or triple mutant At*fer1,3,4* **(A,D)** plants irrigated with either water **(A–C)** or 2 mM Fe-EDDHA **(D–F)** were probed with an anti-ferritin antibody and revealed with a secondary anti-rabbit antibody coupled to the Alexa Fluor® 488 fluorophore. Sections were stained with DAPI to reveal cell nuclei. Ferritin localization appears in green, DAPI fluorescence in blue and chlorophyll auto-fluorescence in red. Scale bars: 10 μm.

mutants and by the numerous genes encoding iron acquisition components that are expressed in this organ (Stacey et al., 2002; Vert et al., 2002; Connolly et al., 2003; Waters et al., 2006). In order to determine in which tissues and cell compartments iron is accumulated in flowers, entire Arabidopsis flowers were stained with Perls/DAB. A strong black precipitate was observed in anthers and mature pollen grains revealing that the male reproductive organ is an important sink for iron in the plant (**Figures 5A,C**). The staining observed on top of the pistil is exclusively produced by pollen grains that are attached to the stigma in open flowers (**Figure 5B**). Thus, the Perls/DAB staining method did not detect iron in floral organs other than the anther, indicating that the anther alone contains large pools of Fe.

In order to investigate where iron is located in the anther, flowers were fixed and thin sections were stained with Perls/DAB. Three stages of pollen development were analyzed: monovacuolated mononucleate pollen (**Figures 6A,B**), binucleate pollen (**Figures 6C,D**), and mature pollen with degenerated tapetum (**Figure 6E**). The number of nuclei in the first two stages was controlled by DAPI staining (**Figures 6B,D**). In all three stages, iron was detected on the surface of the pollen grain, in the exine layer of the pollen coat. In addition, Fe accumulated in the cytoplasm as multiple vesicular structures, both in the pollen grains and in the different anther cell layers, including the endothecium. In all these anther cells, iron-containing compartments likely corresponded to plastids based on their number, size and position (**Figure 6E**). In pollen grains, after the first mitotic division, iron-stained structures tended to organize in a ring surrounding the large loosely condensed vegetative nucleus as identified by DAPI staining (**Figures 6C,D**). This iron organization was lost in mature pollen, showing thereafter a random distribution in the cytosol (**Figure 6E**). Mitochondria and amyloplasts are two potential Fe-rich organelles that were shown to aggregate around the vegetative nucleus (Yamamoto et al., 2003). In order to identify these Fe-rich bodies and potentially discriminate between mitochondria and amyloplasts, we compared the iron pattern in pollen grains with mitochondria and amyloplasts staining. Since it was technically not possible to co-stain Fe and these two organelles on the same section, two successive sections were

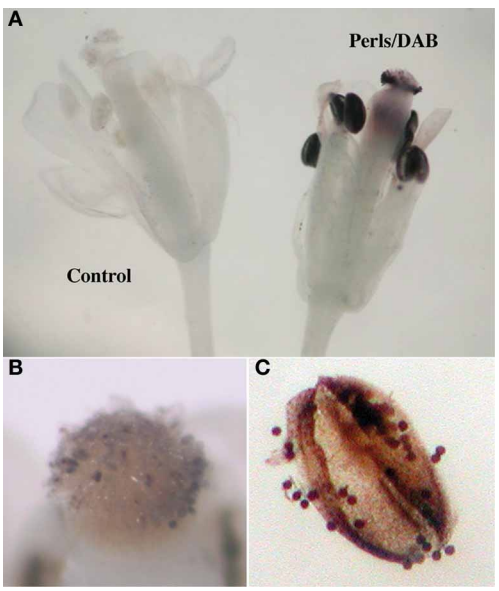

FIGURE 5 | Arabidopsis flowers stained with Perls/DAB. (A) Open mature flowers, **(B)** stigmatic papillae with sticking pollen grains, **(C)** anther with mature pollen grains.

stained with either Perls/DAB (**Figure 7A**) or periodic-acid/Schiff (PAS) (**Figure 7B**), to compare the distribution of Fe and amyloplasts stained with PAS. Another section was stained with DiOC6 for fluorescence imaging of mitochondria (**Figure 7E**). The Fe-rich structures fitted almost exactly with the starch-rich granules (**Figures 7C, D**) and this specific pattern was clearly not comparable to mitochondria, that were smaller and more numerous (**Figure 7E**). Taken together, these observations led us to conclude that in pollen grains Fe is highly concentrated in starch-rich structures corresponding to the amyloplasts.

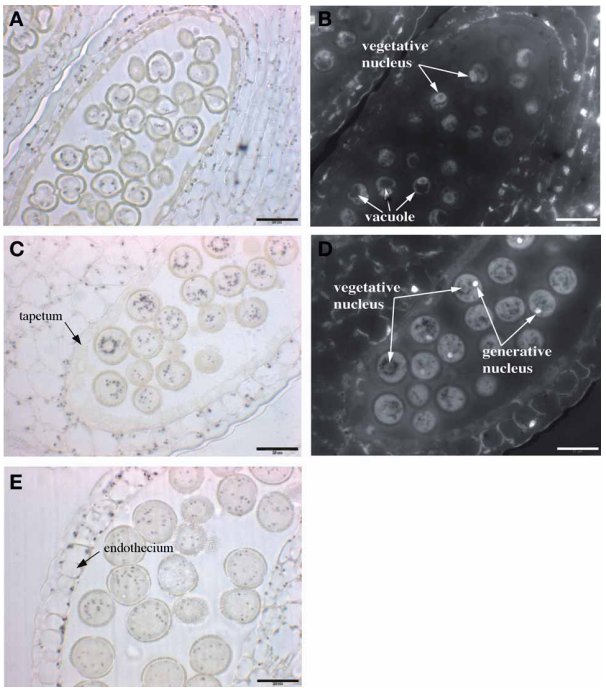

FIGURE 6 | Iron distribution during Arabidopsis pollen development. Sections of anthers at three different stages of pollen development were stained with Perls/DAB and DAPI. **(A,B)** mononuclear pollen grain, **(C,D)** binuclear pollen grain, **(E)** mature pollen grain. **(A,C,E)** Bright field images; **(B,D)** Epifluorescence images from slides **(A,C)**, respectively, showing DAPI-stained vegetative and generative nuclei. Scale bars: 20 μm.

DISCUSSION

Iron, as a cofactor for many cellular functions, is required in many sites within an organ or a cell. Studying Fe homeostasis implies, somehow, having precise information on the localization, amount and dynamics of the Fe pools in the plant. To date, such information is very fragmented and, in some cases, a matter of debate. The Perls/DAB procedure had already been described for the staining of Fe in animal tissues (Nguyen-Legros et al., 1980), but never adapted to plant material. When this procedure was adapted to plant samples, we verified that the Perls/DAB was specific for Fe ions, vs. other metals such as zinc, manganese and copper and we also demonstrated that the Perls/DAB could stain both Fe^{3+} and Fe^{2+} (Roschzttardtz et al., 2009). Potentially, Perls/DAB could thus stain most of the Fe atoms in a cell, except Fe bound to hemes since these structures do not react with these dyes (Nguyen-Legros et al., 1980). Moreover, the staining procedure directly applied to histological sections alleviated the problems of dye penetration in tissues and yielded very high-resolution images of Fe localization in cells, although the major drawback of this technique was that a portion of Fe could be lost during the fixation and dehydration steps. For instance, Fe loosely bound to soluble ligands could be drained out and some compartments such as the vacuole could appear "empty" if they contained Fe under these chemical forms (Roschzttardtz et al., 2011a). We have analyzed Fe localization in source (roots) and sink organs (leaves, flowers, and pollen) and visualized important Fe pools in several sub-cellular compartments: the cell wall, the chloroplast and a compartment in the pollen grain attributed to amyloplasts.

In roots we have shown that the vast majority of iron is located within the central cylinder since only a faint staining was visible in epidermis and cortex. Within the stele, we could also observe that Fe was principally accumulated in the cell walls, in both WT and *frd3* mutant, although in the latter case the overall Fe concentration was much higher. The role of the apoplastic compartment

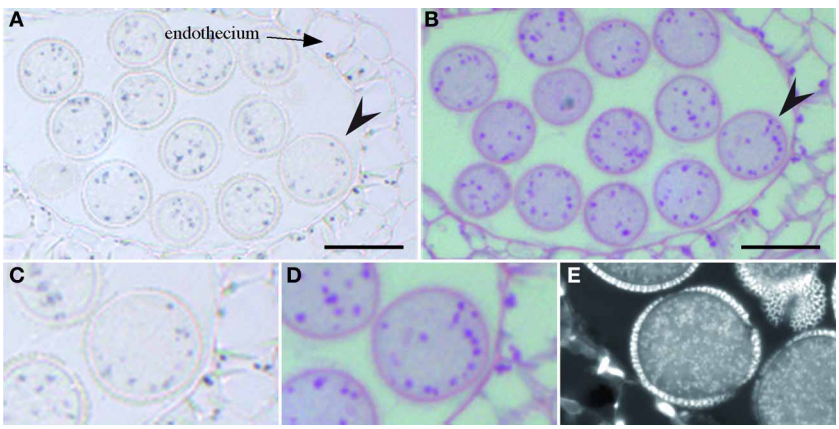

FIGURE 7 | Iron co-localizes with starch in pollen. Serial sections of the same anther were stained with either Perls/DAB **(A,C)**, periodic acid-Schiff **(B,D)** or $DiOC_6$ **(E)**. The arrow heads in **(A,B)** indicate the pollen grain that is magnified in **(C,D)**, respectively. Scale bars: 20 μm.

in Fe homeostasis and nutrition has been a matter of debate in the past. For instance, the capacity of cortical cell walls to bind Fe was estimated to reach 1000 ppm in plants cultivated in the presence of high concentrations of available (Fe-EDTA) iron (Bienfait et al., 1985) although it was later demonstrated that depending on the culture system and Fe source, the amount of apoplastic Fe pool could be overestimated (Strasser et al., 1999). The plants used in this study were grown on soil without added Fe, except in Fe excess conditions. We had chosen these growth conditions to avoid potential artifacts related to the Fe source and availability. Indeed, supplying iron as Fe-EDTA in the culture medium of axenically-grown plants, provoked an important accumulation of Fe in the apoplast of epidermal and cortical cells (**Figure A1**), a pattern that was not observed in the root of soil-grown plants (**Figure 1**). Taken together, our results establish that the apoplast can be a reservoir of Fe, mostly within the stele, and confirm the importance of this compartment in buffering Fe during the process of transport toward the aerial parts.

We have used the *frd3* mutant as a genetic model for Fe over-accumulation in roots (Green and Rogers, 2004). Like in wild type roots, most of the Fe was located in the apoplast and this pattern was particularly visible between the pericycle and the endodermis. This apoplastic accumulation included the endodermis inner half part that is internal to the casparian strip, indicating that Fe diffusion in the extracellular space is efficiently blocked by the casparian strip. A direct consequence of this observation is that Fe must reach the central cylinder via a symplastic route, which in turn suggests that an iron efflux activity is required to export iron from the endodermis and/or pericycle cells toward the apoplastic space of the central cylinder. The Ferroportin 1 (FPN1) transporter represented an appealing candidate to catalyze Fe efflux from the cells, since its expression in roots is also restricted to the central cylinder (Morrissey et al., 2009). This hypothesis was checked by testing whether the FPN1 mutation in the *frd3-7* background could decrease the apoplastic Fe accumulation in the stele. Since this was not the case, the potential role of FPN1 in the efflux of Fe toward the xylem stream in the stele was ruled out (Roschzttardtz et al., 2011b). Taken together, our data on root Fe distribution confirm and reinforce a previous report where it was proposed that the precise function of FRD3 was to facilitate Fe movement between symplastically disconnected tissues (Roschzttardtz et al., 2011b).

Within leaf cells, most of the staining was located in chloroplasts. This result, highly expected given the number of plastidial Fe-proteins, is in good agreement with earlier data that estimated that 70% of the leaf Fe lies in chloroplasts (Shikanai et al., 2003). In leaf tissues from plants grown without added iron, the staining of Fe was intense around the vascular system and very faint in mesophyll cells (**Figure 2**). A similar distribution has been reported in pea (Branton and Jacobson, 1962) and more recently in tobacco leaves (Takahashi et al., 2003), using ^{55}Fe autoradiography and X-ray fluorescence, respectively. Fe-EDDHA supply to the plants provoked an increased abundance of Fe in most of the mesophyll cells as well as the appearance of small sized Fe rich granules in plastids. These Fe deposits were attributed to Fe-ferritin structures, based on the size, 1 μm, (Paramonova et al., 2007), the exact match with ferritin proteins detected by immunofluorescence (**Figure 4**) and the fact that these structures were absent in a *fer1,3,4* triple mutant devoid of ferritin proteins in leaves (**Figure 3**). Interestingly, ferritin-iron was more abundant in the cells associated to the vascular system. Since AtFER1, the main ferritin gene in leaves, is highly expressed in the veins (Tarantino et al., 2003), our results strongly suggest a role of this protein in buffering the excess of Fe during the process of xylem unloading. As part of the mechanism to cope with excess iron, it has recently been shown that chloroplasts can also release a fraction of the Fe pool by the efflux activity of two nicotianamine-Fe transporters, YSL4 and YSL6 (Divol et al., 2013). The mutation of these two genes results in a higher accumulation of Fe and ferritins in plastids and eventually in a higher sensitivity of the *ysl4ysl6* double mutant plants to Fe excess conditions (Divol et al., 2013). It had been previously shown that the loss of ferritin proteins in leaves did not induce a significant modification of Fe content or any macroscopic phenotype in Fe excess conditions (Ravet et al., 2009). Thanks to the Perls/DAB staining, we could show that ferritin-free chloroplasts were still able to accumulate Fe in conditions of excess (**Figure 3**) and, more interestingly, that this loss of ferritins provoked an important modification of the iron distribution at the cellular level with a strong accumulation in the cell walls. This redistribution of Fe outside of the cell could be the result of reduced cell uptake at the plasma membrane or the consequence of increased Fe efflux. Like in root, Ferroportin 1 could be a good candidate to fulfill this efflux function since it is expressed in the vasculature of leaves (Morrissey et al., 2009).

The vacuolar compartment is generally considered as a potential site for Fe accumulation. Such vacuolar storage was indeed found in *Arabidopsis thaliana* embryos, where Fe was detected in globoid structures inside the vacuoles (Lanquar et al., 2005) and this particular Fe pool was further located in the endodermal cell layer (Roschzttardtz et al., 2009). This vacuolar pool, remobilized by the NRAMP3 and NRAMP4 tonoplastic transporters, was shown to be an essential source of Fe during germination (Lanquar et al., 2005). Surprisingly, except in embryos, such a pool of iron was never observed in the tissues and cells studied in the present work. To some extent, this observation can be linked with the function of NRAMP3 and NRAMP4, which in the vacuoles of mesophyll cells is to export manganese and not iron (Lanquar et al., 2010).

In reproductive organs, anthers and pollen grains accumulated most of the plant stainable iron (**Figure 5**) indicating that the male gametophyte is a major sink of Fe. It is worth noticing that the key components of the iron uptake machinery described in roots, the ferric-chelate reductase FRO2, the ferrous iron transporter IRT1 and the citrate effluxer FRD3 are expressed in anthers (Vert et al., 2002; Connolly et al., 2003; Roschzttardtz et al., 2011b). Within the anther, iron accumulated in most of the cell layers, including the epidermis and endothecium, in structures that are compatible in size and number with plastids. Unexpectedly, the tapetum cells did not contain detectable Fe (**Figures 6A,C**). The absence of Fe accumulation in this important nourishing tissue could indicate that Fe is only transiently accumulated in the tapetum, before its delivery to the developing microspore cells, although it cannot be ruled out that Fe did accumulate in the tapetum in earlier stages of development.

As a matter of fact, at the earliest stage considered in this study, the microspore cells (mononuclear vacuolated stage) already contained considerable amounts of Fe in the cytoplasm. The Fe-rich bodies stained in pollen grains surrounding the vegetative nucleus could correspond to mitochondria or amyloplasts, since these two organelles were shown to preferentially accumulate around the vegetative nucleus at the binuclear stage, whereas vacuoles and lipid bodies aggregate around the generative cell (Yamamoto et al., 2003). The comparison of Fe pattern with mitochondria and amyloplasts allowed to discriminate between these two organelles and established that Fe accumulated in amyloplasts. Although not demonstrated in this study, it is very likely that the Fe-rich deposits correspond to ferritins. Indeed, contrary to chloroplasts that only accumulate detectable amounts of ferritins in Fe-excess conditions, amyloplasts have been shown to contain high amounts of ferritins in physiological conditions (Yang et al., 2010). In Arabidopsis *AtFER1* is, among the four ferritin genes, the only one expressed in anthers and pollen, suggesting that this isoform could be involved in Fe storage and accumulation in pollen amyloplasts (Ravet et al., 2008). The role and importance of Fe in pollen amyloplasts remains to be demonstrated, however, it is clear that affecting long distance transport of Fe has an impact on pollen formation, development and viability. For instance, reducing NA concentration in the Arabidopsis quadruple *nas* mutant or in tobacco overexpressing a NA Amino Transferase results in a severe decrease in pollen development, viability and germination, leading to strong decrease in fertility (Takahashi et al., 2003; Schuler et al., 2012). Comparable defects have been reported in the *ysl1ysl3* double mutant (Waters et al., 2006), as well as in *frd3-7* mutant (Roschzttardtz et al., 2011b). Overall, our data have highlighted that anthers are a very important sink for iron, which is stored in amyloplats of anther tissues and pollen grains and, together with other reports on Fe transport related genes, strengthen the importance of Fe in the reproduction process.

In a previous report, we had shown that the nucleolus was an unexpected site of high Fe concentration in plant cells. Fe-rich nucleoli were observed first in pea embryos and then more generally in Arabidopsis and tomato mesophyll cells (Roschzttardtz et al., 2011a). In the present study, we have also detected Fe most likely in the nucleolus in pericycle cells in roots. The presence of Fe in the nucleolus appears thus to be a general feature of this sub-nuclear structure in plants, although the role of this specific pool of Fe is still unknown. Nevertheless, the nucleoli do not always contain high concentrations of Fe and the most striking illustration is the pollen grain. Indeed, the vegetative nucleus has a very large nucleolus that is not stained with Perls/DAB. This observation somehow suggests that Fe not strictly required as a structural element to maintain the nucleolar components together and instead, Fe may be required for the catalytic activity of the nucleolus.

REFERENCES

Bienfait, H. F., Briel, W. V. D., and Mesland-Mul, N. T. (1985). Free space iron pools in roots: generation and mobilization. *Plant Physiol.* 78, 596–600. doi: 10.1104/pp.78.3.596

Branton, D., and Jacobson, L. (1962). Iron transport in pea plants. *Plant Physiol.* 37, 539–545. doi: 10.1104/pp.37.4.539

Briat, J. F., and Lebrun, M. (1999). Plant responses to metal toxicity. *C. R. Acad. Sci. III, Sci. Vie* 322, 43–54. doi: 10.1016/S0764-4469(99)80016-X

Briat, J. F., and Lobreaux, S. (1998). Iron storage and ferritin in plants. *Met. Ions Biol. Syst.* 35, 563–584.

Connolly, E. L., Campbell, N. H., Grotz, N., Prichard, C. L., and Guerinot, M. L. (2003). Overexpression of the FRO2 ferric chelate reductase confers tolerance to growth on low iron and uncovers posttranscriptional control. *Plant Physiol.* 133, 1102–1110. doi: 10.1104/pp.103.025122

Divol, F., Couch, D., Conéjéro, G., Roschzttardtz, H., Mari, S., and Curie, C. (2013). The Arabidopsis yellow stripe4 and 6 transporters control iron release from the chloroplast. *Plant Cell* 25, 1040–1055. doi: 10.1105/tpc.112.107672

Durrett, T. P., Gassmann, W., and Rogers, E. E. (2007). The FRD3-mediated efflux of citrate into the root vasculature is necessary for efficient iron translocation. *Plant Physiol.* 144, 197–205. doi: 10.1104/pp.107.097162

Eide, D., Broderius, M., Fett, J., and Guerinot, M. L. (1996). A novel iron-regulated metal transporter from plants identified by functional expression in yeast. *Proc. Natl Acad. Sci. U.S.A.* 93, 5624–5628. doi: 10.1073/pnas.93.11.5624

Green, L. S., and Rogers, E. E. (2004). FRD3 controls iron localization in Arabidopsis. *Plant Physiol.* 136, 2523–2531. doi: 10.1104/pp.104.045633

Jimenez, S., Morales, F., Abadia, A., Abadia, J., Moreno, M. A., and Gogorcena, Y. (2009). Elemental 2-D mapping and changes in leaf iron and chlorophyll in response to iron re-supply in iron-deficient GF 677 peach-almond hybrid. *Plant Soil* 315, 93–106. doi: 10.1007/s11104-008-9735-9

Kim, S. A., Punshon, T., Lanzirotti, A., Li, L., Alonso, J. M., Ecker, J. R., et al. (2006). Localization of iron in Arabidopsis seed requires the vacuolar membrane transporter VIT1. *Science* 314, 1295–1298. doi: 10.1126/science.1132563

Lanquar, V., Lelievre, F., Bolte, S., Hames, C., Alcon, C., Neumann, D., et al. (2005). Mobilization of vacuolar iron by AtNRAMP3 and AtNRAMP4 is essential for seed germination on low iron. *EMBO J.* 24, 4041–4051. doi: 10.1038/sj.emboj.7600864

Lanquar, V., Ramos, M. S., Lelievre, F., Barbier-Brygoo, H., Krieger-Liszkay, A., Kramer, U., et al. (2010). Export of vacuolar manganese by AtNRAMP3 and AtNRAMP4 is required for optimal photosynthesis and growth under manganese deficiency. *Plant Physiol.* 152, 1986–1999. doi: 10.1104/pp.109.150946

Lobreaux, S., Massenet, O., and Briat, J. F. (1992). Iron induces ferritin synthesis in maize plantlets. *Plant Mol. Biol.* 19, 563–575. doi: 10.1007/BF00026783

Morrissey, J., Baxter, I. R., Lee, J., Li, L. T., Lahner, B., Grotz, N., et al. (2009). The ferroportin metal efflux proteins function in iron and cobalt homeostasis in Arabidopsis. *Plant Cell* 21, 3326–3338. doi: 10.1105/tpc.109.069401

Nagata, N., Saito, C., Sakai, A., Kuroiwa, H., and Kuroiwa, T. (2000). Unique positioning of mitochondria in developing microspores and pollen grains in Pharbitis nil: mitochondria cover the nuclear surface at specific developmental stages. *Protoplasma* 213, 74–82. doi: 10.1007/BF01280507

Nguyen-Legros, J., Bizot, J., Bolesse, M., and Pulicani, J. P. (1980). "Diaminobenzidine black" as a new histochemical demonstration of exogenous iron (author's transl). *Histochemistry* 66, 239–244. doi: 10.1007/BF00495737

Paramonova, N. V., Shevyakova, N. I., and Kuznetsov, V. V. (2007). Ultrastructure of ferritin in the leaves of Mesembryanthemum crystallinum under stress conditions. *Russ. J. Plant Physiolo.* 54, 244–256. doi: 10.1134/S1021443707020136

Ravet, K., Touraine, B., Boucherez, J., Briat, J. F., Gaymard, F., and Cellier, F. (2008). Ferritins control interaction between iron homeostasis and oxidative stress in Arabidopsis. *Plant J.* 57, 400–412. doi: 10.1111/j.1365-313X.2008.03698.x

Ravet, K., Touraine, B., Kim, S. A., Cellier, F., Thomine, S., Guerinot, M. L., et al. (2009). Post-Translational regulation of AtFER2 ferritin in response to intracellular iron trafficking during fruit development in Arabidopsis.

Mol. Plant 2, 1095–1106. doi: 10.1093/mp/ssp041

Robinson, N. J., Procter, C. M., Connolly, E. L., and Guerinot, M. L. (1999). A ferric-chelate reductase for iron uptake from soils. *Nature* 397, 694–697. doi: 10.1038/17800

Rogers, E. E., and Guerinot, M. L. (2002). FRD3, a member of the multidrug and toxin efflux family, controls iron deficiency responses in Arabidopsis. *Plant Cell* 14, 1787–1799. doi: 10.1105/tpc.001495

Roschzttardtz, H., Conejero, G., Curie, C., and Mari, S. (2009). Identification of the endodermal vacuole as the iron storage compartment in the Arabidopsis embryo. *Plant Physiol.* 151, 1329–1338. doi: 10.1104/pp.109.144444

Roschzttardtz, H., Grillet, L., Isaure, M. P., Conejero, G., Ortega, R., Curie, C., et al. (2011a). Plant cell nucleolus as a hot spot for iron. *J. Biol. Chem.* 286, 27863–27866. doi: 10.1074/jbc.C111.269720

Roschzttardtz, H., Seguela-Arnaud, M., Briat, J. F., Vert, G., and Curie, C. (2011b). The FRD3 citrate effluxer promotes iron nutrition between symplastically disconnected tissues throughout Arabidopsis development. *Plant Cell* 23, 2725–2737. doi: 10.1105/tpc.111.088088

Schuler, M., Rellan-Alvarez, R., Fink-Straube, C., Abadia, J., and Bauer, P. (2012). Nicotianamine functions in the Phloem-based transport of iron to sink organs, in pollen development and pollen tube growth in Arabidopsis. *Plant Cell* 24, 2380–2400. doi: 10.1105/tpc.112.099077

Shikanai, T., Muller-Moule, P., Munekage, Y., Niyogi, K. K., and Pilon, M. (2003). PAA1, a P-type ATPase of Arabidopsis, functions in copper transport in chloroplasts. *Plant Cell* 15, 1333–1346. doi: 10.1105/tpc.011817

Stacey, M. G., Koh, S., Becker, J., and Stacey, G. (2002). AtOPT3, a member of the oligopeptide transporter family, is essential for embryo development in Arabidopsis. *Plant Cell* 14, 2799–2811. doi: 10.1105/tpc.005629

Stacey, M. G., Patel, A., McClain, W. E., Mathieu, M., Remley, M., Rogers, E. E., et al. (2008). The Arabidopsis AtOPT3 protein functions in metal homeostasis and movement of iron to developing seeds. *Plant Physiol.* 146, 589–601. doi: 10.1104/pp.107.108183

Strasser, O., Kohl, K., and Romheld, V. (1999). Overestimation of apoplastic Fe in roots of soil grown plants. *Plant Soil* 210, 179–187. doi: 10.1023/A:1004650506592

Takahashi, M., Terada, Y., Nakai, I., Nakanishi, H., Yoshimura, E., Mori, S., et al. (2003). Role of nicotianamine in the intracellular delivery of metals and plant reproductive development. *Plant Cell* 15, 1263–1280. doi: 10.1105/tpc.010256

Tarantino, D., Petit, J. M., Lobreaux, S., Briat, J. F., Soave, C., and Murgia, I. (2003). Differential involvement of the IDRS cis-element in the developmental and environmental regulation of the AtFer1 ferritin gene from Arabidopsis. *Planta* 217, 709–716. doi: 10.1007/s00425-003-1038-z

Vert, G., Grotz, N., Dedaldechamp, F., Gaymard, F., Guerinot, M. L., Briat, J. F., et al. (2002). IRT1, an Arabidopsis transporter essential for iron uptake from the soil and for plant growth. *Plant Cell* 14, 1223–1233. doi: 10.1105/tpc.001388

Waters, B. M., Chu, H. H., Didonato, R. J., Roberts, L. A., Eisley, R. B., Lahner, B., et al. (2006). Mutations in Arabidopsis yellow stripe-like1 and yellow stripe-like3 reveal their roles in metal ion homeostasis and loading of metal ions in seeds. *Plant Physiol.* 141, 1446–1458. doi: 10.1104/pp.106.082586

Wollman, F. A., Minai, L., and Nechushtai, R. (1999). The biogenesis and assembly of photosynthetic proteins in thylakoid membranes. *Biochimica Et Biophysica Acta* 1411, 21–85. doi: 10.1016/S0005-2728(99)00043-2

Yamamoto, Y., Nishimura, M., Hara-Nishimura, I., and Noguchi, T. (2003). Behavior of vacuoles during microspore and pollen development in *Arabidopsis thaliana*. *Plant and Cell Physiology* 44, 1192–1201. doi: 10.1093/pcp/pcg147

Yang, H. X., Fu, X. P., Li, M. L., Leng, X. J., Chen, B., and Zhao, G. H. (2010). Protein association and dissociation regulated by extension peptide: a mode for iron control by phytoferritin in seeds. *Plant Physiol.* 154, 1481–1491. doi: 10.1104/pp.110.163063

Yokosho, K., Yamaji, N., Ueno, D., Mitani, N., and Ma, J. F. (2009). OsFRDL1 is a citrate transporter required for efficient translocation of iron in rice. *Plant Physiol.* 149, 297–305. doi: 10.1104/pp.108.128132

Conflict of Interest Statement: The authors declare that the research was conducted in the absence of any commercial or financial relationships that could be construed as a potential conflict of interest.

Received: 10 May 2013; paper pending published: 17 June 2013; accepted: 20 August 2013; published online: 06 September 2013.

*Citation: Roschzttardtz H, Conéjéro G, Divol F, Alcon C, Verdeil J-L, Curie C and Mari S (2013) New insights into Fe localization in plant tissues. Front. Plant Sci. **4**:350. doi: 10.3389/fpls.2013.00350*

This article was submitted to Plant Nutrition, a section of the journal Frontiers in Plant Science.

APPENDIX

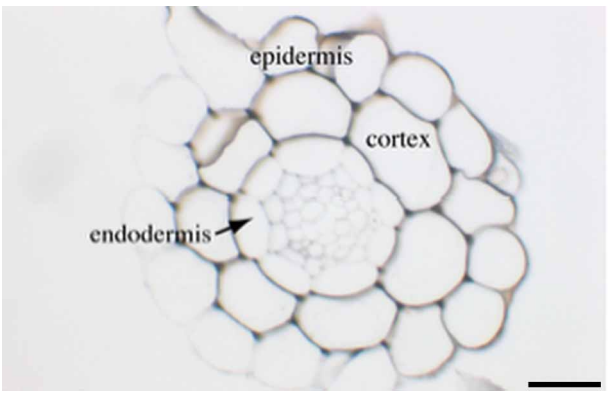

FIGURE A1 | Iron detection in Arabidopsis roots from plants grown in plate. Three-week old wild-type plants grown in MS/2 medium supplemented with 50 μM Fe-EDTA were embedded in Technovit resin and the sections were stained with Perls/DAB. The scale bar represents 50 μm.

frontiers in
PLANT SCIENCE

REVIEW ARTICLE
published: 24 July 2013
doi: 10.3389/fpls.2013.00259

The iron-sulfur cluster assembly machineries in plants: current knowledge and open questions

*Jérémy Couturier[1], Brigitte Touraine[2], Jean-François Briat[2], Frédéric Gaymard[2] and Nicolas Rouhier[1]**

[1] Interactions Arbres/Micro-organismes, Faculté des Sciences, UMR1136 Université de Lorraine-INRA, Vandoeuvre, France
[2] Biochimie et Physiologie Moléculaire des Plantes, Centre National de la Recherche Scientifique-INRA-Université Montpellier 2, Montpellier, France

Edited by:
Gianpiero Vigani, Università degli Studi di Milano, Italy

Reviewed by:
Ruediger Hell, University of Heidelberg, Germany
Janneke Balk, John Innes Centre, UK

***Correspondence:**
Nicolas Rouhier, Université de Lorraine, UMR1136 Université de Lorraine-INRA, Interactions Arbres/Micro-organismes, Faculté des Sciences, Bd des aiguillettes, BP 239,54506 Vandoeuvre, France
e-mail: nicolas.rouhier@univ-lorraine.fr

Many metabolic pathways and cellular processes occurring in most sub-cellular compartments depend on the functioning of iron-sulfur (Fe-S) proteins, whose cofactors are assembled through dedicated protein machineries. Recent advances have been made in the knowledge of the functions of individual components through a combination of genetic, biochemical and structural approaches, primarily in prokaryotes and non-plant eukaryotes. Whereas most of the components of these machineries are conserved between kingdoms, their complexity is likely increased in plants owing to the presence of additional assembly proteins and to the existence of expanded families for several assembly proteins. This review focuses on the new actors discovered in the past few years, such as glutaredoxin, BOLA and NEET proteins as well as MIP18, MMS19, TAH18, DRE2 for the cytosolic machinery, which are integrated into a model for the plant Fe-S cluster biogenesis systems. It also discusses a few issues currently subjected to an intense debate such as the role of the mitochondrial frataxin and of glutaredoxins, the functional separation between scaffold, carrier and iron-delivery proteins and the crosstalk existing between different organelles.

Keywords: iron-sulfur, assembly machineries, iron donor, repair, scaffold proteins, carrier Proteins

GENERAL INTRODUCTION

Plants have a high iron demand, in particular in chloroplasts and mitochondria, to ensure the functionality of many vital processes such as photosynthesis and respiration. Besides, many metabolic pathways require the presence of metalloproteins including those containing iron in the form of Fe-S clusters, heme, siroheme and mono- or bi-nuclear non-heme iron centers (Johnson et al., 2005; Ye et al., 2006b). For instance, sulfur and nitrogen assimilation, chlorophyll catabolism, DNA replication and repair, ribosome biogenesis, tRNA thio-modification or co-enzyme (biotin, lipoic acid, thiamine) synthesis also rely on the functionality of Fe-S proteins (Lill, 2009; Balk and Pilon, 2011). In general, Fe-S proteins perform a wide diversity of functions ranging from electron transfer, (de)hydration reactions, radical-generation or disulfide cleavage (Johnson et al., 2005). In both eukaryotes and prokaryotes, Fe-S proteins are first synthesized in an apoform *via* the cellular translational machinery. The prosthetic group is often required for correct folding or stability of the protein. It should therefore be inserted co-translationally or immediately upon translation of the apo-polypeptides through specific assembly machineries. The precise functioning of these machineries and their regulation by environmental constraints are only poorly understood.

TYPES OF Fe-S CLUSTERS AND INTERCONVERSION

Fe-S clusters are prosthetic groups formed by iron atoms and acid-labile inorganic sulfide. In general, iron atoms are coordinated with the protein backbone *via* thiol groups of cysteinyl residues, but other more rarely encountered ligands are His, Arg, Ser or Glu residues. The most common clusters found in plant proteins are the $[Fe_2S_2]$ and $[Fe_4S_4]$ clusters liganded by four Cys residues, but other examples are found, as the $[Fe_2S_2]$ Rieske-type clusters coordinated by 2 Cys and 2 His residues, the $[Fe_2S_2]$ NEET-type clusters coordinated by 3 Cys and 1 His residues, the $[Fe_3S_4]$ clusters coordinated by 3 Cys and the $[Fe_4S_4]$ clusters with one Cys ligand also serving for ligating siroheme (**Figure 1**) (Johnson et al., 2005; Nechushtai et al., 2012). Some proteins, especially those involved in the Fe-S cluster biogenesis machineries, can assemble different types of cluster *in vitro* and the interconversion observed between these clusters might have a physiological relevance. For example, the *Azotobacter vinelandii* assembly proteins, IscU and $^{(Nif)}$IscA, can accommodate either a $[Fe_2S_2]$ or a $[Fe_4S_4]$ cluster and reversible cycling between these forms is effective *via* the reductive coupling of two $[Fe_2S_2]$ clusters to form a $[Fe_4S_4]$ cluster or, in the case of $^{(Nif)}$IscA, *via* the O_2-induced oxidative cleavage of the $[Fe_4S_4]$ (Chandramouli et al., 2007; Mapolelo et al., 2012b). Another example of interconversion has been described for the bacterial fumarate and nitrate reduction (FNR) regulatory protein. In response to elevated oxygen levels, the dimeric DNA binding form of FNR which binds a $[Fe_4S_4]$ cluster is transformed into a monomeric form with a $[Fe_2S_2]$ cluster that is unable to bind to DNA (Khoroshilova et al., 1997; Zhang et al., 2012). The $[Fe_4S_4]$ cluster in FNR can be regenerated from a cysteine persulfide-coordinated $[Fe_2S_2]$ cluster in the presence of a reductant and ferrous iron. This observation provided some clues about a possible mechanism devoted to the repair of biological $[Fe_4S_4]$ clusters, which represent the vast majority of the cellular Fe-S clusters and are usually

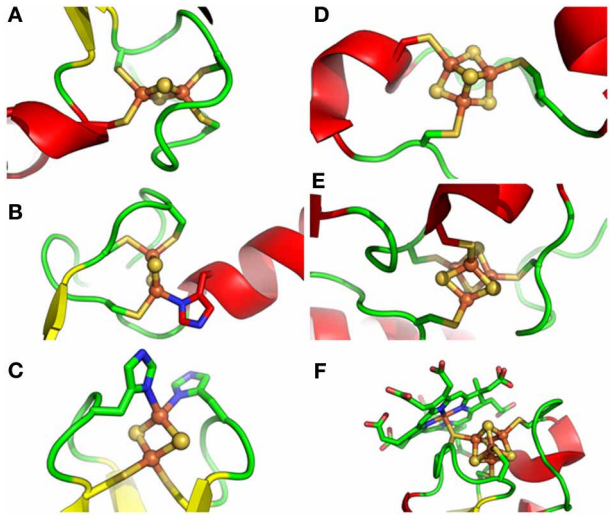

FIGURE 1 | Different types of Fe-S clusters found in proteins from photosynthetic organisms. Schematic representation of Fe-S clusters and their ligands with sulfur, iron and nitrogen atoms colored in yellow, green and blue, respectively. **(A)**. classical [Fe_2S_2] ligated by four cysteines as in ferredoxin from *Cyanidioschyzon merolae*, **(B)**. NEET-type [Fe_2S_2] ligated by three cysteines and one histidine as in *Arabidopsis thaliana* NEET, **(C)**. Rieske-type [Fe_2S_2] ligated by two cysteines and two histidines as in the Rieske protein subunit of the b_6f complex from *Spinacia oleracea*, **(D)**. [Fe_3S_4] ligated by three cysteines as in *Synechocystis sp. PCC 6803* glutamate synthase, **(E)**. [Fe_4S_4] ligated by four cysteines as in the ferredoxin-thioredoxin reductase from *Synechocystis sp. PCC 6803*, and **(F)**. [Fe_4S_4] ligated by four cysteines but with one thiolate ligand serving also for siroheme as in *Nicotiana tabacum* nitrite reductase. PDB codes used for drawing these clusters using Pymol are 3AB5, 3S2Q, 1RFS, 1OFD, 2PU9, and 3B0G, respectively.

more sensitive to oxygen compared to [Fe_2S_2] clusters (Zhang et al., 2012). Altogether, cluster interconversion may represent an efficient way for the maturation or repair of different types of Fe-S proteins or for the regulation of cellular processes in response either to some changes in the intracellular conditions or to extracellular stimuli.

BIOLOGICAL ROLES OF Fe-S PROTEINS

The primary role of Fe-S proteins concerns their involvement in electron transfer reactions, usually as one-electron carriers. Hence, they are major elements for the photosynthetic electron transport chain, being present in the Rieske protein of the b_6f complex and as three [Fe_4S_4] clusters at the level of photosystem I (PSI) directly transferring their electrons to stromal ferredoxins. Several Fe-S clusters also contribute to electron transfer in the respiratory electron transport chain. There are eight Fe-S clusters in complex I: two [Fe_2S_2] and six [Fe_4S_4]; three in complex II: one [Fe_2S_2], one [Fe_3S_4] and one [Fe_4S_4], and a Rieske protein in the bc_1 complex. However, due to the chemical versatility of both iron and sulfur and the structural diversity and electronic properties of Fe-S clusters, they also have several other identified roles. The most documented functions, which will be illustrated by a few examples, are the regulation of gene expression, and the catalytic roles which include substrate binding, activation and/or reduction.

In bacteria, several transcription factors, SoxR, IscR, NsrR and FNR, possess Fe-S cofactors serving for the sensing of cellular changes in superoxide, Fe-S clusters, NO and oxygen contents, respectively (Fleischhacker and Kiley, 2011). Most of these regulatory mechanisms reflect the sensitivity of Fe-S clusters of these transcription factors to reactive species and their subsequent degradation. In eukaryotes, a well-known example is the iron regulatory protein 1 (IRP1) that controls the cellular iron homeostasis. This protein alternates between an active cytosolic aconitase holoform harboring an Fe-S cluster and an apoform that binds iron responsive elements for post-transcriptional regulation (Rouault, 2006). However, although a recombinant aconitase can bind to the 5′UTR of the *Arabidopsis* chloroplastic CuZn superoxide dismutase 2, such regulation does not seem to be a general pathway operating in plants (Arnaud et al., 2007; Moeder et al., 2007).

Besides this sensing function, Fe-S clusters also constitute the reaction center of many enzymes, serving for the binding and/or the activation of the substrate or simply for funneling electrons to the substrate. This is typically illustrated for aconitase for which one Fe atom is involved in the coordination of citrate (Kennedy et al., 1987). Another important and widespread protein family is constituted by radical-SAM enzymes that catalyze the reductive cleavage of *S*-adenosylmethionine (SAM) to generate a 5′-deoxyadenosyl radical which subsequently activates the substrate by abstracting a hydrogen atom (Atta et al., 2010). This radical chemistry is required for many biosynthesis and degradation pathways as for biotin or lipoic acid synthesis. Illustrating the importance of Fe-S clusters, it is worth mentioning the unique cluster chemistry of chloroplastic ferredoxin:thioredoxin reductase and most likely bacterial and archaeal counterparts possessing similar enzymes (Jacquot et al., 2009). Using a catalytic intermediate with two cysteinyl ligands at a unique Fe site, the active-site [Fe_4S_4] cluster promotes the reduction of an intramolecular disulfide bond in thioredoxins by relaying electrons provided by ferredoxins (Walters et al., 2005; Dai et al., 2007).

Finally, several recent examples of [Fe_4S_4] clusters bound to enzymes in DNA metabolism (glycosylases, primases, helicases, helicases/nucleases, polymerases) raised the question of the chemical role of these clusters (Wu and Brosh, 2012). However, this is currently unclear as mutation of the cluster ligands affects the integrity and functioning of some enzymes, whereas there was no measurable effect in other cases.

THE Fe-S CLUSTER ASSEMBLY MACHINERIES

Schematically, the assembly process can be divided into two steps (**Figure 2**). In the first stage, Fe-S clusters are built from iron and sulfur delivered by proteins onto so-called scaffold proteins (comprising U-type scaffold proteins or a SufBCD complex). Then, the subsequent transfer of preformed Fe-S clusters to target recipient apoproteins is achieved with the help of carrier proteins (generally referred to as Nfu proteins or A-type carriers (ATC) called SufA/IscA). The nature of the iron donor is still a matter of debate, whereas sulfur is mobilized *via* the action

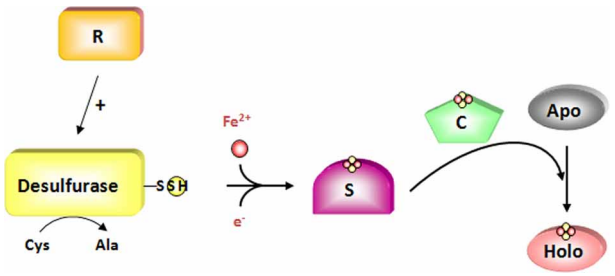

FIGURE 2 | The two-steps of *de novo* assembly of Fe-S clusters. An Fe-S cluster is assembled on scaffold proteins (S) from iron and sulfur sulfane generated as a persulfide on cysteine desulfurase whose activity is regulated by specific proteins (R). For this step, two electrons are required to reduce sulfur sulfane (S^0) into sulfide (S^{2-}). This cluster is subsequently transferred to acceptor apoproteins *via* the action of carrier proteins (C). The cysteine desulfurase is colored in yellow and the regulators in orange. Putative scaffold and carrier proteins are colored in purple and green, respectively.

of pyridoxal-5′-phosphate (PLP)-dependent cysteine desulfurases (SufS, IscS/Nfs) (Lill and Mühlenhoff, 2008). As sulfur is always present in the S^{2-} oxidation state in Fe-S clusters, two electrons are needed to reduce sulfane sulfur (S^0) in the course of cluster assembly (Lill, 2009). Beyond electron donors, a few additional proteins such as ATP-hydrolyzing chaperones or sulfur acceptors are also required for some steps.

The components for Fe-S cluster assembly in eukaryotes and in particular in plants, belong to three systems, namely the SUF (sulfur mobilization), ISC (iron-sulfur cluster) and CIA (cytosolic iron-sulfur cluster assembly) machineries for plastidial, mitochondrial and cytosolic/nuclear Fe-S proteins, respectively (Lill and Mühlenhoff, 2008). In addition, an ISC export machinery links the mitochondrial and the cytosolic machineries (Lill and Mühlenhoff, 2008). Whereas the ISC export and CIA machineries are specific to eukaryotes, the SUF and/or ISC machineries are found in most living organisms. Hence, the prokaryotic systems represent good working models for the plastidial and mitochondrial assembly machineries considering the evolutionary origin of these organelles.

THE MITOCHONDRIAL ISC-LIKE SYSTEM

Overview of the ISC system in bacteria and in mitochondria of non-plant eukaryotes

The ISC-mediated assembly of Fe-S clusters was first described in bacteria (Roche et al., 2013). In *Azotobacter vinelandii* and *E. coli*, the *isc* operon is formed by 7 genes that encode a regulator (IscR), a cysteine desulfurase (IscS), a scaffold protein (IscU), an ATC protein (IscA), a DnaK-like chaperone (HscA), a DnaJ-like co-chaperone (HscB) and an electron donor, a ferredoxin (Johnson et al., 2005). These proteins likely form transient and sequential protein complexes exhibiting a dynamic interplay of protein–protein interactions and associated conformational changes. IscS is a PLP-dependent enzyme extracting the sulfur atom from L-cysteine (Schwartz et al., 2000) and transiently binding a persulfide onto an active-site cysteine. Following the formation of an IscS-IscU complex, the sulfur atom is transferred from IscS to the scaffold protein, IscU. IscU also acts as an Fe acceptor, enabling the assembly of an Fe-S cluster, without dissociation of the IscS-IscU complex. The origin of the iron, which has been suggested to come from frataxin, named CyaY in bacteria, is still uncertain (see section Where do Iron Atoms Come From?). By interacting with IscS and/or IscU, ferredoxin provides the electrons to reduce the sulfur but it could also contribute to the dynamic equilibrium between the $[Fe_2S_2]$ and $[Fe_4S_4]$ cluster-bound forms of IscU by enabling the reductive coupling of two $[Fe_2S_2]^{2+}$ clusters to form a single $[Fe_4S_4]^{2+}$ cluster on IscU (Chandramouli et al., 2007; Kim et al., 2013). The release and transfer of the Fe-S cluster to apo-target proteins is enhanced by the interaction of IscU with HscA and HscB proteins in an ATP-dependent process. HscA and HscB belong to the DnaK/DnaJ chaperones/co-chaperones families, respectively (Hoff et al., 2000). A LPPVK sequence motif in IscU is recognized by HscA and this interaction is regulated by the co-chaperone HscB, whose interaction with IscU involves hydrophobic residues (Hoff et al., 2003; Fuzery et al., 2008). Cluster assembly and release have been shown to be uncoupled.

The cluster built on IscU is delivered to final acceptors with the help of carrier proteins which may provide the necessary specificity. Among putative carrier proteins present in *E. coli* (IscA, SufA, ErpA, NfuA, ApbC and Grx4), IscA and SufA are clearly associated with the ISC and SUF pathways, respectively, in accordance with their presence in the respective gene cluster/operon. In the current model, ErpA, which is required in particular for cluster assembly in two enzymes implicated in isoprenoid synthesis (IspG/H), is connected to both pathways, but it would act in a later step, serving as a relay of IscA or SufA. Quite similarly, NfuA is also connected to both pathways receiving an Fe-S cluster from the IscU or SufBCD scaffold proteins (Py et al., 2012). For other proteins, the situation is more uncertain. There is no clear information on the relationship of ApbC with one of these pathways. For Grx4, the fact that a mutation of individual genes of the isc operon in a *grxD*/*ydhD* recipient mutant strain leads to an aggravating phenotype, is in favor of Grx4 cooperating with the *suf* operon (Butland et al., 2008). Recently, Grx4 was found to cooperate with NfuA for the maturation of MiaB, a radical SAM-dependent enzyme involved in tRNA maturation (Boutigny et al., 2013).

The system found in eukaryotes is quite similar to the bacterial system but it is compartmentalized in mitochondria. Its integrity is required for the functioning of the CIA machinery and there are a few additional actors (Lill et al., 2012). As in bacteria, an $[Fe_2S_2]$ cluster is first synthesized on the Isu1 scaffold protein, prior to its dissociation and transfer to specific ISC targeting factors responsible for its shuttling and efficient insertion into target apoproteins (Mühlenhoff et al., 2003). The *de novo* synthesis on Isu1 requires the Nfs1–Isd11 complex for providing S, the NAD(P)H-ferredoxin reductase (Arh1p) (Li et al., 2001) and ferredoxin (Yah1p in yeast) (Lange et al., 2000) for electron transfer, and possibly frataxin as an iron donor. Although purified Nfs1 can function as a cysteine desulfurase releasing sulfide *in vitro* in the presence of dithiothreitol, it has no activity in the absence of Isd11, which might

have a stabilizing effect (Mühlenhoff et al., 2004; Adam et al., 2006; Wiedemann et al., 2006). Isd11 is a member of the LYR protein family and it has no ortholog in prokaryotes (Richards and van der Giezen, 2006; Atkinson et al., 2011). The dissociation of the cluster from Isu1 requires its interaction with an intermediate chaperone complex comprising Ssq1 and Jac1, the orthologous proteins to HscA and HscB. It also requires additional factors such as the nucleotide exchange factor Mge1 and the monothiol glutaredoxin Grx5 which may transiently coordinate the Fe-S cluster considering the ability of this type of Grxs to bind $[Fe_2S_2]$ clusters into dimers (Rodriguez-Manzaneque et al., 2002; Mühlenhoff et al., 2003; Bandyopadhyay et al., 2008a). These steps are necessary for the maturation of all mitochondrial Fe-S proteins, but also for cytosolic and nuclear Fe-S protein biogenesis, and for transcriptional iron regulation *via* mitochondria. Therefore, these components are named "ISC core proteins."

The maturation of certain Fe-S proteins requires additional specific proteins named ISC targeting factors, selectively interacting with subsets of Fe-S proteins (Lill et al., 2012). These late-acting components do not contribute to extra-mitochondrial processes. Isa proteins together with Iba57 are required for specific Fe-S enzymes, such as the mitochondrial aconitase and two radical SAM enzymes, the biotin and lipoic acid synthases (Gelling et al., 2008; Mühlenhoff et al., 2011; Sheftel et al., 2012). Nfu1 is required for the function of lipoic acid synthase (Navarro-Sastre et al., 2011). For organisms possessing a respiratory complex I, the P-loop NTPase Ind1 is important for its assembly (Bych et al., 2008a; Sheftel et al., 2009). Most ISC components are essential for the viability of yeast and human cells, pointing to the importance of this pathway.

The mitochondrial ISC system in Arabidopsis thaliana

The basic mechanisms of the ISC system described above likely apply for plant mitochondria, as all components, both ISC core and targeting proteins, are found in *Arabidopsis* (**Table 1**) (**Figure 3**) (Balk and Pilon, 2011). The major difference is that some gene families (ISCU, ISCA and NFU) are slightly expanded compared with non-plant eukaryotes. A recombinant *Arabidopsis* cysteine desulfurase, AtNFS1, expressed and purified from *E. coli*, was able to catalyze the release of sulfide from cysteine (Frazzon et al., 2007). Furthermore, AtNFS1 promotes assembly of an Fe-S cluster *in vitro* on a recombinant AtISU1 scaffold protein in a time- and cysteine-dependent manner and it interacts with frataxin (Frazzon et al., 2007; Turowski et al., 2012). In addition to ISU1, two other ISU proteins (AtISU2 and AtISU3) are also located in *Arabidopsis* mitochondria, and all ISUs can complement a yeast Δ*isu1*Δ*nfu1* thermo-sensitive mutant strain (Leon et al., 2005). It is not yet clear which interacting protein is required for AtNFS1 function since the plant ISD11 ortholog has not been

Table 1 | *Arabidopsis thaliana* members of the mitochondrial ISC machinery.

Protein names	AGI numbers	Phenotype(s) of mutant plants	Reference(s)
NFS1	At5g65720	Embryo lethal	Frazzon et al., 2007
SUFE1	At4g26500	Embryo lethal	Xu and Moller, 2006
ISD11	At5g61220	None yet described	
ISU1	At4g22220	Likely embryo-lethal but only knock down by RNAi was achieved	Frazzon et al., 2007
ISU2	At3g01020	None yet described	
ISU3	At4g04080	None yet described	
FH	At4g03240	Embryo lethal	Busi et al., 2006
mFDX1	At4g05450	None yet described	
mFDX2	At4g21090	None yet described	
mFDXR	At432360	None yet described	
HSCA1	At4g37910	None yet described	
HSCA2	At5g09590	None yet described	
HSCB	At5g06410	Reduced seed set, waxless phenotype, inappropriate trichome development, decreased Fe-S enzyme activities	Xu et al., 2009
MGE1a	At4g26780	None yet described	
MGE1b	At5g55200	None yet described	
ISCA2	At2g16710	None yet described	
ISCA3	At2g36260	None yet described	
ISCA4	At5g03905	None yet described	
NFU4	At3g20970	None yet described	
NFU5	At1g51390	None yet described	
IND1-like/INDH	At4g19540	None yet described	
IBA57.1	At4g12130	Embryo lethal	Waller et al., 2012
GRXS15	At3g15660	Sensitivity to H_2O_2	Cheng, 2008

A. thaliana SUFE1 is dual targeted to plastids and mitochondria, AtHSCA and AtHSCB to the mitochondria and the cytosol. For ATCs (ISCA2 to ISCA4), the mitochondrial localization is based only on prediction and has not been experimentally confirmed.

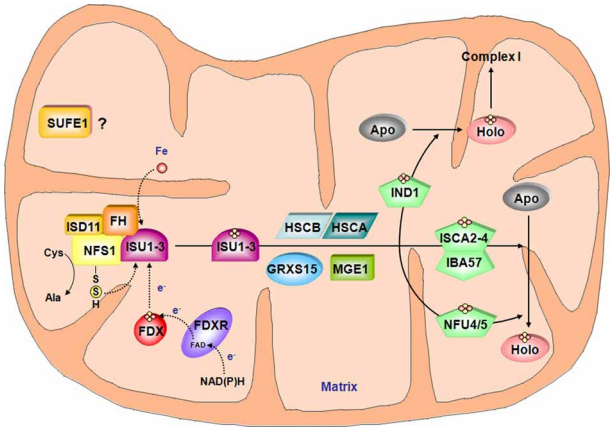

FIGURE 3 | Model for the Fe-S cluster assembly machinery in mitochondria. This scheme has been drawn essentially based on the current models of Fe-S cluster assembly for the bacterial and the mitochondrial yeast ISC machineries. The color code is the same as in **Figure 2**. The complex between the cysteine desulfurase NFS1 and ISD11 mobilizes sulfur from cysteine and frataxin (FH) promotes the interaction with the scaffold protein ISUs and favor sulfur transfer reaction. In addition to iron whose origin is yet unidentified, the Fe-S cluster synthesis on ISUs also requires electrons probably coming from the ferredoxin/ferredoxin reductase system. According to the yeast model, HSCA, HSCB, MGE1 and GRXS15 may be involved in Fe-S cluster release from ISU and subsequent transfer to carrier proteins such as IND1, ISCA2-4/IBA57 couple and NFU4-5 that finally transfer the Fe-S cluster to specific target proteins. Due to its localization in mitochondria and its ability to stimulate *in vitro* the activity of NFS1, SUFE1 may also be involved in sulfur mobilization.

functionally characterized and an additional interacting protein of AtNFS1, AtSUFE1, is found in mitochondria (Xu and Moller, 2006). Although the majority of an overexpressed SUFE1-GFP fusion was found to be localized to plastids, contribution of AtSUFE1 for the mitochondrial ISC machinery is supported by the observation that a plastidial targeted SUFE1 is not sufficient for complementing the embryo lethality of the mutant (Xu and Moller, 2006; Ye et al., 2006a).

As reported above, dissociation of the Fe-S cluster from the Nfs1-Isu1 complex requires accessory proteins in yeast mitochondria. *A. thaliana* HSCB, the yeast Jac1 ortholog, was shown to interact with the scaffold AtISU1 by yeast-two-hybrid and bimolecular fluorescence complementation (BiFc) (Xu et al., 2009). Moreover, it is able to complement a yeast *jac1* mutant strain. One of two abundant mitochondrial HSP70 chaperones, HSCA1 protein, has its ATPase activity stimulated *in vitro* by HSCB. Nevertheless, its involvement in Fe-S cluster assembly in mitochondria has not been investigated yet (Heazlewood et al., 2004). The involvement of the mitochondrial GRXS15 in the process of dissociation remains to be confirmed as this is the only plant monothiol Grx unable to complement the yeast *grx5* mutant (Bandyopadhyay et al., 2008a).

Among specialized targeting factors, very scarce functional information is available, although orthologs are present in *Arabidopsis* (**Table 1**). For NFU members, the mitochondrial localization has only been confirmed for NFU4 (Leon et al., 2003). NFU5 has, however, been identified in two proteomic studies performed with isolated mitochondria (Ito et al., 2006; Tan et al., 2010). From a functional point of view, both *A. thaliana* NFU4 and NFU5 are able to complement the yeast Δ*isu1*Δ*nfu1* thermo-sensitive mutant strain (Leon et al., 2003). Whether they participate to the general assembly pathway or to cluster assembly in specific Fe-S proteins awaits confirmation. The *Arabidopsis* mitochondrial IBA57 is an essential protein and seems to have conserved functions compared to other organisms. In particular, it is able to complement an *E. coli* mutant strain for the ygfZ ortholog by rescuing MiaB activity (Waller et al., 2010, 2012). *A. thaliana* IND1/INDH was found in mitochondria and it is expected, by analogy with other eukaryotes that it plays a role in the maturation of Fe-S proteins in complex I (Bych et al., 2008b). Finally, there is no information about the roles, subcellular localizations and properties of the three putative ATC isoforms (ISCA2 to 4) predicted to be targeted in mitochondria.

THE CHLOROPLASTIC SUF-LIKE SYSTEM

Overview of the SUF system in bacteria

Based on the organization of the *suf* operon in *E. coli*, the SUF system is primarily composed of six proteins. However, the situation is more complex as some bacteria have different operon architectures and other biogenesis factors encoded by isolated genes (Py et al., 2011). From genetic and biochemical investigations performed in *E. coli*, the current view is that SufE and SufS are involved in sulfur mobilization from cysteine. SufB, C and D form a complex where SufB harbors both the *de novo* assembled Fe-S cluster and a flavin redox cofactor, which could transmit the electrons required for reducing the sulfur. The ATC protein SufA likely acts as a carrier protein, but this assumption is challenged by the fact that SufA and ATCs in general can also bind mononuclear iron, sometimes with a good affinity (Fontecave et al., 2005; Lu et al., 2008; Chahal et al., 2009; Gupta et al., 2009; Wollers et al., 2010). A recent study added a higher level of complexity by showing that $SufBC_{(2)}D$ and $SufB_{(2)}C_{(2)}$ complexes harboring a preformed $[Fe_4S_4]$ cluster can serve for the maturation of $[Fe_2S_2]$-containing SufA or ferredoxin (Chahal and Outten, 2012), but also of NfuA (Py et al., 2012). These results support the view that SufBCD complexes, irrespective of their detailed composition, constitute the scaffold system assembling nascent Fe-S clusters which can be loaded on SufA or NfuA carriers for *in vitro* maturation of $[Fe_2S_2]$ enzymes like Fdx. As mentioned earlier, other proteins, not belonging to the *suf* operon, have been functionally associated with some components of the SUF machinery in *E. coli*. For instance, the csdA-csdE couple constitutes an additional cysteine desulfurase-sulfurtransferase system likely fueling the SufBCD complex (Loiseau et al., 2005; Trotter et al., 2009).

In cyanobacteria, Fe-S cluster biogenesis relies both on the ISC and SUF systems but only the latter is essential (Balasubramanian et al., 2006). Important differences with *E. coli* include the presence of a SufR repressor, of four cysteine desulfurases (two IscS, one SufS and one CsdA) and the absence of an IscU prototype. While a *sufA iscA* mutant in *E. coli* is not viable under aerobiosis (Vinella et al., 2009), a similar double mutant in *Synechococcus* sp PCC 7002 has similar growth to the wild type both under

standard and stress conditions (Balasubramanian et al., 2006). The most notable difference is the accumulation of transcripts for some Isc and Suf components in response to iron limitation and to oxidative stress which suggested that SufA and IscA may play regulatory roles in iron and/or redox sensing (Balasubramanian et al., 2006). On the contrary, inactivation of Nfu in this species is lethal pointing to an essential function likely related to PSI assembly as shown by *in vitro* experiments (Balasubramanian et al., 2006; Jin et al., 2008).

The chloroplastic SUF system in Arabidopsis thaliana

A SUF-like system exists in photosynthetic organisms: cyanobacteria, algae and terrestrial plants (**Figure 4**). Some additional assembly proteins have been identified in *A. thaliana* compared to the *E. coli* SUF machinery (**Table 2**). Among the core components, NFS2, SUFB, SUFC and SUFD are encoded by a single gene. There are three plastidial proteins containing a SufE domain. Considering that it is expressed in most tissues, SUFE1 might be the preferential activator of NFS2 in plastids (Ye et al., 2006a). It is worth noting that SUFE1 is unique to plants, having a C-terminal BolA domain that could contribute to its post-translational regulation (see section Post-Translational Control: Does the Grx/BolA Interaction also Constitute a Regulatory Link between Fe-S cluster Biogenesis and Cellular Iron Regulation in Plants?). The other two genes, *SUFE2* and *SUFE3*, have respectively, a specific expression in flowers and a low transcript level in all major plant organs (Murthy et al., 2007). All three SUFE proteins can stimulate NFS2 activity *in vitro*, and SUFE3 also possesses quinolinate synthase activity owing to the presence of a C-terminal NadA domain. No phenotype has yet been described for *sufE2* knock-out (KO) mutant, but the disruption of *SUFE1* and *SUFE3* genes results in arrested embryo development (Xu and Moller, 2006; Murthy et al., 2007). Basically, all KO mutants for these early-acting core components described thus far are embryo-lethal (**Table 2**) (Xu and Moller, 2004, 2006; Hjorth et al., 2005; Murthy et al., 2007; Van Hoewyk et al., 2007; Nagane et al., 2010).

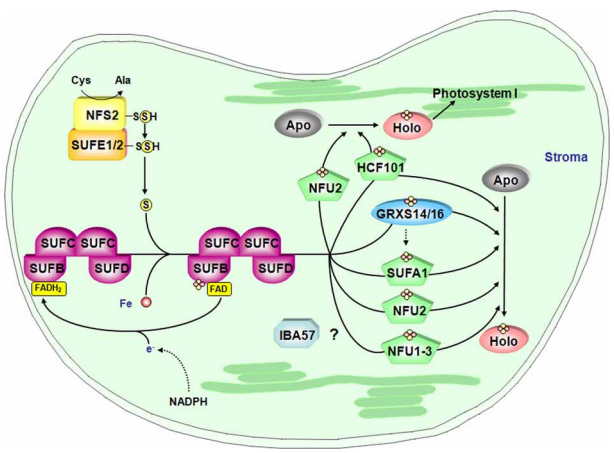

FIGURE 4 | Model for the Fe-S cluster assembly machinery in chloroplasts. This scheme has been drawn essentially based on the current models of Fe-S cluster assembly for the plant plastidial and bacterial SUF assembly machineries. The color code is the same as in **Figure 2**. SUFE1/2 stimulate the cysteine desulfurase activity of NFS2 and transfer the sulfur to SUFB that fulfills scaffold protein function by forming a complex with SUFC and SUFD. The iron source is unknown and electrons may be channeled from NADPH to a SUFB-bound FAD *via* an as yet unidentified flavin reductase. Fe-S cluster transfer to specific proteins is then accomplished by carrier proteins. Hence, NFU2 and HCF101 are involved in the maturation of one or several proteins belonging to PSI and some other stromal proteins. Up to now, target proteins of SUFA1, NFU1 and 3 are not identified. Finally, some plants possess a plastidial isoform of IBA57. By analogy with the mitochondrial isoform, plastidial IBA57 might act as carrier protein in conjunction with SUFA1 but this assumption awaits confirmation. Finally, the role of GRXS14 and GRXS16 is uncertain but they may be involved in Fe-S cluster release from scaffold protein as in mitochondria and/or they could be carrier proteins for the delivery of Fe-S clusters to specific target proteins.

On the contrary, plant KO mutants for most genes coding targeting factors (generally carrier proteins) acting late during Fe-S cluster biogenesis, are viable. This may indicate either that there is redundancy among them or that their function is dispensable i.e., the transfer of preformed clusters from scaffold proteins to acceptor proteins could eventually occur *in vivo* in the absence of carrier proteins, though maybe at lower rates or lower specificities. To date, the only exception is an *hcf101* mutant, whose lethal phenotype might be explained by the essential nature of its targets, i.e., one or several of the three Fe-S proteins of PSI (Lezhneva et al., 2004; Stockel and Oelmuller, 2004). Other proteins have been proposed, based on *in vitro* or *in vivo* data, to participate in the assembly of Fe-S proteins in chloroplasts. For instance, the possible functioning of Grxs as carrier proteins was supported by data showing that two plant chloroplastic Grxs (GRXS14 and S16), which bridge one $[Fe_2S_2]$ cluster per homodimer, can rapidly and stoichiometrically transfer their cluster to an apo Fdx and that they complement a yeast *grx5* mutant (Bandyopadhyay et al., 2008a). Among the three plastidial NFU proteins, NFU1 to NFU3, NFU2 is the best functionally characterized. The domain organization of the plastidial NFU proteins is specific to photosynthetic eukaryote organisms. Nevertheless, both NFU1 and NFU2 are able to restore the growth of an *isu1 nfu1* yeast mutant, when targeted to yeast mitochondria (Leon et al., 2003). The phenotypic and physiological analysis of *nfu2* KO plants indicated that NFU2 contributes to the correct assembly of leaf FDX and PSI (Touraine et al., 2004; Yabe et al., 2004). Concerning ATC proteins, a KO mutant for *AtSUFA1*/*CpISCA* has no visible phenotype, although transcripts are found in most tissues and particularly in leaves (Yabe and Nakai, 2006). Nevertheless, biochemical evidence supported a role of SUFA1 in the SUF machinery. AtSUFA1 is able to transiently bind an $[Fe_2S_2]$ upon *in vitro* reconstitution that can be transferred to an apo-ferredoxin (Abdel-Ghany et al., 2005). On the other hand, the observation of a rapid, unidirectional and intact transfer of an $[Fe_2S_2]$ cluster from *A. thaliana* GRXS14 suggested possible physiological sequential steps for Fe-S cluster shuttling with GRXS14 acting before SUFA1 (Mapolelo et al., 2013).

THE CYTOSOLIC CIA SYSTEM

The CIA machinery is required for the maturation of cytosolic and nuclear Fe-S proteins and is restricted to eukaryotes. Owing

Table 2 | *Arabidopsis thaliana* members of the plastidial assembly machinery.

Protein names	AGI numbers	Phenotype(s) of mutant plants	Reference(s)
NFS2/CpNifS	At1g08490	A RNAi mutant is seedling lethal	Van Hoewyk et al., 2007
SUFE1	At4g26500	Embryo lethal	Xu and Moller, 2006
SUFE2	At1g67810	None yet described	
SUFE3	At5g50210	Embryo lethal	Murthy et al., 2007
SUFB/ NAP1	At4g04770	Strong alleles are embryo-lethal, weak alleles present a perturbation in the phytochrome signal transduction pathway and an impaired chlorophyll degradation	Moller et al., 2001; Nagane et al., 2010
SUFC/ NAP7	At3g10670	Embryo lethal	Xu and Moller, 2004
SUFD/ NAP6	At1g32500	Bleached plants with reduced root growth, defects in plastid morphology and in seed germination	Hjorth et al., 2005
SUFA1/CpISCA	At1g10500	No phenotype	Yabe and Nakai, 2006
NFU1	At4g01940	None yet described	
NFU2	At5g49940	Pale green, dwarf phenotype, inhibition of root growth. Impaired PSI and decreased levels of FDX	Touraine et al., 2004; Yabe et al., 2004
NFU3	At4g25910	None yet described	
HCF101	At3g24430	Strong alleles are seedling-lethal In weak alleles, reduced levels of [4Fe-4S] enzymes (PSI, FTR)	Lezhneva et al., 2004
IBA57.2	At1g60990	None yet described	
GRXS14	At3g54900	Increased carbonylation of plastidial proteins	Cheng et al., 2006
GRXS16	At2g38270	None yet described	

The plastidial localization of all these proteins has been experimentally confirmed. A. thaliana SUFE1 is dual targeted to plastids and mitochondria. There is another putative SUFB gene (At4g04770) but, from EST or transcriptomic data, there is no evidence that it is expressed.

to the absence of a cytosolic cysteine desulfurase, its functioning depends on the mitochondrial ISC machinery. Indeed, it was shown in yeast and human that mitochondrial Nfs1 is required for the assembly of extra-mitochondrial Fe-S proteins (Mühlenhoff et al., 2004; Kispal et al., 2005; Biederbick et al., 2006). Its fundamental role has been emphasized in recent years by the identification of several Fe-S proteins involved in DNA/RNA metabolism (White and Dillingham, 2012; Wu and Brosh, 2012). Whereas most of the CIA components have been first identified in yeast and mammals, orthologs are also present in plants (**Table 3**).

The CIA machinery in yeast and mammals

As already described for ISC and SUF assembly machineries, the first step of the CIA machinery consists of the *de novo* assembly of an Fe-S cluster onto scaffold proteins using three elements, sulfur, iron and electrons. To date, the source of iron is unknown. The sulfur is provided by the mitochondrial ISC machinery in the form of an unidentified sulfur-containing compound that is transported through the membranes (see section The ISC Export Machinery). The required electrons are initially delivered from NADPH and they are channeled through the FAD and FMN cofactors of the NADPH-dependent diflavin reductase Tah18 to the Fe-S protein Dre2 (Zhang et al., 2008; Netz et al., 2010; Banci et al., 2013). Interestingly, the maturation of Dre2 is dependent on the ISC but not on the CIA machinery indicating either that this is the primary Fe-S scaffold or that there is another pathway for the assembly of Fe-S clusters into this protein. However, the fact that it is unable to transfer its Fe-S cluster to target proteins as apo-ferredoxin (Yah1) and apo-isopropylmalate isomerase (Leu1) precluded considering Dre2 as a scaffold protein (Netz et al., 2010). Surprisingly, whereas Tah18 and Dre2 are required for Fe-S cluster assembly on both Nbp35 and Nar1, they are not for Cfd1.

In yeast and human, the scaffold function is ensured by two P-loop NTPases, Nbp35 and Cfd1, which form a tight heterotetrameric complex ligating four [Fe_4S_4] clusters, one at the C-terminus of each protein and two permanent clusters situated in the N-terminal region of the two Nbp35 monomers (Netz et al., 2007, 2012). The transfer of the Fe-S cluster to final acceptor proteins requires additional participants. The maturation of one of them, Nar1, is intriguing since it is both a target and a component of the CIA machinery. Indeed, the biochemical characterization of the yeast protein which exhibits a strong homology to [FeFe] hydrogenases revealed that it can bind two [Fe_4S_4] clusters, one which seems to be permanently present and one which is transferred to recipient proteins (Balk et al., 2004; Urzica et al., 2009). The Cia1 protein, which possesses a WD40 repeat domain, likely facilitates the transfer of the Fe-S cluster to acceptor proteins by interacting with Nar1 (Balk et al., 2005). More recently, two additional components, MET18/MMS19 and MIP18 (MMS19-interacting protein) were shown to bind to the Nar1/Cia1 complex in order to shuttle Fe-S clusters to a specific subset of Fe-S proteins, especially those involved in DNA metabolism (Weerapana et al., 2010; Gari et al., 2012; Stehling et al., 2012).

This quite simple model might well be more complex in mammalian cells considering the identification of a small cytosolic pool of ISC proteins, ISCS and ISCU1, in cultured human cells (Biederbick et al., 2006; Tong and Rouault, 2006). However, there

Table 3 | *Arabidopsis thaliana* members of the CIA and ISC export machineries.

Protein names	AGI numbers	Phenotype(s) of mutant plants	Reference(s)
NAR1/GOLLUM	At4g16440	Embryo lethal	Cavazza et al., 2008; Luo et al., 2012
CIA1	At2g26060	Embryo lethal	Luo et al., 2012
NBP35	At5g50960	Embryo lethal	Bych et al., 2008b
AE7/ MIP18/CIA2	At1g68310	Strong allele is embryo lethal, weak alleles are viable but exhibit highly accumulated DNA damage and cell cycle arrest	Yuan et al., 2010; Luo et al., 2012
MET18/MMS19	At5g48120	No phenotype under standard growth conditions	Luo et al., 2012
DRE2/CIAPIN	At5g18400	Embryo lethal	Bernard et al., 2013
TAH18/ATR3	At3g02280	Embryo lethal	Varadarajan et al., 2010
ATM3/ABCB7	At5g58270	Defects in root growth, chlorophyll content and seedling establishment	Kushnir et al., 2001; Kim et al., 2006; Bernard et al., 2009
ERV1/ALR	At1g49880	Embryo lethal	Carrie et al., 2010

Except ATM3 and ERV1 which code for the two protein components of the ISC machinery, all other genes code for proteins of the CIA machinery. Yeast and human names have been indicated. ATM1 (At4g28630), ATM2 (At4g28620), AE7.2/AEL1 (At3g50845) and AE7.3/AEL2 (At3g09380) genes have not been listed here considering that they are not able to complement atm3 and ae7 mutants. There are putative additional CIA1 (At4g32990) and DRE2 genes (At5g18362) but, from EST or transcriptomic data, there is no evidence that they are expressed.

is no clear evidence for their *in vivo* requirement for Fe-S assembly in this compartment. Besides, some other proteins could belong to the CIA machinery. In yeast, depletion of cytosolic Grx3 and Grx4 clearly affects cytosolic and nuclear Fe-S biogenesis but it also leads to defects in both the mitochondrial ISC machinery and the synthesis of heme and di-iron centers (Mühlenhoff et al., 2010). It has led to the proposal that these Grxs might function both in iron sensing and in intracellular iron delivery. Interestingly, human Dre2/anamorsin/Ciapin-1 was found to interact with the human Grx3 ortholog called PICOT (PKC-interacting cousin of thioredoxin) by yeast two hybrid, confirming previous high throughput data obtained in yeast (Tarassov et al., 2008; Saito et al., 2011). This interaction may also support the observation that Grx3/4 and Dre2 serve for the assembly of the di-ferric Tyr$^{\bullet}$ cofactor in yeast ribonucleotide reductase (Zhang et al., 2011). Overall, based on the strict definition that CIA components are only required for extra-mitochondrial Fe-S biogenesis, it seems that cytosolic monothiol Grxs cannot be considered as a CIA component *per se*. However, (i) the assembly of the Fe-S cluster in yeast Grx3/4 is not dependent on the CIA, similar to Cfd1 and Dre2, (ii) the depletion of Grx3 and 4 in the W303 genetic background is lethal and (iii) Fe-S clusters ligated by glutathione may be physiologically relevant (Mühlenhoff et al., 2010; Qi et al., 2012). These observations put therefore these Grxs at a central position, possibly for the primary building of an Fe-S cluster using the mitochondrial exported sulfur compound, and/or for the subsequent delivery of Fe or Fe-S centers.

The CIA machinery in Arabidopsis thaliana

The CIA machinery in plants should in principle be very similar to the one existing in other eukaryotic organisms, as plants possess orthologs of all identified CIA components except Cfd1 (**Figure 5**) (**Table 3**). Interestingly, except MMS19, all characterized genes are essential. The corresponding KO mutants are embryo-lethal highlighting the importance of one or several cytosolic or nuclear Fe-S enzymes (Bych et al., 2008b; Varadarajan et al., 2010; Luo et al., 2012; Bernard et al., 2013). They are mostly encoded by single genes which are usually constitutively expressed *in planta*.

As in other eukaryotes, the electrons required for Fe-S cluster assembly are probably relayed by a TAH18-DRE2 complex. For instance, the only partner of TAH18 also called ATR3 identified using a yeast 2-hybrid screen is DRE2 (Varadarajan et al., 2010). Interestingly, *A. thaliana* DRE2 can complement the yeast *dre2* mutant strain only upon AtTAH18 co-expression suggesting that it cannot interact with the yeast Tah18 ortholog (Bernard et al., 2013).

In the absence of Cfd1, NBP35 fulfils the scaffold function alone (Bych et al., 2008b; Kohbushi et al., 2009). The *A. thaliana* isoform does not complement a yeast *nbp35* mutant strain, whereas it does partially complement the yeast *cfd1* mutant strain suggesting that it does not have the capacity to interact with yeast Cfd1. The biochemical characterization of AtNBP35 revealed that it is a dimer able to bind a stable $[Fe_4S_4]$ cluster at the N-terminal part of each monomer and a more labile C-terminal $[Fe_4S_4]$ cluster bridged by the two monomers and which can be transferred *in vitro* to a yeast apo-Leu1 (Bych et al., 2008b).

The role of the targeting factors (NAR1, CIA1, AE7/MIP18 and MET18/MMS19) has been investigated recently in plants. The cytosolic aconitase and the nuclear DNA glycosylase ROS1, both containing $[Fe_4S_4]$ clusters, have decreased activities in a weak *ae7* allele, whereas the $[Fe_2S_2]$-containing aldehyde oxidase is unaffected by this mutation (Luo et al., 2012). It suggested that AE7 might be involved preferentially in $[Fe_4S_4]$ cluster maturation. The observed defects in the maintenance of nuclear genome integrity are likely associated with the Fe-S cluster assembly defect in various Fe-S proteins involved in DNA metabolism such as ROS1 (Luo et al., 2012). Using several complementary approaches (yeast two-hybrid, co-immunoprecipitation and BiFc) it was shown that AE7 interacts with both CIA1 and MET18 but not with NAR1, which led to a model slightly different from the one proposed in mammals (**Figure 5**). In contrast to

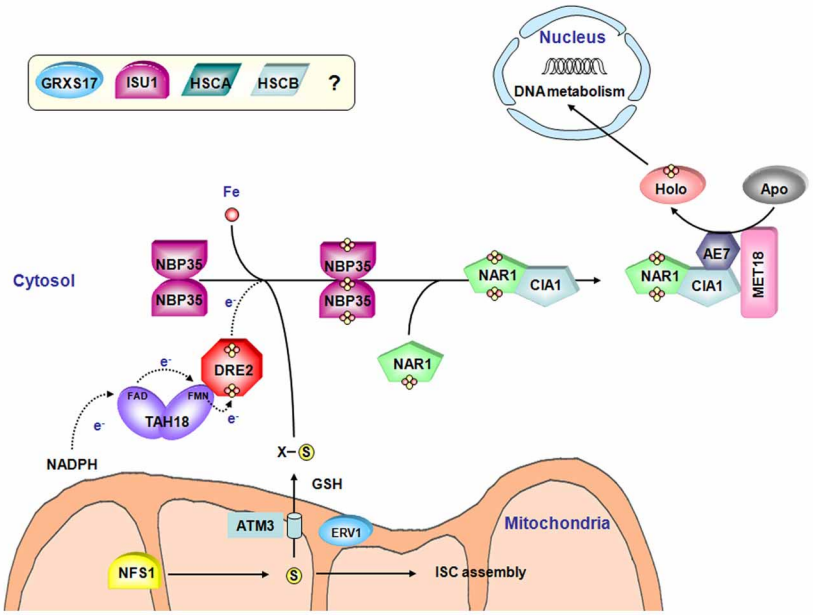

FIGURE 5 | Model for the Fe-S cluster assembly machinery in the cytosol. Both the CIA machinery and the connected ISC export machinery have been represented. The color code is the same as in **Figure 2**. A sulfide compound originating from NFS1 activity and preferentially transported by the ATM3 transporter may represent the sulfur source for Fe-S cluster biogenesis in the cytosol. ERV1, another mitochondrial protein and glutathione are also important for this process although their specific roles are not elucidated. As for organellar assembly machineries, the iron source is also unclear. Based on yeast and human models of the CIA machinery assembly, TAH18 transfers electrons from NADPH to DRE2. In plants, NBP35 constitutes the sole scaffold protein. Then, the Fe-S cluster is transferred to target apoproteins *via* a NAR1-CIA1-AE7-MET18 complex. The involvement of GRXS17 and of ISU1, HSCA and HSCB in the cytosolic Fe-S cluster biogenesis is not yet elucidated.

other partners forming this complex in plants and to *mms19* mutant in human, an *A. thaliana met18* KO mutant is viable and does not exhibit obvious phenotype compared to wild type plants. However, there is a genetic interaction between *AE7* and *MMS19/MET18* because a double mutant is non-viable (Luo et al., 2012). It raises therefore the question of the role of MMS19 in plants. AE7 can either bypass the effect of a MMS19 depletion by interacting with target proteins. Alternatively, proteins targeted by MMS19 are slightly different and do not have vital functions.

A role for the plant ortholog of GRX3/PICOT, named GRXS17, is not yet elucidated. The plant proteins are slightly different from the yeast and human counterparts having one and two additional Grx domains, respectively, being composed of an N-terminal Trx-like domain followed by three successive Grx domains (Couturier et al., 2009). To date, it has been demonstrated that a *grxS17* mutant is hypersensitive to high temperature conditions (Cheng et al., 2011). The authors suggested that GRXS17 might participate to the regulation of redox homeostasis and auxin perception in the temperature-dependent post-embryonic growth but a clear link to Fe-S cluster biogenesis is missing.

Finally, a puzzling piece of data is the observation, using over-expressed fusion proteins with YFP that AtHSCB together with AtHSCA1 and AtISCU1 may also be localized in the cytosol (Xu et al., 2009). Whether they play a role in the biogenesis of cytosol and nuclear Fe-S proteins requires further experimental support, as cleavage of such translational fusions may occur.

INTER-ORGANELLAR TRANSPORT AND SIGNALING

THE ISC EXPORT MACHINERY

The ISC export machinery connects the ISC to the CIA assembly machineries and has been characterized initially in yeast by showing that a deficiency in the mitochondrial Nfs1 and in the Atm1 ABC transporter affected the maturation of cytosolic Fe-S proteins (**Figure 5**) (Kispal et al., 1999). In eukaryote photosynthetic organisms, the SUF machinery and in particular NFS2 is not involved in the function of the CIA or ISC machineries (Van Hoewyk et al., 2007; Bernard et al., 2013). As the components of the ISC export machinery seem to be conserved in all eukaryotes, this system will be discussed in a single part.

As mentioned earlier, the mutation of any single ISC core components in yeast led to a deficiency in the biosynthesis of cytosolic and nuclear Fe-S proteins. Besides, it was shown that similar physiological and cellular defects were observed by (i) deleting or disrupting a mitochondrial ATP-binding cassette transporter, Atm1 in yeast, ABCB7 in human and ATM3 (STA1/ABCB25) in *A. thaliana* (Kispal et al., 1999; Kushnir et al., 2001; Bernard et al., 2009), (ii) deleting the sulfhydryl oxidase Erv1 (Lange et al., 2001) and (iii) decreasing GSH levels (Sipos et al., 2002). In yeast, a depletion in *atm1* or in the gene encoding the first GSH biosynthesis enzyme, *gsh1*, leads to the accumulation of iron in the mitochondrial matrix (Sipos et al., 2002; Kispal et al., 2005). In these mutants, only the maturation of extra-mitochondrial Fe-S proteins was affected. A double *gsh1atm1* mutant is non-viable (Sipos et al., 2002).

There are two other proteins related to ATM3 in *A. thaliana*, ATM1 and ATM2, but none is involved in this process, being unable to complement the yeast mutant (Chen et al., 2007). The *atm3 Arabidopsis* plants are dwarfed and chlorotic, and present defects in root growth, chlorophyll content, seedling establishment and genome integrity (Kushnir et al., 2001; Bernard et al., 2009; Luo et al., 2012). Interestingly, although *Arabidopsis* ATM3 can functionally complement the yeast *atm1* mutant, iron accumulation in mitochondria and iron homeostasis defects in *atm3* mutant plants were not observed (Chen et al., 2007; Bernard et al., 2009). This difference may indicate that the signal produced by the ISC machinery and exported from the mitochondria, though unknown, could be a sulfide compound rather than an Fe-S cluster form. Furthermore, mutants in *ATM3* accumulate cyclic pyranopterin monophosphate, the first intermediate of Moco biosynthesis, and have decreased amounts of Moco (Kim et al., 2006; Teschner et al., 2010). More generally, it is puzzling that yeast *atm1* or *Arabidopsis atm3* KO mutants are viable, whereas there are many essential Fe-S proteins in the cytosol and nucleus, and that mutants for all core CIA genes are lethal. It would suggest that the exported mitochondrial compound is either able to partially diffuse across membranes or that it can be transported by other transporter(s) though with lower efficiency.

Erv1 constitutes one of the principal component of the oxidative protein folding in the intermembrane mitochondrial space (IMS), together with Mia40 (Herrmann and Riemer, 2010). In yeast, *erv1* gene is essential for cell viability and for the biogenesis of functional mitochondria (Lisowsky, 1994). In *A. thaliana*, the disruption of the gene is also lethal (Carrie et al., 2010). Using a conditional *erv1* yeast mutant, Erv1 was shown to be involved in cell division, in the maintenance of mitochondrial genomes and in Fe-S cluster biogenesis (Lisowsky, 1994; Lange et al., 2001). The homologous mammalian protein ALR (augmenter of liver regeneration) is able to complement the yeast mutant indicating they have a conserved function (Lange et al., 2001). Whether the contribution of Erv1/ALR is direct *via* its oxidoreductase activity or an as yet unidentified function, or indirect by ensuring the correct folding of another contributor is not known. The demonstration that GSH is involved in this process would be in favor of a redox mechanism. This is in line with microarray analyses performed in yeast presenting low GSH levels which clearly indicates that one of the primary function of GSH is related to the regulation of iron homeostasis (Kumar et al., 2011). Hence, the redox buffering function described for plants for example may not be as important in yeast, since depletion of the GSH pool in yeast does not dramatically affect the survival of the strain until a certain limit. It was recently observed that the glutathione redox potential in the IMS impacts Mia40 redox state (Kojer et al., 2012) but, on the other hand that Mia40 could bind an Fe-S cluster *in vitro* and possibly *in vivo* (Daithankar et al., 2009). However, the lethal deletion of Mia40 in yeast has not been associated to defects in the maturation of Fe-S proteins and *Arabidopsis mia40* mutant plants have no visible phenotype, although they display a decreased amount of complex I (Chacinska et al., 2004; Carrie et al., 2010). This suggests that the phenotype observed following depletion of Erv1 may not be related to a defect in the folding of a protein required for Fe-S cluster assembly and likely relies on a Mia40-independent function.

MEMBRANE-ANCHORED NEET PROTEINS

MitoNEET is an Fe-S protein present in most living organisms except fungi. It was first identified as a target of piogliazone, an anti-diabetes drug (Colca et al., 2004). It is an outer mitochondrial membrane-anchored protein with one CDGSH domain oriented toward the cytoplasm (Wiley et al., 2007a). The CDGSH domain refers to a 39 amino acid motif [C-X-C-X2-(S/T)-X3-P-X-C-D-G-(S/A/T)-H] which contains the residues involved in Fe-S cluster binding. The mitoNEET proteins are dimers containing one [Fe_2S_2] cluster bound to each monomer and coordinated by 3 Cys and 1 His (Lin et al., 2007; Paddock et al., 2007; Wiley et al., 2007b; Conlan et al., 2009; Nechushtai et al., 2012). Substitution of the His by a Cys stabilizes the cluster and prevents its transfer to acceptor protein, revealing that this atypical coordination involving a single His residue is responsible for the relative instability of the cluster and the ability of mitoNEET to transfer it (Tirrell et al., 2009; Dicus et al., 2010; Conlan et al., 2011; Zuris et al., 2011). Moreover, only an oxidized mitoNEET can transfer its Fe-S cluster to an acceptor protein, revealing that the oxidation state of mitoNEET influences its transfer ability. Hence, it was hypothesized that changes in the cytosolic redox potential, which is normally a reducing environment precluding Fe-S transfer, may favor the transfer of the Fe-S cluster associated to the oxidized form of mitoNEET (Zuris et al., 2011). In agreement with these results, physiological concentrations of NADPH could destabilize the mitoNEET Fe-S cluster and regulate both the cellular level of holo mitoNEET, and/or its ability to transfer its cluster (Zhou et al., 2010; Zuris et al., 2012). Altogether these data, coupled to the existence of fusion proteins composed of a CDGSH domain and a FMN-binding domain in some prokaryotes, support the view of an involvement of mitoNEET protein in redox chemistry either in electron or in Fe-S cluster transfer.

Despite this, the physiological function of mitoNEET remains unclear. It could be linked to mitochondrial and/or cytosolic maturation of Fe-S clusters owing to its capacity to transfer Fe-S clusters (Paddock et al., 2007; Zuris et al., 2011; Nechushtai et al., 2012). More generally the analysis of *mitoNEET*-null mutant mice revealed that mitoNEET modulates the mitochondrial respiratory capacity possibly by controlling the iron content. Indeed, the reduction in mitoNEET expression in adipocytes enhanced both the iron content in the matrix and oxidative stress (Wiley et al., 2007a; Kusminski et al., 2012). In plants, there is a single gene that encodes a protein that is dual targeted to both the chloroplast and mitochondria (Nechushtai et al., 2012). While there is no *A. thaliana* KO plants for AtNEET available (this gene is likely essential), knockdown mutants displayed late greening and early senescence phenotypes and a reduced growth on low Fe level, but on the other hand, plants are insensitive to high Fe levels (Nechushtai et al., 2012). In addition, these plants accumulated higher levels of ROS and iron. Hence, all these results suggested that NEET would participate in Fe or Fe-S distribution between the different sub-cellular compartments, but further experiments

to investigate the effect on the Fe-S cluster assembly are necessary.

EVOLUTION OF [Fe-S] BIOGENESIS SYSTEMS IN PHOTOSYNTHETIC ORGANISMS

Considering the importance of Fe-S proteins for plant physiology and development, we sought to analyze the gene content for these assembly factors in various organisms along the green lineage to understand how gene families are conserved and potential novelties that appeared during evolution. The analysis of several sequenced genomes of photosynthetic organisms from cyanobacteria to higher plants revealed that the proteins are usually encoded by a relatively constant number of genes in all organisms and that core proteins of each machinery are mostly encoded by a single gene copy. However, some gene families have been specifically expanded in a few organisms. Another interesting evolutionary feature of these systems is the appearance of multidomain proteins in some species and the presence of similar protein domains in different assembly factors. Some novelties are detailed below.

Among CIA components, the case of MIP18/AE7 family is intriguing. Indeed, there are generally 1–3 genes coding for AE7-related proteins in all organisms analyzed. When 3 genes are present, they clearly form three separate clades. In *A. thaliana,* which possesses three genes, the phenotypic defects of the *ae7* mutant cannot be rescued by the two paralogs, *AEL1* and *AEL2* (Luo et al., 2012). Interestingly, the only gene present in algae, in the moss *Physcomitrella patens* and in the pteridophyte *Selaginella moellendorffii*, supposed to be the ancestral gene, does not group with the *A. thaliana AE7* gene found to participate in the CIA machinery (**Figure 6**). All angiosperms have at least one *AE7* gene. Genes forming the third clade are found specifically in Brassicaceae suggesting that an additional duplication occurred in the last common ancestor of this plant family. Altogether, these observations raise the question of the involvement of the ancestral gene in Fe-S cluster assembly and of the role of additional genes in organisms having multiple paralogs.

The SUFE family has been expanded in plants and its evolution in the green lineage is particular. The ancestral gene, found in cyanobacteria, encodes a single SufE domain protein and it does correspond to the *SUFE2* gene found in dicots. Gene fusion with a *BOLA* gene (for *SUFE1*) or with a quinolinate synthase *NADA* gene (for *SUFE3*) probably occurred in the ancestor of green algae and has been conserved throughout evolution in accordance with the observation that they are indispensable for plant physiology or development (Xu and Moller, 2006; Ye et al., 2006a; Murthy et al., 2007). Interestingly, a *SUFE2* gene is only found in dicots, except poplar (**Figure 6**). Due to its specific expression in pollen, this gene is probably associated with Fe-S cluster

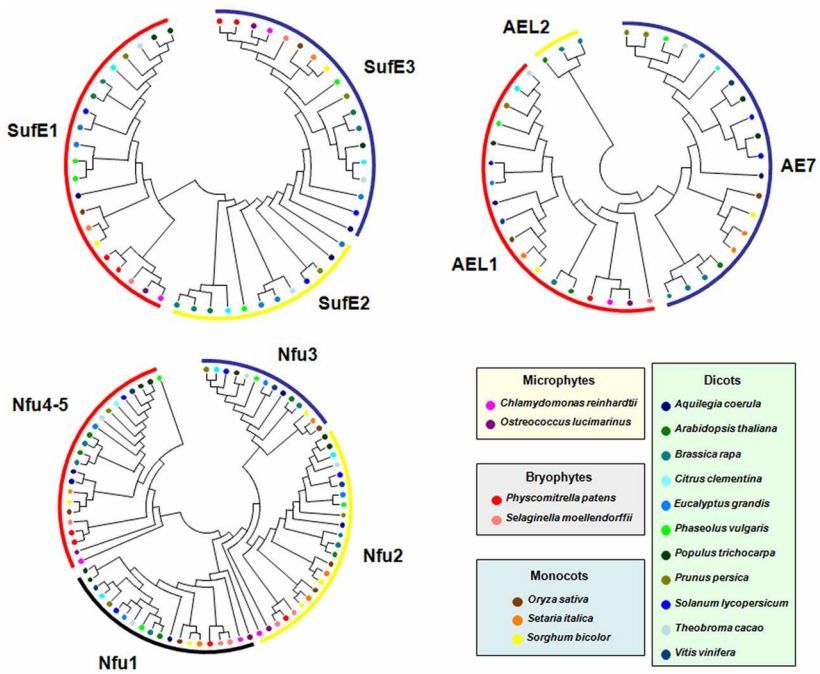

FIGURE 6 | Evolution of selected Fe-S biogenesis components in photosynthetic organisms. Proteins belonging to the SUFE, AE7 and NFU families have been retrieved in 17 other genomes from microphytes, bryophytes, monocots and dicots available in the Phytozome (version 9.1) database (http://www.phytozome.net/) by BLASTP or TBLASTN using Arabidopsis amino acid sequences. The amino acid sequence alignments were done using CLUSTALW and imported into the Molecular Evolutionary Genetics Analysis (MEGA) package version 4.1 for the phylogenetic analysis. Phylogenetic analyses were conducted using the neighbor-joining (NJ) method implemented in MEGA, with the pairwise deletion option for handling alignment gaps, and with the Poisson correction model for distance computation. Bootstrap tests were conducted using 1000 replicates. Branch lengths are proportional to phylogenetic distances. For more clarity, protein names have been removed and replaced by colored circles corresponding to specific organisms.

biogenesis specifically in this organ (Murthy et al., 2007). It may have been replaced by another SUFE protein in monocot flowers and became dispensable in green algae, or non-flowering organisms as *Selaginella* and *Physcomitrella*.

Concerning the NFU family, cyanobacteria have a single protein (NfuA) consisting of a single Nfu domain, whereas eukaryotes have usually two NFU prototypes corresponding to the plastidial NFU1-3 type and to the mitochondrial NFU4-5 type. The NFU1-3 type is typically formed by two Nfu domains, an N-terminal one that conserved the cysteine residues involved in Fe-S cluster binding and a degenerate C-terminal domain without these cysteines. Hence, these genes likely result from a fusion event between two *NFU* genes that took place in the last common ancestor of green algae. The NFU4-5 type is formed by a domain of unknown function of about 90 amino acids at the N-terminus and a single Nfu domain at the C-terminus. Hence, these genes have probably been formed through a different gene reshuffling event compared to *NFU1-3*. Most algae possess two genes of the NFU1-3 type and one gene of the NFU4-5 type, meaning that additional duplication events occurred in some angiosperms, in particular in *A. thaliana* (**Figure 6**). Very interestingly, one of the two NFU1-3 proteins present in some algae possesses, in addition to the two Nfu domains, an N-terminal extension of about 200 amino acids, with a predicted GIY-YIG nuclease domain. In this fusion protein, the Nfu domain may serve as a scaffold for the coordination of a divalent metal ion required for catalysis of the nuclease domain. This kind of sequence is also found in *P. patens* and in *Picea sitchensis*, while it seems to be absent in *S. moellendorffii* and in all other angiosperms analyzed. In this case, the evolutionary scenario is more uncertain. Even more interesting, this domain displays some similarity to the one found at the N-terminus of GRXS16, a Grx isoform specific to photosynthetic organisms. However, the similarity between the nuclease domains of these two proteins is not that strong, which may be explained by the existence of two different ancestral genes in cyanobacteria. Altogether, although the activity and importance of these N-terminal regions will have to be explored, this suggests a functional relationship between the two domains.

With the same idea, we have also noted that HCF101 proteins possess an N-terminal DUF59 domain that is also found in AE7 proteins, suggesting a conserved function of this domain possibly for protein-protein interactions and maybe for the recognition of proteins containing [Fe_4S_4] clusters (Lezhneva et al., 2004; Schwenkert et al., 2010; Luo et al., 2012).

A last intriguing case concerns *IBA57* genes. Most photosynthetic eukaryotes possess one *IBA57.1* gene related to those of α-proteobacteria and one *IBA57.2* gene related to those of cyanobacteria, coding for mitochondrial and plastidial proteins, respectively. Surprisingly, monocots and poplar do not possess the *IBA57.2* gene raising questions about the role and importance of the plastidial isoform for plants. In *A. thaliana*, the mitochondrial isoform is indispensable while no mutant for the *IBA57.2* gene was characterized so far (Waller et al., 2012). As proposed in this study, it is, however, possible that in organisms lacking IBA57.2, IBA57.1 is targeted to both sub-cellular compartments.

CURRENT OPEN QUESTIONS

In this part, we focus on a number of questions about key steps in the assembly process which are the subject of intense research or which should receive attention in the future.

WHERE DO IRON ATOMS COME FROM?

As reported above, the process of sulfur mobilization for Fe-S cluster assembly is well-described and involves cysteine desulfurases conserved throughout kingdoms. In contrast, the origin of iron is still largely unknown. As sulfide and iron are toxic as free entities, the cell has to tightly regulate the intracellular concentrations of both atoms. Moreover, whether there is a sequential or combined delivery of iron and sulfide on scaffold proteins for building an Fe-S cluster is under intense investigation.

The Fe storage proteins, ferritins, which are conserved in most organisms, would have been an obvious iron donor candidate both for heme and Fe-S cluster synthesis, but there is no evidence supporting their involvement (Briat et al., 2010). In *Arabidopsis*, a triple mutant (*atfer1-3-4*) for leaf ferritins has no apparent phenotype (Ravet et al., 2009), whereas mutant plants altered in most biogenesis factors are lethal. Moreover, frataxin-deficient yeast cells expressing the human mitochondrial ferritin still accumulate excess iron in their mitochondria and remained deficient in Fe-S cluster assembly (Sutak et al., 2012).

Much more attention has been paid to frataxin. The *E. coli* CyaY ortholog was shown to interact with the IscU–IscS complex *in vitro* (Adinolfi et al., 2009) and to bind iron with low affinity (Bou-Abdallah et al., 2004; Layer et al., 2006), without involving histidine or cysteine which are classical conserved residues found in iron-binding proteins (Bou-Abdallah et al., 2004; Pastore et al., 2007). It was also reported that the CyaY protein decreased the activity of the IscS cysteine desulfurase, leading to inhibition of the Fe-S cluster assembly (Prischi et al., 2010; Iannuzzi et al., 2011).

The yeast frataxin homologue (Yfh1) interacts physically with both Nfs–Isd11 and Isu1 (Gerber et al., 2003), it binds iron with high affinity (Stemmler et al., 2010; Subramanian et al., 2011) and it is required early in the ISC pathway for Fe-S cluster assembly on Isu1 (Mühlenhoff et al., 2003; Hoff et al., 2003). However, no clear consensus has been reached so far on the mechanistic role of this protein, although it is well-accepted that its primary function in yeast and human mitochondria is in Fe-S protein biogenesis. Frataxin is required for Nfs1–Isd11 desulfurase activity during *in vitro* Fe-S cluster synthesis (Tsai and Barondeau, 2010), but its function is not essential and serves to improve the efficiency of the ISC machinery (Yoon et al., 2012). A direct transfer of frataxin-bound iron to acceptor proteins has been documented (Yoon and Cowan, 2003), but an unambiguous *in vivo* confirmation has not been obtained so far (Mühlenhoff et al., 2002). Very recently, the biochemical and spectroscopic analyses of mouse Nfs1-IscU-Isd11 complexes with or without frataxin indicated that frataxin could control iron entry in the quaternary complex through the activation of Nfs1 cysteine desulfurase activity, at least in mammals (Colin et al., 2013).

Only one frataxin gene coding for an essential mitochondrial protein is found in the *Arabidopsis* genome (Busi et al., 2004). Indeed, contrary to yeast frataxin or *E. coli cyay* mutants which are perfectly viable, a KO mutant is embryo-lethal (Vazzola et al., 2007). A knockdown mutant in *A. thaliana* displayed a strong decrease of the activity of two mitochondrial Fe-S enzymes, namely aconitase and succinate dehydrogenase (Busi et al., 2006). The *atfh-1* plants also present a 1.6 fold elevated total iron content comparatively to wild type plants. It reflects a mitochondrial and possibly plastidial Fe content increase (Martin et al., 2009). Consequently, these plants, which have increased levels of superoxide and other ROS, are also hypersensitive to oxidative stress. Moreover, the analysis of these plants reveals an increase in NO production which helps to maintain low levels of oxidative damage in root cells, concomitant with the induction of the expression of the *FER1* and *FER4* ferritin genes (Martin et al., 2009). The role of plant frataxin in mitochondrial iron homeostasis has recently been reinforced by the demonstration of its involvement in heme synthesis (Maliandi et al., 2011). However, the precise biochemical function of frataxin remains to be determined.

Additional candidates for the iron-delivery function are ATC proteins and Grxs. Several arguments in favor or against the involvement of both proteins can be found in the section (The CIA Machinery in Yeast and Mammals) for Grxs and in the next section (Functional Analysis of NFU and ATC Proteins: How to Differentiate Between Iron Donor, Scaffold or Carrier Functions?) for ATCs.

FUNCTIONAL ANALYSIS OF NFU AND ATC PROTEINS: HOW TO DIFFERENTIATE BETWEEN IRON DONOR, SCAFFOLD OR CARRIER FUNCTIONS?

In the current literature, there is very often confusion between scaffold and carrier functions. Basically, a scaffold protein is the primary site of *de novo* cluster assembly. It interacts directly with the cysteine desulfurase or the persulfide-carrying partner protein (typically SufE) and most of the time it stimulates cysteine desulfurase activity. In contrast, carrier proteins would rather interact with the scaffold proteins or eventually with the chaperones also required for the cluster trafficking. Carrier proteins can generally receive Fe-S clusters from scaffold proteins but the opposite is not true. While it is generally accepted that IscU and SufBCD are scaffold proteins, the exact role of many other components, especially NFU and ATC proteins is not clearly defined.

Similar to human Nfu1 isoform, bacterial NfuA proteins from *E. coli*, *A. vinelandii* and *Synechococcus* sp. PCC 7002 can form $[Fe_4S_4]$ clusters upon reconstitution into dimeric proteins and they are able to transfer *in vitro* their cluster to various acceptor apoproteins, aconitase and PsaC for the cyanobacterial isoform (Tong et al., 2003; Angelini et al., 2008; Bandyopadhyay et al., 2008b; Jin et al., 2008; Py et al., 2012). While Nfu is an essential gene in *Synechococcus* and in human (Balasubramanian et al., 2006; Navarro-Sastre et al., 2011), this is not the case in *A. vinelandii* and *E. coli* since the mutants are viable, although an *A. vinelandii* NfuA mutant becomes lethal under elevated oxygen concentrations (Angelini et al., 2008; Bandyopadhyay et al., 2008b). In *A. thaliana*, inactivating *NFU2* gene resulted in a dwarf phenotype, primarily explained by an impaired PSI accumulation and thus deficient photosynthesis (Touraine et al., 2004; Yabe et al., 2004). A very detailed biochemical and functional analysis was achieved for *E. coli* NfuA, showing that both the degenerate ATC N-terminal domain, which is responsible of protein substrate recognition, and the Nfu domain are important for its *in vivo* function (Py et al., 2012). Considering the definitions detailed above, *E. coli* NfuA is definitely defined as a carrier protein since it has no effect on cysteine desulfurase activities and does not interact with cysteine desulfurases, whereas it can accept an Fe-S cluster from IscU/HscBA or SufBCD scaffold complex proteins (Py et al., 2012).

Concerning ATC proteins, their physiological functions are subject to an intense debate because their *in vitro* biochemical properties (type of bound Fe-S clusters and oligomeric state) do not entirely match *in vivo* analyses. *A. vinelandii* ^{Nif}IscA, and *Erwinia chrysanthemi* SufA are homodimeric proteins binding both labile $[Fe_2S_2]$ and $[Fe_4S_4]$ clusters, whereas *E. coli* IscA and SufA and *A. thaliana* SUFA1 binds $[Fe_2S_2]$ clusters, the former being tetrameric and the two latter dimeric (Ollagnier-de Choudens et al., 2003; Ollagnier-de-Choudens et al., 2004; Cupp-Vickery et al., 2004; Abdel-Ghany et al., 2005; Gupta et al., 2009; Mapolelo et al., 2012b). All Fe-S cluster-bound ATCs can generally efficiently transfer their clusters to usual acceptor proteins and some ATC can reversibly convert between $[Fe_2S_2]^{2+}$ and $[Fe_4S_4]^{2+}$ forms, which is convenient for delivering the correct type of clusters to specific proteins. Besides, several ATCs also bind mononuclear iron with different affinities raising the question of its *in vivo* significance (Cupp-Vickery et al., 2004; Sendra et al., 2007; Lu et al., 2010; Mapolelo et al., 2012a). The demonstration that ATCs do not interact with the cysteine desulfurase systems and that they can accept clusters formed on primary scaffold proteins, but that the opposite in not true, led to define them as carrier proteins. This has been clearly demonstrated for *E. coli* IscU/IscA, *E. coli* SufBCD/SufA or *A. vinelandii* NifU/^{Nif}IscA couples (Ollagnier-de-Choudens et al., 2004; Chahal and Outten, 2012; Mapolelo et al., 2012b). Thus, the current view is that ATC proteins are very versatile, binding mononuclear iron and accepting *in vitro* both types of preassembled clusters from primary scaffolds, and transferring also both types to acceptor proteins. However, the study of organisms depleted for *ATC* genes may help to differentiate between both capacities. Depletion of the mitochondrial Isa1/Isa2 in *S. cerevisiae* and ISCA1/ISCA2 in human or of IscA/SufA in *E. coli* indicated that they are not essential genes and that the proteins are involved in the maturation of $[Fe_4S_4]$proteins but not of $[Fe_2S_2]$proteins (Tan et al., 2009; Mühlenhoff et al., 2011; Sheftel et al., 2012). Similarly, deletion of SufA or IscA in prokaryotes is usually neither detrimental nor lethal, unless mutations are combined or under specific conditions, and depletion of the chloroplastic SUFA1 in *A. thaliana* has no effect when plants are grown under control conditions (Balasubramanian et al., 2006; Yabe and Nakai, 2006; Lu et al., 2008). These observations are not in favor of a role as a general Fe donor since the mutation of such genes would be expected to be lethal.

HOW IS Fe-S CLUSTER BIOGENESIS REGULATED/COORDINATED AT THE CELLULAR AND PLANT SCALE AND BY WHICH PROTEINS/MOLECULES?

The role of *A. thaliana* ATM3 and the whole ISC export machinery in the cross-talk between the mitochondrial ISC system and the cytosolic CIA system has already been discussed previously. Similarly, an involvement of NEET proteins for the regulation of inter-organellar Fe or Fe-S distribution has been proposed but it awaits firm confirmation.

Transcriptional control in response to environmental factors

Fe-S clusters are sensitive to oxygen and some derived reactive species such as superoxide anion, hydrogen peroxide or nitric oxide and their synthesis should be affected by iron and sulfur limitations. Hence, variations of several environmental factors should undoubtedly modulate the functioning of the biogenesis systems but this has been poorly documented to date.

In bacteria, many reports indicate that, when both systems are present, the ISC system behaves as the house-keeping machinery, whereas the SUF system is rather expressed under stress conditions (Lee et al., 2004; Outten et al., 2004; Yeo et al., 2006). In *E. coli*, the expression of both machineries is controlled by the IscR transcriptional regulator, which exists under two forms. An holo-IscR form containing a $[Fe_2S_2]$ cluster has the ability to bind to the promoter of the *isc* operon, repressing its expression (Schwartz et al., 2001). Impairment or loss of its cluster, due to sensitivity to oxygen or iron depletion, converts IscR to an apo-form which is released from the *isc* promoter, leading to the transcriptional activation of the *isc* operon. Incidentally, apo-IscR will activate the *suf* operon through its binding to the *suf* promoter region (Giel et al., 2006; Yeo et al., 2006). Therefore, under conditions of iron limitation and/or oxidative stress, the expression of both the ISC and SUF systems is induced. However, the SufS-SufE couple is less susceptible to H_2O_2-mediated oxidation than the IscS-IscU couple (Dai and Outten, 2012) and the SUF system may rely on an iron-independent flavin reductase system for electron donation instead of an iron-dependent system (FdR-Fdx) for the ISC system. Therefore, the SUF system is likely more adapted to oxidative conditions. It is notable that the *suf* and *isc* operons are also controlled by the OxyR, IHF and Fur transcription factors, but the interplay between all these regulatory mechanisms remains to be precisely investigated. In addition to this transcriptional control, the ISC system is also regulated by a small non-coding RNA, RyhB (Desnoyers et al., 2009). In response to Fe deficiency, RyhB is expressed and it binds to *iscS*, the second cistron of the polycistronic *iscRSUA* mRNA, leading to the cleavage of the downstream *iscSUA* transcript. A model of the genetic regulation of Fe-S cluster assembly systems in *E. coli* can be found in (Roche et al., 2013).

There is growing evidence that some assembly factors, especially carrier proteins, as ErpA and NfuA, are linked to both machineries in *E. coli* and that there is a certain level of redundancy (Py et al., 2011). However, the current view is that there may be different trafficking pathways for a single protein depending on the conditions. Typically the genetic analysis of null mutants for some genes indicated that lethal phenotypes are only observed under specific conditions. For instance, a very nice example concerns the maturation of the IspG and IspH proteins in *E. coli*, two enzymes required for the synthesis of isopentenyl diphosphate. It would necessitate the SufBCD–SufA system under stress conditions, but would use IscU, IscA and then ErpA in this order under aerobic conditions, and IscU and either ErpA or IscA in anaerobic conditions (Vinella et al., 2009).

In eukaryotic cells, and in yeast in particular, the regulation of expression of the genes encoding the various Fe-S cluster biogenesis machineries has not been studied into detail. It is so far unknown if the coordination of their action is mediated through transcriptional control, as in prokaryotes. As an example, it was shown that human *ISCU1/2* are repressed during hypoxia by the microRNA-210, as a way to control mitochondrial metabolism under this condition (Chan et al., 2009).

In plants, although public databases for gene expression can be questioned, almost no report has been published concerning the regulation of the expression of the ISC, SUF or CIA components. None of the above reported transcriptional regulators are encoded in plant or algal genomes. Some studies on isolated genes have been performed showing for example that in *A. thaliana*, *SUFB* gene expression is repressed upon iron starvation but the regulatory mechanisms are not known (Xu et al., 2005). More detailed studies would be important, in particular in the case of the SUF system which is located in the chloroplast, and therefore exposed to important changes in O_2 concentration between day and night, and to oxidative stress under high light intensity conditions. The regulation of expression of the genes encoding the SUF system has been investigated in *Synechocystis* sp. PCC 6803 (Wang et al., 2004), a cyanobacterium with an evolutionary relationship to chloroplasts. A SufR gene regulator possesses a DNA-binding domain and exhibits four highly conserved cysteine residues near its C-terminus enabling the coordination of two $[Fe_4S_4]$ cluster (Shen et al., 2007). Cells grown under oxidative or iron stress conditions have elevated levels of expression of the Suf operon, which are even higher in a null *sufR* mutant. SufR acts therefore as a transcriptional repressor whose activity depends on the presence or absence of an Fe-S cluster. Other information came from work done with the cyanobacterium *Synechococcus* PCC7002. In this organism, it has been proposed that, instead of having direct roles for Fe-S cluster assembly, SufA and IscA could play regulatory roles in iron homeostasis and in the sensing of redox stress (Balasubramanian et al., 2006). Clearly, there is a pressing need to understand whether and how assembly factors are controlled at the transcriptional level. Important conditions to assess would be those leading to iron and sulfur starvation, iron excess, and several other environmental constraints known to generate reactive oxygen or nitrogen species. Besides, the regulation of these genes in plants grown under various regimes of temperature and photoperiod or in response to a light/dark cycle would also bring valuable information to better understand the mechanisms of *de novo* synthesis or repair of Fe-S clusters.

Post-translational control: does the Grx/bola interaction also constitute a regulatory link between Fe-S cluster biogenesis and cellular iron regulation in plants?

BolA has been initially identified in a screen for *E. coli* mutants with altered cell morphology, which in the case of *bolA* mutation results in a round cell shape morphology (Aldea et al., 1988). In addition, BolA seems to be involved in cell protection from stress, cell proliferation or cell-cycle regulation (Kim et al., 2002). More recently, it was demonstrated that human BolA3 is required for the maturation of lipoate-containing 2-oxoacid dehydrogenases and for the assembly of the respiratory chain complexes (Cameron et al., 2011).

In *S. cerevisiae*, genetic and biochemical studies have revealed that Grx3 and Grx4 form a complex with two other proteins named Fra1 and Fra2 (Fe repressor of activation-1 and 2) corresponding to an aminopeptidase P-like protein and a BolA protein, respectively (Kumanovics et al., 2008). By interacting with the transcription factor Aft1p, which controls the expression of iron uptake and storage genes in *S. cerevisiae*, this complex senses the status of the mitochondrial Fe-S cluster biogenesis and regulates in turn Aft1 nuclear localization (Ojeda et al., 2006; Pujol-Carrion et al., 2006; Kumanovics et al., 2008).

However, Aft1 proteins are only present in a specific group of yeast species. For instance, in *Schizosaccharomyces pombe*, iron homeostasis is controlled by other transcription factors as Fep1 and Php4 and their activity is also regulated through a direct interaction with cytosolic monothiol Grxs but a requirement of BolA has not been explored (Mercier and Labbe, 2009; Jbel et al., 2011; Kim et al., 2011). As exemplified for the interaction with Aft1, it has been proposed that the C-terminal region of cytosolic monothiol Grxs constitutes the binding site for most iron responsive transcriptional factors, at least in fungi (Hoffmann et al., 2011).

Based on these observations, it appears crucial to explore whether the Grx-BolA proteins also participate to an iron sensing mechanism in other organisms. First, bioinformatic analyses indicated that both genes are frequently adjacent in prokaryotic genomes that some natural fusion proteins exist in a few microbes and that there is a very strong gene co-occurrence of these genes (Couturier et al., 2009). Moreover, high-throughput screen for interaction partners using yeast two hybrid studies showed that *Drosophila*, yeast and plant Grx and BolA proteins interact (Ho et al., 2002; Giot et al., 2003; Braun et al., 2011) and several biochemical studies have demonstrated that Grx and BolA from *S. cerevisiae*, *E. coli* and human can form $[Fe_2S_2]$-bridged heterodimers (Li et al., 2009, 2011, 2012; Yeung et al., 2011). In addition, recent work on the human mitochondrial BolA1 isoform revealed that it can interact with the mitochondrial Grx5 (Willems et al., 2013).

In plants, genomic analysis revealed the existence of four genes coding for proteins containing a BolA domain. Interestingly, whereas three of these genes code for proteins with a single domain and whose function is unknown, plants possess the chloroplastic SUFE1 protein which is a fusion protein constituted by an N-terminal SufE domain and a C-terminal BolA domain. As the activity of the cysteine desulfurase NFS2 is increased by SUFE1 (Xu and Moller, 2006; Ye et al., 2006a), it is tempting to speculate that plastidial monothiol Grxs could regulate the functioning of the SUF machinery by controlling the SUFE1-dependent NFS2 activity through an interaction with the BolA domain of SUFE1. Another possible regulatory mechanisms would consist of redox-dependent post-translational control of the sulfurtransferase activity as both *E. coli* SufE and CsdE, which do not have a BolA domain, have been shown to interact with a monothiol Grx through an intermolecular disulfide bond (Bolstad et al., 2010; Bolstad and Wood, 2010). Finally, using *in vitro* Fe-S cluster transfer experiments, it was shown that A-type proteins were able to transfer an $[Fe_2S_2]$ cluster to a Grx-BolA heterodimer, whereas, in the absence of BolA, the only cluster transfer observed was in the opposite direction, i.e., from cluster-bound holodimeric forms of glutaredoxins to A-type carriers (Mapolelo et al., 2013). This led to the conclusion that BolA proteins could convert monothiol Grxs from cluster donors to net cluster acceptors. All these data point to the possible involvement of Grx-BolA complexes either in the regulation of Fe-S cluster biogenesis or in the sensing of Fe-S cluster status in organelles where both proteins are simultaneously present.

Are there Fe-S cluster repair mechanisms?

Fe-S clusters in most proteins/enzymes can readily and directly react with oxygen and its derived oxidant molecules as peroxynitrite, superoxide ions, hydrogen peroxide, leading both to enzyme inactivation and to the release of Fe^{2+} (Keyer and Imlay, 1997; Djaman et al., 2004; Imlay, 2006; Jang and Imlay, 2007). This loss can fuel Fenton chemistry, producing even higher levels of toxic reactive oxygen species, which are deleterious to most macromolecules. This underlines quite simply the futile cycle that could occur upon metal release during oxidative stress conditions. This aspect is particularly important to consider in the context of the chloroplast, a sub-cellular compartment producing important levels of reactive oxygen or nitrogen species especially under environmental constraints. Thus, how cells maintain the activity of enzymes with sensitive clusters is a crucial question, because of the essential nature of many Fe-S enzymes for the cellular functioning. The simplest view is that cells, and plastids in particular, need more robust biogenesis pathways, and/or Fe-S reservoirs and/or repair systems. A few *in vivo* experiments have highlighted the existence of repair systems for damaged Fe-S proteins. This was illustrated for dehydratases whose $[Fe_4S_4]$ clusters are rapidly degraded into $[Fe_3S_4]$ forms in contact with univalent oxidants as hydrogen peroxide, superoxide or peroxynitrite (Keyer and Imlay, 1997; Djaman et al., 2004). By assessing in whole cells the disappearance of $[Fe_3S_4]$ EPR signal upon scavenging of hydrogen peroxide, it was concluded that *in vivo* repair systems exist. In bacteria, several genetic or biochemical evidence showed that the bacterial di-iron proteins YtfE belonging to the RIC family, and some ferritins as FtnA or FtnB or the YaaA protein could transiently store released iron (Velayudhan et al., 2007; Bitoun et al., 2008; Overton et al., 2008; Liu et al., 2011). This mechanism could attenuate the Fenton reaction that would occur in the presence of higher intracellular iron levels and could facilitate the re-assembly of the disrupted iron-sulfur clusters. In line with these results, it was found that the iron

stored in FtnA can be retrieved by IscA for the re-assembly of the iron-sulfur cluster in the IscU scaffold protein (Bitoun et al., 2008).

As mentioned previously, additional observations open new perspectives in the understanding of cluster disassembly/reassembly process in particular for O_2-sensitive [Fe_4S_4] clusters and *in vivo* repair mechanisms. Indeed, a cysteine persulfide-coordinated [Fe_2S_2] cluster has been observed in several enzymes as FNR, and most likely in aconitase or biotin synthase upon O_2-mediated disassembly of [Fe_4S_4] (Kennedy and Beinert, 1988; Zhang et al., 2012). For FNR, this intermediate can be used for the re-assembly of an active [Fe_4S_4] cluster pending the presence of iron and a reducing agent. These results have been strengthened by the recently described 3D structure of an [Fe_2S_2] cluster bound by two cysteine persulfides in the hydrogenase maturase HydE from *Thermotoga maritima* (Nicolet et al., 2013).

CONCLUSIONS AND PERSPECTIVES

The assembly of cellular Fe-S clusters in plants is governed by three biogenesis systems, the SUF, ISC and CIA machineries. Contrary to the plastidial SUF machinery which seems to function independently, the maturation of cytosolic and nuclear Fe-S proteins *via* the CIA machinery requires the function of the mitochondrial ISC machinery through an export system likely providing the sulfur source. Whereas the source of sulfur and of electrons required for these machineries has been *a priori* elucidated, how iron is mobilized and delivered is very poorly understood. Moreover, the current knowledge on the precise roles of each identified component is still limited and there is a pressing need to understand the functions of the remaining participants. In particular, whether GRX, ATC and NFU proteins act as scaffold or carrier proteins or eventually as iron donors has not been firmly elucidated so far. It is worth noting that many studies in plants are complicated by the fact that several genes are essential for embryo development. Hence, improving our knowledge on these mechanisms will require the study of knock down or conditional mutants as successfully achieved for AtNFS2 (Van Hoewyk et al., 2007). Another under-explored area of research concerns the regulation of the assembly processes by environmental factors and constraints and the repair mechanisms of damaged Fe-S clusters. A recent study highlighted that a circadian-controlled retrograde pathway from plastid-to-nucleus and involving phytochromes participates in Fe sensing (Salome et al., 2013). This opens interesting perspectives to decipher the signaling pathways and regulatory mechanisms allowing plant cells to adapt to changing conditions.

ACKNOWLEDGMENTS

The work of all authors is currently supported by ANR Grant No. 2010BLAN1616. The authors would like to thank Thomas Roret for his help with the drawing of **Figure 1**.

REFERENCES

Abdel-Ghany, S. E., Ye, H., Garifullina, G. F., Zhang, L., Pilon-Smits, E. A., and Pilon, M. (2005). Iron-sulfur cluster biogenesis in chloroplasts. Involvement of the scaffold protein CpIscA. *Plant Physiol.* 138, 161–172. doi: 10.1104/pp.104.058602

Adam, A. C., Bornhovd, C., Prokisch, H., Neupert, W., and Hell, K. (2006). The Nfs1 interacting protein Isd11 has an essential role in Fe/S cluster biogenesis in mitochondria. *EMBO J.* 25, 174–183. doi: 10.1038/sj.emboj.7600905

Adinolfi, S., Iannuzzi, C., Prischi, F., Pastore, C., Iametti, S., Martin, S. R., et al. (2009). Bacterial frataxin CyaY is the gatekeeper of iron-sulfur cluster formation catalyzed by IscS. *Nat. Struct. Mol. Biol.* 16, 390–396. doi: 10.1038/nsmb.1579

Aldea, M., Hernandez-Chico, C., de la Campa, A. G., Kushner, S. R., and Vicente, M. (1988). Identification, cloning, and expression of bolA, an ftsZ-dependent morphogene of *Escherichia coli*. *J. Bacteriol.* 170, 5169–5176.

Angelini, S., Gerez, C., Ollagnier-de Choudens, S., Sanakis, Y., Fontecave, M., Barras, F., et al. (2008). NfuA, a new factor required for maturing Fe/S proteins in *Escherichia coli* under oxidative stress and iron starvation conditions. *J. Biol. Chem.* 283, 14084–14091. doi: 10.1074/jbc.M709405200

Arnaud, N., Ravet, K., Borlotti, A., Touraine, B., Boucherez, J., Fizames, C., et al. (2007). The iron-responsive element (IRE)/iron-regulatory protein 1 (IRP1)-cytosolic aconitase iron-regulatory switch does not operate in plants. *Biochem. J.* 405, 523–531. doi: 10.1042/BJ20061874

Atkinson, A., Smith, P., Fox, J. L., Cui, T. Z., Khalimonchuk, O., and Winge, D. R. (2011). The LYR protein Mzm1 functions in the insertion of the Rieske Fe/S protein in yeast mitochondria. *Mol. Cell. Biol.* 31, 3988–3996. doi: 10.1128/MCB.05673-11

Atta, M., Mulliez, E., Arragain, S., Forouhar, F., Hunt, J. F., and Fontecave, M. (2010). S-Adenosylmethionine-dependent radical-based modification of biological macromolecules. *Curr. Opin. Struct. Biol.* 20, 684–692. doi: 10.1016/j.sbi.2010.09.009

Balasubramanian, R., Shen, G., Bryant, D. A., and Golbeck, J. H. (2006). Regulatory roles for IscA and SufA in iron homeostasis and redox stress responses in the cyanobacterium *Synechococcus* sp. strain PCC 7002. *J. Bacteriol.* 188, 3182–3191. doi: 10.1128/JB.188.9.3182-3191.2006

Balk, J., Aguilar Netz, D. J., Tepper, K., Pierik, A. J., and Lill, R. (2005). The essential WD40 protein Cia1 is involved in a late step of cytosolic and nuclear iron-sulfur protein assembly. *Mol. Cell. Biol.* 25, 10833–10841. doi: 10.1128/MCB.25.24.10833-10841.2005

Balk, J., Pierik, A. J., Netz, D. J., Mühlenhoff, U., and Lill, R. (2004). The hydrogenase-like Nar1p is essential for maturation of cytosolic and nuclear iron-sulphur proteins. *EMBO J.* 23, 2105–2115. doi: 10.1038/sj.emboj.7600216

Balk, J., and Pilon, M. (2011). Ancient and essential: the assembly of iron-sulfur clusters in plants. *Trends Plant Sci.* 16, 218–226. doi: 10.1016/j.tplants.2010.12.006

Banci, L., Bertini, I., Calderone, V., Ciofi-Baffoni, S., Giachetti, A., Jaiswal, D., et al. (2013). Molecular view of an electron transfer process essential for iron-sulfur protein biogenesis. *Proc. Natl. Acad. Sci. U.S.A.* 110, 7136–7141. doi: 10.1073/pnas.1302378110

Bandyopadhyay, S., Gama, F., Molina-Navarro, M. M., Gualberto, J. M., Claxton, R., Naik, S. G., et al. (2008a). Chloroplast monothiol glutaredoxins as scaffold proteins for the assembly and delivery of [2Fe-2S] clusters. *EMBO J.* 27, 1122–1133. doi: 10.1038/emboj.2008.50

Bandyopadhyay, S., Naik, S. G., O'Carroll, I. P., Huynh, B. H., Dean, D. R., Johnson, M. K., et al. (2008b). A proposed role for the *Azotobacter vinelandii* NfuA protein as an intermediate iron-sulfur cluster carrier. *J. Biol. Chem.* 283, 14092–14099.

Bernard, D. G., Cheng, Y., Zhao, Y., and Balk, J. (2009). An allelic mutant series of ATM3 reveals its key role in the biogenesis of cytosolic iron-sulfur proteins in Arabidopsis. *Plant Physiol.* 151, 590–602. doi: 10.1104/pp.109.143651

Bernard, D. G., Netz, D. J. A., Lagny, T. J., Pierik, A. J., and Balk, J. (2013). Requirements of the cytosolic iron-sulphur cluster assembly pathway in Arabidopsis. *Philos. Trans. Roy. Soc. B.* 368:20120259. doi: 10.1098/rstb.2012.0259

Biederbick, A., Stehling, O., Rosser, R., Niggemeyer, B., Nakai, Y., Elsasser, H. P., et al. (2006). Role of human mitochondrial Nfs1 in cytosolic iron-sulfur protein biogenesis and iron regulation. *Mol. Cell. Biol.* 26, 5675–5687. doi: 10.1128/MCB.00112-06

Bitoun, J. P., Wu, G., and Ding, H. (2008). *Escherichia coli* FtnA acts as an iron buffer for re-assembly of iron-sulfur clusters in response to hydrogen peroxide stress. *Biometals* 21, 693–703. doi: 10.1007/s10534-008-9154-7

Bolstad, H. M., Botelho, D. J., and Wood, M. J. (2010). Proteomic analysis of protein-protein interactions within the Cysteine Sulfinate Desulfinase Fe-S cluster biogenesis system. *J. Proteome Res.* 9, 5358–5369. doi: 10.1021/pr1006087

Bolstad, H. M., and Wood, M. J. (2010). An *in vivo* method for characterization of protein interactions within sulfur trafficking systems of *E. coli*. *J. Proteome Res.* 9, 6740–6751. doi: 10.1021/pr100920r

Bou-Abdallah, F., Adinolfi, S., Pastore, A., Laue, T. M., and Dennis Chasteen, N. (2004). Iron binding and oxidation kinetics in frataxin CyaY of *Escherichia coli*. *J. Mol. Biol.* 341, 605–615. doi: 10.1016/j.jmb.2004.05.072

Boutigny, S., Saini, A., Baidoo, E. E., Yeung, N., Keasling, J. D., and Butland, G. (2013). Physical and functional interactions of a monothiol glutaredoxin and an iron sulfur cluster carrier protein with the sulfur-donating radical S-adenosyl-L-methionine enzyme MiaB. *J. Biol. Chem*. 288, 14200–14211. doi: 10.1074/jbc.M113.460360

Braun, P., Carvunis, A. R., Charloteaux, B., Dreze, M., Ecker, J. R., Hill, D. E., et al. (2011). Evidence for network evolution in an Arabidopsis interactome map. *Science* 333, 601–607. doi: 10.1126/science.1203877

Briat, J. F., Duc, C., Ravet, K., and Gaymard, F. (2010). Ferritins and iron storage in plants. *Biochim. Biophys. Acta* 1800, 806–814. doi: 10.1016/j.bbagen.2009.12.003

Busi, M. V., Maliandi, M. V., Valdez, H., Clemente, M., Zabaleta, E. J., Araya, A., et al. (2006). Deficiency of *Arabidopsis thaliana* frataxin alters activity of mitochondrial Fe-S proteins and induces oxidative stress. *Plant J.* 48, 873–882. doi: 10.1111/j.1365-313X.2006.02923.x

Busi, M. V., Zabaleta, E. J., Araya, A., and Gomez-Casati, D. F. (2004). Functional and molecular characterization of the frataxin homolog from *Arabidopsis thaliana*. *FEBS Lett.* 576, 141–144. doi: 10.1016/j.febslet.2004.09.003

Butland, G., Babu, M., Diaz-Mejia, J. J., Bohdana, F., Phanse, S., Gold, B., et al. (2008). eSGA: *E. coli* synthetic genetic array analysis. *Nat. Methods* 5, 789–795. doi: 10.1038/nmeth.1239

Bych, K., Kerscher, S., Netz, D. J., Pierik, A. J., Zwicker, K., Huynen, M. A., et al. (2008a). The iron-sulphur protein Ind1 is required for effective complex I assembly. *EMBO J.* 27, 1736–1746. doi: 10.1038/emboj.2008.98

Bych, K., Netz, D. J., Vigani, G., Bill, E., Lill, R., Pierik, A. J., et al. (2008b). The essential cytosolic iron-sulfur protein Nbp35 acts without Cfd1 partner in the green lineage. *J. Biol. Chem.* 283, 35797–35804. doi: 10.1074/jbc.M807303200

Cameron, J. M., Janer, A., Levandovskiy, V., Mackay, N., Rouault, T. A., Tong, W. H., et al. (2011). Mutations in iron-sulfur cluster scaffold genes NFU1 and BOLA3 cause a fatal deficiency of multiple respiratory chain and 2-oxoacid dehydrogenase enzymes. *Am. J. Hum. Genet.* 89, 486–495. doi: 10.1016/j.ajhg.2011.08.011

Carrie, C., Giraud, E., Duncan, O., Xu, L., Wang, Y., Huang, S., et al. (2010). Conserved and novel functions for *Arabidopsis thaliana* MIA40 in assembly of proteins in mitochondria and peroxisomes. *J. Biol. Chem.* 285, 36138–36148. doi: 10.1074/jbc.M110.121202

Cavazza, C., Martin, L., Mondy, S., Gaillard, J., Ratet, P., and Fontecilla-Camps, J. C. (2008). The possible role of an [FeFe]-hydrogenase-like protein in the plant responses to changing atmospheric oxygen levels. *J. Inorg. Biochem.* 102, 1359–1365. doi: 10.1016/j.jinorgbio.2008.01.027

Chacinska, A., Pfannschmidt, S., Wiedemann, N., Kozjak, V., Sanjuan Szklarz, L. K., Schulze-Specking, A., et al. (2004). Essential role of Mia40 in import and assembly of mitochondrial intermembrane space proteins. *EMBO J.* 23, 3735–3746. doi: 10.1038/sj.emboj.7600389

Chahal, H. K., Dai, Y., Saini, A., Ayala-Castro, C., and Outten, F. W. (2009). The SufBCD Fe-S scaffold complex interacts with SufA for Fe-S cluster transfer. *Biochemistry* 48, 10644–10653. doi: 10.1021/bi901518y

Chahal, H. K., and Outten, F. W. (2012). Separate FeS scaffold and carrier functions for SufB(2)C(2) and SufA during *in vitro* maturation of [2Fe2S] Fdx. *J. Inorg. Biochem.* 116, 126–134. doi: 10.1016/j.jinorgbio.2012.06.008

Chan, S. Y., Zhang, Y. Y., Hemann, C., Mahoney, C. E., Zweier, J. L., and Loscalzo, J. (2009). MicroRNA-210 controls mitochondrial metabolism during hypoxia by repressing the iron-sulfur cluster assembly proteins ISCU1/2. *Cell Metab.* 10, 273–284. doi: 10.1016/j.cmet.2009.08.015

Chandramouli, K., Unciuleac, M. C., Naik, S., Dean, D. R., Huynh, B. H., and Johnson, M. K. (2007). Formation and properties of [4Fe-4S] clusters on the IscU scaffold protein. *Biochemistry* 46, 6804–6811. doi: 10.1021/bi6026659

Chen, S., Sanchez-Fernandez, R., Lyver, E. R., Dancis, A., and Rea, P. A. (2007). Functional characterization of AtATM1, AtATM2, and AtATM3, a subfamily of Arabidopsis half-molecule ATP-binding cassette transporters implicated in iron homeostasis. *J. Biol. Chem.* 282, 21561–21571. doi: 10.1074/jbc.M702383200

Cheng, N. H. (2008). AtGRX4, an Arabidopsis chloroplastic monothiol glutaredoxin, is able to suppress yeast grx5 mutant phenotypes and respond to oxidative stress. *FEBS Lett.* 582, 848–854. doi: 10.1016/j.febslet.2008.02.006

Cheng, N. H., Liu, J. Z., Brock, A., Nelson, R. S., and Hirschi, K. D. (2006). AtGRXcp, an Arabidopsis chloroplastic glutaredoxin, is critical for protection against protein oxidative damage. *J. Biol. Chem.* 281, 26280–26288. doi: 10.1074/jbc.M601354200

Cheng, N. H., Liu, J. Z., Liu, X., Wu, Q., Thompson, S. M., Lin, J., et al. (2011). Arabidopsis monothiol glutaredoxin, AtGRXS17, is critical for temperature-dependent postembryonic growth and development via modulating auxin response. *J. Biol. Chem.* 286, 20398–20406. doi: 10.1074/jbc.M110.201707

Colca, J. R., McDonald, W. G., Waldon, D. J., Leone, J. W., Lull, J. M., Bannow, C. A., et al. (2004). Identification of a novel mitochondrial protein ("mitoNEET") cross-linked specifically by a thiazolidinedione photoprobe. *Am. Physiol. Endocrinol. Metab.* 286, E252–E260. doi: 10.1152/ajpendo.00424.2003

Colin, F., Martelli, A., Clemancey, M., Latour, J. M., Gambarelli, S., Zeppieri, L., et al. (2013). Mammalian frataxin controls sulfur production and iron entry during de novo Fe4S4 cluster assembly. *J. Am. Chem. Soc.* 135, 733–740. doi: 10.1021/ja308736e

Conlan, A. R., Axelrod, H. L., Cohen, A. E., Abresch, E. C., Zuris, J., Yee, D., et al. (2009). Crystal structure of Miner1: the redox-active 2Fe-2S protein causative in Wolfram Syndrome 2. *J. Mol. Biol.* 392, 143–153. doi: 10.1016/j.jmb.2009.06.079

Conlan, A. R., Paddock, M. L., Homer, C., Axelrod, H. L., Cohen, A. E., Abresch, E. C., et al. (2011). Mutation of the His ligand in mitoNEET stabilizes the 2Fe-2S cluster despite conformational heterogeneity in the ligand environment. *Acta Crystallogr. D Biol. Crystallogr.* 67, 516–523. doi: 10.1107/S0907444911011577

Couturier, J., Jacquot, J. P., and Rouhier, N. (2009). Evolution and diversity of glutaredoxins in photosynthetic organisms. *Cell. Mol. Life Sci.* 66, 2539–2557. doi: 10.1007/s00018-009-0054-y

Cupp-Vickery, J. R., Silberg, J. J., Ta, D. T., and Vickery, L. E. (2004). Crystal structure of IscA, an iron-sulfur cluster assembly protein from *Escherichia coli*. *J. Mol. Biol.* 338, 127–137. doi: 10.1016/j.jmb.2004.02.027

Dai, S., Friemann, R., Glauser, D. A., Bourquin, F., Manieri, W., Schürmann, P., et al. (2007). Structural snapshots along the reaction pathway of ferredoxin-thioredoxin reductase. *Nature* 448, 92–96. doi: 10.1038/nature05937

Dai, Y., and Outten, F. W. (2012). The *E. coli* SufS-SufE sulfur transfer system is more resistant to oxidative stress than IscS-IscU. *FEBS Lett.* 586, 4016–4022. doi: 10.1016/j.febslet.2012.10.001

Daithankar, V. N., Farrell, S. R., and Thorpe, C. (2009). Augmenter of liver regeneration: substrate specificity of a flavin-dependent oxidoreductase from the mitochondrial intermembrane space. *Biochemistry* 48, 4828–4837. doi: 10.1021/bi900347v

Desnoyers, G., Morissette, A., Prevost, K., and Masse, E. (2009). Small RNA-induced differential degradation of the polycistronic mRNA iscRSUA. *EMBO J.* 28, 1551–1561. doi: 10.1038/emboj.2009.116

Dicus, M. M., Conlan, A., Nechushtai, R., Jennings, P. A., Paddock, M. L., Britt, R. D., et al. (2010). Binding of histidine in the (Cys)3(His)1-coordinated [2Fe-2S] cluster of human mitoNEET. *J. Am. Chem. Soc.* 132, 2037–2049. doi: 10.1021/ja909359g

Djaman, O., Outten, F. W., and Imlay, J. A. (2004). Repair of oxidized iron-sulfur clusters in *Escherichia coli*. *J. Biol. Chem.* 279, 44590–44599. doi: 10.1074/jbc.M406487200

Fleischhacker, A. S., and Kiley, P. J. (2011). Iron-containing

transcription factors and their roles as sensors. *Curr. Opin. Chem. Biol.* 15, 335–341. doi: 10.1016/j.cbpa.2011.01.006

Fontecave, M., Choudens, S. O., Py, B., and Barras, F. (2005). Mechanisms of iron-sulfur cluster assembly: the SUF machinery. *J. Biol. Inorg. Chem.* 10, 713–721. doi: 10.1007/s00775-005-0025-1

Frazzon, A. P., Ramirez, M. V., Warek, U., Balk, J., Frazzon, J., Dean, D. R., et al. (2007). Functional analysis of Arabidopsis genes involved in mitochondrial iron-sulfur cluster assembly. *Plant Mol. Biol.* 64, 225–240. doi: 10.1007/s11103-007-9147-x

Fuzery, A. K., Tonelli, M., Ta, D. T., Cornilescu, G., Vickery, L. E., and Markley, J. L. (2008). Solution structure of the iron-sulfur cluster cochaperone HscB and its binding surface for the iron-sulfur assembly scaffold protein IscU. *Biochemistry* 47, 9394–9404. doi: 10.1021/bi800502r

Gari, K., Leon Ortiz, A. M., Borel, V., Flynn, H., Skehel, J. M., and Boulton, S. J. (2012). MMS19 links cytoplasmic iron-sulfur cluster assembly to DNA metabolism. *Science* 337, 243–245. doi: 10.1126/science.1219664

Gelling, C., Dawes, I. W., Richhardt, N., Lill, R., and Mühlenhoff, U. (2008). Mitochondrial Iba57p is required for Fe/S cluster formation on aconitase and activation of radical SAM enzymes. *Mol. Cell. Biol.* 28, 1851–1861. doi: 10.1128/MCB.01963-07

Gerber, J., Muhlenhoff, U., and Lill, R. (2003). An interaction between frataxin and Isu1/Nfs1 that is crucial for Fe/S cluster synthesis on Isu1. *EMBO Rep.* 4, 906–911. doi: 10.1038/sj.embor.embor918

Giel, J. L., Rodionov, D., Liu, M., Blattner, F. R., and Kiley, P. J. (2006). IscR-dependent gene expression links iron-sulphur cluster assembly to the control of O2-regulated genes in *Escherichia coli*. *Mol. Microbiol.* 60, 1058–1075. doi: 10.1111/j.1365-2958.2006.05160.x

Giot, L., Bader, J. S., Brouwer, C., Chaudhuri, A., Kuang, B., Li, Y., et al. (2003). A protein interaction map of *Drosophila melanogaster*. *Science* 302, 1727–1736. doi: 10.1126/science.1090289

Gupta, V., Sendra, M., Naik, S. G., Chahal, H. K., Huynh, B. H., Outten, F. W., et al. (2009). Native *Escherichia coli* SufA, coexpressed with SufBCDSE, purifies as a [2Fe-2S] protein and acts as an Fe-S transporter to Fe-S target enzymes. *J. Am. Chem. Soc.* 131, 6149–6153. doi: 10.1021/ja807551e

Heazlewood, J. L., Tonti-Filippini, J. S., Gout, A. M., Day, D. A., Whelan, J., and Millar, A. H. (2004). Experimental analysis of the Arabidopsis mitochondrial proteome highlights signaling and regulatory components, provides assessment of targeting prediction programs, and indicates plant-specific mitochondrial proteins. *Plant Cell* 16, 241–256. doi: 10.1105/tpc.016055

Herrmann, J. M., and Riemer, J. (2010). The intermembrane space of mitochondria. *Antioxid. Redox Signal.* 13, 1341–1358. doi: 10.1089/ars.2009.3063

Hjorth, E., Hadfi, K., Zauner, S., and Maier, U. G. (2005). Unique genetic compartmentalization of the SUF system in cryptophytes and characterization of a SufD mutant in *Arabidopsis thaliana*. *FEBS Lett.* 579, 1129–1135. doi: 10.1016/j.febslet.2004.12.084

Ho, Y., Gruhler, A., Heilbut, A., Bader, G. D., Moore, L., Adams, S. L., et al. (2002). Systematic identification of protein complexes in *Saccharomyces cerevisiae* by mass spectrometry. *Nature* 415, 180–183. doi: 10.1038/415180a

Hoff, K. G., Cupp-Vickery, J. R., and Vickery, L. E. (2003). Contributions of the LPPVK motif of the iron-sulfur template protein IscU to interactions with the Hsc66-Hsc20 chaperone system. *J. Biol. Chem.* 278, 37582–37589. doi: 10.1074/jbc.M305292200

Hoff, K. G., Silberg, J. J., and Vickery, L. E. (2000). Interaction of the iron-sulfur cluster assembly protein IscU with the Hsc66/Hsc20 molecular chaperone system of *Escherichia coli*. *Proc. Natl. Acad. Sci. U.S.A.* 97, 7790–7795. doi: 10.1073/pnas.130201997

Hoffmann, B., Uzarska, M. A., Berndt, C., Godoy, J. R., Haunhorst, P., Lillig, C. H., et al. (2011). The multidomain thioredoxin-monothiol glutaredoxins represent a distinct functional group. *Antioxid. Redox Signal.* 15, 19–30. doi: 10.1089/ars.2010.3811

Iannuzzi, C., Adinolfi, S., Howes, B. D., Garcia-Serres, R., Clemancey, M., Latour, J. M., et al. (2011). The role of CyaY in iron sulfur cluster assembly on the *E. coli* IscU scaffold protein. *PLoS ONE* 6:e21992. doi: 10.1371/journal.pone.0021992

Imlay, J. A. (2006). Iron-sulphur clusters and the problem with oxygen. *Mol. Microbiol.* 59, 1073–1082. doi: 10.1111/j.1365-2958.2006.05028.x

Ito, J., Heazlewood, J. L., and Millar, A. H. (2006). Analysis of the soluble ATP-binding proteome of plant mitochondria identifies new proteins and nucleotide triphosphate interactions within the matrix. *J. Proteome Res.* 5, 3459–3469. doi: 10.1021/pr060403j

Jacquot, J. P., Eklund, H., Rouhier, N., and Schurmann, P. (2009). Structural and evolutionary aspects of thioredoxin reductases in photosynthetic organisms. *Trends Plant Sci.* 14, 336–343. doi: 10.1016/j.tplants.2009.03.005

Jang, S., and Imlay, J. A. (2007). Micromolar intracellular hydrogen peroxide disrupts metabolism by damaging iron-sulfur enzymes. *J. Biol. Chem.* 282, 929–937. doi: 10.1074/jbc.M607646200

Jbel, M., Mercier, A., and Labbe, S. (2011). Grx4 monothiol glutaredoxin is required for iron limitation-dependent inhibition of Fep1. *Eukaryot. Cell* 10, 629–645. doi: 10.1128/EC.00015-11

Jin, Z., Heinnickel, M., Krebs, C., Shen, G., Golbeck, J. H., and Bryant, D. A. (2008). Biogenesis of iron-sulfur clusters in photosystem I: holo-NfuA from the cyanobacterium *Synechococcus* sp. PCC 7002 rapidly and efficiently transfers [4Fe-4S] clusters to apo-PsaC *in vitro*. *J. Biol. Chem.* 283, 28426–28435. doi: 10.1074/jbc.M803395200

Johnson, D. C., Dean, D. R., Smith, A. D., and Johnson, M. K. (2005). Structure, function, and formation of biological iron-sulfur clusters. *Annu. Rev. Biochem.* 74, 247–281. doi: 10.1146/annurev.biochem.74.082803.133518

Kennedy, M. C., and Beinert, H. (1988). The state of cluster SH and S2- of aconitase during cluster interconversions and removal. A convenient preparation of apoenzyme. *J. Biol. Chem.* 263, 8194–8198.

Kennedy, M. C., Werst, M., Telser, J., Emptage, M. H., Beinert, H., and Hoffman, B. M. (1987). Mode of substrate carboxyl binding to the [4Fe-4S]+ cluster of reduced aconitase as studied by 17O and 13C electron-nuclear double resonance spectroscopy. *Proc. Natl. Acad. Sci. U.S.A.* 84, 8854–8858. doi: 10.1073/pnas.84.24.8854

Keyer, K., and Imlay, J. A. (1997). Inactivation of dehydratase [4Fe-4S] clusters and disruption of iron homeostasis upon cell exposure to peroxynitrite. *J. Biol. Chem.* 272, 27652–27659. doi: 10.1074/jbc.272.44.27652

Khoroshilova, N., Popescu, C., Munck, E., Beinert, H., and Kiley, P. J. (1997). Iron-sulfur cluster disassembly in the FNR protein of *Escherichia coli* by O2: [4Fe-4S] to [2Fe-2S] conversion with loss of biological activity. *Proc. Natl. Acad. Sci. U.S.A.* 94, 6087–6092. doi: 10.1073/pnas.94.12.6087

Kim, D. Y., Bovet, L., Kushnir, S., Noh, E. W., Martinoia, E., and Lee, Y. (2006). AtATM3 is involved in heavy metal resistance in Arabidopsis. *Plant Physiol.* 140, 922–932. doi: 10.1104/pp.105.074146

Kim, J. H., Frederick, R. O., Reinen, N. M., Troupis, A. T., and Markley, J. L. (2013). [2Fe-2S]-Ferredoxin binds directly to cysteine desulfurase and supplies an electron for iron-sulfur cluster assembly but is displaced by the scaffold protein or bacterial frataxin. *J. Am. Chem. Soc.* 135, 8117–8120. doi: 10.1021/ja401950a

Kim, K. D., Kim, H. J., Lee, K. C., and Roe, J. H. (2011). Multi-domain CGFS-type glutaredoxin Grx4 regulates iron homeostasis via direct interaction with a repressor Fep1 in fission yeast. *Biochem. Biophys. Res. Commun.* 408, 609–614. doi: 10.1016/j.bbrc.2011.04.069

Kim, M. J., Kim, H. S., Lee, J. K., Lee, C. B., and Park, S. D. (2002). Regulation of septation and cytokinesis during resumption of cell division requires uvi31+, a UV-inducible gene of fission yeast. *Mol. Cells* 14, 425–430.

Kispal, G., Csere, P., Prohl, C., and Lill, R. (1999). The mitochondrial proteins Atm1p and Nfs1p are essential for biogenesis of cytosolic Fe/S proteins. *EMBO J.* 18, 3981–3989. doi: 10.1093/emboj/18.14.3981

Kispal, G., Sipos, K., Lange, H., Fekete, Z., Bedekovics, T., Janaky, T., et al. (2005). Biogenesis of cytosolic ribosomes requires the essential iron-sulphur protein Rli1p and mitochondria. *EMBO J.* 24, 589–598. doi: 10.1038/sj.emboj.7600541

Kohbushi, H., Nakai, Y., Kikuchi, S., Yabe, T., Hori, H., and Nakai, M. (2009). Arabidopsis cytosolic Nbp35 homodimer can assemble both [2Fe-2S] and [4Fe-4S] clusters in two distinct domains. *Biochem. Biophys. Res. Commun.* 378, 810–815. doi: 10.1016/j.bbrc.2008.11.138

Kojer, K., Bien, M., Gangel, H., Morgan, B., Dick, T. P., and Riemer, J. (2012). Glutathione redox potential in the mitochondrial intermembrane space is linked to the cytosol and impacts the Mia40 redox state. *EMBO J.* 31, 3169–3182. doi: 10.1038/emboj.2012.165

Kumanovics, A., Chen, O. S., Li, L., Bagley, D., Adkins, E. M., Lin, H., et al. (2008). Identification of FRA1 and FRA2 as genes involved in regulating the yeast iron regulon in response to decreased mitochondrial iron-sulfur cluster synthesis. *J. Biol. Chem.* 283, 10276–10286. doi: 10.1074/jbc.M801160200

Kumar, C., Igbaria, A., D'Autreaux, B., Planson, A. G., Junot, C., Godat, E., et al. (2011). Glutathione revisited: a vital function in iron metabolism and ancillary role in thiol-redox control. *EMBO J.* 30, 2044–2056. doi: 10.1038/emboj.2011.105

Kushnir, S., Babiychuk, E., Storozhenko, S., Davey, M. W., Papenbrock, J., De Rycke, R., et al. (2001). A mutation of the mitochondrial ABC transporter Sta1 leads to dwarfism and chlorosis in the Arabidopsis mutant starik. *Plant Cell* 13, 89–100.

Kusminski, C. M., Holland, W. L., Sun, K., Park, J., Spurgin, S. B., Lin, Y., et al. (2012). MitoNEET-driven alterations in adipocyte mitochondrial activity reveal a crucial adaptive process that preserves insulin sensitivity in obesity. *Nat. Med.* 18, 1539–1549. doi: 10.1038/nm.2899

Lange, H., Kaut, A., Kispal, G., and Lill, R. (2000). A mitochondrial ferredoxin is essential for biogenesis of cellular iron-sulfur proteins. *Proc. Natl. Acad. Sci. U.S.A.* 97, 1050–1055. doi: 10.1073/pnas.97.3.1050

Lange, H., Lisowsky, T., Gerber, J., Muhlenhoff, U., Kispal, G., and Lill, R. (2001). An essential function of the mitochondrial sulfhydryl oxidase Erv1p/ALR in the maturation of cytosolic Fe/S proteins. *EMBO Rep.* 2, 715–720. doi: 10.1093/embo-reports/kve161

Layer, G., Ollagnier-de Choudens, S., Sanakis, Y., and Fontecave, M. (2006). Iron-sulfur cluster biosynthesis: characterization of *Escherichia coli* CYaY as an iron donor for the assembly of [2Fe-2S] clusters in the scaffold IscU. *J. Biol. Chem.* 281, 16256–16263. doi: 10.1074/jbc.M513569200

Lee, J. H., Yeo, W. S., and Roe, J. H. (2004). Induction of the sufA operon encoding Fe-S assembly proteins by superoxide generators and hydrogen peroxide: involvement of OxyR, IHF and an unidentified oxidant-responsive factor. *Mol. Microbiol.* 51, 1745–1755. doi: 10.1111/j.1365-2958.2003.03946.x

Leon, S., Touraine, B., Briat, J. F., and Lobreaux, S. (2005). Mitochondrial localization of *Arabidopsis thaliana* Isu Fe-S scaffold proteins. *FEBS Lett.* 579, 1930–1934. doi: 10.1016/j.febslet.2005.02.038

Leon, S., Touraine, B., Ribot, C., Briat, J. F., and Lobreaux, S. (2003). Iron-sulphur cluster assembly in plants: distinct NFU proteins in mitochondria and plastids from *Arabidopsis thaliana*. *Biochem. J.* 371, 823–830. doi: 10.1042/BJ20021946

Lezhneva, L., Amann, K., and Meurer, J. (2004). The universally conserved HCF101 protein is involved in assembly of [4Fe-4S]-cluster-containing complexes in *Arabidopsis thaliana* chloroplasts. *Plant J.* 37, 174–185. doi: 10.1046/j.1365-313X.2003.01952.x

Li, H., Mapolelo, D. T., Dingra, N. N., Keller, G., Riggs-Gelasco, P. J., Winge, D. R., et al. (2011). Histidine 103 in Fra2 is an iron-sulfur cluster ligand in the [2Fe-2S] Fra2-Grx3 complex and is required for *in vivo* iron signaling in yeast. *J. Biol. Chem.* 286, 867–876. doi: 10.1074/jbc.M110.184176

Li, H., Mapolelo, D. T., Dingra, N. N., Naik, S. G., Lees, N. S., Hoffman, B. M., et al. (2009). The yeast iron regulatory proteins Grx3/4 and Fra2 form heterodimeric complexes containing a [2Fe-2S] cluster with cysteinyl and histidyl ligation. *Biochemistry* 48, 9569–9581. doi: 10.1021/bi901182w

Li, H., Mapolelo, D. T., Randeniya, S., Johnson, M. K., and Outten, C. E. (2012). Human glutaredoxin 3 forms [2Fe-2S]-bridged complexes with human BolA2. *Biochemistry* 51, 1687–1696. doi: 10.1021/bi2019089

Li, J., Saxena, S., Pain, D., and Dancis, A. (2001). Adrenodoxin reductase homolog (Arh1p) of yeast mitochondria required for iron homeostasis. *J. Biol. Chem.* 276, 1503–1509. doi: 10.1074/jbc.M007198200

Lill, R. (2009). Function and biogenesis of iron-sulphur proteins. *Nature* 460, 831–838. doi: 10.1038/nature08301

Lill, R., Hoffmann, B., Molik, S., Pierik, A. J., Rietzschel, N., Stehling, O., et al. (2012). The role of mitochondria in cellular iron-sulfur protein biogenesis and iron metabolism. *Biochim. Biophys. Acta* 1823, 1491–1508. doi: 10.1016/j.bbamcr.2012.05.009

Lill, R., and Mühlenhoff, U. (2008). Maturation of iron-sulfur proteins in eukaryotes: mechanisms, connected processes, and diseases. *Annu. Rev. Biochem.* 77, 669–700. doi: 10.1146/annurev.biochem.76.052705.162653

Lin, J., Zhou, T., Ye, K., and Wang, J. (2007). Crystal structure of human mitoNEET reveals distinct groups of iron sulfur proteins. *Proc. Natl. Acad. Sci. U.S.A.* 104, 14640–14645. doi: 10.1073/pnas.0702426104

Lisowsky, T. (1994). ERV1 is involved in the cell-division cycle and the maintenance of mitochondrial genomes in *Saccharomyces cerevisiae*. *Curr. Genet.* 26, 15–20. doi: 10.1007/BF00326299

Liu, Y., Bauer, S. C., and Imlay, J. A. (2011). The YaaA protein of the *Escherichia coli* OxyR regulon lessens hydrogen peroxide toxicity by diminishing the amount of intracellular unincorporated iron. *J. Bacteriol.* 193, 2186–2196. doi: 10.1128/JB.00001-11

Loiseau, L., Ollagnier-de Choudens, S., Lascoux, D., Forest, E., Fontecave, M., and Barras, F. (2005). Analysis of the heteromeric CsdA-CsdE cysteine desulfurase, assisting Fe-S cluster biogenesis in *Escherichia coli*. *J. Biol. Chem.* 280, 26760–26769. doi: 10.1074/jbc.M504067200

Lu, J., Bitoun, J. P., Tan, G., Wang, W., Min, W., and Ding, H. (2010). Iron-binding activity of human iron-sulfur cluster assembly protein hIscA1. *Biochem. J.* 428, 125–131. doi: 10.1042/BJ20100122

Lu, J., Yang, J., Tan, G., and Ding, H. (2008). Complementary roles of SufA and IscA in the biogenesis of iron-sulfur clusters in *Escherichia coli*. *Biochem. J.* 409, 535–543. doi: 10.1042/BJ20071166

Luo, D., Bernard, D. G., Balk, J., Hai, H., and Cui, X. (2012). The DUF59 family gene AE7 acts in the cytosolic iron-sulfur cluster assembly pathway to maintain nuclear genome integrity in Arabidopsis. *Plant Cell* 24, 4135–4148. doi: 10.1105/tpc.112.102608

Maliandi, M. V., Busi, M. V., Turowski, V. R., Leaden, L., Araya, A., and Gomez-Casati, D. F. (2011). The mitochondrial protein frataxin is essential for heme biosynthesis in plants. *FEBS J.* 278, 470–481. doi: 10.1111/j.1742-4658.2010.07968.x

Mapolelo, D. T., Zhang, B., Naik, S. G., Huynh, B. H., and Johnson, M. K. (2012a). Spectroscopic and functional characterization of iron-bound forms of *Azotobacter vinelandii*(Nif)IscA. *Biochemistry* 51, 8056–8070. doi: 10.1021/bi300664j

Mapolelo, D. T., Zhang, B., Naik, S. G., Huynh, B. H., and Johnson, M. K. (2012b). Spectroscopic and functional characterization of iron-sulfur cluster-bound forms of *Azotobacter vinelandii*(Nif)IscA. *Biochemistry* 51, 8071–8084. doi: 10.1021/bi3006658

Mapolelo, D. T., Zhang, B., Randeniya, S., Albetel, A. N., Li, H., Couturier, J., et al. (2013). Monothiol glutaredoxins and A-type proteins: partners in Fe-S cluster trafficking. *Dalton Trans.* 42, 3107–3115. doi: 10.1039/c2dt32263c

Martin, M., Colman, M. J., Gomez-Casati, D. F., Lamattina, L., and Zabaleta, E. J. (2009). Nitric oxide accumulation is required to protect against iron-mediated oxidative stress in frataxin-deficient Arabidopsis plants. *FEBS Lett.* 583, 542–548. doi: 10.1016/j.febslet.2008.12.039

Mercier, A., and Labbe, S. (2009). Both Php4 function and subcellular localization are regulated by iron via a multistep mechanism involving the glutaredoxin Grx4 and the exportin Crm1. *J. Biol. Chem.* 284, 20249–20262. doi: 10.1074/jbc.M109.009563

Moeder, W., Del Pozo, O., Navarre, D. A., Martin, G. B., and Klessig, D. F. (2007). Aconitase plays a role in regulating resistance to oxidative stress and cell death in Arabidopsis and *Nicotiana benthamiana*. *Plant Mol. Biol.* 63, 273–287. doi: 10.1007/s11103-006-9087-x

Moller, S. G., Kunkel, T., and Chua, N. H. (2001). A plastidic ABC protein involved in intercompartmental communication of light signaling. *Genes Dev.* 15, 90–103. doi: 10.1101/gad.850101

Mühlenhoff, U., Balk, J., Richhardt, N., Kaiser, J. T., Sipos, K., Kispal, G., et al. (2004). Functional characterization of the eukaryotic cysteine desulfurase Nfs1p from *Saccharomyces cerevisiae*. *J. Biol. Chem.* 279, 36906–36915. doi: 10.1074/jbc.M406516200

Mühlenhoff, U., Gerber, J., Richhardt, N., and Lill, R. (2003). Components involved in assembly and dislocation of iron-sulfur clusters on the scaffold protein Isu1p. *EMBO J.* 22, 4815–4825. doi: 10.1093/emboj/cdg446

Mühlenhoff, U., Molik, S., Godoy, J. R., Uzarska, M. A., Richter, N., Seubert, A., et al. (2010). Cytosolic monothiol glutaredoxins function in intracellular iron sensing and trafficking via their bound iron-sulfur cluster. *Cell Metab.* 12, 373–385. doi: 10.1016/j.cmet.2010.08.001

Mühlenhoff, U., Richhardt, N., Ristow, M., Kispal, G., and Lill, R. (2002). The yeast frataxin homolog Yfh1p plays a specific role in the

maturation of cellular Fe/S proteins. *Hum. Mol. Genet.* 11, 2025–2036. doi: 10.1093/hmg/11.17.2025

Mühlenhoff, U., Richter, N., Pines, O., Pierik, A. J., and Lill, R. (2011). Specialized function of yeast Isa1 and Isa2 proteins in the maturation of mitochondrial [4Fe-4S] proteins. *J. Biol. Chem.* 286, 41205–41216. doi: 10.1074/jbc.M111.296152

Murthy, N. M., Ollagnier-de-Choudens, S., Sanakis, Y., Abdel-Ghany, S. E., Rousset, C., Ye, H., et al. (2007). Characterization of *Arabidopsis thaliana* SufE2 and SufE3: functions in chloroplast iron-sulfur cluster assembly and Nad synthesis. *J. Biol. Chem.* 282, 18254–18264. doi: 10.1074/jbc.M701428200

Nagane, T., Tanaka, A., and Tanaka, R. (2010). Involvement of AtNAP1 in the regulation of chlorophyll degradation in *Arabidopsis thaliana*. *Planta* 231, 939–949. doi: 10.1007/s00425-010-1099-8

Navarro-Sastre, A., Tort, F., Stehling, O., Uzarska, M. A., Arranz, J. A., Del Toro, M., et al. (2011). A fatal mitochondrial disease is associated with defective NFU1 function in the maturation of a subset of mitochondrial Fe-S proteins. *Am. J. Hum. Genet.* 89, 656–667. doi: 10.1016/j.ajhg.2011.10.005

Nechushtai, R., Conlan, A. R., Harir, Y., Song, L., Yogev, O., Eisenberg-Domovich, Y., et al. (2012). Characterization of Arabidopsis NEET reveals an ancient role for NEET proteins in iron metabolism. *Plant Cell* 24, 2139–2154. doi: 10.1105/tpc.112.097634

Netz, D. J., Pierik, A. J., Stumpfig, M., Bill, E., Sharma, A. K., Pallesen, L. J., et al. (2012). A bridging [4Fe-4S] cluster and nucleotide binding are essential for function of the Cfd1-Nbp35 complex as a scaffold in iron-sulfur protein maturation. *J. Biol. Chem.* 287, 12365–12378. doi: 10.1074/jbc.M111.328914

Netz, D. J., Pierik, A. J., Stumpfig, M., Muhlenhoff, U., and Lill, R. (2007). The Cfd1-Nbp35 complex acts as a scaffold for iron-sulfur protein assembly in the yeast cytosol. *Nat. Chem. Biol.* 3, 278–286. doi: 10.1038/nchembio872

Netz, D. J., Stumpfig, M., Dore, C., Muhlenhoff, U., Pierik, A. J., and Lill, R. (2010). Tah18 transfers electrons to Dre2 in cytosolic iron-sulfur protein biogenesis. *Nat. Chem. Biol.* 6, 758–765. doi: 10.1038/nchembio.432

Nicolet, Y., Rohac, R., Martin, L., and Fontecilla-Camps, J. C. (2013). X-ray snapshots of possible intermediates in the time course of synthesis and degradation of protein-bound Fe4S4 clusters. *Proc. Natl. Acad. Sci. U.S.A.* 110, 7188–7192. doi: 10.1073/pnas.1302388110

Ojeda, L., Keller, G., Mühlenhoff, U., Rutherford, J. C., Lill, R., and Winge, D. R. (2006). Role of glutaredoxin-3 and glutaredoxin-4 in the iron regulation of the Aft1 transcriptional activator in *Saccharomyces cerevisiae*. *J. Biol. Chem.* 281, 17661–17669. doi: 10.1074/jbc.M602165200

Ollagnier-de Choudens, S., Nachin, L., Sanakis, Y., Loiseau, L., Barras, F., and Fontecave, M. (2003). SufA from Erwinia chrysanthemi. Characterization of a scaffold protein required for iron-sulfur cluster assembly. *J. Biol. Chem.* 278, 17993–18001. doi: 10.1074/jbc.M300285200

Ollagnier-de-Choudens, S., Sanakis, Y., and Fontecave, M. (2004). SufA/IscA: reactivity studies of a class of scaffold proteins involved in [Fe-S] cluster assembly. *J. Biol. Inorg. Chem.* 9, 828–838. doi: 10.1007/s00775-004-0581-9

Outten, F. W., Djaman, O., and Storz, G. (2004). A suf operon requirement for Fe-S cluster assembly during iron starvation in *Escherichia coli*. *Mol. Microbiol.* 52, 861–872. doi: 10.1111/j.1365-2958.2004.04025.x

Overton, T. W., Justino, M. C., Li, Y., Baptista, J. M., Melo, A. M., Cole, J. A., et al. (2008). Widespread distribution in pathogenic bacteria of di-iron proteins that repair oxidative and nitrosative damage to iron-sulfur centers. *J. Bacteriol.* 190, 2004–2013. doi: 10.1128/JB.01733-07

Paddock, M. L., Wiley, S. E., Axelrod, H. L., Cohen, A. E., Roy, M., Abresch, E. C., et al. (2007). MitoNEET is a uniquely folded 2Fe 2S outer mitochondrial membrane protein stabilized by pioglitazone. *Proc. Natl. Acad. Sci. U.S.A.* 104, 14342–14347. doi: 10.1073/pnas.0707189104

Pastore, C., Franzese, M., Sica, F., Temussi, P., and Pastore, A. (2007). Understanding the binding properties of an unusual metal-binding protein–a study of bacterial frataxin. *FEBS J.* 274, 4199–4210. doi: 10.1111/j.1742-4658.2007.05946.x

Prischi, F., Konarev, P. V., Iannuzzi, C., Pastore, C., Adinolfi, S., Martin, S. R., et al. (2010). Structural bases for the interaction of frataxin with the central components of iron-sulphur cluster assembly. *Nat. Commun.* 1, 95. doi: 10.1038/ncomms1097

Pujol-Carrion, N., Belli, G., Herrero, E., Nogues, A., and de la Torre-Ruiz, M. A. (2006). Glutaredoxins Grx3 and Grx4 regulate nuclear localisation of Aft1 and the oxidative stress response in *Saccharomyces cerevisiae*. *J. Cell. Sci.* 119, 4554–4564. doi: 10.1242/jcs.03229

Py, B., Gerez, C., Angelini, S., Planel, R., Vinella, D., Loiseau, L., et al. (2012). Molecular organization, biochemical function, cellular role and evolution of NfuA, an atypical Fe-S carrier. *Mol. Microbiol.* 86, 155–171. doi: 10.1111/j.1365-2958.2012.08181.x

Py, B., Moreau, P. L., and Barras, F. (2011). Fe-S clusters, fragile sentinels of the cell. *Curr. Opin. Microbiol.* 14, 218–223. doi: 10.1016/j.mib.2011.01.004

Qi, W., Li, J., Chain, C. Y., Pasquevich, G. A., Pasquevich, A. F., and Cowan, J. A. (2012). Glutathione complexed Fe-S centers. *J. Am. Chem. Soc.* 134, 10745–10748. doi: 10.1021/ja302186j

Ravet, K., Touraine, B., Boucherez, J., Briat, J. F., Gaymard, F., and Cellier, F. (2009). Ferritins control interaction between iron homeostasis and oxidative stress in Arabidopsis. *Plant J.* 57, 400–412. doi: 10.1111/j.1365-313X.2008.03698.x

Richards, T. A., and van der Giezen, M. (2006). Evolution of the Isd11-IscS complex reveals a single alpha-proteobacterial endosymbiosis for all eukaryotes. *Mol. Biol. Evol.* 23, 1341–1344. doi: 10.1093/molbev/msl001

Roche, B., Aussel, L., Ezraty, B., Mandin, P., Py, B., and Barras, F. (2013). Iron/sulfur proteins biogenesis in prokaryotes: formation, regulation and diversity. *Biochim. Biophys. Acta* 1827, 455–469. doi: 10.1016/j.bbabio.2012.12.010

Rodriguez-Manzaneque, M. T., Tamarit, J., Belli, G., Ros, J., and Herrero, E. (2002). Grx5 is a mitochondrial glutaredoxin required for the activity of iron/sulfur enzymes. *Mol. Biol. Cell* 13, 1109–1121. doi: 10.1091/mbc.01-10-0517

Rouault, T. A. (2006). The role of iron regulatory proteins in mammalian iron homeostasis and disease. *Nat. Chem. Biol.* 2, 406–414. doi: 10.1038/nchembio807

Saito, Y., Shibayama, H., Tanaka, H., Tanimura, A., Matsumura, I., and Kanakura, Y. (2011). PICOT is a molecule which binds to anamorsin. *Biochem. Biophys. Res. Commun.* 408, 329–333. doi: 10.1016/j.bbrc.2011.04.033

Salome, P. A., Oliva, M., Weigel, D., and Kramer, U. (2013). Circadian clock adjustment to plant iron status depends on chloroplast and phytochrome function. *EMBO J.* 32, 511–523. doi: 10.1038/emboj.2012.330

Schwartz, C. J., Djaman, O., Imlay, J. A., and Kiley, P. J. (2000). The cysteine desulfurase, IscS, has a major role *in vivo* Fe-S cluster formation in *Escherichia coli*. *Proc. Natl. Acad. Sci. U.S.A.* 97, 9009–9014. doi: 10.1073/pnas.160261497

Schwartz, C. J., Giel, J. L., Patschkowski, T., Luther, C., Ruzicka, F. J., Beinert, H., et al. (2001). IscR, an Fe-S cluster-containing transcription factor, represses expression of *Escherichia coli* genes encoding Fe-S cluster assembly proteins. *Proc. Natl. Acad. Sci. U.S.A.* 98, 14895–14900. doi: 10.1073/pnas.251550898

Schwenkert, S., Netz, D. J., Frazzon, J., Pierik, A. J., Bill, E., Gross, J., et al. (2010). Chloroplast HCF101 is a scaffold protein for [4Fe-4S] cluster assembly. *Biochem. J.* 425, 207–214. doi: 10.1042/BJ20091290

Sendra, M., Ollagnier de Choudens, S., Lascoux, D., Sanakis, Y., and Fontecave, M. (2007). The SUF iron-sulfur cluster biosynthetic machinery: sulfur transfer from the SUFS-SUFE complex to SUFA. *FEBS Lett.* 581, 1362–1368. doi: 10.1016/j.febslet.2007.02.058

Sheftel, A. D., Stehling, O., Pierik, A. J., Netz, D. J., Kerscher, S., Elsasser, H. P., et al. (2009). Human ind1, an iron-sulfur cluster assembly factor for respiratory complex I. *Mol. Cell. Biol.* 29, 6059–6073. doi: 10.1128/MCB.00817-09

Sheftel, A. D., Wilbrecht, C., Stehling, O., Niggemeyer, B., Elsasser, H. P., Mühlenhoff, U., et al. (2012). The human mitochondrial ISCA1, ISCA2, and IBA57 proteins are required for [4Fe-4S] protein maturation. *Mol. Biol. Cell* 23, 1157–1166. doi: 10.1091/mbc.E11-09-0772

Shen, G., Balasubramanian, R., Wang, T., Wu, Y., Hoffart, L. M., Krebs, C., et al. (2007). SufR coordinates two [4Fe-4S]2+, 1+ clusters and functions as a transcriptional repressor of the sufBCDS operon and an autoregulator of sufR in cyanobacteria. *J. Biol. Chem.* 282, 31909–31919. doi: 10.1074/jbc.M705554200

Sipos, K., Lange, H., Fekete, Z., Ullmann, P., Lill, R., and Kispal, G. (2002). Maturation of cytosolic iron-sulfur proteins requires glutathione. *J. Biol.*

Chem. 277, 26944–26949. doi: 10.1074/jbc.M200677200

Stehling, O., Vashisht, A. A., Mascarenhas, J., Jonsson, Z. O., Sharma, T., Netz, D. J., et al. (2012). MMS19 assembles iron-sulfur proteins required for DNA metabolism and genomic integrity. *Science* 337, 195–199. doi: 10.1126/science.1219723

Stemmler, T. L., Lesuisse, E., Pain, D., and Dancis, A. (2010). Frataxin and mitochondrial FeS cluster biogenesis. *J. Biol. Chem.* 285, 26737–26743. doi: 10.1074/jbc.R110.118679

Stockel, J., and Oelmuller, R. (2004). A novel protein for photosystem I biogenesis. *J. Biol. Chem.* 279, 10243–10251. doi: 10.1074/jbc.M309246200

Subramanian, P., Rodrigues, A. V., Ghimire-Rijal, S., and Stemmler, T. L. (2011). Iron chaperones for mitochondrial Fe-S cluster biosynthesis and ferritin iron storage. *Curr. Opin. Chem. Biol.* 15, 312–318. doi: 10.1016/j.cbpa.2011.01.003

Sutak, R., Seguin, A., Garcia-Serres, R., Oddou, J. L., Dancis, A., Tachezy, J., et al. (2012). Human mitochondrial ferritin improves respiratory function in yeast mutants deficient in iron-sulfur cluster biogenesis, but is not a functional homologue of yeast frataxin. *Microbiologyopen* 1, 95–104. doi: 10.1002/mbo3.18

Tan, G., Lu, J., Bitoun, J. P., Huang, H., and Ding, H. (2009). IscA/SufA paralogues are required for the [4Fe-4S] cluster assembly in enzymes of multiple physiological pathways in *Escherichia coli* under aerobic growth conditions. *Biochem. J.* 420, 463–472. doi: 10.1042/BJ20090206

Tan, Y. F., O'Toole, N., Taylor, N. L., and Millar, A. H. (2010). Divalent metal ions in plant mitochondria and their role in interactions with proteins and oxidative stress-induced damage to respiratory function. *Plant Physiol.* 152, 747–761.

Tarassov, K., Messier, V., Landry, C. R., Radinovic, S., Serna Molina, M. M., Shames, I., et al. (2008). An *in vivo* map of the yeast protein interactome. *Science* 320, 1465–1470. doi: 10.1126/science.1153878

Teschner, J., Lachmann, N., Schulze, J., Geisler, M., Selbach, K., Santamaria-Araujo, J., et al. (2010). A novel role for Arabidopsis mitochondrial ABC transporter ATM3 in molybdenum cofactor biosynthesis. *Plant Cell* 22, 468–480. doi: 10.1105/tpc.109.068478

Tirrell, T. F., Paddock, M. L., Conlan, A. R., Smoll, E. J. Jr., Nechushtai, R., Jennings, P. A., et al. (2009). Resonance Raman studies of the (His)(Cys)3 2Fe-2S cluster of MitoNEET: comparison to the (Cys)4 mutant and implications of the effects of pH on the labile metal center. *Biochemistry* 48, 4747–4752. doi: 10.1021/bi900028r

Tong, W. H., Jameson, G. N., Huynh, B. H., and Rouault, T. A. (2003). Subcellular compartmentalization of human Nfu, an iron-sulfur cluster scaffold protein, and its ability to assemble a [4Fe-4S] cluster. *Proc. Natl. Acad. Sci. U.S.A.* 100, 9762–9767. doi: 10.1073/pnas.1732541100

Tong, W. H., and Rouault, T. A. (2006). Functions of mitochondrial ISCU and cytosolic ISCU in mammalian iron-sulfur cluster biogenesis and iron homeostasis. *Cell Metab.* 3, 199–210. doi: 10.1016/j.cmet.2006.02.003

Touraine, B., Boutin, J. P., Marion-Poll, A., Briat, J. F., Peltier, G., and Lobreaux, S. (2004). Nfu2: a scaffold protein required for [4Fe-4S] and ferredoxin iron-sulphur cluster assembly in Arabidopsis chloroplasts. *Plant J.* 40, 101–111. doi: 10.1111/j.1365-313X.2004.02189.x

Trotter, V., Vinella, D., Loiseau, L., Ollagnier de Choudens, S., Fontecave, M., and Barras, F. (2009). The CsdA cysteine desulphurase promotes Fe/S biogenesis by recruiting Suf components and participates to a new sulphur transfer pathway by recruiting CsdL (ex-YgdL), a ubiquitin-modifying-like protein. *Mol. Microbiol.* 74, 1527–1542. doi: 10.1111/j.1365-2958.2009.06954.x

Tsai, C. L., and Barondeau, D. P. (2010). Human frataxin is an allosteric switch that activates the Fe-S cluster biosynthetic complex. *Biochemistry* 49, 9132–9139. doi: 10.1021/bi1013062

Turowski, V. R., Busi, M. V., and Gomez-Casati, D. F. (2012). Structural and functional studies of the mitochondrial cysteine desulfurase from *Arabidopsis thaliana*. *Mol. Plant* 5, 1001–1010. doi: 10.1093/mp/sss037

Urzica, E., Pierik, A. J., Muhlenhoff, U., and Lill, R. (2009). Crucial role of conserved cysteine residues in the assembly of two iron-sulfur clusters on the CIA protein Nar1. *Biochemistry* 48, 4946–4958. doi: 10.1021/bi900312x

Van Hoewyk, D., Abdel-Ghany, S. E., Cohu, C. M., Herbert, S. K., Kugrens, P., Pilon, M., et al. (2007). Chloroplast iron-sulfur cluster protein maturation requires the essential cysteine desulfurase CpNifS. *Proc. Natl. Acad. Sci. U.S.A.* 104, 5686–5691. doi: 10.1073/pnas.0700774104

Varadarajan, J., Guilleminot, J., Saint-Jore-Dupas, C., Piegu, B., Chaboute, M. E., Gomord, V., et al. (2010). ATR3 encodes a diflavin reductase essential for Arabidopsis embryo development. *New Phytol.* 187, 67–82. doi: 10.1111/j.1469-8137.2010.03254.x

Vazzola, V., Losa, A., Soave, C., and Murgia, I. (2007). Knockout of frataxin gene causes embryo lethality in Arabidopsis. *FEBS Lett.* 581, 667–672. doi: 10.1016/j.febslet.2007.01.030

Velayudhan, J., Castor, M., Richardson, A., Main-Hester, K. L., and Fang, F. C. (2007). The role of ferritins in the physiology of *Salmonella enterica* sv. Typhimurium: a unique role for ferritin B in iron-sulphur cluster repair and virulence. *Mol. Microbiol.* 63, 1495–1507. doi: 10.1111/j.1365-2958.2007.05600.x

Vinella, D., Brochier-Armanet, C., Loiseau, L., Talla, E., and Barras, F. (2009). Iron-sulfur (Fe/S) protein biogenesis: phylogenomic and genetic studies of A-type carriers. *PLoS Genet.* 5:e1000497. doi: 10.1371/journal.pgen.1000497

Waller, J. C., Alvarez, S., Naponelli, V., Lara-Nunez, A., Blaby, I. K., Da Silva, V., et al. (2010). A role for tetrahydrofolates in the metabolism of iron-sulfur clusters in all domains of life. *Proc. Natl. Acad. Sci. U.S.A.* 107, 10412–10417. doi: 10.1073/pnas.0911586107

Waller, J. C., Ellens, K. W., Alvarez, S., Loizeau, K., Ravanel, S., and Hanson, A. D. (2012). Mitochondrial and plastidial COG0354 proteins have folate-dependent functions in iron-sulphur cluster metabolism. *J. Exp. Bot.* 63, 403–411. doi: 10.1093/jxb/err286

Walters, E. M., Garcia-Serres, R., Jameson, G. N., Glauser, D. A., Bourquin, F., Manieri, W., et al. (2005). Spectroscopic characterization of site-specific [Fe(4)S(4)] cluster chemistry in ferredoxin:thioredoxin reductase: implications for the catalytic mechanism. *J. Am. Chem. Soc.* 127, 9612–9624. doi: 10.1021/ja051909q

Wang, T., Shen, G., Balasubramanian, R., McIntosh, L., Bryant, D. A., and Golbeck, J. H. (2004). The sufR gene (sll0088 in Synechocystis sp. strain PCC 6803) functions as a repressor of the sufBCDS operon in iron-sulfur cluster biogenesis in cyanobacteria. *J. Bacteriol.* 186, 956–967. doi: 10.1128/JB.186.4.956-967.2004

Weerapana, E., Wang, C., Simon, G. M., Richter, F., Khare, S., Dillon, M. B., et al. (2010). Quantitative reactivity profiling predicts functional cysteines in proteomes. *Nature* 468, 790–795. doi: 10.1038/nature09472

White, M. F., and Dillingham, M. S. (2012). Iron-sulphur clusters in nucleic acid processing enzymes. *Curr. Opin. Struct. Biol.* 22, 94–100. doi: 10.1016/j.sbi.2011.11.004

Wiedemann, N., Urzica, E., Guiard, B., Muller, H., Lohaus, C., Meyer, H. E., et al. (2006). Essential role of Isd11 in mitochondrial iron-sulfur cluster synthesis on Isu scaffold proteins. *EMBO J.* 25, 184–195. doi: 10.1038/sj.emboj.7600906

Wiley, S. E., Murphy, A. N., Ross, S. A., van der Geer, P., and Dixon, J. E. (2007a). MitoNEET is an iron-containing outer mitochondrial membrane protein that regulates oxidative capacity. *Proc. Natl. Acad. Sci. U.S.A.* 104, 5318–5323. doi: 10.1073/pnas.0701078104

Wiley, S. E., Paddock, M. L., Abresch, E. C., Gross, L., van der Geer, P., Nechushtai, R., et al. (2007b). The outer mitochondrial membrane protein mitoNEET contains a novel redox-active 2Fe-2S cluster. *J. Biol. Chem.* 282, 23745–23749. doi: 10.1074/jbc.C700107200

Willems, P., Wanschers, B. F., Esseling, J., Szklarczyk, R., Kudla, U., Duarte, I., et al. (2013). BOLA1 is an aerobic protein that prevents mitochondrial morphology changes induced by glutathione depletion. *Antioxi. Redox Signal.* 18, 129–138. doi: 10.1089/ars.2011.4253

Wollers, S., Layer, G., Garcia-Serres, R., Signor, L., Clemancey, M., Latour, J. M., et al. (2010). Iron-sulfur (Fe-S) cluster assembly: the SufBCD complex is a new type of Fe-S scaffold with a flavin redox cofactor. *J. Biol. Chem.* 285, 23331–23341. doi: 10.1074/jbc.M110.127449

Wu, Y., and Brosh, R. M. Jr. (2012). DNA helicase and helicase-nuclease enzymes with a conserved iron-sulfur cluster. *Nucleic Acids Res.* 40, 4247–4260. doi: 10.1093/nar/gks039

Xu, X. M., Adams, S., Chua, N. H., and Moller, S. G. (2005). AtNAP1 represents an atypical SufB protein in Arabidopsis plastids. *J. Biol. Chem.* 280, 6648–6654. doi: 10.1074/jbc.M413082200

Xu, X. M., Lin, H., Latijnhouwers, M., and Moller, S. G. (2009).

Dual localized AtHscB involved in iron sulfur protein biogenesis in Arabidopsis. *PLoS ONE* 4:e7662. doi: 10.1371/journal.pone.0007662

Xu, X. M., and Moller, S. G. (2004). AtNAP7 is a plastidic SufC-like ATP-binding cassette/ATPase essential for Arabidopsis embryogenesis. *Proc. Natl. Acad. Sci. U.S.A.* 101, 9143–9148. doi: 10.1073/pnas.0400799101

Xu, X. M., and Moller, S. G. (2006). AtSufE is an essential activator of plastidic and mitochondrial desulfurases in Arabidopsis. *EMBO J.* 25, 900–909. doi: 10.1038/sj.emboj.7600968

Yabe, T., Morimoto, K., Kikuchi, S., Nishio, K., Terashima, I., and Nakai, M. (2004). The Arabidopsis chloroplastic NifU-like protein CnfU, which can act as an iron-sulfur cluster scaffold protein, is required for biogenesis of ferredoxin and photosystem I. *Plant Cell* 16, 993–1007. doi: 10.1105/tpc.020511

Yabe, T., and Nakai, M. (2006). Arabidopsis AtIscA-I is affected by deficiency of Fe-S cluster biosynthetic scaffold AtCnfU-V. *Biochem. Biophys. Res. Commun.* 340, 1047–1052. doi: 10.1016/j.bbrc.2005.12.104

Ye, H., Abdel-Ghany, S. E., Anderson, T. D., Pilon-Smits, E. A., and Pilon, M. (2006a). CpSufE activates the cysteine desulfurase CpNifS for chloroplastic Fe-S cluster formation. *J. Biol. Chem.* 281, 8958–8969. doi: 10.1074/jbc.M512737200

Ye, H., Pilon, M., and Pilon-Smits, E. A. (2006b). CpNifS-dependent iron-sulfur cluster biogenesis in chloroplasts. *New Phytol.* 171, 285–292. doi: 10.1111/j.1469-8137.2006.01751.x

Yeo, W. S., Lee, J. H., Lee, K. C., and Roe, J. H. (2006). IscR acts as an activator in response to oxidative stress for the suf operon encoding Fe-S assembly proteins. *Mol. Microbiol.* 61, 206–218. doi: 10.1111/j.1365-2958.2006.05220.x

Yeung, N., Gold, B., Liu, N. L., Prathapam, R., Sterling, H. J., Willams, E. R., et al. (2011). The *E. coli* monothiol glutaredoxin GrxD forms homodimeric and heterodimeric FeS cluster containing complexes. *Biochemistry* 50, 8957–8969. doi: 10.1021/bi2008883

Yoon, H., Golla, R., Lesuisse, E., Pain, J., Donald, J. E., Lyver, E. R., et al. (2012). Mutation in the Fe-S scaffold protein Isu bypasses frataxin deletion. *Biochem. J.* 441, 473–480. doi: 10.1042/BJ20111637

Yoon, T., and Cowan, J. A. (2003). Iron-sulfur cluster biosynthesis. Characterization of frataxin as an iron donor for assembly of [2Fe-2S] clusters in ISU-type proteins. *J. Am. Chem. Soc.* 125, 6078–6084. doi: 10.1021/ja027967i

Yuan, Z., Luo, D., Li, G., Yao, X., Wang, H., Zeng, M., et al. (2010). Characterization of the AE7 gene in Arabidopsis suggests that normal cell proliferation is essential for leaf polarity establishment. *Plant J.* 64, 331–342. doi: 10.1111/j.1365-313X.2010.04326.x

Zhang, B., Crack, J. C., Subramanian, S., Green, J., Thomson, A. J., Le Brun, N. E., et al. (2012). Reversible cycling between cysteine persulfide-ligated [2Fe-2S] and cysteine-ligated [4Fe-4S] clusters in the FNR regulatory protein. *Proc. Natl. Acad. Sci. U.S.A.* 109, 15734–15739. doi: 10.1073/pnas.1208787109

Zhang, Y., Liu, L., Wu, X., An, X., Stubbe, J., and Huang, M. (2011). Investigation of *in vivo* diferric tyrosyl radical formation in *Saccharomyces cerevisiae* Rnr2 protein: requirement of Rnr4 and contribution of Grx3/4 AND Dre2 proteins. *J. Biol. Chem.* 286, 41499–41509. doi: 10.1074/jbc.M111.294074

Zhang, Y., Lyver, E. R., Nakamaru-Ogiso, E., Yoon, H., Amutha, B., Lee, D. W., et al. (2008). Dre2, a conserved eukaryotic Fe/S cluster protein, functions in cytosolic Fe/S protein biogenesis. *Mol. Cell. Biol.* 28, 5569–5582. doi: 10.1128/MCB.00642-08

Zhou, T., Lin, J., Feng, Y., and Wang, J. (2010). Binding of reduced nicotinamide adenine dinucleotide phosphate destabilizes the iron-sulfur clusters of human mitoNEET. *Biochemistry* 49, 9604–9612. doi: 10.1021/bi101168c

Zuris, J. A., Ali, S. S., Yeh, H., Nguyen, T. A., Nechushtai, R., Paddock, M. L., et al. (2012). NADPH inhibits [2Fe-2S] cluster protein transfer from diabetes drug target MitoNEET to an apo-acceptor protein. *J. Biol. Chem.* 287, 11649–11655. doi: 10.1074/jbc.M111.319731

Zuris, J. A., Harir, Y., Conlan, A. R., Shvartsman, M., Michaeli, D., Tamir, S., et al. (2011). Facile transfer of [2Fe-2S] clusters from the diabetes drug target mitoNEET to an apo-acceptor protein. *Proc. Natl. Acad. Sci. U.S.A.* 108, 13047–13052. doi: 10.1073/pnas.1109986108

Conflict of Interest Statement: The authors declare that the research was conducted in the absence of any commercial or financial relationships that could be construed as a potential conflict of interest.

Received: 16 May 2013; accepted: 25 June 2013; published online: 24 July 2013.
*Citation: Couturier J, Touraine B, Briat J-F, Gaymard F and Rouhier N (2013) The iron-sulfur cluster assembly machineries in plants: current knowledge and open questions. Front. Plant Sci. **4**:259. doi: 10.3389/fpls.2013.00259*
This article was submitted to Frontiers in Plant Nutrition, a specialty of Frontiers in Plant Science.

frontiers in
PLANT SCIENCE

PERSPECTIVE ARTICLE
published: 02 October 2013
doi: 10.3389/fpls.2013.00357

Toward new perspectives on the interaction of iron and sulfur metabolism in plants

Ilaria Forieri[1,2], *Markus Wirtz*[1] *and Rüdiger Hell*[1]*

[1] Department of Molecular Biology of Plants, Centre for Organismal Studies Heidelberg, University of Heidelberg, Heidelberg, Germany
[2] The Hartmut Hoffmann-Berling International Graduate School of Molecular and Cellular Biology, University of Heidelberg, Heidelberg, Germany

Edited by:
Katrin Philippar, Ludwig Maximilian University of Munich, Germany

Reviewed by:
Agnieszka Sirko, Institute of Biochemistry and Biophysics; Polish Academy of Sciences, Poland
Hong-Qing Ling, Institute of Genetics and Developmental Biology, Chinese Academy of Sciences, China

***Correspondence:**
Rüdiger Hell, Department of Molecular Biology of Plants, Centre for Organismal Studies Heidelberg, University of Heidelberg, Im Neuenheimer Feld 360, 69120 Heidelberg, Germany
e-mail: ruediger.hell@cos.uni-heidelberg.de

The deficiency of nutrients has been extensively investigated because of its impact on plant growth and yield. So far, the effects of a combined nutrient limitation have rarely been analyzed, although such situations are likely to occur in agroecosystems. Iron (Fe) is a prerequisite for many essential cellular functions. Its availability is easily becoming limiting for plant growth and thus higher plants have evolved different strategies to cope with Fe deficiency. Sulfur (S) is an essential macro-nutrient and the responses triggered by shortage situations have been well characterized. The interaction between these two nutrients is less investigated but might be of particular importance because most of the metabolically active Fe is bound to S in Fe–S clusters. The biosynthesis of Fe–S clusters requires the provision of reduced S and chelated Fe in a defined stoichiometric ratio, strongly suggesting coordination between the metabolisms of the two nutrients. Here the available information on interactions between Fe and S nutritional status is evaluated. Experiments with *Arabidopsis thaliana* and crop plants indicate a co-regulation and point to a possible role of Fe–S cluster synthesis or abundance in the Fe/S network.

Keywords: iron–sulfur clusters, nutrient sensing, transceptor, sulfate transporter, iron transport

INTRODUCTION

Iron (Fe) is an essential nutrient for plants because of its role as cofactor of many proteins (Balk and Pilon, 2011). Its availability strongly affects plant growth and yield. Thus complex regulatory networks have evolved to tightly balance its uptake, transport, metabolization, and storage during changes of supply and demand. Most of the Fe in plant cells is required in the chloroplasts and in the mitochondria. Several proteins that belong to the electron transport chains in both cellular compartments contain Fe as cofactor, mainly conjugated with sulfur (S) to form the Fe–S clusters. Thus, the biosynthesis of these clusters requires simultaneously reduced S in form of cysteine and of chelated Fe. The provision of the substrates must be tightly regulated for two reasons: (1) in order to meet the plant's changing demands for Fe–S clusters and (2) to avoid potentially toxic free Fe and sulfide. The strong requirement for reduced Fe and cysteine in stoichiometric amounts to synthesize Fe–S clusters indicates the development of cross-regulatory mechanisms between the two pathways. Indeed preliminary nutrient deficiency studies suggest such a co-regulation but the signals generated by deficiency of S or Fe that are needed to regulate the other pathway have not been addressed so far (Zuchi et al., 2009; Astolfi et al., 2010, 2012). In this respect, an important difference between both nutrients should be noted that may give rise to different regulatory patterns: The major sinks of Fe are heme and Fe–S clusters. In contrast, only a small amount of reduced S is part of cofactors (like Fe–S clusters) and soluble low molecular weight compounds like glutathione, while the bulk is intrinsically bound in proteins in form of cysteine and methionine. Thus, sulfur deficiency does not only limit synthesis of Fe–S cluster containing proteins (Fe–S proteins) but also translation in general. In chloroplasts, the most abundant Fe–S proteins are ferredoxin, photosystem I (PSI), and cytochrome b_6f complex. Other Fe–S proteins are present in the stroma, including nitrite reductase, sulfite reductase, and adenosine 5′-phosphosulfate reductase (APR). In mitochondria, major Fe–S proteins are complex I, II, and III of the respiratory chain and aconitase in the citric acid cycle. Thus it seems reasonable to assume that the demand of Fe and S for the biosynthesis of Fe–S clusters in the organelles constitutes a feedback signal that co-ordinates the uptake and reduction of both nutrients. In support of this perspective, retrograde signals have been suggested that regulate the uptake and metabolism of Fe during Fe deficiency (Vigani et al., 2013). Such retrograde feedback signals have also been proposed for the S assimilatory pathway (Hell and Wirtz, 2011; Chan et al., 2013).

UPTAKE AND REDUCTION STRATEGIES AND REGULATION OF THE PATHWAYS

Although Fe is one of the most abundant elements in earth's crust, its availability is highly restricted in alkaline and calcareous soil, because of Fe^{3+} precipitation. Thus Fe can easily become a major constraint for plant growth and higher plants have developed strategies to regulate its homeostasis (Hindt and Guerinot, 2012). One of the prime targets in this respect is the control of iron acquisition in the root. All dicotyledonous and non-graminaceous monocotyledonous plants mobilize iron via the so-called Strategy I or reduction strategy, which is based on soil acidification to increase Fe solubility and reduction of Fe^{3+} to Fe^{2+} before the uptake. In *Arabidopsis thaliana*, the first step is catalyzed by members of the *Arabidopsis* H^+-ATPase family AHA, while

the ferric-chelate reductase oxidase FRO2 reduces Fe^{3+} prior to the uptake into root epidermal cells by iron-regulated transporter 1 (IRT1), a divalent metal transporter. Roots of Strategy II plants from the Poaceae use the extrusion of phytosiderophores to chelate Fe^{3+} and import the resulting complexes (Kobayashi and Nishizawa, 2012). In Strategy I plants, two networks are known to control the regulation of the Fe uptake machinery, based on the transcription factors FIT (FER-like iron deficiency induced) and POPEYE, respectively (Ivanov et al., 2012). The permease in chloroplast 1 (PIC1) has been characterized as plastidic Fe importer in *Arabidopsis* (Duy et al., 2007), whereas the mitochondrial iron transporter MIT1 has been identified in rice (Bashir et al., 2011). In acidic and anaerobic conditions, Fe overload can cause severe damage to plant cells, because free Fe catalyzes the formation of reactive oxygen species (ROS). Thus, the concentration of free Fe ions must be tightly regulated. In this regard, the ferritins in plastids and probably also in mitochondria play a fundamental role in the storage of Fe, in the first case preventing photo-oxidative damage (Briat et al., 2010; Tarantino et al., 2010). In the mitochondria, also frataxin might be involved in the protection against oxidative damage (Busi et al., 2006). However, the bulk of Fe is usually bound as metabolically active Fe in Fe–S clusters. The assembly of Fe–S clusters with their apoproteins involves numerous genes and takes place in plastids, mitochondria, and the cytosol (Balk and Pilon, 2011). Thus, the whole plant and cellular metabolism of Fe is well characterized, while sensing and signaling mechanisms still need to be understood.

Unlike Fe, the macro-nutrient S cannot be reduced by plants in the rhizosphere and must be first taken up in the root plasmalemma in form of sulfate by sulfate transporters (SULTR). The expression of high-affinity SULTR1;1 is highly up-regulated in S deficiency conditions. Further members of the SULTR family mediate its allocation in the leaf cells and import into plastids (Cao et al., 2013) where the assimilation takes place (Takahashi et al., 2011). Following activation the resulting adenosine 5′-phosphosulfate is reduced by APR to sulfite which is further reduced to sulfide. Free sulfide can have strong negative impact on cells because it interacts with free thiols on the surface of proteins, with metals such as copper and iron and inhibits the cytochrome *c* of the respiratory chain (Birke et al., 2012). Cysteine represents the main source of S in a reduced form and is fundamental for the biosynthesis of methionine, Fe–S clusters and the redox compound glutathione. The hetero-oligomeric cysteine synthase complex has been identified as an internal sensor for free sulfide to control the flux toward cysteine. In general, the metabolism of S including uptake and APR expression and activity is believed to be regulated by the availability of sulfate in the soil and the internal demand for reduced sulfur. Different regulators of sulfur metabolism have been identified, but the signal transduction toward supply and demand as well as coordination with other assimilatory pathways are unknown (Takahashi et al., 2011).

EVIDENCES FOR AN INTERACTION BETWEEN IRON AND SULFUR METABOLISM

The effect of the combined shortage of Fe and S has rarely been subjected to studies but provides first hints for a possible co-regulation of their metabolism and particularly the formation of the Fe–S clusters. In tomato plants S deficiency limits the capacity to cope with Fe shortage, preventing the induction of *FRO1* and reducing the activity of IRT1 (Zuchi et al., 2009). From nutrient starvation experiments with the Strategy II plant barley also a positive correlation between the S nutritional status of the plant and its capability of coping with Fe deficiency emerged. One of the first responses to Fe deficiency in the Poaceae is the extrusion of phytosiderophores in the root rhizosphere in order to chelate and solubilize Fe^{3+} (Kobayashi and Nishizawa, 2012). Phytosiderophores are derived from nicotianamine that is synthesized from three molecules of *S*-adenosyl-methionine, thus representing another possible junction between Fe and S metabolism. Under S deficiency conditions the release of phytosiderophores was reduced but when barley plants were re-supplied with sulfate, the release of phytosiderophores was increased (Astolfi et al., 2010, 2012). The impact of Fe deprivation on the sulfur assimilation pathway has been recently investigated in durum wheat (Ciaffi et al., 2013). Here Fe shortage triggered several responses that are associated with S deficiency. The expression of genes encoding high-affinity SULTR was up-regulated in the root, as well as of several genes of the S metabolic pathway. These studies have followed a nutritional approach in crop plants and have focused on the changes that occur in the uptake and assimilation processes, supporting the idea of a co-regulation of Fe and S metabolism.

EVIDENCES FROM *Arabidopsis thaliana*

The model plant *Arabidopsis* is well investigated with respect to Fe and S metabolism. A double nutrient limitation strategy would allow to identify the target genes of potential co-regulation and to connect them to the so far known signal transduction chains of Fe and S metabolism. However, microarray data comprising systematic combinations of Fe and S starvation regimes are currently not available in public databases.

The potential impact of a double nutrient shortage approach for Fe and S was tested by growing *Arabidopsis thaliana* plants (Col-0 ecotype) in media that were supplemented with different concentrations of sulfate and of Fe in order to obtain four different growth conditions, named +Fe/+S, −Fe/+S, +Fe/−S, and −Fe/−S. The gene expression of *IRT1* and *SULTR1;1* that are primarily involved in the uptake strategies, was analyzed (**Figure 1**).

The expression of *IRT1* was induced (4.5-fold) in the roots of plants grown in −Fe/+S condition. This expected increase in *IRT1* expression under Fe deficiency was lower when plants were exposed to the double starvation (**Figure 1A**), which might be explained by a decreased requirement of Fe for Fe–S cluster synthesis under −S. In agreement with this, the +Fe/−S treatment caused a 50-fold down-regulation of the expression of the *IRT1* gene from its basal level. Interestingly, Fe deficiency resulted in a 2.5-fold decreased transcript level of the high-affinity SULTR, *SULTR1;1*, when compared to full supply of both nutrients, suggesting that decreased Fe–S cluster synthesis rate and/or accumulation of Fe–S cluster precursors, can affect this sulfate uptake system under −Fe/+S conditions. S depletion induced the expression of *SULTR1;1* by approximately 70-fold irrespective of the Fe supply (**Figure 1B**). This indicates that the demand of cysteine for translation triggers the typical S deficiency response in

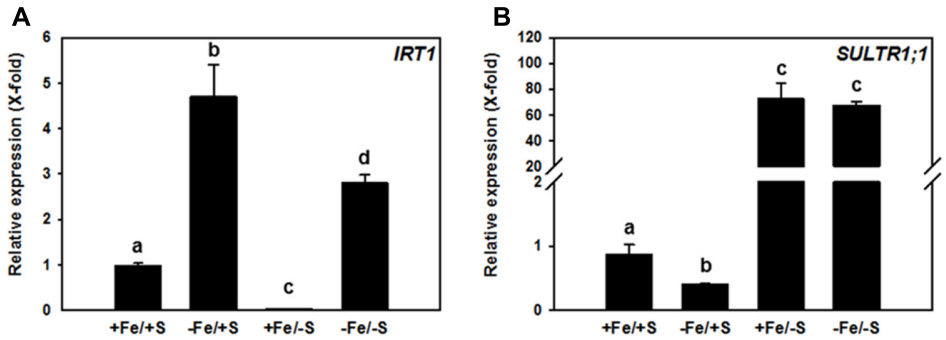

FIGURE 1 | Relative transcript abundance of *IRT1* (A) and *SULTR1;1* (B) in roots of 7-week-old *Arabidopsis thaliana* Col-0 plants grown upon different Fe and sulfate supply. Two weeks old plants were transferred to 6 l boxes containing half strength Hoagland medium with combined Fe and S supply (+Fe = 10 μM FeHBED Iron [*N,N′*-di-(2-hydroxybenzyl)-ethylenediamine-*N,N′*-diacetic acid], −Fe = 0.1 μM FeHBED, +S = 500 μM $MgSO_4$, −S = 1 μM $MgSO_4$) and grown for 5 weeks under short day conditions (8.5 h day light, 50% relative humidity, and 0.1 mmol m^{-2} s^{-1} light intensity). Total RNA was extracted from roots (PeqLAB) and converted into cDNA (Fermentas). The absolute transcript abundance of *IRT1* and *SULTR1;1* was measured by quantitative real-time PCR and normalized against the expression value of the reference gene *TIP41-like* (*At4g34270*). Means ± SD of four replicates are shown. Different letters indicate statistical significance ($P < 0.05$, ANOVA followed by Student–Newman–Keuls test).

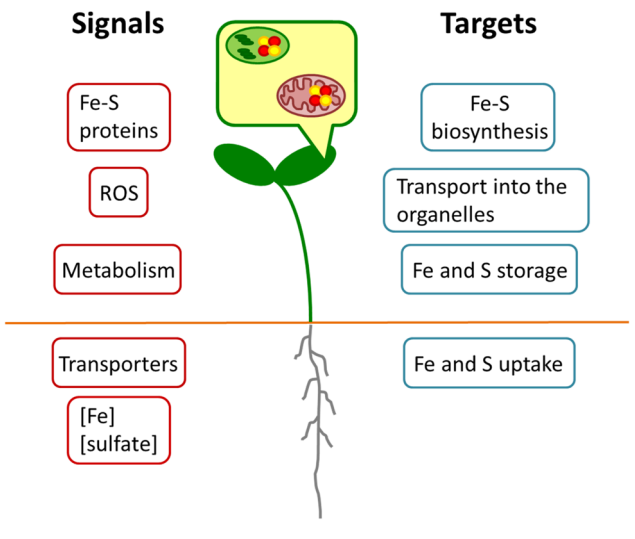

FIGURE 2 | Schematic model for regulatory interactions between Fe and S metabolism. Different putative Fe or S signals (red) may originate in the organelles or whole cells of root or shoot. Targets (blue) may comprise metabolic processes at expression or protein levels.

roots and can overcome the signal generated by decreased demand of cysteine for Fe–S clusters synthesis under −Fe condition.

Altogether, these results point toward a co-regulation between the pathways as the limitation of one nutrient influences the uptake of the other one. Such a co-regulation is very likely the outcome of a complex remodeling of the whole plant metabolism upon nutrient limitation as it is known for the prolonged deficiency of the single nutrients (Schuler et al., 2011). Hence, many different signals might contribute to this regulation as outlined in **Figure 2**. A primary signal might come from the sensing of the Fe and S concentrations or even their ratio in either the root environment or the cytosol of root cells. No such sensor has been identified yet, but an intriguing option would be the transporter/receptor (or "transceptor") concept as described for nitrate uptake (Wang et al., 2012). ROS could be another common signal, since excess of Fe and deficiency of S are known to result in their accumulation (Noctor et al., 2011) and this may also apply to imbalances between the metabolized nutrients. Different studies have indicated that the citric acid cycle is affected upon Fe deficiency (Vigani, 2012). Upon S deprivation, significant changes in the citric acid cycle have also been reported (Nikiforova et al., 2005). Thus, intermediates of the cycle or modulations of energy charge might function as signals for the co-regulation.

The lack of the precursors for the biosynthesis of Fe–S clusters in mitochondria and plastids might constitute an important feedback signal that leads to an overall adjustment of the metabolism. The Fe–S proteins might give rise to a signal for the co-regulation, but when the cluster biosynthesis is impaired, the apoproteins might be degraded and the break-down products might constitute a signal for the metabolic co-regulation. Interestingly, in bacteria Fe–S clusters with transcription factors as apoproteins often serve as sensors, mostly for reactive oxygen (Fleischhacker and Kiley, 2011). The iron regulatory protein 1 (IRP1) that controls the cellular iron homeostasis in mammals and changes between an active cytosolic aconitase with an Fe–S cluster and an apoform that binds iron responsive elements for post-transcriptional regulation is another example of Fe–S cluster sensing but is not present in plants (Arnaud et al., 2007).

All these signals are expected to converge into several plant responses (**Figure 2**). Important targets are the uptake of Fe and S, their transport into organelles, their storage and the actual synthesis of Fe–S clusters. Data mining of earlier microarray analyses of Fe starved *Arabidopsis* (Schuler et al., 2011) pointed to a co-expression cluster of sulfur metabolism-related genes including *APR* and *SULTR* isoforms and the vacuolar sulfate exporters *SULTR4;1* and *SULTR4;2* in leaves, which was interpreted as a necessity of rebalancing the metabolism of S under

these conditions (Ivanov et al., 2012). Such a requirement to actively maintain homeostasis of Fe and S metabolism might be the case also for the double nutrient deficiency. It should be taken into consideration, however, that the expression of genes represents only one side of the coin. In Fe and S uptake (e.g., *IRT1*; *SULTR1;1*) numerous post-transcriptional regulatory mechanisms have been observed that can modulate the responses to nutrient deficiency (Takahashi et al., 2011; Hindt and Guerinot, 2012). On the other hand, the enzymatic activity of Fe–S proteins (e.g., APR or aconitase) might be compromised due to the lack of precursors for the biosynthesis of the clusters. As it was already shown by different studies (for overview, see Vigani, 2012), the functionality of several enzymes in the root mitochondria is impaired by Fe starvation. The simultaneous lack of S might exacerbate this effect.

CONCLUSION

In this perspective the available information on single and combined nutrient limitation with emphasis on *Arabidopsis thaliana* was evaluated and a model of co-regulation between Fe and S metabolism was developed. The model was corroborated by the expression of the two key genes for the uptake of Fe (*IRT1*) and of S (*SULTR1;1*) that correlated with the nutrient supply and was differentially regulated in case of double nutrient deprivation. We conclude that a co-regulation between Fe and S metabolism exists and that Fe–S cluster availability is in accordance with a function in sensing and signaling of combined Fe and S deficiencies.

ACKNOWLEDGMENT

Ilaria Forieri is supported by the Marie Curie Initial Training Network BIONUT.

REFERENCES

Arnaud, N., Ravet, K., Borlotti, A., Touraine, B., Boucherez, J., Fizames, C., et al. (2007). The iron-responsive element (IRE)/iron-regulatory protein 1 (IRP1)–cytosolic aconitase iron-regulatory switch does not operate in plants. *Biochem. J.* 405, 523–531. doi: 10.1042/BJ20061874

Astolfi, S., Zuchi, S., Hubberten, H.-M., Pinton, R., and Hoefgen, R. (2010). Supply of sulphur to S-deficient young barley seedlings restores their capability to cope with iron shortage. *J. Exp. Bot.* 61, 799–806. doi: 10.1093/jxb/erp346

Astolfi, S., Zuchi, S., Neumann, G., Cesco, S., Di Toppi, L. S., and Pinton, R. (2012). Response of barley plants to Fe deficiency and Cd contamination as affected by S starvation. *J. Exp. Bot.* 63, 1241–1250. doi: 10.1093/jxb/err344

Balk, J., and Pilon, M. (2011). Ancient and essential: the assembly of iron–sulfur clusters in plants. *Trends Plant Sci.* 16, 218–226. doi: 10.1016/j.tplants.2010.12.006

Bashir, K., Ishimaru, Y., Shimo, H., Nagasaka, S., Fujimoto, M., Takanashi, H., et al. (2011). The rice mitochondrial iron transporter is essential for plant growth. *Nat. Commun.* 2, 322. doi: 10.1038/ncomms1326

Birke, H., Haas, F. H., De Kok, L. J., Balk, J., Wirtz, M., and Hell, R. (2012). Cysteine biosynthesis, in concert with a novel mechanism, contributes to sulfide detoxification in mitochondria of *Arabidopsis thaliana*. *Biochem. J.* 445, 275–283.

Briat, J.-F., Duc, C., Ravet, K., and Gaymard, F. (2010). Ferritins and iron storage in plants. *Biochim. Biophys. Acta* 1800, 806–814. doi: 10.1016/j.bbagen.2009.12.003

Busi, M. V., Maliandi, M. V., Valdez, H., Clemente, M., Zabaleta, E. J., Araya, A., et al. (2006). Deficiency of *Arabidopsis thaliana* frataxin alters activity of mitochondrial Fe–S proteins and induces oxidative stress. *Plant J.* 48, 873–882. doi: 10.1111/j.1365-313X.2006.02923.x

Cao, M.-J., Wang, Z., Wirtz, M., Hell, R., Oliver, D. J., and Xiang, C.-B. (2013). SULTR3;1 is a chloroplast-localized sulfate transporter in *Arabidopsis thaliana*. *Plant J.* 73, 607–616. doi: 10.1111/tpj.12059

Chan, K. X., Wirtz, M., Phua, S. Y., Estavillo, G. M., and Pogson, B. J. (2013). Balancing metabolites in drought: the sulfur assimilation conundrum. *Trends Plant Sci.* 18, 18–29. doi: 10.1016/j.tplants.2012.07.005

Ciaffi, M., Paolacci, A. R., Celletti, S., Catarcione, G., Kopriva, S., and Astolfi, S. (2013). Transcriptional and physiological changes in the S assimilation pathway due to single or combined S and Fe deprivation in durum wheat (*Triticum durum* L.) seedlings. *J. Exp. Bot.* 64, 1663–1675. doi: 10.1093/jxb/ert027

Duy, D., Wanner, G., Meda, A. R., Von Wiren, N., Soll, J., and Philippar, K. (2007). PIC1, an ancient permease in *Arabidopsis* chloroplasts, mediates iron transport. *Plant Cell* 19, 986–1006. doi: 10.1105/tpc.106.047407

Fleischhacker, A. S., and Kiley, P. J. (2011). Iron-containing transcription factors and their roles as sensors. *Curr. Opin. Chem. Biol.* 15, 335–341. doi: 10.1016/j.cbpa.2011.01.006

Hell, R., and Wirtz, M. (2011). Molecular biology, biochemistry and cellular physiology of cysteine metabolism in *Arabidopsis thaliana*. *Arabidopsis Book* 9, e0154. doi: 10.1199/tab.0154

Hindt, M. N., and Guerinot, M. L. (2012). Getting a sense for signals: regulation of the plant iron deficiency response. *Biochim. Biophys. Acta* 1823, 1521–1530. doi: 10.1016/j.bbamcr.2012.03.010

Ivanov, R., Brumbarova, T., and Bauer, P. (2012). Fitting into the harsh reality: regulation of iron-deficiency responses in dicotyledonous plants. *Mol. Plant* 5, 27–42. doi: 10.1093/mp/ssr065

Kobayashi, T., and Nishizawa, N. K. (2012). Iron uptake, translocation, and regulation in higher plants. *Annu. Rev. Plant Biol.* 63, 131–152. doi: 10.1146/annurev-arplant-042811-105522

Nikiforova, V. J., Kopka, J., Tolstikov, V., Fiehn, O., Hopkins, L., Hawkesford, M. J., et al. (2005). Systems rebalancing of metabolism in response to sulfur deprivation, as revealed by metabolome analysis of *Arabidopsis* plants. *Plant Physiol.* 138, 304–318. doi: 10.1104/pp.104.053793

Noctor, G., Queval, G., Mhamdi, A., Chaouch, S., and Foyer, C. H. (2011). Glutathione. *Arabidopsis Book* 9, e0142. doi: 10.1199/tab.0142

Schuler, M., Keller, A., Backes, C., Philippar, K., Lenhof, H.-P., and Bauer, P. (2011). Transcriptome analysis by GeneTrail revealed regulation of functional categories in response to alterations of iron homeostasis in *Arabidopsis thaliana*. *BMC Plant Biol.* 11:87. doi: 10.1186/1471-2229-11-87

Takahashi, H., Kopriva, S., Giordano, M., Saito, K., and Hell, R. (2011). Sulfur assimilation in photosynthetic organisms: molecular functions and regulations of transporters and assimilatory enzymes. *Annu. Rev. Plant Biol.* 62, 157–184. doi: 10.1146/annurev-arplant-042110-103921

Tarantino, D., Santo, N., Morandini, P., Casagrande, F., Braun, H.-P., Heinemeyer, J., et al. (2010). AtFer4 ferritin is a determinant of iron homeostasis in *Arabidopsis thaliana* heterotrophic cells. *J. Plant Physiol.* 167, 1598–1605. doi: 10.1016/j.jplph.2010.06.020

Vigani, G. (2012). Discovering the role of mitochondria in the iron deficiency-induced metabolic responses of plants. *J. Plant Physiol.* 169, 1–11. doi: 10.1016/j.jplph.2011.09.008

Vigani, G., Zocchi, G., Bashir, K., Philippar, K., and Briat, J.-F. (2013). Signals from chloroplasts and mitochondria for iron homeostasis regulation. *Trends Plant Sci.* 18, 305–311. doi: 10.1016/j.tplants.2013.01.006

Wang, Y.-Y., Hsu, P.-K., and Tsay, Y.-F. (2012). Uptake, allocation and signaling of nitrate. *Trends Plant Sci.* 17, 458–467. doi: 10.1016/j.tplants.2012.04.006

Zuchi, S., Cesco, S., Varanini, Z., Pinton, R., and Astolfi, S. (2009). Sulphur deprivation limits Fe-deficiency responses in tomato plants. *Planta* 230, 85–94. doi: 10.1007/s00425-009-0919-1

Conflict of Interest Statement: The authors declare that the research was conducted in the absence of any commercial or financial relationships that could be construed as a potential conflict of interest.

Received: 24 May 2013; paper pending published: 21 June 2013; accepted: 23 August 2013; published online: 02 October 2013.

Citation: Forieri I, Wirtz M and Hell R (2013) Toward new perspectives on the interaction of iron and sulfur metabolism in plants. Front. Plant Sci. ***4****:357. doi: 10.3389/fpls.2013.00357*

This article was submitted to Plant Nutrition, a section of the journal Frontiers in Plant Science.

frontiers in
PLANT SCIENCE

PERSPECTIVE ARTICLE
published: 31 May 2013
doi: 10.3389/fpls.2013.00169

Searching iron sensors in plants by exploring the link among 2′-OG-dependent dioxygenases, the iron deficiency response and metabolic adjustments occurring under iron deficiency

Gianpiero Vigani[1], Piero Morandini[2] and Irene Murgia[2]*

[1] *Dipartimento di Scienze Agrarie ed Ambientali-Produzioni, Territorio, Agroenergia, Università degli Studi di Milano, Milano, Italy*
[2] *Dipartimento di Bioscienze, Università degli Studi di Milano, Milano, Italy*

Edited by:
Jean-Francois Briat, Centre National de la Recherche Scientifique, France

Reviewed by:
Wolfgang Schmidt, Academia Sinica, Taiwan
Sabine Lüthje, University of Hamburg, Germany

***Correspondence:**
Irene Murgia, Dipartimento di Bioscienze, Università degli Studi di Milano, Via Celoria 26, 20133 Milano, Italy
e-mail: irene.murgia@unimi.it

Knowledge accumulated on the regulation of iron (Fe) homeostasis, its intracellular trafficking and transport across various cellular compartments and organs in plants; storage proteins, transporters and transcription factors involved in Fe metabolism have been analyzed in detail in recent years. However, the key sensor(s) of cellular plant "Fe status" triggering the long-distance shoot–root signaling and leading to the root Fe deficiency responses is (are) still unknown. Local Fe sensing is also a major task for roots, for adjusting the internal Fe requirements to external Fe availability: how such sensing is achieved and how it leads to metabolic adjustments in case of nutrient shortage, is mostly unknown. Two proteins belonging to the 2′-OG-dependent dioxygenases family accumulate several folds in Fe-deficient *Arabidopsis* roots. Such proteins require Fe(II) as enzymatic cofactor; one of their subgroups, the HIF-P4H (hypoxia-inducible factor-prolyl 4-hydroxylase), is an effective oxygen sensor in animal cells. We envisage here the possibility that some members of the 2′-OG dioxygenase family may be involved in the Fe deficiency response and in the metabolic adjustments to Fe deficiency or even in sensing Fe, in plant cells.

Keywords: *Arabidopsis thaliana*, iron sensor, HIF (hypoxia-inducible factor), 2′-OG-dependent dioxygenase, prolyl 4-hydroxylase

INTRODUCTION

Iron is an essential micronutrient for plants although it is potentially toxic, when present in a free, non-complexed form. A recent review on that subject (Kobayashi and Nishizawa, 2012) details the knowledge accumulated on the regulation of plant Fe homeostasis, its intracellular trafficking and transport across cellular compartments and organs under various conditions of Fe supply, unveiling a complex net of molecular interactions. Beside the intensification of Fe-uptake strategies activated by plants under Fe-limiting conditions, root cells reprogram their metabolism to better cope with shortage of Fe (Vigani et al., 2012). Low Fe content triggers a high energy request to sustain the increased rate of Fe uptake from the soil, and at the same time it impairs the function of mitochondria and chloroplasts which provide energy to the cells. Thus, cells must increase the rate of alternative energy-providing pathways, such as glycolysis, Krebs cycle, or pentose phosphate pathway (López-Millán et al., 2000, 2012; Li et al., 2008; Vigani and Zocchi, 2009; Donnini et al., 2010; Rellán-Álvarez et al., 2010; Vigani, 2012a). To date, however, the sensors of plant "Fe status" triggering the signal transduction pathways, which eventually induce transcription factors such as the *Arabidopsis* FIT1, are still unknown and represent a challenging issue in plant science (Vigani et al., 2013). Efforts to fill up such gap of knowledge have been made by different research groups since years (Schmidt and Steinbach, 2000); recently, it has been demonstrated that localized Fe supply stimulates lateral root formation through the AUX1 auxin importer, which is proposed as a candidate for integrating the local Fe status in auxin signaling (Giehl et al., 2012).

2′-OG Fe(II)-DEPENDENT DIOXYGENASES AND PROLYL 4-HYDROXYLASES

It has been recently observed that some similarities might exist between the metabolic reprogramming occurring in Fe-deficient roots and that one occurring in tumor cells (Vigani, 2012b). In tumor cells, such reprogramming is known as "Warburg-effect" in which glucose is preferentially converted to lactate by enhancing glycolysis and fermentative reactions rather than completely oxidized by oxidative phosphorylation (OXOPHOS; Brahimi-Horn et al., 2007). Also in root cells a low Fe availability causes a decrease of OXOPHOS activity and induction of glycolysis and anaerobic reactions (Vigani, 2012b). The Warburg-effect in animal cells is mediated by hypoxia-inducible factor (HIF1), a heterodimeric complex whose α subunit is inducible by hypoxia. Under normoxic conditions, HIFα is post-translationally modified via the hydroxylation of proline residues by prolyl 4-hydroxylases (P4H); such modification leads to the proteasome-mediated degradation of HIFα. Under hypoxic conditions, however, such hydroxylation cannot occur because P4H enzymes belong to the 2-oxoglutarate Fe(II)-dependent dioxygenase family which have molecular oxygen and oxoglutarate as co-substrates; in other words, the lack of oxygen inhibits the P4H enzymatic activity, HIFα escapes degradation, it translocates to the nucleus where it can therefore form a

dimer with HIFβ subunit; the complex then activates the cascade of hypoxia-responsive gene expression pathways (Myllyharju, 2003; Ken and Costa, 2006; Semenza, 2007).

Prolyl 4-hydroxylases are present in animal as well as in plant cells. In animal cells, P4H are classified into two categories: the collagen-type-P4H and the above cited HIF-P4H. The first class is localized within the lumen of the endoplasmic reticulum and it catalyzes the hydroxylation of proline residues within -X-Pro-Gly- sequences in collagen and in collagen-type proteins (Myllyharju, 2003), thus stabilizing their triple helical structure at body temperature (Myllyharju, 2003). These P4Hs are $\alpha_2\beta_2$ tetramers and their catalytic site is located in the α subunit (Myllyharju, 2003; Tiainen et al., 2005). Three aa residues, His-412, Asp-414, and His-483, are the binding sites for Fe(II) in the human α(I) subunit (Myllyharju, 2003). The second class of P4H is localized in cytoplasm and it is responsible for hydroxylation of a proline residue in the HIFα subunit, under normoxic conditions, as described above. The K_m values of HIF-P4Hs for O_2 are slightly above atmospheric concentration, making such proteins effective O_2 sensors (Hirsilä et al., 2003). A novel role has also been uncovered for a human collagen-type-P4H, as regulator of Argonaute2 stability with consequent influence on RNA interference mechanisms (Qi et al., 2008).

Several genes similar to P4H are present in plants; for instance, 13 P4H have been identified in *Arabidopsis* and named AtP4H1–AtP4H13 (Vlad et al., 2007a,b); with the exception of AtP4H11 and AtP4H12, the three binding residues for Fe(II) (two His and one Asp) as well as the Lys residues binding the 2-oxoglutarate, are all conserved in such P4Hs (Vlad et al., 2007a). The different isoforms are more expressed in roots than in shoots and they show different pattern of expression in response to various stresses (hypoxia, anoxia, and mechanical wounding ; Vlad et al., 2007a,b).

Cloning and biochemical characterization of two of them, i.e., AtP4H1, encoded by At2g43080 gene (Hieta and Myllyharju, 2002) and At4PH2, encoded by At3g06300 gene (Tiainen et al., 2005) show that substrate specificity varies: recombinant AtP4H1 effectively hydroxylates poly(L-proline) and other synthetic peptides with K_m values lower than those for AtP4H2, thus suggesting different physiological roles between the two. Recombinant AtP4H1 can also effectively hydroxylate human HIFα-like peptides and collagen-like peptides, whereas recombinant AtP4H2 cannot (Hieta and Myllyharju, 2002; Tiainen et al., 2005). Their K_m for Fe(II) are 16 and 5 μM, respectively (Hieta and Myllyharju, 2002; Tiainen et al., 2005).

Two proteins belonging to the 2′-OG dioxygenase family, encoded by At3g12900 and At3g13610 genes, accumulate several folds in Fe-deficient roots, when compared to Fe-sufficient ones (Lan et al., 2011). The protein encoded by At3g13610 gene, named F6′H1, is involved in the synthesis of coumarins via the phenylpropanoid pathway, as it catalyzes the ortho-hydroxylation of feruloyl CoA, which is the precursor of scopoletin (Kai et al., 2008). Scopoletin and its β-glucoside scopolin accumulate in *Arabidopsis* roots and, at lower levels, also in shoots (Kai et al., 2006).

A severe reduction of scopoletin levels can be observed in the KO mutants for the At3g13610 gene (Kai et al., 2008). One of the responses to Fe deficiency, is the induction of the phenylpropanoid pathway (Lan et al., 2011). Phenolics can facilitate the reutilization of root apoplastic Fe (Jin et al., 2007a,b) and a phenolic efflux transporter PEZ1 located in the stele has been identified in rice (Ishimaru et al., 2011). The secretion of phenolic compounds can, moreover, selectively modify the soil microbial population in the surroundings of the roots, which in turn can favor acquisition of Fe by production of siderophores as well as auxin-like compounds (Jin et al., 2006, 2008, 2010).

Plant 2′-OG dioxygenases are also involved in synthesis of phytosiderophores such as Ids3 from barley, which is induced by Fe deficiency and it catalyzes the hydroxylation step from 2′-deoxymugeinic acid (DMA) to mugeinic acid (MA; Kobayashi et al., 2001).

2′-OG Fe(II)-DEPENDENT DIOXYGENASES, Fe DEFICIENCY RESPONSE AND METABOLIC REPROGRAMMING: IS THERE A COMMON LINK?

Given the above premises, it is possible that a link among P4H activity, and more generally among 2′-OG Fe(II)-dependent dioxygenase activities, the Fe deficiency responses and the metabolic reprogramming occurring during Fe deficiency exists in higher plants. If such a link exists for a given 2′-OG Fe(II)-dependent dioxygenase, at least two possible scenarios could be predicted for such enzyme (**Figure 1**):

(a) If, for a given sub-cellular localization, the K_m of such enzyme for Fe is close to the physiological concentration of the LIP (labile iron pool, consisting of free redox-active Fe ions), then the enzyme activity is strongly affected by Fe fluctuations, similarly to the above described HIF-P4H, which is an effective sensor for O_2 (Hirsilä et al., 2003). Upon reduction of Fe availability below the physiological LIP, its enzymatic activity should be indeed drastically reduced or fully inhibited; reduction or complete lack of enzymatic product might, in turn, triggers the "Fe deficiency" signaling. The enzyme might therefore act as true Fe sensor (**Figure 1**, upper panel, right).

Although the Fe-dependent transcriptional regulation of such an Fe sensor enzyme might be not expected, it cannot be excluded *a priori*: for example, chitin recognition is dependent not only on the presence of specific receptors, but also on the expression of extracellular chitinases, which are essential for the production of smaller chito-oligosaccharides from chitin hydrolysis, in animal (Gorzelanny et al., 2010; Vega and Kalkum, 2012) as well as in plant systems (Shibuya and Minami, 2001; Wan et al., 2008). These smaller, diffusible molecules induce, in turn, the expression of several defense protein, among which also chitinase activities. Chitinase is thus both an example of a crucial enzyme for the signal production but also an integral part of the response.

(b) If, for a given sub-cellular localization, the K_m for Fe of such an enzyme is instead far below the physiological LIP, the enzyme might still be active under Fe deficiency. Additionally, if transcriptional/translational up-regulation occurs under Fe deficiency, accumulation of protein and increased total enzymatic activity might be observed. The enzyme might be involved in the Fe response/metabolic adjustment occurring under Fe deficiency, without being itself a Fe sensor (**Figure 1**, lower panel, right).

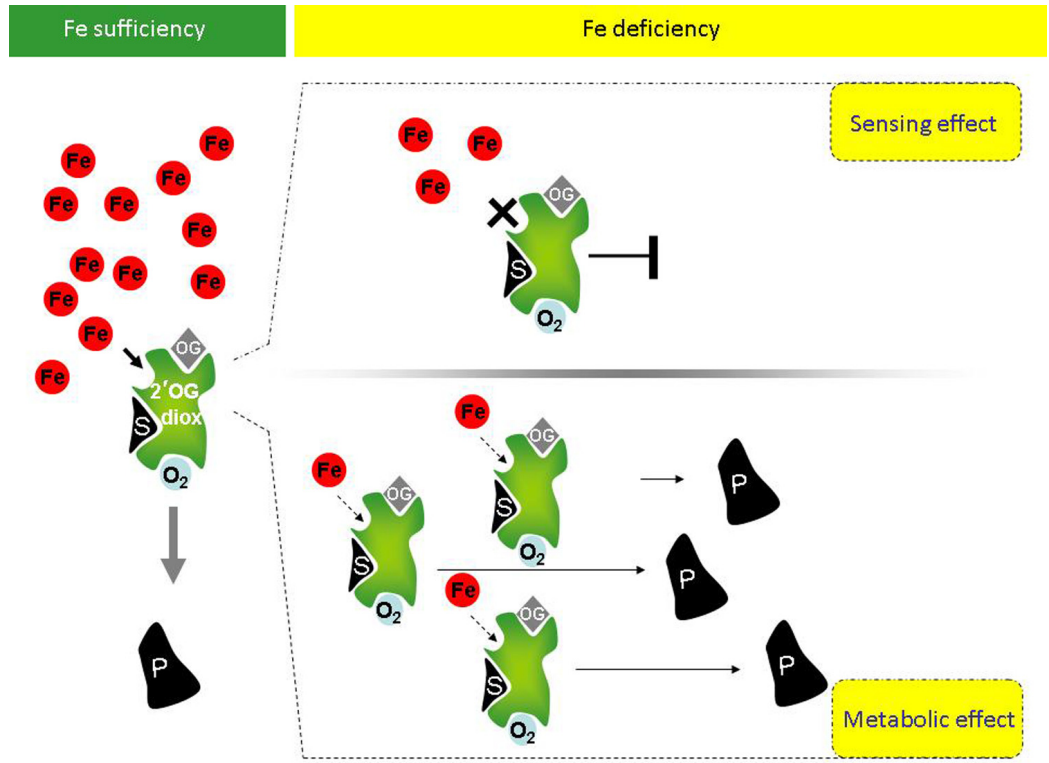

FIGURE 1 | Potential involvement of plant 2′-OG-dioxygenases in Fe sensing, in the Fe deficiency responses and in the metabolic reprogramming occurring under Fe deficiency. Under Fe sufficiency, in presence of the co-factors O_2 and oxoglutarate (OG), 2′-OG-dioxygenases (in green) can catalyze the dioxygenase reaction leading to production of product P from substrate S. Under Fe deficiency, however, at least two scenarios can occur, depending on the K_m of a given 2′-OG-dioxygenase for Fe. If the K_m is close to the physiological concentration of the labile iron pool (LIP; free redox-active Fe ions), upon reduction of Fe availability, the enzymatic activity of the 2′-OG-dioxygenase is drastically reduced or fully inhibited and the reduction or complete lack of enzymatic product can be itself a signal of "Fe deficiency" triggering the Fe deficiency response cascades (upper panel, right). If instead K_m is far below the physiological LIP, the enzyme might still be active (lower panel, right). Not only, if transcriptional/translational up-regulation of such 2′-OG-dioxygenase takes place under Fe deficiency, then an increased total enzymatic activity can lead to higher production of product P (lower panel, right). Product P, in turn, could be involved in the Fe response/metabolic adjustments occurring under Fe deficiency.

This second scenario is supported by the evidence that the *Arabidopsis* 2′-OG-dioxygenase F6′H1 (described in previous paragraph) which accumulates in Fe-deficient roots (Lan et al., 2011) is indeed possibly involved in the Fe response/metabolic adjustment occurring under Fe deficiency: *Arabidopsis* mutants KO for the At3g13610 gene (coding for F6′H1) have indeed altered root phenotype under Fe deficiency (I. Murgia, unpublished observations).

Such a link among 2′-OG Fe(II)-dependent dioxygenase activity, the Fe deficiency responses and the metabolic reprogramming occurring during Fe deficiency can be explored first by analyzing the transcriptional co-regulation of 2′-OG-dependent dioxygenase genes with genes involved in the Fe deficiency response or in the metabolic reprogramming. The bioinformatic approach of our choice was already described (Beekwilder et al., 2008; Menges et al., 2008; Berri et al., 2009; Murgia et al., 2011) and successfully applied in *Arabidopsis* and rice. Such analysis identifies genes which are co-regulated in large microarray datasets; in this case, it provides candidate genes potentially involved in Fe metabolism, among the 2′-OG-dioxygenase family members. Although transcript levels do not equal protein levels (or activities), there is nevertheless evidence for correlation between the two in many organisms (Vogel and Marcotte, 2012). This approach is not only simple on a genomic scale, but it has proved useful to identify candidate genes in the past, which were then validated by experimental approaches (e.g., Beekwilder et al., 2008; Murgia et al., 2011; Møldrup et al., 2012).

Arabidopsis possesses almost one hundred annotated 2′-OG dioxygenase genes which make such analysis not immediate; we therefore restricted the analysis to the AtP4H subclass (with the exclusion of AtP4H8, AtP4H12, and AtP4H13 because the corresponding genes were not available in the Affymetrix microarray data set most commonly used). As pivot bioinformatic analysis, we analyzed the correlation of such AtP4H subclass with two gene groups. The first group consisted of a list of 25 Fe-homeostasis/trafficking/transport related genes, described in recent reviews on this subject (Conte and Walker, 2011; Kobayashi and Nishizawa, 2012). The second group consisted of an equal number of genes coding for enzymes possibly involved in the metabolic adjustments under Fe deficiency, such as those catalyzing the synthesis of pyruvate (Pyr). It is indeed known that several glycolitic genes are overexpressed in roots of Fe-deficient

plants (Thimm et al., 2001): different isoforms of hexokinase (HXK), phosphoglyceratekinase, enolase (ENO), phosphoglycerate mutase (iPGAM), were therefore considered. Also, genes coding for enzymes involved in the consumption of Pyr by non-OXOPHOS reactions and whose expression is affected by Fe deficiency, such as alcohol dehydrogenase (ADH), lactate dehydrogenase (LDH), and malate dehydrogenase, were also considered (Thimm et al., 2001). Last, the genes coding for the four isoforms of *Arabidopsis* phospho*enol*pyruvate carboxylase (PEPC; PPC1, 2, 3, 4; Sanchez et al., 2006) were also included in the second group, since PEPC is strongly induced in several dicotyledonous plants under Fe deficiency (Vigani, 2012a) and PEPC is supposed to play a central role in the metabolic reprogramming occurring in Fe-deficient root cells (Zocchi, 2006).

As positive controls, the two 2′-OG-dioxygenases encoded by At3g12900 and At3g13610 and accumulating in Fe-deficient roots (Lan et al., 2011) whereas, as negative control, the ferritin gene whose expression is known to be repressed under Fe deficiency (Murgia et al., 2002), were included. The full list of genes for which the correlation analysis has been performed, is reported in **Table 1**.

The resulting Pearson's correlation coefficients, calculated by using either linear or logarithmic expression values (Menges et al., 2008; Murgia et al., 2011) are reported in **Table 2**, if above a defined threshold ($\geq$0.60 or ≤ -0.60); genes for which none of the Pearson's coefficient fulfilled this condition, were not included in **Table 2** (AtP4H3, AtP4H9, AtP4H10 and AtP4H11).

In accordance with results obtained by iTRAQ (isobaric peptide tags for relative and absolute quantitation) analysis of Fe-deficient roots (Lan et al., 2011), both At3g12900 and At3g136100 show positive correlation with genes actively involved in the Fe deficiency response, such as iron-regulated transporter 1 (IRT1; Vert et al., 2002), ferric-chelate oxidase reductase (FRO2; Connolly et al., 2003) CYP82C4 (Murgia et al., 2011), ferroportin/iron-regulated (IREG2; Morrissey et al., 2009) metal tolerance protein (MTP3; Arrivault et al., 2006)(**Table 2**); viceversa, they show no significant correlation with the ferritin genes since their correlation values fall within the $[-0.3 + 0.02]$ range (data not shown).

According to such results, the AtP4H genes could be divided into three classes:

Class 1: positive or negative correlation with metabolic genes only (At3g28490, At2g43080, and At5g18900).

Class 2: positive correlation with Fe-related genes and positive or negative correlation with metabolic genes (At2g17720 and At3g06300, beside the positive control At3g13610).

Class 3: no significant correlation (positive or negative) with any of the genes tested (At1g20270, At4g33910, At5g66060, At4g35820).

Genes in class 1 might be not involved in the plant response to improve Fe uptake and trafficking in order to alleviate Fe deficiency symptoms.

Genes in class 2 might be the ones linking the stimulation of Fe deficiency response with the metabolic adaptations triggered by Fe deficiency (**Figure 1**) whereas genes in class 3 might contain the candidate Fe sensor(s) (**Figure 1**).

Regarding the genes in class 2, it is interesting to notice that beside with the Fe-related genes, the positive control At3g13610 is positively correlated with PPC3 and ENO1, the At3g06300 gene coding for P4H2 (Tiainen et al., 2005) is positively correlated with PPC1, PPC3, ENO1, and also negatively correlated with a malate dehydrogenase family member whereas the At2g17720 gene coding

Table 1 | List of genes for which the correlation analysis with 2′-OG-dependent dioxygenases has been performed.

Fe homeostasis genes		Metabolic genes	
IRT1	At4g19690	HXK1	At4g29130
IRT2	At4g19680	HXK2	At2g19860
AHA2	At4g30190	HXK4	At3g20040
NAS1	At5g04950	HKL1	At1g50460
NAS2	At5g56080	HXL3	At4g37840
NAS3	At1g09240	PPC1	At1g53310
NAS4	At1g56430	PPC2	At2g42600
CYP82C4	At4g31940	PPC3	At3g14940
IREG2	At5g03570	PPC4	At1g68750
MTP3	At3g58810	PGK	At1g79550
Popeye	At3g47640	PGK1	At3g12780
Brutus	At3g18290	LDH	At4g17260
NRAMP3	At2g23150	ENO1	At1g74030
NRAMP4	At5g67330	ENOC	At2g29560
FRO3	At1g23020	ENO2	At2g36530
FRO7	At5g49740	iPGAM	At1g09780
FRD3	At3g08040	PGM	At1g78050
ILR3	At5g54680	PDC2	At5g54960
YSL1	At4g24120	PDC3	At5g01330
ZIF1	At5g13740	G6PD4	At1g09420
VIT1	At2g01770	MMDH2	At3g15020
Fer1	At5g01600	mal dehydr family	At3g53910
Fer2	At3g11050	mal dehydr family	At4g17260
Fer3	At3g56090	mal dehydr family	At5g58330
Fer4	At2g40300	ADH1	At1g77120
		ADH transcrip factor	At2g44730
		ADH transcrip factor	At3g24490

Genes in the left column are known to be involved in the Fe deficiency response, in regulation of Fe homeostasis or Fe trafficking. Genes in the right column are involved in glycolysis or in the consumption of pyruvate by non-OXOPHOS reactions; genes coding for the four isoforms of Arabidopsis phosphoenolpyruvate carboxylase (PEPC; PPC1, 2, 3, 4) have been also included. IRT, iron-regulated transporter; AHA, Arabidopsis H^+-ATPase; NAS, nicotianamine synthase; CYP82C4, cytochrome P450 82C4; IREG, ferroportin/iron-regulated; MTP3, metal tolerance protein; NRAMP, natural resistance-associated macrophage protein; FRO, ferric-chelate oxidase reductase; FRD, ferric reductase defective; ILR, IAA-leucine resistant; YSL, yellow stripe-like; ZIF, zinc induced facilitator; VIT, vacuolar iron transporter; Fer, ferritin; HXK1, hexokinase; HXL, hexokinase-like; PPC, phosphoenolpyruvate carboxylase; PGK, phosphoglyceratekinase; LDH, lactate dehydrogenase; ENO, enolase; ENOC, cytosolic enolase; iPGAM, phosphoglycerate mutase; PGM, phosphoglycerate/bisphosphoglycerate mutase; PDC, pyruvate decarboxylase; G6PD4, glucose-6-phosphate dehydrogenase; MMDH, mitochondrial malate dehydrogenase; mal dehydr family, malate dehydrogenase family; ADH, alcohol dehydrogenase.

Table 2 | Correlation analysis of Arabidopsis thaliana 2′-OG dioxygenase genes with genes involved in Fe deficiency response or with genes possibly involved in metabolic reprogramming during Fe deficiency.

	AGI code	2′-OG-dioxyg At3g12900		2′-OG-dioxyg At3g13610		P4H-1 At2g43080		P4H-2 At3g06300		P4H-4 At5g18900		P4H-5 At2g17720		P4H-6 At3g28490	
		lin	log	lin	log	lin	log	lin	log	lin	log	lin	log	lin	log
IRT1	At4g19690	**0.69**	0.23	**0.74**	**0.69**	0.21	0.21	0.54	0.55	0.10	0.11	0.36	0.53	−0.02	0.05
AHA2	At4g30190	0.22	0.09	**0.67**	**0.69**	0.35	0.31	**0.76**	**0.71**	0.18	0.22	**0.76**	**0.79**	−0.07	−0.07
CYP82C4	At4g31940	0.54	0.47	**0.61**	0.56	0.30	0.33	0.40	0.43	0.16	0.22	0.27	0.37	−0.04	−0.13
IREG2	At5g03570	**0.73**	0.42	**0.79**	0.59	0.26	0.22	**0.64**	0.55	0.23	0.31	0.41	0.51	−0.02	−0.08
MTP3	At3g58810	**0.77**	0.27	**0.83**	**0.70**	0.30	0.37	**0.62**	**0.66**	0.16	0.23	0.40	0.58	−0.04	−0.10
HXK4	At3g20040	0.25	0.22	0.32	0.25	0.24	0.27	0.29	0.37	0.26	0.02	0.17	0.26	**0.72**	0.06
HXL3	At4g37840	0.01	0.05	−0.06	−0.03	0.13	0.05	−0.08	−0.06	0.32	0.11	−0.05	−0.06	**0.66**	0.35
PPC1	At1g53310	0.03	−0.06	0.41	0.55	0.19	0.22	**0.60**	**0.63**	0.03	0.10	**0.73**	**0.70**	−0.10	−0.06
PPC3	At3g14940	0.23	0.21	**0.78**	**0.73**	0.35	0.27	**0.69**	0.58	0.19	0.23	0.58	0.58	0.02	0.03
PPC4	At1g68750	0.01	0.08	−0.04	0.10	0.13	0.05	−0.05	0.08	0.35	0.08	0.00	0.13	**0.78**	0.21
PGK1	At3g12780	−0.13	−0.11	−0.50	−0.41	**−0.67**	**−0.69**	−0.49	−0.46	**−0.66**	**−0.74**	−0.33	−0.30	−0.09	−0.03
ENO1	At1g74030	0.14	0.03	**0.72**	0.59	0.37	0.31	**0.67**	0.59	0.12	0.06	0.54	0.49	−0.05	−0.01
iPGAM	At1g09780	0.07	0.03	0.47	0.51	0.04	0.10	0.54	0.56	−0.21	−0.32	**0.61**	**0.62**	−0.07	−0.03
Mal. d. fam.	At5g58330	−0.19	−0.23	−0.56	−0.49	**−0.70**	**−0.67**	**−0.61**	**−0.61**	−0.59	**−0.60**	−0.47	−0.47	−0.08	0.02

For each gene pair, the Pearson's correlation coefficient, from logarithmic or linear analysis, is reported. Coefficients with values ≥0.60 or ≤−0.60 are highlighted in gray.

for P4H5 is positively correlated with PPC1 and iPGAM (Zhao and Assmann, 2011).

Interestingly, PPC1 and PPC3 are mainly expressed in root tissues and their expression is affected by abiotic stress when compared with PPC2, which is considered to cover an housekeeping role (Sanchez et al., 2006), whereas ENO1 encodes the plastid-localized isoform of phospho*enol*pyruvate (PEP)-ENO (Prabhakar et al., 2009); PEP is further metabolized to Pyr by pyruvate kinase (PK). PEP and Pyr represent essential precursors for anaerobic reaction. PEP is fed into the schikimate pathway, which is localized within the plastid stroma (Herrmann and Weaver, 1999) and which is essential for a large variety of secondary products. Pyr can also act as precursor for several plastid-localized pathways, among which the mevalonate-independent way of isoprenoid biosynthesis (Lichtenthaler, 1999). Plastid-MEP (2-*C*-methyl-D-erythritol 4-phosphate) pathways might be responsible for the synthesis of a signal molecule putatively involved in the regulation of Fe homeostasis (Vigani et al., 2013).

Such analysis is preliminary and needs to be extended to all 2′-OG-dioxygenase gene family members. Genes candidate as Fe sensors can be further analyzed experimentally, insofar that loss-of function mutants lacking the "Fe sensing" function should display a Fe deficiency response, even in Fe-sufficient conditions (see **Figure 1**, upper panel, right).

FUTURE DIRECTIONS

Elucidation of nutrient sensing and signaling is a major issue in plant physiology and crop production, with potential impact in the design of new biofortification strategies for improving yields as well as the nutritional value of crops of interest (Murgia et al., 2012; Schachtman, 2012). In *Arabidopsis*, a major sensor of nitrate is the nitrate transporter NRT1.1, which is the first representative of plant "transceptors," thus indicating their dual nutrient transport/signaling function (Gojon et al., 2011). Transceptors, whose feature is that transport and sensing activity can be uncoupled, have been described in animals and yeasts (Thevelein and Voordeckers, 2009; Kriel et al., 2011) and more active transceptors have been postulated also in plants (Gojon et al., 2011).Three major global challenges faced by agriculture are food and energy production as well as environmental compatibility (Ehrhardt and Frommer, 2012). Advancements in the area of nutrient sensing and signaling can positively contribute solutions to all these three challenges and the extensive analysis of the complete 2′-OG-dioxygenase gene family, based on pilot analysis described in the present perspective, could be a novel way to pursue these advancements.

ACKNOWLEDGMENTS

Gianpiero Vigani and Irene Murgia were supported by FIRB, Futuro in Ricerca 2012 (project code RBFR127WJ9) funded by MIUR. Gianpiero Vigani was further supported by "Dote Ricerca": FSE, Regione Lombardia. We are grateful to Prof. Shimizu Bun-Ichi (Graduate School of Life Science, Toyo University, Japan) for kindly providing *Arabidopsis* At3g13610 KO mutant seeds and to Luca Mizzi (Milano University, Italy) for developing the programs to compute the correlation coefficients.

REFERENCES

Arrivault, S., Senger, T., and Krämer, U. (2006). The *Arabidopsis* metal tolerance protein AtMTP3 maintains metal homeostasis by mediating Zn exclusion from the shoot under Fe deficiency and Zn oversupply. *Plant J.* 46, 861–879. doi: 10.1111/j.1365-313X.2006.02746.x

Beekwilder, J., van Leeuwen, W., van Dam, N. M., Bertossi, M., Grandi, V., Mizzi, L., et al. (2008). The impact of the absence of aliphatic glucosinolates on insect herbivory in *Arabidopsis*. *PLoS ONE* 3:e2068. doi: 10.1371/journal.pone.0002068

Berri, S., Abbruscato, P., Faivre-Rampant, O., Brasiliero, A. C. M., Fumasoni, I., Mizzi, L., et al. (2009). Characterization of WRKY co-regulatory networks in rice and *Arabidopsis*. *BMC Plant Biol.* 9:120. doi: 10.1186/1471-2229-9-120

Brahimi-Horn, M. C., Chiche, J., and Pouyessegur, J. (2007). Hypoxia signalling controls metabolic demand. *Curr. Opin. Cell Biol.* 19, 223–229. doi: 10.1016/j.ceb.2007.02.003

Connolly, E., Campbell, N. H., Grotz, N., Prichard, C. L., and Guerinot, M. L. (2003). Overexpression of the FRO2 ferric chelate reductase confers tolerance to growth on low iron and uncovers posttranscriptional control. *Plant Physiol.* 133, 1102–1110. doi: 10.1104/pp.103.025122

Conte, S. S., and Walker, E. L. (2011). Transporter contributing to iron trafficking in plants. *Mol. Plant* 4, 464–476. doi: 10.1093/mp/ssr015

Donnini, S., Prinsi, B., Negri, A. S., Vigani, G., Espen, L., and Zocchi, G. (2010). Proteomic characterization of iron deficiency responses in *Cucumis sativus* L. roots. *BMC Plant Biol.* 10:268. doi: 10.1186/1471-2229-10-268

Ehrhardt, D. W., and Frommer, W. B. (2012). New technologies for 21 century plant science. *Plant Cell* 24, 374–394. doi: 10.1105/tpc.111.093302

Giehl, R. F. H., Lima, J. E., and von Wiren, N. (2012). Localized iron supply triggers lateral root elongation in *Arabidopsis* by altering the AUX1-mediated auxin distribution. *Plant Cell* 24, 33–49. doi: 10.1105/tpc.111.092973

Gojon, A., Krouk, G., Perrine-Walker, F., and Laugier, E. (2011). Nitrate transceptor(s) in plants. *J. Exp. Bot.* 62, 2299–2308. doi: 10.1093/jxb/erq419

Gorzelanny, C., Pöppelmann, P., Pappelbaum, K., Moerschbacher, B. M., and Schneider, S. W. (2010). Human macrophage activation triggered by chitotriosidase-mediated chitin and chitosan degradation. *Biomaterials* 31, 8556–8563. doi: 10.1016/j.biomaterials.2010.07.100

Herrmann, K. M., and Weaver, L. M. (1999). The shikimate pathway. *Annu. Rev. Plant Physiol. Plant Mol. Biol.* 50, 473–503. doi: 10.1146/annurev.arplant.50.1.473

Hieta, R., and Myllyharju, J. (2002). Cloning and characterization of a low molecular weight prolyl 4-hydroxylase from *Arabidopsis thaliana*. *J. Biol. Chem.* 277, 23965–23971. doi: 10.1074/jbc.M201865200

Hirsilä, M., Koivunen, P., Günzler, V., Kivirikko, K. I., and Myllyharju, J. (2003). Characterization of the human prolyl 4-hydroxylases that modify the hypoxia-inducible factor. *J. Biol. Chem.* 278, 30772–30780. doi: 10.1074/jbc.M304982200

Ishimaru, Y., Kakei, Y., Shimo, H., Bashir, K., Sato, Y., Uozumi, N., et al. (2011). A rice phenolic efflux transporter is essential for solubilizing precipitated apoplastic iron in the plant stele. *J. Biol. Chem.* 286, 24649–24655. doi: 10.1074/jbc.M111.221168

Jin, C. W., He, Y. F., Tang, C. X., Wu, P., and Zheng, S. J. (2006). Mechanisms of microbially enhanced Fe acquisition in red clover (*Trifolium pratense* L.). *Plant Cell Environ.* 29, 888–897. doi: 10.1111/j.1365-3040.2005.01468.x

Jin, C. W., Li, G. X., Yu, X. H., and Zheng, S. J. (2010). Plant Fe status affects the composition of siderophore-secreting microbes in the rhizosphere. *Ann. Bot.* 105, 835–841. doi: 10.1093/aob/mcq071

Jin, C. W., You, G. Y., He, Y. F., Tang, C., Wu, P., and Zheng, S. J. (2007a). Iron deficiency-induced secretion of phenolics facilitates the reutilization of root apoplastic iron in red clover. *Plant Physiol.* 144, 278–285. doi: 10.1104/pp.107.095794

Jin, C. W., He, X. X., and Zheng, S. J. (2007b). The iron-deficiency induced phenolics accumulation may involve in regulation of Fe(III) chelate reductase in red clover. *Plant Signal. Behav.* 2, 327–332. doi: 10.4161/psb.2.5.4502

Jin, C. W., You, G. Y., and Zheng, S. J. (2008). The iron deficiency-induced phenolics secretion plays multiple important roles in plant iron acquisition underground. *Plant Signal. Behav.* 3, 60–61. doi: 10.4161/psb.3.1.4902

Kai, K., Mizutani, M., Kawamura, N., Yamamoto, R., Tamai, M., Yamaguchi, H., et al. (2008). Scopoletin is biosynthesised via ortho-hydroxylation of feruloyl CoA by a 2-oxoglutarate-dependent dioxygenase in *Arabidopsis thaliana*. *Plant J.* 55, 989–999. doi: 10.1111/j.1365-313X.2008.03568.x

Kai, K., Shimizu, B., Mizutani, M., Watanabe, K., and Sakata, K. (2006). Accumulation of coumarins in *Arabidopsis thaliana*. *Phytochemistry* 67, 379–386. doi: 10.1016/j.phytochem.2005.11.006

Ken, Q., and Costa, M. (2006). Hypoxia-inducible factor-1 (HIF-1). *Mol. Pharmacol.* 70, 1469–1480. doi: 10.1124/mol.106.027029

Kobayashi, T., Nakanishi, H., Takahashi, M., Kawasaki, S., Nishizawa, N. K., and Mori, S. (2001). In vivo evidence that Ids3 from *Hordeum vulgare* encodes a dioxygenase that converts 2′deoxymugineic acid to mugineic acid in transgenic rice. *Planta* 212, 864–871. doi: 10.1007/s004250000453

Kobayashi, T., and Nishizawa, N. K. (2012). Iron uptake, translocation, and regulation in higher plants. *Annu. Rev. Plant Biol.* 63, 131–152. doi: 10.1146/annurev-arplant-042811-105522

Kriel, J., Haesendonckx, S., Rubio-Texeira, M., Van Zeebroeck, G., and Thevelein, J. M. (2011). From transporter to transceptor: signalling from transporter provokes re-evaluation of complex trafficking and regulatory control. *Bioessays* 33, 870–879. doi: 10.1002/bies.201100100

Lan, P., Li, W., Wen, T. N., Shiau, J. Y., Wu, Y. C., Lin, W., et al. (2011). iTRAQ protein profile analysis of *Arabidopsis* roots reveals new aspects critical for iron homeostasis. *Plant Physiol.* 155, 821–834. doi: 10.1104/pp.110.169508

Li, J., Wu, X., Hao, S., Wang, X., and Ling, H. (2008). Proteomic response to iron deficiency in tomato root. *Proteomics* 8, 2299–2311. doi: 10.1002/pmic.200700942

Lichtenthaler, H. K. (1999). The 1-dideoxy-D-xylulose-5-phosphate pathway of isoprenoid biosynthesis in plants. *Annu. Rev. Plant Physiol. Plant Mol. Biol.* 50, 47–65. doi: 10.1146/annurev.arplant.50.1.47

López-Millán, A. F., Grusak, M. A., and Abadía, J. (2012). Carboxylate metabolism change induced by Fe deficiency in barley, a strategy II plant species. *J. Plant Physiol.* 169, 1121–1124. doi: 10.1016/j.jplph.2012.04.010

López-Millán, A. F., Morales, F., Andaluz, S., Gogorcena, Y., Abadia, A., De Las Rivas, J., et al. (2000). Responses of sugar beet roots to iron deficiency. Changes in carbon assimilation and oxygen use. *Plant Physiol.* 124, 885–898. doi: 10.1104/pp.124.2.885

Menges, M., Dóczi, R., Okrész, L., Morandini, P., Mizzi, L., Soloviev, M., et al. (2008). Comprehensive gene expression atlas for the *Arabidopsis* MAP kinase signalling pathways. *New Phytol.* 179, 643–662. doi: 10.1111/j.1469-8137.2008.02552.x

Møldrup, M. E., Salomonsen, B., and Halkier, B. A. (2012). Engineering of glucosinolate biosynthesis: candidate gene identification and validation. *Methods Enzymol.* 515, 291–313. doi: 10.1016/B978-0-12-394290-6.00020-3

Morrissey, J., Baxter, I. R., Lee, L., Lahner, B., Grotz, N., Kaplan, J., et al. (2009). The ferroportin metal efflux proteins function in iron and cobalt homeostasis in *Arabidopsis*. *Plant Cell* 21, 3326–3338. doi: 10.1105/tpc.109.069401

Murgia, I., Arosio, P., Tarantino, D., and Soave, C. (2012). Crops biofortification for combating "hidden hunger" for iron. *Trends Plant Sci.* 17, 47–55. doi: 10.1016/j.tplants.2011.10.003

Murgia, I., Delledonne, M., and Soave, C. (2002). Nitric oxide mediates iron-induced ferritin accumulation in *Arabidopsis*. *Plant J.* 30, 521–528. doi: 10.1046/j.1365-313X.2002.01312.x

Murgia, I., Tarantino, D., Soave, C., and Morandini, P. (2011). The *Arabidopsis* CYP82C4 expression is dependent on Fe availability and the circadian rhythm and it correlates with genes involved in the early Fe-deficiency response. *J. Plant Physiol.* 168, 894–902. doi: 10.1016/j.jplph.2010.11.020

Myllyharju, J. (2003). Prolyl-hydroxylases, the key enzymes of collagen biosynthesis. *Matrix Biol.* 22, 15–24. doi: 10.1016/S0945-053X(03)00006-4

Prabhakar, V., Löttgert, T., Gigolashvili, T., Bell, K., Flügge, U. I., and Häusler, R. E. (2009). Molecular and functional characterization of the plastid-localized phosphoenolpyruvate enolase (ENO1) from *Arabidopsis thaliana*. *FEBS Lett.* 583, 983–991. doi: 10.1016/j.febslet.2009.02.017

Qi, H. H., Ongushaha, P. P., Myllyharju, J., Cheng, D., Pakkamen, O., Shi, Y., et al. (2008). Prolyl 4-hydroxylation regulates Argonaute2 stability. *Nature* 455, 421–424. doi: 10.1038/nature07186

Rellán-Álvarez, R., Andaluz, S., Rodríguez-Celma, J., Wohlgrmuth, G., Zocchi, G., Álvarez- Fernández, A., et al. (2010). Changes in the proteomic and metabolic profiles of *Beta vulgaris* root tips in response to iron deficiency and resupply. *BMC Plant*

Biol. 10:120. doi: 10.1186/1471-2229-10-120

Sanchez, R., Flores, A., and Cejudo, F. J. (2006). *Arabidopsis* phosphoenolpyruvate carboxylase genes encode immunologically unrelated polypeptides and are differentially expressed in response to drought and salt stress. *Planta* 223, 901–909. doi: 10.1007/s00425-005-0144-5

Schachtman, D. P. (2012). Recent advances in nutrient sensing and signalling. *Mol. Plant* 5, 1170–1172. doi: 10.1093/mp/sss109

Schmidt, W., and Steinbach, S. (2000). Sensing iron-a whole plant approach. *Ann. Bot.* 86, 589–593. doi: 10.1006/anbo.2000.1223

Semenza, G. L. (2007). Hypoxia-inducible factor 1 (HIF-1) pathway. *Sci. STKE* 2007, cm8. doi: 10.1126/stke.4072007cm8

Shibuya, N., and Minami, E. (2001). Oligosaccharide signalling for defence responses in plant. *Physiol. Mol. Plant Pathol.* 59, 223–233. doi: 10.1006/pmpp.2001.0364

Thevelein, J. M., and Voordeckers, K. (2009). Functioning and evolutionary significance of nutrient transceptors. *Mol. Biol. Evol.* 26, 2047–2414. doi: 10.1093/molbev/msp168

Thimm, O., Essigmann, B., Kloska, S., Altmann, T., and Buckhout, T. J. (2001). Response of *Arabidopsis* to iron deficiency stress as revealed by microarray analysis. *Plant Physiol.* 127, 1030–1043. doi: 10.1104/pp.010191

Tiainen, P., Myllyharju, J., and Koivunen, P. (2005). Characterization of a second *Arabidopsis* thaliana prolyl 4-hydroxylase with distinct substrate specificity. *J. Biol. Chem.* 280, 1142–1148. doi: 10.1074/jbc.M411109200

Vega, K., and Kalkum, M. (2012). Chitin, chitinase responses, and invasive fungal infections. *Int. J. Microbiol.* 2012:920459. doi: 10.1155/2012/920459

Vert, G., Grotz, N., Dédaldéchamp, F., Gaymard, F., Guerinot, M. L., Briat, J. F., et al. (2002). IRT1, an *Arabidopsis* transporter essential for iron uptake from the soil and for plant growth. *Plant Cell* 14, 1223–1233. doi: 10.1105/tpc.001388

Vigani, G. (2012a). Discovering the role of mitochondria in the iron deficiency-induced metabolic responses of plants. *J. Plant Physiol.* 169, 1–11.

Vigani, G. (2012b). Does a similar metabolic reprogramming occur in Fe-deficient plant cells and animal tumor cells? *Front. Plant Sci.* 3:47. doi: 10.3389/fpls.2012.00047

Vigani, G., Donnini, S., and Zocchi, G. (2012). "Metabolic adjustment under Fe deficiency in roots of dicotiledonous plants," in *Iron Deficiency and Its Complication,* ed. Y. Dincer, (Hauppauge: Nova Science Publishers Inc.), 1–27. doi: 10.1016/j.jplph.2011.09.008

Vigani, G., and Zocchi, G. (2009). The fate and the role of mitochondria in Fe-deficient roots of strategy I plants. *Plant Signal. Behav.* 5, 375–379. doi: 10.4161/psb.4.5.8344

Vigani, G., Zocchi, G., Bashir, K., Philippar, K., and Briat, J. F. (2013). Signal from chloroplasts and mitochondria for iron homeostasis regulation. *Trends Plant Sci.* doi: 10.1016/j.tplants.2013.01.006 [Epub ahead of print].

Vlad, F., Spano, T., Vlad, D., Daher, F. B., Ouelhadj, A., and Kalaitzis, P. (2007a). *Arabidopsis* prolyl hydroxylases are differently expressed in response to hypoxia, anoxia and mechanical wounding. *Physiol. Plant.* 130, 471–483. doi: 10.1111/j.1399-3054.2007.00915.x

Vlad, F., Spano, T., Vlad, D., Daher, F. B., Ouelhadj, A., Fragkostefanakis, S., et al. (2007b). Involvement of *Arabidopsis* Prolyl 4 hydroxylases in hypoxia, anoxia and mechanical wounding. *Plant Signal. Behav.* 2, 368–369. doi: 10.4161/psb.2.5.4462

Vogel, C., and Marcotte, E. M. (2012). Insights into the regulation of protein abundance from proteomic and transcriptomic analyses. *Nat. Rev. Genet.* 13, 227–232. doi: 10.1038/nrg3185

Wan, J., Zhang, X. C., and Stacey, G. (2008). Chitin signaling and plant disease resistance. *Plant Signal. Behav.* 3, 831–833. doi: 10.4161/psb.3.10.5916

Zhao, Z., and Assmann, S. M. (2011). The glycolytic enzyme, phosphoglycerate mutase, has critical roles in stomatal movement, vegetative growth, and pollen production in *Arabidopsis thaliana*. *J. Exp. Bot.* 62, 5179–5189. doi: 10.1093/jxb/err223

Zocchi, G. (2006). "Metabolic changes in iron-stressed dicotyledonous plants," in *Iron Nutrition in Plants and Rhizospheric Microorganisms*, eds L. L. Barton and J. Abadía (Dordrecht: Springer), 359–370. doi: 10.1007/1-4020-4743-6_18

Conflict of Interest Statement: The authors declare that the research was conducted in the absence of any commercial or financial relationships that could be construed as a potential conflict of interest.

Received: 25 February 2013; paper pending published: 18 March 2013; accepted: 13 May 2013; published online: 31 May 2013.

Citation: Vigani G, Morandini P and Murgia I (2013) Searching iron sensors in plants by exploring the link among 2′-OG-dependent dioxygenases, the iron deficiency response and metabolic adjustments occurring under iron deficiency. Front. Plant Sci. ***4****:169. doi: 10.3389/fpls.2013.00169*

This article was submitted to Frontiers in Plant Nutrition, a specialty of Frontiers in Plant Science.

frontiers in
PLANT SCIENCE

MINI REVIEW ARTICLE
published: 06 September 2013
doi: 10.3389/fpls.2013.00348

Mitochondrial iron transport and homeostasis in plants

Anshika Jain and Erin L. Connolly*

Department of Biological Sciences, University of South Carolina, Columbia, SC, USA

Edited by:
Gianpiero Vigani, Università degli Studi di Milano, Italy

Reviewed by:
Elsbeth L. Walker, University of Massachusetts, Amherst, USA
Michael A. Grusak, United States Department of Agriculture-Agricultural Research Service Children's Nutrition Research Center, USA

***Correspondence:**
Erin L. Connolly, University of South Carolina, 715 Sumter Street, Columbia, SC 29208, USA
e-mail: erinc@biol.sc.edu

Iron (Fe) is an essential nutrient for plants and although the mechanisms controlling iron uptake from the soil are relatively well understood, comparatively little is known about subcellular trafficking of iron in plant cells. Mitochondria represent a significant iron sink within cells, as iron is required for the proper functioning of respiratory chain protein complexes. Mitochondria are a site of Fe–S cluster synthesis, and possibly heme synthesis as well. Here we review recent insights into the molecular mechanisms controlling mitochondrial iron transport and homeostasis. We focus on the recent identification of a mitochondrial iron uptake transporter in rice and a possible role for metalloreductases in iron uptake by mitochondria. In addition, we highlight recent advances in mitochondrial iron homeostasis with an emphasis on the roles of frataxin and ferritin in iron trafficking and storage within mitochondria.

Keywords: iron, mitochondria, plant, iron transporter, frataxin, ferritin

INTRODUCTION

Iron is an essential micronutrient for virtually all organisms, including plants. Indeed, photosynthetic organisms are distinguished by the high iron requirement of photosynthetic complexes. Although iron is generally quite abundant in the soil, it has a low bioavailability in aerobic environments at neutral to basic pH and as a result, approximately 30% of the world's soils are considered iron-limiting for plant growth. Iron deficiency represents an enormous problem in human populations as well, with approximately two billion people afflicted (Wu et al., 2002). Plant foods (especially staples like rice, maize, and wheat) tend to be poor sources of dietary iron and thus significant interest surrounds efforts to develop crop varieties with elevated levels of bioavailable iron.

Despite its importance, iron can be toxic when it accumulates to high levels within cells. It catalyzes the formation of hydroxyl radicals that can damage cellular components like DNA and proteins (Halliwell et al., 1992). Thus iron metabolism is carefully regulated to ensure adequate supply of iron while avoiding toxicity associated with its over-accumulation. Organelles like chloroplasts and mitochondria are thought to play a central role in the cellular iron economy of a plant cell. This is because iron serves as an essential cofactor for many enzymes involved in the electron transport chain in mitochondria and in the photosynthetic complexes found in chloroplasts. Indeed, recent work has shown that iron deficiency results in significant changes in the structure and function of mitochondria (Vigani et al., 2009; Vigani and Zocchi, 2009). PS1–LHC1 supercomplexes also exhibit structural and functional alterations under iron limited conditions (Yadavalli et al., 2012). Thus, iron deficiency affects respiratory and photosynthetic output. However, excessive iron exacerbates the generation of reactive oxygen species (ROS) in these redox centers, which can have exceedingly deleterious effects on cells. Thus, mitochondrial and chloroplast iron metabolism are of particular importance to cellular iron homeostasis (Nouet et al., 2011; Vigani et al., 2013).

The chloroplasts and mitochondria are unique organelles in that they are thought to have evolved via endosymbiosis. As a result, both organelles are surrounded by two membranes; the outer membrane resembles eukaryotic membranes while the inner resembles prokaryotic membranes. Thus, it follows that these two organelles may utilize prokaryotic and/or eukaryotic type iron transport systems (Shimoni-Shor et al., 2010). It is usually assumed that Fe may pass freely across the outer membrane of both organelles via porins. It is also important to note that there is little known about the speciation of cytosolic Fe although it is assumed that there is very little free Fe present in the cytosol (Hider and Kong, 2013). Thus, the Fe species that are available for transport into subcellular compartments are unclear at this time.

A variety of proteins are known to be involved in the maintenance of mitochondrial iron homeostasis **(Figure 1)**. The recent discovery and characterization of rice MIT (mitochondrial iron transporter), which is involved in iron uptake by mitochondria, and the mitochondrial iron chaperone, frataxin (FH) has demonstrated the significance of mitochondrial iron uptake and trafficking/distribution to plant growth and development (Busi et al., 2006; Bashir et al., 2011b; Maliandi et al., 2011; Vigani, 2012). Other key players responsible for maintaining mitochondrial iron homeostasis are the iron–sulfur cluster (ISC) synthesis machinery, which accepts iron from FH and mediates the synthesis of Fe–S clusters to serve as cofactors for various proteins in the mitochondria and cytosol (Lill et al., 2012). It is thought that mitochondria also contain the iron storage protein ferritin, which serves to store iron and protect against Fe-catalyzed ROS production (Briat et al., 2010). Mitochondria also supply iron and sulfur to the cytoplasmic iron–sulfur cluster assembly machinery (CIA; Balk and Pilon, 2011). While the sulfur scaffold is likely exported to the cytosol via an ABC transporter, ATM3 (Bernard et al., 2009), putative transporters required for iron efflux are still unknown. The recent discovery of a mitochondrial iron exporter (MIE) in mice (ATP-binding cassette B8, ABCB8) and its role in CIA-mediated Fe–S synthesis has provided new insight into understanding of

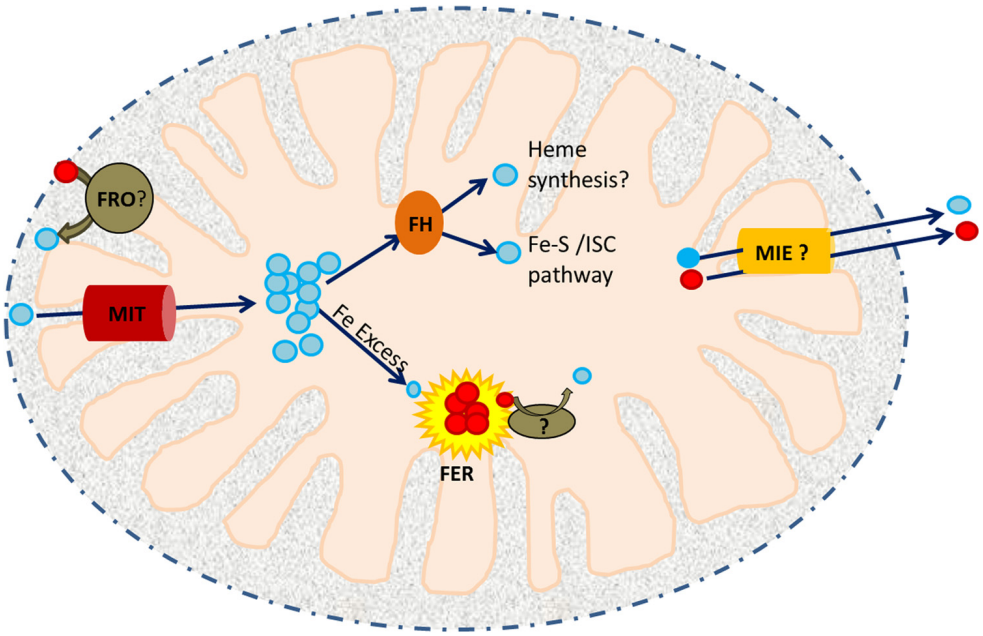

FIGURE 1 | A working model of iron trafficking and utilization in plant mitochondria. Cytosolic Fe^{3+} (red circles) may be reduced to Fe^{2+} (blue circles) by a member of the ferric reductase oxidase (FRO) family within the inter-membrane space (IMS). Ferrous iron is then translocated across the inner membrane by MIT. In the mitochondrial matrix, it is received by an iron chaperone, frataxin (FH). FH distributes this Fe to ISC assembly proteins and possibly to the heme biosynthetic machinery. Excess Fe^{2+} is stored in FER4. Iron released from FER4 upon Fe deficiency may require the activity of another reductase prior to its utilization/remobilization. Mitochondrial iron exporters (MIEs) are postulated to function in mitochondrial iron export for delivery of iron to CIA.

intracellular iron homeostasis (Ichikawa et al., 2012) and may facilitate the identification of MIE proteins in other species. Finally, a recent report showed that the YSL4 and YSL6 (yellow stripe-like) transporters are involved in iron release from chloroplasts of *Arabidopsis*, suggesting a possible role for other members of the YSL family in mitochondrial iron efflux (Divol et al., 2013). In this review, we discuss in detail the roles of the iron transporter (MIT), metalloreductases, FH and ferritin in mitochondrial iron homeostasis.

MITOCHONDRIAL IRON TRANSPORTERS

Mitochondrial iron transporters are conserved proteins that belong to the mitochondrial carrier family (MCF; Wiesenberger et al., 1991; Metzendorf et al., 2009; Bashir et al., 2011a,b). This family consists of small (∼30 kDa) proteins that localize to the mitochondrial inner membrane and are involved in solute transport (e.g., keto acids, nucleotides, amino acids, etc.) into the mitochondrial matrix (Kunji and Robinson, 2006). MCF proteins were first characterized in yeast and their crystal structure shows the presence of a tripartite structure with a total of six transmembrane helices. Amino acid residues responsible for substrate recognition are found in helices II, IV and VI.

The first set of mitochondrial iron transporters (MRS3 and MRS4 for mitochondrial RNA splicing) were discovered in yeast as multicopy suppressors of the *mrs2* phenotype (Waldherr et al., 1993) and subsequently shown to function in Fe import (Foury and Roganti, 2002). Mitochondrial iron transporters (named Mitoferrins) have since been identified and characterized in zebrafish, humans, and Drosophila (Shaw et al., 2006; Metzendorf et al., 2009; Paradkar et al., 2009). Later, a mitochondrial iron transporter was identified in rice and named MIT (Bashir et al., 2011b). Similar to zebrafish mitoferrin, rice *MIT* is able to rescue the poor growth phenotype of the yeast *mrs3/4* mutant under iron deficiency, indicating the functional similarity of these proteins. *MIT* is an essential gene as the *mit* knockout mutant shows an embryo lethal phenotype. *mit* knockdown mutants exhibit a slow growth phenotype, reduced chlorophyll concentration and poor seed yield. In addition, these mutants show reduced mitochondrial iron concentration while total iron concentration is elevated, indicating that iron is mislocalized in *mit* loss-of-function lines (Bashir et al., 2011b). In the absence of *MIT*, the gene encoding vacuolar iron transporter1 (*VIT1*) is upregulated, suggesting that excess cytosolic iron may be directed toward vacuoles. MIT plays an important role in seed development and its expression level is positively regulated by iron availability. *MIT* is expressed throughout development, consistent with the idea that it is essential for mitochondrial iron metabolism.

Previous studies conducted in yeast and mammals have demonstrated an adverse effect of loss of mitochondrial iron transport on heme and Fe–S cluster synthesis (Zhang et al., 2005; Shaw et al., 2006; Zhang et al., 2006). In rice, partial loss of MIT results in decreased total and mitochondrial aconitase activity, indicating that the effect on Fe–S cluster synthesis affects not only mitochondrial Fe–S proteins but also cytosolic Fe–S cluster proteins. However, the role of MIT in heme synthesis has yet to be determined. Interestingly, the fact that *mit* loss-of-function

lines show altered chlorophyll concentration and altered ferritin expression supports the idea of cross-talk between mitochondrial and chloroplastic iron homeostasis.

Yeast MRS3/4 are thought to serve as high affinity ferrous ion transporters which are essential in the absence of other low affinity mitochondrial iron transporters (Froschauer et al., 2009). Thus, low affinity iron uptake systems may be present at the plant mitochondrial membrane. The recent discovery of siderophore (2,5-DHBA)-mediated iron delivery to mammalian mitochondria has introduced the possibility of such an alternative pathway for iron transport into the mitochondria (Devireddy et al., 2010). 2,5-DHBA is synthesized by a short chain dehydrogenase/reductase family member (BDH2). BLAST searches of the *Arabidopsis* and rice genomes indicate that these genomes code for 3 and 13 BDH2 homologs respectively. Characterization of these homologs may give interesting insights into the mitochondrial iron trafficking pathways in plants.

PUTATIVE MITOCHONDRIAL FERRIC REDUCTASES

The recent characterization of *Arabidopsis* FRO7 (ferric reductase oxidase 7), a chloroplast-localized member of the FRO family, demonstrated that this protein functions to reduce ferric iron to ferrous iron at the surface of the chloroplast for subsequent uptake into the organelle (Jeong et al., 2008). A similar hypothesis has been suggested for mitochondria based on the predicted localization of FRO3 and FRO8 to mitochondria (Jeong and Connolly, 2009). Whereas *FRO3-GUS* promoter lines show expression throughout seedlings with highest expression in vasculature, expression of *FRO8* is restricted to shoots during senescence (Mukherjee et al., 2006; Jeong and Connolly, 2009). This suggests that the two mitochondrial FROs may be involved in reducing Fe^{3+} at different stages of development. *FRO3* has been widely used as an iron deficiency marker (Mukherjee et al., 2006). Nevertheless, the exact role of *FRO3 in planta* remains elusive. It is important to note that although mitochondrial homologs of FRO3 have been identified in other organisms (FRE5 in yeast) there is no evidence to date that these proteins function in mitochondrial iron metabolism (Jeong and Connolly, 2009).

Rice possesses only two FRO family members, *OsFRO1* and *OsFRO2*, neither of which has been shown to localize to mitochondria (Victoria Fde et al., 2012; Vigani, 2012). Thus, iron uptake by mitochondria of grass species such as rice may differ from non-grass species, like *Arabidopsis*. It is possible that iron uptake by rice mitochondria utilizes a non-reductive iron uptake pathway and/or the rice genome may encode other types of reductases capable of reducing iron. In the future, it will be critical to determine the redox state of iron transported across the outer and inner membranes of the mitochondria.

FRATAXIN

Mitochondria are known to facilitate two major iron utilization pathways in the cell: heme synthesis and Fe–S cluster biogenesis. It has been suggested that the mitochondrial compartment contains micromolar concentrations of chelatable iron (Petrat et al., 2001). Maintaining this iron in a soluble and non-toxic form presents a challenge given the alkaline pH and the continuous production of ROS within the mitochondrial matrix under normal conditions (Park et al., 2002). Thus, the existence of mitochondrial iron chaperones and chelators was postulated (Flatmark and Romslo, 1975). Mitochondrial ferritin and FH have been implicated in iron storage and control of iron homeostasis in the mitochondrial matrix (Babcock et al., 1997; Corsi et al., 2002).

Frataxin is a conserved mitochondrial protein found in bacteria, yeast, mammals, and plants (Busi et al., 2006). FH was first identified in humans, where its deficiency was reported to cause an autosomal recessive cardio-neurodegenerative disease known as Friedreich's ataxia (Campuzano et al., 1996). Functional studies in yeast revealed the role of FH (mYfh1p) in mitochondrial iron homeostasis (Babcock et al., 1997). Loss of yeast mYfh1p results in impaired iron export from the mitochondria. This is primarily due to the accumulation of iron as amorphous ferric phosphate nanoparticles, which are unavailable for physiological purposes (Lesuisse et al., 2003). Thus, although the *yfh1* mutant exhibits iron overload, it suffers from iron deficiency and thus upregulates the iron uptake machinery (Santos et al., 2010). Lack of FH also results in iron-induced oxidative damage of mtDNA and reduced activity of mitochondrial Fe–S cluster proteins which thus affects respiration (Foury, 1999). FH has been reported to bind to the ISC assembly complex suggesting its importance in Fe–S cluster biogenesis (Gerber et al., 2003). It directly interacts with a scaffold protein, Isu (iron–sulfur cluster U) in an iron-dependent manner and facilitates the transfer of iron to Isu during Fe–S cluster assembly. Because of the capacity of FH to bind iron and transfer it to Isu via a direct protein–protein interaction, FH is considered a mitochondrial iron chaperone (Philpott, 2012).

The first FH homolog identified in a photosynthetic organism was *Arabidopsis* AtFH (Busi et al., 2004); *AtFH* functionally complements the yeast FH mutant. *AtFH* is essential as loss-of-function mutants exhibit an embryo lethal phenotype (Vazzola et al., 2007). The knock-down mutant shows elevated levels of iron and ROS in the mitochondrial compartment (Martin et al., 2009). The oxidative stress observed in *atfh* mutants is accompanied by an increase in nitric oxide (NO) production. NO, a potent antioxidant, protects the cell by directly scavenging peroxide radicals (Beligni and Lamattina, 1999) and by inducing the expression of ferritin genes (*FER1* and *FER4*) to sequester free iron (Murgia et al., 2002; Martin et al., 2009).

Like its yeast ortholog, AtFH also functions as a mitochondrial iron chaperone. *atfh* mutants show reduced activity of two Fe–S cluster containing enzymes, mitochondrial aconitase and succinate dehydrogenase, while the activity of malate dehydrogenase (a non-Fe–S containing enzyme) is not altered. This indicates that FH likely plays a role in Fe–S cluster biogenesis and/or assembly of the Fe–S moiety with mitochondrial proteins in *Arabidopsis*. Indeed, it was shown that AtFH plays an instrumental role in Fe–S cluster biogenesis in plant mitochondria (Turowski et al., 2012). AtFH interacts with a cysteine desulfurase, AtNfs1m (which is known to supply S for the biogenesis of Fe–S clusters), and modulates its kinetic properties. AtNfs1m exhibits a 50-fold increase in its cysteine desulfurase activity in the presence of AtFH (Turowski et al., 2012). This interaction thus links the accumulation of iron (bound to FH) with Fe–S cluster production in a mitochondrion.

In animal systems, FH appears to be involved in the biogenesis of heme-containing proteins. FH was shown to interact

with and deliver iron to ferrochelatase (FC) in the last step of heme synthesis in human mitochondria (Yoon and Cowan, 2004). Reduced FH expression in human cells results in reduced levels of heme-a and reduced cytochrome c oxidase activity (Napoli et al., 2007). In plants, however, there is no strong evidence to support the presence of FC in mitochondria. In fact, studies in various families of plants have clearly demonstrated the exclusive localization of FC to plastids (Cornah et al., 2002; Masuda et al., 2003). Therefore, it is possible that heme synthesis in plants occurs exclusively in plastids, some of which is then exported to the cytosol and mitochondria (van Lis et al., 2005; Tanaka and Tanaka, 2007; Mochizuki et al., 2010). Despite this, AtFH deficient plants show a decrease in total heme content, an altered expression of genes (*FC2*, *HEMA1*, *HEMA2*, *GSA1*, *GSA2*, *HEMB2*, *HEMF2*) which are involved in the heme biosynthetic pathway and a reduction in the activity of mitochondrial catalase, which is a heme-containing protein. Reduced catalase activity in *atfh* is rescued via supplementation with exogenous hemin (Maliandi et al., 2011). Taken together, these data indicate that in plants, FH plays important roles in protection against oxidative stress and in the biogenesis of Fe–S cluster and heme-containing proteins (Maliandi et al., 2011).

MITOCHONDRIAL FERRITIN

Metal homeostasis in plants is accomplished via a set of elegantly regulated mechanisms that control various aspects of iron metabolism (including uptake, efflux, chelation, and storage). Ferritins are clearly essential to overall iron homeostasis as they function in iron sequestration and thus serve to prevent oxidative damage (Zhao et al., 2002; Arosio et al., 2009; Ravet et al., 2009). Ferritins are localized to both chloroplasts and mitochondria, two major sites for ROS production. Plant ferritins are conserved proteins that oligomerize to form a hollow sphere. They exhibit ferroxidase activity and oxidize Fe^{2+} and store it within the ferritin core in the form of hydrous ferric oxides along with phosphates (Arosio et al., 2009). Ferritin can accommodate 2,000–4,000 Fe^{3+} atoms per ferritin molecule (Carrondo, 2003). The molecular mechanism underlying the release of iron from ferritins is not very well understood. *In vitro* studies in animals suggest that release of Fe requires iron chelators or reducing agents. In contrast, *in vivo* studies in animals have demonstrated the release of Fe by proteolytic degradation of ferritin protein (Briat et al., 2010). To date, the process is not described in plant systems.

Plant ferritins are primarily localized to plastids, as opposed to animal ferritins which are usually cytoplasmic. Mitochondrial localization of ferritins was first reported in mammals (Levi et al., 2001). Subsequently, mitochondrial ferritins were also identified in plants (Zancani et al., 2004; Tarantino et al., 2010a). *Arabidopsis* possesses four ferritin (FER1–4) proteins, all of which are known to be localized to chloroplasts. Ferritin4 (AtFER4) is unique in that it contains dual targeting signals and is therefore found in mitochondria as well as chloroplasts (Tarantino et al., 2010a). This protein is detected in mitochondria in the aerial portion of plants only after exposure to excess iron. Although the *atfer4* mutant does not exhibit any severe phenotypes, callus cultures prepared from the *atfer4* mutant show reduced cell and vacuole size, damaged plasma membranes, accumulation of H_2O_2, higher cell death and reduction of O_2 consumption, in addition to elevated cellular and mitochondrial iron concentrations (Tarantino et al., 2010b).

Loss of *AtFER4* also results in increased *FRO3* expression both in control as well as excess Fe conditions. This suggests that loss of *AtFER4* triggers sensing of mitochondrial iron deficiency despite the fact that mitochondrial iron levels are elevated in *atfer4*. This may also result in damage to electron transport chain components, which is consistent with the diminished O_2 consumption rate of *atfer4* mutants. These observations indicate that although *AtFER4* is responsible for proper cellular iron homeostasis and subcellular iron trafficking, it is dispensable for protection against the oxidative stress in photosynthetic tissue (Tarantino et al., 2010a).

CONCLUSION

Recent studies have begun to shed light on the machinery involved in mitochondrial iron uptake, storage, and trafficking/utilization. In particular, studies of mitochondrial iron transporters, chaperones, and storage proteins have set the stage for future investigations in this area (see **Figure 1**). Such studies will be critical to efforts to understand both organellar iron homeostasis and the mechanisms employed by plants to coordinate and prioritize Fe utilization by the various iron containing compartments of the cell. These studies will contribute to the development of a comprehensive understanding of iron homeostasis in plants, which should enable efforts to develop crop varieties with improved tolerance of growth on iron-limited soils and elevated levels of bioavailable iron in support of improved sustainability in agriculture and reductions in the incidence of iron deficiency in humans, respectively.

ACKNOWLEDGMENT

The authors are grateful to Grandon Wilson for critical reading of the manuscript and gratefully acknowledge support from the US NSF (IOS 0919739).

REFERENCES

Arosio, P., Ingrassia, R., and Cavadini, P. (2009). Ferritins: a family of molecules for iron storage, antioxidation, and more. *Biochim. Biophys. Acta* 7, 589–599. doi: 10.1016/j.bbagen.2008.09.004

Babcock, M., De Silva, D., Oaks, R., Davis-Kaplan, S., Jiralerspong, S., Montermini, L., et al. (1997). Regulation of mitochondrial iron accumulation by Yfh1p, a putative homolog of frataxin. *Science* 276, 1709–1712. doi: 10.1126/science.276.5319.1709

Balk, J., and Pilon, M. (2011). Ancient and essential: the assembly of iron–sulfur clusters in plants. *Trends Plant Sci.* 16, 218–226. doi: 10.1016/j.tplants.2010.12.006

Bashir, K., Ishimaru, Y., and Nishizawa, N. K. (2011a). Identification and characterization of the major mitochondrial Fe transporter in rice. *Plant Signal. Behav.* 6, 1591–1593. doi: 10.4161/psb.6.10.17132

Bashir, K., Ishimaru, Y., Shimo, H., Nagasaka, S., Fujimoto, M., Takanashi, H., et al. (2011b). The rice mitochondrial iron transporter is essential for plant growth. *Nat. Commun.* 2, 322. doi: 10.1038/ncomms1326

Beligni, M., and Lamattina, L. (1999). Is nitric oxide toxic or protective? *Trends Plant Sci.* 4, 299–300. doi: 10.1016/S1360-1385(99)01451-X

Bernard, D. G., Cheng, Y., Zhao, Y., and Balk, J. (2009). An allelic mutant series of ATM3 reveals its key role in the biogenesis of cytosolic iron–sulfur proteins in *Arabidopsis*. *Plant Physiol.* 151, 590–602. doi: 10.1104/pp.109.143651

Briat, J.-F., Duc, C., Ravet, K., and Gaymard, F. (2010). Ferritins and iron storage in plants. *Biochim.*

Biophys. Acta 1800, 806–814. doi: 10.1016/j.bbagen.2009.12.003

Busi, M. V., Maliandi, M. V., Valdez, H., Clemente, M., Zabaleta, E. J., Araya, A., et al. (2006). Deficiency of *Arabidopsis thaliana* frataxin alters activity of mitochondrial Fe–S proteins and induces oxidative stress. *Plant J.* 48, 873–882. doi: 10.1111/j.1365-313X.2006.02923.x

Busi, M. V., Zabaleta, E. J., Araya, A., and Gomez-Casati, D. F. (2004). Functional and molecular characterization of the frataxin homolog from *Arabidopsis thaliana*. *FEBS Lett.* 576, 141–144. doi: 10.1016/j.febslet.2004.09.003

Campuzano, V., Montermini, L., Molto, M. D., Pianese, L., Cossee, M., Cavalcanti, F., et al. (1996). Friedreich's ataxia: autosomal recessive disease caused by an intronic GAA triplet repeat expansion. *Science* 271, 1423–1427. doi: 10.1126/science.271.5254.1423

Carrondo, M. A. (2003). Ferritins, iron uptake and storage from the bacterioferritin viewpoint. *EMBO J.* 22, 1959–1968. doi: 10.1093/emboj/cdg215

Cornah, J. E., Roper, J. M., Pal Singh, D., and Smith, A. G. (2002). Measurement of ferrochelatase activity using a novel assay suggests that plastids are the major site of haem biosynthesis in both photosynthetic and non-photosynthetic cells of pea (*Pisum sativum* L.). *Biochem. J.* 362, 423–432.

Corsi, B., Cozzi, A., Arosio, P., Drysdale, J., Santambrogio, P., Campanella, A., et al. (2002). Human mitochondrial ferritin expressed in HeLa cells incorporates iron and affects cellular iron metabolism. *J. Biol. Chem.* 277, 22430–22437. doi: 10.1074/jbc.M105372200

Devireddy, L. R., Hart, D. O., Goetz, D. H., and Green, M. R. (2010). A mammalian siderophore synthesized by an enzyme with a bacterial homolog involved in enterobactin production. *Cell* 141, 1006–1017. doi: 10.1016/j.cell.2010.04.040

Divol, F., Couch, D., Conejero, G., Roschzttardtz, H., Mari, S., and Curie, C. (2013). The *Arabidopsis* YELLOW STRIPE LIKE4 and 6 transporters control iron release from the chloroplast. *Plant Cell* 25, 1040–1055. doi: 10.1105/tpc.112.107672

Flatmark, T., and Romslo, I. (1975). Energy-dependent accumulation of iron by isolated rat liver mitochondria. Requirement of reducing equivalents and evidence for a unidirectional flux of Fe(II) across the inner membrane. *J. Biol. Chem.* 250, 6433–6438.

Foury, F. (1999). Low iron concentration and aconitase deficiency in a yeast frataxin homologue deficient strain. *FEBS Lett.* 456, 281–284. doi: 10.1016/S0014-5793(99)00961-8

Foury, F., and Roganti, T. (2002). Deletion of the mitochondrial carrier genes MRS3 and MRS4 suppresses mitochondrial iron accumulation in a yeast frataxin-deficient strain. *J. Biol. Chem.* 277, 24475–24483. doi: 10.1074/jbc.M111789200

Froschauer, E. M., Schweyen, R. J., and Wiesenberger, G. (2009). The yeast mitochondrial carrier proteins Mrs3p/Mrs4p mediate iron transport across the inner mitochondrial membrane. *Biochim. Biophys. Acta* 1788, 1044–1050. doi: 10.1016/j.bbamem.2009.03.004

Gerber, J., Muhlenhoff, U., and Lill, R. (2003). An interaction between frataxin and Isu1/Nfs1 that is crucial for Fe/S cluster synthesis on Isu1. *EMBO Rep.* 4, 906–911. doi: 10.1038/sj.embor.embor918

Halliwell, B., Gutteridge, J. M., and Cross, C. E. (1992). Free radicals, antioxidants, and human disease: where are we now? *J. Lab. Clin. Med.* 119, 598–620.

Hider, R. C., and Kong, X. (2013). Iron speciation in the cytosol: an overview. *Dalton Trans.* 42, 3220–3229. doi: 10.1039/c2dt32149a

Ichikawa, Y., Bayeva, M., Ghanefar, M., Potini, V., Sun, L., Mutharasan, R. K., et al. (2012). Disruption of ATP-binding cassette B8 in mice leads to cardiomyopathy through a decrease in mitochondrial iron export. *Proc. Natl. Acad. Sci. U.S.A.* 109, 4152–4157. doi: 10.1073/pnas.1119338109

Jeong, J., Cohu, C., Kerkeb, L., Pilon, M., Connolly, E. L., and Guerinot, M. L. (2008). Chloroplast Fe(III) chelate reductase activity is essential for seedling viability under iron limiting conditions. *Proc. Natl. Acad. Sci. U.S.A.* 105, 10619–10624. doi: 10.1073/pnas.0708367105

Jeong, J., and Connolly, E. L. (2009). Iron uptake mechanisms in plants: functions of the FRO family of ferric reductases. *Plant Sci.* 176, 709–714.

Kunji, E. R., and Robinson, A. J. (2006). The conserved substrate binding site of mitochondrial carriers. *Biochim. Biophys. Acta* 1757, 1237–1248. doi: 10.1016/j.bbabio.2006.03.021

Lesuisse, E., Santos, R., Matzanke, B. F., Knight, S. A., Camadro, J. M., and Dancis, A. (2003). Iron use for haeme synthesis is under control of the yeast frataxin homologue (Yfh1). *Hum. Mol. Genet.* 12, 879–889.

Levi, S., Corsi, B., Bosisio, M., Invernizzi, R., Volz, A., Sanford, D., et al. (2001). A human mitochondrial ferritin encoded by an intronless gene. *J. Biol. Chem.* 276, 24437–24440. doi: 10.1074/jbc.C100141200

Lill, R., Hoffmann, B., Molik, S., Pierik, A. J., Rietzschel, N., Stehling, O., et al. (2012). The role of mitochondria in cellular iron–sulfur protein biogenesis and iron metabolism. *Biochim. Biophys. Acta* 1823, 1491–1508. doi: 10.1016/j.bbamcr.2012.05.009

Maliandi, M. V., Busi, M. V., Turowski, V. R., Leaden, L., Araya, A., and Gomez-Casati, D. F. (2011). The mitochondrial protein frataxin is essential for heme biosynthesis in plants. *FEBS J.* 278, 470–481. doi: 10.1111/j.1742-4658.2010.07968.x

Martin, M., Colman, M. J., Gomez-Casati, D. F., Lamattina, L., and Zabaleta, E. J. (2009). Nitric oxide accumulation is required to protect against iron-mediated oxidative stress in frataxin-deficient *Arabidopsis* plants. *FEBS Lett.* 583, 542–548. doi: 10.1016/j.febslet.2008.12.039

Masuda, T., Suzuki, T., Shimada, H., Ohta, H., and Takamiya, K. (2003). Subcellular localization of two types of ferrochelatase in cucumber. *Planta* 217, 602–609. doi: 10.1007/s00425-003-1019-2

Metzendorf, C., Wu, W., and Lind, M. I. (2009). Overexpression of *Drosophila* mitoferrin in l(2)mbn cells results in dysregulation of Fer1HCH expression. *Biochem. J.* 421, 463–471. doi: 10.1042/BJ20082231

Mochizuki, N., Tanaka, R., Grimm, B., Masuda, T., Moulin, M., Smith, A. G., et al. (2010). The cell biology of tetrapyrroles: a life and death struggle. *Trends Plant Sci.* 15, 488–498. doi: 10.1016/j.tplants.2010.05.012

Mukherjee, I., Campbell, N. H., Ash, J. S., and Connolly, E. L. (2006). Expression profiling of the *Arabidopsis* ferric chelate reductase (FRO) gene family reveals differential regulation by iron and copper. *Planta* 223, 1178–1190. doi: 10.1007/s00425-005-0165-0

Murgia, I., Delledonne, M., and Soave, C. (2002). Nitric oxide mediates iron-induced ferritin accumulation in *Arabidopsis*. *Plant J.* 30, 521–528. doi: 10.1046/j.1365-313X.2002.01312.x

Napoli, E., Morin, D., Bernhardt, R., Buckpitt, A., and Cortopassi, G. (2007). Hemin rescues adrenodoxin, heme a and cytochrome oxidase activity in frataxin-deficient oligodendroglioma cells. *Biochim. Biophys. Acta* 1772, 773–780. doi: 10.1016/j.bbadis.2007.04.001

Nouet, C., Motte, P., and Hanikenne, M. (2011). Chloroplastic and mitochondrial metal homeostasis. *Trends Plant Sci.* 16, 395–404. doi: 10.1016/j.tplants.2011.03.005

Paradkar, P. N., Zumbrennen, K. B., Paw, B. H., Ward, D. M., and Kaplan, J. (2009). Regulation of mitochondrial iron import through differential turnover of mitoferrin 1 and mitoferrin 2. *Mol. Cell. Biol.* 29, 1007–1016. doi: 10.1128/MCB.01685-08

Park, S., Gakh, O., Mooney, S. M., and Isaya, G. (2002). The ferroxidase activity of yeast frataxin. *J. Biol. Chem.* 277, 38589–38595. doi: 10.1074/jbc.M206711200

Petrat, F., De Groot, H., and Rauen, U. (2001). Subcellular distribution of chelatable iron: a laser scanning microscopic study in isolated hepatocytes and liver endothelial cells. *Biochem. J.* 356, 61–69. doi: 10.1042/0264-6021:3560061

Philpott, C. C. (2012). Coming into view: eukaryotic iron chaperones and intracellular iron delivery. *J. Biol. Chem.* 287, 13518–13523. doi: 10.1074/jbc.R111.326876

Ravet, K., Touraine, B., Boucherez, J., Briat, J.-F., Gaymard, F., and Cellier, F. (2009). Ferritins control interaction between iron homeostasis and oxidative stress in *Arabidopsis*. *Plant J.* 57, 400–412. doi: 10.1111/j.1365-313X.2008.03698.x

Santos, R., Lefevre, S., Sliwa, D., Seguin, A., Camadro, J. M., and Lesuisse, E. (2010). Friedreich ataxia: molecular mechanisms, redox considerations, and therapeutic opportunities. *Antioxid. Redox Signal.* 13, 651–690. doi: 10.1089/ars.2009.3015

Shaw, G. C., Cope, J. J., Li, L., Corson, K., Hersey, C., Ackermann, G. E., et al. (2006). Mitoferrin is essential for erythroid iron assimilation. *Nature* 440, 96–100. doi: 10.1038/nature04512

Shimoni-Shor, E., Hassidim, M., Yuval-Naeh, N., and Keren, N. (2010). Disruption of Nap14, a plastid-localized non-intrinsic ABC protein in *Arabidopsis thaliana* results in the over-accumulation of transition metals and in aberrant chloroplast structures. *Plant Cell Environ.* 33, 1029–1038. doi: 10.1111/j.1365-3040.2010.02124.x

Tanaka, R., and Tanaka, A. (2007). Tetrapyrrole biosynthesis in higher plants. *Annu. Rev. Plant Biol.* 58, 321–346. doi: 10.1146/annurev.arplant.57.032905.105448

Tarantino, D., Casagrande, F., Soave, C., and Murgia, I. (2010a). Knocking

out of the mitochondrial AtFer4 ferritin does not alter response of *Arabidopsis* plants to abiotic stresses. *J. Plant Physiol.* 167, 453–460. doi: 10.1016/j.jplph.2009.10.015

Tarantino, D., Santo, N., Morandini, P., Casagrande, F., Braun, H. P., Heinemeyer, J., et al. (2010b). AtFer4 ferritin is a determinant of iron homeostasis in *Arabidopsis thaliana* heterotrophic cells. *J. Plant Physiol.* 167, 1598–1605. doi: 10.1016/j.jplph.2010.06.020

Turowski, V. R., Busi, M. V., and Gomez-Casati, D. F. (2012). Structural and functional studies of the mitochondrial cysteine desulfurase from *Arabidopsis thaliana*. *Mol. Plant* 5, 1001–1010. doi: 10.1093/mp/sss037

van Lis, R., Atteia, A., Nogaj, L. A., and Beale, S. I. (2005). Subcellular localization and light-regulated expression of protoporphyrinogen IX oxidase and ferrochelatase in *Chlamydomonas reinhardtii*. *Plant Physiol.* 139, 1946–1958. doi: 10.1104/pp.105.069732

Vazzola, V., Losa, A., Soave, C., and Murgia, I. (2007). Knockout of frataxin gene causes embryo lethality in *Arabidopsis*. *FEBS Lett.* 581, 667–672. doi: 10.1016/j.febslet.2007.01.030

Victoria Fde, C., Bervald, C. M., Da Maia, L. C., De Sousa, R. O., Panaud, O., and De Oliveira, A. C. (2012). Phylogenetic relationships and selective pressure on gene families related to iron homeostasis in land plants. *Genome* 55, 883–900. doi: 10.1139/gen-2012-0064

Vigani, G. (2012). Discovering the role of mitochondria in the iron deficiency-induced metabolic responses of plants. *J. Plant Physiol.* 169, 1–11. doi: 10.1016/j.jplph.2011.09.008

Vigani, G., Maffi, D., and Zocchi, G. (2009). Iron availability affects the function of mitochondria in cucumber roots. *New Phytol.* 182, 127–136. doi: 10.1111/j.1469-8137.2008.02747.x

Vigani, G., and Zocchi, G. (2009). The fate and the role of mitochondria in Fe-deficient roots of strategy I plants. *Plant Signal. Behav.* 4, 375–379. doi: 10.4161/psb.4.5.8344

Vigani, G., Zocchi, G., Bashir, K., Philippar, K., and Briat, J.-F. (2013). Signals from chloroplasts and mitochondria for iron homeostasis regulation. *Trends Plant Sci.* 18, 305–311. doi: 10.1016/j.tplants.2013.01.006

Waldherr, M., Ragnini, A., Jank, B., Teply, R., Wiesenberger, G., and Schweyen, R. (1993). A multitude of suppressors of group II intron-splicing defects in yeast. *Curr. Genet.* 24, 301–306. doi: 10.1007/BF00336780

Wiesenberger, G., Link, T. A., Von Ahsen, U., Waldherr, M., and Schweyen, R. J. (1991). MRS3 and MRS4, two suppressors of mtRNA splicing defects in yeast, are new members of the mitochondrial carrier family. *J. Mol. Biol.* 217, 23–37. doi: 10.1016/0022-2836(91)90608-9

Wu, A. C., Lesperance, L., and Bernstein, H. (2002). Screening for iron deficiency. *Pediatr. Rev.* 23, 171–178. doi: 10.1542/pir.23-5-171

Yadavalli, V., Jolley, C. C., Malleda, C., Thangaraj, B., Fromme, P., and Subramanyam, R. (2012). Alteration of proteins and pigments influence the function of photosystem I under iron deficiency from *Chlamydomonas reinhardtii*. *PLoS ONE* 7:e35084. doi: 10.1371/journal.pone.0035084

Yoon, T., and Cowan, J. A. (2004). Frataxin-mediated iron delivery to ferrochelatase in the final step of heme biosynthesis. *J. Biol. Chem.* 279, 25943–25946. doi: 10.1074/jbc.C400107200

Zancani, M., Peresson, C., Biroccio, A., Federici, G., Urbani, A., Murgia, I., et al. (2004). Evidence for the presence of ferritin in plant mitochondria. *Eur. J. Biochem.* 271, 3657–3664. doi: 10.1111/j.1432-1033.2004.04300.x

Zhang, Y., Lyver, E. R., Knight, S. A., Lesuisse, E., and Dancis, A. (2005). Frataxin and mitochondrial carrier proteins, Mrs3p and Mrs4p, cooperate in providing iron for heme synthesis. *J. Biol. Chem.* 280, 19794–19807. doi: 10.1074/jbc.M500397200

Zhang, Y., Lyver, E. R., Knight, S. A., Pain, D., Lesuisse, E., and Dancis, A. (2006). Mrs3p, Mrs4p, and frataxin provide iron for Fe–S cluster synthesis in mitochondria. *J. Biol. Chem.* 281, 22493–22502. doi: 10.1074/jbc.M604246200

Zhao, G., Ceci, P., Ilari, A., Giangiacomo, L., Laue, T. M., Chiancone, E., et al. (2002). Iron and hydrogen peroxide detoxification properties of DNA-binding protein from starved cells. A ferritin-like DNA-binding protein of *Escherichia coli*. *J. Biol. Chem.* 277, 27689–27696. doi: 10.1074/jbc.M202094200

Conflict of Interest Statement: The authors declare that the research was conducted in the absence of any commercial or financial relationships that could be construed as a potential conflict of interest.

Received: 05 June 2013; accepted: 18 August 2013; published online: 06 September 2013.

*Citation: Jain A and Connolly EL (2013) Mitochondrial iron transport and homeostasis in plants. Front. Plant Sci. **4**:348. doi: 10.3389/fpls.2013.00348*

This article was submitted to Plant Nutrition, a section of the journal Frontiers in Plant Science.

frontiers in
PLANT SCIENCE

ORIGINAL RESEARCH ARTICLE
published: 16 August 2013
doi: 10.3389/fpls.2013.00316

Mitochondrial ferritin is a functional iron-storage protein in cucumber (*Cucumis sativus*) roots

Gianpiero Vigani[1], Delia Tarantino[2] and Irene Murgia[2]*

[1] *Dipartimento di Scienze Agrarie e Ambientali – Produzione, Territorio, Agroenergia, Università degli Studi di Milano, Milano, Italy*
[2] *Dipartimento di Bioscienze, Università degli Studi di Milano, Milano, Italy*

Edited by:
Graziano Zocchi, Università degli Studi di Milano, Italy

Reviewed by:
Luigi Palmieri, Università degli Studi di Bari Aldo Moro, Italy
Francisco J. Romera, University of Cordoba, Spain

***Correspondence:**
Irene Murgia, Dipartimento di Bioscienze, Università degli Studi di Milano, Via Celoria 26, 20133 Milano, Italy
e-mail: irene.murgia@unimi.it

In plants, intracellular Fe trafficking must satisfy chloroplasts' and mitochondrial demands for Fe without allowing its accumulation in the organelles in dangerous redox-active forms. Protein ferritin is involved in such homeostatic control, however its functional role in mitochondria, differently from its role in chloroplasts, is still matter of debate. To test ferritin functionality as a 24-mer Fe-storage complex in mitochondria, cucumber seedlings were grown under different conditions of Fe supply (excess, control, deficiency) and mitochondria were purified from the roots. A ferritin monomer of around 25 KDa was detected by SDS-PAGE in Fe-excess root mitochondria, corresponding to the annotated Csa5M215130/XP_004163524 protein: such a monomer is barely detectable in the control mitochondria and not at all in the Fe-deficient ones. Correspondingly, the ferritin 24-mer complex is abundant in root mitochondria from Fe-excess plants and it stores Fe as Fe(III): such a complex is also detectable, though to a much smaller extent, in control mitochondria, but not in Fe-deficient ones. Cucumber ferritin Csa5M215130/XP_004163524 is therefore a functional Fe(III)-store in root mitochondria and its abundance is dependent on the Fe nutritional status of the plant.

Keywords: *Cucumis sativus*, ferritin, iron homeostasis, iron-storage protein, mitochondria, micronutrients, O_2 consumption, roots

INTRODUCTION

The detailed understanding of molecular mechanisms regulating plant nutrient homeostasis is of the highest priority and represents one of the hundred most relevant questions facing plant research (Grierson et al., 2011). Keeping iron (Fe) homeostasis under control is particularly relevant for plants due to its essential role in many house-keeping cellular functions, but also to its toxicity as catalyst of the Fenton reaction, when in a free form (Winterbourn, 1995; Briat et al., 2010). A picture is now emerging of how the Fe deficiency responses, uptake, transport and distribution to various plant organs, together with its intracellular trafficking and storage, are finely tuned on the availability of soluble Fe in the soil by a complex net of signal transduction pathways (Vigani et al., 2009; Murgia et al., 2009; Conte and Walker, 2011; Ramirez et al., 2011; Kobayashi and Nishizawa, 2012; Vigani et al., 2013a,b; Thomine and Vert, 2013).

The intra-organellar partitioning of Fe under various nutritional conditions is intriguing: the question of whether modifications of mitochondrial and chloroplastic Fe metabolism, in response to alteration in the plant Fe status, represent a source of retrograde signals necessary to regulate the nuclear gene expression, has been posed (Vigani et al., 2013a). For that, metabolic changes in organelles occurring under various conditions of Fe supply should be documented in detail (Vigani et al., 2013a). Investigation of mitochondria from roots is particularly attractive, since the lack of photosynthetically active chloroplasts might reduce the complexity of the retrograde signals involved. Moreover, roots are directly involved in uptake of Fe from soil and their mitochondria provide chemical energy for such a process.

An extra layer of complexity involving plant Fe nutrition is given by the necessity to prevent Fe accumulation in dangerous, redox-active forms, in the organelles as well as in the cytosol. Ferritin protein, by forming a 24-mer cage-like structure able to store Fe in a safe, bioavailable form, is involved in such intracellular control of Fe trafficking and homeostasis, in both plant and animal cells (Arosio et al., 2009; Briat et al., 2009). In plants, ferritin is targeted to chloroplasts (Briat et al., 2009) but its localization to mitochondria has been also documented in Arabidopsis and in pea (Zancani et al., 2004; Tarantino et al., 2010a,b).

The characterization of Arabidopsis *atfer4* mutants knock-out for the ferritin isoform, targeted also to mitochondria (Tarantino et al., 2010a,b), posed the question of whether the role of the mitochondrial-targeted AtFER4 is a sort of ancestral relict, replaced by other still unknown regulatory mechanisms of Fe homeostasis, during the evolution to green plants. On the other side, a relevant role of human mitochondrial ferritin (Levi et al., 2001) as protectant against oxidative stress in various cell types (Campanella et al., 2009; Wang et al., 2011) but also in improving respiratory function in yeast mutants deficient in [Fe-S] cluster biogenesis (Sutak et al., 2012), is emerging.

Taken together, this evidence prompted us to investigate whether ferritin is functional in the mitochondria of cucumber (*Cucumis sativus*) roots, that is, if it can truly store Fe(III), as a 24-mer complex.

MATERIALS AND METHODS

PLANT GROWTH CONDITIONS AND PURIFICATION OF ROOT MITOCHONDRIA

Seeds of cucumber (*Cucumis sativus* L. cv. Marketmore) were sown in Agriperlite, watered with 0.1 mM $CaSO_4$, allowed to germinate in the dark at 26°C for 3 d, and then transferred to a nutrient solution with the following composition: 2 mM $Ca(NO)_3$, 0.75 mM K_2SO_4, 0.65 mM $MgSO_4$, 0.5 mM KH_2PO_4, 10 μM H_3BO_3, 1 μM $MnSO_4$, 0.5 μM $CuSO_4$, 0.5 μM $ZnSO_4$, 0.05 μM $(NH_4)Mo_7O_{24}$, and Fe(III)-EDTA at the following concentrations: 0 mM (Fe deficiency), 0.05 mM (Control), 0.5 mM (Fe excess). The pH was adjusted to 6.0–6.2 with NaOH. Aerated hydroponic cultures were maintained in a growth chamber with a day: night regime of 16:8 h and 200 μE $m^{-2}s^{-1}$ photosynthetically active radiation (PAR) at the plant level. The temperature ranged from 18°C (in the dark) to 24°C (in the light).

Mitochondria were purified from cucumber roots according to Balk et al. (1999) and Vigani et al. (2009), with few modifications. 10 days old roots were homogenized with a mortar and pestle in 0.4 M mannitol, 25 mM MOPS pH 7.8, 1 mM EGTA, 8 mM cysteine, and 0.1% (w/v) bovine serum albumin (BSA). The filtered homogenized plant material (total extract, TE) was centrifuged 5 min at 4000 g and the pellet was used as an enriched plastids fraction (P). The supernatant was re-centrifuged 15 min at 12,000 g to pellet mitochondria whereas the supernatant fraction constitutes the so-called PMS (post-mitochondria supernatant fraction). The crude mitochondrial pellet was resuspended in RB buffer (0.4 M mannitol, 10 mM Tricine pH 7.2, 1 mM EGTA) and lightly homogenized with a potter; mitochondria were further purified on a 40, 28, and 13.5% (v/v) Percoll (Pharmacia) step gradient in RB buffer. The fraction at the 28/40% interface (purified mitochondria) was collected and washed by differential centrifugation in RB buffer.

NATIVE GEL ELECTROPHORESIS AND WESTERN BLOT ANALYSIS

Purified mitochondrial proteins were loaded on a non-denaturing polyacrylamide gel (3% [w/v] stacking, 5.5% [w/v] separating) after heating at 65°C for 7 min. The gel was run for 5 h at 25 mA (on ice); then the gel was rinsed in water and incubated in potassium ferrous cyanide solution [2% KFe(II)CN, 2% HCl], 1 h in the dark. The gel was washed four times in H_2O, 15 min each, with gentle shaking and incubated overnight in a diaminobenzidine (DAB) solution (0.05% DAB, 18 mM H_2O_2 in PBS at pH 7.4) without shaking.

SDS-PAGE was performed according to Vigani et al. (2009) with the following antibodies: spinach anti-Toc33 (Rödiger et al., 2010) at 1:1000 dilution, maize anti-porin (Balk and Leaver, 2001) at 1:2000 dilution, Arabidopsis anti-ATFER1 (Murgia et al., 2007) at 1:2000 and an anti-rabbit conjugated with alkaline phosphatase as secondary antibody. Protein quantification was determined according to Vigani et al. (2009).

RT-PCR

Roots apices and true second leaves from 10 days old plants grown under Fe-excess were sampled and RNA extracted with Trizol reagent (Gibco). RT-PCR reactions were performed by using Access RT-PCR kit (Promega), 60 ng total RNA/reaction.

Cucsafor1:5′-CCACCACACACACACGC-3′
Cucsarev1:5′-ATTGTCTCTGTCAAAGTAGGC-3′
Cucsarev2: 5′-TTGGCCAAACCCTTGAGTGC-3′
Cucsarev3: 5′-CCATTGCAAAAAAAGCATCTCC-3′
Cucsarev4: 5′-GAGCTCCATTGCATATAAGGC-3′

For Cucsafor1-Cucsarev1: 1 mM $MgSO_4$ final conc., annealing at 61°C; for Cucsafor1-Cucsarev2: 1.5 mM $MgSO_4$ final conc., annealing at 61°C; for Cucsafor1-Cucsarev3: 1.5 mM $MgSO_4$ final conc., annealing at 57–67°C; for Cucsafor1-Cucsarev4: 1 mM $MgSO_4$ final conc., annealing at 61–67°C.

MISCELLANOUS

Total Chl, Chla and Chlb content was determined according to Lichtenthaler (1987). Fe content in purified mitochondria was determined by ICP-MS spectroscopy (Variant).

F_0F_1ATP synthase and G6PDH activities were performed according to Camacho-Pereira et al. (2009).

O_2 consumption and use of KCN and SHAM (salicylhydroxamic acid) was measured on root apices from 10 days-old plants according to Vigani et al. (2009).

Protein sequence alignment was performed with Multalin version 5.4.1 (Corpet, 1988) at http://multalin.toulouse.inra.fr/multalin/.

RESULTS

Fe-DEFICIENT AND Fe-EXCESS ROOT TIPS SHOW AN INCREASE IN THE O_2 CONSUMPTION RATES

Cucumber seedlings were grown in hydroponic medium for 10 days in a complete nutrient solution containing 0, 50, or 500 μM Fe(III)-EDTA (Fe deficiency, control, excess) (**Figure 1A**). Fe deficient plants showed the typical symptoms of chlorosis in leaves, while leaves from both control or Fe excess plants were green; length of root apparatus was reduced in Fe-deficient plants (**Figures 1A**,**B**). Accordingly, total Chl content was very low in the Fe-deficient leaves (**Figure 1C**), while no significant differences in total Chl nor in Chla/Chlb content, could be detected between Fe-excess and control leaves (**Figure 1C**).

Root tips are the most metabolically active parts of the roots and indeed they are the main site displaying Fe uptake in which Strategy I activities are strongly induced (Landsberg, 1986; Vigani et al., 2012) Both Fe-deficient and Fe-excess root tips show higher O_2 consumption rates than control root tips (**Figure 1D**). Moreover, the addition of KCN and SHAM (inhibitors of the respiratory O_2 consumption) did not completely block the O_2 consumption, differently from what was observed in control root tips where such inhibitors almost completely abolished it (**Figure 1D**). Such residual O_2 consumption in root tissues of Fe deficient as well as of Fe-excess plants, not attributable to the mitochondrial respiratory chain activity, has been already described in cucumber (Vigani et al., 2009).

PURITY OF MITOCHONDRIA ISOLATED FROM CUCUMBER ROOTS

A one step-gradient protocol was applied for purifying mitochondria from seedling roots grown in the different conditions of Fe supply. Since it is well established that ferritin accumulates in plastids of plants grown under Fe-excess, all the different

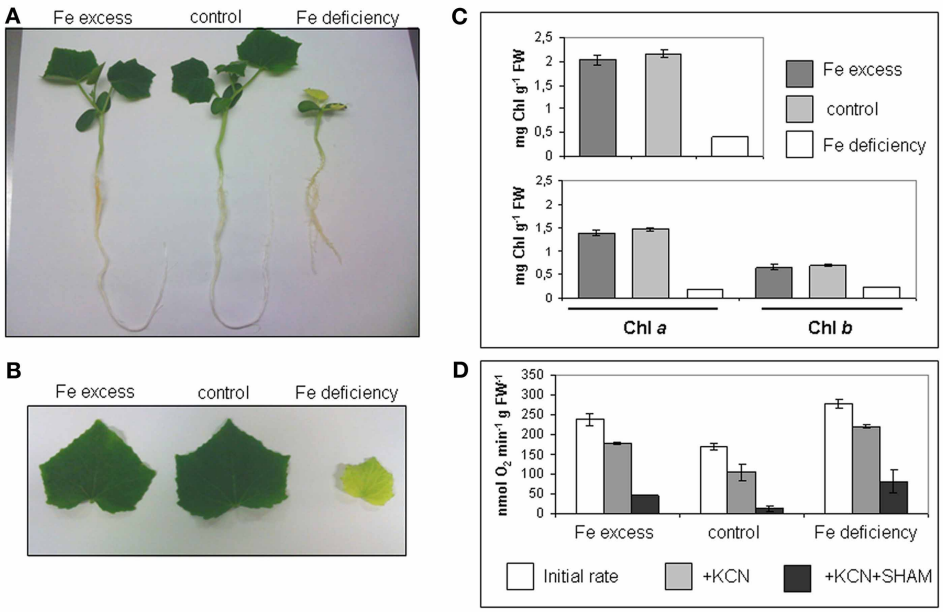

FIGURE 1 | Cucumber seedlings under different conditions of Fe supply. (A) 10 days-old cucumber seedlings grown in hydroponic medium containing either 500 μM Fe(III)-EDTA (Fe excess), 50 μM Fe(III)-EDTA (control), or with no added Fe in the medium (Fe deficiency). **(B)** Leaves of cucumber seedlings grown as in **(A)**. **(C)** Chl content (mg g^{-1} FW) of seedlings leaves, grown as in **(A)**; upper panel: total Chl content; lower panel: Chl*a* and Chl*b* content. Bars represent mean values ± SE from 4 independent samples of 3–4 leaves each **(D)** O_2 consumption in seedlings roots, grown as in **(A)**; for each condition (Fe excess, control, Fe deficiency), the initial rate and the rates after addition of KCN or KCN + SHAM are provided. Bars represent mean values ± SE from 6 independent samples of 10 root tips each.

fractions collected during isolation of mitochondria from Fe-excess roots, i.e., the TE, the plastid enriched fraction (P), the purified mitochondria (M) and the post-mitochondrial supernatant (PMS) (Balk et al., 2004) were tested with two different enzymatic assays as well as with different antibodies (in SDS-PAGE experiments), in order to exclude any contamination of the purified mitochondrial fractions with intact plastids. Activity of F_0F_1ATP synthase enzyme, a marker used for mitochondria (Camacho-Pereira et al., 2009) was measured in the four isolated fractions TE, P, M, and PMS (**Figure 2A**). F_0F_1ATP synthase activity is highest in the M fraction (0.79 U mg^{-1} prot), and, as expected, also in the TE fraction (0.56 U mg^{-1} prot) (**Figure 2A**). A 40% reduction of enzyme activity is observed in PMS fraction containing the cytosol (0.35 U mg^{-1}prot) whereas it is almost undetectable in the P fraction (0.05 U mg^{-1} prot) (**Figure 2A**). Glucose 6 phosphate dehydrogenase (G6PDH) is localized both in cytosol and in the plastids' stroma (Camacho-Pereira et al., 2009) therefore it can be used as a cytosolic and plastidial enzyme marker; its activity is undetectable in M fraction (**Figure 2B**), whereas it is highest in the PMS (8.95 U mg^{-1}prot), followed by P (6.70 U mg^{-1}prot), and TE (4.20 U mg^{-1} prot) (**Figure 2B**). The two enzyme assays confirmed that the purified mitochondria are not contaminated by the cytosolic fraction nor from integral, undisrupted plastids, since in that case the G6PDH enzymatic activity should have been detected also in the mitochondrial fraction. Furthermore, the plastid marker Toc33 protein (Rödiger et al., 2010) accumulated only in the P fraction (**Figure 2C**), whereas porin (Balk and Leaver, 2001) accumulated, as expected, in the M fraction and, to lesser extent, in the P fraction (**Figure 2C**).

A FERRITIN 24-mer COMPLEX ACCUMULATES IN THE ROOT MITOCHONDRIA FROM Fe-EXCESS PLANTS AND IT STORES Fe(III)

The genome of the Chinese Long cultivar of cucumber (line 9930) was first annotated in 2009 and then reassembled and reannotated (Huang et al., 2009; Li et al., 2011) (www.icugi.org/cgi-bin/ICuGI/index.cgi). According to that annotation, a unique ferritin protein sequence, named Csa5M215130 (259 aa), is encoded by the cucumber genome (**Figure 3**). The genome of a North-European cultivar (B10) has been also sequenced (Wóycicki et al., 2011) and again, a unique ferritin gene has been identified, LOC101221012 with three different transcript variants, the protein sequences of which are deposited in the NCBI database: XP_004148174 (259 aa), XP_004163524 identical to Csa5M215130 (259 aa) and XP_004163525 (241 aa) (**Figure 3**). XP_004148174 and XP_004163524 differ by two aa at position 180–181 (**Figure 3**), whereas XP_004163525 lacks a 18 aa stretch at position 104 (**Figure 3**). A further sequencing of the cucumber genome has been made available at Phytozome (http://www.phytozome.net), a comparative hub for plant genome analysis (Goodstein et al., 2012). According to this, the cucumber genome possesses a single ferritin gene Cucsa144440 with its primary transcript coding for a protein identical to Csa5M215130/XP_004163524.

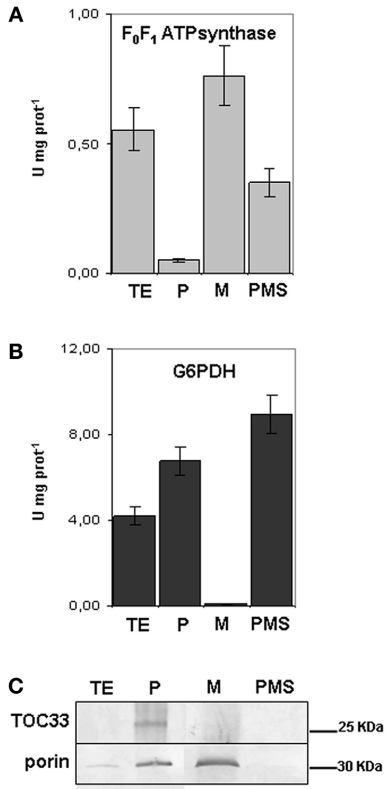

FIGURE 2 | Purity of mitochondria isolated from cucumber roots. (A) F_0F_1 ATPsynthase activity, expressed as Units mg^{-1} protein in the different fractions obtained during purification of mitochondria: total extract (TE), enriched plastids (P), mitochondria (M) and the post- mitochondria supernatant fraction (PMS). Bars represent the mean values ± SE from 4 independent samples of 30–50 μg protein each. **(B)** Glucose 6-phosphate dehydrogenase activity (G6PDH) in TE, P, M and PMS fraction. Bars represent the mean values ± SE from 4 independent samples of 30–50 μg protein each. **(C)** SDS-PAGE, followed by western blot analysis, of TE, P, M and PMS fractions; equal protein quantity (12 μg) was loaded in each lane.

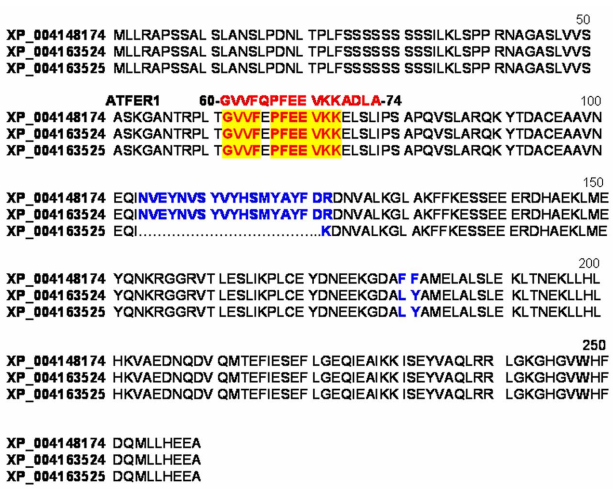

FIGURE 3 | Sequence alignment of the three predicted cucumber ferritin protein variants of the unique ferritin gene: XP_004148174, XP_004163524 identical to Csa5M215130 and XP_004163525. In blue are the aa residues differing among the three sequences; highlighted in red are the aa identical to those in the 16-aa peptide GVVFQPFEEVKKADL used as antigen for raising the anti-ATFER1 antibody.

To investigate ferritin localization and its physiological role in root mitochondria, quantification of Fe content, by ICP-MS analysis, in mitochondria purified from roots of plants grown under different conditions of Fe supply, was first performed.

Total Fe in mitochondria from Fe-excess roots is 718.92 nmol mg^{-1} prot, more than two-fold higher than in control ones (309.77 nmol mg^{-1} prot) (**Figure 4A**); this result confirms that growth of cucumber plants under Fe-excess treatment is effective in perturbing the Fe content of their mitochondria, beside their function, such as the described increase in O_2 consumption (**Figure 1D**). Total Fe content is, instead, dramatically reduced in mitochondria purified from Fe-deficient plants; nevertheless, such Fe-deficient mitochondria are still able to perform their respiratory function (**Figure 1D**) thus suggesting that mitochondria are still functional in such stress conditions.

The mitochondria purified from control, Fe-excess or Fe-deficient roots were then analyzed by western blot with the Arabidopsis anti-ATFER1 ferritin antibody (Murgia et al., 2007), raised against the 16-aa antigen peptide GVVFQPFEEVKKADL corresponding to aa 60–74 in the Arabidopsis ATFER1 sequence; such an antibody is appropriate for the detection of cucumber ferritin since both Csa5M215130/XP_004163524, as well as XP_004148174 and XP_004163525, would show an 11/16 aa match with such a peptide (**Figure 3**).

As a positive control, crude protein TE from pea seeds (rich in ferritin) was used (**Figure 4B**); pea ferritin is indeed detected by the anti-ATFER1 antibody (Murgia et al., 2007).

A single band of around 25 KDa could be detected, the accumulation of which is dependent on Fe-content of the mitochondria, being strong in Fe-excess mitochondria, still detectable in control mitochondria and undetectable in Fe-deficient ones (**Figure 4B**). Equal loading of protein content for each sample was confirmed through hybridization with anti-porin antibody (**Figure 4B**) (Vigani and Zocchi, 2010).

The Fe-excess, control and Fe-deficient mitochondria, tested above, were also analyzed by native gel electrophoresis followed by Prussian blue staining, which stains Fe in the oxidized form Fe(III), and DAB/H_2O_2 enhancement (Luscieti et al., 2010). Recombinant human ferritin 24-mer complex (around 500 kDa) served as a positive control. A band of higher molecular weight than the recombinant human ferritin complex is clearly detected in Fe-excess mitochondria; such band is fairly weak in control mitochondria and undetectable in Fe-deficient ones (**Figure 4C**).

Identity of the ferritin detected in Fe-excess mitochondria (**Figures 4B,C**) could be unambiguously attributed to Csa5M215130/XP_004163524. Indeed, based on gene and predicted coding sequences of XP004163524 (annotated at NCBI as ferritin-3, chloroplast-like, transcript variant 1 (LOC101221012) (**Figure 5**), of XP004163525 (annotated at NCBI as ferritin-3, chloroplast-like, transcript variant 2) (**Figure S1**) and of

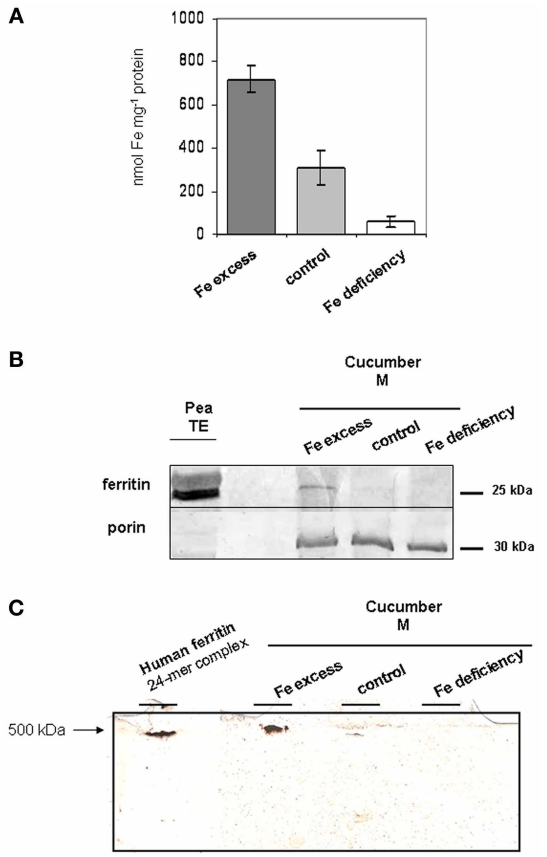

FIGURE 4 | Fe and ferritin content in mitochondria from cucumber roots grown under different conditions of Fe supply. (A) Total Fe content in mitochondria purified from Fe-excess, control, or Fe-deficiency roots, quantified by ICP-MS. Each bar represents the mean value ± SE from 4 independent samples consisting of 60–200 μg mitochondria each. **(B)** SDS-PAGE and western blot analysis of mitochondria purified from Fe-excess, control, or Fe-deficiency root. 15 μg proteins were loaded in each lane. As positive control, 34 μg total extract (TE) from pea seeds, rich in ferritin, has been loaded in leftmost lane. **(C)** native PAGE analysis, followed by Prussian blue/DAB stain of mitochondria purified from Fe-excess, control or Fe-deficiency root; 40 μg proteins were loaded in each lane. As positive control, 48 μg proteins recombinant human ferritin consisting of a 24-mer of around 500 KDa, was also loaded in the far left lane.

XP_004148174 (annotated at NCBI as ferritin-3, chloroplast-like) (**Figure S2**) five different primers Cucsafor1, Cucsarev1-rev4 were designed for RT-PCR experiments with RNA purified from either roots or leaves from Fe-excess cucumber plants (thus accumulating ferritin). Results show that RT-PCR with the following pairs: Cucsafor1-Cucsarev1 and Cucsafor1-Cucsarev2, amplified, respectively a fragment of 436 and 470 bp (**Figure 5B**, left panel), as expected from an mRNA coding for XP004163524 (**Figure 5A**) but not from an mRNA coding for XP004163525 (**Figure S1**). Moreover, RT-PCR with the Cucsafor1-Cucsarev4 primer pair amplified a fragment of 612 bp (**Figure 5B**, right panel), expected from an mRNA coding for XP004163524 (**Figure 5A**) but not from an mRNA coding for XP_004148174 (**Figure S2**); amplification of such fragment, in roots and in leaves, has been obtained not only at the optimal annealing temperature for that primer pair (61°C), but also at more stringent conditions, i.e., with annealing temperatures up to 67°C (**Figure 5B**, right panel). Viceversa, RT-PCR with Cucsafor1-Cucsarev3 primer pair (**Figure S2**) performed with RNA extractions from different roots and leaf samples, could not amplify any fragment expected from the mRNA coding for XP_004148174 (data not shown).

The transcription of a single mRNA coding for cucumber ferritin in roots as well as in green leaves with consequent translation of a unique ferritin protein, strongly suggests that cucumber ferritin is "dual targeted" in both mitochondria and chloroplasts (Carrie and Small, 2013). PSort (http://psort.hgc.jp/form2.html), MitoProtII (http://ihg.gsf.de/ihg/mitoprot.html) and TargetP (http://www.cbs.dtu.dk/services/TargetP/) programs are three widely used bioinformatic tools predicting subcellular localization of a given protein sequence and cleavage site of the corresponding transit peptide (Nakai and Kanehisa, 1991; Claros and Vincens, 1996; Emanuelsson et al., 2007). Such programs, when applied to the three putative protein variants Csa5M215130/XP_004163524, XP_004148174 and XP_004163525, for prediciting the mitochondrial localization, give different results: MitoProtII scores are indeed, respectively: 0.82, 0.79, 0.80; PSort scores are 0.47 for all the three sequences whereas TargetP scores are below 0.1 for all the three sequences. The predictions of the cleavage site for the transit peptide are also quite different among the three programs, being of 68 aa with MitoProtII, 32 aa with PSort and 50 aa with TargetP. Variability of such results is not surprising, since it is widely known that such bioinformatic predictors proved extremely problematic for dual targeted proteins (Pujol et al., 2007; Berglund et al., 2009; Carrie and Small, 2013).

A 14 bp Iron Dependent Regulatory Sequence (IDRS) is present in the promoter region of the Arabidopsis AtFer1 gene and is responsible for the AtFer1 transcriptional repression under low Fe supply. On the contrary, Fe treatment releases the IDRS-mediated transcriptional repression of the AtFer1 gene via a NO-dependent mechanism, and AtFer1 ferritin transcript can therefore accumulate (Petit et al., 2001; Murgia et al., 2002; Arnaud et al., 2006).

A 14-bp sequence, 64% identical to the AtFer1 IDRS, is present in the promoter region of the cucumber ferritin gene LOC101221012/Csa5M215130/Cucsa144440, at position -199 from ATG start (**Figure 5A**), similarly to what is observed for the AtFer1 IDRS sequence (Petit et al., 2001).

DISCUSSION

The scientific relevance in focusing on plant nutrients and their homeostasis is not confined to the potential long-term benefits in agriculture: indeed, a better understanding of Fe homeostasis can have positive impacts and can offer new solutions for combatting malnutrition (Grierson et al., 2011). Such knowledge can assist the exploitation of new strategies for the production of plants biofortified for Fe and for reducing Fe deficiency anaemia, a severe burden for populations in developing countries mostly affecting children and women (Murgia et al., 2012).

Elucidation of the role of mitochondria in plant Fe homeostasis is a challenging issue (Vigani et al., 2013a). Despite the

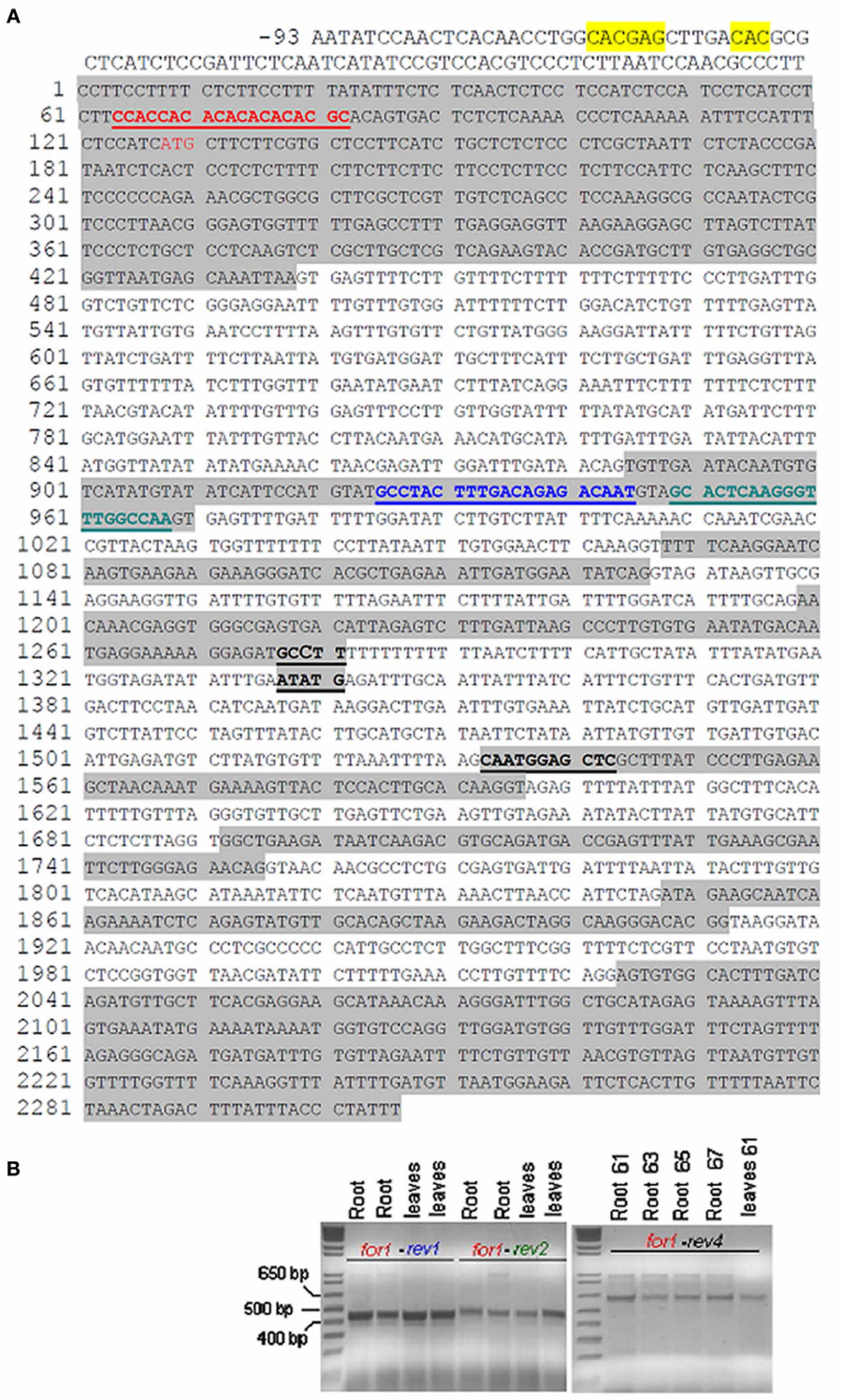

FIGURE 5 | Gene and predicted coding sequence of cucumber ferritin protein XP004163524 (reported at NCBI as ferritin-3, chloroplastic-like, transcript variant 1, LOC101221012). (A) IDRS-like sequence in gene promoter is highlighted in yellow; ATG start is in red color; exons are highlighted in gray. Positions of primers Cucsafor1 (in red), Cucsarev1 (in blue), Cucsarev2 (in green), Cucsarev4 (in black) are underlined; **(B)** left panel: RT-PCR reactions with primer pairs Cucsafor1-Cucsa-rev1 and Cucsafor1-Cucsa-rev2, with either two independent RNA extracts from Fe-excess cucumber roots or two independent RNA extracts from Fe-excess leaves. The Kb ladder Plus (Invitrogen) has been loaded in the far left lane. Right panel: RT-PCR reactions with primer pair Cucsafor1-Cucsa-rev4, with RNA purified from Fe-excess roots at 61, 63, 65, 67 anneal. temp., or with RNA purified from Fe-excess leaves at 61°C anneal. temp.

fact that mitochondria are strongly affected by Fe deficiency, they in fact display a high level of functional flexibility, which allows them to guarantee cell viability under Fe shortage (Vigani, 2012).

The present work confirms the localization of the ferritin in mitochondria of cucumber roots, as already observed in Arabidopsis and pea (Zancani et al., 2004; Tarantino et al., 2010a,b); its abundance is strictly dependent on the total Fe content in mitochondria which, in turn, is dependent on the availability of Fe in the growth medium.

A unique mRNA transcribed from LOC101221012 cucumber gene, coding for the ferritin protein named alternatively Csa5M215130 or XP_004163524 by two different sequencing consortia (Li et al., 2011; Wóycicki et al., 2011) has been identified in Fe-excess cucumber roots and leaves; moreover, such mRNA is 100% identical to the primary transcript of the ferritin gene named Cucsa144440 in the Phytozome hub (Goodstein et al., 2012). Results in the present work show that a single Fe-dependent ferritin isoform, named Csa5M215130/XP_004163524 accumulates in cucumber roots. Since no other transcripts are detected in green leaves of Fe-excess cucumber plants, such ferritin protein is most probably dual-targeted to both chloroplasts and mitochondria and represents an example of the so-called "ambiguous targeting" (Peeters and Small, 2001; Carrie and Small, 2013).

The presence, in LOC101221012/Cucsa144440 gene promoter ferritin, of an IDRS-like stretch, is suggestive of a common regulatory mechanism for the Fe-dependent expression of the two ferritin genes in Arabidopsis and in cucumber.

The results shown in the present work strongly suggest that the detected multimer complex is truly the 24-mer ferritin complex Csa5M215130/XP_004163524; indeed, as observed for the monomer, the abundance of the multimer complex is also dependent on the mitochondrial Fe content and results obtained in native gel are consistent with its expected weight (around 600 KDa).

In conclusion, for the first time proof that ferritin is a functional Fe-storage protein in cucumber mitochondria is provided: the 24-mer ferritin complex indeed truly binds Fe(III).

Such results open the way to further investigations about the possible physiological relevance of ferritin as a root protectant against various oxidative stresses which may arise during adverse field conditions.

ACKNOWLEDGMENTS

We are grateful to P. Arosio and co-workers for providing recombinant human ferritin and for support during preliminary experiments and to R. B. Klösgen and M. Jakob for providing Toc33. Gianpiero Vigani and Irene Murgia were supported by FIRB 2012 (MIUR, RBFR127WJ9).

SUPPLEMENTARY MATERIAL

The Supplementary Material for this article can be found online at: http://www.frontiersin.org/Plant_Nutrition/10.3389/fpls.2013.00316/abstract

Figure S1 | Predicted coding sequence for XP004163525 protein.

Figure S2 | Predicted coding sequence for XP_004148174 protein.

REFERENCES

Arnaud, N., Murgia, I., Boucherez, J., Briat, J. F., Cellier, F., and Gaymard, F. (2006). An iron-induced Nitric Oxide burst precedes ubiquitin-dependent protein degradation for *Arabidopsis AtFer1* ferritin gene expression. *J. Biol. Chem.* 281, 23579–23588. doi: 10.1074/jbc.M602135200

Arosio, P., Ingrassia, R., and Cavadini, P. (2009). Ferritins: a family of molecules for iron storage, antioxidation and more. *Biochim. Biophys. Acta* 1790, 589–599. doi: 10.1016/j.bbagen.2008.09.004

Balk, J., and Leaver, C. J. (2001). The PET1-CMS mitochondrial mutation in sunflower is associated with premature programmed cell death and cytochrome c release. *Plant Cell* 13, 1803–1818.

Balk, J., Leaver, C. J., and McCabe, P. F. (1999). Translocation of cytochrome c from the mitochondria to the cytosol occurs during heat-induced programmed cell death in cucumber plants. *FEBS Lett.* 463, 151–154. doi: 10.1016/S0014-5793(99)01611-7

Balk, J., Pierik, A. J., Netz, D. J. A., Mühlenhoff, U., and Lill, R. (2004). The hydrogenase-like Nar1p is essential for maturation of cytosolic and nuclear iron–sulphur proteins. *EMBO J.* 23, 2105–2115. doi: 10.1038/sj.emboj.7600216

Berglund, A. K., Spanning, E., Biverstahl, H., Maddalo, G., Tellgren-Roth, C., Maler, L., et al. (2009). Dual targeting to mitochondria and chloroplasts: characterization of Thr-tRNA synthetase targeting peptide. *Mol. Plant* 2, 1298–1309. doi: 10.1093/mp/ssp048

Briat, J. F., Duc, C., Ravet, K., and Gaymard, F. (2009). Ferritins and iron storage in plants. *Biochem. Biophys. Acta* 1800, 806–814. doi: 10.1016/j.bbagen.2009.12.003

Briat, J. F., Ravet, K., Arnaud, N., Duc, C., Boucherez, J., Touraine, B., et al. (2010). New insights into ferritin synthesis and function highlight a link between iron homeostasis and oxidative stress in plants. *Ann. Bot.* 105, 811–822. doi: 10.1093/aob/mcp128

Camacho-Pereira, J., Meyer, L. E., Machado, L. B., Oliveira, M. F., and Galina, A. (2009). Reactive oxygen species production by potato tuber mitochondria is modulated by mitochondrially bound hexokinase activity. *Plant Physiol.* 146, 1099–1110.

Campanella, A., Rovelli, E., Santambrogio, P., Cozzi, A., Taroni, F., and Levi, S. (2009). Mitochondrial ferritin limits oxidative damage regulating mitochondrial iron availability: hypothesis for a protective role in Friedreich ataxia. *Hum. Mol. Genet.* 18, 1–11. doi: 10.1093/hmg/ddn308

Carrie, C., and Small, I. (2013). A revaluation of dual-targeting of proteins to mitochondria and chloroplasts. *Biochim. Biophys. Acta* 1833, 253–259. doi: 10.1016/j.bbamcr.2012.05.029

Claros, M. G., and Vincens, P. (1996). Computational methods to predict mitochondrially imported proteins and their targeting sequences. *Eur. J. Biochem.* 241, 779–786. doi: 10.1111/j.1432-1033.1996.00779.x

Conte, S. S., and Walker, E. L. (2011). Transporter contributing to iron trafficking in plants. *Mol. Plant* 4, 464–476. doi: 10.1093/mp/ssr015

Corpet, F. (1988). Multiple sequence alignment with hierarchical clustering. *Nucleic Acids Res.* 16, 10881–10890. doi: 10.1093/nar/16.22.10881

Emanuelsson, O., Brunak, S., von Heijne, G., and Nielsen, H. (2007). Locating proteins in the cell using TargetP, SignalP, and related tools. *Nat. Protoc.* 2, 953–971. doi: 10.1038/nprot.2007.131

Goodstein, D. M., Shu, S., Howson, R., Neupane, R., Hayes, R. D., Fazo, J., et al. (2012). Phytozome: a comparative platform for green plant genomics. *Nucleic Acids Res.* 40, D1178–D1186. doi: 10.1093/nar/gkr944

Grierson, C. S., Barnes, S. R., Chase, M. W., Clarke, M., Grierson, D., Edwards, K. J., et al. (2011). One hundred important questions facing plant science research. *New Phytol.* 192, 6–12. doi: 10.1111/j.1469-8137.2011.03859.x

Huang, S., Li, R., Zhang, Z., Li, L., Gu, X., Fan, W., et al. (2009). The genome of the cucumber Cucumis sativus L. *Nat. Genet.* 41, 1275–1281. doi: 10.1038/ng.475

Kobayashi, T., and Nishizawa, N. K. (2012). Iron uptake, translocation,

and regulation in higher plants. *Ann. Rev. Plant Biol.* 63, 131–152. doi: 10.1146/annurev-arplant-042811-105522

Landsberg, E. C. (1986). Function of rhizodermal transfer cells in the Fe stress response mechanism of Capsicum annuum L. *Plant Physiol.* 82, 511–517. doi: 10.1104/pp.82.2.511

Levi, S., Corsi, B., Bosisio, M., Invernizzi, R., Volz, A., Sanford, D., et al. (2001). A human mitochondrial ferritin encoded by an intronless gene. *J. Biol. Chem.* 276, 24437–24440. doi: 10.1074/jbc.C100141200

Li, Z., Zhang, Z., Yan, P., Huang, S., Fei, Z., and Lin, K. (2011). RNA-Seq improves annotation of protein-coding genes in the cucumber genome. *BMC Genomics* 12:540. doi: 10.1186/1471–2164-12-540

Lichtenthaler, H. K. (1987). Chlorophyll and carotenoids: pigments of photosynthetic biomembranes. *Methods Enzymol.* 148, 350–382. doi: 10.1016/0076-6879(87)48036-1

Luscieti, S., Santambrogio, P., Langlois d'Estaintot, B., Granier, T., Cozzi, A., Poli, M., et al. (2010). Mutant ferritin L-chains that cause neurodegeneration act in a dominant-negative manner to reduce ferritin iron incorporation. *J. Biol. Chem.* 285, 11948–11957. doi: 10.1074/jbc.M109.096404

Murgia, I., Arosio, P., Tarantino, D., and Soave, C. (2012). Crops biofortification for combating "hidden hunger" for iron. *Trends Plant Sci.* 17, 47–55. doi: 10.1016/j.tplants.2011.10.003

Murgia, I., Delledonne, M., and Soave, C. (2002). Nitric oxide mediates iron-induced ferritin accumulation in *Arabidopsis. Plant J.* 30, 521–528. doi: 10.1046/j.1365-313X.2002.01312.x

Murgia, I., Tarantino, D., and Soave, C. (2009) Mitochondrial iron metabolism in plants: frataxin comes into play. *Plant Soil* 325, 5–14. doi: 10.1007/s11104-009-0038-6

Murgia, I., Vazzola, V., Tarantino, D., Cellier, F., Ravet, K., Briat, J. F., et al. (2007). Knock-out of the ferritin *AtFer1* causes earlier onset of age-dependent leaf senescence in *Arabidopsis*. *Plant Physiol. Biochem.* 45, 898–907. doi: 10.1016/j.plaphy.2007.09.007

Nakai, K., and Kanehisa, M. (1991) Expert system for predicting protein localization sites in gram-negative bacteria. *Proteins* 11, 95–110. doi: 10.1002/prot.340110203

Peeters, N., and Small, I. (2001) Dual targeting to mitochondria and chloroplasts. *Biochim. Biophys. Acta* 1541, 54–63. doi: 10.1016/S0167-4889(01)00146-X

Petit, J. M., van Wuytswinkel, O., Briat, J. F., and Lobreaux, S. (2001). Characterization of an iron-dependent regulatory sequence involved in the transcriptional control of *AtFer1* and *ZmFer1* plant ferritin genes by iron. *J. Biol. Chem.* 276, 5584–5590. doi: 10.1074/jbc.M005903200

Pujol, C., Marechal-Drouard, L., and Duchene, A. M. (2007) How can organellar protein N-terminal sequences be dual targeting signals? *In silico* analysis and mutagesis approach. *J. Mol. Biol.* 369, 356–367. doi: 10.1016/j.jmb.2007.03.015

Ramirez, L., Simontacchi, M., Murgia, I., Zabaleta, E., and Lamattina, L. (2011). Nitric Oxide, Nitrosyl Iron complexes, ferritin and frataxin: a well equipped team to preserve plant iron homeostasis. *Plant Sci.* 181, 582–592. doi: 10.1016/j.plantsci.2011.04.006

Rödiger, A., Baudisch, B., and Klosgen, R. B. (2010). Simultaneous isolation of intact mitochondria and chloroplast from a single pulping of plant tissue. *J. Plant Physiol.* 167, 620–624. doi: 10.1016/j.jplph.2009.11.013

Sutak, R., Seguin, A., Garcia-Serres, R., Oddou, J. L., Dancis, A., Tachezy, J., et al. (2012). Human mitochondrial ferritin improves respiratory function in yeast mutants deficient in iron–sulfur cluster biogenesis, but is not a functional homologue of yeast frataxin. *Microbiologyopen* 1, 95–104. doi: 10.1002/mbo3.18

Tarantino, D., Casagrande, F., Soave, C., and Murgia, I. (2010a). Knocking out of the mitochondrial AtFer4 ferritin does not alter response of Arabidopsis plants to abiotic stresses. *J. Plant Physiol.* 167, 453–460. doi: 10.1016/j.jplph.2009.10.015

Tarantino, D., Santo, N., Morandini, P., Casagrande, F., Braun, H. P., Heinemeyer, J., et al. (2010b). AtFer4 ferritin is a determinant of iron homeostasis in Arabidopsis thaliana heterotrophic cells. *J. Plant Physiol.* 167, 1598–1605. doi: 10.1016/j.jplph.2010.06.020

Thomine, S., and Vert, G. (2013). Iron transport in plants: better safe than sorry. *Curr. Opin. Plant Biol.* 6, 1–6.

Vigani, G. (2012). Discovering the role of mitochondria in the iron deficiency-induced metabolic responses of plants. *J. Plant Physiol.* 169, 1–11. doi: 10.1016/j.jplph.2011.09.008

Vigani, G., Chittò, A., De Nisi, P., and Zocchi, G. (2012). cDNA-AFLP analysis reveals a set of new genes differentially expressed in response to Fe deficiency in cucumber (*Cucumis sativus* L.) root apexes. *Biol. Plant* 56, 502–508. doi: 10.1007/s10535-012-0050-1

Vigani, G., Maffi, D., and Zocchi, G. (2009). Iron availability affects the function of mitochondria in cucumber roots. *New Phytol.* 182, 127–136. doi: 10.1111/j.1469-8137.2008.02747.x

Vigani, G., Zocchi, G., Bashir, K., Philippar, K., and Briat, J. F. (2013a). Signal from chloroplasts and mitochondria for iron homeostasis regulation. *Trends Plant Sci.* 18, 305–311. doi: 10.1016/j.tplants.2013.01.006

Vigani, G., Morandini, P., and Murgia, I. (2013b). Searching iron sensors in plants by exploring the link among 2′OG-dependent dioxygenases, the iron deficiency response and metabolic adjustments occurring under iron deficiency. *Front. Plant Sci.* 4:169. doi: 10.3389/fpls.2013.00169

Vigani, G., and Zocchi, G. (2010). Effect of Fe deficiency on mitochondrial alternative NAD(P)H dehydrogenases in cucumber roots. *J. Plant Physiol.* 167, 666–669. doi: 10.1016/j.jplph.2009.12.006

Wang, L., Yang, H., Zhao, S., Sato, H., Konishi, Y., Beach, T. G., et al. (2011). Expression and localization of mitochondrial ferritin mRNA in Alzheimer's Disease cerebral cortex. *PLoS ONE* 6:e22325. doi: 10.1371/journal.pone.0022325

Winterbourn, C. C. (1995). Toxicity of iron and hydrogen peroxide: the Fenton reaction. *Toxicol. Lett.* 82/83, 969–974. doi: 10.1016/0378-4274(95)03532-X

Wóycicki, R., Witkowicz, J., Gawroński, P., Dąbrowska, J., Lomsadze, A., Pawełkowicz, M., et al. (2011). The genome sequence of the North-European cucumber (*Cucumis sativus* L.) unravels evolutionary adaptation mechanisms in plants. *PLoS ONE* 6:e22728. doi: 10.1371/journal.pone.0022728

Zancani, M., Peresson, M., Biroccio, A., Federici, G., Urbani, A., Murgia, I., et al. (2004). Evidence for the presence of ferritin in plant mitochondria. *Eur. J. Biochem.* 271, 3657–3664. doi: 10.1111/j.1432-1033.2004.04300.x

Conflict of Interest Statement: The authors declare that the research was conducted in the absence of any commercial or financial relationships that could be construed as a potential conflict of interest.

Received: 23 May 2013; accepted: 28 July 2013; published online: 16 August 2013.
*Citation: Vigani G, Tarantino D and Murgia I (2013) Mitochondrial ferritin is a functional iron-storage protein in cucumber (Cucumis sativus) roots. Front. Plant Sci. **4**:316. doi: 10.3389/fpls.2013.00316*
This article was submitted to Plant Nutrition, a section of the journal Frontiers in Plant Science.

frontiers in
PLANT SCIENCE

ORIGINAL RESEARCH ARTICLE
published: 27 August 2013
doi: 10.3389/fpls.2013.00326

Fe deficiency differentially affects the vacuolar proton pumps in cucumber and soybean roots

Marta Dell'Orto*, Patrizia De Nisi, Gianpiero Vigani and Graziano Zocchi

Dipartimento di Scienze Agrarie, Alimentari e Ambientali, Università degli Studi di Milano, Milano, Italy

Edited by:
Jean-Francois Briat, Centre National de la Recherche Scientifique, France

Reviewed by:
Javier Abadía, Consejo Superior de Investigaciones Científicas, Spain
Richard Bligny, Commissariat à l'Energie Atomique et aux Energies Alternatives, France

****Correspondence:***
Marta Dell'Orto, Dipartimento di Scienze Agrarie, Alimentari e Ambientali, Università degli Studi di Milano, Via Celoria 2, 20133 Milano, Italy
e-mail: marta.dellorto@unimi.it

Iron uptake in dicots depends on their ability to induce a set of responses in root cells including rhizosphere acidification through H^+ extrusion and apoplastic Fe(III) reduction by Fe(III)-chelate reductase. These responses must be sustained by metabolic rearrangements aimed at providing the required NAD(P)H, ATP and H^+. Previous results in Fe-deficient cucumber roots showed that high H^+ extrusion is accompanied by increased phosphoenolpyruvate carboxylase (PEPC) activity, involved in the cytosol pH-stat; moreover ^{31}P-NMR analysis revealed increased vacuolar pH and decreased vacuolar [inorganic phosphate (Pi)]. The opposite was found in soybean: low rhizosphere acidification, decreased PEPC activity, vacuole acidification, and increased vacuolar [Pi]. These findings, highlighting a different impact of the Fe deficiency responses on cytosolic pH in the two species, lead to hypothesize different roles for H^+ and Pi movements across the tonoplast in pH homeostasis. The role of vacuole in cytosolic pH-stat involves the vacuolar H^+-ATPase (V-ATPase) and vacuolar H^+-pyrophosphatase (V-PPase) activities, which generating the ΔpH and $\Delta\psi$, mediate the transport of solutes, among which Pi, across the tonoplast. Fluxes of Pi itself in its two ionic forms, $H_2PO_4^-$ predominating in the vacuole and HPO_4^{2-} in the cytosol, may be involved in pH homeostasis owing to its pH-dependent protonation/deprotonation reactions. Tonoplast enriched fractions were obtained from cucumber and soybean roots grown with or without Fe. Both V-ATPase and V-PPase activities were analyzed and the enrichment and localization of the corresponding proteins in root tissues were determined by Western blot and immunolocalization. V-ATPase did not change its activity and expression level in response to Fe starvation in both species. V-PPase showed a different behavior: in cucumber roots its activity and abundance were decreased, while in Fe-deficient soybean roots they were increased. The distinct role of the two H^+ pumps in Pi fluxes between cytoplasm and vacuole in Fe-deficient cucumber and soybean root cells is discussed.

Keywords: V-ATPase, V-PPase, Fe deficiency, cucumber, soybean

INTRODUCTION

Among Strategy I plants (dicots and non-graminaceous monocots) there is an inter- and intra-specific variability in susceptibility to lime-induced Fe deficiency, despite a similar demand for Fe. This variability is strongly related to the ability of plants to enhance the activities involved in the so-called reduction based Strategy I (Marschner et al., 1986; Schmidt, 2006; Kim and Guerinot, 2007; Ivanov et al., 2012), residing at the root cell plasma membrane (PM), which consists of three main steps: (1) acidification of the root apoplast and rhizosphere, mainly due to the enhanced H^+ extrusion driven by the plasma membrane H^+-ATPase (PM-ATPase); (2) reduction of the extracellular Fe^{3+} to Fe^{2+}, which is the only form transported into the root by these species, by means of Fe(III)-chelate reductase (FC-R) which utilizes NAD(P)H as reducing substrate; (3) Fe^{2+} transport into the root symplast by IRT1, a member of the ZIP family.

The variability found among plants in the ability to induce these activities under Fe deficiency is particularly wide for H^+ extrusion (Schmidt, 1999) rather than for FC-R, since Fe(III) reduction is an obligatory step in Fe acquisition by Strategy I plants; in fact, differences were found among differently tolerant species also in the ability to modify the metabolism in order to provide NAD(P)H, ATP and H^+ necessary to sustain the reduction-based response (Zocchi, 2006).

Moreover, a wide variability has been also found among dicots in the production and secretion of compounds facilitating the uptake of Fe, such as flavins and phenolics (Rodríguez-Celma et al., 2013).

In Fe-deficient cucumber plants the high induction of the Strategy I responses is concomitant with the increase in carbohydrate catabolism, through the up-regulation of glycolysis and oxidative pentose phosphate pathway (Rabotti et al., 1995; Espen et al., 2000), providing ATP and reducing equivalents. Moreover, in such conditions, phosphoenolpyruvate carboxylase (PEPC) activity results to be enhanced even more than the primary responses (De Nisi and Zocchi, 2000), leading to PEP consumption (with further increase in the glycolysis rate) and synthesis of organic acids, which are protogenic. Indeed, PEPC activity has been

recognized to play a fundamental role in balancing cytoplasmic pH (Davies, 1973), which, in Fe-deficient cucumber roots, is subject to alkalization due to the exceptionally high rate of H^+ extrusion. Intriguingly, a strong PEPC induction upon Fe deficiency was found in plants with high H^+ extrusion activity such as sugar beet (López-Millán et al., 2000), bean (Bienfait et al., 1989), *Capsicum annuum* (Landsberg, 1986). On the contrary, in plants which do not induce H^+-ATPase activity under Fe starvation, or which induce it at a low rate such as *Medicago ciliaris* (M'sehli et al., 2009a,b) or soybean (Zocchi et al., 2007), PEPC activity and expression level only are weakly or not induced.

Thus, comparing the responses to Fe deficiency in two dicotyledonous plants, cucumber, and soybean, it arises that their different ability to induce the Strategy I responses and in particular apoplast acidification, is accompanied by different degree in the activation of the carbohydrate catabolism, especially in the induction of PEPC (De Nisi and Zocchi, 2000; Zocchi et al., 2007). Accordingly, data from *in vivo* ^{31}P-NMR studies conducted on Fe deficient roots of these two species (Espen et al., 2000; Zocchi et al., 2007) showed some interesting differences: (a) the cytoplasm pH was kept almost constant in root cells of both species, suggesting that efficient pH-stat mechanisms are functioning; conversely, the vacuolar pH increased in cucumber, characterized by active H^+ extrusion to the apoplast, while it was lowered in soybean roots under Fe deficiency; this is consistent with the role of vacuole in cytosolic pH homeostasis under various stresses (Martinoia et al., 2007); (b) moreover, while in Fe-deficient cucumber roots a dramatic fall in the vacuolar inorganic phosphate (Pi) concentration occurred, soybean showed a strong increase of the Pi concentration in the vacuole. These findings led Zocchi et al. (2007) to hypothesize that, besides the already established role of PM-ATPase and PEPC in the pH-stat mechanism under Fe deficiency (Zocchi, 2006 and references therein), also the movements of Pi in its two inorganic forms, $H_2PO_4^-$ predominating in the vacuole and HPO_4^{2-} in the cytosol, across the tonoplast could cooperate in balancing the cytosolic pH, thanks to the buffering activity exerted by its pH-dependent protonation/deprotonation reactions. Little is known about Pi transport across the tonoplast, as no carriers nor channels have been identified so far. What is known is that its entrance into the vacuole has been demonstrated to be driven by the H^+ gradient generated across the tonoplast by the two vacuolar proton pumps (Massonneau et al., 2000; Ohnishi et al., 2007): the vacuolar H^+-ATPase (V-ATPase, EC 3.6.3.14) and the vacuolar H^+-pyrophosphatase (V-PPase, EC 3.6.1.1), which actively transport H^+ inside the vacuolar lumen hydrolyzing ATP and inorganic pyrophosphate (PPi), respectively, thus generating the electrochemical potential difference (ΔpH and $\Delta\psi$) which mediates the secondary active transport of solutes (among which Pi) across the tonoplast (Maeshima, 2001; Hedrich and Marten, 2006; Schumacher, 2006).

Thus, the activity and expression of V-ATPase and V-PPase are expected to be differently regulated in cucumber and soybean in response to Fe deficiency. For this reason, the aim of this work was to characterize how the activities of the vacuolar proton pumps change in cucumber and soybean roots grown under Fe deficiency.

MATERIALS AND METHODS

PLANT MATERIAL AND GROWTH CONDITIONS

Seeds of cucumber (*Cucumis sativus* L., cv. Marketmore 76) and soybean (*Glycine max* L. cv. Elvir from Pioneer, Italy) were sown in wet agriperlite and allowed to germinate in the dark at 26°C for 3 days (cucumber) or 18°C for 6 days (soybean). Seedlings were transferred to a nutrient solution with the following composition: 2 mM $Ca(NO)_3$, 0.75 mM K_2SO_4, 0.65 mM $MgSO_4$, 0.5 mM KH_2PO_4, 10 μM H_3BO_3, 1 μM $MnSO_4$, 0.5 μM $ZnSO_4$, 0.05 μM $(NH_4)Mo_7O_{24}$, and 0.1 mM Fe-EDTA (when added). The pH was brought to 6.0–6.2 with NaOH. Plants in hydroponic cultures were maintained in a growth chamber with a day/night regime of 16/8 h at 24/18°C and a PPFD of 200 μmol m^{-2} s^{-1}. The nutrient solution was changed weekly.

ISOLATION OF TONOPLAST-ENRICHED VESICLES

Vacuolar membrane vesicles were isolated from roots of plants grown for 8 days (cucumber) and 11 days (soybean) in the presence or in the absence of Fe, according to Rea and Poole (1985) with some modifications. About 25 g of roots were homogenized using mortar and pestle in 4 mL/g (fresh weight) of a buffer containing 250 mM sorbitol, 25 mM Tris-Mes pH 7.4, and 5 mM Na-EDTA. Just prior to use, 1 mM DTT and 2 mM PMSF were added to the buffer. The homogenate was filtered through four layers of gauze and centrifuged at 12,000 *g* for 15 min. The supernatant was then centrifuged at 80,000 *g* for 30 min. The pellet was resuspended in 3 mL of a resuspension medium (RM) containing 1.1 M glycerol, 2.5 mM Tris-Mes pH 7.4, 5 mM Na-EDTA, 1 mM DTT, and 0.1 mM PMSF and layered over a 10/23% discontinuous sucrose gradient prepared in RM. After centrifugation at 80,000 *g* (r_{max}) for 2 h in a swinging bucket rotor (SW40), vesicles sedimented at the interface between 10 and 23% sucrose were collected, diluted with three volumes of RM and centrifuged at 80,000 *g* for 30 min. The pellet was finally resuspended in about 150 μL of RM. The vesicles were either used immediately or frozen under liquid N_2 and stored at −80°C until use. Protein concentration was determined by the Bradford method using BSA as the standard (Bradford, 1976).

MEASUREMENT OF H^+-ATPase AND H^+-PPase ACTIVITIES

The activity of the V-ATPase was measured as the rate of ADP-dependent NADH oxidation in a coupled lactate dehydrogenase-pyruvate kinase reaction and ATP-regenerating system at 25°C according to Ward and Sze (1992) with modifications. The reaction mixture (1 mL) contained 25 mM MOPS-BTP buffer pH 7.0, 50 mM KCl, 250 mM sucrose, 3 mM ATP, 1 mM PEP, 0.25 mM NADH, 4.5 mM $MgSO_4$, 0.015% Lubrol, 6 U/mL pyruvate kinase and 12 U/mL lactate dehydrogenase, 20 μg membrane protein. Sodium molybdate 0.1 mM was added to the reaction medium to inhibit acid phosphatase activity. The rate of NADH oxidation was measured as the decrease in A_{340} with time. The assay was performed in the presence and in the absence of 50 mM K-nitrate (a specific inhibitor of the V-type ATPase) and the difference between these two activities was attributed to the vacuolar ATPase. Analog results were obtained using bafilomycin as V-ATPase inhibitor. The degree of purity of the tonoplast membrane preparations was also assessed by measuring marker enzymes for mitochondria

(azide-sensitive H^+-ATPase) and PM (vanadate-sensitive H^+-ATPase) contamination according to Rabotti and Zocchi (1994): around 60% of the total activity was nitrate-sensitive (tonoplast), the remaining 40% was almost totally vanadate-sensitive activity, while the azide-sensitive activity was negligible.

The activity of the V-PPase was measured as the rate of liberation of Pi from PPi in a reaction volume of 250 μl by the Ames (1966) method. According to Rea and Poole (1985) with some modifications, the assay medium consisted of 15 μg membrane protein, 40 mM Tris-Mes pH 8.0, 50 mM KCl, 0.1% Lubrol, 3 mM Na-PPi and 3 mM $MgSO_4$, 0.1 mM Na_2MoO_4 (to inhibit acid phosphatase activity). PPase activity was calculated as half the rate of Pi liberation (1 mol of PPi = 2 mol of Pi).

WESTERN BLOTTING ANALYSIS

Tonoplast enriched fractions extracted from roots of plants grown in the presence and in the absence of Fe were loaded on a discontinuous SDS-polyacrylamide gel (3.75% [w/v] acrylamide stacking gel, and 10% [w/v] acrylamide separating gel). For each sample 10 μg of total protein were loaded.

After SDS-PAGE, the electrophoretic transfer to nitrocellulose membrane filters (Sigma) was performed using a semi-dry blotting system in 10 mM cyclohexylamino-1-propane sulphonic acid (pH 11.0 with NaOH) and 10%(v/v) methanol for 1.5 h at room temperature at 0.8 mA cm^{-2}. After blotting, the membrane was incubated for 1 h in TBS-T buffer (Tris Buffered Saline, 0.1% Tween-20, 5% commercial dried skimmed milk). Polyclonal antibodies raised against a 100 kDa peptide (ELVEINANNDKLQRSYNELC) corresponding to the V-ATPase subunit a and a 73 kDa peptide (CDLVGKIERNIPEDDPRN) corresponding to the V-PPase (Maeshima and Yoshida, 1989; Maeshima, 2001; Kobae et al., 2004) were used. The incubation in primary antibody, diluted 1:1500 in TBS, was carried out for 2 h at room temperature. After rinsing with TBS-T, membranes were incubated at room temperature for 2 h with a 1:10000 diluted secondary antibody (alkaline phosphatase-conjugated anti-rabbit IgG, Sigma). After rinsing in TBS-T membranes were incubated in 5-bromo-4-chloro-3-indolyl phosphate and nitroblue tetrazolium (FAST BCIP/NBT, Sigma).

IMMUNOLOCALIZATION OF VACUOLAR PROTON PUMPS

Apical segments from roots of both 8-day-old cucumber and 11-day-old soybean plants grown in the presence and in the absence of Fe were fixed at 4°C in 100 mM sodium phosphate buffer (pH 7.0) containing 4% paraformaldehyde (w/v), then dehydrated through an ethanol-tertiary butanol series and embedded in paraffin (Paraplast plus, Sigma) as described by Dell'Orto et al. (2002). Serial sections of 5 μm were cut with a microtome up to a distance from the tip of about 1500 μm. Sections were mounted on polylysine-treated slides, deparaffinized in xylene and rehydrated through an ethanol series.

Immunological detection was performed as in Dell'Orto et al. (2002) with some modifications. Sections were incubated for 30 min at room temperature in 3% H_2O_2, then blocked for 1 h in TBS (150 mM NaCl, 25 mM Tris-HCl, pH 7.6) with 2% BSA (w/v). Sections were incubated overnight at 4°C in the same polyclonal antibodies used for Western blot after dilution 1:200 (anti-V-ATPase) and 1:300 (anti-V-PPase) in TBS with 0.5% BSA. After 3 × 5 min washes in TBS, sections were incubated 2 h at room temperature with a biotinylated secondary antibody (anti-rabbit IgG biotin conjugate developed against goat, Sigma) diluted 1:200 in TBS with 0.5% BSA. After 3 × 5 min washes in TBS sections were incubated 30 min in extravidin-peroxidase (ExtrAvidin Peroxidase Staining Kit, Sigma) diluted 1:20. After 3 × 5 min washes in TBS sections were incubated 3–5 min in 0.05 M acetate buffer pH 5.0 containing 5% dimethylformamide, 0.04% 3-amino-9-ethylcarbazole (AEC) and 0.015% H_2O_2 and finally washed in distilled water.

RESULTS

Cucumber and soybean plants grown in Fe-deprived nutrient solution for 8 and 11 days, respectively, showed highly chlorotic leaves and the typical Fe deficiency responses already described in previous works at the root level (Rabotti et al., 1995; Espen et al., 2000; Zocchi et al., 2007): in cucumber, a strong increase in both Fe reduction and H^+ extrusion, by induction of FC-R and PM-ATPase activities respectively, enhanced activity of glycolytic enzymes and PEPC; in soybean, increased Fe reduction activity but weak acidification of the nutrient solution, no induction of the PM-ATPase activity, only slight increase of glycolytic enzymes and decrease of PEPC activity (data not shown).

For this reason, in order to investigate the role played by the two vacuolar H^+ pumps in the pH-stat mechanism under Fe deficiency, vacuolar membrane vesicles were isolated from roots of both 8-day-old cucumber and 11-day-old soybean plants grown in the presence and in the absence of Fe. The V-ATPase activity, determined as the difference between ATP hydrolysis in the presence and in the absence of 50 mM K-nitrate (nitrate-sensitive ATPase) was around 60% of the total ATPase activity for both cucumber and soybean preparations and is shown in **Table 1**. Both in cucumber and in soybean roots this activity is diminished under Fe deficiency. The V-PPase (**Table 2**) shows a similar behavior as the V-ATPase in Fe-deficient cucumber roots, lowering its phosphohydrolytic activity and thus contributing to the vacuole alkalization. On the contrary, in Fe-deficient soybean roots this activity is kept at the same level of the control or even slightly increased.

In order to verify whether the H^+ pump activities are regulated, under Fe deficiency, by decreasing their synthesis, Western bolt analysis was performed on tonoplast enriched fractions using

Table 1 | Nitrate-sensitive H^+-ATPase activity determined on tonoplast enriched fractions isolated from roots of 8-day-old cucumber and 11-day-old soybean plants grown in the presence (control) and in the absence of iron (−Fe).

ATPase activity (nmol NADH mg^{-1} prot min^{-1})			
	Control	**−Fe**	**%**
Cucumber			
	453 ± 31	290 ± 18	−36
Soybean			
	168 ± 12	94 ± 8	−44

Results are the mean values (±SE) of four experiments.

Table 2 | Vacuolar H$^+$-PPase activity determined on tonoplast enriched fractions isolated from roots of 8-day-old cucumber and 11-day-old soybean plants grown in the presence (control) and in the absence of iron (−Fe).

	PPase activity (nmol PPi mg^{-1} prot min^{-1})		
	Control	**−Fe**	**%**
Cucumber			
	215 ± 15	129 ± 11	−40
Soybean			
	179 ± 15	194 ± 11	+8

Results are the mean values (±SE) of four experiments.

two polyclonal antibodies raised against the V- PPase polypeptide and the a subunit of the V-ATPase, respectively. For what concerns the V-ATPase (**Figure 1**) the antibody recognized a polypeptide with a molecular mass of about 95 kDa. The results are consistent with the measured activities, showing a decrease in the protein level in Fe-deficient roots of both cucumber and soybean. Also the V-PPase polypeptide level reflects the activity changes found under Fe deficiency, showing a decreased level of protein in cucumber roots and an accumulation in soybean (**Figure 1**).

Moreover, by using the same antibodies, an *in situ* immunological detection of V-ATPase and V-PPase proteins has been performed on subapical root sections of cucumber and soybean plants grown in the presence and in the absence of Fe (**Figures 2** and **3**) in order to localize this response at the histological level. Root sections in **Figures 2** and **3** were cut at 500–900 μm from the tips, corresponding to the elongation zone. Root sections treated without the primary antibody appeared not stained, indicating that aspecific reactions attributable to the secondary antibody or to extravidin-peroxidase complex did not occur (data not shown).

Overall, it is evident that growth in the absence of Fe leads to the proliferation of root hairs in cucumber (**Figures 2A,C** and **3A,C**) and to increased root diameter in soybean (**Figures 2B,D** and **3B,D**). This is in agreement with the well documented occurrence of root morphological modifications such as swollen root tips and root hairs formation in several Fe-deficient Strategy I plants (Schmidt, 1999; Dell'Orto et al., 2002). Under control growth conditions, the V-ATPase accumulated mainly in the external cell layers of root sections from both cucumber and soybean plants (**Figures 2A,B**). When grown in the absence of Fe, both cucumber and soybean root sections show a markedly reduced level of the V-ATPase (**Figures 2C,D**). The V-PPase protein is widely accumulated in root sections from the control cucumber plants (**Figure 3A**) staining all cortex layers, while under Fe deficiency a strong decrease in V-PPase protein expression occurs (**Figure 3C**), even more drastic than what detected by immunoblot analysis; soybean plants show a lower steady-state level of the V-PPase protein in the same root zone, but under Fe deficiency the PPase is strongly intensified, localizing particularly at the external cell layers and at the endodermis, suggesting an increase expression of the protein, in agreement with the Western blot result.

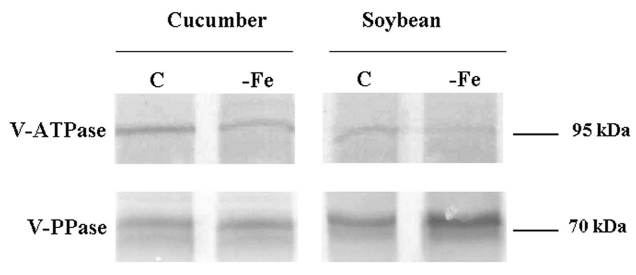

FIGURE 1 | Western blot analysis of proteins (10 μL per lane) present in tonoplast-enriched membrane vesicle fractions isolated from cucumber (left) and soybean (right) roots grown in the presence (C) and in the absence (−Fe) of Fe. Immunostaining was performed using polyclonal antibodies raised against the V-ATPase a subunit and the V-PPase polypeptide respectively.

DISCUSSION

It is becoming more and more evident that, beyond the obligatory step of Fe reduction, the response efficiency in adapting to Fe low availability in Strategy I plants resides on other mechanisms which can be differently regulated in different genotypes. In particular, the highly differentiated aptitude to acidify the apoplast and the rhizosphere, by inducing the PM-ATPase activity, appears to explain the different tolerance exhibited by different genotypes to calcareous soils (Schmidt, 1999; Ksouri et al., 2006; M'sehli et al., 2009b).

By comparing the response to Fe deficiency in two Strategy I species, cucumber and soybean, it emerged that the different aptitudes to induce the PM-ATPase are accompanied by other differences, related to the root cell vacuolar composition: in cucumber roots, in which PM-ATPase and PEPC activities are strongly induced, the vacuole undergoes an alkalization and a depletion of Pi, while in soybean, in which PM-ATPase and PEPC are weakly and/or not induced, the vacuolar pH is decreased and the Pi concentration increased (Espen et al., 2000; Zocchi et al., 2007). Thus, besides the already established role of PM-ATPase and PEPC in the pH-stat mechanism under Fe deficiency (Zocchi, 2006 and references therein), also the movements of Pi across the tonoplast could cooperate in balancing the cytosolic pH, thanks to the buffering activity exerted by its pH-dependent protonation/deprotonation reactions. So, to explain the different movements of Pi in soybean and cucumber, we hypothesized that in Fe-deficient soybean roots the net influx of Pi toward the vacuole would be sustained by the increased H^+ pumping activity of V-ATPase and/or V-PPase. On the contrary, in Fe-deficient cucumber roots we expected a decreased activity of the vacuolar proton pumps, perhaps to counterbalance the strong H^+ consumption by PM-ATPase and leading to a release of H_2PO^- which, by deprotonation in the cytosol, would cooperate in buffering the cytosolic pH.

To test these hypotheses, tonoplast-enriched fractions were extracted from roots of cucumber and soybean plants grown in the presence and in the absence of Fe. In cucumber roots, Fe starvation induced a reduced activity of both the nitrate-sensitive ATPase and the PPase (**Tables 1** and **2**), as expected considering the high ATP and H^+ consumption by PM-ATPase and the increased vacuolar pH detected under these conditions (Rabotti and Zocchi,

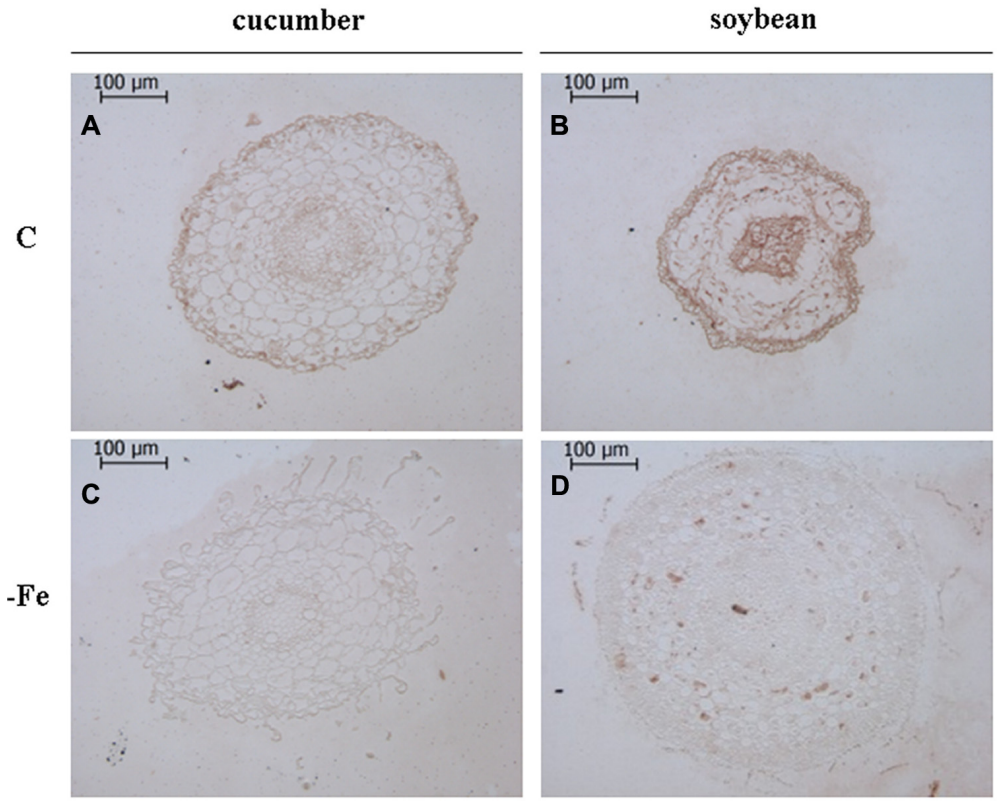

FIGURE 2 | Immunolocalization of V-ATPase in cross sections of 8-day-old cucumber and 11-day-old soybean roots. C: control (Fe-sufficient) cucumber **(A)** and soybean **(B)** root sections; −Fe: Fe-deficient cucumber **(C)** and soybean **(D)** root sections. Root sections were cut at 500–900 µm from the tips, corresponding to the elongation zone. The sections treated without the primary antibody appeared not stained, indicating the absence of any aspecific reaction (data not shown).

1994; Espen et al., 2000). This finding fits well with the scenario depicted in **Figure 4A**, resuming all the data available so far for cucumber: the increased PM-ATPase activity induces the alkalinization of the cytoplasm pH which, in turn, activates the PEPC (Zocchi, 2006). Moreover, the high need for H^+ is in part fulfilled also by the increased glycolysis rate; in part by the lower H^+ transport into the vacuole due to the reduced vacuolar pump activity, in part, as a consequence, by the net efflux of $H_2PO_3^-$, which, at the cytosolic pH is subject to dissociation into H^+ and HPO_3^{2-} (the pKa being 6.8).

For Fe-deficient soybean the proposed scenario is different, as shown in **Figure 4B**. In soybean roots the activity of the vacuolar pumps are differently affected by Fe deficiency: unexpectedly the V-ATPase activity is lowered more or less at the same degree as in cucumber, despite the low activity of the antagonistic PM-ATPase, showing to be not responsible for the acidification of the vacuole detected by Zocchi et al. (2007). On the contrary, the slight increase of the V-PPase activity found in Fe-deficient soybean roots, besides fitting well with the already mentioned vacuole acidification, is in agreement with several works reporting the increase of such activity under mineral deficiencies and various other stresses which affect the ATP synthesis rate (Maeshima, 2000 and references therein). In fact PPi, despite its high-energy phosphoanhydride bond, is indeed a low-cost substrate, generated as a by-product of several metabolic processes characteristic of actively growing cells, such as the synthesis of proteins, nucleic acid, and cellulose (Maeshima, 2000; Gaxiola et al., 2007). Thus, the ability of soybean roots to induce the V-PPase rather than the V-ATPase activity in response to a stress condition, which deeply affects the mitochondrial efficiency and thus the ATP supply (Vigani, 2012), could be interpreted as a metabolic plasticity leading to an alternative adaptive mechanism. In soybean roots, differently to what happens in cucumber the glycolysis rate does not increase significantly (Zocchi et al., 2007).

Protein amounts of V-ATPase subunit a and V-PPase were slightly reduced in the tonoplast fractions extracted from Fe-deficient cucumber roots (**Figure 1**). Thus, the observed reduction in the activity of both tonoplast H^+ pumps can be, at least in part, attributed to changes in the expression of the encoding genes or in the amounts of proteins. As well, the amount of V-ATPase subunit a detected by Western blot in Fe-deficient soybean roots was lowered (**Figure 1**), consistently with the specific activity, while the amount of V-PPase (**Figure 1**), whose activity was found to be increased by Fe starvation, was higher. This is not an obvious result since it has been found, especially for the V-PPase, that the activity changes in response to nutritional stresses are due to post-translational modulation rather than to increased amount of

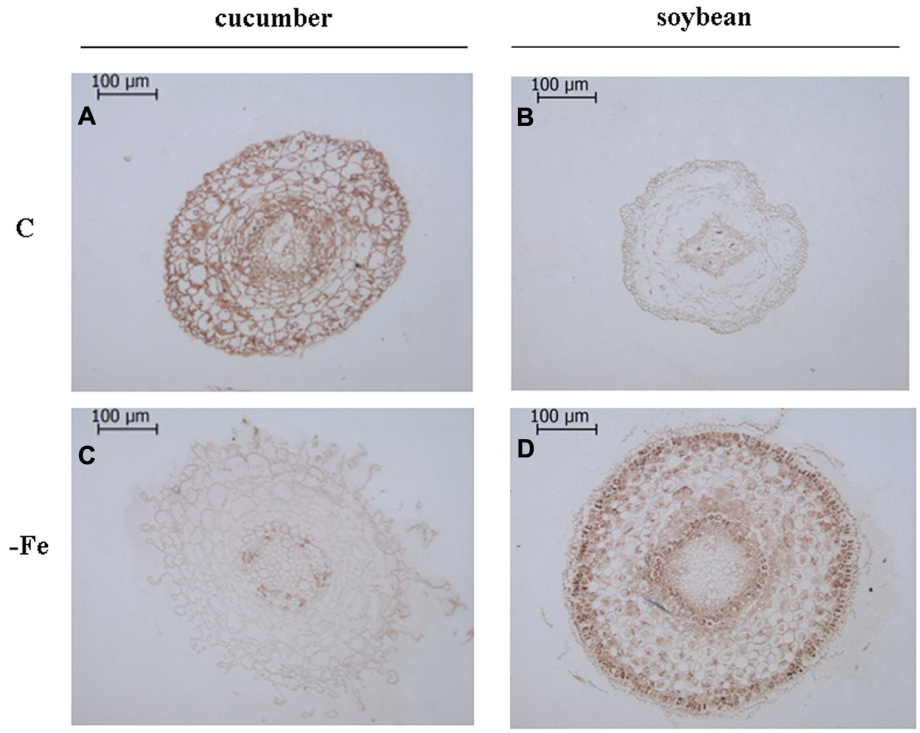

FIGURE 3 | Immunolocalization of V-PPase in cross sections of 8-day-old cucumber and 11-day-old soybean roots. C: control (Fe-sufficient) cucumber **(A)** and soybean **(B)** root sections; −Fe: Fe-deficient cucumber **(C)** and soybean **(D)** root sections. Root sections were cut at 500–900 µm from the tips, corresponding to the elongation zone. The sections treated without the primary antibody appeared not stained, indicating the absence of any aspecific reaction (data not shown).

the proteins (Maeshima, 2000; Ohnishi et al., 2007; Kabała and Janicka-Russak, 2011).

Several post-translational regulation mechanisms have been proposed both for V-ATPase and for V-PPase in plants: one of the possible mechanisms involved in the regulation of V-ATPase is reversible phosphorylation (Liu et al., 2004; McCubbin et al., 2004; Hong-Hermesdorf et al., 2006); moreover, a phosphorylation-dependent specific interaction with 14-3-3 protein has been found to be involved (Klychnikov et al., 2007). Since a putative 14-3-3 interaction motif has been identified also in V-PPase from *Vitis vinifera*, the existence of a coordinated regulation of the three H^+ pumps involved in pH-homeostasis in the cytosol can be postulated (Gaxiola et al., 2007). The post-translational regulation of plant V-ATPase has been reviewed by Ratajczak (2000).

It has been found that in young growing tissues in which the anabolism is high, such as for instance seedling hypocotyls, the V-PPase activity determined on vacuolar membrane fraction was higher respect to the V-ATPase activity, due to a higher content of the former enzyme, this being consistent with the availability of large amounts of PPi in such tissues. On the contrary, in mature cells, in which the anabolism decreases leading to a lower PPi availability, V-PPase activity has been found to be lower than that of V-ATPase (Maeshima, 2000 and references therein). In this work the immunohistochemical technique allowed us to localize the changes in protein amounts in the root portion in which the response to Fe deficiency actually occurs, i.e., the sub apical region, corresponding to the elongation zone, characterized by actively growing tissues and thus by a high anabolic activity. Under Fe-sufficient conditions the relative enrichment of the V-PPase protein respect to the V-ATPase could be seen only in cucumber roots; while in soybean roots the V-ATPase seems to be more expressed than the V-PPase. Moreover, the differences found between Fe-sufficient and Fe-deficient roots in the expression level of the two proteins appear to be stronger than what evidenced by western blot. This could be probably explained by the fact that the tonoplast enriched fraction was obtained from the whole root system, leading to a dilution effect in the control samples, since the two proton pumps, but especially the V-PPase, are particularly expressed in the actively growing tissues (Nakanishi and Maeshima, 1998; Maeshima, 2000; Gaxiola et al., 2007) as the root meristems and elongation zones are. With this regard, the immunohistochemical approach seems provide better assessment, since it allows to detect the expression of the two proton pumps in a more limited region, in which the Strategy I responses actually take place (Dell'Orto et al., 2002; Schmidt et al., 2003).

Overall, the results obtained in this work, together with those previously reported by Espen et al. (2000) and Zocchi et al. (2007) suggest that cucumber and soybean, although both adopting the Strategy I for Fe uptake, follow different models for what concerns the metabolic adaptations needed to sustain the response to Fe

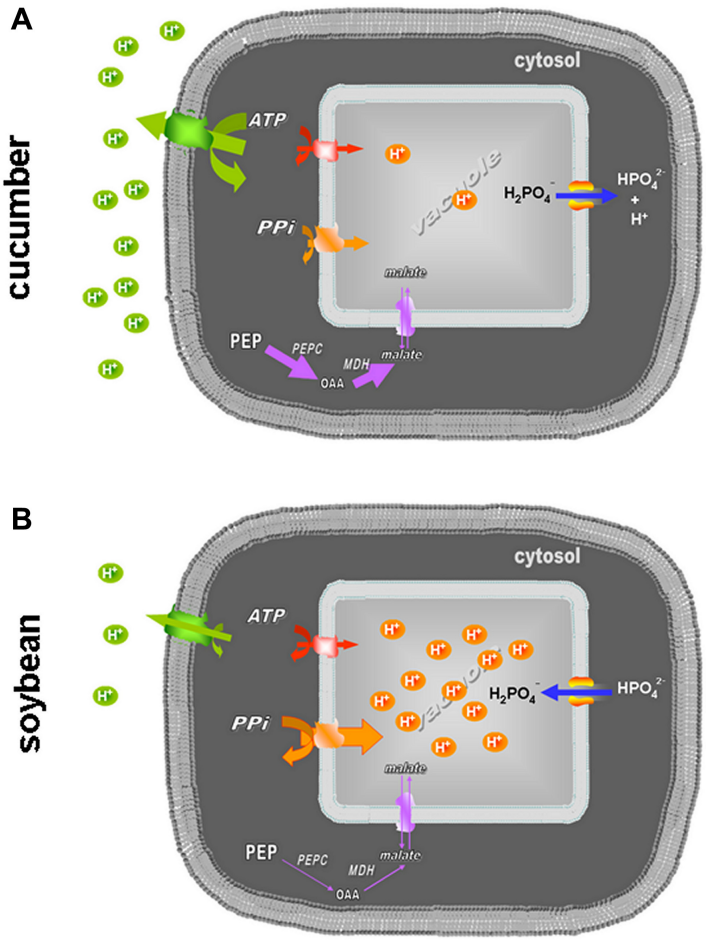

FIGURE 4 | Representation of the different roles of the vacuolar proton pumps and Pi movements across the tonoplast in cucumber (A) and soybean (B) roots under Fe deficiency. The activities of the PM-ATPase, V-ATPase, V-PPase, and PEPC are visualized as differently marked lines; the net Pi fluxes are described through the arrow orientation.

starvation. In particular these two species resulted to differently manage the cellular pH homeostasis by differently modulating the V-PPase and, as a consequence, by differently regulating the Pi fluxes across the tonoplast.

It is still to be elucidated how the vacuolar proton pumps regulation is coordinated with that of the other activities involved in the pH-stat of the cell, i.e., the PM-ATPase and the PEPC. Moreover, also the fluxes of malate produced by PEPC across the tonoplast could be involved in the cytosolic pH homeostasis as proposed by Martinoia et al. (2007) and by **Figure 4**, since under Fe deficiency the malate concentration is strongly increased in several dicotyledonous species, among which cucumber (Rabotti et al., 1995). Future work should then be addressed to elucidate the role of malate and the regulation of the vacuolar malate transporter, since acidification of the plant cytosol has been found to stimulate the expression of the gene encoding for it in *Arabidopsis* (*At*tDT; Hurth et al., 2005).

ACKNOWLEDGMENT

We wish to thank Dr. Maeshima (Nagoya University, Japan) for the kind gift of the antibodies against V-ATPase and V-PPase.

REFERENCES

Ames, B., and N. (1966). Assay of inorganic phosphate, totals phosphate, and phosphatases. *Methods Enzymol.* 8, 115–118. doi: 10.1016/0076-6879(66)08014-5

Bienfait, H. F., Lubberding, H. J., Heutink, P., Lindner, L., Visser, J., Kaptein, R., et al. (1989). Rhizosphere acidification by iron deficient bean plants: the role of trace amounts of divalent metal ions. *Plant Physiol.* 90, 359–364. doi: 10.1104/pp.90.1.359

Bradford, M. M. (1976). A rapid and sensitive method for the quantitation of microgram quantities of protein utilizing the principle of protein-dye binding. *Anal. Biochem.* 72, 248–254. doi: 10.1016/0003-2697(76)90527-3

Davies, D. D. (1973). Control of and by pH. *Symp. Soc. Exp. Biol.* 27, 513–520.

Dell'Orto, M., Pirovano, L., Villalba, J. M., González Reyes, J. A., and Zocchi, G. (2002). Localization of the plasma membrane H^+-ATPase in Fe-deficient cucumber roots by immunodetection. *Plant Soil* 241, 11–17. doi: 10.1023/A:1016030514200

De Nisi, P., and Zocchi, G. (2000). Phosphoenolpyruvate carboxylase in cucumber (*Cucumis sativus* L.) roots under iron deficiency: activity and kinetic characterization.

J. Exp. Bot. 51, 1903–1909. doi: 10.1093/jexbot/51.352.1903

Espen, L., Dell'Orto, M., De Nisi, P., and Zocchi, G. (2000). Metabolic responses in cucumber (*Cucumis sativus* L.) roots under Fe deficiency: a 31P-nuclear magnetic resonance in vivo study. *Planta* 210, 985–992. doi: 10.1007/s004250050707

Gaxiola, R. A., Palmgren, M. G., and Schumacher, K. (2007). Plant proton pumps. *FEBS Lett.* 581, 2204–2214. doi: 10.1016/j.febslet.2007.03.050

Hedrich, R., and Marten, I. (2006). 30-year progress of membrane transport in plants. *Planta* 224, 725–739. doi: 10.1007/s00425-006-0341-x

Hong-Hermesdorf, A., Brux, A., Gruber, A., Gruber, G., and Schumacher, K. (2006). A WNK kinase binds and phosphorylates V-ATPase subunit C. *FEBS Lett.* 580, 932–939. doi: 10.1016/j.febslet.2006.01.018

Hurth, M. A., Suh, S. J., Kretzschmar, T., Geis, T., Bregante, M., Gambale, F., et al. (2005). Impaired pH homeostasis in *Arabidopsis*, lacking the vacuolar dicarboxylate transporter and analysis of carboxylic acid transport across the tonoplast.*Plant Physiol.* 137, 901–910. doi: 10.1104/pp.104.058453

Ivanov, R., Brumbarova, T., and Bauer, P. (2012). Fitting into the harsh reality: regulation of iron deficiency responses in dicotyledonous plants. *Mol. Plant* 5, 27–42. doi: 10.1093/mp/ssr065

Landsberg, E. C. (1986). Function of rhizodermal transfer cells in Fe stress response mechanism of *Capsicum annum* L. *Plant Physiol.* 82, 511–517. doi: 10.1104/pp.82.2.511

Kabała, K., and Janicka-Russak, M. (2011). Differential regulation of vacuolar H^+-ATPase and H^+-PPase in *Cucumis sativus* roots by zinc and nickel. *Plant Sci.* 180, 531–539. doi: 10.1016/j.plantsci.2010.11.013

Kim, S. A., and Guerinot, M. L. (2007). Mining iron: iron uptake and transport in plants. *FEBS Lett.* 581, 2273–2280. doi: 10.1016/j.febslet.2007.04.043

Klychnikov, O. I., Lill, K. W., Li, H., and de Boer, A. H. (2007). The V-ATPase from etiolated barley (*Hordeum vulgare* L.) shoots is activated by blue light and interacts with 14-3-3 proteins. *J. Exp. Bot.* 58, 1013–1023. doi: 10.1093/jxb/erl261

Kobae, Y., Uemura, T., Sato, M. H., Ohnishi, M., Mimura, T., and Maeshima, M. (2004). Zinc transporter of *Arabidopsis thaliana* AtMTP1 is localized to vacuolar membranes and implicated in zinc homeostasis. *Plant Cell Physiol.* 45, 1749–1758. doi: 10.1093/pcp/pci015

Ksouri, R., M'rah, S., Gharsalli, M., and Lachaâl, M. (2006). Biochemical responses to true and bicarbonate induced iron deficiency in grapevine genotypes. *J. Plant Nutr.* 29, 305–315. doi: 10.1080/01904160500476897

Landsberg, E. C. (1986). Function of rhizodermal transfer cells in Fe stress response mechanism of *Capsicum annum* L. *Plant Physiol.* 82, 511–517. doi: 10.1104/pp.82.2.511

Liu, G. S., Chen, S., Chen, J., and Wang, X. C. (2004). Identification of the phosphorylation site of the V-ATPase subunit A in maize roots. *Acta Bot. Sin.* 46, 428–435.

López-Millán, A. F., Morales, F., Andaluz, S., Gogorcena, Y., Abadía, A., De Las Rivas, J., et al. (2000). Responses of sugar beet roots to iron deficiency. Changes in carbon assimilation and oxygen use. *Plant Physiol.* 124, 885–897. doi: 10.1104/pp.124.2.885

Maeshima, M. (2000). Vacuolar H^+-pyrophosphatase. *Biochim. Biophys. Acta* 1465, 37–51. doi: 10.1016/S0005-2736(00)00130-9

Maeshima, M. (2001). Tonoplast transporters: organization and function. *Annu. Rev. Plant Physiol. Plant Mol. Biol.* 52, 469–497. doi: 10.1146/annurev.arplant.52.1.469

Maeshima, M., and Yoshida, S. (1989). Purification and properties of vacuolar membrane proton-translocating inorganic pyrophosphatase from mung bean. *J. Biol. Chem.* 264, 20068–20073.

Marschner, H., Römheld, V., and Kissel, M. (1986). Different strategies in higher plants in mobilization and uptake of iron. *J. Plant Nutr.* 9, 695–713. doi: 10.1080/01904168609363475

Martinoia, E., Maeshima, M., and Neuhaus, H. E. (2007). Vacuolar transporters and their essential role in plant metabolism. *J. Exp. Bot.* 58, 83–102. doi: 10.1093/jxb/erl183

Massonneau, A., Martinoia, E., Dietz, K.-J., and Mimura, T. (2000). Phosphate uptake across the tonoplast of intact vacuoles isolated from suspension-cultured cells of *Catharanthus roseus* (L.) G. Don. *Planta* 211, 390–395. doi: 10.1007/s004250000297

McCubbin, A. G., Ritchie, S. M., Swanson, S. J., and Gilroy, S. (2004). The calcium-dependent protein kinase HvCDPK1 mediates the gibberellic acid response of barley aleurone through regulation of vacuolar function. *Plant J.* 39, 206–218. doi: 10.1111/j.1365-313X.2004.02121.x

M'sehli, W., Dell'Orto, M., Donnini, S., De Nisi, P., Zocchi, G., Abdelly, C., et al. (2009a). Variability of metabolic responses and antioxidant defense in two lines of *Medicago ciliaris* to Fe deficiency. *Plant Soil* 320, 219–230. doi: 10.1007/s11104-008-9887-7

M'sehli, W., Dell'Orto, M., De Nisi, P., Donnini, S., Abdelly, C., Zocchi, G., et al. (2009b). Responses of two ecotypes of *Medicago ciliaris* to direct and bicarbonate-induced iron deficiency conditions. *Acta Physiol. Plant.* 31, 667–673. doi: 10.1007/s11738-009-0288-1

Nakanishi, Y., and Maeshima, M. (1998). Molecular cloning of vacuolar H^+-pyrophosphatase and its developmental expression in growing hypocotyl of mung bean. *Plant Physiol.* 116, 589–597. doi: 10.1104/pp.116.2.589

Ohnishi, M., Mimura, T., Tsujimura, T., Mitsuhashi, N., Washitani-Nemoto, S., Maeshima, M., et al. (2007). Inorganic phosphate uptake in intact vacuoles isolated from suspension-cultured cells of *Catharanthus roseus* (L.) G. Don under varying Pi status. *Planta* 225, 711–718. doi: 10.1007/s00425-006-0379-9

Rabotti, G., De Nisi, P., and Zocchi, G. (1995). Metabolic implications in the biochemical responses to iron deficiency in cucumber (*Cucucmis sativus* L.) roots. *Plant Physiol.* 107, 1195–1199. doi: 10.1104/pp.107.4.1195

Rabotti, G., and Zocchi, G. (1994). Plasma membrane-bound H^+-ATPase and reductase activities in Fe-deficient cucumber roots. *Physiol. Plant.* 90, 779–785. doi: 10.1111/j.1399-3054.1994.tb02537.x

Ratajczak, R. (2000). Structure, function, and regulation of the plant vacuolar H.-translocating ATPase. *Biochim. Biophys. Acta* 1465, 17–36. doi: 10.1016/S0005-2736(00)00129-2

Rea, P. A., and Poole, R. J. (1985). Proton-translocating inorganic pyrophosphatase in red beet (*Beta vulgaris* L.) tonoplast vesicles. *Plant Physiol.* 77, 46–52. doi: 10.1104/pp.77.1.46

Rodríguez-Celma, J., Lin, W. D., Fu, G. M., Abadía, J., López-Míllán, A. F., and Schmidt, W. (2013). Mutually exclusive alterations in secondary metabolism are critical for the uptake of insoluble iron compounds by *Arabidopsis* and *Medicago truncatula*. *Plant Physiol.* doi: 10.1104/pp.113.220426 [Epub 2013 Jun 4].

Schmidt, W. (1999). Mechanisms and regulation of reduction based iron uptake in plants. *New Phytol.* 141, 1–26. doi: 10.1046/j.1469-8137.1999.00331.x

Schmidt, W. (2006). "Iron stress responses in roots of Strategy I plants," in *Iron Nutrition in Plants and Rhizospheric Microorganisms*, eds L. L. Barton and J. Abadía (Dordrecht: Springer), 229–250.

Schmidt, W., Michalke, W., and Schikora, A. (2003). Proton pumping by tomato roots. Effect of Fe deficiency and hormones on the activity and distribution of plasma membrane H^+-ATPase in rhizodermal cells. *Plant Cell Environ.* 26, 361–370. doi: 10.1046/j.1365-3040.2003.00967.x

Schumacher, K. (2006). Endomembrane proton pumps: connecting membrane and vesicle transport. *Curr. Opin. Plant Biol.* 9, 595–600. doi: 10.1016/j.pbi.2006.09.001

Vigani, G. (2012). Discovering the role of mitochondria in the iron deficiency-induced metabolic responses of plants. *J. Plant Physiol.* 169, 1–11. doi: 10.1016/j.jplph.2011.09.008

Ward, J. M., and Sze, H. (1992). Subunit composition and organization of the vacuolar H^+-ATPase from oat roots. *Plant Physiol.* 99, 170–179. doi: 10.1104/pp.99.1.170

Zocchi, G. (2006). "Metabolic changes in iron-stressed dicotyledonous plants," in *Iron Nutrition in Plants and Rhizospheric Microorganisms*, eds L. L. Barton and J. Abadía (Dordrecht: Springer), 359–370.

Zocchi, G., De Nisi, P., Dell'Orto, M., Espen, L., and Marino Gallina, P. (2007). Iron deficiency differently affects metabolic responses in soybean roots. *J. Exp. Bot.* 58, 993–1000. doi: 10.1093/jxb/erl259

Conflict of Interest Statement: The authors declare that the research was conducted in the absence of any commercial or financial relationships that could be construed as a potential conflict of interest.

Received: 04 June 2013; paper pending published: 17 June 2013; accepted: 01 August 2013; published online: 27 August 2013.

Citation: Dell'Orto M, De Nisi P, Vigani G and Zocchi G (2013) Fe deficiency differentially affects the vacuolar proton pumps in cucumber and soybean roots. Front. Plant Sci. ***4****:326. doi: 10.3389/fpls.2013.00326*

This article was submitted to Plant Nutrition, a section of the journal Frontiers in Plant Science.

frontiers in
PLANT SCIENCE

ORIGINAL RESEARCH ARTICLE
published: 26 July 2013
doi: 10.3389/fpls.2013.00283

Arabidopsis thaliana Yellow Stripe1-Like4 and Yellow Stripe1-Like6 localize to internal cellular membranes and are involved in metal ion homeostasis

S. S. Conte[1†], H. H. Chu[2†], D. Chan-Rodriguez[1,3], T. Punshon[2], K. A. Vasques[3,4], D. E. Salt[5] and E. L. Walker[1]*

[1] Biology, University of Massachusetts, Amherst, MA, USA
[2] Biology, Dartmouth College, Hanover, NH, USA
[3] Plant Biology Graduate Program, University of Massachusetts, Amherst, MA, USA
[4] Biogen-Idec, Cambridge, MA, USA
[5] Institute of Biological and Environmental Sciences, University of Aberdeen, Aberdeen, Scotland

Edited by:
Gianpiero Vigani, Università degli Studi di Milano, Italy

Reviewed by:
Graziano Zocchi, Università degli Studi di Milano, Italy
Jian F. Ma, Okayama University, Japan

***Correspondence:**
E. L. Walker, Biology, University of Massachusetts, Amherst, 611 North Pleasant St., Amherst, 01003 MA, USA
e-mail: ewalker@bio.umass.edu
† These authors have contributed equally to this work.

Several members of the Yellow Stripe1-Like (YSL) family of transporter proteins are able to transport metal-nicotianamine (NA) complexes. Substantial progress has been made in understanding the roles of the Arabidopsis YSLs that are most closely related to the founding member of the family, ZmYS1 (e.g., AtYSL1, AtYSL2 and AtYSL3), but there is little information concerning members of the other two well-conserved YSL clades. Here, we provide evidence that AtYSL4 and AtYSL6, which are the only genes in Arabidopsis belong to YSL Group II, are localized to vacuole membranes and to internal membranes resembling endoplasmic reticulum. Both single and double mutants for YSL4 and YSL6 were rigorously analyzed, and have surprisingly mild phenotypes, in spite of the strong and wide-ranging expression of YSL6. However, in the presence of toxic levels of Mn and Ni, plants with mutations in YSL4 and YSL6 and plants overexpressing GFP-tagged YSL6 showed growth defects, indicating a role for these transporters in heavy metal stress responses.

Keywords: nickel, nicotianamine, yellow stripe-like, metal transporters, manganese, iron, tonoplast, endomembrane

INTRODUCTION

Members of the Yellow Stripe Like (YSL) family of transporters are required for normal iron, zinc, manganese and copper movement in both vegetative and reproductive tissues (DiDonato et al., 2004; Koike et al., 2004; Roberts et al., 2004; Schaaf et al., 2004; Murata et al., 2006; Gendre et al., 2007; Aoyama et al., 2009; Curie et al., 2009; Inoue et al., 2009; Lee et al., 2009; Chu et al., 2010; Sasaki et al., 2011; Zheng et al., 2011, 2012). Work on the YSL family started with cloning of the maize *Yellow stripe1* (*ZmYS1*) gene (Curie et al., 2001). Transport through YS1 is the primary route by which roots of grasses take up iron from the soil. The grasses, a group that includes most of the world's staple grains (e.g., rice, wheat and corn), use a chelation strategy for primary iron uptake. In response to iron starvation, grasses secrete phytosiderophores (PS), which are non-proteinogenic amino acid derivatives of the mugineic acid (MA) family that form stable chelates with Fe(III) (Tagaki et al., 1984). This accomplishes solubilization of the otherwise nearly insoluble soil iron. The *ZmYS1* gene encodes a protein that is distantly related to the Oligopeptide Transporter (OPT) family of proteins (Curie et al., 2001; Yen et al., 2001) and functionally complements yeast strains that are defective in iron uptake when grown on medium containing Fe(III)-PS complexes.

Although non-grass plant species neither synthesize nor efficiently use PS, Yellow Stripe1-Like (YSL) proteins are found in monocots and dicots, as well as gymnosperms, ferns and mosses. The major physiological role of the YSLs appears to be in the movement of metals bound to the ubiquitous plant metal chelator, nicotianamine (NA). It has been well-established that several YSL proteins are indeed able to transport metal-NA complexes (DiDonato et al., 2004; Koike et al., 2004; Roberts et al., 2004; Schaaf et al., 2004; Le Jean et al., 2005; Murata et al., 2006; Gendre et al., 2007; Harada et al., 2007) and that NA is essential for long-distance transport of metals throughout the plant body (Schuler et al., 2012). NA is capable of forming complexes with manganese (Mn), Fe(II), cobalt (Co), zinc (Zn), nickel (Ni) and copper (Cu) in increasing order of affinity (Anderegg and Ripperger, 1989). However, little is known about the role of NA in intracellular transport of metals. Pich et al. used an NA-specific antibody to localize NA in the vacuoles of Fe-loaded tomato cells, which suggests a role for NA in the vacuolar storage of excess Fe (Pich et al., 2001). Recently, Haydon et al. showed that overexpression of the transporter Zinc Induced Facilitator1 (ZIF1) caused an increase in vacuolar NA in roots with a concomitant increase in vacuolar Zn, thus implicating NA in the vacuolar storage of Zn (Haydon et al., 2012). Because YSLs are known metal-NA transport proteins, it is reasonable that members of the YSL family could participate in the intracellular transport of NA.

Now that several plant genomes have been sequenced, it is clear that higher plants possess four distinct, well-conserved groups

of YSL proteins, and that one of these is unique to grass species (Curie et al., 2009; Yordem et al., 2011). Substantial progress has been made in understanding the roles of the YSLs that are most closely related to ZmYS1 [e.g., AtYSL1, AtYSL2 and AtYSL3 (DiDonato et al., 2004; Waters et al., 2006; Chu et al., 2010) and OsYSL2 (Koike et al., 2004; Inoue et al., 2006; Ishimaru et al., 2010)], but there is little information concerning members of the other two conserved YSL clades. The most basal clade of the YSL family tree contains YSLs from the moss *Physcomitrella patens*, the lycophyte *Selaginella moellendorffii*, OsYSL5 and 6 from rice, HvYSL5 from barley and AtYSL4 and 6 from Arabidopsis (Yordem et al., 2011; Zheng et al., 2011). Details about the members of this group have just begun to emerge. Interestingly, Jaquinod et al. identified AtYSL4 and AtYSL6 as members of the tonoplast proteome (Jaquinod et al., 2007). The barley protein, HvYSL5, was found to localize either to vesicles or the tonoplast based on bombardment of onion skin cells with the ORF of *HvYSL5* fused to *smGFP* (Zheng et al., 2011). Localization of the rice protein, OsYSL6, was inconclusive; bombardment experiments indicated that regardless of whether GFP was fused to the N- or C-terminus, the GFP signal appeared cytoplasmic (Sasaki et al., 2011). Very recently, Divol et al. (2013) used immunofluorescence imaging to conclude that the Arabidopsis AtYSL4 and AtYSL6 proteins are located in plastids. Taken together, these localization data suggest that YSLs in the most basal clade may play roles in the intracellular transport of metal chelates.

In this study, we investigated the role of the two closely related Arabidopsis group II YSL genes, *AtYSL4* (AT5G41000) and *AtYSL6* (AT3G27020). *AtYSL4* and *AtYSL6* mRNAs are abundantly expressed in Arabidopsis, especially during seed germination, but surprisingly, neither null single (*ysl4* and *ysl6*) mutants nor the *ysl4ysl6* double mutant exhibits strong visible phenotypes. The levels of several transition metals are modestly perturbed in both single and double mutants, but localization of metals in the seeds is unaltered. Using transient transformation of GFP fusions into poorly-conserved cytosolic domains of the proteins, we observed a pattern that is consistent with localization of AtYSL4 and AtYSL6 to vacuolar membranes within the cell. When the same YSL6mid GFP construct was stably transformed into Arabidopsis, we observed a pattern of fluorescence consistent with localization to internal membranes resembling the endoplasmic reticulum. Loss of *AtYSL4*, *AtYSL6* or both confers almost no measurable phenotypic change other than an alteration in the plants' sensitivity to excess manganese. When excess Mn and Ni are added to iron deficient medium, alterations in root growth occur in both mutant and overexpressing plants. Taken together, these data indicate a role for AtYSL4 and AtYSL6 in intracellular transport of metal-NA complexes.

MATERIALS AND METHODS

PLANT GROWTH

Plate-grown plants

Seeds were sterilized in eppendorf tubes (1.5 mL) or a 15 mL falcon tube depending on the quantity and suspected level of contamination of the seeds. Seeds were soaked in 70% ethanol and 0.05% Triton X-100 for 10 min with occasional vortexing, then three times with 100% ethanol. Seeds were gently placed onto sterile Whatman paper and allowed to dry. They were then either imbibed in sterile 0.1% agarose at 4°C for 3–5 days, or were plated, wrapped in foil, and stored at 4°C for 3 days prior to transfer to the growth chamber Plants were grown on sterile 1X MS agar medium with or without antibiotics. Plates were placed in an upright position so that the roots grew along the surface rather than inside the agar, which allowed for easy transfer. Plates were placed in an incubator at 22°C with 16 h of light and 8 h of darkness.

Soil-grown plants

Seeds imbibed in distilled water at 4C in the dark for 3 days, and then were sown directly onto Metro-Mix (Sungro Horticulture) treated with Gnatrol (Valent Biosciences) to control fungus gnats. Growth chamber conditions were the same as for plate-grown plants.

AtYSL4 AND *AtYSL6* EXPRESSION ANALYSIS USING RT-PCR

Plant parts were ground in 1.5 mL tubes using RNase-free disposable pestles (VWR, Batavia, Illinois). Total RNA was isolated using the RNeasy plant mini kit (Qiagen, Valencia, CA), followed by DNase treatment using the DNA-free kit (Ambion, Austin, Texas). The total RNA concentration was quantified using a spectrophotometer (260 nm; Beckman DU640B, Fullerton, CA), and confirmation of RNA quality was performed by visualization on a 1X TBE gel stained with ethidium bromide.

QUANTITATIVE RT-PCR

RNA isolation and RT reactions were performed as described (Waters et al., 2006). Quantitative real-time PCR was also performed as described (Chu et al., 2010). YSL4- and YSL6-specific primer sequences were as follows: for AtYSL4, oAtYSL4.qPCR Fw (5′-TCGTTCCACTTCGCAAGGTGATG-3′) and oAtYSL4.qPCR Rev (5′-ACATTGCTGTAGCGGTTCCACTG-3′); for AtYSL6, oAtYSL6.qPCR Fw (5′-TCGTTCCGTTACGCAAGGTG-3′) and oAtYSL6.qPCR Rev (5′-AGCTCCAGTGTTGGTGTGGAAG-3′).

PROMOTER::GUS CONSTRUCTS

The *AtYSL4* promoter region containing 785 bp upstream of the *AtYSL4* initiating ATG was cloned to create a C-terminal translational fusion to the GUS reporter gene. The *AtYSL6* promoter region containing 601 bp upstream of the *AtYSL6* initiating ATG was cloned to create a C-terminal translational fusion to the GUS reporter gene. The *AtYSL4p*::GUS and *AtYSL6p*::GUS constructs were then stably introduced into Arabidopsis using the floral dip method (Clough and Bent, 1998). T1 seeds were germinated on 1X MS medium with 50 μM kanamycin to select for transformants, and seedlings were transferred to soil 7 days after germination.

PREPARATION OF SAMPLES FOR MINERAL ANALYSIS

For soil-grown plants, leaf samples were collected 20 days after sowing and dried in an oven at 60°C. ICP-MS was performed as described previously (Lahner et al., 2003).

CONSTRUCTION OF GFP-MID TAGGED PROTEINS

AtYSL4 (At5g41000) and *AtYSL6* (At3g27020) cDNAs were amplified by RT-PCR using Platinum *Taq* DNA Polymerase High

Fidelity (Invitrogen, Carlsbad, CA). *AtYSL4* cDNA was amplified using the primers 5′-TCTGAGAGTGAGAGGAATCACTGAAAA-3′ and 5′-GTCTCGGATGGTCTAAAGTACATACAAATGGGTG-3′. *AtYSL6* cDNA was amplified using the primers 5′-GCTAAAACATGGGGACGGAGATCCC-3′ and 5′-CTCTCTCTTGCTGAGGACGGTCCAAA-3′. *AtYSL4* and *AtYSL6* cDNA were then cloned into the Gateway vector pCR8/GW/TOPO (Invitrogen, Carlsbad, CA). Using the "megaprimer" method, *smGFP* (Davis and Vierstra, 1998) was incorporated into *AtYSL4* between position 1053 and 1054 in the cDNA (corresponding to amino acid position 351) and *AtYSL6* between position 1086 and 1087 in the cDNA (corresponding to amino acid position 362). Based on protein structure predictions, these positions correspond to extracellular loops that are weakly conserved among YSLs. The primers 5′-GCAACAAAAGCTCCAGACAAGGGATCCAAGGAGATATAACAATGA-3′ and 5′-GTCGGTAAAGACAGGTAGGTTGTGTTTGTATAGTTCATCCATGCCAT-3′ (for *AtYSL4*), and 5′-CAATCTACCCATTGTTACCGACGGGATCCAAGGAGATATAACAATGA-3′ and 5′-GAAGCTTCACTGTCATCTACACCTTTGTATAGTTCATCCATGCCAT-3′ (for *AtYSL6*) were used to amplify the plasmid psmGFP (CD3-326, available from ABRC) to create megaprimers containing the smGFP sequence flanked by specific YSL sequences. These megaprimers were gel purified and used in a modified site-directed mutagenesis protocol to introduce the smGFP sequence into the AtYSL4 and AtYSL6 clones described above. This was accomplished using 440 ng of purified megaprimers, 50 ng of target vector (either *YSL4* or *YSL6* cDNA in pCR8/GW/TOPO, described above), 0.6 mM dNTP mix, 1X Phusion HF buffer (New England Biolabs, Ipswich, MA), 0.25 μl of Phusion enzyme (New England Biolabs, Ipswich, MA), and the following PCR conditions: an initial denaturation at 98°C for 2 min, followed by 18 cycles of 98°C for 50 s, 50°C for 50 s, and 72°C for 5 min, followed by a final elongation of 72°C for 7 min. After DpnI digestion to remove the methylated parent plasmid, 2 ml of each reaction was used to transform TOP10™ chemically competent *E. coli* (Invitrogen, Carlsbad, CA). Positive clones were verified by restriction digestion and sequencing to ensure incorporation of the full smGFP sequence. An LR recombination reaction was then performed to transfer *AtYSL4-GFPmid* and *AtYSL6-GFPmid* into the vector pB7WG2 (Karimi et al., 2002) for subsequent transient expression in Arabidopsis protoplasts in addition to stable expression in Arabidopsis plants.

PROTOPLAST ISOLATION AND TRANSFORMATION

Protoplasts were isolated using the Tape-Arabidopsis Sandwich method (Wu et al., 2009). Transformations were carried out using 5×10^4 protoplasts in 200 μL of MMg solution (0.4 M mannitol, 15 mM $MgCl_2$, 4 mM MES pH 5.7) mixed with 30 μg of plasmid DNA at room temperature. An equal volume of freshly prepared transformation solution [40% w/v PEG (MW 4000), 0.1 M $CaCl_2$, 0.2 M mannitol] was added and allowed to incubate for 7 min. Protoplasts were then carefully washed three times with modified W5 solution (154 mM NaCl, 125 mM $CaCl_2$, 5 mM KCl, 5 mM glucose, 2 mM MES pH 5.7), resuspended in 200–500 μL modified W5, and incubated at room temperature in Mattek™ dishes for 16 to 24 h. *AtYSL4-GFPmid* or *AtYSL6-GFPmid* in pB7GW2 was co-transformed with CD3-976, which is available from TAIR (www.arabidopsis.org) and contains γ-TIP fused to mCherry.

STAINING OF PROTOPLASTS WITH FM-464

The lipophilic dye FM-464 was applied to transformed protoplasts at a final concentration of 100 μM for 10 min on ice. The dye was then washed off, and protoplasts were incubated at RT for 1 h to allow the dye to penetrate the cells prior to confocal imaging.

PLANT TRANSFORMATION

All constructs to be used in plant transformation experiments were transferred to *Agrobacterium tumefaciens* GV3101 via electroporation. *Arabidopsis thaliana* plants were transformed by Agrobacterium-mediated transformation using the floral dip method (Clough and Bent, 1998). Primary transformants were selected by spraying with the herbicide Finale (Bayer, Research Triangle Park, NC). Individual progeny of selfed primary transformants were examined by confocal microscopy.

CONFOCAL MICROSCOPIC ANALYSIS

Protoplasts were imaged using a Zeiss LSM 510 Meta Confocal System equipped with a 63x oil immersion objective. An argon 488 nm laser was used for excitation of GFP and a HeNe 543 laser was used for excitation of FM-464 and mCherry. Emission of GFP was collected between 505 and 530 nm and emission of FM-464 and mCherry was collected between 585 and 615 nm.

DETERMINATION OF ROOT GROWTH RATE

Seeds were plated directly onto medium containing 1% phytoagar, and imbibed for 72 h at 4C in the dark. Plates were then transferred into the growth chamber and allowed to grow vertically. Photographs of the plates were taken every 24 h, and successive images were aligned using ImageJ. The difference in root length over successive 24 h periods was recorded and used to calculate the root growth rate in mm/h.

RESULTS

EXPRESSION OF *AtYSL4* AND *AtYSL6*

To understand the level of expression of *AtYSL4* and *AtYSL6* relative to other members of the YSL family, we performed quantitative RT-PCR (**Figure 1**). *AtYSL6* is strongly expressed in both shoots and roots, and its mRNA is present at levels similar to *AtYSL3*. *AtYSL4* mRNA is expressed at lower levels, and it is expressed at similar levels in both shoots and roots. Because mRNA levels for *AtYSL1*, *AtYSL2*, and *AtYSL3* decrease in plants that have been grown under iron deficiency, we examined the level of *AtYSL4* and *AtYSL6* mRNA in iron deficient plants. The mRNA levels for *AtYSL4* and *AtYSL6* are not strongly affected by iron deficiency (**Figure 1**). Semi-quantitative RT-PCR (not shown) indicates that *AtYSL4* and *AtYSL6* mRNA levels are also not strongly affected by deficiency for other transition metals.

PATTERN OF *AtYSL4* AND *AtYSL6* EXPRESSION

In order to determine the cell type specific expression of *AtYSL4* and *AtYSL6*, we constructed β-glucuronidase (GUS) reporter constructs containing the promoter sequences of

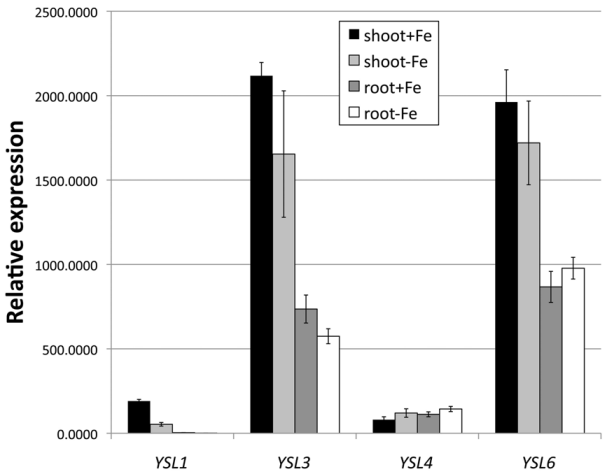

FIGURE 1 | Expression of AtYSL1, AtYSL3, AtYSL4 and AtYSL6 by quantitative RT-PCR. Plants were grown on MS medium for 10 days and then transferred to MS and MS lacking iron for 5 days. mRNA levels were quantified in both shoots and roots.

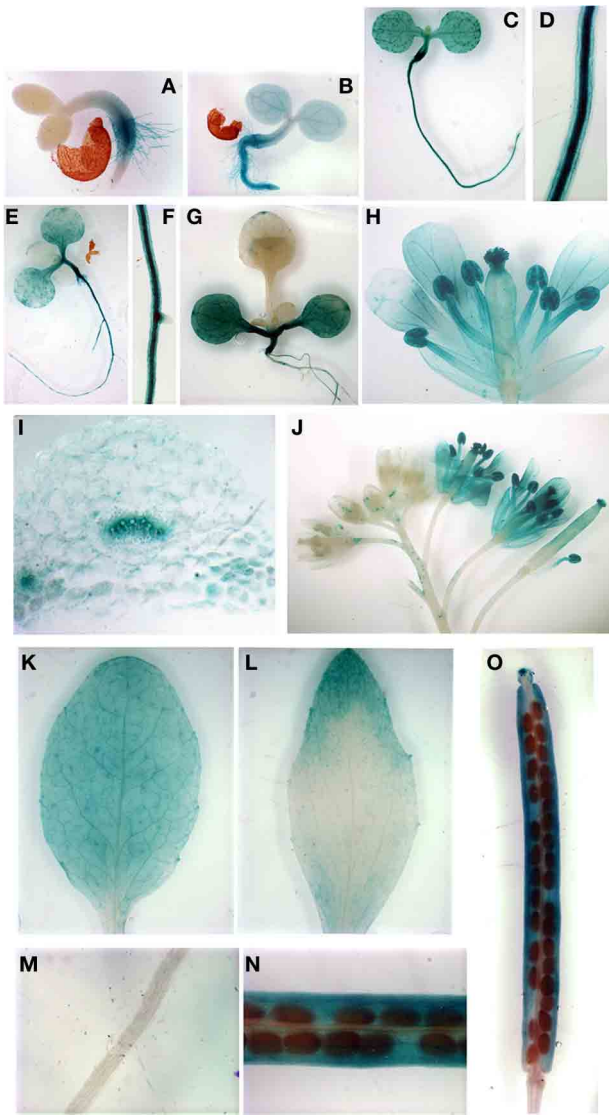

FIGURE 2 | Histochemical staining of AtYSL4 promoter-GUS reporter plants. (A) Seedling at 48 h **(B)** Seedling at 72 h **(C)** Seedling at 5 days **(D)** Root of 5-day-old seedling **(E)** Seedling at 8 days **(F)** Root of 8-day-old seedling **(G)** Seedling at 11 days **(H)** Flower at 36 days **(I)** Cross-section of rosette leaf at 36 days **(J)** Flowers at 36 days illustrating mature and immature flowers **(K)** Rosette leaf at 37 days **(L)** Cauline leaf at 37 days **(M)** Root at 24 days **(N,O)** Siliques at 24 days.

AtYSL4 or *AtYSL6* fused in-frame to GUS (*AtYSL4p:GUS* and *AtYSL6p:GUS*). In germinating seedlings, *AtYSL4p:GUS* was expressed strongly in roots and root hairs at 48 h post-germination (**Figure 2A**); by 72 h, *AtYSL4p:GUS* expression had spread to cotyledons (**Figures 2B,C**) where it remained strong at 11 d post-germination (**Figure 2E**). Only minimal *AtYSL4p:GUS* expression was detected in true leaves (**Figures 2E,G**). Expression was also strong in flowers, especially older flowers, sepals and pollen (**Figures 2H,J**). A cross-section through a rosette leaf revealed that *AtYSL4p:GUS* expression was associated with xylem tissues (**Figure 2I**). In rosette leaves, expression was low and diffuse in interveinal regions (**Figure 2K**), and in cauline leaves, expression was restricted to older areas of the leaf (**Figure 2L**). In fruits, *AtYSL4p:GUS* was expressed most strongly in the veins of the siliques, with only weak expression in the developing seeds (**Figures 2N,O**). Expression was absent from roots at 24 d (**Figure 2M**).

AtYSL6p:GUS plants exhibited stronger staining in roots of very young developing seedlings as compared to *AtYSL4p:GUS* plants (**Figures 3A,B**), and by 5, 8 and 11 d, expression was evident in both cotyledons and true leaves (**Figures 3C,E,G**). Most of the cells in mature rosette leaves showed strong *AtYSL6p:GUS* expression, including very strong staining in the vasculature (**Figure 3K**). A rosette leaf cross section revealed that *AtYSL6p:GUS* expression was associated with xylem tissues (**Figure 3I**). Similar to *AtYSL4*, *AtYSL6* was expressed in the older regions of cauline leaves (**Figure 3L**), albeit more strongly than what was observed for *AtYSL4*. However, *AtYSL6* was not as strongly expressed in sepals and anther filaments, and expression was not completely restricted to older flowers (**Figures 3H,J**). *AtYSL6* expression in young roots was more diffuse than *AtYSL4*, and the expression was more closely associated with the root vasculature (compare **Figures 2D,F** with **Figures 3D,F**). Roots at 24 d expressed *AtYSL6p:GUS* in all tissue layers (**Figure 3M**). Similar to *AtYSL4*, *AtYSL6* was expressed in veins of siliques but was also evident to some extent in the developing seeds themselves (**Figures 3N,O**).

LOCALIZATION OF AtYSL4 AND AtYSL6 PROTEINS

Although several YSLs are known to localize to the plasma membrane (DiDonato et al., 2004; Aoyama et al., 2009; Inoue et al., 2009; Lee et al., 2009; Chu et al., 2010), a proteomics study of Arabidopsis vacuoles identified AtYSL4 and AtYSL6 in the tonoplast proteome (Jaquinod et al., 2007). To investigate this, we used Arabidopsis protoplasts to transiently express

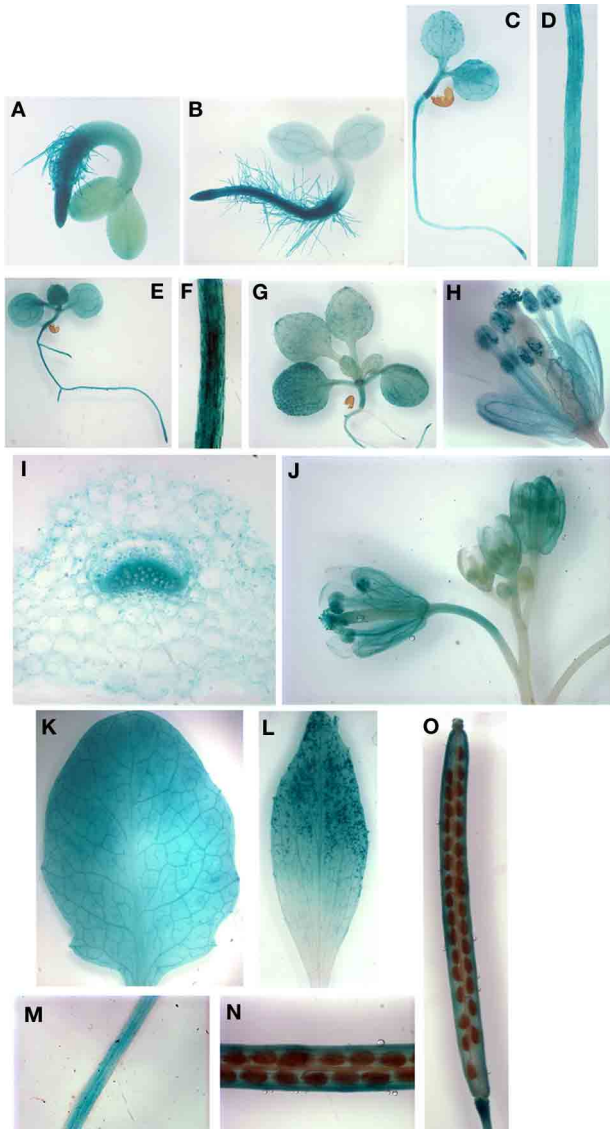

FIGURE 3 | Histochemical staining of AtYSL6 promoter-GUS reporter plants. (A) Seedling at 48 h **(B)** Seedling at 72 h **(C)** Seedling at 5 days **(D)** Root of 5-day-old seedling **(E)** Seedling at 8 days **(F)** Root of 8-day-old seedling **(G)** Seedling at 11 days **(H)** Flower at 27 days **(I)** Cross-section of rosette leaf at 27 days **(J)** Flowers at 24 days illustrating mature and immature flowers **(K)** Rosette leaf at 27 days **(L)** Cauline leaf at 37 days **(M)** Root at 24 days **(N,O)** Siliques at 24 days.

GFP-tagged AtYSL4 and AtYSL6. When protoplasts were transformed with either AtYSL4 or AtYSL6 tagged with GFP at the C-terminus, very few cells became labeled. Indeed, we were unable to observe fluorescence signals in the case of AtYSL6. In the small number of YSL4-GFP transformants identified, we observed fluorescent label accumulating within the ER (data not shown). Based on these findings, we tentatively concluded that end-labeled AtYSL4 and AtYSL6 were being abnormally processed, and we constructed versions of AtYSL4 and AtYSL6 that contain GFP labels in non-conserved regions within each protein (AtYSL4-GFPmid and AtYSL6-GFPmid). We then co-transformed protoplasts with either *AtYSL4-GFPmid* or *AtYSL6-GFPmid* in addition to γ*-TIP-mCherry*, which served as a vacuolar marker. In a separate experiment, we stained protoplasts transformed with *AtYSL6-GFPmid* with FM-464 to provide a marker for internal membranes. It was evident that GFPmid-tagged AtYSL4 localized to the tonoplast membrane, based on colocalization with γ-TIP-mCherry (**Figure 4**, **Top row**). Additionally, AtYSL6 also localized to the tonoplast membrane, based on colocalization with γ-TIP-mCherry and FM-464 (**Figure 4**, **middle and bottom rows**, respectively).

The *AtYSL6-GFPmid* construct was also used to stably transform Arabidopsis plants. The resulting transgenic plants were morphologically normal, indicating that overexpression of this membrane protein did not cause serious problems with the endomembrane system. In the stable transformants, the GFP signal was most readily observed in the guard cells (**Figures 5A–I**) Notably, not every cell contained fluorescent material, in spite of the fact that the *AtYSL6-GFPmid* construct was driven by a constitutive promoter. Most often, the signal appeared as a bright spot in each guard cell that did not coincide with the chloroplasts (**Figures 5A–C**). To identify the bright spots, which are positioned similarly to guard cell nuclei, we used DAPI stain (**Figures 5D–F**). From this analysis we observed that the green fluorescence was positioned around the nuclei in the guard cells. The signal is not coming from the nuclear envelope, since often it does not completely surround the nucleus. Probably the signal emanates from the endoplasmic reticulum (ER) surrounding nuclei. Another commonly observed pattern of fluorescence was more diffuse staining of internal membranous networks that may be ER (**Figures 5G–I**). Finally, we often observed fluorescence in bright bodies similar to the small vacuoles that we had observed in protoplasts. These bright bodies were observed in pavement (leaf epidermal) cells (**Figures 5J–L**), in root cells (not shown) and in root hairs (**Figures 5M–O**) Consistent with our observations in transiently transformed protoplasts, we never observed fluorescence associated with the large central vacuole in any cell.

CHARACTERIZATION OF *ysl4* AND *ysl6* MUTANT ALLELES

In order to understand the *in planta* functions of AtYSL4 and AtYSL6, we obtained mutant alleles from the SALK collection of sequence-indexed T-DNA insertions (Alonso et al., 2003). A single insertion line (SALK_025447; *ysl4-2*) was confirmed for AtYSL4, in which the T-DNA is inserted in the fifth exon (**Figure 6A**). The line SALK_006995 is annotated as an insertion into *AtYSL4*, but we were not able to amplify flanking sequences from this line, and thus concluded that the line is likely misannotated. Two alleles were identified with T-DNA insertions in *AtYSL6* (SALK_119560; *ysl6-4* and SALK_093392; *ysl6-5*). These insertions were in the first intron and last exon, respectively (**Figure 6A**). To determine whether these T-DNA insertions caused loss of function mutations, RT-PCR was performed on plants homozygous for each allele (**Figure 6B**). No *AtYSL4* mRNA was detected in the leaves of *ysl4-2* plants, and no *AtYSL6* mRNA was detected in the leaves of *ysl6-4* and *ysl6-5* plants, although small amounts of contaminating gDNA were detected in these

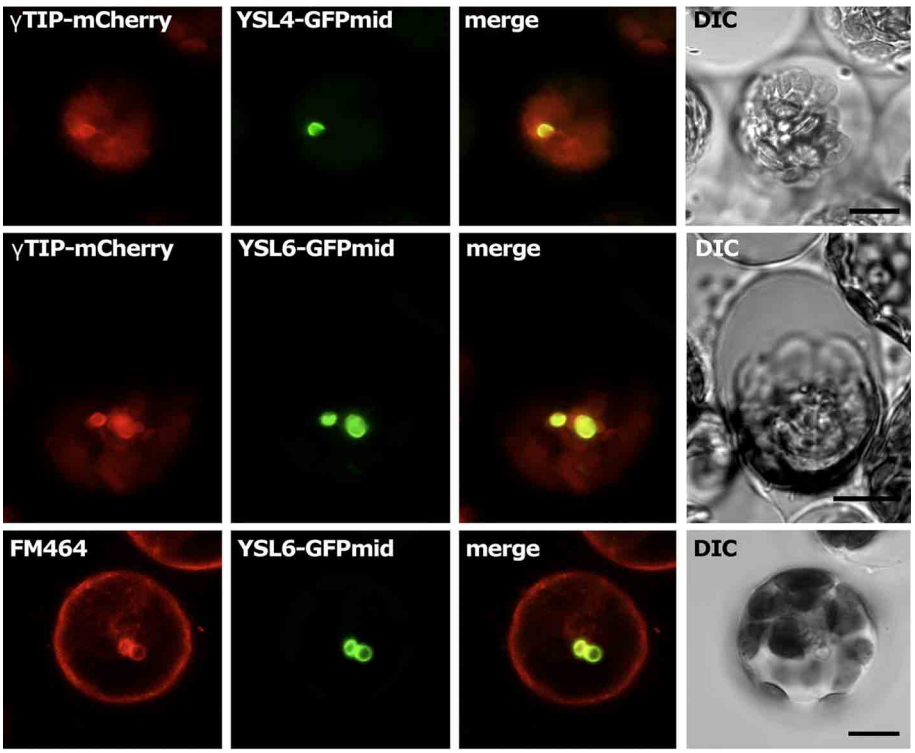

FIGURE 4 | Subcellular localization of AtYSL4 and AtYSL6 in protoplasts. Each horizontal row of four images shows (left to right) red fluorescence, green fluorescence, merged red and green images, and differential interference contrast. **Top row:** protoplast co-transformed with *AtYSL4-GFPmid* and γ-*TIP-mCherry*. **Middle row:** protoplast co-transformed with *AtYSL6-GFPmid* and γ-*TIP-mCherry*. **Bottom row:** protoplast transformed with *AtYSL6-GFPmid* and stained with the membrane-selective dye FM-464. Scale bar = 10 um.

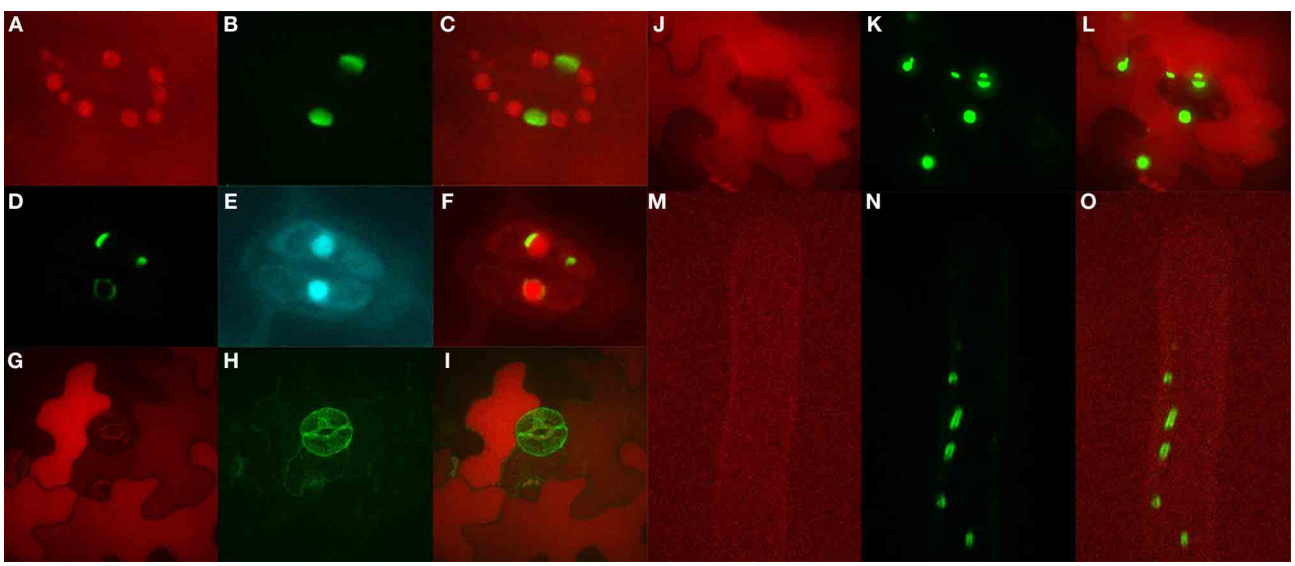

FIGURE 5 | Subcellular localization of AtYSL6 in stably transformed plants. The AtYSL6-GFPmid construct, controlled by a ubiquitin promoter, was stably transformed into Arabidopsis plants. **(A)** Red fluorescence of guard cell chloroplasts. **(B)** Green fluorescence in guard cells from **(A)**. **(C)** Overlay of **(A,B). (D)** Green fluorescence in guard cells. **(E)** DAPI fluorescence in guard cells from **(D)**. **(F)** Overlay of **(D,E)**. **(G)** Red autofluorescence in leaf epidermis and guard cells. **(H)** Green fluorescence in cells from **(G)**. **(I)** Overlay of **(G,H)**. **(J)** Red autofluorescence in leaf epidermis and guard cells. **(K)** Green fluorescence in cells from **(J). (L)** Overlay of **(J,K)**. **(M)** Red autofluorescence in a root hair. **(N)** Green fluorescence in root hair from **(M)**. **(O)** Overlay of **(M,N)**.

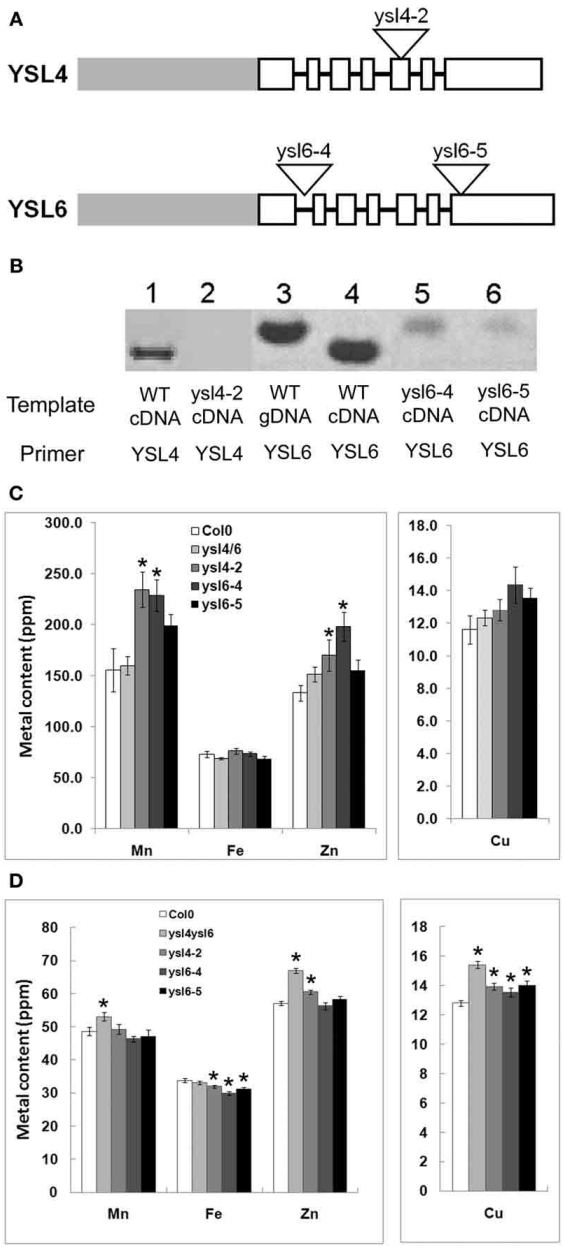

FIGURE 6 | ysl4-2, ysl6-4 and ysl6-5 null mutants. (A) Schematic representation of the structure of AtYSL4 and AtYSL6. Gray bars represent promoter regions. White boxes represent exons. Black lines represent introns (not to scale). Triangles represent insertion sites of T-DNAs in the Salk T-DNA insertion mutants, ysl4-2 (SALK_025447), ysl6-4 (SALK_119560), and ysl6-5 (SALK_093392). **(B)** Detection of AtYSL4 and AtYSL6 mRNA. RT-PCR was performed using RNA extracted from the leaves of wild type (WT), ysl4-2, ysl6-4, ysl6-5, and ysl4ysl6 plants. WT genomic DNA (gDNA) was also included as a control. Lane 1: WT cDNA with AtYSL4 specific primers. Lane 2: ysl4-2 cDNA with AtYSL4 specific primers. Lane 3: WT gDNA with AtYSL6 specific primers. Lane 4: WT cDNA with YSL6 specific primers. Lane 5: ysl6-4 cDNA with YSL6 specific primers. Lane 6: ysl6-5 cDNA with AtYSL6 specific primers. **(C)** and **(D)** ICP-MS determination of metal concentrations of Col-0, ysl4-2, ysl6-4, ysl6-5, and ysl4ysl6. Results are given as ppm. Error bars represent standard error. Each sample contains 10 replicates. Asterisks indicate $P < 0.05$ by *t*-test. **(C)** Metal concentrations of leaves. **(D)** Metal concentrations of seeds.

samples. Thus, each of these T-DNA insertions appears to have caused a null mutation.

We determined the metal levels of each single mutant and the *ysl4ysl6* double mutants using ICP-MS (**Figures 6C,D**). In leaves of plants grown in soil, some statistically significant differences in metal levels were observed, but these did not form a clear pattern. For example, *ysl6-4* mutants had elevated levels of Mn and Zn, yet *ysl6-5* mutants had no significant differences from WT Col-0 plants. Homozygous *ysl4-2* plants also had high Mn and Zn in leaves. Interestingly, however, the *ysl4ysl6* double mutant plants had normal levels of all four metals (Mn, Fe, Zn, and Cu) in leaves.

In the seeds of the mutant plants, more consistent changes in metal levels were observed (**Figure 6D**). The *ysl4-2* mutant seeds had elevated levels of Zn and Cu and a decreased level of Fe. Both *ysl6-4* and *ysl6-5* mutant seeds had low Fe and elevated Cu. In the *ysl4ysl6* double mutant seeds, Zn and Cu were higher than normal, similar to the *ysl4* and *ysl6* single mutants. However, Fe levels in the seeds of the *ysl4ysl6* double mutants were not significantly different from WT Col-0 despite the single mutants' low seed Fe. The double mutants had elevated Mn levels, which were also not observed in any of the single mutants. The altered metal accumulation phenotypes observed in these mutants suggest that, as expected, AtYSL4 and AtYSL6 play roles in metal ion homeostasis in Arabidopsis.

No obvious growth defects were noted in the single mutants when grown in soil or on MS agar plates (data not shown), so we identified double mutants that were homozygous for both *ysl4-2* and *ysl6-5*. Like the single mutants, the *ysl4ysl6* double mutants had no obvious growth defects when grown in soil or on MS agar plates (data not shown). We then tested for differential tolerance or sensitivity to metal deficiency in plants either germinated directly on plates lacking Fe, Cu, Mn, or Zn (**Figure 7**), or in seedlings germinated on plates with normal nutrients, and then transferred to plates lacking one metal (**Figure 8**). No differences in growth or appearance were identified.

We next examined whether *ysl4-2*, *ysl6-5* and *ysl4ysl6* mutants were differentially affected by high levels of iron in the growth medium. Seeds were plated directly onto medium containing either no additional Fe, 500 μM Fe-citrate, or 500 μM Na-citrate. Our initial experiment indicated that, although single mutants were not affected, *ysl4ysl6* double mutants were more sensitive to 500 μM Fe-citrate based on chlorosis and smaller seedling size (**Figure 9A**). This is finding is consistent with the results presented recently by Divol et al. (Divol et al., 2013). However, we discovered that the addition of 500 μM Fe-citrate caused the pH of the medium to decrease from 5.7–4.0. We thus set up an additional experiment in which we buffered the growth medium such that plates containing 500 μM Fe-citrate remained at pH 5.7. After 2 weeks of growth, we did not observe any differences in seedling appearance on these plates, and there were no measurable differences in chlorophyll content (**Figures 9B–D**). Thus, without the lowered pH brought about by the inclusion of high concentrations of Fe-citrate in the medium, the double mutant plants were not unusually sensitive to excess Fe.

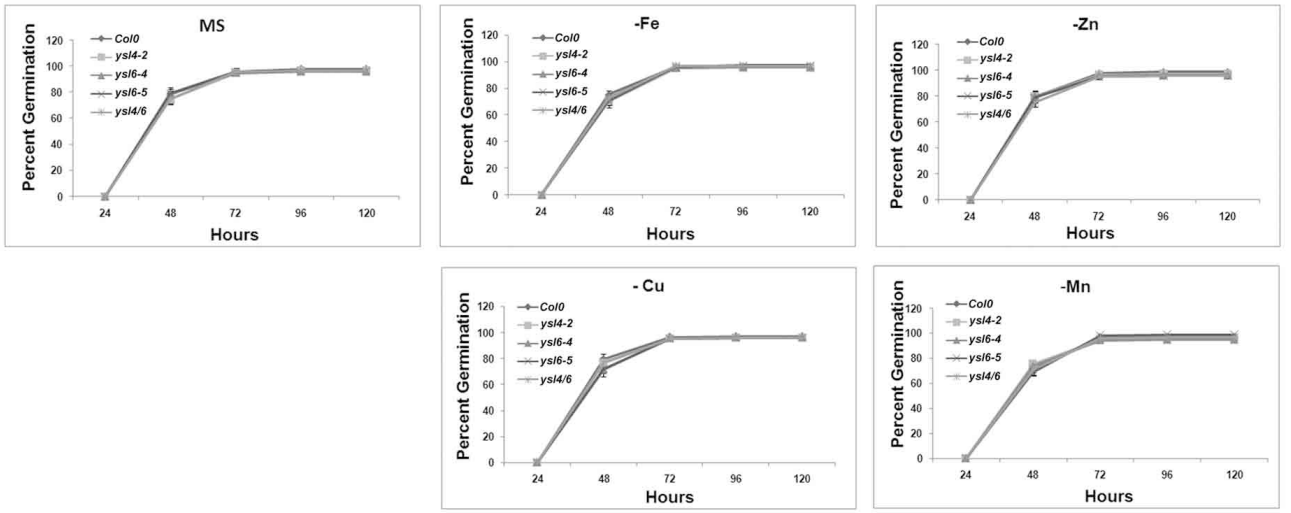

FIGURE 7 | Germination response to metal deficiency. Seeds of ysl6-4, ysl6-5, ysl4-2 or the ysl4ysl6 double mutant were germinated on complete MS medium or MS medium lacking Fe, Zn, Cu, or Mn. Germination (scored as emergence of the radicle) was scored every 24 h. Three replicates of 100 seeds each were scored. Error bars indicate standard error of the mean.

LOCALIZATION OF METALS IN *ysl4* AND *ysl6* MUTANT SEEDS

Because altered seed metal levels were observed using ICP-MS, we examined whether metals were also mis-localized in the seeds of the mutants. We used synchrotron x-ray fluorescence microtomography (SXFM) to visualize metals directly in the seeds of *ysl4-2*, *ysl6-4*, *ysl6-5* and the double mutant *ysl4ysl6* (**Figure 10**). Fe localizes to the provascular strands of the hypocotyl, radicle and cotyledons; Mn to the abaxial (lower) epidermis of the cotyledons; and Zn and Cu localize throughout the embryo in a diffuse pattern (Kim et al., 2006). The patterns of metal localization in the single and double mutants were unaltered, indicating that AtYSL4 and AtYSL6 are not required for proper localization of metals in Arabidopsis seeds, even though the levels of these metals are altered in the mutants (**Figure 6D**).

INTERACTION OF AtYSL4 AND AtYSL6 WITH AtYSL1 AND AtYSL3

It has been established that loss of AtYSL1 and AtYSL3 causes altered metal accumulation in the seeds (Waters et al., 2006; Chu et al., 2010). Because the weak phenotypes of the *ysl4*, *ysl6*, and *ysl4ysl6* mutants were difficult to interpret, we constructed double mutants of *ysl1ysl4*, *ysl1ysl6* and *ysl3ysl6*. Previously, we have shown that *ysl1ysl3* double mutants have severe developmental defects that include chlorosis, male infertility, impaired or aborted seed development, and altered levels of metals in both vegetative structures and seeds (Waters et al., 2006; Chu et al., 2010). Single *ysl1* mutants have mild phenotypes that include low iron in seeds and elevated NA levels (Le Jean et al., 2005), while single *ysl3* mutants are not distinguishable from WT plants. Neither *ysl1ysl4*, *ysl1ysl6* nor *ysl3ysl6* plants displayed strong phenotypes either on soil or MS agar plates (data not shown). Plants had normal chlorophyll levels and normal fertility (data not shown). Additionally, metal localization was not disrupted in either the *ysl1ysl6* or the *ysl3ysl6* double mutant lines based on SXFM experiments (**Figure 10**).

SINGLE MUTANTS *ysl4-2, ysl6-4, ysl6-5* AND THE DOUBLE MUTANT *ysl4ysl6* ARE SENSITIVE TO HIGH LEVELS OF MANGANESE

Recently, Sasaki *et al.* uncovered a Mn-sensitivity phenotype in rice *OsYSL6* knockout lines. This finding prompted us to examine *AtYSL4* and *AtYSL6* mutants for manganese sensitivity phenotypes. After 21 days of growth, we measured the fresh weights of mutant and wild-type plants grown on MS agar plates containing 0, 1, and 1.5 mM additional Mn. We found that at 1 mM additional Mn, *ysl4-2*, *ysl6-4*, *ysl6-5* and *ysl4ysl6* double mutants had significant decreases in fresh weight compared to Col-0 (**Figure 11**). At 1.5 mM additional Mn, all plants were severely affected, with only *ysl6-5* showing a significantly lower fresh weight compared to Col-0. When the plants grown for an additional 2 weeks on 1/2X MS plates supplemented with 1 mM Mn, the double mutant plants became green, and grew larger than either single mutants or WT Col0 (**Figure 12**). Double mutant plants transformed with the *YSL6midGFP* construct did not show growth recovery, but remained small and yellow on 1 mM Mn (**Figure 12**). Since the *YSL6midGFP* construct restores a WT phenotype (poor growth during prolonged exposure to 1 mM Mn), it appears to be functional *in vivo*.

We also measured the rate of root growth in early seedlings exposed to 1 mM $MnSO_4$, as well as 90 um $NiCl_2$ and 500 uM $ZnSO_4$, to see whether mutation of *YSL4* and *YSL6* or overexpression of *YSL6midGFP* would affect the plants' ability to grow in the presence of toxic levels of these metals (**Figure 13**). To force the plants to take up excess Mn, Zn, or Ni, we included plates that were prepared with no iron. Under these iron deficient conditions, plants are expected to up-regulate *IRT1* expression, which leads to increase uptake of iron, and of other IRT1 substrates like Mn, Ni and Zn (Baxter et al., 2008).

One of the two lines of plants overexpressing YSL6midGFP had an increased root growth rate on 1/2MS medium (**Figure 13A**). On 1/2X MS containing added Mn, there was a

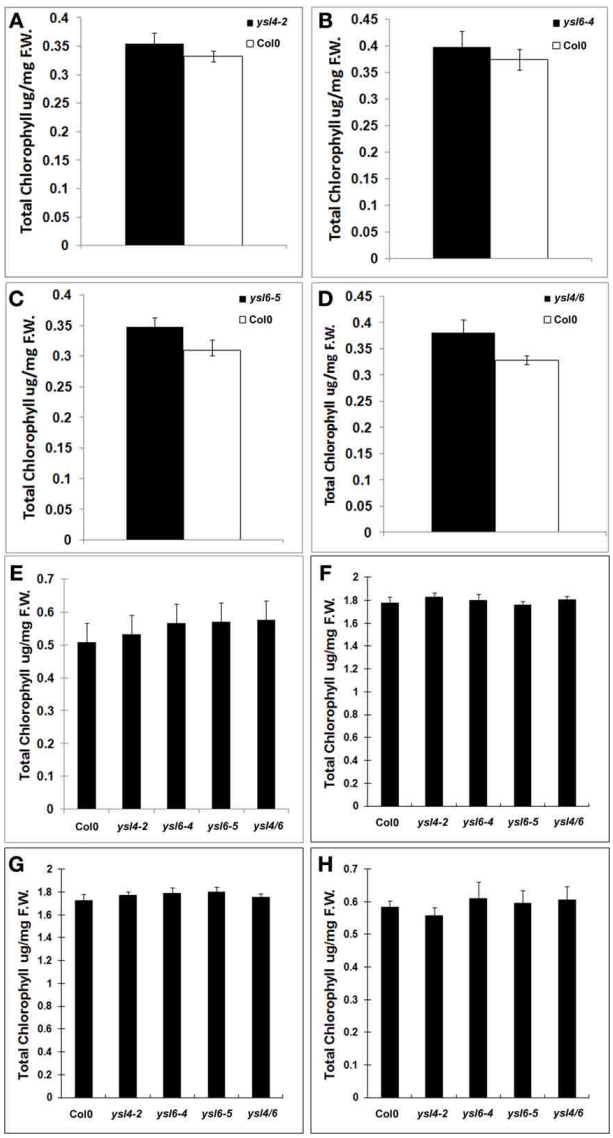

FIGURE 8 | Metal starvation response in seedlings of Col-0, ysl4-2, ysl6-4, ysl6-5, and ysl4ysl6. (A–D) Seedlings were grown on MS medium lacking Fe for 5 days and then chlorophyll levels were measured. **(A)** Chlorophyll levels of Col-0 and ysl4-2. **(B)** Chlorophyll levels of Col-0 and ysl6-4. **(C)** Chlorophyll levels of Col-0 and ysl6-5. **(D)** Chlorophyll levels of Col-0 and ysl4ysl6. **(E–H)** Plants were grown on MS plates for 10 days, and then transferred to MS without Fe, Zn, Cu, or Mn for 14 days. The total chlorophyll content of the shoot system was measured. **(E)** Chlorophyll levels of plants grown on MS medium lacking Fe. **(F)** Chlorophyll levels of plants grown on MS medium lacking Zn. **(G)** Chlorophyll levels of plants grown on MS medium lacking Cu. **(H)** Chlorophyll levels of plants grown on MS medium lacking Mn.

trend (**Figure 13B**; not statistically significant) of decreased root growth rate for the YSL6midGFP plants, but no trends or significant differences were noted on 1/2XMS containing added Ni (not shown). When iron was withdrawn from the medium, however, both mutants and over-expressing plants showed marked changes in root growth rates (**Figures 13D,E**). In the presence of either Mn or Ni, the *ysl4* mutants and the *ysl4ysl6* double mutants had increased root growth rates, while *AtYSL6-GFPmid* overexpressing plants had decreased root growth rates. We did not observe any significant differences in the growth rates of mutant or over-expressing plants exposed to 500 uM Zn (not shown).

Transport of metals by AtYSL4 and AtYSL6

We tested transporter activity of AtYSL4 and AtYSL6 using yeast functional complementation assays, but neither protein could alleviate the iron-limited growth defect of *fet3fet4* yeast (**Figure 14**). Because successful complementation will only occur if heterologous proteins are expressed on the yeast plasma membrane, it is reasonable that vacuolar proteins AtYSL4 and AtYSL6 would not correct the *fet3fet4* growth defect. Indeed, HvYSL5, which belongs to the same group as AtYSL4 and AtYSL6 and was shown to localize to vesicles in barley cells, was unable to complement *fet3fet4* yeast in the presence of 20 mM Fe-NA (Zheng et al., 2011). The use of other transport assay systems will be required in order to characterize the transport activity of these proteins.

DISCUSSION

AtYSL4 AND AtYSL6 ARE ASSOCIATED WITH INTERNAL MEMBRANES AND SMALL VACUOLES

In this paper, we provide evidence to indicate that two members of the Arabidopsis YSL family, AtYSL4 and AtYSL6, function at internal membranes. All previously characterized YSL proteins are located on the plasma membrane (DiDonato et al., 2004; Aoyama et al., 2009; Inoue et al., 2009; Lee et al., 2009; Chu et al., 2010) or on PM associated vesicles (Zheng et al., 2011). Interestingly, the localization pattern of OsYSL6, which belongs to the same group as AtYSL4 and AtYSL6, could not be definitely determined. In transient transformation experiments, the GFP signal accumulated throughout the cell regardless of whether OsYSL6 was tagged at the C-terminus or the N-terminus (Sasaki et al., 2011). Using GFPmid tagged proteins, which have GFP inserted in non-conserved central region of each protein, we have shown that AtYSL4-GFPmid and AtYSL6-GFPmid localize to the vacuolar membrane based on co-localization with γ-TIP-mCherry. Additionally, AtYSL6-GFPmid co-localized with FM-464, a lipophilic membrane stain that can efficiently label vacuolar membranes (Kutsuna and Hasezawa, 2002). In stably transformed plants, fluorescence from the *AtYSL6-GFPmid* construct was also observed on diffuse internal membranes, possibly the ER. The *AtYSL6-GFPmid* construct appears to be functional, since stably transformed plants that overexpress this construct do not have growth defects under normal growth conditions, but do show distinct metal-related phenotypes.

Vacuoles are an important site for storage of metals, with more than 90% of the zinc in the cell and approximately 50% of the iron in the cell sequestered in the vacuoles (Lanquar et al., 2010). In Arabidopsis, the vacuolar transporter MTP1 is required for plant responses to Zn excess, implying that vacuolar sequestration of Zn is critical for preventing cellular damage caused by excess Zn (Kobae et al., 2004; Desbrosses-Fonrouge et al., 2005). The vacuole also serves as an important storage place for iron during embryo development. In stage VI wild type embryos, the

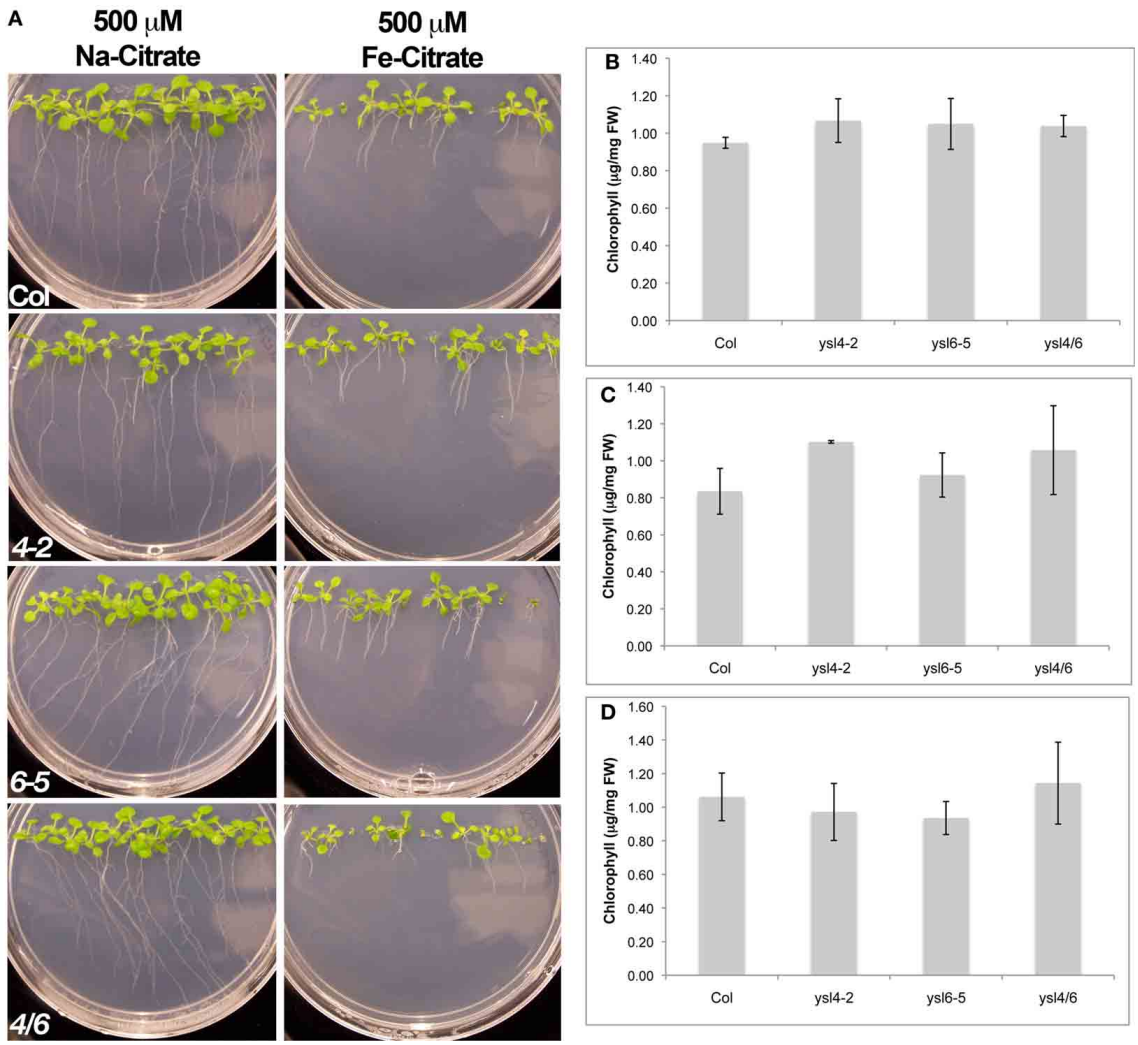

FIGURE 9 | Response of Col-0, ysl4-2, ysl6-5 and ysl4ysl6 to Fe-citrate excess. (A) Plants were grown vertically for two weeks on medium containing either 500 mM Na-Citrate or 500 mM FeCitrate prior to photographing. **(B)** Plants were grown for 2 weeks on regular MS medium (no additives, pH 5.7) before measuring chlorophyll content. **(C)** Plants were grown for 2 weeks on MS medium containing 500 mM NaCitrate (pH 5.7) before measuring chlorophyll content. **(D)** Plants were grown for 2 weeks on MS medium that was adjusted to pH 5.7 after addition of 500 mM Fe-Citrate. Chlorophyll content was measured as in **(B,C)**. For **(B–D)**, chlorophyll content of three batches of seedlings was measured and averaged. Error bars indicate ±SD.

main pool of Fe is held in the vacuoles of cells surrounding the pro-vascular system (Kim et al., 2006). Loss of the vacuolar iron importer VIT1 caused a redistribution of iron to a single sub-epidermal cell layer in the cotyledon, although the iron remained in vacuoles (Roschzttardtz et al., 2009). This finding suggests the existence of other vacuolar Fe import systems. AtNRAMP4, which is known to be involved in remobilization of vacuolar Fe during germination (Lanquar et al., 2005), co-localizes with γ-TIP (Bolte et al., 2011). γ-TIP has recently been shown to label structures embedded inside the protein storage vacuole (PSV) of dry Arabidopsis seeds(Bolte et al., 2011), and γ-TIP has been found associated with globoid structures in dry seeds of tobacco (Jiang et al., 2001). Because AtYSL4 and AtYSL6 also co-localize with γ-TIP, it is possible that they also function within PSVs. The Metal Tolerance Proteins, MTP1 and MTP3 are responsible for transporting zinc into vacuoles (Desbrosses-Fonrouge et al., 2005; Arrivault et al., 2006). Recently ZIF1 was identified as a transporter that can move NA into vacuoles. Thus, metal NA complexes are expected to occur in vacuoles, and the existence of tonoplast transporters capable of moving metal-NA complexes across this membrane is logical.

Vacuolar sequestration or excess heavy metals is particularly important during iron deficiency, when increased activity of the IRT1 transporter causes excessive uptake of Mn, Ni, and Zn, as well as some other heavy metals, if they are present in the growth medium(Eide et al., 1996; Korshunova et al., 1999; Baxter et al., 2008) In Arabidopsis, the tonoplast-localized Metal Transport Protein3 (MTP3) is critical for moving excess Zn accumulated during iron deficiency into the vacuole (Arrivault et al., 2006). MTP3 is positively regulated by iron deficiency, and also by excess

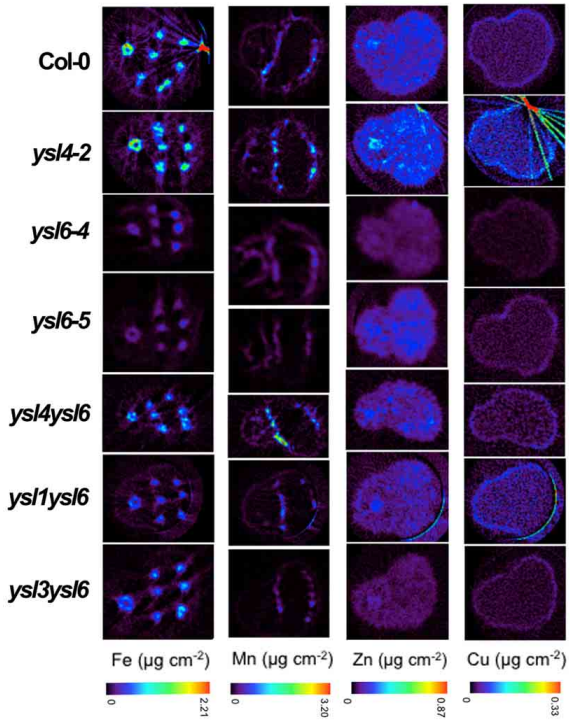

FIGURE 10 | Synchrotron X-ray Fluorescence (SXRF) Computed Microtomography showing the distribution of Fe, Mn, Zn, and Cu in Col-0 and ysl mutant lines. Tomograms (virtual cross sections) were collected via SXRF computed microtomography from intact, dry Arabidopsis seed. All seeds are oriented with the radicle at left and cotyledons at right.

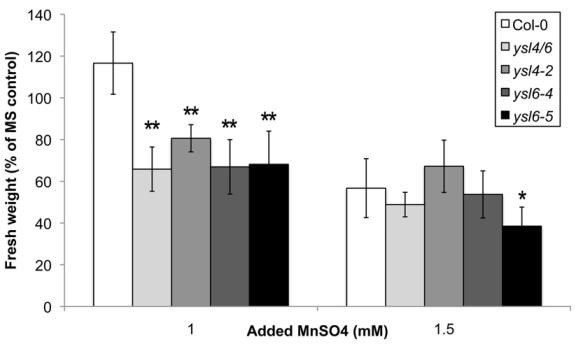

FIGURE 11 | Manganese sensitivity of *ysl* mutants. Seeds of Col-0, *ysl4ysl6* double mutants, *ysl4-2*, *ysl6-4* and *ysl6-5* single mutants were sown onto MS medium containing either 0, 1.0 or 1.5 mM excess MnSO4 and grown for 21 days. Fresh weights were measured by weighing batches of 5 seedlings each. Weights are expressed as a percentage of the weights of seedlings grown under the control condition (MS medium without excess MnSO4). $n = 3$–5 batches of seedlings. $^{*}p \leq 0.05$ and > 0.01, $^{**}p \leq 0.01$.

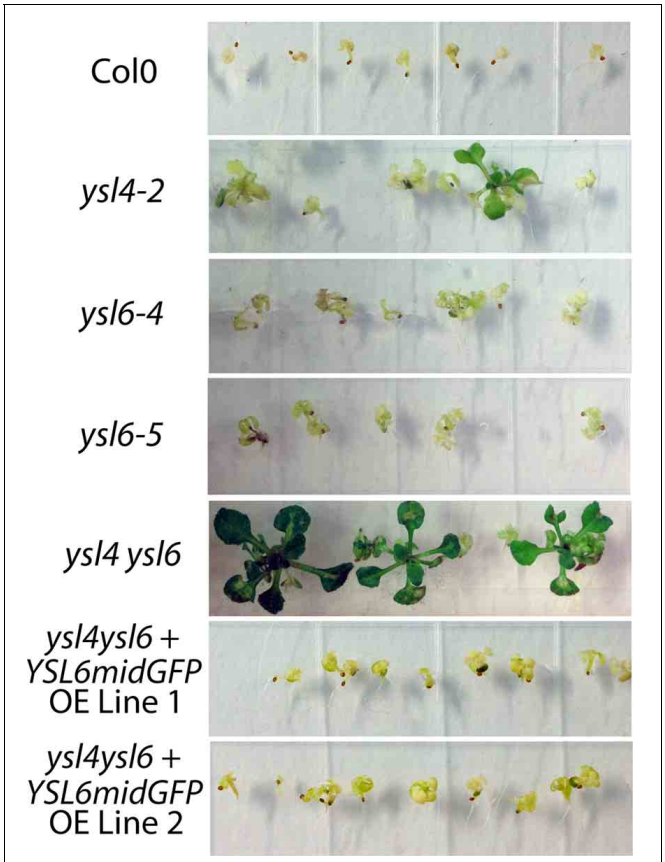

FIGURE 12 | Prolonged growth of mutants and YSL6-midGFP-OE complemented mutants on excess Mn. Seeds of Col0, *ysl4-2*, *ysl6-4* and *ysl6-5* single mutants, *ysl4ysl6* double mutants and two independent lines of *ysl4ysl6* double mutants transformed with a construct over expressing the AtYSL6midGFPconstruct (YSL6midGFP) were sown onto 1/2X MS medium containing 1.0 mM excess MnSO4 and grown for 35 days.

Zn and Co. In the absence of MTP3, plants grown under Fe deficiency are unable to sequester Zn in the roots, resulting in increased Zn accumulation in the shoots.

Metal transporters are also found in the endomembrane system, where they are responsible for providing metals to metalloproteins located in the ER and/or Golgi. For example, the copper transporter RAN1 is required for biogenesis of ethylene receptors (Binder et al., 2010) and the probable zinc transporter IAR1 is required for the activity of ER localized IAA-amino acid conjugate hydrolases(Lasswell et al., 2000). The Golgi-localized P-type ATPase, ECA3, is required for growth under Mn deficiency, while the prevacuolar compartment (PVC) localized manganese transporter MTP11 is required for maintaining correct levels of Mn in tissues, and for growth on excess Mn (Delhaize et al., 2007).

The model best supported by the data presented here is that AtYSL4 and AtYSL6 participate in the provision of Mn and Ni to proteins located in internal cellular compartments. Loss of *YSL4* and *YSL6* function allowed improved long term development of shoots grown on excess Mn (**Figure 12**), and improved growth of roots exposed to excess Mn and excess Ni (**Figure 13**), while over-expression of *YSL6* caused decreased growth of roots on excess Mn or Ni. This suggests that, when Mn or Ni are plentiful in the cytoplasm, these YSLs promote transport of excess metals into intracellular compartments, causing impaired growth. If the role of the YSLs were in Mn or Zn sequestration

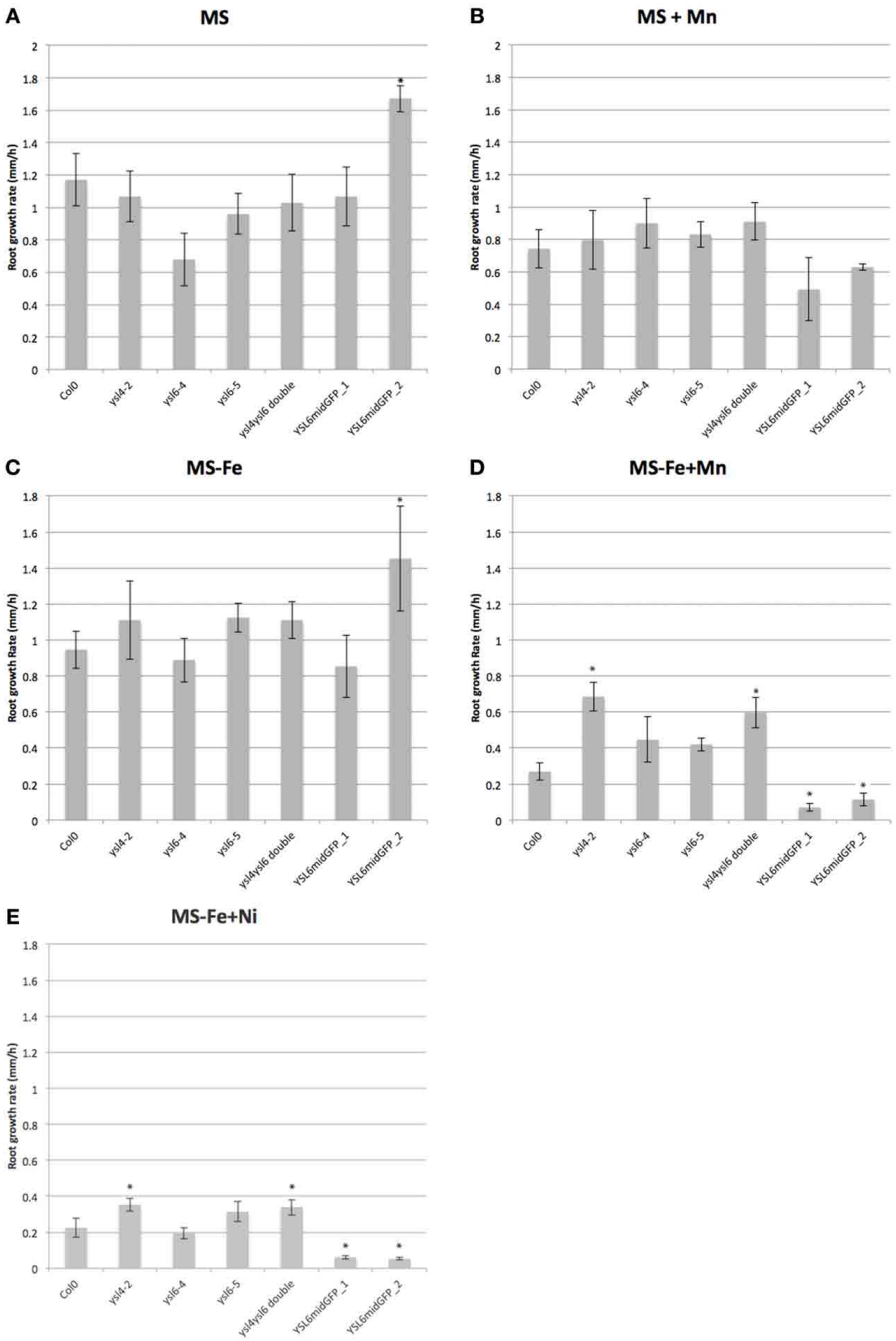

FIGURE 13 | Growth of mutants and YSL6-midGFP-OE plants on excess metals. Root growth rate during the 24 h period between 24 h and 48 h post-germination is presented. Photographs of the plates were taken every 24 h, and used to determine the growth rate for each 24 h period (see Materials and Methods). Plants were germinated and grown vertically on plates containing. **(A)** 1/2X MS (MS). **(B)** 1/2X MS + 1 mM MnSO4 (MS + Mn). **(C)** 1/2X MS without added iron (MS-Fe). **(D)** 1/2X MS without added iron and with 1 mM MnSO4 (MS−Fe+Mn). **(E)** 1/2X MS without added iron and with 90 uM NiCl2 (MS−Fe+Ni). $^*p \leq 0.05$.

(similar to the role of MTP3), we would expect the opposite phenotype: *ysl4* and *ysl6* mutants would be expected to have diminished growth in conditions of metal excess, and over-expressors would be expected to have better growth in metal excess.

In a recent publication, Divol et al. (2013) raised polyclonal antibodies against AtYSL6, and used these in immunofluorescence microscopy to conclude that AtYSL6 is localized to plastids. In our experiments using GFP-tagged AtYSL6, we never observed green fluorescence signals associated

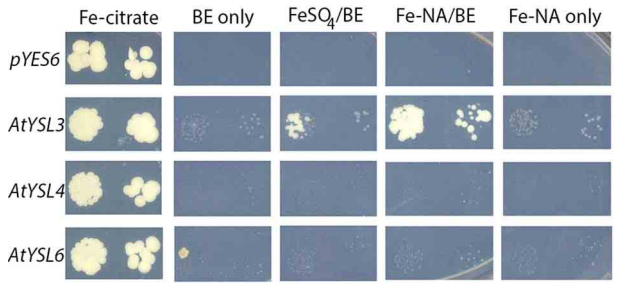

FIGURE 14 | Neither *AtYSL4* nor *AtYSL6* is able to complement *fet3fet4*. These experiments were performed as described (Chu et al. 2010). *fet3fet4* yeast (derived from DEY1453) transformed with *pGEV* and *pYES6/CT* empty vector (top row) or constructs containing *AtYSL3* (middle row), *AtYSL4* (third row), and AtYSL6 (bottom row) were plated onto SD-TRP medium containing 50 mM Fe-Citrate (first column), 0 mM iron + 10 nM beta-estradiol (BE) (second column), 5 mM FeSO4 + 10 nM BE (third column), 5 mM Fe-NA complex +10 nM BE (fourth column), or 5 mM Fe-NA complex without BE (last column). Pairs of spots correspond to 100 and 1000 fold dilutions of the original cultures. Plates were photographed after 10 days of growth.

with chloroplasts. Instead, we observed fluorescence signals on the vacuole membrane, and on other, undefined internal membranes in stably transformed plants. The *YSL6midGFP* construct used in our studies appears to be functional, since it complements the phenotype of the *ysl4ysl6* double mutant plants, conferring poor growth during prolonged exposure to 1 mM Mn. In these stably transformed plants, we often observed chloroplasts, which have strong red autofluorescence, but never observed any indication of green GFP fluorescence signal (see, for example, **Figure 5**). Additional work will be needed to resolve why the different techniques used for localization of AtYSL4 and AtYSL6 showed such marked differences.

It is interesting to note Divol et al.'s examination of vacuolar iron using Perl's/DAB staining in 2D imbibed embryos. In these embryos, Fe mobilization from vacuolar storage has commenced. *ysl4ysl6* double mutants have higher than normal vacuolar Fe while YSL6 over-expressing plants have lower than normal vacuolar Fe during this time(Divol et al., 2013). This pattern is consistent with YSL4 and YSL6 as vacuolar effluxers of iron (or Fe-NA complexes) during germination. We note, however, that no consistent germination effects in the *ysl4*, *ysl6* or *ysl4ysl6* double mutants were noted in spite of extensive investigation during the course of our studies (**Figure 10**, and data not shown).

TRANSPORT OF METALS BY AtYSL4 AND AtYSL6

Several lines of evidence indicate that AtYSL4 and AtYSL6 function in metal ion transport. First, mutants (either single or double) have altered metal accumulation patterns in shoots or in seeds. This suggests that, like other YSL proteins, AtYSL4 and AtYSL6 transport metals. *ysl4* and *ysl6* single mutants, along with the *ysl4ysl6* double mutant, are sensitive to high levels of manganese. Under conditions that increase the expression of the promiscuous transporter IRT1, both mutants and overexpressing plants exhibit altered rates of root elongation. Mutant plants (*ysl4* and *ysl4ysl6* double mutants) display increased root growth under these conditions, while YSL6-GFPmid overexpressing plants have decreased root elongation under these conditions. Indeed, when single (*ysl4-2, ysl6-4,* or *ysl6-5*) or double mutants are grown for 21 days on 1 mM Mn, they accumulate less shoot mass. This, combined with their vacuolar/endomembrane system localization patterns, suggests a role for AtYSL4 and AtYSL6 in sequestration or release of heavy metals such as manganese and nickel from the plant endomembrane system and vacuole.

Divol et al. (2013) reported that *ysl4ysl6* double mutants are sensitive to excess Fe in the growth medium. We also observed sensitivity of the double mutant to Fe-Citrate, but show here that 500 uM Fe-citrate used in the experiment also causes a dramatic lowering of the pH of the medium. When pH of the medium is buffered to 5.7, as is usual for Arabidopsis growth, the sensitivity phenotype of the double mutant was not observed. Since Fe solubility is strongly affected by pH, the amount of soluble iron is likely higher on the un-buffered plates than the buffered ones, making it difficult to experimentally separate the effect of Fe vs. the effect of pH. Thus, while YSL4 and YSL6 may have roles in internal Fe transport, experimental evidence for this is not completely clear. Direct measurement of transport activity, which has not been achieved yet, would help to elucidate this point.

ACKNOWLEDGMENTS

We thank Teddi Bloniarz for her expert assistance with greenhouse and growth chamber, Daneyal Farouq for assistance with image quantification, and Dr. Lawrence Winship for his critical evaluation of our micrographs. This work was funded by the National Science Foundation (IOS0847687).

REFERENCES

Alonso, J. M., Stepanova, A. N., Leisse, T. J., Kim, C. J., Chen, H., Shinn, P., et al. (2003). Genome-wide insertional mutagenesis of *Arabidopsis thaliana*. *Science* 301, 653–657. doi: 10.1126/science.1086391

Anderegg, G., and Ripperger, H. (1989). Correlation between metal complex formation and biological activity of nicotianamine analogues. *J. Chem. Soc. Chem. Commun.* 10, 647–650. doi: 10.1039/c39890000647

Aoyama, T., Kobayashi, T., Takahashi, M., Nagasaka, S., Usuda, K., Kakei, Y., et al. (2009). OsYSL18 is a rice iron(III)-deoxymugineic acid transporter specifically expressed in reproductive organs and phloem of lamina joints. *Plant Mol. Biol.* 70, 681–692. doi: 10.1007/s11103-009-9500-3

Arrivault, S., Senger, T., and Kramer, U. (2006). The Arabidopsis metal tolerance protein AtMTP3 maintains metal homeostasis by mediating Zn exclusion from the shoot under Fe deficiency and Zn oversupply. *Plant J.* 46, 861–879. doi: 10.1111/j.1365-313X.2006.02746.x

Baxter, I. R., Vitek, O., Lahner, B., Muthukumar, B., Borghi, M., Morrissey, J., et al. (2008). The leaf ionome as a multivariable system to detect a plant's physiological status. *Proc. Natl. Acad. Sci. U.S.A.* 105, 12081–12086. doi: 10.1073/pnas.0804175105

Binder, B. M., Rodriguez, F. I., and Bleecker, A. B. (2010). The copper transporter RAN1 is essential for biogenesis of ethylene receptors in Arabidopsis. *J. Biol. Chem.* 285, 37263–37270. doi: 10.1074/jbc.M110.170027

Bolte, S., Lanquar, V., Soler, M. N., Beebo, A., Satiat-Jeunemaitre, B., Bouhidel, K., et al. (2011). Distinct lytic vacuolar compartments are embedded inside the protein storage vacuole of dry and germinating *Arabidopsis thaliana* seeds. *Plant Cell Physiol.* 52, 1142–1152. doi: 10.1093/pcp/pcr065

Chu, H. H., Chiecko, J., Punshon, T., Lanzirotti, A., Lahner, B., Salt, D. E., et al. (2010). Successful reproduction requires the function of Arabidopsis YELLOW STRIPE-LIKE1 and YELLOW STRIPE-LIKE3 metal-nicotianamine transporters in both vegetative and reproductive structures. *Plant Physiol.* 154, 197–210. doi: 10.1104/pp.110.159103

Clough, S. J., and Bent, A. F. (1998). Floral dip: a simplified method for Agrobacterium-mediated transformation of *Arabidopsis thaliana*. *Plant J.* 16, 735–743. doi: 10.1046/j.1365-313x.1998.00343.x

Curie, C., Cassin, G., Couch, D., Divol, F., Higuchi, K., Le Jean, M., et al. (2009). Metal movement within the plant: contribution of nicotianamine and yellow stripe 1-like transporters. *Ann. Bot. (Lond.)* 103, 1–11. doi: 10.1093/aob/mcn207

Curie, C., Panaviene, Z., Loulergue, C., Dellaporta, S. L., Briat, J. F., and Walker, E. L. (2001). Maize *yellow stripe1* encodes a membrane protein directly involved in Fe(III) uptake. *Nature* 409, 346–349. doi: 10.1038/35053080

Davis, S. J., and Vierstra, R. D. (1998). Soluble, highly fluorescent variants of green fluorescent protein (GFP) for use in higher plants. *Plant Mol. Biol.* 36, 521–528. doi: 10.1023/A:1005991617182

Delhaize, E., Gruber, B. D., Pittman, J. K., White, R. G., Leung, H., Miao, Y. S., et al. (2007). A role for the AtMTP11 gene of Arabidopsis in manganese transport and tolerance. *Plant J.* 51, 198–210. doi: 10.1111/j.1365-313X.2007.03138.x

Desbrosses-Fonrouge, A., Voigt, K., Schroder, A., Arrivault, S., Thomine, S., and Kramer, U. (2005). *Arabidopsis thaliana* MTP1 is a Zn transporter in the vacuolar membrane which mediates Zn detoxification and drives leaf Zn accumulation. *FEBS Lett* 579, 4165–4174. doi: 10.1016/j.febslet.2005.06.046

DiDonato, R. J. Jr., Roberts, L. A., Sanderson, T., Eisley, R. B., and Walker, E. L. (2004). Arabidopsis Yellow Stripe-Like2 (YSL2): a metal-regulated gene encoding a plasma membrane transporter of nicotianamine-metal complexes. *Plant J.* 39, 403–414. doi: 10.1111/j.1365-313X.2004.02128.x

Divol, F., Couch, D., Conejero, G., Roschzttardtz, H., Mari, S., and Curie, C. (2013). The Arabidopsis Yellow Stripe LIKE4 and 6 transporters control iron release from the chloroplast. *Plant Cell* 25, 1040–1055. doi: 10.1105/tpc.112.107672

Eide, D., Broderius, M., Fett, J., and Guerinot, M. L. (1996). A novel iron-regulated metal transporter from plants identified by functional expression in yeast. *Proc. Natl. Acad. Sci. U.S.A.* 93, 5624–5628. doi: 10.1073/pnas.93.11.5624

Gendre, D., Czernic, P., Conejero, G., Pianelli, K., Briat, J. F., Lebrun, M., et al. (2007). TcYSL3, a member of the YSL gene family from the hyperaccumulator Thlaspi caerulescens, encodes a nicotianamine-Ni/Fe transporter. *Plant J.* 49, 1–15. doi: 10.1111/j.1365-313X.2006.02937.x

Harada, E., Sugase, K., Namba, K., Iwashita, T., and Murata, Y. (2007). Structural element responsible for the Fe(III)-phytosiderophore specific transport by HvYS1 transporter in barley. *FEBS Lett.* 581, 4298–4302. doi: 10.1016/j.febslet.2007.08.011

Haydon, M. J., Kawachi, M., Wirtz, M., Hillmer, S., Hell, R., and Kramer, U. (2012). Vacuolar nicotianamine has critical and distinct roles under iron deficiency and for zinc sequestration in Arabidopsis. *Plant Cell.* 24, 724–737. doi: 10.1105/tpc.111.095042

Inoue, H., Aoyama, T., Takahashi, M., Nakanishi, H., Mori, S., and Nisjozawa, N. (2006). Rice OsYSL2 and OsYSL15 are involved in the uptake and translocation of iron. *Plant Cell Physiol.* 47, S231–S231.

Inoue, H., Kobayashi, T., Nozoye, T., Takahashi, M., Kakei, Y., Suzuki, K., et al. (2009). Rice OsYSL15 Is an Iron-regulated Iron(III)-Deoxymugineic acid transporter expressed in the roots and is essential for iron uptake in early growth of the seedlings. *J. Biol. Chem.* 284, 3470–3479. doi: 10.1074/jbc.M806042200

Ishimaru, Y., Masuda, H., Bashir, K., Inoue, H., Tsukamoto, T., Takahashi, M., et al. (2010). Rice metal-nicotianamine transporter, OsYSL2, is required for the long-distance transport of iron and manganese. *Plant J.* 62, 379–390. doi: 10.1111/j.1365-313X.2010.04158.x

Jaquinod, M., Villiers, F., Kieffer-Jaquinod, S., Hugouvieux, V., Bruley, C., Garin, J., et al. (2007). A proteomics dissection of *Arabidopsis thaliana* vacuoles isolated from cell culture. *Mol. Cell Proteomics* 6, 394–412.

Jiang, L., Phillips, T. E., Hamm, C. A., Drozdowicz, Y. M., Rea, P. A., Maeshima, M., et al. (2001). The protein storage vacuole: a unique compound organelle. *J. Cell Biol.* 155, 991–1002. doi: 10.1074/mcp.M600250-MCP200

Karimi, M., Inze, D., and Depicker, A. (2002). GATEWAY vectors for Agrobacterium-mediated plant transformation. *Trends Plant Sci.* 7, 193–195. doi: 10.1016/S1360-1385(02)02251-3

Kim, S. A., Punshon, T., Lanzirotti, A., Li, L., Alonso, J. M., Ecker, J. R., et al. (2006). Localization of iron in Arabidopsis seed requires the vacuolar membrane transporter VIT1. *Science* 314, 1295–1298. doi: 10.1126/science.1132563

Kobae, Y., Uemura, T., Sato, M., Ohnishi, M., Mimura, T., Nakagawa, T., et al. (2004). Zinc transporter of *Arabidopsis thaliana* AtMTP1 is localized to vacuolar membranes and implicated in zinc homeostasis. *Plant Cell Physiol.* 45, 1749–1758. doi: 10.1093/pcp/pci015

Koike, S., Inoue, H., Mizuno, D., Takahashi, M., Nakanishi, H., Mori, S., et al. (2004). OsYSL2 is a rice metal-nicotianamine transporter that is regulated by iron and expressed in the phloem. *Plant J.* 39, 415–424. doi: 10.1111/j.1365-313X.2004.02146.x

Korshunova, Y. O., Eide, D., Clark, W. G., Guerinot, M. L., and Pakrasi, H. B. (1999). The IRT1 protein from *Arabidopsis thaliana* is a metal transporter with a broad substrate range. *Plant Mol. Biol.* 40, 37–44. doi: 10.1023/A:1026438615520

Kutsuna, N., and Hasezawa, S. (2002). Dynamic organization of vacuolar and microtubule structures during cell cycle progression in synchronized tobacco BY-2 cells. *Plant Cell Physiol.* 43, 965–973. doi: 10.1093/pcp/pcf138

Lahner, B., Gong, J., Mahmoudian, M., Smith, E. L., Abid, K. B., Rogers, E. E., et al. (2003). Genomic scale profiling of nutrient and trace elements in *Arabidopsis thaliana*. *Nat. Biotechnol.* 21, 1215–1221. doi:10.1038/nbt865

Lanquar, V., Lelievre, F., Bolte, S., Hames, C., Alcon, C., Neumann, D., et al. (2005). Mobilization of vacuolar iron by AtNRAMP3 and AtNRAMP4 is essential for seed germination on low iron. *Embo J.* 24, 4041–4051. doi: 10.1038/sj.emboj.7600864

Lanquar, V., Schnell Ramos, M., Lelievre, F., Barbier-Brygoo, H., Krieger-Liszkay, A., Kramer, U., et al. (2010). Export of vacuolar manganese by AtNRAMP3 and AtNRAMP4 is required for optimal photosynthesis and growth under manganese deficiency. *Plant Physiol.* 152, 1986–1999. doi: 10.1104/pp.109.150946

Lasswell, J., Rogg, L. E., Nelson, D. C., Rongey, C., and Bartel, B. (2000). Cloning and characterization of IAR1, a gene required for auxin conjugate sensitivity in Arabidopsis. *Plant Cell* 12, 2395–2408.

Lee, S., Chiecko, J. C., Kim, S. A., Walker, E. L., Lee, Y., Guerinot, M. L., et al. (2009). Disruption of OsYSL15 leads to iron inefficiency in rice plants. *Plant Physiol.* 150, 786–800. doi: 10.1104/pp.109.135418

Le Jean, M., Schikora, A., Mari, S., Briat, J. F., and Curie, C. (2005). A loss-of-function mutation in AtYSL1 reveals its role in iron and nicotianamine seed loading. *Plant J.* 44, 769–782. doi: 10.1111/j.1365-313X.2005.02569.x

Murata, Y., Ma, J. F., Yamaji, N., Ueno, D., Nomoto, K., and Iwashita, T. (2006). A specific transporter for iron(III)-phytosiderophore in barley roots. *Plant J.* 46, 563–572. doi: 10.1111/j.1365-313X.2006.02714.x

Pich, A., Manteuffel, R., Hillmer, S., Scholz, G., and Schmidt, W. (2001). Fe homeostasis in plant cells: does nicotianamine play multiple roles in the regulation of cytoplasmic Fe concentration? *Planta* 213, 967–976. doi: 10.1007/s004250100573

Roberts, L. A., Pierson, A. J., Panaviene, Z., and Walker, E. L. (2004). Yellow stripe1. Expanded roles for the maize iron-phytosiderophore transporter. *Plant Physiol.* 135, 112–120. doi: 10.1104/pp.103.037572

Roschzttardtz, H., Conejero, G., Curie, C., and Mari, S. (2009). Identification of the endodermal vacuole as the iron storage compartment in the Arabidopsis embryo. *Plant Physiol.* 151, 1329–1338. doi: 10.1104/pp.109.144444

Sasaki, A., Yamaji, N., Xia, J., and Ma, J. F. (2011). OsYSL6 is involved in the detoxification of excess manganese in rice. *Plant Physiol.* 157, 1832–1840. doi: 10.1104/pp.111.186031

Schaaf, G., Ludewig, U., Erenoglu, B. E., Mori, S., Kitahara, T., and Wirén, N. V. (2004). ZmYS1 functions as a proton-coupled symporter for phytosiderophore- and nicotianamine-chelated metals. *J. Biol. Chem.* 279, 9091–9096. doi: 10.1074/jbc.M311799200

Schuler, M., Rellan-Alvarez, R., Fink-Straube, C., Abadia, J., and Bauer, P. (2012). Nicotianamine functions in the Phloem-based

transport of iron to sink organs, in pollen development and pollen tube growth in Arabidopsis. *Plant Cell* 24, 2380–2400. doi: 10.1105/tpc.112.099077

Tagaki, S., Nomoto, K., and Takemoto, T. (1984). Physiological aspect of mugineic acid, a possible phytosiderophore of graminaceous plants. *J. Plant Nutr.* 7, 469–477. doi: 10.1080/01904168409363213

Waters, B. M., Chu, H. H., Didonato, R. J., Roberts, L. A., Eisley, R. B., Lahner, B., et al. (2006). Mutations in Arabidopsis *yellow stripe-like1* and *yellow stripe-like3* reveal their roles in metal ion homeostasis and loading of metal ions in seeds. *Plant Physiol.* 141, 1446–1458. doi: 10.1104/pp.106.082586

Wu, F. H., Shen, S. C., Lee, L. Y., Lee, S. H., Chan, M. T., and Lin, C. S. (2009). Tape-Arabidopsis Sandwich - a simpler Arabidopsis protoplast isolation method. *Plant Methods* 5, 16. doi: 10.1186/1746-4811-5-16

Yen, M.-R., Tseng, Y.-H., and Saier, M. H. Jr. (2001). Maize *Yellow Stripe1*, and iron-phytosiderophore uptake transporter, is a member of the oligopeptide transporter (OPT) family. *Microbiology* 147, 2881–2883.

Yordem, B. K., Conte, S. S., Ma, J. F., Yokosho, K., Vasques, K. A., Gopalsamy, S. N., et al. (2011). Brachypodium distachyon as a new model system for understanding iron homeostasis in grasses: phylogenetic and expression analysis of Yellow Stripe-Like (YSL) transporters. *Ann. Bot.* 108, 821–833. doi: 10.1093/aob/mcr200

Zheng, L., Fujii, M., Yamaji, N., Sasaki, A., Yamane, M., Sakurai, I., et al. (2011). Isolation and characterization of a barley yellow stripe-like gene, HvYSL5. *Plant Cell Physiol.* 52, 765–774. doi: 10.1105/tpc.112.103820

Zheng, L., Yamaji, N., Yokosho, K., and Ma, J. F. (2012). YSL16 is a phloem-localized transporter of the copper-nicotianamine complex that is responsible for copper distribution in rice. *Plant Cell* 24, 3767–3782. doi: 10.1093/pcp/pcr009

Conflict of Interest Statement: The authors declare that the research was conducted in the absence of any commercial or financial relationships that could be construed as a potential conflict of interest.

Received: 29 May 2013; accepted: 10 July 2013; published online: 26 July 2013.

*Citation: Conte SS, Chu HH, Chan-Rodriguez D, Punshon T, Vasques KA, Salt DE and Walker EL (2013) Arabidopsis thaliana Yellow Stripe1-Like4 and Yellow Stripe1-Like6 localize to internal cellular membranes and are involved in metal ion homeostasis. Front. Plant Sci. **4**:283. doi: 10.3389/fpls.2013.00283*

This article was submitted to Frontiers in Plant Nutrition, a specialty of Frontiers in Plant Science.

frontiers in
PLANT SCIENCE

REVIEW ARTICLE
published: 02 September 2013
doi: 10.3389/fpls.2013.00337

Iron economy in *Chlamydomonas reinhardtii*

Anne G. Glaesener[1], Sabeeha S. Merchant[1,2] and Crysten E. Blaby-Haas[1]*

[1] Department of Chemistry and Biochemistry, University of California, Los Angeles, Los Angeles, CA, USA
[2] Institute of Genomics and Proteomics, David Geffen School of Medicine at the University of California, Los Angeles, CA, USA

Edited by:
Jean-Francois Briat, Centre National de la Recherche Scientifique, France

Reviewed by:
Francis-André Wollman, Centre National de la Recherche Scientifique/UPMC/IBPC, France
Francois-Yves Bouget, Centre National de la Recherche Scientifique, France

***Correspondence:**
Crysten E. Blaby-Haas, Department of Chemistry and Biochemistry, University of California, Box 951569, 607 Charles E. Young Drive East, Los Angeles, CA 90095-1569, USA
e-mail: cblaby@chem.ucla.edu

While research on iron nutrition in plants has largely focused on iron-uptake pathways, photosynthetic microbes such as the unicellular green alga *Chlamydomonas reinhardtii* provide excellent experimental systems for understanding iron metabolism at the subcellular level. Several paradigms in iron homeostasis have been established in this alga, including photosystem remodeling in the chloroplast and preferential retention of some pathways and key iron-dependent proteins in response to suboptimal iron supply. This review presents our current understanding of iron homeostasis in Chlamydomonas, with specific attention on characterized responses to changes in iron supply, like iron-deficiency. An overview of frequently used methods for the investigation of iron-responsive gene expression, physiology and metabolism is also provided, including preparation of media, the effect of cell size, cell density and strain choice on quantitative measurements and methods for the determination of metal content and assessing the effect of iron supply on photosynthetic performance.

Keywords: photosynthesis, transcriptome, ferredoxin, respiration, ferroxidases, photo-oxidative stress, acidocalcisome

INTRODUCTION

Although iron is relatively abundant in the earth's crust, inadequate access to this micronutrient often chronically limits photosynthesis in the ocean and on land. In oxygen-rich surface waters and neutral to alkaline soil, iron is present predominately in poorly soluble complexes, such as ferric oxides. The low bioavailability of iron complexes creates a major obstacle for photosynthetic organisms. Estimates indicate that iron limits phytoplankton growth in 40% of ocean waters (Moore et al., 2002) and that 30% of arable land is too alkaline for optimal iron uptake (Chen and Barak, 1982). This suggests that poor iron bioavailability causes consequential impacts on food chains, carbon sequestration and oxygen production.

Single-celled algae present a unique system for investigating how photosynthetic organisms respond to and cope with suboptimal iron nutrition. Specifically, in a laboratory setting, studying the subcellular response of plants to a deficient iron status can be complicated by the individual nutritional profile of each cell, tissue and organ type. Single-celled algae, on the other hand, such as the well-characterized green alga *Chlamydomonas reinhardtii* (referred herein as Chlamydomonas), are routinely grown in liquid cultures where the cell population and exposure to nutrients can be more homogenous. Chlamydomonas has been studied in the laboratory for well over 60 years as a convenient single-celled reference for understanding fundamental aspects of photosynthesis (Rochaix, 2002), including its specific relation to metal metabolism [reviewed in Merchant et al. (2006)]. The common laboratory strains are derived from a soil isolate, therefore, the natural environment of Chlamydomonas is close to that of land plants. Additionally, although the last common ancestor between Chlamydomonas and land plants such as Arabidopsis existed at least 700 million years ago (Becker, 2013), the photosynthetic apparatus are virtually identical. However, there are several metabolic differences; Chlamydomonas can oxidize acetate and exploits alternative bioenergetic routes such as hydrogen photoproduction and fermentation (Grossman et al., 2007).

This review focuses on our present understanding of iron nutrition in Chlamydomonas and on the preparation and use of iron-deficient and -limited media and common techniques to study physiology, gene expression and metabolism in Chlamydomonas. An effort is also made to point out caveats associated with these types of studies for all investigators to consider.

IRON NUTRITION IN CHLAMYDOMONAS

Like land plants, algae have two especially iron-rich organelles, the chloroplast and the mitochondrion. Both organelles house numerous iron-dependent proteins whose functions are essential in the electron transfer pathways of the bioenergetic membranes in those compartments. In addition, iron is a component of many proteins involved in other essential processes such as reactive oxygen detoxification, fatty acid metabolism, and amino acid biosynthesis. Assuming a 1:1 stoichiometry of the electron transfer complexes [dimers for photosystem II (PSII) and the cytochrome b_6f complex and a monomer for photosystem I (PSI)], linear electron flow from PSII to ferredoxin is estimated to require 30 iron ions (if plastocyanin is present, and 31 iron atoms if cytochrome c_6 is present) (Blaby-Haas and Merchant, 2013). Again assuming 1:1 stoichiometry (monomers for complexes I, II, and IV, and a dimer for complex III), mitochondrial electron transport requires 50 iron atoms, over half contained within complex I (Xu et al., 2013). Although electron transfer in respiration appears to require more iron than does photosynthesis, the chloroplast is the dominant sink for iron in the oxygen-evolving plant cell, where this cofactor is

concentrated in the abundant iron-dependent proteins of the thylakoid membrane.

The contribution of iron-dependent proteins in other cellular compartments to the cellular iron quota may be relatively small, but they are also essential for fitness or survival. These enzymes participate in DNA synthesis and repair [ribonucleotide reductase (cytosol) and DNA glycosylases (nucleus)], metabolite synthesis [cytochrome P450s (endoplasmic reticulum), aldehyde oxidase (cytosol), xanthine dehydrogenase (cytosol)], molybdopterin synthesis [Cnx2 (cytosol)], fatty acid metabolism [fatty acid desaturases (endoplasmic reticulum)] and reactive oxygen species detoxification [peroxidases (multiple compartments including peroxisome, Golgi, and cytosol)], just to name a few. Therefore, a delicate balance exists to ensure an appropriate amount of iron or iron-bound cofactor such as heme is present throughout the cell for the maturation of each iron-dependent protein.

As a facultative photoheterotroph, Chlamydomonas can generate ATP from either photosynthesis or respiration depending on the presence of light and carbon source. This characteristic provides a unique and powerful experimental system to explore the effect of iron status on bioenergetic metabolism and vice versa. In particular, during the two major trophic states, photoautotrophic and photoheterotrophic, Chlamydomonas cells respond to iron status with acutely different physiologies (**Figure 1**). During the photoheterotrophic state, the cells are provided with light, CO_2, and acetate. When iron becomes a limiting resource, competition for iron acquisition between the chloroplast and the mitochondria ensues. In response, the cell maintains respiration while decreasing the photosynthetic contribution to the bioenergetics of the cell, a phenomenon that may rely on preferential allocation of iron to the mitochondrion or recycling of iron from the chloroplast to the mitochondrion. In contrast, in the absence of acetate, photosynthetic activity is maintained, as seen by a less pronounced decrease in chlorophyll (Chl) content and maintenance of the maximum quantum efficiency of PSII (expressed by F_v/F_m) (**Figures 1A,B**) (Terauchi et al., 2010; Urzica et al., 2012).

To understand these phenomena and discover the underlying mechanisms, the study of iron homeostasis in Chlamydomonas is routinely performed in the context of four graded iron nutrition stages: excess, replete, deficient and limited. These states were delineated by the evaluation of phenotype and iron-responsive gene expression in response to controlled medium iron content (described in more detail in the following sections and summarized in **Table 1**).

Specifically, components of the iron-uptake pathway are routinely used as sentinel genes for iron status. In contrast to land plants, the main iron uptake pathway in Chlamydomonas (based on transcript and protein abundance) is the fungal-like ferroxidase-dependent ferric transporter complex consisting of FOX1 (the ferroxidase) and FTR1 (the permease) (**Figure 2**). The copper-containing enzyme FOX1 catalyzes the oxidation of Fe(II) to Fe(III), similar to the yeast and human enzymes, Fet3p and ceruloplasmin, respectively (Herbik et al., 2002; La Fontaine et al., 2002). FOX1 is presumed to form a complex with the permease FTR1, which transports the ferric iron provided by FOX1 into the cytosol (Terzulli and Kosman, 2010). *FOX1* expression responds quickly to changes in iron nutrition ahead of any observable effects on physiology and thus provides a convenient and robust marker for iron status (**Figure 3**).

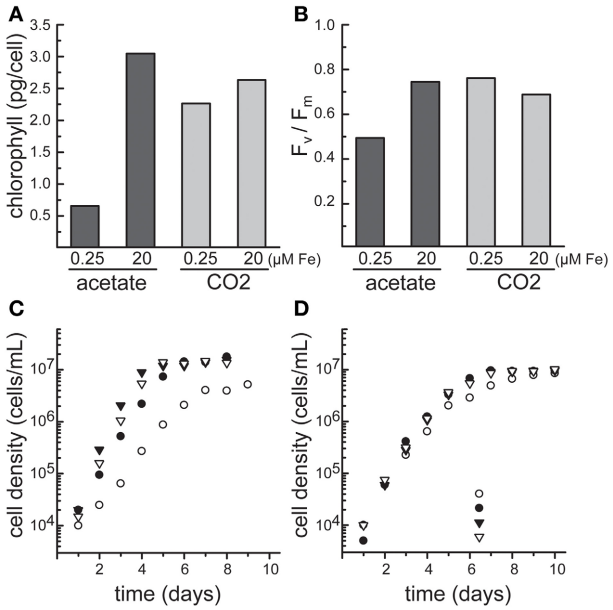

FIGURE 1 | The growth of Chlamydomonas CC-4532 in response to iron supplementation depends on the carbon source. Cells were cultured in TAP for photoheterotrophic growth (acetate) or TP for photoautotrophic growth (CO_2) using the revised trace metal supplement (Kropat et al., 2011) at 24°C and shaken at 180 rpm under continuous illumination of 70–80 μmol/m^{2}s, and bubbled with sterile air. **(A)** Determination of chlorophyll content and **(B)** maximum quantum efficiency of photosystem II (F_v/F_m). Aliquots of cells grown photoheterotrophic (dark gray) and photoautotrophic (light gray) were removed from the culture during the logarithmic growth phase (~4 × 10^6 cells/ml). **(C)** Photoheterotrophically and **(D)** photoautotrophically grown cells at 0.25 μM (open circles), 1 μM (filled circles), 20 μM (filled inverted triangles) and 200 μM Fe (filled inverted triangles) were counted with a hemocytomer for estimation of growth rates.

It should be noted that the following iron nutrition stages are described for cells grown photoheterotrophically (light and acetate). The same stages can be described for phototrophic cells (light and CO_2), but the iron concentration thresholds are distinct, as is the cellular response to those concentrations. These stages are also likely distinct for cells grown purely heterotrophically (dark and acetate), but this phenomenon has not yet been systematically studied.

STAGE 1: IRON EXCESS

In the iron excess stage (200 μM medium iron content), the cells will over-accumulate iron, as compared to the iron-replete stage (Long and Merchant, 2008; Terauchi et al., 2010). This observation is in contrast to the copper-excess situation where the cells only take up as much copper as needed despite over 500-fold excess in the medium (Page et al., 2009). Although the culture does not display any visible phenotype associated with iron excess, the cells are unable to grow at high photon flux density (500 μmol/m^{2}s at the surface of a petri dish) (Long and

Table 1 | Summary of the iron nutrition stages in Chlamydomonas distinguished by phenotype and sentinel gene expression.

	Photoheterotrophic				Photoautotrophic		
	Excess	**Replete**	**Deficient**	**Limited**	**Replete**	**Deficient**	**Limited**
Fe in the media (μM)	200	20	1–3	0–0.5	20	1–3	0–0.5
Growth	Impaired only under light stress			Impaired			Slightly impaired
Fe atoms/cell ($\times 10^7$)	50–100	8–20	2–12	1–4	14	6–9	3
FOX1 expression	Basal	Basal	Up	Up	Basal	Up	Up
Chl content (pg/cell)		2.3–2.5	1.8–2	0.6–1.2	2.6	2.6	1.8

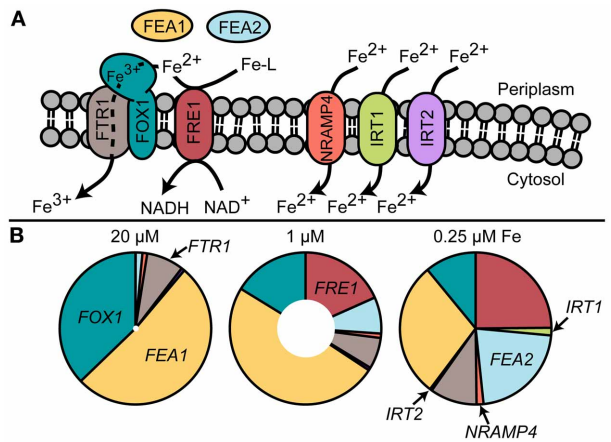

FIGURE 2 | (A) Known and putative iron uptake pathways in Chlamydomonas and **(B)** transcript abundance of uptake components estimated by RNA-Seq (Urzica et al., 2012). The inner white circles represent total transcript abundance relative to 0.25 μM iron.

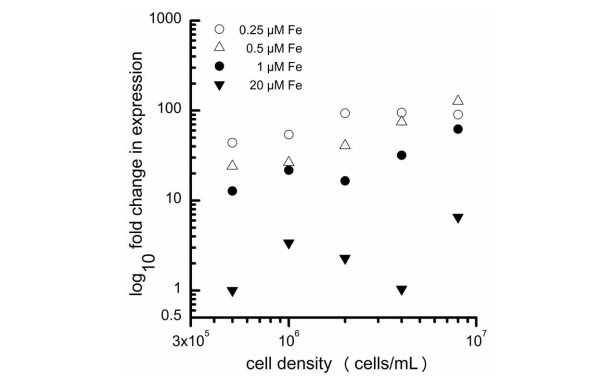

FIGURE 3 | Expression of *FOX1* depends both on extracellular iron content (0.25 μM, open circles; 0.5 μM, filled triangles; 1 μM, filled circles; 20 μM, filled inverted triangles) and the number of cells per mL. The increased expression of *FOX1*during growth of the batch culture likely reflects the reduced Fe availability on a per cell basis. Adapted from Urzica et al. (2012).

Merchant, 2008). This result suggests that the higher iron content of the cells, which is 2- to 5-fold higher than in replete cells, exacerbates damage caused by photo-oxidative stress and that there may be a pool of reactive iron in the chloroplast. In contrast to mammals and higher plants, iron excess does not affect the abundance of ferritin in Chlamydomonas, leading to the conclusion that ferritin is not the major iron storage molecule in the cell (Busch et al., 2008; Long et al., 2008). For Chlamydomonas, there are no known mechanisms for iron export, presumably because this high iron concentration is not typically experienced in nature and there is no need to establish pathways to deal with the excess.

Based on Mössbauer spectroscopy of iron-replete cells, Semin et al. found that Chlamydomonas cells contain an unusally high amount of ferrous iron. The authors have postulated that instead of typical iron storage proteins such as ferritin or siderophores, which would bind ferric iron, iron is stored in vacuoles as in yeast (Semin et al., 2003). This compartment may in fact be the acidocalcisome, which is an acidic, calcium- and polyphosphate-rich, membrane-bound, lysosome-related organelle (Ruiz et al., 2001; Docampo et al., 2005). Indeed, in the green alga *Dunaliella salina* and the red alga *Cyanidium caldarium*, intracellular iron is found in acidic vacuoles (Paz et al., 2007; Nagasaka and Yoshimura, 2008).

STAGE 2: IRON REPLETE

The standard growth medium for Chlamydomonas contains 18–20 μM iron (depending on the trace supplement) (Hutner et al., 1950; Kropat et al., 2011). In both trace mixes, iron is supplied as an EDTA chelate, which is used to maintain iron in solution, thereby facilitating uptake. However, it should be mentioned that for the Hutner's trace mix, 18 μM iron is the concentration of iron added to the mix, but because of ferric iron precipitation during preparation, there is batch-to-batch variation, and the concentration of soluble iron may be closer to 10 μM (Kropat et al., 2011). Recently, a revised trace metal supplement for Chlamydomonas was formulated (Kropat et al., 2011). Using the cellular content of metals during growth in the replete condition, the trace metal composition was adjusted to supply a 3-fold excess of each nutrient. Some components not utilized by Chlamydomonas found in the Hunter's trace mix were removed, such as cobalt and boron, and the concentrations of other metals, such as zinc and manganese were reduced. Several benefits are apparent with use of the new formulation. The cells have an increased growth rate, and the supplement is more stable and less time consuming to prepare. Instead of combining the mineral nutrients into a single stock, each component is stored separately and added freshly while preparing media. In terms of iron nutrition, the greatest benefit of the revised mix is the absence of iron precipitation (over a 5 years period).

As the culture reaches stationary growth, the cells in replete medium have consumed (depending on the strain) 10–30% of the medium iron content (Kropat et al., 2011; Page et al., 2012). This "luxury" consumption is characterized by basal low level expression of the genes encoding the high-affinity FOX1/FTR1 ferric iron transporter and negligible expression of the putative secondary iron transporters NRAMP4, IRT1, and IRT2 (Urzica et al., 2012). In the replete stage, Chl concentration has been measured at roughly 2.5 pg/cell Chl (Moseley et al., 2002; Page et al., 2012; Urzica et al., 2012). However, the ratio of Chl per cell or Chl per protein is affected by the incident illumination and the strain genotype.

STAGE 3: IRON DEFICIENT

As the iron content of the medium is reduced to around 1–3 μM, the cells begin to experience iron deficiency. The expression of iron uptake pathways is dramatically induced. Increased abundance of FOX1 at either mRNA or protein levels is commonly used as a sentinel marker for iron-deficiency. Well characterized primers for qPCR and antibodies for immunoblot analysis are available (Herbik et al., 2002; La Fontaine et al., 2002; Allen et al., 2007a). At this concentration of iron supply, the cells are usually not chlorotic and photosynthetic complex abundance is generally not affected (Moseley et al., 2002). Of course, depending on genotype, in some strains the lower end of this concentration range may result already in symptoms of limitation (see below), such as marginal chlorosis and a very mild impact on abundance of photosynthetic complexes. In general, this stage is differentiated from the iron-limited state by the lack of a growth phenotype.

Despite the absence of chlorosis in the iron-deficient state, spectroscopic measurements revealed some changes within the chloroplast. Specifically, fluorescence rise and decay kinetics (Kautsky curves) indicate that re-oxidation of the plastoquinone (PQ) pool is slower in the iron-deficiency situation (Moseley et al., 2002). This has been attributed to some loss of function of iron-containing electron transfer complexes downstream of the PQ pool, such as the cytochrome b_6f complex, PSI or ferredoxin. The relatively exposed [4Fe-4S] clusters of PSI are prime candidates.

Structural changes in the PSI-LHCI complex accompany iron deficiency, presumably to compensate for reduced PSI function. These modifications to the complex result in reduced energy transfer from the accessory antenna to the reaction center (Moseley et al., 2002). This results both from dissociation of PsaK, a connector between PSI and LHCI, from PSI and proteolysis of individual Lhca subunits in LHCI (Ben-Shem et al., 2003; Naumann et al., 2005). The signal transduction pathway leading to the structural modification of PSI-LHCI is not known, nor is the mechanism of PsaK and Lhca degradation. Mixing experiments indicate that degradation does result from induced proteolysis (Moseley et al., 2002). One idea that has been put forward regarding sensing of iron status by PSI is that it may occur by occupancy of the Chl binding sites in PsaK. If these sites are low affinity, they may be sensitive indicators of flux through the Chl biosynthetic pathway, which is dependent on iron at the rate-limiting step catalyzed by aerobic cyclase (Tottey et al., 2003).

Based on genome-wide expression profiling using RNA-Seq methodology, 78 genes displayed at least a 2-fold difference in transcript abundance between this stage (1 μM Fe) and the replete stage (Urzica et al., 2012). Since many organisms occupy a niche that allows them to survive in just barely sufficient iron, the transcriptome of this state is clearly relevant to the impact of marginal iron nutrition on crop yields and primary productivity. The two largest functional groups (for this particular dataset) represented in the iron-deficient stage encode proteins with known or predicted function in metal transport (17%) and the redox/stress response (25%). This includes the upregulation of genes involved in iron transport, like the ferric reductase *FRE1*, the high-affinity iron-uptake system (comprising *FOX1* and *FTR1*), the transcripts for the algal-specific proteins FEA1 and FEA2, and the putative secondary iron transporters *NRAMP4* and *IRT2*. The expression of a Mn-dependent superoxide dismutase is also highly induced. The transcripts of only four genes were significantly reduced in abundance during this condition. One of these is *FDX5*, an anaerobically-induced chloroplast-targeted ferredoxin which contains a [2Fe-2S] cluster (Jacobs et al., 2009). The reduction of *FDX5* transcript abundance may serve to spare iron.

The large proportion of redox/stress-related transcripts at this stage of iron nutrition, which is visually asymptomatic, may reflect an anticipatory response to incipient stress associated with changes in light harvesting and reduced rate of electron transfer downstream of the PQ pool. Additionally, these transcripts may be related to compromised PSI, which can produce superoxide by the photoreduction of oxygen. Solvent-exposed iron-sulfur clusters are particularly sensitive to superoxide and are consequently destroyed releasing ferric iron. If not immediately chelated, the free iron can react with hydrogen peroxide creating the hydroxyl radical, a highly cytotoxic molecule, which cannot be detoxified enzymatically. Indeed, expression of the two ferritin genes in Chlamydomonas is induced during iron deficiency. The ferritins localize to the chloroplast, but only ferritin1 appears to increase in abundance in response to iron-deficiency (Busch et al., 2008; Long et al., 2008). Although ferritins are typically regarded as iron storage complexes, neither of the two Chlamydomonas complexes appears to contain significant amounts of iron when cells were grown in iron-deficient medium, leading to the conclusion that ferritin buffers instead of stores iron liberated within the chloroplast. As a unicellular organism, iron homeostasis is focused on distribution at a sub-cellular level, including partitioning to the mitochondria vs. the chloroplast, and this may account for the unique response of ferritin within the chloroplast.

STAGE 4: IRON LIMITATION

As the iron content of the medium is reduced below about 0.5 μM, cells enter the iron-limited stage, where cell growth is inhibited due to limiting nutritional supply of iron. Although the iron transport pathways are still highly expressed, and at a higher level than in the deficiency state (**Figure 3**), the cells are markedly chlorotic, corresponding to a decrease in Chl of about 2- to 4-fold, and the growth rate is reduced (**Figure 1**). Concurrently, multiple iron-containing proteins in the chloroplast are reduced in abundance. These include PSI (12 iron atoms), the cytochrome

b_6f complex (12 iron atoms) and ferredoxin (2 iron atoms), and as a result, iron-limited cells exhibit a severe block in photosynthesis (Moseley et al., 2002; Page et al., 2012; Urzica et al., 2012). The noticeable loss of iron-bound photosynthetic complexes is generally only seen for cells grown in media containing acetate as carbon source, whereas photoautotrophically grown cultures maintain photosynthetic performance and retain these complexes for an extended period of time during iron-limitation. During photoheterotrophic iron-limited growth, subunits of respiratory complexes localized in the mitochondria change in abundance, as shown by immunoblot analysis and comparative quantitative proteomics (Naumann et al., 2007; Terauchi et al., 2010). The abundance of complex I subunits is decreased, whereas subunits of complexes III and IV increase. In the absence of acetate, abundances of respiratory complexes remain unchanged during iron-limitation.

Urzica et al. found a large number of genes with increased transcript abundance (at least 2-fold difference; 2050 genes) during this stage (0.25 μM) relative to iron replete, underscoring the stress induced by iron limitation (Urzica et al., 2012). As seen in the iron-deficient dataset, the most dramatically increased transcripts are those involved in iron transport and those encoding Mn-dependent superoxide dismutase (Urzica et al., 2012). The large number of differentially abundant transcripts during this condition also highlights the value of studying the transcriptome of the iron-deficient state, where only 78 RNAs are significantly changed in abundance. It is more likely that these 78 RNAs include the direct targets of iron nutrition acclimation rather than secondary stress responses. Indeed, several transcriptome studies of iron-starved land plants have had to contend with large sets of transcripts with changed abundance (Thimm et al., 2001; Zheng et al., 2009). The mechanical stress of transferring plants from iron-sufficient to -deprived medium (Buckhout et al., 2009) and the cumulative response from different cell types and tissue often obscures the primary iron responses.

COMMON METHODS FOR STUDYING IRON NUTRITION IN CHLAMYDOMONAS

Three basic techniques are generally used to generate poor iron nutrition in the laboratory. The first is to limit the available iron in the medium by chelators. For work with yeasts like *S. cerevisiae* and *Schizosaccharomyces pombe*, iron-chelators such as 2,2′-dipyridyl and bathophenanthroline disulfonic acid, are often used to generate a state of poor iron nutrition *in vivo* (Eide et al., 1996; Pelletier et al., 2005; Mercier et al., 2006; Jo et al., 2009). Some studies with plants like *Arabidopsis thaliana* have combined the use of chelators like ferrozine with the strategy of creating iron deficiency by omitting iron from the media (Vert et al., 2002; Lanquar et al., 2005; Yang et al., 2010). For Chlamydomonas, some studies have used the chelators ferrozine and ethylenediamine-N,N′-bis(2-hydroxyphenyl)acetic acid (EDDHA) (Xue et al., 1998; Weger, 1999; Weger and Espie, 2000; Rubinelli et al., 2002). However, when using chelators or evaluating studies that solely used chelators to achieve iron depletion, several caveats should be kept in mind. As with all metal chelators, these molecules are not specific to iron and will bind other metal ions (Kroll et al., 1957; Stookey, 1970), possibly leading to observations not specifically caused by iron depletion. In addition, the cells may be able to compete with the chelator leading to slower iron uptake, which may affect how the cells respond as compared to an actual omission of iron from the media. In some ways, however, the use of chelators could be a more appropriate approach to the study of iron homeostasis, because in most environments poor iron nutrition is due to competition between iron uptake pathways and natural ligands in contrast to the absence of iron.

The second technique is to limit intracellular iron by using an iron-transport mutant. This approach has not been routinely employed for work with Chlamydomonas but is commonly used in other organisms such as yeast and land plants. In *A. thaliana*, a mutant of the iron transporter *IRT1* was used to elucidate the role of iron-nutrition on lateral root development (Giehl et al., 2012), gene expression (Wang et al., 2007), and circadian rhythm (Hong et al., 2013; Salomé et al., 2013). In the yeast *S. cerevisiae*, the *fet3 fet4* double mutant, lacking both the high and low affinity iron transport pathway, is very sensitive to poor iron nutrition (Dix et al., 1994). This mutant has been used to study siderophore uptake (Lesuisse et al., 1998) and to investigate the relationship between iron homeostasis and an anti-malaria drug (Emerson et al., 2002). Although the use of iron transport mutants is a convenient method to achieve cellular iron depletion, iron will likely enter the cell via other routes and uptake of other metal ions can be affected in the mutant.

The third and preferable approach is to control the amount of iron added to the medium, described in more detail in section Preparing Media. Of course, in each of these cases, one has to worry about whether deficiency in one metal affects the intracellular concentration of other metal ions. For instance, non-selective transporters may be induced, which will inadvertently bring in multiple metal ions. The cell may purposefully change the concentration of other metals as seen for iron and manganese and for zinc and copper levels in Chlamydomonas (Allen et al., 2007b; Malasarn et al., 2013). Therefore, it is imperative to measure all intracellular metal concentrations during iron nutrition experiments (see section Metal Measurement).

PREPARING MEDIA

Chlamydomonas is routinely cultured in a simple, defined medium where the concentration of metal ions can be selectively controlled. Popular media include Sueoka's high salt medium (HS or HSM) and Tris-phosphate medium (TP), both of which can be supplemented with the carbon source acetate (HSMA and TAP, respectively). The largest difference between the two media is the presence of Tris(hydroxymethyl)aminomethane (Tris) in TP and a roughly 14-fold higher concentration of potassium and phosphate in HSM. TAP/TP has a higher capacity to buffer pH changes in the culture compared to HSMA/HSM, which should be considered when choosing a medium, since the pH of the medium affects the availability of iron. Both types of media are routinely used for iron nutrition studies in Chlamydomonas. Indeed, TAP and HSM are generally used to compare photoheterotrophic and photoautotrophic growth. However, because the compositions of the two media are different, using TAP and TP or HSMA and HSM is preferred.

Because of high metabolic demand for iron, iron depletion in laboratory media is relatively easy to accomplish in Chlamydomonas. However, several precautions should be followed to ensure that the amount of iron in the medium is tightly controlled and the experiments are therefore reproducible, i.e., the only iron present is that which is consciously added. Most recent iron metabolism studies of Chlamydomonas employ the media preparation methods detailed in (Quinn and Merchant, 1998) for achieving copper deficiency. In summary, the use of clean glassware and plasticware is of paramount importance. All culture flasks and reusable plasticware are rinsed at least twice with 6 N HCl to displace metal ions and rinsed six times with MilliQ-purified water to remove the HCl. High-purity chemicals are used to make iron-free stock solutions, which are stored in metal-free plasticware. Certificates of analysis specifying the trace metal composition are generally available before purchase of the stock chemicals and can be used to estimate the amount of contaminating metals in the prepared medium. These chemicals should be kept separate from other laboratory chemicals to avoid accidental metal contamination. The preparation of solid iron-deficient media requires washing of the agar with EDTA to remove contaminating metal ions (**Figure 4**). At all times, effort should be made to avoid contamination with metals (wear gloves, no metal spatulas and protection from dust). Ideally, iron-deficient media prepared in glass flasks should be used immediately. It is recommended that the media not be stored for more than a couple of days. Even though the flasks are acid washed, there will be residual metal ions remaining in the glass, which will leach into the medium over time (Cox, 1994).

The use of pH

Alkaline pH is commonly employed in iron nutrition experiments with soil-grown plants that rely on acidification and reduction to solubilize iron (i.e., Strategy I plants). This strategy has not been generally applied to Chlamydomonas, because of the ease with which the iron concentration in the medium can be controlled.

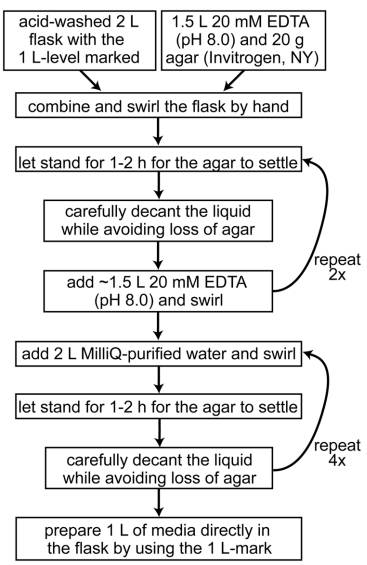

FIGURE 4 | Workflow for the preparation of iron-depleted solid growth media for Chlamydomonas.

STRAINS

The genotype of each "wild-type" Chlamydomonas strain can have a noticeable effect on a strain's tolerance to poor iron nutrition. Most of the commonly used laboratory strains appear to be descendants of a cross between two divergent spores from the original isolate, and the resulting progeny may have one or the other of two distinct haplotypes at any given locus (Gallaher et al., manuscript in preparation). In practice, this means that even closely related strains, such as CC-4402 and CC-4532, can have thousands of SNPs relative to each other, and will exhibit observable phenotypic differences (**Figure 5**).

The largest difference between strains in terms of iron nutrition is the presence or absence of a cell wall. Some researchers have chosen to employ a cell wall-less strain in their studies to avoid overestimation of iron uptake rates caused by iron bound to the cell wall (Lynnes et al., 1998). However, it was later found that two key components of the iron assimilation pathway are soluble proteins secreted to the periplasmic space between the plasma membrane and cell wall. Expression of the genes encoding these algal-specific proteins, *FEA1* and *FEA2*, is significantly induced during iron deficiency, and in a cell wall-less strain, these proteins are lost to the medium (Allen et al., 2007a). Although we do not know the function of these periplasmic proteins, it is hypothesized that they may bind iron and may serve to concentrate iron (whether Fe(II) or Fe(III) is not known) in proximity to the plasma membrane assimilatory transporters. A significant consequence of the loss of the FEA proteins into the medium is increased sensitivity of these strains to iron depletion (strain CC-425 in **Figure 5**).

CELL SIZE

Metal and Chl content are commonly reported on a per cell basis for Chlamydomonas. This convention can complicate comparisons of iron homeostasis studies employing different Chlamydomonas strains or cells grown under different growth regimes as cell size can vary between laboratory strains and growth conditions. Cell size was reported to be affected by trophic status (Terauchi et al., 2010), nutrient stress (Zhang et al., 2002; Kropat et al., 2011), CO_2 concentration (Vance and Spalding,

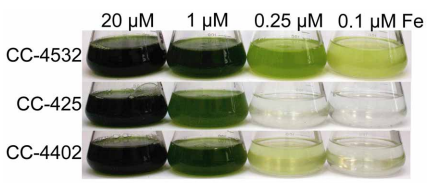

FIGURE 5 | Growth of different Chlamydomonas strains in response to iron supply. CC-4532 and CC-4402 are cell wall-containing strains, whereas CC-425 represents a cell wall-less strain. Cultures were inoculated at 1×10^4 cells/mL and grown for 10 days in TAP (Tris-acetate-phosphate) supplemented with iron to the indicated concentrations at 24°C and shaken at 180 rpm under constant illumination of 60–80 µmol/m^2s.

2005), HSM compared to TAP media (Fischer et al., 2006), light quality (Murakami et al., 1997), light intensity (Matsumura et al., 2003) as well as during the cell cycle (Umen, 2005). Additionally, cell size can vary between mutant and parent. For instance, a ferritin knockdown mutant was found to be almost 2-fold bigger in size than the wild-type strain (Busch et al., 2008).

CELL DENSITY

In general, it is advisable to control for cell density rigorously during sampling of cells for molecular analyses so that external iron concentration can be used as a proxy for intracellular iron content. A typical laboratory culture of Chlamydomonas will consume iron equivalent to about 3 μM as it goes from inoculation to stationary phase (Page et al., 2012). Therefore, in medium containing iron in this concentration range (or lower), expression of the nutritional iron regulon is dependent on the cell density (**Figure 3**). As the cells in culture divide, the ratio of medium iron per cell decreases, and expression of genes involved in iron assimilation steadily increases (Urzica et al., 2012). This relationship is not evident in medium containing excess iron (see 20 μM samples in **Figure 3**) where the *FOX1* marker gene is expressed at a very low basal level. Interestingly, in fully replete media, during logarithmic phase, the demand for intracellular iron exceeds the capacity of the iron uptake and metabolism pathway, resulting in transient iron deficiency (Page et al., 2012).

METAL MEASUREMENT

Element quantification based on inductively coupled plasma in combination with mass spectrometry (ICP-MS) or optical emission spectroscopy (ICP-OES) enables investigators to measure multiple metals within a sample. For mass spectrometry based detection, the plasma is used to ionize the atoms, which are then separated on the basis of their mass to charge ratio (Husted et al., 2011). For detection by OES, atoms in the sample are excited by argon plasma and emit light at their characteristic wavelengths, which is used to identify the elements in the sample (Hou and Jones, 2000).

Theoretical detection limits of ICP-MS for most elements are at about 10 parts per trillion (ppt). When measuring complex biological samples, one has to consider matrix effects caused by the cell material, and measuring a standard curve in the cell paste is recommended to verify that matrix effects are negligible. The theoretical limit for ICP-OES is typically two- to three orders of magnitude higher than for ICP-MS with most elements detected at 1–10 parts per billion (ppb). Both detection methods have a linear dynamic detection range over several orders of magnitude (usually a linear dynamic range of 10^6 to 10^7) (Pröfrock and Prange, 2012).

Yet the use of ICP-MS for iron quantification has a limitation with respect to sensitivity when argon is used to generate the plasma. Polyatomic interferences, mainly due to argon oxide, have the same mass as the most abundant Fe isotope, ^{56}Fe, and prohibit accurate measurement (Vogl et al., 2003). Therefore, in order to measure the iron content in a sample, a less abundant isotope of iron (^{57}Fe) can be measured. Another possibility is to use helium or hydrogen as a collision gas, which reduces the occurrence of interfering polyatomic complexes (Niemelä et al., 2003). However, depending on the tuning of the collision gases, the background equivalent concentration (BEC) can be as high as 2 ppb. Therefore, to be able to measure accurate iron concentrations, the concentration of the sample has to be above the background level. Newer ICP-MS instruments utilize a combination of collision/reaction cell technologies with quadrupole or octupole mass analyzer to minimize interferences even further (Yip and Sham, 2007; Cvetkovic et al., 2010).

Because of the wide dynamic range, both the concentration of iron in the medium (1116 ppb) and in the cells can be quantified by either ICP-MS or ICP-OES. ICP-MS measurements (Agilent 7500) for different Chlamydomonas strains grown photoheterotrophically in iron-replete (20 μM) media range between 5 and 40 × 10^7 Fe atoms per cell (corresponding to 46 and 371 ppb, when digested cell paste equivalent to 1 × 10^7 cells/mL is measured) (Kropat et al., 2011). The cellular iron content of the strain CC-125 is reduced from 12–25 × 10^7 Fe atoms per cell to about 5 × 10^7 Fe atoms per cell within 24 h of transfer from iron replete to iron-minus medium (Page et al., 2012). This iron content corresponds to about 110–230 ppb for iron-replete and 46 ppb Fe for iron starved cells (for sample preparation, see **Figure 6**).

As mentioned in section Cell Size, the cell size can vary between strains and growth conditions, and the calculation of metal content on a per cell basis, even though broadly used, is not ideal for comparisons between experiments conducted

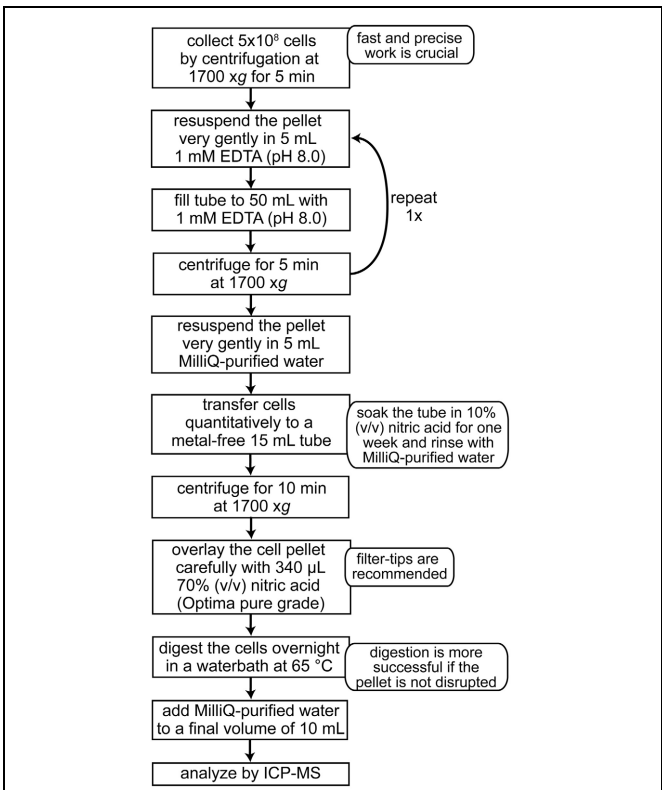

FIGURE 6 | Sample preparation of Chlamydomonas cells for metal analysis by ICP-MS.

with different strains or under different growth conditions. Normalization based on the amount of other elements measured from the same sample would be desirable, but this normalization method should also be performed with caution, and efforts made to ensure that the chosen element's concentration does not change between test conditions. For instance, phosphorous content is commonly used to normalize the metal content between samples. However, Chlamydomonas manganese-deficient cells contain less phosphorous than replete cells (Allen et al., 2007b). The measurement of total organic carbon for normalization purposes may be a likely alternative.

METHODS FOR MONITORING PHOTOSYNTHETIC PARAMETERS

Chlorophyll assay

Interveinal chlorosis is a classic symptom of poor iron nutrition in plants and is indeed a convenient indicator of iron status in agriculture (Mengel, 1994). It was originally attributed to the impact of low iron supply on the function of an iron-dependent step in Chl biosynthesis (Brown, 1956), but there may also be programmed degradation of Chl-containing proteins (Spiller et al., 1982; Moseley et al., 2002).

Unlike in land plants, the extent of chlorosis is dependent on the growth mode of Chlamydomonas cultures—photoheterotrophic vs. photoautotrophic. As a result, chlorosis by itself is not an absolute indicator of iron status. As mentioned above, the photosynthetic machinery is maintained longer in iron-limited cells grown in the light without acetate, while in the presence of acetate, degradation is apparent at early stages of suboptimal iron nutrition (**Figures 1A,B**) (Terauchi et al., 2010; Urzica et al., 2012).

For the measurement of Chl content, quantitative extraction of all Chl molecules from the cell is important. For Chlamydomonas this is routinely achieved with 80% (v/v) acetone in methanol (**Figure 7**) (Porra et al., 1989; Moseley et al., 2000). Chl *a* and *b* concentrations are estimated according to the method of Porra et al. (1989). Even though the extinction coefficients in that method were determined for 80% acetone in aqueous solution, the estimation is accurate enough for comparing strains or conditions. In addition, extraction of Chl with 100% methanol has also been used in Chlamydomonas (Lynnes et al., 1998).

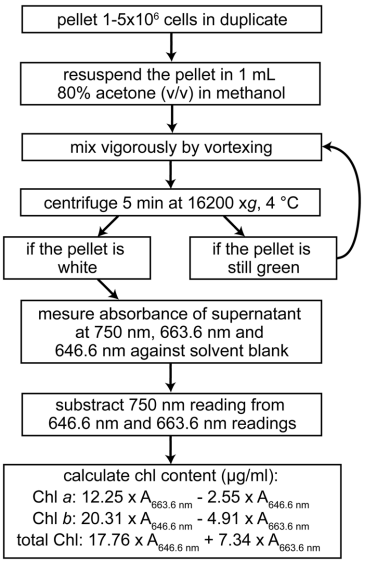

FIGURE 7 | Workflow for the spectrophotometric determination of the chlorophyll content of Chlamydomonas cells. Calculations are based on Porra et al. (1989).

Chlorophyll fluorescence

Chlorophyll fluorescence is a fast, non-destructive way of characterizing the photosynthetic status of a cell. Absorbed photons generate excited Chls that can participate in photochemistry, dissipate the absorbed energy as heat (non-photochemical quenching) or return to the ground state accompanied by emission of light, referred to as Chl fluorescence. Since these individual fates of the excited state are mutually exclusive, the measurement of Chl fluorescence can be used to assess the efficiency of photochemical and non-photochemical quenching in the reaction center [the reader is encouraged to see (Maxwell and Johnson, 2000) and (Baker, 2008) for more details].

To probe the effect of iron nutrition on photosynthetic performance, Moseley et al. measured Chl fluorescence induction and decay kinetics of Chlamydomonas cells grown photoheterotrophically under different iron nutrition stages. The cells were dark-adapted for at least 5 min and exposed to actinic light with a photon flux density of $\sim$60 μmol/m^{2}s, using an open FluorCam detector to record the resulting fluorescence emission (Moseley et al., 2002). During dark-adaptation, the absence of photons and the consequent absence of electron output from PSII causes the Q_A pool (the primary quinone electron acceptor of PSII) to become maximally oxidized. When these cells are exposed to actinic light, the Kautsky effect is observed: a fast increase in Chl fluorescence due to initial reduction of Q_A followed by a slow decay due to its subsequent re-oxidization. Photoheterotrophic iron-deficient Chlamydomonas cells (1 μM Fe in the growth medium) display a slower fluorescence decay rate compared to iron replete cells, indicative of a reduced rate of Q_A re-oxidation, possibly caused by impaired function of iron-containing complexes downstream of the PQ pool (Moseley et al., 2002). The slower decay rate is exacerbated in iron-limited cells (0.25 μM Fe in the media) and accompanied by a slower rate of Q_A reduction and a higher fluorescence yield suggesting impairment of PSII in addition to downstream electron transfer (Moseley et al., 2002).

The measurement of Chl fluorescence can also be used to determine photosynthetic parameters which help to determine the photosynthetic status of a cell. The ratio F_v/F_m (maximum quantum efficiency of PSII) is a frequently used parameter, its value is relatively constant but decreases in stressed cells. Using a Hansatech FMS2 pulse-modulated fluorometer, Terauchi et al. measured the fluorescence of Chlamydomonas cells grown in the presence of different iron concentrations under both photoautotrophic and photoheterotrophic conditions. Cells were dark-adapted for 15 min and subsequently filtered onto 13-mm diameter Milipore AP20 glass fiber filters prior to measurement (Terauchi et al., 2010). F_v is defined as the difference between F_m and F_0, with F_0 as the minimum fluorescence of the sample after dark-adaptation and F_m the maximal Chl fluorescence after illumination with actinic light (Baker, 2008). Insufficient iron

nutrition during photoheterotrophic growth of Chlamydomonas cells results in decreased F_v/F_m from 0.7–0.74 in iron-replete to 0.67 and 0.54 in 0.2 and 0.1 μM Fe in the growth media, respectively. This decrease was not observed during iron-limitation in photoautotrophic growth conditions, indicating maintenance of photochemistry during this trophic growth regime (**Figure 1B**) (Terauchi et al., 2010).

77 K fluorescence

Low-temperature (77 K) fluorescence emission spectra of whole Chlamydomonas cells or isolated thylakoid membranes are generally composed of major fluorescence bands around 685 and 715 nm, which correspond to fluorescence emitted from Chl in light-harvesting antennae connected with PSII (685 nm) and connected with PSI (715 nm) (Murata, 1968). This technique can be used to analyze changes in the interactions between light-harvesting antennae and the photosynthetic reaction centers. Functional disconnection of antennae from PSII or PSI appears as a shift in the fluorescence peaks, because LHC antennae not connected to photosystems show a different fluorescence maximum than those connected (Wollman and Bennoun, 1982). An increase in the amplitude of the PSI peak illustrates a state 1-to-state 2 transition, which is the reversible transfer of a fraction of LHCII antenna from PSII to PSI (Wollman and Delepelaire, 1984).

Low-temperature fluorescence spectra have revealed that poor iron nutrition affects the light harvesting antennae associated with both photosystems (Moseley et al., 2002; Naumann et al., 2005). During iron-deficient photoheterotrophic growth, the amplitude of the LHCI/PSI peak increases and shifts toward 705 nm, which indicates a reduced energy transfer between the antennae and the reaction centers (higher amplitude) and a disconnection of LHCI antennae from PSI (shift). If the iron concentration in the media is further reduced (0.1 μM), the LHCII antennae are also disconnected from PSII as indicated by a shift of the 685 nm peak toward 680 nm (Moseley et al., 2002). In contrast, in the absence of acetate, the amplitude of the LCHI/PSI peak decreases, and there is only a small shift after extended iron-deplete growth (Busch et al., 2008).

Low temperature 77 K fluorescence has also been applied to characterize mutants involved in the iron deficiency response. In the *pgrl1-28* knock-down mutant for example, the antennae disconnection is more sensitive to iron-deficiency. An increase in amplitude and a small blue shift (from 713 to 709 nm) was observed for the mutant but not the wild-type at 3 μM Fe in the media (Petroutsos et al., 2009).

FUTURE DIRECTION

The role of iron in the metabolism of Chlamydomonas has been studied extensively; however, several questions remain to be investigated. Most iron nutrition studies have focused on growth in the presence of light and acetate. An outstanding question relates to the relationship between iron nutrition and carbon metabolism. Several studies have noted that the response of Chlamydomonas to iron status can vary drastically depending on whether acetate is present or not. Both the physiology as evaluated with growth kinetics, iron uptake and photosynthetic efficiency, and the transcriptome have revealed markedly different phenomena. How carbon source impacts the decision to maintain photosynthesis is not known. The relationship between Chlamydomonas iron metabolism and heterotrophic growth (in the dark with acetate) or anaerobiosis have been largely left uninvestigated.

How iron status is linked to changes in transcription is also unknown for Chlamydomonas. A number of transcription factors and regulatory proteins are known components of iron homeostasis in land plants (Vigani et al., 2013), but the extent to which there is overlap in the iron-regulatory networks between green algae and land plants is unknown. The recent iron-nutrition transcriptome of Chlamydomonas has provided some targets, which include eleven putative transcription regulators whose mRNA abundance is increased in iron-limited cells (Urzica et al., 2012). Of these putative regulators is a potential functional ortholog of the *A. thaliana* E3 ubiquitin ligase BTS and a bHLH transcription factor orthologous to bHLH115. However, as of yet, the functions of these putative regulators have not been confirmed in Chlamydomonas. Multiple types of iron-responsive elements (FeREs) have been uncovered (Deng and Eriksson, 2007; Fei et al., 2009, 2010), suggesting the involvement of more than one transcription factor. Also, the different responses to iron nutrition depending on carbon source suggest that the iron-regulatory network in Chlamydomonas may be complex.

ACKNOWLEDGMENTS

This work was supported by the Division of Chemical Sciences, Geosciences, and Biosciences, Office of Basic Energy Sciences of the U.S Department of Energy (DE-FD02-04ER15529). Crysten E. Blaby-Haas acknowledges support from an Individual Kirschstein National Research Service Award (GM100753). We would like to thank Janette Kropat, Rikard Fristedt, Sean Gallaher, and Ian Blaby for critical review of the manuscript.

REFERENCES

Allen, M. D., del Campo, J. A., Kropat, J., and Merchant, S. S. (2007a). *FEA1*, *FEA2*, and *FRE1*, encoding two homologous secreted proteins and a candidate ferrireductase, are expressed coordinately with *FOX1* and *FTR1* in iron-deficient *Chlamydomonas reinhardtii*. *Eukaryot. Cell* 6, 1841–1852. doi: 10.1128/EC.00205-07

Allen, M. D., Kropat, J., Tottey, S., del Campo, J. A., and Merchant, S. S. (2007b). Manganese deficiency in Chlamydomonas results in loss of photosystem II and MnSOD function, sensitivity to peroxides, and secondary phosphorus and iron deficiency. *Plant Physiol.* 143, 263–277. doi: 10.1104/pp.106.088609

Baker, N. R. (2008). Chlorophyll fluorescence: a probe of photosynthesis *in vivo*. *Annu. Rev. Plant Biol.* 59, 89–113. doi: 10.1146/annurev.arplant.59.032607.092759

Becker, B. (2013). Snow ball earth and the split of Streptophyta and Chlorophyta. *Trends Plant Sci.* 18, 180–183.

Ben-Shem, A., Frolow, F., and Nelson, N. (2003). Crystal structure of plant photosystem I. *Nature* 426, 630–635. doi: 10.1038/nature02200

Blaby-Haas, C. E., and Merchant, S. S. (2013). "Sparing and salvaging metals in chloroplasts," in *Encyclopedia of Inorganic and Bioinorganic Chemistry. Metals in Cells*, eds V. Culotta, and R. A. Scott (Chichester: John Wiley and Sons Ltd.) (in press).

Brown, J. (1956). Iron chlorosis. *Ann. Rev. Plant Physiol.* 7, 171–190.

Buckhout, T. J., Yang, T. J. W., and Schmidt, W. (2009). Early iron-deficiency-induced transcriptional changes in *Arabidopsis* roots as revealed by microarray analyses. *BMC Genomics* 10:147. doi: 10.1186/1471–2164-10-147

Busch, A., Rimbauld, B., Naumann, B., Rensch, S., and Hippler, M. (2008). Ferritin is required for rapid remodeling of the photosynthetic apparatus and minimizes photooxidative stress in response to iron availability in *Chlamydomonas reinhardtii*. *Plant J.* 55, 201–211. doi: 10.1111/j.1365-313X.2008.03490.x

Chen, Y., and Barak, P. (1982). Iron nutrition of plants in calcareous soils. *Adv. Agron.* 35, 217–240.

Cox, C. D. (1994). Deferration of laboratory media and assays for ferric and ferrous ions. *Methods Enzymol.* 235, 315–329. doi: 10.1016/0076-687935150-3

Cvetkovic, A., Menon, A. L., Thorgersen, M. P., Scott, J. W., Poole, F. L. 2nd., Jenney, F. E. Jr., et al. (2010). Microbial metalloproteomes are largely uncharacterized. *Nature* 466, 779–782. doi: 10.1038/nature09265

Deng, X., and Eriksson, M. (2007). Two iron-responsive promoter elements control expression of FOX1 in *Chlamydomonas reinhardtii*. *Eukaryot. Cell* 6, 2163–2167. doi: 10.1128/EC.00324-07

Dix, D. R., Bridgham, J. T., Broderius, M. A., Byersdorfer, C. A., and Eide, D. J. (1994). The *FET4* gene encodes the low affinity Fe(II) transport protein of *Saccharomyces cerevisiae*. *J. Biol. Chem.* 269, 26092–26099.

Docampo, R., de Souza, W., Miranda, K., Rohloff, P., and Moreno, S. N. (2005). Acidocalcisomes - conserved from bacteria to man. *Nat. Rev. Microbiol.* 3, 251–261. doi: 10.1038/nrmicro1097

Eide, D., Broderius, M., Fett, J., and Guerinot, M. L. (1996). A novel iron-regulated metal transporter from plants identified by functional expression in yeast. *Proc. Natl. Acad. Sci. U.S.A.* 93, 5624–5628.

Emerson, L. R., Nau, M. E., Martin, R. K., Kyle, D. E., Vahey, M., and Wirth, D. F. (2002). Relationship between chloroquine toxicity and iron acquisition in *Saccharomyces cerevisiae*. *Antimicrob. Agents Chemother.* 46, 787–796. doi: 10.1128/AAC.46.3.787-796.2002

Fei, X., Eriksson, M., Li, Y., and Deng, X. (2010). A novel negative fe-deficiency-responsive element and a TGGCA-type-like FeRE control the expression of FTR1 in *Chlamydomonas reinhardtii*. *J. Biomed. Biotechnol.* 2010:790247. doi: 10.1155/2010/790247

Fei, X., Eriksson, M., Yang, J., and Deng, X. (2009). An Fe deficiency responsive element with a core sequence of TGGCA regulates the expression of FEA1 in *Chlamydomonas reinharditii*. *J. Biochem.* 146, 157–166. doi: 10.1093/jb/mvp056

Fischer, B. B., Wiesendanger, M., and Eggen, R. I. L. (2006). Growth condition-dependent sensitivity, photodamage and stress response of *Chlamydomonas reinhardtii* exposed to high light conditions. *Plant Cell Physiol.* 47, 1135–1145. doi: 10.1093/pcp/pcj085

Giehl, R. F. H., Lima, J. E., and von Wirén, N. (2012). Localized iron supply triggers lateral root elongation in *Arabidopsis* by altering the AUX1-mediated Auxin distribution. *Plant cell* 24, 33–49. doi: 10.1105/tpc.111.092973

Grossman, A. R., Croft, M., Gladyshev, V. N., Merchant, S. S., Posewitz, M. C., Prochnik, S., et al. (2007). Novel metabolism in Chlamydomonas through the lens of genomics. *Curr. Opin. Plant Biol.* 10, 190–198. doi: 10.1016/j.pbi.2007.01.012

Herbik, A., Bölling, C., and Buckhout, T. J. (2002). The involvement of a multicopper oxidase in iron uptake by the green algae *Chlamydomonas reinhardtii*. *Plant Physiol.* 130, 2039–2048. doi: 10.1104/pp.013060

Hong, S., Kim, S. A., Guerinot, M. L., and McClung, C. R. (2013). Reciprocal interaction of the circadian clock with the iron homeostasis network in Arabidopsis. *Plant Physiol.* 161, 893–903. doi: 10.1104/pp.112.208603

Hou, X., and Jones, B. T. (2000). "Inductively coupled plasma-optical emission spectrometry," in *Encyclopedia of Analytical Chemistry*, ed R. A. Meyers (Chichester: John Wiley and Sons Ltd.), 9468–9485.

Husted, S., Persson, D. P., Laursen, K. H., Hansen, T. H., Pedas, P., Schiller, M., et al. (2011). The role of atomic spectrometry in plant science. *J. Anal. At. Spectrom.* 26, 52–79. doi: 10.1039/c0ja00058b

Hutner, S. H., Provasoli, L., Schatz, A., and Haskins, C. P. (1950). Some approaches to the study of the role of metals in the metabolism of microorganisms. *Proc. Am. Phil. Soc.* 94, 152–170.

Jacobs, J., Pudollek, S., Hemschemeier, A., and Happe, T. (2009). A novel, anaerobically induced ferredoxin in *Chlamydomonas reinhardtii*. *FEBS Lett.* 583, 325–329. doi: 10.1016/j.febslet.2008.12.018

Jo, W. J., Kim, J. H., Oh, E., Jaramillo, D., Holman, P., Loguinov, A. V., et al. (2009). Novel insights into iron metabolism by integrating deletome and transcriptome analysis in an iron deficiency model of the yeast *Saccharomyces cerevisiae*. *BMC Genomics* 10:130. doi: 10.1186/1471–2164-10-130

Kroll, H., Knell, M., Powers, J., and Simonian, J. (1957). A phenolic analog of ethylenediaminetetraacetic acid. *J. Am. Chem. Soc.* 79, 2024–2025. doi: 10.1021/ja01565a075

Kropat, J., Hong-Hermesdorf, A., Casero, D., Ent, P., Castruita, M., Pellegrini, M., et al. (2011). A revised mineral nutrient supplement increases biomass and growth rate in *Chlamydomonas reinhardtii*. *Plant J.* 66, 770–780. doi: 10.1111/j.1365-313X.2011.04537.x

La Fontaine, S., Quinn, J. M., Nakamoto, S. S., Page, M. D., Göhre, V., Moseley, J. L., et al. (2002). Copper-dependent iron assimilation pathway in the model photosynthetic eukaryote *Chlamydomonas reinhardtii*. *Eukaryot. Cell* 1, 736–757. doi: 10.1128/EC.1.5.736-757.2002

Lanquar, V., Lelièvre, F., Bolte, S., Hamès, C., Alcon, C., Neumann, D., et al. (2005). Mobilization of vacuolar iron by AtNRAMP3 and AtNRAMP4 is essential for seed germination on low iron. *EMBO J.* 24, 4041–4051. doi: 10.1038/sj.emboj.7600864

Lesuisse, E., Simon-Casteras, M., and Labbe, P. (1998). Siderophore-mediated iron uptake in *Saccharomyces cerevisiae*: the *SIT1* gene encodes a ferrioxamine B permease that belongs to the major facilitator superfamily. *Microbiology* 144, 3455–3462. doi: 10.1099/00221287-144-12-3455

Long, J. C., and Merchant, S. S. (2008). Photo-oxidative stress impacts the expression of genes encoding iron metabolism components in Chlamydomonas. *Photochem. Photobiol.* 84, 1395–1403. doi: 10.1111/j.1751-1097.2008.00451.x

Long, J. C., Sommer, F., Allen, M. D., Lu, S. F., and Merchant, S. S. (2008). *FER1* and *FER2* encoding two ferritin complexes in *Chlamydomonas reinhardtii* chloroplasts are regulated by iron. *Genetics* 179, 137–147. doi: 10.1534/genetics.107.083824

Lynnes, J. A., Derzaph, T. L. M., and Weger, H. G. (1998). Iron limitation results in induction of ferricyanide reductase and ferric chelate reductase activities in *Chlamydomonas reinhardtii*. *Planta* 204, 360–365. doi: 10.1007/s004250050267

Malasarn, D., Kropat, J., Hsieh, S. I., Finazzi, G., Casero, D., Loo, J. A., et al. (2013). Zinc deficiency impacts CO_2 assimilation and disrupts copper homeostasis in *Chlamydomonas reinhardtii*. *J. Biol. Chem.* 288, 10672–10683. doi: 10.1074/jbc.M113.455105

Matsumura, K., Yagi, T., and Yasuda, K. (2003). Role of timer and sizer in regulation of *Chlamydomonas* cell cycle. *Biochem. Biophys. Res. Commun.* 306, 1042–1049. doi: 10.1016/S0006-291X(03)01089-1

Maxwell, K., and Johnson, G. N. (2000). Chlorophyll fluorescence - a practical guide. *J. Exp. Bot.* 51, 659–668. doi: 10.1093/jexbot/51.345.659

Mengel, K. (1994). Iron availability in plant tissues - iron chlorosis on calcareous soils. *Plant Soil* 165, 275–283. doi: 10.1007/BF00008070

Merchant, S. S., Allen, M. D., Kropat, J., Moseley, J. L., Long, J. C., Tottey, S., et al. (2006). Between a rock and a hard place: trace element nutrition in Chlamydomonas. *Biochim. Biophys. Acta* 1763, 578–594. doi: 10.1016/j.bbamcr.2006.04.007

Mercier, A., Pelletier, B., and Labbé, S. (2006). A Transcription factor cascade involving Fep1 and the CCAAT-binding factor Php4 regulates gene expression in response to iron deficiency in the fission yeast *Schizosaccharomyces pombe*. *Eukaryot. Cell* 5, 1866–1881. doi: 10.1128/EC.00199-06

Moore, J. K., Doney, S. C., Glover, D. M., and Fung, I. Y. (2002). Iron cycling and nutrient-limitation patterns in surface waters of the World Ocean. *Deep Sea Res. II* 49, 463–507. doi: 10.1016/S0967-064500109-6

Moseley, J. L., Allinger, T., Herzog, S., Hoerth, P., Wehinger, E., Merchant, S., et al. (2002). Adaptation to Fe-deficiency requires remodeling of the photosynthetic apparatus. *EMBO J.* 21, 6709–6720. doi: 10.1093/emboj/cdf666

Moseley, J. L., Quinn, J., Eriksson, M., and Merchant, S. (2000). The *Crd1* gene encodes a putative di-iron enzyme required for photosystem I accumulation in copper deficiency and hypoxia in *Chlamydomonas reinhardtii*. *EMBO J.* 19, 2139–2151. doi: 10.1093/emboj/19.10.2139

Murakami, A., Fujita, Y., Nemson, J. A., and Melis, A. (1997). Chromatic regulation in *Chlamydomonas reinhardtii*: time course of photosystem stoichiometry adjustment following a shift in growth light quality. *Plant Cell Physiol.* 38, 188–193.

Murata, N. (1968). Fluorescence of chlorophyll in photosynthetic systems. IV. Induction of various emissions at low temperatures. *Bioenergetics* 162, 106–121. doi: 10.1016/0005-272890219-3

Nagasaka, S., and Yoshimura, E. (2008). External iron regulates polyphosphate content in the acidophilic, thermophilic alga *Cyanidium caldarium*. *Biol. Trace Elem. Res.* 125, 286–289. doi: 10.1007/s12011-008-8177-9

Naumann, B., Busch, A., Allmer, J., Ostendorf, E., Zeller, M., Kirchhoff, H., et al. (2007). Comparative quantitative proteomics to investigate the remodeling of bioenergetic pathways under iron deficiency in *Chlamydomonas reinhardtii*. *Proteomics* 7, 3964–3979. doi: 10.1002/pmic.200700407

Naumann, B., Stauber, E. J., Busch, A., Sommer, F., and Hippler, M. (2005). N-terminal processing of Lhca3 is a key step in remodeling of the photosystem I-light-harvesting complex under iron deficiency in *Chlamydomonas reinhardtii*. *J. Biol. Chem.* 280, 20431–20441. doi: 10.1074/jbc.M414486200

Niemelä, M., Perämäki, P., Kola, H., and Piispanen, J. (2003). Determination of arsenic, iron and selenium in moss samples using hexapole collision cell, inductively coupled plasma-mass spectrometry. *Anal. Chim. Acta* 493, 3–12. doi: 10.1016/S0003-267000819-5

Page, M. D., Allen, M. D., Kropat, J., Urzica, E. I., Karpowicz, S. J., Hsieh, S. I., et al. (2012). Fe sparing and Fe recycling contribute to increased superoxide dismutase capacity in iron-starved *Chlamydomonas reinhardtii*. *Plant Cell* 24, 2649–2665. doi: 10.1105/tpc.112.098962

Page, M. D., Kropat, J., Hamel, P. P., and Merchant, S. S. (2009). Two *Chlamydomonas* CTR copper transporters with a novel cys-met motif are localized to the plasma membrane and function in copper assimilation. *Plant Cell* 21, 928–943. doi: 10.1105/tpc.108.064907

Paz, Y., Shimoni, E., Weiss, M., and Pick, U. (2007). Effects of iron deficiency on iron binding and internalization into acidic vacuoles in *Dunaliella salina*. *Plant Physiol.* 144, 1407–1415. doi: 10.1104/pp.107.100644

Pelletier, B., Trott, A., Morano, K. A., and Labbé, S. (2005). Functional characterization of the iron-regulatory transcription factor Fep1 from *Schizosaccharomyces pombe*. *J. Biol. Chem.* 280, 25146–25161. doi: 10.1074/jbc.M502947200

Petroutsos, D., Terauchi, A. M., Busch, A., Hirschmann, I., Merchant, S. S., Finazzi, G., et al. (2009). PGRL1 participates in iron-induced remodeling of the photosynthetic apparatus and in energy metabolism in *Chlamydomonas reinhardtii*. *J. Biol. Chem.* 284, 32770–32781. doi: 10.1074/jbc.M109.050468

Porra, R. J., Thompson, W. A., and Kriedemann, P. E. (1989). Determination of accurate extinction coefficients and simultaneous equations for assaying chlorophylls *a* and *b* extracted with four different solvents: verification of the concentration of chlorophyll standards by atomic absorption spectroscopy. *Bioenergetics* 975, 384–394. doi: 10.1016/S0005-272880347-0

Pröfrock, D., and Prange, A. (2012). Inductively Coupled Plasma–Mass Spectrometry (ICP-MS) for quantitative analysis in environmental and life sciences: a review of challenges, solutions, and trends. *Appl. Spectrosc.* 66, 843–868. doi: 10.1366/12-06681

Quinn, J. M., and Merchant, S. S. (1998). Copper-responsive gene expression during adaptation to copper deficiency. *Methods Enzymol.* 297, 263–279. doi: 10.1016/S0076-687997020-687997023

Rochaix, J.-D. (2002). *Chlamydomonas*, a model system for studying the assembly and dynamics of photosynthetic complexes. *FEBS Lett.* 529, 34–38. doi: 10.1016/S0014-579303181-2

Rubinelli, P., Siripornadulsil, S., Gao-Rubinelli, F., and Sayre, R. T. (2002). Cadmium- and iron-stress-inducible gene expression in the green alga *Chlamydomonas reinhardtii*: evidence for H43 protein function in iron assimilation. *Planta* 215, 1–13. doi: 10.1007/s00425-001-0711-3

Ruiz, F. A., Marchesini, N., Seufferheld, M., Govindjee, and Docampo, R. (2001). The polyphosphate bodies of *Chlamydomonas reinhardtii* possess a proton-pumping pyrophosphatase and are similar to acidocalcisomes. *J. Biol. Chem.* 276, 46196–46203. doi: 10.1074/jbc.M105268200

Salomé, P. A., Oliva, M., Weigel, D., and Krämer, U. (2013). Circadian clock adjustment to plant iron status depends on chloroplast and phytochrome function. *EMBO J.* 32, 511–523. doi: 10.1038/emboj.2012.330

Semin, B. K., Davletshina, L. N., Novakova, A. A., Kiseleva, T. Y., Lanchinskaya, V. Y., Aleksandrov, A. Y., et al. (2003). Accumulation of ferrous iron in *Chlamydomonas reinhardtii*. Influence of CO_2 and anaerobic induction of the reversible hydrogenase. *Plant Physiol.* 131, 1756–1764. doi: 10.1104/pp.102.018200

Spiller, S. C., Castelfranco, A. M., and Castelfranco, P. A. (1982). Effects of iron and oxygen on chlorophyll biosynthesis I. *In vivo* observations on iron and oxygen-deficient plants. *Plant Physiol.* 69, 107–111. doi: 10.1104/pp.69.1.107

Stookey, L. L. (1970). Ferrozine - a new spectrophotometric reagent for iron. *Anal. Chem.* 42, 779–781. doi: 10.1021/ac60289a016

Terauchi, A. M., Peers, G., Kobayashi, M. C., Niyogi, K. K., and Merchant, S. S. (2010). Trophic status of *Chlamydomonas reinhardtii* influences the impact of iron deficiency on photosynthesis. *Photosynth. Res.* 105, 39–49. doi: 10.1007/s11120-010-9562-8

Terzulli, A., and Kosman, D. J. (2010). Analysis of the high-affinity iron uptake system at the *Chlamydomonas reinhardtii* plasma membrane. *Eukaryot. Cell* 9, 815–826. doi: 10.1128/EC.00310-09

Thimm, O., Essigmann, B., Kloska, S., Altmann, T., and Buckhout, T. J. (2001). Response of Arabidopsis to iron deficiency stress as revealed by microarray analysis. *Plant Physiol.* 127, 1030–1043. doi: 10.1104/pp.010191

Tottey, S., Block, M. A., Allen, M., Westergren, T., Albrieux, C., Scheller, H. V., et al. (2003). *Arabidopsis* CHL27, located in both envelope and thylakoid membranes, is required for the synthesis of protochlorophyllide. *Proc. Natl. Acad. Sci. U.S.A.* 100, 16119–16124. doi: 10.1073/pnas.2136793100

Umen, J. D. (2005). The elusive sizer. *Curr. Opin. Cell Biol.* 17, 435–441. doi: 10.1016/j.ceb.2005.06.001

Urzica, E. I., Casero, D., Yamasaki, H., Hsieh, S. I., Adler, L. N., Karpowicz, S. J., et al. (2012). Systems and *trans*-system level analysis identifies conserved iron deficiency responses in the plant lineage. *Plant Cell* 24, 3921–3948. doi: 10.1105/tpc.112.102491

Vance, P., and Spalding, M. H. (2005). Growth, photosynthesis, and gene expression in *Chlamydomonas* over a range of CO_2 concentrations and CO_2/O_2 ratios: CO_2 regulates multiple acclimation states. *Can. J. Bot.* 83, 796–809. doi: 10.1139/b05-064

Vert, G., Grotz, N., Dédaldéchamp, F., Gaymard, F., Guerinot, M. L., Briat, J.-F., et al. (2002). IRT1, an arabidopsis transporter essential for iron uptake from the soil and for plant growth. *Plant Cell* 14, 1223–1233. doi: 10.1105/tpc.001388

Vigani, G., Zocchi, G., Bashir, K., Philippar, K., and Briat, J.-F. (2013). Signals from chloroplasts and mitochondria for iron homeostasis regulation. *Trends Plant Sci.* 8, 305–311. doi: 10.1016/j.tplants.2013.01.006

Vogl, J., Klingbeil, P., Pritzkow, W., and Riebe, G. (2003). High accuracy measurements of Fe isotopes using hexapole collision cell MC-ICP-MS and isotope dilution for certification of reference materials. *J. Anal. Atom. Spectrom.* 18, 1125–1132. doi: 10.1039/B301812A

Wang, H.-Y., Klatte, M., Jakoby, M., Bäumlein, H., Weisshaar, B., and Bauer, P. (2007). Iron deficiency-mediated stress regulation of four subgroup Ib *BHLH* genes in *Arabidopsis thaliana*. *Planta* 226, 897–908. doi: 10.1007/s00425-007-0535-x

Weger, H. G. (1999). Ferric and cupric reductase activities in the green alga *Chlamydomonas reinhardtii*: Experiments using iron-limited chemostats. *Planta* 207, 377–384. doi: 10.1007/s004250050495

Weger, H. G., and Espie, G. S. (2000). Ferric reduction by iron-limited *Chlamydomonas* cells interacts with both photosynthesis and respiration. *Planta* 210, 775–781. doi: 10.1007/s004250050679

Wollman, F.-A., and Bennoun, P. (1982). A new chlorophyll-protein complex related to photosystem I in *Chlamydomonas reinhardii*. *Bioenergetics* 680, 352–360. doi: 10.1016/0005-272890149-9

Wollman, F.-A., and Delepelaire, P. (1984). Correlation between changes in light energy distribution and changes in thylakoid membrane polypeptide phosphorylation in *Chlamydomonas reinhardtii*. *J. Cell Biol.* 98, 1–7. doi: 10.1083/jcb.98.1.1

Xu, W., Barrientos, T., and Andrews, N. C. (2013). Iron and copper in mitochondrial diseases. *Cell Metab.* 17, 319–328. doi: 10.1016/j.cmet.2013.02.004

Xue, X., Collins, C. M., and Weger, H. G. (1998). The energetics of

extracellular Fe(III) reduction by iron-limited *Chlamydomonas reinhardtii* (Chlorophyta). *J. Phycol.* 34, 939–944. doi: 10.1046/j.1529-8817.1998.340939.x

Yang, T. J. W., Lin, W.-D., and Schmidt, W. (2010). Transcriptional profiling of the Arabidopsis iron deficiency response reveals conserved transition metal homeostasis networks. *Plant Physiol.* 152, 2130–2141. doi: 10.1104/pp.109.152728

Yip, Y.-c., and Sham, W.-c. (2007). Application of collision/reaction-cell technology in isotope dilution mass spectrometry. *Trends Anal. Chem.* 26, 727–743. doi: 10.1016/j.trac.2007.03.007

Zhang, L., Happe, T., and Melis, A. (2002). Biochemical and morphological characterization of sulfur-deprived and H2-producing *Chlamydomonas reinhardtii* (green alga). *Planta* 214, 552–561. doi: 10.1007/s004250100660

Zheng, L., Huang, F., Narsai, R., Wu, J., Giraud, E., He, F., et al. (2009). Physiological and transcriptome analysis of iron and phosphorus interaction in rice seedlings. *Plant Physiol.* 151, 262–274. doi: 10.1104/pp.109.141051

Conflict of Interest Statement: The authors declare that the research was conducted in the absence of any commercial or financial relationships that could be construed as a potential conflict of interest.

Received: 24 May 2013; paper pending published: 17 June 2013; accepted: 09 August 2013; published online: 02 September 2013.

*Citation: Glaesener AG, Merchant SS and Blaby-Haas CE (2013) Iron economy in Chlamydomonas reinhardtii. Front. Plant Sci. **4**:337. doi: 10.3389/fpls.2013.00337*

This article was submitted to Plant Nutrition, a section of the journal Frontiers in Plant Science.

frontiers in
PLANT SCIENCE

REVIEW ARTICLE
published: 13 September 2013
doi: 10.3389/fpls.2013.00359

Iron: an essential micronutrient for the legume–rhizobium symbiosis

Ella M. Brear[1], David A. Day[2] and Penelope M. C. Smith[1]*

[1] School of Biological Sciences, The University of Sydney, Sydney, NSW, Australia
[2] School of Biological Sciences, Flinders University, Bedford Park, Adelaide, SA, Australia

Edited by:
Khurram Bashir, The University of Tokyo, Japan

Reviewed by:
Stephane Mari, Institut National pour la Recherche Agronomique, France
Stephan Clemens, University of Bayreuth, Germany
Federico José Battistoni, Instituto de Investigaciones Biológicas Clemente Estable, Uruguay

***Correspondence:**
Penelope M. C. Smith, School of Biological Sciences, Macleay Building A12, The University of Sydney, Sydney, NSW 2006, Australia
e-mail: penny.smith@sydney.edu.au

Legumes, which develop a symbiosis with nitrogen-fixing bacteria, have an increased demand for iron. Iron is required for the synthesis of iron-containing proteins in the host, including the highly abundant leghemoglobin, and in bacteroids for nitrogenase and cytochromes of the electron transport chain. Deficiencies in iron can affect initiation and development of the nodule. Within root cells, iron is chelated with organic acids such as citrate and nicotianamine and distributed to other parts of the plant. Transport to the nitrogen-fixing bacteroids in infected cells of nodules is more complicated. Formation of the symbiosis results in bacteroids internalized within root cortical cells of the legume where they are surrounded by a plant-derived membrane termed the symbiosome membrane (SM). This membrane forms an interface that regulates nutrient supply to the bacteroid. Consequently, iron must cross this membrane before being supplied to the bacteroid. Iron is transported across the SM as both ferric and ferrous iron. However, uptake of Fe(II) by both the symbiosome and bacteroid is faster than Fe(III) uptake. Members of more than one protein family may be responsible for Fe(II) transport across the SM. The only Fe(II) transporter in nodules characterized to date is GmDMT1 (*Glycine max* divalent metal transporter 1), which is located on the SM in soybean. Like the root plasma membrane, the SM has ferric iron reductase activity. The protein responsible has not been identified but is predicted to reduce ferric iron accumulated in the symbiosome space prior to uptake by the bacteroid. With the recent publication of a number of legume genomes including *Medicago truncatula* and *G. max,* a large number of additional candidate transport proteins have been identified. Members of the NRAMP (natural resistance-associated macrophage protein), YSL (yellow stripe-like), VIT (vacuolar iron transporter), and ZIP (Zrt-, Irt-like protein) transport families show enhanced expression in nodules and are expected to play a role in the transport of iron and other metals across symbiotic membranes.

Keywords: legume–rhizobium symbiosis, nitrogen fixation, nodule, iron, symbiosome, bacteroid, symbiosome membrane

INTRODUCTION

All plants require the micronutrient iron for optimum growth. However, legumes, which develop symbiotic relationships with nitrogen-fixing bacteria, have an increased demand for the micronutrient (Tang et al., 1990a). Both the plant and bacteria individually have an innate requirement, but it is also essential for the establishment, development, and function of the symbiosis (O'Hara, 2001). This review will focus on the role of iron in the legume–rhizobium symbiosis, specifically iron movement within the symbiotic organ, the nodule. We will also describe how the analysis of legume genomes and transcriptomes will enhance the identification of iron transporters in the nodule.

THE IMPORTANCE OF LEGUMES

Symbiotic nitrogen fixation (SNF) by rhizobia, housed within legume nodules, converts abundant but biologically unavailable atmospheric nitrogen to ammonia. Thus the ability of legumes to obtain fixed nitrogen from the bacteroid offers a growth advantage as soil nitrogen often limits plant growth (Graham and Vance, 2003). Not only is the symbiosis beneficial to the legume, SNF introduces approximately 40 million tonnes of nitrogen into agricultural soils each year (Herridge et al., 2008). This injection of nitrogen can be utilized by subsequent crops and reduces reliance on application of synthetic nitrogen fertilizer for enhanced crop yields.

THE DEVELOPMENT OF THE LEGUME–RHIZOBIUM SYMBIOSIS

Development of the symbiosis results in the production of a new plant organ, the root nodule, where SNF occurs. The induction of nodule organogenesis involves a signaling exchange between free-living soil bacteria and the legume host (Popp and Ott, 2011). This signaling dialog produces specificity to the interaction and ultimately results in attachment of rhizobia to the legume root hair cells and prepares the legume for infection (Schultze and Kondorosi, 1998).

Rhizobia attached to a root hair are transported toward root cortical cells, within an infection thread before being released into

root cortical cells where they are surrounded by a plant-derived membrane, the symbiosome membrane (SM) that separates them from the plant cell cytoplasm (Whitehead and Day, 1997). Rhizobia once differentiated into their symbiotic nitrogen fixing form are called bacteroids. The bacteroid, SM and the space surrounding the bacteroid, the symbiosome space, together comprise the symbiosome.

Rhizobia are released into root cortical cells from the infection thread via a process that shares similarities to exocytosis (Limpens et al., 2009; Ivanov et al., 2012). During release the rhizobia become encapsulated by the infection thread membrane, which is continuous with the plant plasma membrane (Whitehead and Day, 1997). To accommodate bacterial infection and proliferation, it is estimated that 21,500 μm^2 of SM is synthesized per infected cell (Roth and Stacey, 1989). Following initial formation, the composition of the SM reflects its plasma membrane origin, but modifications to its composition are continually made for the membranes specialized new role (Verma et al., 1978; Fortin et al., 1985). This modification includes synthesis and incorporation of new lipids and proteins, and is mediated by the secretory pathway (Catalano et al., 2004). The importance of the secretory pathway to nodule formation in *Medicago truncatula* is emphasized by secretory proteins making up 62% of all proteins expressed in nodules (Maunoury et al., 2010). The identity of the SM can be described as a mosaic that changes throughout development (Limpens et al., 2009). Following symbiosome formation and until senescence the SM is labeled with the known plasma membrane SNARE protein SYP132 (Limpens et al., 2009). Later, during symbiosome differentiation to senescence the late endosomal marker, Rab7 (Limpens et al., 2009), labels the SM. Vacuolar SNAREs are also acquired on the SM during senescence (Limpens et al., 2009).

The mature nodule is composed of the central infection zone, containing infected and uninfected cells, surrounded by layers of cells termed the cortex (Udvardi and Poole, 2013). Metabolites are transported to the nodule through the vasculature, which terminates in the cortex (Udvardi and Poole, 2013). Nodules can be divided into two types, determinant and indeterminant (**Figure 1**). Soybean and *Lotus japonicus* produce determinant nodules, which are spherical and contain bacteroids all at approximately the same developmental stage (Udvardi and Poole, 2013). Whereas indeterminant nodules, which develop on *M. truncatula*, *Pisum sativum*, and clover, are characterized by elongated or branched structures with meristems that remain throughout the life of the nodule. Unlike determinant nodules, which contain an infected region that matures and senesces together, indeterminant nodules are segmented into developmental zones a meristematic zone, an invasion zone where rhizobia are first released, a transition zone where bacteroids differentiate, a nitrogen fixation zone and a zone of senescence closest to the root (Udvardi and Poole, 2013).

The symbiosome can be thought of as a plant organelle with a specialized function for nitrogen fixation. Thus the symbiosome is expected to have unique properties that may change throughout nodule development to meet the requirements of differentiating bacteroids, nitrogen fixation and senescence (Whitehead and Day, 1997). Within the symbiosome, the bacteroid is reliant on the legume for the supply of a carbon source and all the other nutrients essential for bacterial metabolism and nitrogen fixation, apart from nitrogen itself (Udvardi and Day, 1997). All nutrients transported to the bacteroid must first cross the SM, allowing the legume to remain in control of the symbiosis.

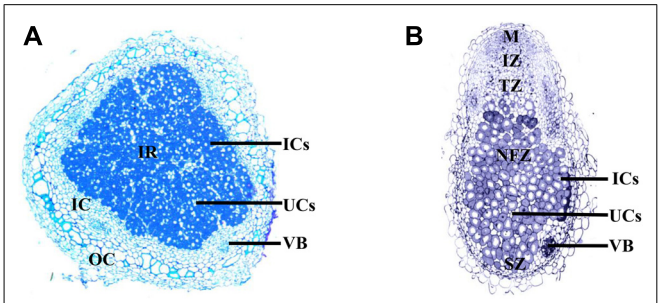

FIGURE 1 | Longitudinal cross section of the determinant soybean nodule (A), compared to a longitudinal cross section of the indeterminant *M. truncatula* nodule (B). The determinant soybean nodule consists of a central infected region (IR), composed of infected cells (ICs; dark) dispersed between uninfected cells (UCs; light); surrounding the IR is the inner cortex (IC), which includes the vascular bundles surrounded by parenchyma cells; the outer cortex (OC), encapsulates the nodule. The meristem of the indeterminant *M. truncatula* nodule remains active throughout nodule development, allowing continual growth. As a result the nodule is divided into sequential zones of development, including the meristem (M); invasion zone (IZ), where rhizobia infect divided cortical cells; a transition zone (TZ), composed of infected cells containing differentiating bacteria; a nitrogen fixation zone (NFZ) and a zone of senescence (SZ) close to the root. Images courtesy of Aleksandr Gavrin.

IRON DEFICIENCY AND THE LEGUME–RHIZOBIUM SYMBIOSIS

Legumes involved in a nitrogen-fixing symbiosis have a greater requirement for iron (Tang et al., 1990a). The rate of nitrogen fixation in *Phaseolus vulgaris* L. nodules is positively correlated with increasing nodule iron concentrations (Slatni et al., 2008). Under iron deficient conditions soybean and peanut with active nodules have a heightened response to iron deficiency (O'Hara et al., 1988; Terry et al., 1991). Iron stress induces the secretion of H^+ into the rhizosphere and the activity of Fe(III) reductase in soybean, to enhance iron uptake from the soil (Terry et al., 1991). Lupins require a greater supply of iron when relying on SNF for the supply of nitrogen when compared to plants grown with nitrogen fertilizer (Tang et al., 1990b).

Iron deficiency can affect both the legume host and the rhizobia individually or can have a direct affect on their interaction. All legumes are affected by iron deficiency, but the effect on the symbiosis varies between legume species. Studies on iron deficiency and nodule formation have been conducted for peanut, chickpea, lupin, lentil, soybean, and French bean (Tang et al., 1990b). Iron deficiency affected either nodule initiation or later development. When *Lupinus angustifolius* L. is grown under iron deficiency, fewer nodules form, indicating an effect on nodule initiation (Tang et al., 1990a). In contrast iron deficiency does not affect the initiation of nodules in peanuts, common bean and soybean, but rather affects later nodule development (O'Hara et al., 1988; Soerensen et al., 1988; Slatni et al., 2011). Peanuts grown under iron deficiency have lower concentrations of leghemoglobin, a delayed onset of nitrogen fixation and up to 215 times fewer bacteroids

within the infected region (O'Hara et al., 1988), indicating an effect on the differentiation of rhizobia and the development of the resulting bacteroids.

When *Lupinus angustifolius* L. plants were grown in a split root system so that the effect of reduced metabolite supply from the shoot could be distinguished from the direct affects of iron deficiency on the symbiosis, iron was not translocated from an uninoculated root exposed to sufficient iron to the roots exposed to iron deficiency and there was no affect of foliar application of iron on nodule development, suggesting that the signaling of iron deficiency is not systemic (Tang et al., 1990b). However, in the same experiment peanut showed enhanced nodule initiation, development, and nitrogen fixation following application of foliar iron compared to an iron deficient control (O'Hara et al., 1988).

REQUIREMENT FOR IRON IN THE SYMBIOSIS

The requirement for iron by legumes with an active symbiosis is large because many symbiotic proteins incorporate iron. Iron is required by the very numerous bacteroids for the synthesis of the nitrogen-fixing enzyme, nitrogenase, as well as cytochromes, ferredoxin, and hydrogenase (Guerinot, 1991; Delgado et al., 1998; O'Hara, 2001; Dixon and Kahn, 2004; Peters and Szilagyi, 2006). This requirement for iron by the symbiosis is highlighted by the proportion of iron within the nodule compared to other plant organs. At nodule maturity soybean nodules have the highest iron concentration, approximately 44% of the iron within soybean plants is present in the nodule compared to 31% in leaves, 7% in seed, and 5% in roots (Burton et al., 1998). At seed maturity, the seed has the highest iron concentration of all organs approximately 35% compared to 27% in the nodule, 23% in leaves, 9% in roots, and 3% in the stem (Burton et al., 1998).

Nitrogenase is a metalloenzyme, which catalyses the conversion of atmospheric dinitrogen to ammonia. Iron is essential in the two components that make up nitrogenase. The iron protein is the smaller component, which is reduced and provides electrons to the molybdenum-iron protein, a larger, heterotetrameric component that contains the catalytic site (Dixon and Kahn, 2004). At the catalytic site, dinitrogen binds and is reduced (Peters and Szilagyi, 2006). Both the iron protein and the molybdenum-iron protein are sensitive to oxygen.

Other iron-containing proteins essential for the symbiosis include ferredoxin, a non-heme protein, involved in transferring electrons and reducing the iron component of nitrogenase (Dixon and Kahn, 2004), and cytochrome components of the bacterial respiratory electron transport chain, essential for providing the energy for nitrogen fixation (Delgado et al., 1998).

There is a conflicting requirement for oxygen by the bacteroid. Nitrogenase is extremely sensitive to oxygen, thus the nodule must maintain low oxygen concentrations while maintaining oxygen supply for bacterial metabolism (Appleby, 1984). As well as an oxygen diffusion barrier in the cortex, infected cells synthesize leghemoglobin to bind oxygen and facilitate diffusion to the bacteroids, while maintaining oxygen concentrations at microaerobic levels for both respiration and nitrogen fixation (Appleby, 1984). Leghemoglobin is present within the cytoplasm of infected cells, at a concentration of approximately 3 mM (Bergersen and Appleby, 1981). Whether leghemoglobin is present within the symbiosome space is controversial (Appleby, 1984). However, if present it is found at low concentrations, approximately 200–500 μM (Bergersen and Appleby, 1981). The apoprotein and heme moiety, both components of leghemoglobin are synthesized by the plant (O'Brian, 1996). Iron is incorporated into the protoporphyrin ring by iron chelatase during the final stage of the tetrapyrrole biosynthetic pathway, resulting in the formation of protoheme (Vavilin and Vermaas, 2002). This protoheme is then incorporated into the apoprotein synthesized in the plant cytoplasm (Verma et al., 1979). An estimated 24% of soluble iron within the nodule is present within leghemoglobin (Ragland and Theil, 1993), thus iron plays an important role in maintaining the nodule environment for the symbiosis.

IRON SUPPLY TO THE NODULE

Iron is transported throughout the plant within the xylem, where it is maintained as a ferric citrate complex due to the low pH of the xylem (Cline et al., 1982). There is evidence for transport of ferric citrate in a number of plant species including the legume, soybean (Tiffin, 1970; Lopez-Millan et al., 2000). Tri-iron (III), tri-citrate (Fe_3Cit_3) is the main iron citrate species transported in tomato xylem exudates (Rellan-Alvarez et al., 2010). As well as iron movement within the xylem, nodules may also take up ferrous iron directly, as there is a ferric chelate reductase on the surface of *Phaseolus vulgaris* L. nodules (Slatni et al., 2009). Analysis of an iron efficient common bean variety with antibodies raised against a H^+-ATPase and *Arabidopsis* IRT1 (iron transporter 1), suggests that immunologically related proteins are present in nodule cortex cells in response to iron deficiency and that direct uptake of iron from the rhizosphere may complement supply from the plant when iron availability is limiting (Slatni et al., 2012). However, when the localization of iron was observed within the indeterminant *M. truncatula* nodule, no iron was localized at the epidermis of the nodule (Rodriguez-Haas et al., 2013), suggesting that direct uptake of iron from the rhizosphere by the nodule is not the main route of iron acquisition.

IRON CONCENTRATIONS ACROSS NODULE DEVELOPMENT

Throughout nodule development, the concentration and distribution of iron within the nodule fluctuates as the role of the symbiotic organ changes over time. Rodriguez-Haas et al. (2013) recently monitored iron distribution in indeterminant *M. truncatula* nodules using synchrotron-based X-ray fluorescence and their results enhance previously proposed theories about iron movement within the nodule.

The nodule meristem is characterized by low concentrations of iron (Rodriguez-Haas et al., 2013). During the early stages of soybean nodule development the concentration of the iron storage protein ferritin increases, reaching maximum concentration 12 days after inoculation (DAI) with rhizobia (Ragland and Theil, 1993). Within the nodule, ferritin accumulates in both infected and uninfected cells (Lucas et al., 1998). This accumulation is proposed to concentrate iron ready for incorporation into nitrogenase and leghemoglobin, beginning around 12 DAI (Ragland and Theil, 1993). Iron concentration within the nodule increases greatly between 12 and 15 DAI,

remaining constant until 36 DAI (Ragland and Theil, 1993). Iron is abundant within the apoplast of zone II, while in zone III, the region of nitrogen fixation, iron becomes incorporated into infected cells (Rodriguez-Haas et al., 2013). Many of the iron-containing symbiotic proteins are synthesized within the bacteroid so following iron incorporation into infected cells iron must then transverse both the symbiosome and bacteroid membrane.

Iron concentrations within the determinant soybean nodule began to decrease 39 DAI (Burton et al., 1998). During senescence, at approximately 77 DAI, the decline in iron concentration is met with an increase in ferritin, which is thought to complex iron produced from the breakdown of leghemoglobin and nitrogenase, ready for remobilization to the seed (Burton et al., 1998; Lucas et al., 1998). Iron remobilization from the senescing *M. truncatula* nodule is supported by accumulation of iron around vessels near the senescing zone (Rodriguez-Haas et al., 2013).

IRON MOVEMENT WITHIN THE NODULE

Within the nodule, iron must be directed to the cells and organelles that synthesize iron-containing proteins. In the case of nitrogenase and cytochromes of the bacteroid respiratory chain, iron must firstly enter the infected cells of the nodule and then transverse the SM before being taken up by the bacteroid from the symbiosome space. Iron is also required in the cytoplasm of infected cells for incorporation into leghemoglobin, as well as in very numerous mitochondria that line the periphery of these cells (Wittenberg et al., 1996). The movement of iron throughout the plant relies on the strict control of redox state and chelate formation, to avoid iron toxicity and precipitation (Kobayashi and Nishizawa, 2012). Evidence for how iron is transported across the numerous nodule membranes to the bacteroid is limited but what is known is presented below.

IRON UNLOADING FROM THE XYLEM

Although iron unloading from xylem vessels has not been directly studied in nodules, it may have similarities to iron transport from xylem to leaf mesophyll cells. Iron (III)-citrate is transported to the shoot in xylem vessels and is released into the apoplast (Brüggemann et al., 1993).

FROM VASCULATURE TO INFECTION ZONE

A number of cell layers, including one or two layers of distributing, boundary and pericycle cells, separate the vascular bundle from the infected zone in soybean nodules (Guinel, 2009). Little is known about iron movement between the xylem and infected cells, both symplastic and apoplastic routes are postulated (**Figure 2**).

The presence of plasmodesmata connections between all cell layers from pericycle cells, adjacent to xylem, to infected cells suggests a possible route for symplastic transport to infected cells in soybean nodules (Brown et al., 1995). Symplastic transport within the nodule would require the reduction of iron (III) and dissociation from citrate (Brüggemann et al., 1993). The resulting iron (II) then could be chelated to nicotianamine (NA) and imported into the cell via members of the yellow stripe-like (YSL) transporter family or taken up directly as ferrous iron via members of the natural resistance-associated macrophage protein (NRAMP) or ZIP (Zrt-, Irt-like protein) transporter families prior to chelation to NA (Kobayashi and Nishizawa, 2012). The iron(II)-NA chelate could then be readily transferred via symplastic route. Despite the presence of plasmodesmata connections between cells spanning from xylem to infected cell, the movement of symplastic and apoplastic dyes within *M. truncatula* nodules suggests a barrier to symplastic continuity (Bederska et al., 2012). There appears to be a requirement for localized apoplastic transport within the pericycle, surrounding the xylem and prior to uptake into the infected cell (Bederska et al., 2012).

Alternatively Fe(III)-citrate, could be transported apoplastically toward the infected region. The slightly acidic pH of the apoplast would promote the oxidation of iron and the formation of Fe(III)-citrate. In *M. truncatula* nodules, Rodriguez-Haas et al. (2013), using synchrotron-based X-ray fluorescence, observed a thread-like distribution of iron around cells in the nodule parenchyma and particularly in zone II, suggesting iron is moving in the apoplast. Confirmation of the route of iron movement between the vasculature and infection zone will enable predictions about transport proteins involved in iron transport toward and into symbiosomes.

IRON TRANSPORT INTO THE INFECTED CELL

Iron transport into *Lotus japonicus* infected cells is enhanced by efflux of citrate via LjMATE1 (*Lotus japonicus* multidrug and toxic compound extrusion 1; Takanashi et al., 2013; **Figure 3**), suggesting that it occurs as a ferric citrate complex. LjMATE1 is expressed exclusively in infected cells early in development and catalyses efflux of citrate when expressed in *Xenopus* oocytes (Takanashi et al., 2013). When expression of LjMATE1 was reduced by RNAi, nitrogenase activity and leghemoglobin concentration were significantly decreased compared to control nodules (Takanashi et al., 2013), apparently as a result of less iron in infected cells. This decrease in leghemoglobin synthesis and nitrogenase activity was accompanied by increased concentrations of iron at the nodule–root junction and the vascular bundle of nodules. The early expression of LjMATE1 and its importance to concentrating iron within the infected region of nodules, suggests that citrate efflux into the apoplast of the infected region is important for iron import into these cells. In this context, LjMATE1 may play a similar role to FRD3, a MATE family member in *Arabidopsis* (Roschzttardtz et al., 2011). *frd3* mutants show iron deficiency in leaves even though iron uptake from the soil is constitutively active. FRD3 is a citrate effluxer and is thought to release citrate into the apoplast, to chelate iron and make it more soluble, to enable transport into the cytoplasm (Roschzttardtz et al., 2011). The protein/s responsible for transport across the plasma membrane of infected cells in soybean and other legumes are not known. A member of the Zrt-, Irt-like protein (ZIP) or NRAMP family may be involved but this would require reduction of Fe(III) by a ferric-chelate reductase before uptake (**Figure 3**). As iron is likely to be imported into infected cells from the apoplast in *M. truncatula* (Rodriguez-Haas et al., 2013), it is likely that similar transporter families are involved in uptake in indeterminant nodules. Transcriptome studies of *M. truncatula* suggest that expression of members of these families is enhanced in nodules (Benedito et al., 2008).

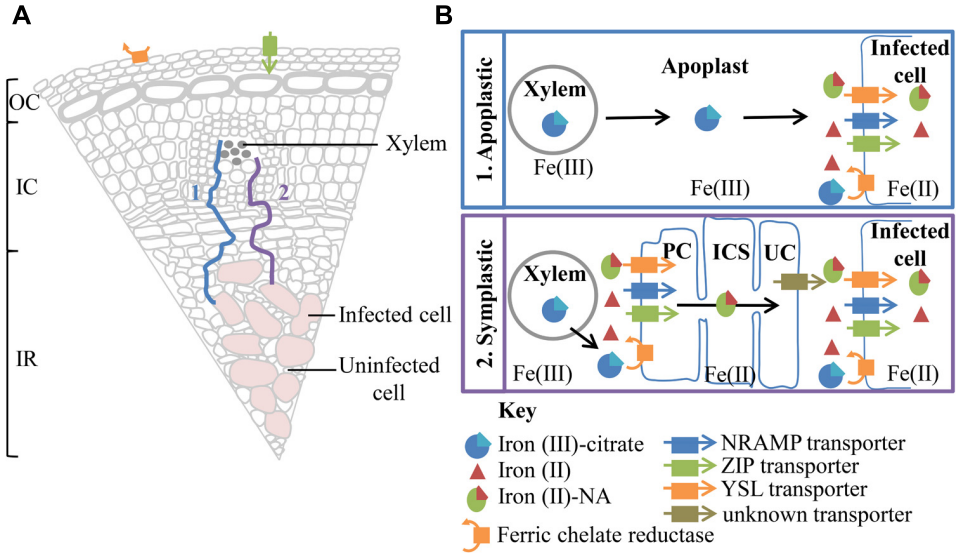

FIGURE 2 | A summary of possible transport pathways for iron from the xylem to the infected cell (A) and a more detailed depiction of the iron species and transporters involved (B). (A) The majority of iron entering the nodule is derived from iron citrate, translocated within the xylem. However, the presence of a ferric chelate reductase and a ZIP family, transporter related to *A. thaliana* IRT1, on the surface of the nodule, suggests a mechanism for direct iron uptake from the soil. The nodule is divided into three main sections the outer cortex (OC), inner cortex (IC), and infected region (IR). The xylem and infected cells are separated by a number of cell layers. Movement of iron to the infected cell could be either via an apoplastic (1) or symplastic (2) route. **(B)** Apoplastic transport involves the unloading of ferric citrate from the xylem into the apoplast. Ferric-citrate diffuses through the apoplast toward the infected cell, stabilized by the low pH. Uptake by the infected cells involve the reduction of ferric iron to ferrous iron. The resulting ferrous iron could then be imported into the infected cell by a member of the NRAMP or ZIP transporter family. Alternatively ferrous iron could chelate to nicotianamine (NA) and be imported into the infected cell via a member of the YSL transporter family. A symplastic path to the infected cell would require the initial reduction of ferric citrate by a ferric chelate reductase, localized on cells surrounding the xylem, possibly a pericycle cell (PC). Ferrous iron could then be imported into the cell via similar transport mechanisms utilized for uptake into the infected cell, highlighted above. Iron could move symplastically through the pericycle cells, inner cortex cells (ICS) and uninfected cells (UC) as a ferrous iron-NA chelate. Uninfected cells neighboring the infected cells possibly efflux ferrous iron-Na or dissociated ferrous iron. Now in the apoplast the ferrous iron could be oxidized and chelated to citrate to increase solubility. However, for import into the infected cell ferric iron must be reduced to ferrous iron.

IRON TRANSPORT ACROSS THE SYMBIOSOME MEMBRANE

Iron can cross the SM as both Fe(III) and Fe(II) (Moreau et al., 1995, 1998; LeVier et al., 1996; **Figure 3**). This was indicated by uptake of radiolabeled ferric and ferrous iron by isolated soybean symbiosomes. Inhibition of ferrous iron transport into symbiosomes by Cu(II) suggests that the protein responsible may not be specific for iron. The uptake of ferrous iron [Fe(II)] was faster than that of ferric iron [Fe(III); Moreau et al., 1998). Whether uptake of ferrous iron is favored by the symbiosome within the natural nodule environment is yet to be determined and will most likely depend on the concentrations of Fe(II) and Fe(III) in the infected cell cytosol. Unlike the soil environment, where iron is found in an oxidized state, the nodule cytosol provides conditions for maintaining iron in its reduced ferrous state (Moreau et al., 1995). This environment is created by the slightly acidic pH, microaerobic environment and the abundance of reducing molecules such as ascorbate and glutathione in the nodule infected cells. Ferric chelate reductase activity has been identified on the SM (LeVier et al., 1996). Initially it was thought that the reductase activity occurred on the cytoplasmic side of the SM, where Fe(III)-citrate, which is present at high concentrations within the nodule, is reduced before uptake into the symbiosome (LeVier et al., 1996). However, Moreau et al. (1998) postulated that the reductase activity was present within the symbiosome space based on the discovery of ferrous iron transport across the SM and the orientation of the plasma membrane reductase (outside the plasma membrane). The protein responsible for the ferric chelate reductase activity has not been identified to date, but two out of nine genes encoding ferric chelate reductase proteins (Glyma15g13090 and Glyma16g03770) are expressed in nodules at a higher level compared to root tissue (Libault et al., 2010; Severin et al., 2010; see **Table 1**). Due to their nodule expression, these proteins are potential candidates for the ferric chelate reductase activity of the SM. It will be interesting to determine their localization and role in iron movement within the nodule. The current model of iron transport across the SM postulates that both ferrous and ferric iron can be transported across the SM, although a transporter for Fe(III)-citrate has not been characterized in dicot plants (**Figure 3**). According to this model, ferric iron is reduced to ferrous iron within the symbiosome space by the SM ferric chelate reductase. The resulting ferrous iron could either be transported out of the symbiosome space into the bacteroid or into the infected cell cytosol (Moreau et al., 1998).

A ferrous iron transporter, *Glycine max* divalent metal transporter 1 (GmDMT1), with homology to the NRAMP transporter family, has been identified on the SM of soybean (Kaiser et al., 2003; **Figure 3**). GmDMT1 was able to complement the yeast iron transport mutant *fet3fet4* (Kaiser et al., 2003). Rates of Fe(II)

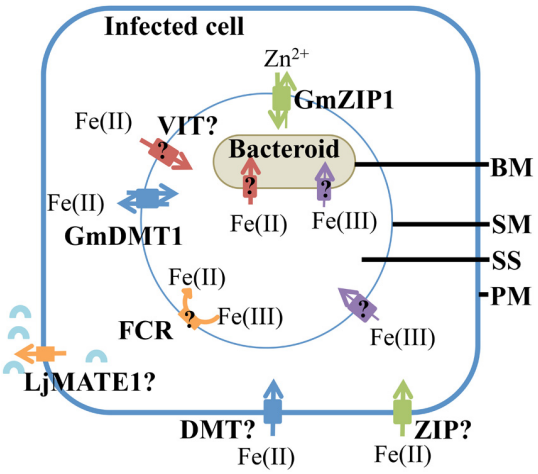

FIGURE 3 | Iron uptake into the infected cell and transport into the symbiosome. Ferrous iron transport into the infected cells, across the plasma membrane (PM) could me mediated by transporters belonging to the NRAMP, ZIP, or YSL family. A citrate effluxer, LjMATE1 is expressed in infected cells, it is predicted to release citrate (blue arc) into the apoplast surrounding infected cells to aid in iron uptake. It is likely to make iron in the apoplast more soluble. Both ferrous and ferric iron are transported across the symbiosome membrane (SM) and bacteroid membrane (BM). However, ferrous iron is taken up more rapidly. A ferric iron transporter, GmDMT1, is present on the SM, but it may not be the only ferrous iron transporter on the SM. Members of the VIT and ZIP transporter families are possible ferrous iron transporters on the SM. Although ferric iron is thought to cross the SM, no plant transporters are known to transport iron-citrate. Ferric chelate reductase activity (FCR) is present on the SM, however, the orientation on the SM has not been confirmed. Within the symbiosome space (SS) ferric iron could chelate siderophores produced by the bacteroid. Ferrous and ferric iron are transported across the bacteroid membrane (BM), but the transporters responsible have not been identified.

uptake by the yeast were similar to the kinetics observed for ferrous uptake into symbiosomes (Moreau et al., 1998). The ability of GmDMT1 to partially complement the zinc uptake mutant (ZHY3) and the ability of excess manganese to interrupt the uptake of ferrous iron, suggests that GmDMT1 is not specific for iron transport. Given ferrous iron uptake was inhibited by copper II in assays with isolated symbiosomes (Moreau et al., 1998) it would be interesting to determine if GmDMT1 also transports copper II.

Although there is evidence that ferrous iron is transported across the SM and that GmDMT1 is present on the SM, this does not prove GmDMT1's role in iron uptake into the symbiosome. The ability of GmDMT1 to complement a yeast mutant for iron transport on the plasma membrane, *fet3fet4*, suggests involvement in import of iron into the cell. However, the direction of transport into the symbiosome is similar to transport across the vacuolar membrane and therefore would be similar to efflux from the cell. Thus the orientation of GmDMT1 on the SM must be determined and its importance in iron uptake investigated, perhaps through RNAi disruption.

Members of the ZIP family of transporters, GmZIP1, are involved in iron transport in some plants and GmZIP1 has been detected on the SM (Moreau et al., 2002; **Figure 3**). However, there is no evidence so far that GmZIP1 transports iron and yeast complementation suggests a role in zinc transport (Moreau et al., 2002). The ZIP family of transporters and their possible role in iron transport within the nodule will be discussed later.

IRON AND THE SYMBIOSOME SPACE

It appears that the majority of iron transported into symbiosomes is not directly incorporated into the bacteroid (LeVier et al., 1996). Rather, the symbiosome space appears to be a storage site for iron within the nodule. The concentration of non-heme iron within the symbiosome space is estimated to be approximately 0.5–2.5 mM, and is thought to be complexed with siderophores derived from the bacteroid (Wittenberg et al., 1996), this represents approximately 7–20% of total non-heme iron extracted from whole nodules. The symbiosome space has a lower pH than the plant cytosol owing to the action of both symbiotic partners (Pierre et al., 2013). An H^+-ATPase localized to the SM pumps protons from the plant cytoplasm into the symbiosome space, while the bacteroid also contributes protons to the symbiosome space through the action of the electron transport chain (Udvardi and Day, 1997). Pierre et al. (2013) estimated the pH of the symbiosome space to range between 4.5 and 5 using acidotropic probes. The low pH of the symbiosome space would promote the stabilization of ferric chelates such as ferric citrate (Cline et al., 1982).

IRON UPTAKE BY THE BACTEROID

The majority of the symbiotically important iron-containing proteins are synthesized within the bacteroid. Consequently iron must be taken up by the bacteroid from the symbiosome space. Regulation of iron uptake has been extensively studied in free-living rhizobia. However, whether bacteroids within the symbiosome use the same iron uptake mechanisms as their free-living counterparts is still to be determined (Fabiano and O'Brian, 2012). A number of transcriptome studies comparing gene expression between free-living rhizobia and symbiotic bacteroids at different developmental stages have been conducted for a range of rhizobial strains (Barnett et al., 2004; Becker et al., 2004; Capela et al., 2006; Chang et al., 2007), but detailed comparisons of iron uptake into free-living bacteria and nitrogen-fixing bacteroids are lacking. Regulation of iron uptake by free-living, culture grown rhizobia has been extensively studied and role of iron responsive transcriptional regulators, such as IrrA and rirA, and the genes that they control under both iron deficient and sufficient conditions determined (Viguier et al., 2005; Todd et al., 2006). Many of the genes controlled by the regulators include genes for siderophore production, heme biosynthesis, and transporters such as a ferric siderophore ATP-binding cassette (ABC) transporter (Viguier et al., 2005; Todd et al., 2006).

Free-living rhizobia have a number of mechanisms to take up and compete for scarce iron from the soil. These include the release of ferric iron chelating siderophores, the reduction of ferric iron to ferrous iron followed by uptake of the resulting ferric iron, and the ability to utilize iron from heme compounds (Fabiano and O'Brian, 2012). Evidence for similar mechanisms of uptake into bacteroids is discussed below.

Ferrous iron

Isolated bacteroids can take up ferrous iron (LeVier et al., 1996; Moreau et al., 1998; **Figure 3**) and at a faster rate than ferric

Table 1 | Ferric chelate reductase family members encoded in the Soybean genome.

	Transcriptome				TMD	Homology to AtFRO2 (% similarity)
	Severin et al. (2010)		Libault et al. (2010)			
	Root	Nodule	Root	Nodule		
Glyma05g02600	1	0	0	0	8	30.57
Glyma07g07380	44	0	366	0	8	56.55
Glyma09g02170	0	0	3	0	9	29.93
Glyma10g37600	15	0	529	0	9	50.00
Glyma10g37610	1	1	16	0	9	49.79
Glyma15g13090	0	0	5	11	9	29.66
Glyma16g03770	0	11	0	93	9	55.43
Glyma17g09260	2	0	17	0	9	29.82
Glyma18g47060	0	0	0	0	9	54.81

A comparison of each reductase's expression in root and nodule tissue from two soybean transcriptome studies is presented (Libault et al., 2010; Severin et al., 2010). A prediction of the number of transmembrane domains (TMD) was analyzed by SOSUI (http://bp.nuap.nagoya-u.ac.jp/sosui/sosui_submit.html). Homology to AtFRO2, a characterized, ferric chelate reductase present in the outer root layers of A. thaliana, was calculated by a clustalW alignment.

iron. A homolog of the transporter involved in ferrous iron uptake, *Escherichia coli,* FeoB (Hantke, 2003) has been identified in *Bradyrhizobium japonicum* but has not been characterized (Fabiano and O'Brian, 2012).

Ferric iron chelates

One of the most common mechanisms for iron uptake uses low molecular weight, high affinity ferric iron ligands called siderophores. The formation of the siderophore-ferric iron chelate solubilizes ferric iron, allowing uptake. Rhizobia can either take up siderophores synthesized *de novo* and released or can scavenge siderophores produced by other soil microbes. The type of siderophore synthesized is not a characteristic of rhizobial strain (Guerinot, 1994), but fall into three major classes of siderophores including α-hydroxycarboxylates, catecholates, and hydroxamates (Miethke and Marahiel, 2007). Siderophore–ferric iron complexes are actively transported across the outer and cytoplasmic membrane of gram negative rhizobia. Ferric iron–siderophore complexes bind to TonB-dependent receptors on the outer membrane and are actively transported into the pericycle following activation by a cytoplasmic membrane complex (TonB–ExbBD), which couples the outer membrane to the proton motive force of the cytoplasmic membrane (Lim, 2010). Following release into the pericycle, the siderophore complex is taken up into the cytoplasm by ABC importers (Faraldo-Gomez and Sansom, 2003). Within the cytoplasm, the siderophore complex is dissociated by the reduction of ferric iron to ferrous iron (Matzanke et al., 2004). A ferric reductase has been identified in *B. japonicum* (Small and O'Brian, 2011).

Under iron limiting conditions, free-living rhizobia express TonB-dependent receptors after activation by the iron response regulator (Irr; Small et al., 2009). In contrast, active transport of siderophores by bacteroids appears to be unnecessary for the symbiosis. Evidence for this includes down regulation of expression of siderophore and heme TonB-dependent receptors and TonB itself, as well as Irr (Yeoman et al., 2000; Chang et al., 2007; Small et al., 2009) and ABC transporters (Barnett et al., 2004) in bacteroids. Mutations in ABC transporters, TonB-dependent receptors and TonB itself, have no affect on the function of the established symbiosis (Lynch et al., 2001; Nienaber et al., 2001; Wexler et al., 2001). This suggests that bacteroids do not require high affinity siderophore uptake to obtain iron during the symbiosis. However, *Sinorhizobium meliloti* have increased nodule occupancy under iron limiting conditions, compared to mutant strains with impaired siderophore uptake systems (Battistoni et al., 2002b). The ability of rhizobia to take up iron chelated to siderophores appears to provide a competitive advantage and may affect the effectiveness of the resulting symbiosis.

Although the proteins essential for siderophore uptake in rhizobia do not appear to be essential for the symbiosis, iron-binding chromophores have been identified within the symbiosome space (Wittenberg et al., 1996). Wittenberg et al. (1996) isolated the siderophore complexes from nodules infected with three different bradyrhizobial strains. The size and optical spectra of the isolated siderophore complexes differed between strains and it was hypothesized that the siderophores were of bacteroid origin.

Another ferric-chelating compound utilized by some rhizobia for iron uptake is citrate. Citrate has a lower affinity for iron than classic siderophores and is released by cells experiencing iron limitation. A strain of *B. japonicum* (61A152), a symbiotic partner of soybean, secretes citrate under iron limitation and was able to take up radiolabeled iron citrate (Guerinot et al., 1990). The mechanism of ferric citrate uptake by rhizobia has not been characterized but it possibly shares similarities with the ferric citrate uptake mechanisms of *E. coli,* another gram negative bacterium. *E. coli* utilize a similar mechanism for uptake of ferric citrate and ferric-siderophore chelates, requiring a TonB-dependent receptor on the outer membrane and a member of the ABC transporter family for transport across the cytoplasmic membrane (Enz et al., 2000).

Like their free-living counterparts, isolated *B. japonicum* bacteroids can take up ferric citrate complexes labeled with ^{59}Fe (Moreau et al., 1995). However, uptake of Fe(III)-chelates across the bacteroid membrane is very slow compared with uptake of ferrous iron (LeVier et al., 1996; Moreau et al., 1998). If ferric chelates are not the major source of iron transported into bacteroids, it raises the issue of why bacteroids produce siderophores. It is not known whether bacteroids experience iron limitation in the symbiotic environment. However, the reduced expression of proteins involved in siderophore synthesis and ferric siderophore uptake suggests not only that ferric iron chelates are not the major form of iron transported to the bacteroid, but also that the bacteroid, does not experience iron stress like free-living rhizobia. Ferric iron may have a greater importance as the iron storage form within the symbiosome space (LeVier et al., 1996), where it is captured by siderophores after transport across the SM so it remains sequestered within the symbiosome space (Wittenberg et al., 1996). The stored ferric iron could then be reduced to ferrous iron prior to uptake by the bacteroid (LeVier et al., 1996).

Heme uptake

As mentioned earlier, leghemoglobin is abundant within the nodule. Like pathogenic bacteria that infect animals, free-living rhizobia are able to utilize leghemoglobin, heme, and hemoglobin as iron sources when iron is limiting (Noya et al., 1997). Bacteroids do not have contact with the pool of leghemoglobin found within infected cells (Wittenberg et al., 1996) and therefore it is probably not a major source of iron during symbiosis. However, leghemoglobin may be of importance during nodule senescence (Noya et al., 1997) because the nodule cytosol becomes acidic and this promotes the dissociation of heme from leghemoglobin (Herrada et al., 1993). Also, the membranes within the nodule including the SM degrade and rhizobia could utilize this pool of newly available heme or the heme could be released into the rhizosphere following degradation of the nodule (Noya et al., 1997). The mechanism used by rhizobia to take up heme appears to be similar to transport mechanisms used for siderophore uptake (Noya et al., 1997). Further evidence for the ability of rhizobia to utilize heme as an iron source is shown by the discovery of a putative high affinity heme-binding outer membrane protein (Battistoni et al., 2002a). However, like mechanisms for siderophore uptake, mutations in heme transport proteins do not affect the symbiosis (Nienaber et al., 2001;Wexler et al., 2001), suggesting heme uptake is not essential for iron supply to the bacteroid.

SENESCENCE AND REMOBILIZATION OF IRON IN THE NODULE

During nodule senescence, membranes degrade and iron is released, inhibiting nitrogen fixation and thereby triggering further senescence. Iron present within leghemoglobin plays a key role in promoting senescence of the nodule. When the nodule begins to senesce, the nodule cytosol becomes more acidic, promoting autoxidation of leghemoglobin and production of superoxide anions and hydrogen peroxide (Herrada et al., 1993). Hydrogen peroxide is known to dissociate iron from leghemoglobin and this free iron can degrade membranes within the nodule (Herrada et al., 1993). This is a problem for indeterminant nodules because within the one nodule there are regions undergoing senescence, while other regions are actively fixing nitrogen. It has been postulated that the increase in ferritin observed within younger infected regions close to senescing zones might restrict the spread of iron-induced senescence and prolong nitrogen fixation (Strozycki et al., 2007). This differs from determinant nodules where the whole nodule senesces at the same time. However, the observation that ferritin increases in the cortex of senescing lupin nodules may also be to contain iron spread during senescence (Lucas et al., 1998).

At the time of nodule senescence, formation of the seed becomes the priority for the legume and the high concentrations of iron in the nodule provide a ready supply of iron for the seed (Burton et al., 1998). The available iron may include iron from leghemoglobin, which is known to decrease in the nodule at senescence (Puppo et al., 1991). During the period of seed filling nodules were shown to lose between 40 and 58% of radiolabeled iron, thus nodules may contribute to a large proportion of seed iron if all this iron is transported to the seed (Burton et al., 1998). This iron may be transported to the seed as a NA-chelate in the phloem (Curie et al., 2009).

A protein potentially involved in the redistribution of nodule iron is *L. japonicas* NA synthase 2 (LjNAS2; Hakoyama et al., 2009). NA synthase catalyses the formation of NA, a phytosiderophore precursor that is present in all plants and forms complexes with a range of metals including Fe(II) and Fe(III) (Curie et al., 2009). LjNAS2 is expressed in nodule vascular bundles, is nodule specific and its expression reaches a maximum at 24 DAI (Hakoyama et al., 2009). Suppression of LjNAS2 expression specifically by RNAi silencing did not have an affect on nitrogen fixation, suggesting that LjNAS2 is not involved in iron supply to the nodule (Hakoyama et al., 2009). This phenotype could possibly indicate the redundancy of LjNAS2. However, only one other NAS, LjNAS1, is encoded in the *L. japonicas* genome (Hakoyama et al., 2009). LjNAS1 has 62.3% amino acid homology to LjNAS2, but unlike LjNAS2, LjNAS1 is expressed predominantly in cotyledons, leaves, and stems, with expression in nodules very low (Hakoyama et al., 2009). Due to the low nodule expression of LjNAS1, the phenotype observed due to suppression of LjNAS2, suggests LjNAS2's role is not redundant. Hakoyama et al. (2009) hypothesize that LjNAS2 may play a role in remobilization of iron from the nodule at senescence and this is supported by the late expression of LjNAS2 during nodule development. Future studies observing LjNAS2 knockdown phenotypes during nodule senesces and seed maturation may enable the role of LjNAS2 to be further dissected. If iron is remobilized from nodules, chelated to NA, members of the YSL family may play a role. A number of which are expressed in nodules and will be discussed later (Libault et al., 2010; Severin et al., 2010).

POTENTIAL IRON TRANSPORTERS WITHIN THE NODULE

There are clear roles for iron transport within the nodules and we can predict where they should be localized, but only one nodule iron transporter, DMT1, has been functionally characterized and it is localized to the SM. Transcriptome analysis of the recently available legume genomes allows us to identify genes with nodule enhanced expression and, together with our knowledge of transporter function in our systems, to predict proteins with important roles in iron transport in the nodule. Movement of iron into

infected cells, for example, is likely to occur via a transporter involved in uptake into the cell, such as ZIP and NRAMP family members. Movement of iron into the symbiosome, on the other hand, could occur via an efflux transporter, such as the vacuolar iron transporter (VIT) family. Members of the YSL family are candidates for remobilization of iron from the nodule and possibly for ferrous iron chelate transport into the symbiosome. Here we will summarize the transcriptome information from soybean to highlight genes encoding possible iron transport proteins important in nodules.

THE ZIP FAMILY

Members of the ZIP transporter family can transport cadmium, zinc, copper, manganese, and iron in a diverse range of organisms (Hall and Guerinot, 2007). Members of this transporter family include the yeast zinc transporters Zrt1p and Zrt2p and the plant iron transporters AtIRT1, MtZIP6, and PsRIT1 (Vert et al., 2002; Cohen et al., 2004; Lopez-Millan et al., 2004). MtZIP6 can transport both iron and zinc (Lopez-Millan et al., 2004). The direction of transport is generally into the cellular cytoplasm, including transport across the plasma membrane into the cytosol and transport across organelle membranes into the cytosol (Hall and Guerinot, 2007). On this basis, ZIP transporters could be involved in transport of iron into infected cells or out of the SM. However, the first ZIP family member to be characterized in soybean, GmZIP1, appears to transport zinc in the opposite direction to all other ZIP family members because GmZIP1-specific antibodies inhibited zinc transport into isolated symbiosomes (Moreau et al., 2002). This suggests that the orientation on the SM may not follow transporter orientation seen for the PM or organelles, or that GmZIP1 allows bidirectional transport, because when it is expressed in yeast, it catalyzed import of zinc across the PM.

The *G. max* genome encodes 19 ZIP family members, with all but six expressed in nodules (**Table 2**). Five of these, Glyma14g37560, Glyma20g06210 (GmZIP1), Glyma15g41620, Glyma13g10790, and Glyma06g05460, have increased expression in nodules compared with other plant tissues. Analysis of nodule microsomal fractions using antibodies directed against AtIRT suggested at least three members of the ZIP family were expressed in nodules, although only one protein band could be identified in SM preparations, presumably corresponding to GmZIP1 (Moreau et al., 2002). This supports a role for ZIP proteins on membranes other than the SM in nodules and these might be responsible for transport of iron.

Table 2 | Expression of the ZRT, IRT-like (ZIP) family transporters encoded in the soybean genome.

	Transcriptome				TMD	Homology to MtZIP6 (% similarity)	Homology to AtIRT1 (% similarity)
	Severin et al. (2010)		Libault et al. (2010)				
	Root	Nodule	Root	Nodule			
Glyma02g13950	0	0	0	0	8	48	53
Glyma04g05410	2	1	0	0	4	42	39
Glyma06g05460	217	83	128	332	6	41	42
Glyma07g34930	40	0	38	0	8	73	59
Glyma08g17530	19	5	4	13	8	45	44
Glyma08g44010	8	5	19	2	9	19	23
Glyma11g27900	3	5	19	6	9	40	40
Glyma13g10780	0	0	0	0	-	44	40
Glyma13g10790	447	36	55	79	4	48	45
Glyma13g41330	46	6	247	1	9	20	21
Glyma14g37560	1	42	9	69	8	41	39
Glyma15g04090	59	24	141	43	9	18	20
Glyma15g04100	1	0	1	0	9	18	20
Glyma15g41620	25	16	4	42	8	46	44
Glyma17g34660	11	10	26	16	9	43	39
Glyma18g06740	4	7	19	14	8	41	39
Glyma18g08760	4	7	11	1	9	19	22
Glyma20g02770	97	0	255	0	8	74	61
Glyma20g06210	29	36	6	48	8	48	44

A comparison of each ZIP transporters expression in root and nodule tissue from two soybean transcriptome studies is presented (Libault et al., 2010; Severin et al., 2010). A prediction of the number of transmembrane domains (TMD) for each protein was analyzed using SOSUI (http://bp.nuap.nagoya-u.ac.jp/sosui/sosui_submit.html). Homology to characterized ferrous iron transporters of the ZIP family, MtZIP6 and AtIRT1 was calculated by a clustalW alignment.

NRAMP FAMILY OF TRANSPORTERS

The NRAMP transporter family are present in bacteria, plants, fungi, and mammals and are involved in general metal ion transport (including ferrous iron), driven by a proton gradient (Nevo and Nelson, 2006). In plants, NRAMP proteins can transport iron (Lanquar et al., 2005), manganese (Cailliatte et al., 2010; Lanquar et al., 2010; Sasaki et al., 2012), cobalt (Cailliatte et al., 2010), cadmium (Sasaki et al., 2012), and aluminum (Xia et al., 2010), and often have broad specificity. AtNRAMP3 and AtNRAMP4 are H^+ metal symporters responsible for iron and Mn mobilization from the vacuole (Lanquar et al., 2005, 2010). Many of the PM localized transporters are involved in transport of metals other than iron (Cailliatte et al., 2010; Sasaki et al., 2012), but peanut AhNRAMP1 is likely to be involved in iron acquisition from the soil (Xiong et al., 2012). Plant NRAMP proteins are generally involved in import into the cytoplasm, although there is some argument over the direction of transport of the mammalian NRAMP1 that suggests it could act as an exporter.

In the soybean genome, 17 genes are predicted to encode members of the NRAMP/DMT protein family (**Table 3**). Four of these are homologs of EIN2, a regulator of the ethylene-signaling pathway in *Arabidopsis* (Alonso et al., 1999) and are unlikely to be involved in metal ion transport. Ten of the classical NRAMP genes are expressed in nodules, with expression of three genes, Glyma04g04660, Glyma06g04720, and Glyma17g18010, enhanced in nodules compared with roots (**Table 3**). Glyma17g18010 corresponds to GmDMT1, the ferrous iron transporter localized on the SM (Kaiser et al., 2003). The three proteins have higher similarity to AtNRAMP3 than any other soybean family members (**Table 3**).

Based on the characterization of known NRAMP/DMT proteins, NRAMP/DMT homologs could be involved in metal ion transport across a number of membranes within the nodule. Similarity to AtNRAMP3 and 4 suggests they maybe localized to the vacuole or SM where they could re-mobilize stored iron. Since there is debate about the direction of transport of NRAMP1 in macrophages it is possible that NRAMP proteins expressed in nodules like GmDMT1 could participate in remobilization of iron from the symbiosome or uptake into the symbiosome (**Figure 3**). Other NRAMP proteins could be present on the plasma membrane of infected cells and mediate uptake into the infected cell (**Figure 3**).

THE VACUOLAR IRON TRANSPORTER FAMILY

Since uptake into the symbiosome involves efflux from the plant cell, we could predict that iron transporters present on the vacuolar membrane in other organisms could play a role in iron uptake into the symbiosome. Members of the VIT family are involved in the uptake of Fe(II) into the vacuole for storage. In yeast, CCC1 (Lapinskas et al., 1996; Li et al., 2001) and in *Arabidopsis*

Table 3 | Expression of members of the NRAMP transporter family encoded in the soybean genome.

	Transcriptome				TMD	Homology to AtNRAMP3 (% similarity)
	Severin et al. (2010)		Libault et al. (2010)			
	Root	Nodule	Root	Nodule		
Glyma01g39790	3	1	9	3	10	77
Glyma03g33850	6	3	29	26	11	18
Glyma04g04660	5	79	15	94	11	70
Glyma05g21780	7	3	23	7	9	75
Glyma06g04720	3	35	11	114	11	71
Glyma06g12190	82	4	263	4	11	36
Glyma07g02680	3	0	6	1	11	37
Glyma07g06490	0	0	0	0	11	64
Glyma08g23320	16	8	35	6	11	37
Glyma10g06610	7	6	39	40	11	20
Glyma11g05500	5	1	14	6	10	78
Glyma13g20810	11	5	53	42	11	19
Glyma13g44710	2	0	1	0	11	34
Glyma15g00590	2	1	4	3	12	35
Glyma16g03090	0	0	0	0	11	65
Glyma17g18010	14	32	63	63	9	75

A comparison of each NRAMP transporter's expression in root and nodule tissue from two soybean transcriptome studies is presented (Libault et al., 2010; Severin et al., 2010). A prediction of the number of transmembrane domains (TMD) for each protein was analyzed using SOSUI (http://bp.nuap.nagoya-u.ac.jp/sosui/sosui_submit.html). Homology to a characterized ferrous iron transporter of the NRAMP family, AtNRAMP3, was calculated by a clustalW alignment.

VIT1 (Kim et al., 2006), fulfill this role. In plants the VIT family includes two different groups, those with close homology to VIT1 and those with similarity to Nodulin21 from soybean (Delauney et al., 1990). Iron transport activity has not been proved for members of the Nodulin21 group although mutation of one member in *Lotus japonicus,* LjSEN1, blocks nitrogen fixation (Hakoyama et al., 2012), and some of the *Arabidopsis* members are regulated by iron availability (Gollhofer et al., 2011).

LjSEN1 is expressed specifically in infected cells of the nodule and the protein it encodes is proposed to be a ferrous iron transporter based on its distant homology to AtVIT1 (Kim et al., 2006) and CCC1 (Li et al., 2001). The development of symbiosomes is affected in *sen1* nodules. Infected cells at 8 DAI had multiple vacuoles and large symbiosomes with a seemingly large symbiosome space surrounding the bacteroids. Expression of *LjSEN1* in *S. cerevisiae* did not increase iron concentrations within transformed yeast cells (Hakoyama et al., 2012). However, this may be attributed to the expected localization of LjSEN1 to vacuoles within the yeast cell, rather than the cell membrane. Complementation studies expressing AtVIT1 in Δ*ccc1* yeast mutants provided evidence that AtVIT1 localizes to the vacuolar membrane in yeast. Thus LjSEN1 would also be predicted to localize to the vacuolar membrane in yeast and would not mediate iron uptake into yeast. It will be interesting to find the location of SEN1 in the nodule and to test for ferrous iron transport in Δ*ccc1* yeast mutants (Hakoyama et al., 2012).

The soybean genome encodes 20 members of the VIT family. Only two are closely related to VIT1. Expression of two of the Nodulin21-like genes, Glyma05g25010 and Glyma08g08120, is very high in nodules and not detected in any other tissue (**Table 4**). They have greater similarity to LjSEN1 than to AtVIT1 (**Table 4**). Due to the importance of LjSEN1 to the symbiosis, Glyma05g25010 and Glyma08g08120 are interesting candidates as possible essential iron transporters for the symbiosis.

THE YSL FAMILY

The YSL family of transporters forms a distinct group in the oligopeptide (OPT) superfamily with less than 20% similarity to other members (Curie et al., 2009; Ueno et al., 2009). The founding member of the YSL transporter family is ZmYS1, which is a symporter coupled to proton transport, and its expression is enhanced under iron deficiency (Roberts et al., 2004; Schaaf et al.,

Table 4 | Expression of members of the vacuolar iron transporter (VIT) family encoded in the soybean genome.

	Transcriptome				TMD	Homology to AtVit1 (% similarity)	Homology to LjSEN1 (% similarity)
	Severin et al. (2010)		Libault et al. (2010)				
	Root	Nodule	Root	Nodule			
Glyma01g36530	0	0	0	0	4	21	52
Glyma02g09110	18	1	2	19	4	22	51
Glyma05g24980	0	0	0	2	5	19	52
Glyma05g24990	0	0	0	1	5	20	54
Glyma05g25000	0	1	8	0	4	20	65
Glyma05g25010	0	761	16	2134	5	19	65
Glyma05g34430	5	8	3	6	5	81	22
Glyma08g05230	5	3	10	2	5	82	22
Glyma08g08070	10	0	0	8	4	12	36
Glyma08g08090	6	1	0	17	4	19	54
Glyma08g08100	3	0	0	8	5	19	54
Glyma08g08110	0	0	3	0	4	21	63
Glyma08g08120	0	192	3	801	4	21	62
Glyma08g19390	3	0	1	7	4	19	52
Glyma10g37030	1	0	0	1	4	24	57
Glyma11g08830	0	0	0	1	5	20	54
Glyma15g05610	0	0	0	1	3	19	50
Glyma16g28340	21	4	9	61	4	22	52
Glyma18g46245	0	0	–	–	5	22	17
Glyma20g30580	0	3	–	–	4	21	55

A comparison of each transporter's expression in root and nodule tissue from two soybean transcriptome studies is presented (Libault et al., 2010; Severin et al., 2010). A prediction of the number of transmembrane domains (TMD) each protein has was analyzed by SOSUI (http://bp.nuap.nagoya-u.ac.jp/sosui/sosui_submit.html). Homology to two VIT family members, AtVIT1, a characterized ferrous iron transporter and LjSEN1, which is essential for nitrogen fixation in L. japonicus, were calculated by a clustalW alignment.

2004). YS1 is able to transport Fe(III) complexed to the phytosiderophores deoxymugineic acid (DMA) and mugeneic acid (MA), as well as Fe(II) and Fe(III) complexed to NA, although the Fe(II) complex is transported more readily (Roberts et al., 2004; Schaaf et al., 2004). In monocots, the family mediates the uptake of Fe(III)-phytosiderophore complexes from the rhizosphere (Ueno et al., 2009). Dicots also contain members of the YSL family, but, because they do not take up siderophore complexes from the soil, it is thought that they specialize in long distance transport of Fe(II)-NA within the plant (Ueno et al., 2009). YSL family members can also transport Cu (Roberts et al., 2004), Ni (Gendre et al., 2007), and Mn (Sasaki et al., 2011) complexed to PS. Most YSL transporters characterized are localized to the plasma membrane and are involved in uptake of metals. AtYSL4 and 6 are the exceptions as they are localized to the chloroplast membrane. However, their direction of transport – out of the chloroplast to reduce iron toxicity – is analogous to that of the plasma membrane transporters (Divol et al., 2013).

Iron remobilization from the nodule will involve transporters that are expressed later in nodule development, during seed formation. The identification of a NA synthase in *Lotus japonicus* nodules and its expression later in nodule development suggests that iron is redistributed from the nodule chelated to NA (Hakoyama et al., 2009). This makes YSL family members candidates for iron remobilization from the nodule during senescence.

Fifteen YSL family members are encoded in the soybean genome. Of these, Glyma11g31870 has essentially nodule specific expression while expression of eight other members of the family has been detected in nodules (**Table 5**). In soybean, the transcriptome has been studied at only one time-point – that of mature N-fixing nodules – and so genes with enhanced expression during nodule senescence may not be obvious.

CONCLUDING REMARKS AND FUTURE DIRECTIONS

Iron transport in the roots and nodules of symbiotic legumes is clearly very complex, involving many cell types, some unique to nodules, and transport both into and out of cells and organelles. Transport across the specialized SM is especially intriguing and of special significance to nitrogen fixation. Given the importance of iron to the symbiosis and the symbiosis to sustainable agriculture, it is important that we understand the processes involved in iron acquisition, storage, and mobilization.

Our knowledge of transporters in nodules to date is derived from classical genetic approaches including screening for sequence homology to known iron transporters (for example *GmZIP1* and *GmDMT1;* Moreau et al., 2002; Kaiser et al., 2003) or the identification of genes involved in certain mutant phenotypes (e.g., LjSEN1; Hakoyama et al., 2012). Recent advances in genome sequencing, transcriptomics, and proteomics, open new avenues for identifying transport functions. In particular, the large scale sequencing of *M. truncatula*, *Lotus japonicus*, and *G. max* genomes has resulted in an explosion in the list of genes encoding membrane proteins (Benedito et al., 2010), many of them highly expressed in nodules and some of them probable iron transporters. The challenge is to functionally characterize these transporters and to identify their location and roles within nodules.

Table 5 | Expression of the YSL family transporters encoded in the soybean genome.

	Transcriptome				TMD	Homology to AtYSL1 (% similarity)
	Severin et al. (2010)		Libault et al. (2010)			
	Root	Nodule	Root	Nodule		
Glyma04g41020.1	6	4	15	18	12	64
Glyma06g13820.1	5	5	22	37	14	64
Glyma09g29410.1	2	1	7	2	14	53
Glyma09g41800.1	0	0	0	0	10	45
Glyma10g31610.1	0	0	1	0	13	71
Glyma11g31870.1	0	25	2	7	12	52
Glyma13g10410.1	0	1	3	2	11	68
Glyma16g05850.1	21	6	91	47	12	54
Glyma16g33840.1	14	4	123	99	13	53
Glyma17g26520.1	0	0	1	2	15	62
Glyma19g26500.1	27	8	90	58	13	54
Glyma20g00690.1	0	0	0	0	14	48
Glyma20g00700.1	0	0	0	0	11	48
Glyma20g16600.1	0	0	0	0	12	73
Glyma20g35980.1	0	2	6	7	13	71

A comparison of each YSL transporter's expression in root and nodule tissue from two soybean transcriptome studies is presented (Libault et al., 2010; Severin et al., 2010). A prediction of the number of transmembrane domains (TMD) for each protein was analyzed by SOSUI (http://bp.nuap.nagoya-u.ac.jp/sosui/sosui_submit.html). Homology to AtYSL1, a characterized ferrous iron transporter of the YSL family, was calculated by a clustalW alignment.

REFERENCES

Alonso, J. M., Hirayama, T., Roman, G., Nourizadeh, S., and Ecker, J. R. (1999). EIN2, a bifunctional transducer of ethylene and stress responses in *Arabidopsis*. *Science* 284, 2148–2152. doi: 10.1126/science.284.5423.2148

Appleby, C. A. (1984). Leghemoglobin and rhizobium respiration. *Annu. Rev. Plant Physiol. Plant Mol. Biol.* 35, 443–478. doi: 10.1146/annurev.pp.35.060184.002303

Barnett, M. J., Tolman, C. J., Fisher, R. F., and Long, S. R. (2004). A dual-genome Symbiosis Chip for coordinate study of signal exchange and development in a prokaryote-host interaction. *Proc. Natl. Acad. Sci. U.S.A.* 101, 16636–16641. doi: 10.1073/pnas.0407269101

Battistoni, F., Platero, R., Duran, R., Cerveñansky, C., Battistoni, J., Arias, A., et al. (2002a). Identification of an iron-regulated, hemin-binding outer membrane protein in *Sinorhizobium meliloti*. *Appl. Environ. Microbiol.* 68, 5877–5881. doi: 10.1128/AEM.68.12.5877-5881.2002

Battistoni, F., Platero, R., Noya, F., Arias, A., and Fabiano, E. (2002b). Intracellular Fe content influences nodulation competitiveness of *Sinorhizobium meliloti* strains as inocula of alfalfa. *Soil Biol. Biochem.* 34, 593–597. doi: 10.1016/S0038-0717(01)00215-2

Becker, A., Berges, H., Krol, E., Bruand, C., Ruberg, S., Capela, D., et al. (2004). Global changes in gene expression in *Sinorhizobium meliloti* 1021 under microoxic and symbiotic conditions. *Mol. Plant Microbe Interact.* 17, 292–303. doi: 10.1094/mpmi.2004.17.3.292

Bederska, M., Borucki, W., and Znojek, E. (2012). Movement of fluorescent dyes Lucifer Yellow (LYCH) and carboxyfluorescein (CF) in *Medicago truncatula* Gaertn. roots and root nodules. *Symbiosis* 58, 183–190. doi: 10.1007/s13199-013-0221-7

Benedito, V. A., Li, H., Dai, X., Wandrey, M., He, J., Kaundal, R., et al. (2010). Genomic inventory and transcriptional analysis of *Medicago truncatula* transporters. *Plant Physiol.* 152, 1716–1730. doi: 10.1104/pp.109.148684

Benedito, V. A., Torres-Jerez, I., Murray, J. D., Andriankaja, A., Allen, S., Kakar, K., et al. (2008). A gene expression atlas of the model legume *Medicago truncatula*. *Plant J.* 55, 504–513. doi: 10.1111/j.1365-313X.2008.03519.x

Bergersen, F. J., and Appleby, C. A. (1981). Leghemoglobin within bacteroid enclosing membrane envelopes from soybean root nodules. *Planta* 152, 534–543. doi: 10.1007/bf00380824

Brown, S. M., Oparka, K. J., Sprent, J. I., and Walsh, K. B. (1995). Symplastic transport in soybean root nodules. *Soil Biol. Biochem.* 27, 387–399. doi: 10.1016/0038-0717(95)98609-R

Brüggemann, W., Maas-Kantel, K., and Moog, P. (1993). Iron uptake by leaf mesophyll cells: The role of the plasma membrane-bound ferric-chelate reductase. *Planta* 190, 151–155. doi: 10.1007/bf00196606

Burton, J. W., Harlow, C., and Theil, E. C. (1998). Evidence for reutilization of nodule iron in soybean seed development. *J. Plant Nutr.* 21, 913–927. doi: 10.1080/01904169809365453

Cailliatte, R., Schikora, A., Briat, J., Mari, S., and Curie, C. (2010). High-affinity manganese uptake by the metal transporter NRAMP1 is essential for *Arabidopsis* growth in low manganese conditions. *Plant Cell* 22, 904–917. doi: 10.1105/tpc.109.073023

Capela, D., Filipe, C., Bobilk, C., Batut, J., and Bruand, C. (2006). *Sinorhizobium meliloti* differentiation during symbiosis with alfalfa: a transcriptomic dissection. *Mol. Plant Microbe Interact.* 19, 363–372. doi: 10.1094/mpmi-19-0363

Catalano, C. M., Lane, W. S., and Sherrier, D. J. (2004). Biochemical characterization of symbiosome membrane proteins from *Medicago truncatula* root nodules. *Electrophoresis* 25, 519–531. doi: 10.1002/elps.200305711

Chang, W. S., Franck, W. L., Cytryn, E., Jeong, S., Joshi, T., Emerich, D. W., et al. (2007). An oligonucleotide microarray resource for transcriptional profiling of *Bradyrhizobium japonicum*. *Mol. Plant Microbe Interact.* 20, 1298–1307. doi: 10.1094/mpmi-20-10-1298

Cline, G. R., Powell, P. E., Szaniszlo, P. J., and Reid, C. P. P. (1982). Comparison of the abilities of hydroxamic, synthetic, and other natural organic acids to chelate iron and other ions in nutrient solution. *Soil Sci. Soc. Am. J.* 46, 1158–1164. doi: 10.2136/sssaj1982.03615995004600060008x

Cohen, C. K., Garvin, D. F., and Kochian, L. V. (2004). Kinetic properties of a micronutrient transporter from *Pisum sativum* indicate a primary function in Fe uptake from the soil. *Planta* 218, 784–792. doi: 10.1007/s00425-003-1156-7

Curie, C., Cassin, G., Couch, D., Divol, F., Higuchi, K., Jean, M., et al. (2009). Metal movement within the plant: contribution of nicotianamine and yellow stripe 1-like transporters. *Ann. Bot.* 103, 1–11. doi: 10.1093/aob/mcn207

Delauney, A. J., Cheon, C. I., Snyder, P. J., and Verma, D. P. S. (1990). A nodule-specific sequence encoding a methionine-rich polypeptide, nodulin-21. *Plant Mol. Biol.* 14, 449–451.

Delgado, M. J., Bedmar, E. J., and Downie, J. A. (1998). "Genes involved in the formation and assembly of rhizobial cytochromes and their role in symbiotic nitrogen fixation," in *Advances in Microbial Physiology*, Vol. 40, ed. R. K. Poole (Waltham: Academic Press), 191–231.

Divol, F., Couch, D., Conéjéro, G., Roschzttardtz, H., Mari, S., and Curie, C. (2013). The *Arabidopsis* YELLOW STRIPE LIKE4 and 6 transporters control iron release from the chloroplast. *Plant Cell* 25, 1040–1055. doi: 10.1105/tpc.112.107672

Dixon, R., and Kahn, D. (2004). Genetic regulation of biological nitrogen fixation. *Nat. Rev. Microbiol.* 2, 621–631. doi: 10.1038/nrmicro954

Enz, S., Mahren, S., Stroeher, U. H., and Braun, V. (2000). Surface signaling in ferric citrate transport gene induction: interaction of the FecA, FecR, and FecI regulatory proteins. *J. Bacteriol.* 182, 637–646. doi: 10.1128/jb.182.3.637-646.2000

Fabiano, E., and O'Brian, M. R. (2012). "Mechanisms and regulation of iron homeostasis in the rhizobia," in *Molecular Aspects of Iron Metabolism in Pathogenic and Symbiotic Plant–Microbe Associations*, eds D. Expert and M. R. O'Brian (Dordrecht: Springer), 41–86.

Faraldo-Gomez, J. D., and Sansom, M. S. P. (2003). Acquisition of siderophores in Gram-negative bacteria. *Nat. Rev. Mol. Cell Biol.* 4, 105–116. doi: 10.1038/nrm1015

Fortin, M. G., Zelechowska, M., and Verma, D. P. S. (1985). Specific targeting of membrane nodulins to the bacteroid-enclosing compartment in soybean nodules. *EMBO J.* 4, 3041–3046.

Gendre, D., Czernic, P., Conejero, G., Pianelli, K., Briat, J. F., Lebrun, M., et al. (2007). TcYSL3, a member of the YSL gene family from the hyperaccumulator *Thlaspi caerulescens*, encodes a nicotianamine-Ni/Fe transporter. *Plant J.* 49, 1–15. doi: 10.1111/j.1365-313X.2006.02937.x

Gollhofer, J., Schlawicke, C., Jungnick, N., Schmidt, W., and Buckhout, T. J. (2011). Members of a small family of nodulin-like genes are regulated under iron deficiency in roots of *Arabidopsis thaliana*. *Plant Physiol. Biochem.* 49, 557–564. doi: 10.1016/j.plaphy.2011.02.011

Graham, P. H., and Vance, C. P. (2003). Legumes: importance and constraints to greater use. *Plant Physiol.* 131, 872–877. doi: 10.1104/pp.017004

Guerinot, M. L. (1991). Iron uptake and metabolism in the rhizobia legume symbiosis. *Plant Soil* 130, 199–209. doi: 10.1007/bf00011874

Guerinot, M. L. (1994). Microbial iron transport. *Annu. Rev. Microbiol.* 48, 743–772. doi: 10.1146/annurev.micro.48.1.743

Guerinot, M. L., Meidl, E. J., and Plessner, O. (1990). Citrate as a siderophore in *Bradyrhizobium japonicum*. *J. Bacteriol.* 172, 3298–3303.

Guinel, F. C. (2009). Getting around the legume nodule: I. The structure of the peripheral zone in four nodule types. *Botany* 87, 1117–1138. doi: 10.1139/b09-074

Hakoyama, T., Niimi, K., Yamamoto, T., Isobe, S., Sato, S., Nakamura, Y., et al. (2012). The integral membrane protein SEN1 is required for symbiotic nitrogen fixation in *Lotus japonicus* nodules. *Plant Cell Physiol.* 53, 225–236. doi: 10.1093/pcp/pcr167

Hakoyama, T., Watanabe, H., Tomita, J., Yamamoto, A., Sato, S., Mori, Y., et al. (2009). Nicotianamine synthase specifically expressed in root nodules of *Lotus japonicus*. *Planta* 230, 309–317. doi: 10.1007/s00425-009-0944-0

Hall, B. P., and Guerinot, M. L. (2007). "The role of zip family members in iron transport," in *Iron Nutrition in Plant and Rhizospheric Microorganisms*, eds L. L. Barton and J. Abadia (Dordrecht: Springer), 311–326.

Hantke, K. (2003). Is the bacterial ferrous iron transporter FeoB a living fossil? *Trends Microbiol.* 11, 192–195. doi: 10.1016/s0966-842x(03)00100-8

Herrada, G., Puppo, A., Moreau, S., Day, D. A., and Rigaud, J. (1993). How is leghemoglobin involved in peribacteroid membrane degradation during nodule senescence? *FEBS Lett.* 326, 33–38. doi: 10.1016/0014-5793(93)81755-o

Herridge, D. F., Peoples, M. B., and Boddey, R. M. (2008). Global inputs of biological nitrogen fixation in agricultural systems. *Plant Soil* 311, 1–18. doi: 10.1007/s11104-008-9668-3

Ivanov, S., Fedorova, E. E., Limpens, E., De Mita, S., Genre, A., Bonfante, P., et al. (2012). Rhizobium–legume symbiosis shares an exocytotic pathway required for arbuscule formation. *Proc. Natl. Acad. Sci. U.S.A.* 109, 8316–8321. doi: 10.1073/pnas.1200407109

Kaiser, B. N., Moreau, S., Castelli, J., Thomson, R., Lambert, A., Bogliolo, S., et al. (2003). The soybean NRAMP homologue, GmDMT1, is a symbiotic divalent metal transporter capable of ferrous iron transport. *Plant J.* 35, 295–304. doi: 10.1046/j.1365-313X.2003.01802.x

Kim, S. A., Punshon, T., Lanzirotti, A., Li, L. T., Alonso, J. M., Ecker, J. R., et al. (2006). Localization of iron in *Arabidopsis* seed requires the vacuolar membrane transporter VIT1. *Science* 314, 1295–1298. doi: 10.1126/science.1132563

Kobayashi, T., and Nishizawa, N. K. (2012). Iron uptake, translocation, and regulation in higher plants. *Annu. Rev. Plant Biol.* 63, 131–152.

Lanquar, V., Lelievre, F., Bolte, S., Hames, C., Alcon, C., Neumann, D., et al. (2005). Mobilization of vacuolar iron by AtNRAMP3 and AtNRAMP4 is essential for seed germination on low iron. *EMBO J.* 24, 4041–4051. doi: 10.1038/sj.emboj.7600864

Lanquar, V., Ramos, M. S., Lelievre, F., Barbier-Brygoo, H., Krieger-Liszkay, A., Kramer, U., et al. (2010). Export of vacuolar manganese by AtNRAMP3 and AtNRAMP4 is required for optimal photosynthesis and growth under manganese deficiency. *Plant Physiol.* 152, 1986–1999. doi: 10.1104/pp.109.150946

Lapinskas, P. J., Lin, S. J., and Culotta, V. C. (1996). The role of the *Saccharomyces cerevisiae* CCC1 gene in the homeostasis of manganese ions. *Mol. Microbiol.* 21, 519–528. doi: 10.1111/j.1365-2958.1996.tb02561.x.

LeVier, K., Day, D. A., and Guerinot, M. L. (1996). Iron uptake by symbiosomes from soybean root nodules. *Plant Physiol.* 111, 893–900.

Li, L. T., Chen, O. S., Ward, D. M., and Kaplan, J. (2001). CCC1 is a transporter that mediates vacuolar iron storage in yeast. *J. Biol. Chem.* 276, 29515–29519. doi: 10.1074/jbc.M103944200

Libault, M., Farmer, A., Joshi, T., Takahashi, K., Langley, R. J., Franklin, L. D., et al. (2010). An integrated transcriptome atlas of the crop model *Glycine max*, and its use in comparative analyses in plants. *Plant J.* 63, 86–99. doi: 10.1111/j.1365-313X.2010.04222.x

Lim, B. L. (2010). TonB-dependent receptors in nitrogen-fixing nodulating bacteria. *Microbes Environ.* 25, 67–74. doi: 10.1264/jsme2.ME10102

Limpens, E., Ivanov, S., Van Esse, W., Voets, G., Fedorova, E., and Bisseling, T. (2009). Medicago N-2-fixing symbiosomes acquire the endocytic identity marker Rab7 but delay the acquisition of vacuolar identity. *Plant Cell* 21, 2811–2828. doi: 10.1105/tpc.108.064410

Lopez-Millan, A. F., Ellis, D. R., and Grusak, M. A. (2004). Identification and characterization of several new members of the ZIP family of metal ion transporters in *Medicago truncatula*. *Plant Mol. Biol.* 54, 583–596. doi: 10.1023/B:PLAN.0000038271.96019.aa

Lopez-Millan, A. F., Morales, F., Abadia, A., and Abadia, J. (2000). Effects of iron deficiency on the composition of the leaf apoplastic fluid and xylem sap in sugar beet. Implications for iron and carbon transport. *Plant Physiol.* 124, 873–884. doi: 10.1104/pp.124.2.873

Lucas, M. M., Sype, G., Hérouart, D., Hernández, M. J., Puppo, A., and Felipe, M. R. (1998). Immunolocalization of ferritin in determinate and indeterminate legume root nodules. *Protoplasma* 204, 61–70. doi: 10.1007/BF01282294

Lynch, D., O'brien, J., Welch, T., Clarke, P., Cuiv, P. O., Crosa, J. H., et al. (2001). Genetic organization of the region encoding regulation, biosynthesis, and transport of rhizobactin 1021, a siderophore produced by *Sinorhizobium meliloti*. *J. Bacteriol.* 183, 2576–2585. doi: 10.1128/jb.183.8.2576-2585.2001

Matzanke, B. F., Anemuller, S., Schunemann, V., Trautwein, A. X., and Hantke, K. (2004). FhuF, part of a siderophore-reductase system. *Biochemistry* 43, 1386–1392. doi: 10.1021/bi0357661

Maunoury, N., Redondo-Nieto, M., Bourcy, M., Van De Velde, W., Alunni, B., Laporte, P., et al. (2010). Differentiation of symbiotic cells and endosymbionts in *Medicago truncatula* nodulation are coupled to two transcriptome-switches. *PLoS ONE* 5:e9519. doi: 10.1371/journal.pone.0009519

Miethke, M., and Marahiel, M. A. (2007). Siderophore-based iron acquisition and pathogen control. *Microbiol. Mol. Biol. Rev.* 71, 413–451. doi: 10.1128/mmbr.00012-07

Moreau, S., Day, D. A., and Puppo, A. (1998). Ferrous iron is transported across the peribacteroid membrane of soybean nodules. *Planta* 207, 83–87. doi: 10.1007/s004250050458

Moreau, S., Meyer, J. M., and Puppo, A. (1995). Uptake of iron by symbiosomes and bacteroids from soybean nodules. *FEBS Lett.* 361, 225–228.

Moreau, S., Thomson, R. M., Kaiser, B. N., Trevaskis, B., Guerinot, M. L., Udvardi, M. K., et al. (2002). GmZIP1 encodes a symbiosis-specific zinc transporter in soybean. *J. Biol. Chem.* 277, 4738–4746. doi: 10.1074/jbc.M106754200

Nevo, Y., and Nelson, N. (2006). The NRAMP family of metal-ion transporters. *Biochim. Biophys. Acta* 1763, 609–620. doi: 10.1016/j.bbamcr.2006.05.007

Nienaber, A., Hennecke, H., and Fischer, H. M. (2001). Discovery of a haem uptake system in the soil bacterium *Bradyrhizobium japonicum*. *Mol. Microbiol.* 41, 787–800. doi: 10.1046/j.1365-2958.2001.02555.x

Noya, F., Arias, A., and Fabiano, E. (1997). Heme compounds as iron sources for nonpathogenic *Rhizobium* bacteria. *J. Bacteriol.* 179, 3076–3078.

O'Brian, M. R. (1996). Heme synthesis in the rhizobium–legume symbiosis: a palette for bacterial and eukaryotic pigments. *J. Bacteriol.* 178, 2471–2478.

O'Hara, G. W. (2001). Nutritional constraints on root nodule bacteria affecting symbiotic nitrogen fixation: a review. *Aust. J. Exp. Agric.* 41, 417–433. doi: 10.1071/ea00087

O'Hara, G. W., Dilworth, M. J., Boonkerd, N., and Parkpian, P. (1988). Iron-deficiency specifically limits nodule development in peanut inoculated with Bradyrhizobium sp. *New Phytol.* 108, 51–57. doi: 10.1111/j.1469-8137.1988.tb00203.x

Peters, J. W., and Szilagyi, R. K. (2006). Exploring new frontiers of nitrogenase structure and mechanism. *Curr. Opin. Chem. Biol.* 10, 101–108. doi: 10.1016/j.cbpa.2006.02.019

Pierre, O., Engler, G., Hopkins, J., Brau, F., Boncompagni, E., and Hérouart, D. (2013). Peribacteroid space acidification: a marker of mature bacteroid functioning in *Medicago truncatula* nodules. *Plant Cell Environ.* doi: 10.1111/pce.12116.

Popp, C., and Ott, T. (2011). Regulation of signal transduction and bacterial infection during root nodule symbiosis. *Curr. Opin. Plant Biol.* 14, 458–467. doi: 10.1016/j.pbi.2011.03.016

Puppo, A., Herrada, G., and Rigaud, J. (1991). Lipid peroxidation in peribacteroid membranes from french-bean nodules. *Plant Physiol.* 96, 826–830. doi: 10.1104/pp.96.3.826

Ragland, M., and Theil, E. C. (1993). Ferritin (Messenger-RNA, protein) and iron concentrations during soybean nodule development. *Plant Mol. Biol.* 21, 555–560. doi: 10.1007/bf00028813

Rellan-Alvarez, R., Giner-Martinez-Sierra, J., Orduna, J., Orera, I., Rodriguez-Castrillon, J. A., Garcia-Alonso, J. I., et al. (2010). Identification of a tri-iron(III), tri-citrate complex in the xylem sap of iron-deficient tomato resupplied with iron: new insights into plant iron long-distance transport. *Plant Cell Physiol.* 51, 91–102. doi: 10.1093/pcp/pcp170

Roberts, L. A., Pierson, A. J., Panaviene, Z., and Walker, E. L. (2004). Yellow stripe1. Expanded roles for the maize iron-phytosiderophore transporter. *Plant Physiol.* 135, 112–120. doi: 10.1104/pp.103.037572

Rodriguez-Haas, B., Finney, L., Vogt, S., Gonzalez-Melendi, P., Imperial, J., and Gonzalez-Guerrero, M. (2013). Iron distribution through the developmental stages of *Medicago truncatula* nodules. *Metallomics* 5, 1247–1253. doi: 10.1039/C3MT00060E

Roschzttardtz, H., Séguéla-Arnaud, M., Briat, J.-F., Vert, G., and Curie, C. (2011). The FRD3 citrate effluxer promotes iron nutrition between symplastically disconnected tissues throughout *Arabidopsis* development. *Plant Cell* 23, 2725–2737. doi: 10.1105/tpc.111.088088

Roth, L. E., and Stacey, G. (1989). Bacterium release into host-cells of the nitrogen-fixing soybean nodules-the symbiosome membrane comes from 3 sources. *Eur. J. Cell Biol.* 49, 13–23.

Sasaki, A., Yamaji, N., Xia, J. X., and Ma, J. F. (2011). OsYSL6 is involved in the detoxification of excess manganese in rice. *Plant Physiol.* 157, 1832–1840. doi: 10.1104/pp.111.186031

Sasaki, A., Yamaji, N., Yokosho, K., and Ma, J. F. (2012). Nramp5 Is a major transporter responsible for manganese and cadmium uptake in rice. *Plant Cell* 24, 2155–2167. doi: 10.1105/tpc.112.096925

Schaaf, G., Ludewig, U., Erenoglu, B. E., Mori, S., Kitahara, T., and Von Wiren, N. (2004). ZmYS1 functions as a proton-coupled symporter for phytosiderophore- and nicotianamine-chelated metals. *J. Biol. Chem.* 279, 9091–9096. doi: 10.1074/jbc.M311799200

Schultze, M., and Kondorosi, A. (1998). Regulation of symbiotic root nodule development. *Annu. Rev. Genet.* 32, 33–57. doi: 10.1146/annurev.genet.32.1.33

Severin, A. J., Woody, J. L., Bolon, Y. T., Joseph, B., Diers, B. W., Farmer, A. D., et al. (2010). RNA-Seq Atlas of *Glycine max*: a guide to the soybean transcriptome. *BMC Plant Biol.* 10:160. doi: 10.1186/1471-2229-10-160

Slatni, T., Dell'orto, M., Ben Salah, I., Vigani, G., Smaoui, A., Gouia, H., et al. (2012). Immunolocalization

of H^+-ATPase and IRT1 enzymes in N2-fixing common bean nodules subjected to iron deficiency. *J. Plant Physiol.* 169, 242–248. doi: 10.1016/j.jplph.2011.10.003

Slatni, T., Krouma, A., Aydi, S., Chaiffi, C., Gouia, H., and Abdelly, C. (2008). Growth, nitrogen fixation and ammonium assimilation in common bean (*Phaseolus vulgaris* L) subjected to iron deficiency. *Plant Soil* 312, 49–57. doi: 10.1007/s11104-007-9481-4

Slatni, T., Krouma, A., Gouia, H., and Abdelly, C. (2009). Importance of ferric chelate reductase activity and acidification capacity in root nodules of N2-fixing common bean (*Phaseolus vulgaris* L.) subjected to iron deficiency. *Symbiosis* 47, 35–42. doi: 10.1007/BF03179968

Slatni, T., Vigani, G., Salah, I. B., Kouas, S., Dell'orto, M., Gouia, H., et al. (2011). Metabolic changes of iron uptake in N2-fixing common bean nodules during iron deficiency. *Plant Sci.* 181, 151–158. doi: 10.1016/j.plantsci.2011.04.015

Small, S. K., and O'Brian, M. R. (2011). The *Bradyrhizobium japonicum* frcB gene encodes a diheme ferric reductase. *J. Bacteriol.* 193, 4088–4094. doi: 10.1128/jb.05064-11

Small, S. K., Puri, S., Sangwan, I., and O'brian, M. R. (2009). Positive control of ferric siderophore receptor gene expression by the Irr protein in *Bradyrhizobium japonicum*. *J. Bacteriol.* 191, 1361–1368. doi: 10.1128/jb.01571-08

Soerensen, K. U., Terry, R. E., Jolley, V. D., Brown, J. C., and Vargas, M. E. (1988). The interaction of iron-stress response and root-nodules in iron efficient and inefficient soybeans. *J. Plant Nutr.* 11, 853–862. doi: 10.1080/01904168809363850

Strozycki, P. M., Szczurek, A., Lotocka, B., Figlerowicz, M., and Legocki, A. B. (2007). Ferritins and nodulation in *Lupinus luteus*: iron management in indeterminate type nodules. *J. Exp. Bot.* 58, 3145–3153. doi: 10.1093/jxb/erm152

Takanashi, K., Yokosho, K., Saeki, K., Sugiyama, A., Sato, S., Tabata, S., et al. (2013). LjMATE1: a citrate transporter responsible for iron supply to the nodule infection zone of *Lotus japonicus*. *Plant Cell Physiol.* doi: 10.1093/pcp/pct019

Tang, C. X., Robson, A. D., and Dilworth, M. J. (1990a). The role of iron in nodulation and nitrogen-fixation in *Lupinus angustifolius* L. *New Phytol.* 114, 173–182. doi: 10.1111/j.1469-8137.1990.tb00388.x

Tang, C. X., Robson, A. D., and Dilworth, M. J. (1990b). A split-root experiment shows that iron is required for nodule initiation in *Lupinus angustifolius* L. *New Phytol.* 115, 61–67. doi: 10.1111/j.1469-8137.1990.tb00922.x

Terry, R. E., Soerensen, K. U., Jolley, V., and Brown, J. C. (1991). The role of active *Bradyrhizobium japonicum* in iron stress response of soybeans. *Plant Soil* 130, 225–230. doi: 10.1007/bf00011877

Tiffin, L. O. (1970). Translocation of iron citrate and phosphorous in xylem exudate of soybean. *Plant Physiol.* 45, 280–283. doi: 10.1104/pp.45.3.280

Todd, J. D., Sawers, G., Rodionov, D. A., and Johnston, A. W. B. (2006). The *Rhizobium leguminosarum* regulator IrrA affects the transcription of a wide range of genes in response to Fe availability. *Mol. Genet. Genomics* 275, 564–577. doi: 10.1007/s00438-006-0155-y

Udvardi, M., and Poole, P. S. (2013). Transport and metabolism in legume–rhizobia symbioses. *Annu. Rev. Plant Biol.* 64, 781–805. doi: 10.1146/annurev-arplant-050312-120235

Udvardi, M. K., and Day, D. A. (1997). Metabolite transport across symbiotic membranes of legume nodules. *Annu. Rev. Plant Physiol. Plant Mol. Biol.* 48, 493–523. doi: 10.1146/annurev.arplant.48.1.493

Ueno, D., Yamaji, N., and Ma, J. F. (2009). Further characterization of ferric-phytosiderophore transporters ZmYS1 and HvYS1 in maize and barley. *J. Exp. Bot.* 60, 3513–3520. doi: 10.1093/jxb/erp191

Vavilin, D. V., and Vermaas, W. F. J. (2002). Regulation of the tetrapyrrole biosynthetic pathway leading to heme and chlorophyll in plants and cyanobacteria. *Physiol. Plant.* 115, 9–24. doi: 10.1034/j.1399-3054.2002.1150102.x

Verma, D. P. S., Ball, S., Guerin, C., and Wanamaker, L. (1979). Leghemoglobin biosynthesis in soybean root nodules. Characterisation of the nascent and released peptides and the relative rate of synthesis of the major leghemoglobins. *Biochemistry* 18, 476–483. doi: 10.1021/bi00570a016

Verma, D. P. S., Kazazian, V., Zogbi, V., and Bal, A. K. (1978). Isolation and Characterization of the membrane envelope enclosing the bacteroids in soybean root nodules. *J. Cell. Biol.* 78, 919–936.

Vert, G., Grotz, N., Dedaldechamp, F., Gaymard, F., Guerinot, M. L., Briat, J. F., et al. (2002). IRT1, an *Arabidopsis* transporter essential for iron uptake from the soil and for plant growth. *Plant Cell* 14, 1223–1233. doi: 10.1105/tpc.001388

Viguier, C., Cuiv, P. O., Clarke, P., and O'connell, M. (2005). RirA is the iron response regulator of the rhizobactin 1021 biosynthesis and transport genes in *Sinorhizobium meliloti* 2011. *FEMS Microbiol. Lett.* 246, 235–242. doi: 10.1016/j.femsle.2005.04.012

Wexler, M., Yeoman, K. H., Stevens, J. B., De Luca, N. G., Sawers, G., and Johnston, A. W. B. (2001). The *Rhizobium leguminosarum* tonB gene is required for the uptake of siderophore and haem as sources of iron. *Mol. Microbiol.* 41, 801–816. doi: 10.1046/j.1365-2958.2001.02556.x.

Whitehead, L. F., and Day, D. A. (1997). The peribacteroid membrane. *Physiol. Plant.* 100, 30–44. doi: 10.1034/j.1399-3054.1997.1000103.x

Wittenberg, J. B., Wittenberg, B. A., Day, D. A., Udvardi, M. K., and Appleby, C. A. (1996). Siderophore-bound iron in the peribacteriod space of soybean root nodules. *Plant. Soil* 178, 161–169. doi: 10.1007/bf00011579

Xia, J., Yamaji, N., Kasai, T., and Ma, J. F. (2010). Plasma membrane-localized transporter for aluminum in rice. *Proc. Natl. Acad. Sci. U.S.A.* 107, 18381–18385. doi: 10.1073/pnas.1004949107

Xiong, H. C., Kobayashi, T., Kakei, Y., Senoura, T., Nakazono, M., Takahashi, H., et al. (2012). AhNRAMP1 iron transporter is involved in iron acquisition in peanut. *J. Exp. Bot.* 63, 4437–4446. doi: 10.1093/jxb/ers117

Yeoman, K. H., Wisniewski-Dye, F., Timony, C., Stevens, J. B., Deluca, N. G., Downie, J. A., et al. (2000). Analysis of the *Rhizobium leguminosarum* siderophore-uptake gene fhuA: differential expression in free-living bacteria and nitrogen-fixing bacteroids and distribution of an fhuA pseudogene in different strains. *Microbiology* 146, 829–837.

Conflict of Interest Statement: The authors declare that the research was conducted in the absence of any commercial or financial relationships that could be construed as a potential conflict of interest.

Received: 24 May 2013; accepted: 26 August 2013; published online: 13 September 2013.

*Citation: Brear EM, Day DA and Smith PMC (2013) Iron: an essential micronutrient for the legume–rhizobium symbiosis. Front. Plant Sci. **4**:359. doi: 10.3389/fpls.2013.00359*

This article was submitted to Plant Nutrition, a section of the journal Frontiers in Plant Science.